NASA Technical Memorandum 84560

Aerodynamic Characteristics of a Series of Twin-Inlet Air-Breathing Missile Configurations

III - Axisymmetric and Two-Dimensional Inlets at Subsonic-Transonic Speeds

Clyde Hayes

MARCH 1983

NASA

NASA Technical Memorandum 84560

Aerodynamic Characteristics of a Series of Twin-Inlet Air-Breathing Missile Configurations

III - Axisymmetric and Two-Dimensional Inlets at Subsonic-Transonic Speeds

Clyde Hayes
Langley Research Center
Hampton, Virginia

NASA

National Aeronautics
and Space Administration

Scientific and Technical
Information Branch

1983

SUMMARY

A series of air-breathing missile configurations has been investigated to provide a data base for the design of such missiles. The model could be configured with either twin axisymmetric or two-dimensional inlets. Three circumferential inlet locations were investigated: 90°, 115°, and 135° from the top center. Two vertical wing locations, as well as wingless configurations, were used. Three tail configurations were formed by locating the tail surfaces either on the inlet fairing or on fairings on the body. The surfaces were deflected to provide pitch control. Two-dimensional inlets with extended compression surfaces, used to improve the angle-of-attack performance of the inlets for wingless configurations, were also investigated. NASA Technical Memorandum 84558 covers the twin axisymmetric inlet configurations at supersonic speeds, and NASA Technical Memorandum 84559 covers two-dimensional inlet configurations at supersonic speeds. This report covers both inlet types at subsonic-transonic speeds, without internal flow, and simulates the boost configuration of an air-breathing missile. Results of the subsonic-transonic part of the investigation indicate that, as with the data at supersonic speeds, the pitching-moment curves were nonlinear but did not exhibit a large margin of longitudinal stability at high angles of attack with the wing on. The model had marginal lateral-directional stability for most configurations. The X-tail, however, resulted in lateral-directional stability for the entire range of angle of attack. With the wing added, the model had reduced longitudinal stability and required positive pitch-control deflection for trim at angles of attack up to 16° for the model with the inlet orientation angle of 115° and for the entire range of angle of attack for an inlet orientation angle of 135°. The X-tail configuration did not have the beneficial effects compared with the tri-tail, as with the supersonic tests, since the nonlinearity of the pitching-moment curves was not as extreme at subsonic speeds. The effect of inlet extensions added to the body-inlet-tail configuration to improve the inlet performance at high angle of attack was generally small. The effect of removing the inlet covers from the two-dimensional inlets (with ducts blocked) was small, except for an increase in axial force (drag) of as much as 50 percent at an angle of attack of 0°.

INTRODUCTION

During the past several years, several air-breathing missile configurations have been investigated in the Langley Unitary Plan Wind Tunnel. These include one-, two-, and four-inlet configurations with various wing and tail arrangements. The results of these investigations have been reported in references 1 through 7. Although the data from these specific missile programs have contributed to an air-breathing configuration data base, a broader data base is needed to better predict the aerodynamic characteristics of candidate configurations and to better design an air-breathing configuration to meet desired aerodynamic specifications. To provide a broader data base, a series of models, which incorporates a wider range of configuration variables, has been designed and tested.

The model could be configured with axisymmetric or two-dimensional single or twin inlets. The single inlet was located at the bottom of the body, whereas the twin inlets could be located circumferentially from 90° to 135° from the top

center. Two vertical wing locations were available to properly locate the wing relative to the inlets at the 115° and 135° inlet orientation angles to provide favorable interference between the wing and inlet at positive angles of attack. Tail surfaces could be mounted on the inlet fairing and/or on fairings on the body to provide several tail configurations. The tail surfaces could be deflected to provide pitch control. The two-dimensional inlets could be configured with extended compression surfaces intended to improve the angle-of-attack performance of the inlets for the wingless configuration.

The present investigation covers tests of the twin-inlet configurations, both axisymmetric and two-dimensional inlets. The inlets were located at circumferential locations of 90°, 115°, and 135° from the top center. The wing was located above the model center line with the inlets located in the 115° position and at the model center line with the inlets in the 135° position. The wing was not used with the inlets located in the 90° position. Three tail configurations were used. A tri-tail configuration with a vertical surface at the top center of the body and a surface mounted on each of the two inlet fairings was tested at all three inlet orientation angles. With the inlets located in the 135° position, the single vertical surface was replaced by two surfaces in the upper 45° position to form an X-tail configuration. Also, at the inlet orientation angle of 135° and with the two upper surfaces at 45°, the two lower surfaces were replaced by a single lower surface to form an inverted tri-tail configuration. The tests included body-inlet, body-inlet-wing, body-inlet-tail, and body-inlet-wing-tail configurations.

The supersonic tests were performed in the high Mach number test section of the Langley Unitary Plan Wind Tunnel at Mach numbers of 2.50, 2.95, 3.50, and 3.95. The inlets were operating with flow through the model to simulate ramjet operation. The subsonic tests were conducted at Mach numbers of 0.60, 0.80, and 0.95 in the 7- by 10-Foot Transonic Wind Tunnel at the David Taylor Naval Ship Research and Development Center. The internal ducts were closed, and there was no flow through the model to simulate rocket boost.

Longitudinal aerodynamic characteristics, lateral-directional stability, pitch-control effectiveness, and trim characteristics were obtained.

Because a large volume of data was obtained in this investigation, the data are presented in three reports: Reference 8 covers the twin axisymmetric inlet configurations at supersonic speeds, reference 9 covers the twin two-dimensional inlet configurations at supersonic speeds, and this report covers both inlet configurations at subsonic-transonic speeds. The results of an investigation of the single-inlet configurations are presented in reference 10.

SYMBOLS

The coefficients of forces and moments are referred to both the body axis and stability axis systems, where appropriate. Aerodynamic moments are taken about a point on the model center line at a distance downstream of the model nose equal to 50 percent of the body length (fig. 1). All coefficients are based on the cross-sectional area and the diameter of the body.

A cross-sectional area of basic body, 0.00456 m^2

C_A axial-force coefficient, $\frac{\text{Axial force}}{qA}$

$C_{A,i}$ internal-flow axial-force coefficient, $\frac{\text{Internal-flow axial force}}{qA}$

C_D drag coefficient, $\frac{\text{Drag}}{qA}$

C_L lift coefficient, $\frac{\text{Lift}}{qA}$

C_l rolling-moment coefficient, $\frac{\text{Rolling moment}}{qAd}$

C_{l_β} $= \left(\frac{\Delta C_l}{\Delta\beta}\right)_{\beta=0^\circ,5^\circ}$

C_m pitching-moment coefficient, $\frac{\text{Pitching moment}}{qAd}$

C_N normal-force coefficient, $\frac{\text{Normal force}}{qA}$

C_n yawing-moment coefficient, $\frac{\text{Yawing moment}}{qAd}$

C_{n_β} $= \left(\frac{\Delta C_n}{\Delta\beta}\right)_{\beta=0^\circ,5^\circ}$

C_Y side-force coefficient, $\frac{\text{Side force}}{qA}$

C_{Y_β} $= \left(\frac{\Delta C_Y}{\Delta\beta}\right)_{\beta=0^\circ,5^\circ}$

d body diameter, 0.0762 m

L/D lift-drag ratio

M free-stream Mach number

M.S. model station

m/m_∞ inlet mass-flow ratio (ratio of inlet mass flow to mass flow at free-stream conditions through a stream tube of cross-sectional area equal to inlet projected area)

q free-stream dynamic pressure, Pa

x,y,y_1,y_2,y_3 coordinates of inlet configurations (figs. 1(c) and 1(d))

α angle of attack, deg

β angle of sideslip, deg

δ_p tail deflection in pitch direction, deg (positive deflection with leading edge up)

ϕ_I inlet orientation angle, measured from model top center line, deg (figs. 1(a) and 1(b))

2-D two-dimensional

Configuration designations (various components shown in fig. 1):

B_1 body

I_1 twin circular inlets (axisymmetric inlets)

I_2 twin rectangular inlets (two-dimensional inlets)

I_{2c} twin rectangular inlets with inlet covers installed

I_3 twin rectangular extended inlets

I_{3c} twin rectangular extended inlets with inlet covers installed

T tail

T_1 tri-tail, one surface at top center and one on each of the inlet fairings

T_2 X-tail, two surfaces at upper 45° positions and two surfaces at inlet fairing; used only with $\phi_I = 135°$

T_3 inverted tri-tail, two surfaces at upper 45° position and one surface at bottom center line

W_1 wing, located at center-line position for $\phi_I = 135°$ and upper position for $\phi_I = 115°$; not used in combination with $\phi_I = 90°$

MODEL DESCRIPTION

Details of the model are presented in figure 1 and photographs in figure 2. The body was an ogive cylinder approximately 14 diameters long. An inlet of either the axisymmetric or rectangular two-dimensional type was located on each side of the body, separated from the body by boundary-layer diverters. The ducts extended downstream of the inlets to a point where they would turn and dump into the combustor. Beyond this point, the external geometry of the inlets consisted of tapered fairings, which extended back to the model base and provided support for two lower tail surfaces. Other tail surfaces could be attached to the body by means of fairings, which provided the necessary support and represented the volume that would be required for tail control actuators.

The inlet ducts dumped into a common passage within the body. The internal flow was kept separate from the balance cavity to facilitate measurement of the internal flow and the balance-cavity axial-force and drag corrections. A rake at the exit of

the duct was used to measure the flow conditions needed to compute the forces due to the internal flow.

The inlets and inlet fairings could be rotated in the circumferential direction about the model center line. The rectangular inlets each had a boundary-layer bleed slot which removed boundary layer from the compression surface and dumped it overboard. The axisymmetric inlets had no boundary-layer control. The wing used in the tests was located so that its pressure field would enhance the angle-of-attack performance of the inlets. The vertical location of the wing depended on the inlet orientation, and for inlets located on each side 90° from the top center line, the wing could not be used.

An extended inlet configuration was also investigated. This configuration consisted of the rectangular two-dimensional inlet with the compression surface extended forward to station 28.829 to enhance the angle-of-attack performance in the absence of a wing. The shorter of the two-dimensional inlet configurations was tested with and without a wing, whereas the extended inlets were not tested with the wing.

The airfoil of the wing consisted of an upper surface having a wedge leading and trailing edge with a flat center section and a lower surface that was flat from leading to trailing edge. The airfoils for the tail surfaces were similar, consisting of straight-line segments, but were symmetrical (figs. 1(e) and 1(f)).

Two types of tail surfaces were used, one designed to fit on the inlet fairings and the other to fit to the body in conjunction with a fairing. When the lines of each tail surface type are projected to the body surface (fig. 1(f)), their planforms are identical. The tail arrangements available depended on the inlet orientation. At all inlet orientations, a tri-tail was used, with a surface on each inlet fairing and a top vertical surface. With the inlets located at 135° from the top center, an X-tail configuration was formed by substituting two surfaces at the upper 45° for the single vertical surface. An inverted tri-tail configuration was also formed by substituting a single vertical surface at the bottom for the inlet fairing-mounted surfaces. For pitch-control deflection, all tail surfaces except the vertical surfaces were deflected. The tail-surface deflection angle was measured in the plane normal to the tail-surface hinge line.

For the tests with the internal ducts closed (subsonic Mach numbers), plugs were installed in each of the ducts. For the two-dimensional inlets, inlet covers were simulated by pieces inserted in the inlets with the outer surface flush with the inlet leading edges. Tests were also run without the inlet covers, but with the ducts closed, to measure the effect of inlet covers. All the closed-duct axisymmetric tests were run without inlet covers.

TESTS

The subsonic-transonic part of the investigation was conducted in the 7- by 10-Foot Transonic Wind Tunnel at the David Taylor Naval Ship Research and Development Center. The tunnel is a continuous-flow, closed-loop facility capable of operating over a Mach number range from 0.4 to 1.17 and over a dynamic-pressure range corresponding to an altitude range from sea level to 40 000 ft. A description of the facility is given in reference 11. The tests were performed at Mach numbers of 0.60, 0.80, and 0.95.

The internal ducts were blocked at the point where the flow would enter the body, and there was no internal flow for the subsonic tests. The tube used in the supersonic tests to separate the internal flow from the balance cavity was removed and the entire cavity was treated as a balance chamber. The cavity pressure was measured by two static-pressure tubes that were attached to the sting and terminated near the balance. Forces and moments were measured by a sting-mounted six-component balance, furnished by NASA.

Three inlet configurations were tested: axisymmetric I_1, rectangular two-dimensional I_2, and extended two-dimensional I_3. Configurations having inlet orientation angles ϕ_I of 90°, 115°, and 135° were used. Each combination of inlet type and inlet orientation angle could be configured as body-inlet, body-inlet-tail, body-inlet-wing, and body-inlet-wing-tail configurations. The entire matrix of configurations was not covered because of the limited test time available. The inlets with $\phi_I = 90°$ and the I_3 inlets at all inlet orientation angles were not designed to be used in combination with the wing. The inverted tri-tail T_3, which was tested at supersonic speeds (refs. 8 and 9), was not tested at subsonic speeds. The various tail configurations are shown in figure 1(g). Pitch-control deflections of 0° and ±10° were used.

Tests were made at angles of attack ranging from about -5° to 28°. Some runs were terminated at lower angles of attack because of the balance limits. To obtain lateral-directional stability, runs at angles of sideslip of 0° and 5° were made. Angles of attack and sideslip have been corrected for deflection of the sting and balance due to aerodynamic loads. The axial-force and drag data have been adjusted to free-stream static pressure acting over the model base, including the balance cavity and internal duct exit.

Tests were conducted at Reynolds numbers of 8.5, 9.5, and 10.0×10^6 per meter and at Mach numbers of 0.60, 0.80, and 0.95, respectively. All tests were made with the boundary-layer transition point fixed by means of transition strips. The transition strips were located 3.66 cm aft of the body nose and 1.78 cm in a streamwise direction from the leading edges of the wing, tail surfaces, and inlets. The transition strips were 0.325 cm wide and consisted of No. 90 sand grains on the aerodynamic surfaces and No. 100 sand grains on the nose.

PRESENTATION OF RESULTS

The results of this investigation are presented in the figures as indicated in the following table:

ϕ_I, deg	Wing	Tail	δ_p, deg	Variable	Effect measured	Figure
			Axisymmetric inlets I_1			
Varies	Off	T_1	0	Inlet orientation	Longitudinal	3
Varies	On	T_1	0	Inlet orientation	Longitudinal	4
90	Off	T_1	0	Model components	Longitudinal	5
115	On and off	T_1	0	Model components	Longitudinal	6
135	On and off	T_1	0	Model components	Longitudinal	7
135	On and off	T_2	0	Model components	Longitudinal	8
135	Off	T_1 and T_2	0	Tail configuration	Longitudinal	9
135	On	T_1 and T_2	0	Tail configuration	Longitudinal	10
90	Off	T_1	Varies	Pitch-control deflection	Pitch-control effectiveness	11
115	Off	T_1	Varies	Pitch-control deflection	Pitch-control effectiveness	12
135	Off	T_1	Varies	Pitch-control deflection	Pitch-control effectiveness	13

ϕ_I, deg	Wing	Tail	δ_p, deg	Variable	Effect measured	Figure
Axisymmetric inlets I_1 - Concluded						
115	On	T_1	Varies	Pitch-control deflection	Pitch-control effectiveness	14
135	On	T_1	Varies	Pitch-control deflection	Pitch-control effectiveness	15
Varies	On	T_1	0	Inlet orientation	Lateral-directional	16
90	Off	T_1	0	Model components	Lateral-directional	17
115	On and off	T_1	0	Model components	Lateral-directional	18
135	On and off	T_1	0	Model components	Lateral-directional	19
135	On and off	T_2	0	Model components	Lateral-directional	20
135	On	T_1 and T_2	0	Tail configuration	Lateral-directional	21
Two-dimensional inlets I_2						
Varies	Off	T_1	0	Inlet orientation	Longitudinal	22
Varies	On	T_1	0	Inlet orientation	Longitudinal	23
90	Off	T_1	0	Model components	Longitudinal	24
115	On and off	T_1	0	Model components	Longitudinal	25
135	On and off	T_1	0	Model components	Longitudinal	26
135	On and off	T_2	0	Model components	Longitudinal	27
135	Off	T_1 and T_2	0	Tail configuration	Longitudinal	28
135	On	T_1 and T_2	0	Tail configuration	Longitudinal	29
90	Off	T_1	Varies	Pitch-control deflection	Pitch-control effectiveness	30
115	Off	T_1	Varies	Pitch-control deflection	Pitch-control effectiveness	31
135	Off	T_1	Varies	Pitch-control deflection	Pitch-control effectiveness	32
135	Off	T_2	Varies	Pitch-control deflection	Pitch-control effectiveness	33
115	On	T_1	Varies	Pitch-control deflection	Pitch-control effectiveness	34
135	On	T_1	Varies	Pitch-control deflection	Pitch-control effectiveness	35
135	On	T_2	Varies	Pitch-control deflection	Pitch-control effectiveness	36
Varies	On	T_1	0	Inlet orientation	Lateral-directional	37
90	Off	T_1	0	Model components	Lateral-directional	38
115	On and off	T_1	0	Model components	Lateral-directional	39
135	On and off	T_1	0	Model components	Lateral-directional	40
135	On and off	T_2	0	Model components	Lateral-directional	41
135	On	T_1 and T_2	0	Tail configuration	Lateral-directional	42
90	Off	T_1	0	Inlet covers	Longitudinal	43
115	On	T_1	0	Inlet covers	Longitudinal	44
135	On	T_2	0	Inlet covers	Longitudinal	45
90	Off	T_1	0	Inlet covers	Lateral-directional	46
115	On	T_1	0	Inlet covers	Lateral-directional	47
135	On	T_2	0	Inlet covers	Lateral-directional	48
Two-dimensional extended inlets I_3						
Varies	Off	T_1	0	Inlet orientation	Longitudinal	49
Varies	Off	T_1	0	Inlet orientation	Lateral-directional	50

DISCUSSION OF RESULTS

The effects of inlet orientation angle ϕ_I on the longitudinal aerodynamic characteristics for the configurations with axisymmetric inlets I_1 are presented in figures 3 and 4, and for those with 2-D inlets I_{2c} in figures 22 and 23. At all three inlet orientation angles, the body-inlet-tail configurations were stable. Although the configurations were stable throughout the angle-of-attack range of the tests, there was a continual increase in the slope of the pitching-moment curve with increasing angle of attack. With the addition of the wing (ϕ_I = 115° and 135° only) the model became less stable and was unstable at negative and small angles of attack, becoming neutrally stable and then stable as the angle of attack was further increased.

As with the supersonic tests (refs. 8 and 9), the longitudinal stability decreased with rotation of the inlets and fairings downward (increasing ϕ_I). The variation of stability at subsonic speeds, however, is more like that which would be

expected from the variation of the planform area of the aft end of the model, than at the supersonic tests for which there was very little difference in the longitudinal stability between the configurations for $\phi_I = 90°$ and $\phi_I = 115°$.

The effect of various model components on the longitudinal aerodynamic characteristics is shown in figures 5 through 8 for the axisymmetric inlets (figs. 24 through 27 for 2-D inlets). The trends are similar to those at supersonic speeds; the pitching-moment curves tended to be nonlinear and stability increased with increasing angle of attack. The body-inlet configurations were unstable at low angles of attack and became stable at angles of attack above about 12°. Adding the tail resulted in longitudinal stability for the range of angle of attack of the tests. Adding the wing to the body-inlet or body-inlet-tail configuration resulted in a positive increment in pitching moment and lift or normal force. This effect is probably caused by the high pressure field ahead of the nonflowing inlets reacting on the wing. This effect is somewhat less for the 2-D inlet configurations, which was expected because the pressure field ahead of the 2-D inlets with inlet covers installed was expected to be less than that ahead of the axisymmetric inlets. The smaller axial force for the 2-D inlet configurations compared with the axisymmetric-inlet configurations indicates that this is true.

The variation of pitching moment with angle of attack for the body-inlet-wing-tail configuration was similar to that at supersonic speeds. The slope increased in the negative direction with increasing angle of attack. At supersonic speeds, however, the model was near neutrally stable near 0° angle of attack and then became stable as the angle of attack was increased. At subsonic speeds, however, the model was unstable near 0° angle of attack, the change of the slope of the pitching-moment curve was more gradual, and the model became stable at a higher angle of attack.

The effect of tail configuration on longitudinal aerodynamic characteristics is shown in figures 9 and 10 (axisymmetric inlets) and figures 28 and 29 (2-D inlets) as a comparison of T_1 and T_2, with $\phi_I = 135°$. Without the wing, the greatest effect was increased longitudinal stability and a straightened pitching-moment curve. This effect of making the pitching-moment curve more linear was not as great as for the supersonic tests (refs. 8 and 9), as the nonlinearity of the pitching-moment curve is not as great at subsonic speeds. With the addition of the wing, the model had less longitudinal stability with the X-tail than with the tri-tail.

To consider the effect of the various components on the lift or normal force, the pitch control and trim characteristics should be considered. Pitch-control data are presented in figures 11 through 15 (axisymmetric inlets) and figures 30 through 36 (2-D inlets). The data include longitudinal characteristics with pitch-control deflections δ_p of 0° and -10° for the body-inlet-tail configuration and 0° and 10° for the body-inlet-wing-tail configuration, as the effect of the wing is a pitch-up increment in pitching moment and requires a positive tail deflection for trim at 0° angle of attack. The body-inlet-tail configurations could be trimmed at angles of attack ranging from about 11° at $\phi_I = 90°$ (fig. 11) to about 17° at $\phi_I = 135°$ (fig. 13) with the tri-tail T_1 and $\delta_p = -10°$. This was similar to the same configuration at supersonic speeds with $\delta_p = -20°$. Although the subsonic data show greater longitudinal stability, this is compensated for by greater pitch-control effectiveness. The configuration $B_1I_1T_1$ with $\phi_I = 90°$ had a trimmed C_N value of about 2.8 compared with about 3.7 for the same configuration at supersonic speeds and at the same trimmed angle of attack. Increasing ϕ_I from 90° to 135° resulted in an increase in the trim angle of attack to about 17.5° and a corresponding normal-force coefficient of about 3.7. With the 2-D inlets the longitudinal stability level was less than with the axisymmetric inlets, and the slope of

the normal-force curves increased. Although tail deflections resulted in about the same increment in pitching-moment coefficient, the resulting trim angles of attack were greater, and the corresponding normal force was greater. At $M = 0.60$ and $\phi_I = 90°$ the trim angle of attack was about 13° with the 2-D inlets, compared with 11° with the axisymmetric inlets, and the corresponding value of normal-force coefficient was about 5 compared with 2.8. With the wing added (figs. 14 and 15), the model had reduced longitudinal stability and an increment of positive pitching moment compared with the model without a wing. At $\phi_I = 115°$, there was a trim point at about 16° angle of attack with $\delta_p = 0°$, and a positive value of δ_p was required to trim the model at angles of attack below about 16°. At $\phi_I = 135°$, a positive value of δ_p was required for trim at any angle of attack. Generally, the increments of pitching-moment coefficient and normal-force coefficient due to δ_p were about the same with or without the wing.

The effect of inlet orientation angle on the lateral-directional stability characteristics for the tri-tail configuration with wings is shown in figure 16 (axisymmetric inlets) and figure 37 (2-D inlets). As the reduction in planform area due to increasing inlet orientation angle is accompanied by an increase in lateral area at the aft end of the model, an increase in directional stability should result from an increase in ϕ_I. The data show this trend, although the comparison is made only for $\phi_I = 115°$ and 135°. Generally, the $\phi_I = 115°$ configuration was stable directionally at angles of attack to about 12° and the $\phi_I = 135°$ configuration was stable at angles of attack to about 16°. Both configurations were laterally stable for the entire range of angle of attack.

The effect of the various model components on the lateral-directional stability is shown in figures 17 through 20 (axisymmetric inlets) and figures 38 through 41 (2-D inlets). Generally, the trends at subsonic speeds were similar to those at supersonic speeds. The body-inlet was directionally unstable and laterally stable except for $\phi_I = 135°$, where at low angles of attack the model had near neutral lateral stability. Adding the tri-tail T_1 increased the directional stability near 0° angle of attack. As the angle of attack was increased, C_{n_β} decreased and the body-inlet-tail configuration became directionally unstable at angles of attack as low as 14° ($\phi_I = 90°$). With the wing installed, the trend was similar, becoming directionally unstable at high angles of attack. With the X-tail T_2 (figs. 20 and 41), the variation of C_{n_β} with angle of attack was similar to that with T_1. However, at about 10° angle of attack, C_{n_β} began to increase and the model with T_2 was both laterally and directionally stable for the entire range of angle of attack.

The effects of removing the inlet covers from the 2-D inlets on the longitudinal aerodynamic characteristics are shown in figures 43 through 45, and the lateral-directional characteristics are shown in figures 46 through 48. The effect on pitching moment was a small positive increment. With $\phi_I = 90°$ (no wing), the change in pitching moment was equivalent to about a 2° change in trim angle of attack. With $\phi_I = 115°$, the wing added, and T_1 and with $\phi_I = 135°$, the wing added, and T_2, the increment in pitching moment was about half that at $\phi_I = 90°$. The only other effect on the longitudinal aerodynamic characteristics was a substantial increase (≈50 percent) in axial force (or drag) near $\alpha = 0°$. The drag decreased as the angle of attack increased, and at angles of attack near 20°, the increment was about half that at 0° angle of attack. The effect on lateral-directional stability was generally small, as shown in figures 46 through 48.

The effects of inlet orientation angle ϕ_I, on the longitudinal aerodynamic characteristics of the model with the extended 2-D inlets ($B_1I_{3c}T_1$) are presented in figure 49. The effect of extending the inlets can be seen by comparing the data of figure 49 with those of figure 22. The effect is seen to be small, with some decrease in longitudinal stability, but there is very little effect on normal force. The lateral-directional stability of configuration $B_1I_{3c}T_1$ is shown in figure 50. The model was directionally stable at angles of attack to about 14° for $\phi_I = 90°$, and at angles of attack to about 24° at $\phi_I = 135°$. The model was generally stable laterally, but at angles of attack below about 6° for $\phi_I = 135°$, the model was near neutrally stable or slightly unstable. Comparisons with $B_1I_{2c}T_1$ data can be made only at $\phi_I = 90°$ (fig. 38). These comparisons show very little difference in lateral-directional stability.

Comparison of the data for the axisymmetric-inlet configuration (figs. 3 through 21) with the data for the 2-D inlet (figs. 22 through 48) gives an indication of the effect of inlet configuration. Comparison of $B_1I_1T_1$ (fig. 3) data with those of $B_1I_{2c}T_1$ (fig. 22) shows that at $\phi_I = 90°$, I_{2c} was less stable longitudinally and had greater values of normal-force coefficient, but for $\phi_I = 135°$, the stability levels were comparable. With I_2, the axial-force coefficient was about 50 percent greater than that with I_{2c}. Removing the inlet cover from I_{2c} increased the axial-force coefficient C_A at $\alpha = 0°$ to about the same as with the axisymmetric inlet I_1, but C_A decreased as the angle of attack was increased. At high angles of attack, I_2 had slightly less axial force than I_1. With the wing added for $\phi_I = 115°$ and 135°, the difference in the longitudinal aerodynamic characteristics of configuration $B_1I_1W_1T_1$ (figs. 6 and 7) and $B_1I_{2c}W_1T_1$ (figs. 25 and 26) was small. At angles of attack to about 12°, the 2-D inlet configuration was somewhat more stable. At $\phi_I = 135°$, the 2-D inlet configuration had slightly more normal force at angles of attack above about 16°, but at $\phi_I = 115°$, there was essentially no difference in normal force. Similarly, there was very little difference in the lateral-directional stability of the two different inlet configurations.

Comparison of parts (a), (b), and (c) of each data figure gives an indication of the effect of free-stream Mach number. Generally, the effect on longitudinal or lateral-directional stability was small. Some increase in normal force at angles of attack and an increase in axial-force coefficient was a result of increasing the free-stream Mach number from 0.60 to 0.95. The increase in axial-force coefficient was about 0.15 without the wing and about 0.075 for the winged configurations.

Comparisons of the supersonic data from references 8 and 9 with the subsonic data of this report show the effect of both free-stream Mach number and of the internal flow on the closed-duct condition. At subsonic speeds, the variation of pitching moment with angle of attack was gradual. At supersonic speeds the model became very stable at high angles of attack, but at subsonic speeds it tended to remain unstable, or nearly unstable. Generally, the difference in the variation of longitudinal stability with angle of attack was at high angles of attack, above those at which the boost configuration would normally operate.

CONCLUDING REMARKS

A series of air-breathing missile configurations has been investigated to provide a data base for the design of such missiles. The model could be configured with either twin axisymmetric or two-dimensional inlets. Three circumferential inlet locations were investigated: 90°, 115°, and 135° from the top center. Two vertical wing locations, as well as wingless configurations, were used. Three tail config-

urations were formed by locating the tail surfaces either on the inlet fairings or on fairings on the body. The surfaces were deflected to provide pitch control. Two-dimensional inlets with extended compression surfaces, used to improve the angle-of-attack performance of the inlets for wingless configurations, were also investigated. NASA Technical Memorandum 84558 covers the twin axisymmetric inlet configurations at supersonic speeds, and NASA Technical Memorandum 84559 covers the two-dimensional inlet configurations at supersonic speeds. This report covers both inlet types at subsonic-transonic speeds without internal flow, and simulates the boost configuration of an air-breathing missile. As a result of the subsonic-transonic part of the investigation, the following general trends may be observed:

1. As with the data at supersonic Mach numbers, the pitching-moment curves were nonlinear, but did not exhibit the large margins of longitudinal stability at high angles of attack with the wing on.

2. The model had marginal lateral-directional stability for most configurations. The X-tail, however, resulted in lateral-directional stability for the entire range of angle of attack.

3. With the wing added, the model had reduced longitudinal stability and required positive pitch-control deflection for trim at angles of attack to 16° for the model with the inlet orientation angle of 115°, and for the entire angle-of-attack range for the inlet orientation angle of 135°.

4. The X-tail configuration did not have the beneficial effects compared with the tri-tail, as was the case with the supersonic tests, because the nonlinearity of the pitching-moment curve was not as extreme at subsonic speeds.

5. The effect of inlet extensions, added to the body-inlet-tail configuration to improve the inlet performance at high angles of attack, was generally small.

6. The effect of removing the inlet covers from the two-dimensional inlets (with ducts closed) was small, except for an increase in axial force (or drag) of as much as 50 percent at an angle of attack of 0°.

Langley Research Center
National Aeronautics and Space Administration
Hampton, VA 23665
November 3, 1982

REFERENCES

1. Sawyer, Wallace C.; and Hayes, Clyde: Stability and Control Characteristics of an Air-Breathing Missile Configuration Having a Forward Located Inlet. NASA TM X-3391, 1976.

2. Hayes, Clyde; and Monta, William J.: Aerodynamic Characteristics of a 1/4-Scale Model of MORASS Missile Configurations at Supersonic Speeds. NASA TM X-3354, 1976.

3. Hayes, Clyde: Aerodynamic Characteristics of 1/4-Scale Model of ALRAAM Missile Configuration at Supersonic Speeds. NASA TM-74075, 1977.

4. Hayes, Clyde; and Sawyer, Wallace C.: Aerodynamic Characteristics of a Model Simulating the Gainful (SA-6) Missile at Supersonic Mach Numbers. NASA TM X-3493, 1977.

5. Hayes, Clyde; and Sawyer, Wallace C.: Aerodynamic Characteristics of a Series of Air-Breathing Missile Configurations Investigated as Part of the SASS Program. NASA TM-80139, 1979.

6. Hayes, Clyde: Supersonic Aerodynamic Characteristics of a Twin-Inlet Advanced Intercept Air-to-Air Missile (AIAAM) Configuration. NASA TM-83178, 1981.

7. Hayes, Clyde: Aerodynamic Characteristics of a Supersonic Single-Inlet Missile Configuration Investigated as Part of the Advanced Intercept Air-to-Air Missile (AIAAM) Program. NASA TM-83177, 1981.

8. Hayes, Clyde: Aerodynamic Characteristics of a Series of Twin-Inlet Air-Breathing Missile Configurations. I - Axisymmetric Inlets at Supersonic Speeds. NASA TM-84558, 1983.

9. Hayes, Clyde: Aerodynamic Charcteristics of a Series of Twin-Inlet Air-Breathing Missile Configurations. II - Two-Dimensional Inlets at Supersonic Speeds. NASA TM-84559, 1983.

10. Hayes, Clyde: Aerodynamic Characteristics of a Series of Single-Inlet Air-Breathing Missile Configurations. NASA TM-84557, 1983.

11. ASED Staff: Transonic Wind-Tunnel Facility at the Naval Ship Research and Development Center. Rept. ASED 332, U.S. Navy, June 1975.

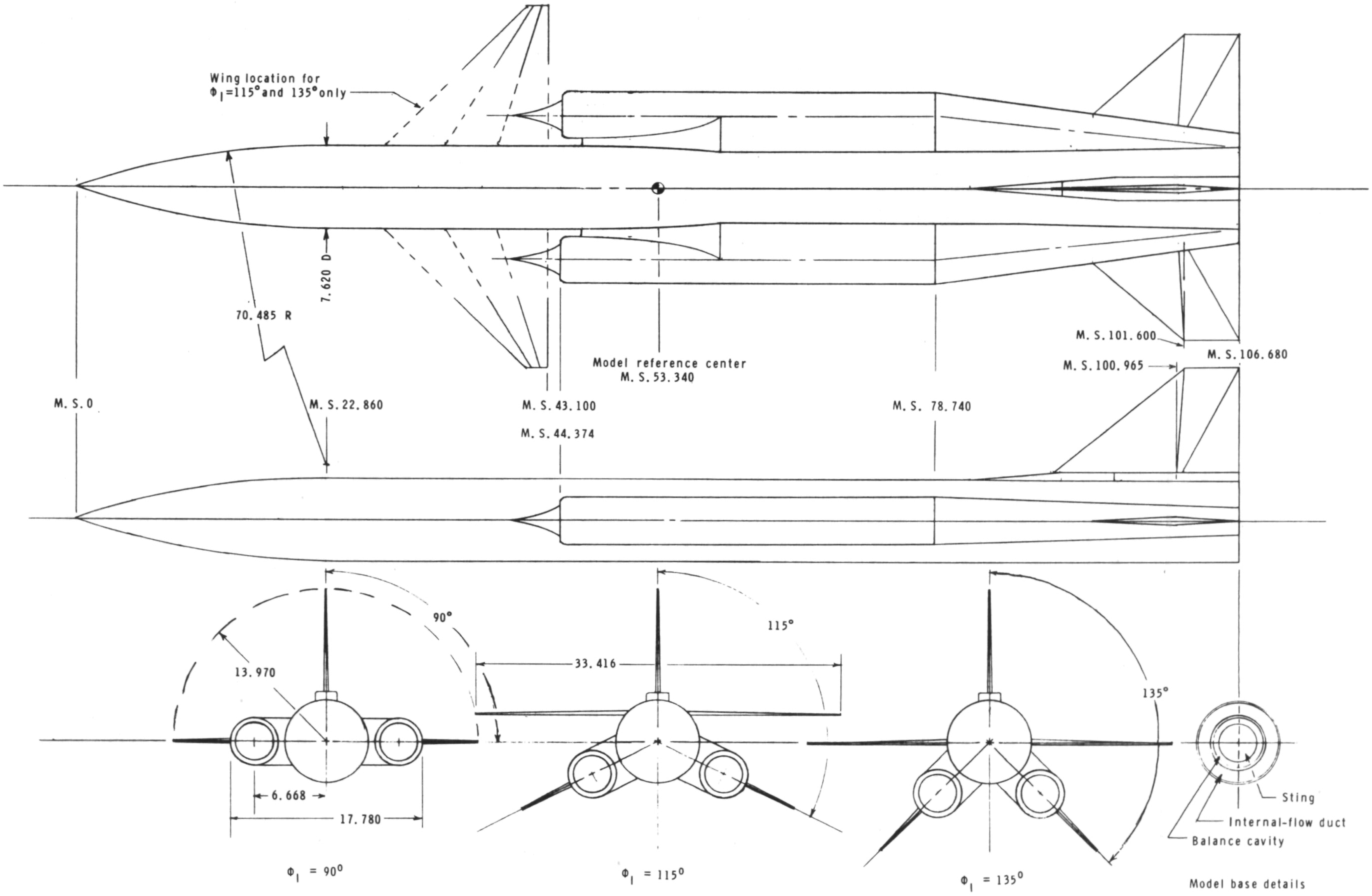

(a) General arrangement of twin axisymmetric inlet I_1 configuration.

Figure 1.- Details of model. All linear dimensions are in centimeters.

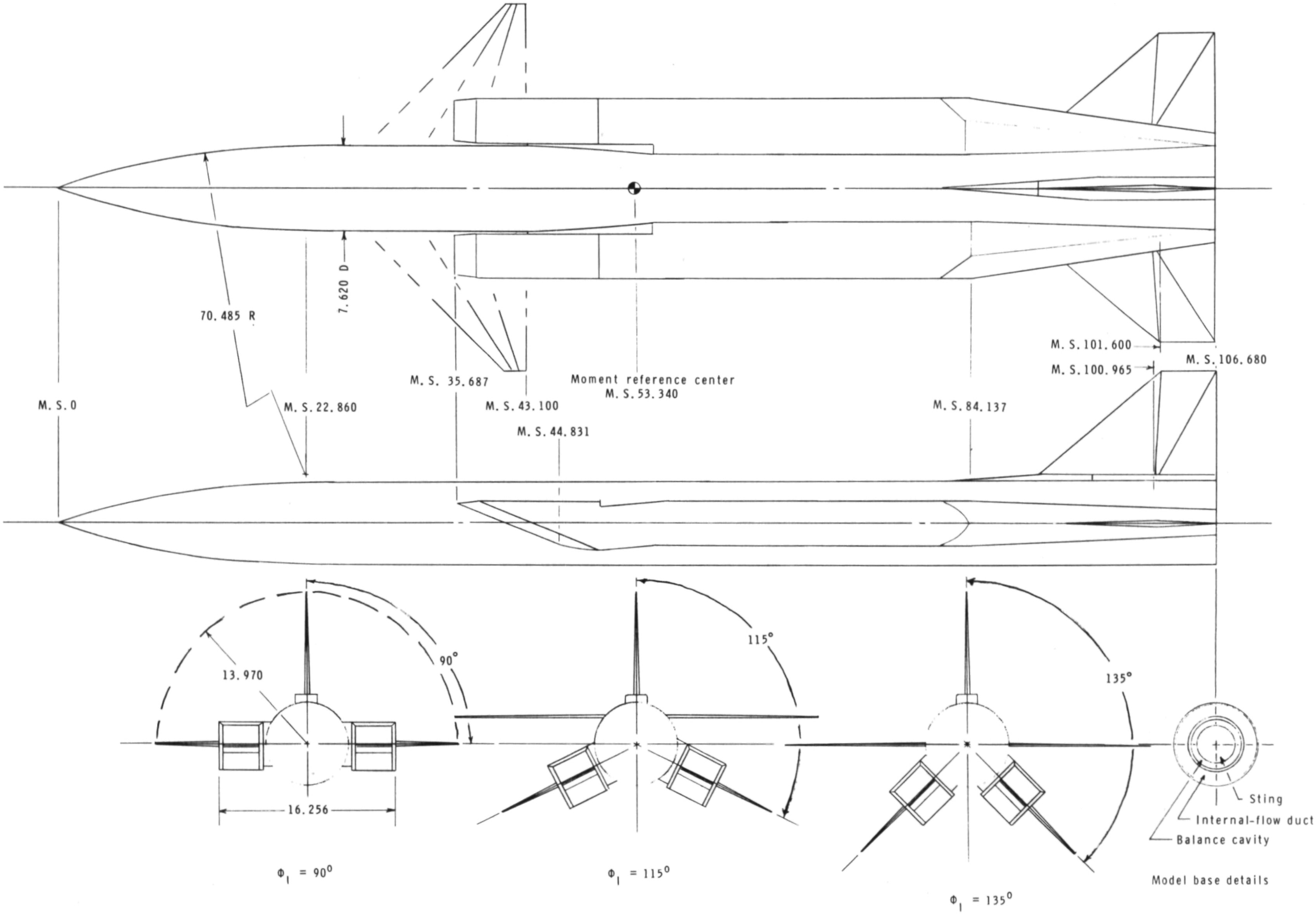

(b) General arrangement of twin two-dimensional inlet I_2 configuration.

Figure 1.- Continued.

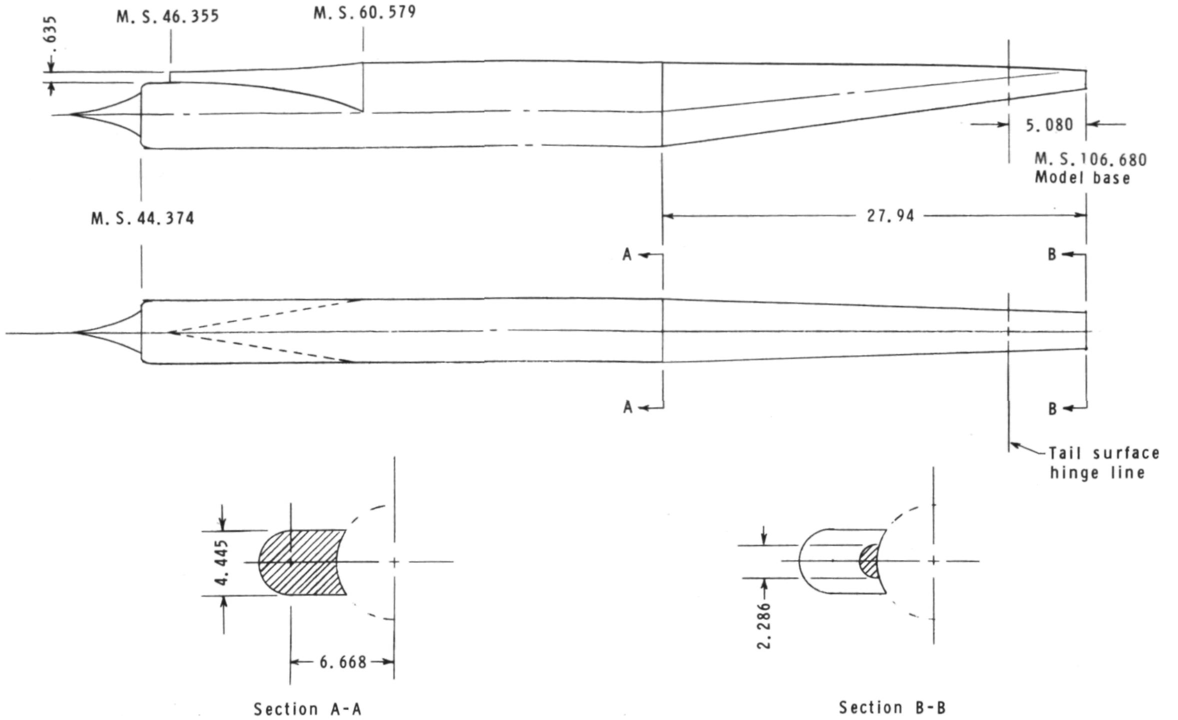

Inlet and inlet fairing

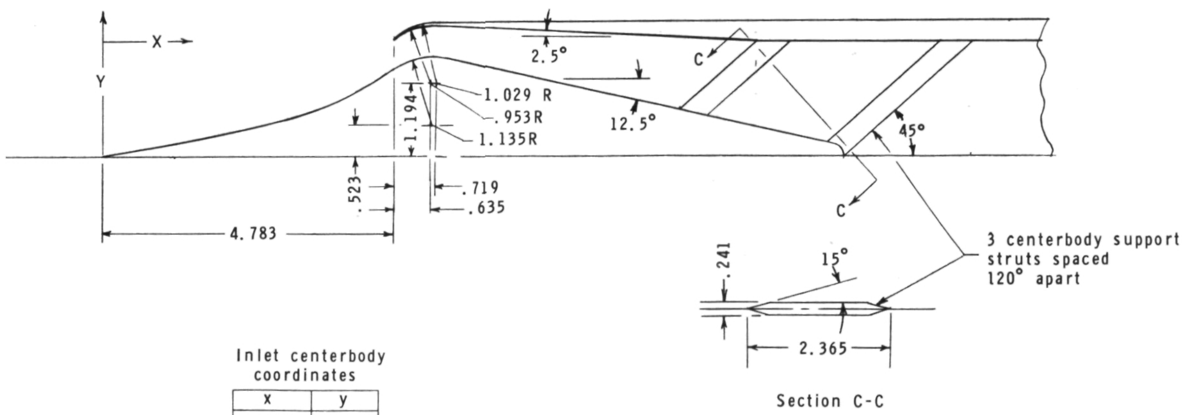

Inlet centerbody coordinates

x	y
.000	.000
1.260	.229
1.712	.325
2.347	.460
2.819	.579
3.185	.688
3.475	.785
3.815	.914
4.061	1.024
4.252	1.128
4.783	1.463
5.664	1.631
13.020	.000

Inlet (×4)

(c) Axisymmetric inlet and inlet fairing.

Figure 1.- Continued.

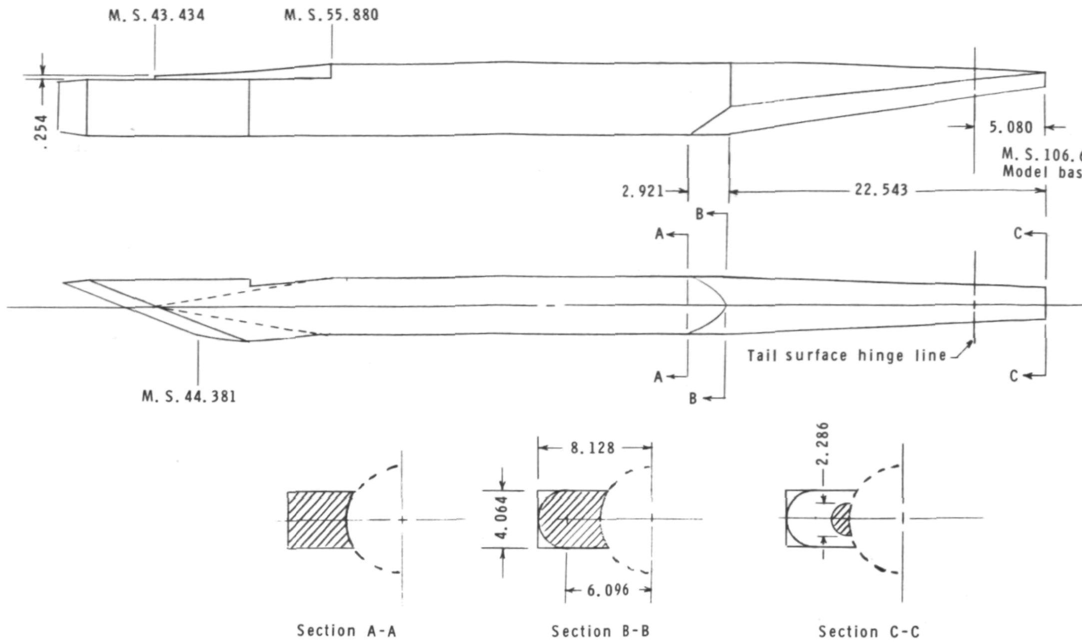

Inlet and inlet fairing

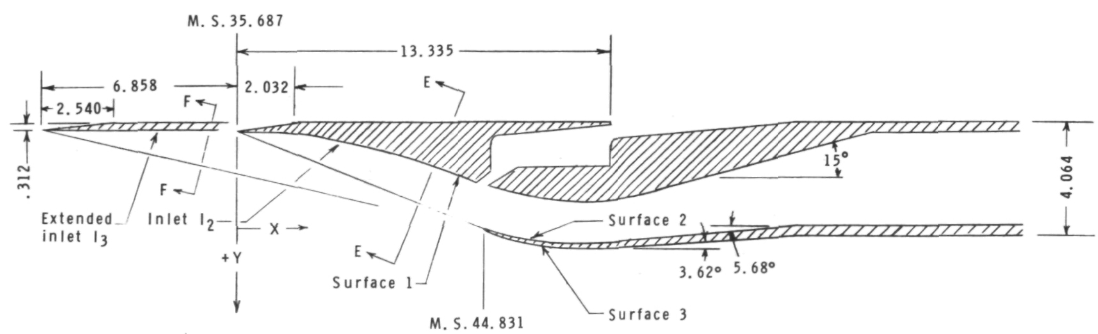

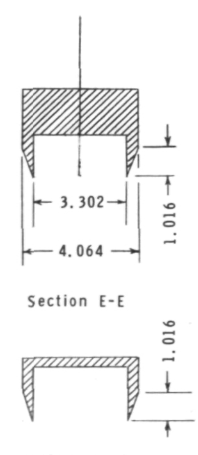

Inlet surface coordinates

Surface 1	
x	y_1
000	000
1. 920	000
3. 861	. 340
4. 491	. 462
5. 039	. 592
5. 519	. 716
5. 936	. 846
6. 320	. 973
8. 964	1. 941
9. 144	1. 981
9. 906	2. 286
10. 922	2. 489
11. 938	2. 515
12. 573	2. 477
13. 335	2. 388

Straight line

Boundary layer

Bleed slot

Surfaces 2 and 3		
x	y_2	y_3
9. 144	4. 073	4. 073
9. 502	4. 196	4. 270
9. 863	4. 305	4. 412
10. 221	4. 399	4. 526
10. 582	4. 478	4. 620
10. 940	4. 544	4. 699
11. 300	4. 592	4. 757
11. 659	4. 625	4. 798
12. 017	4. 646	4. 826
12. 377	4. 646	4. 844
12. 736	4. 633	4. 844
14. 011	4. 600	4. 826

Inlet (×2)

(d) Two-dimensional inlet and inlet fairing.

Figure 1.- Continued.

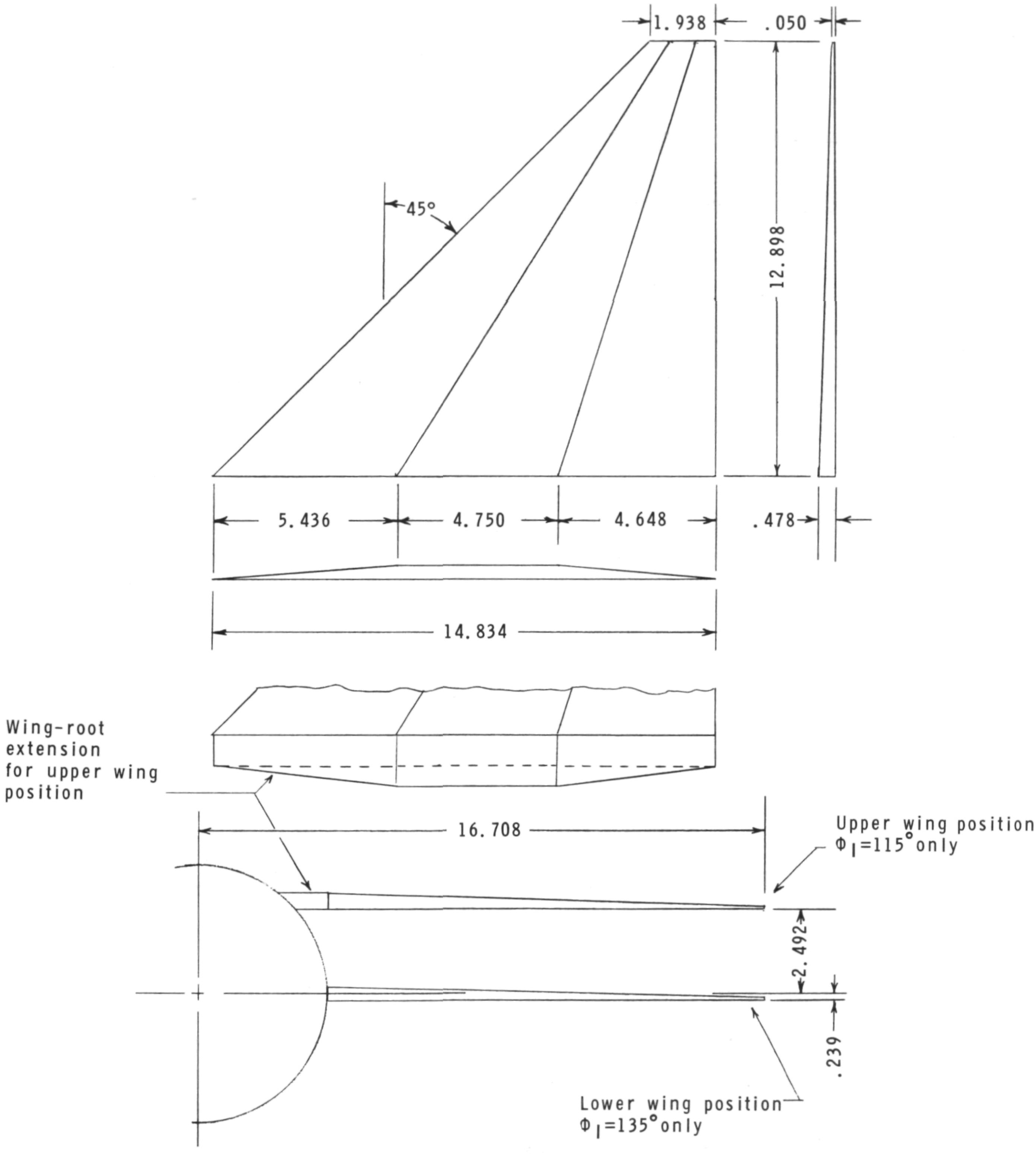

(e) Wing.

Figure 1.- Continued.

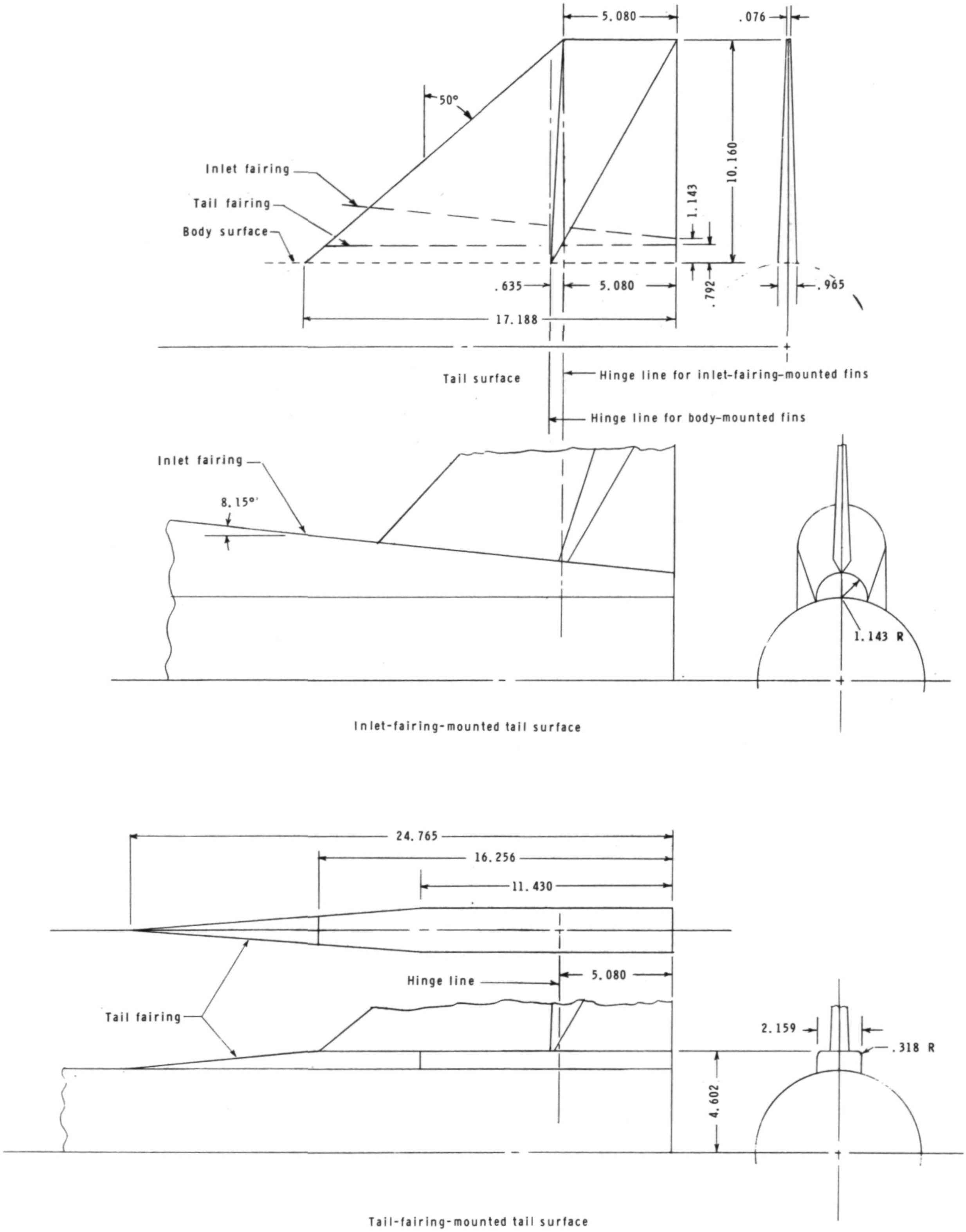

(f) Tail.

Figure 1.- Continued.

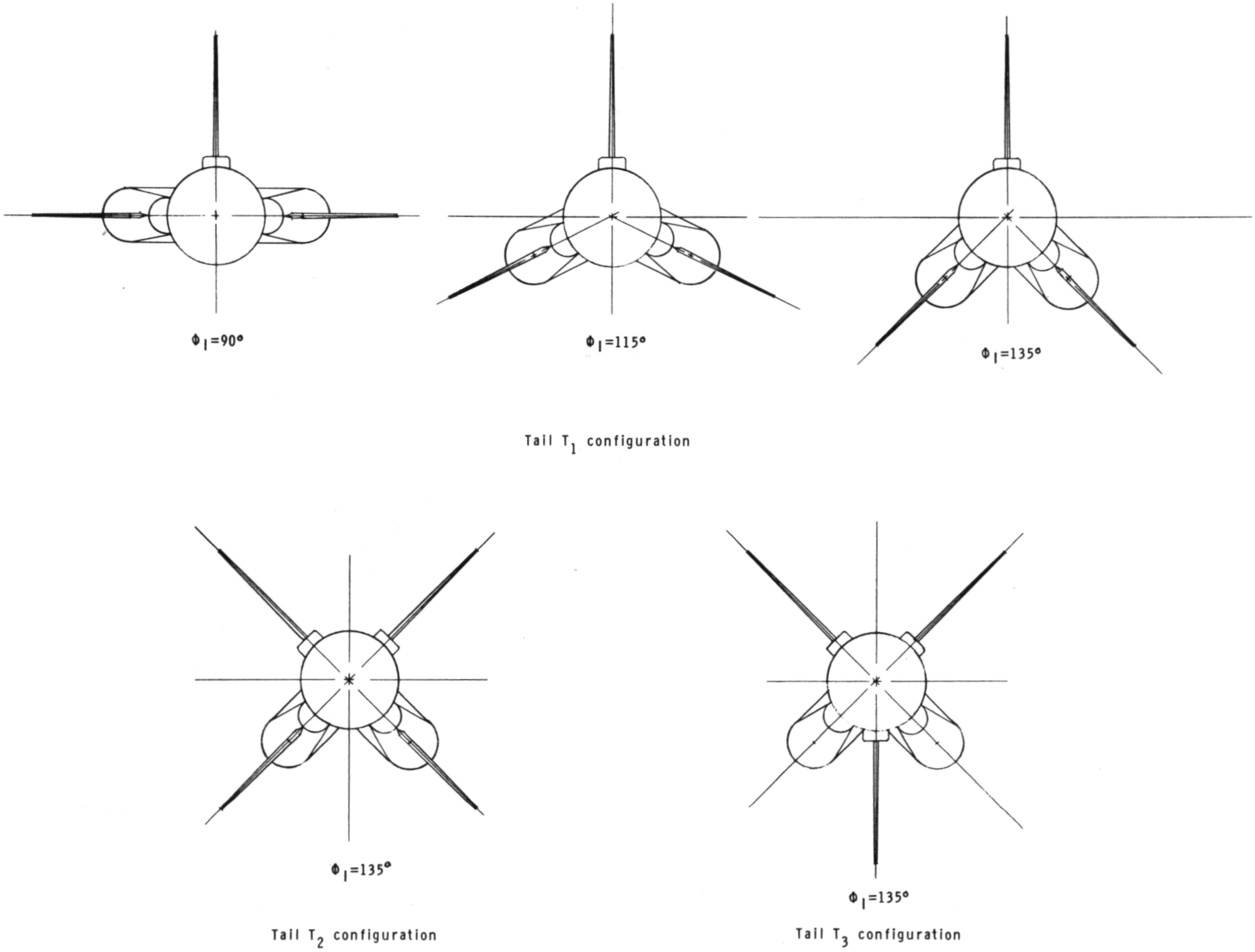

(g) Arrangement of tail configurations.

Figure 1.- Concluded.

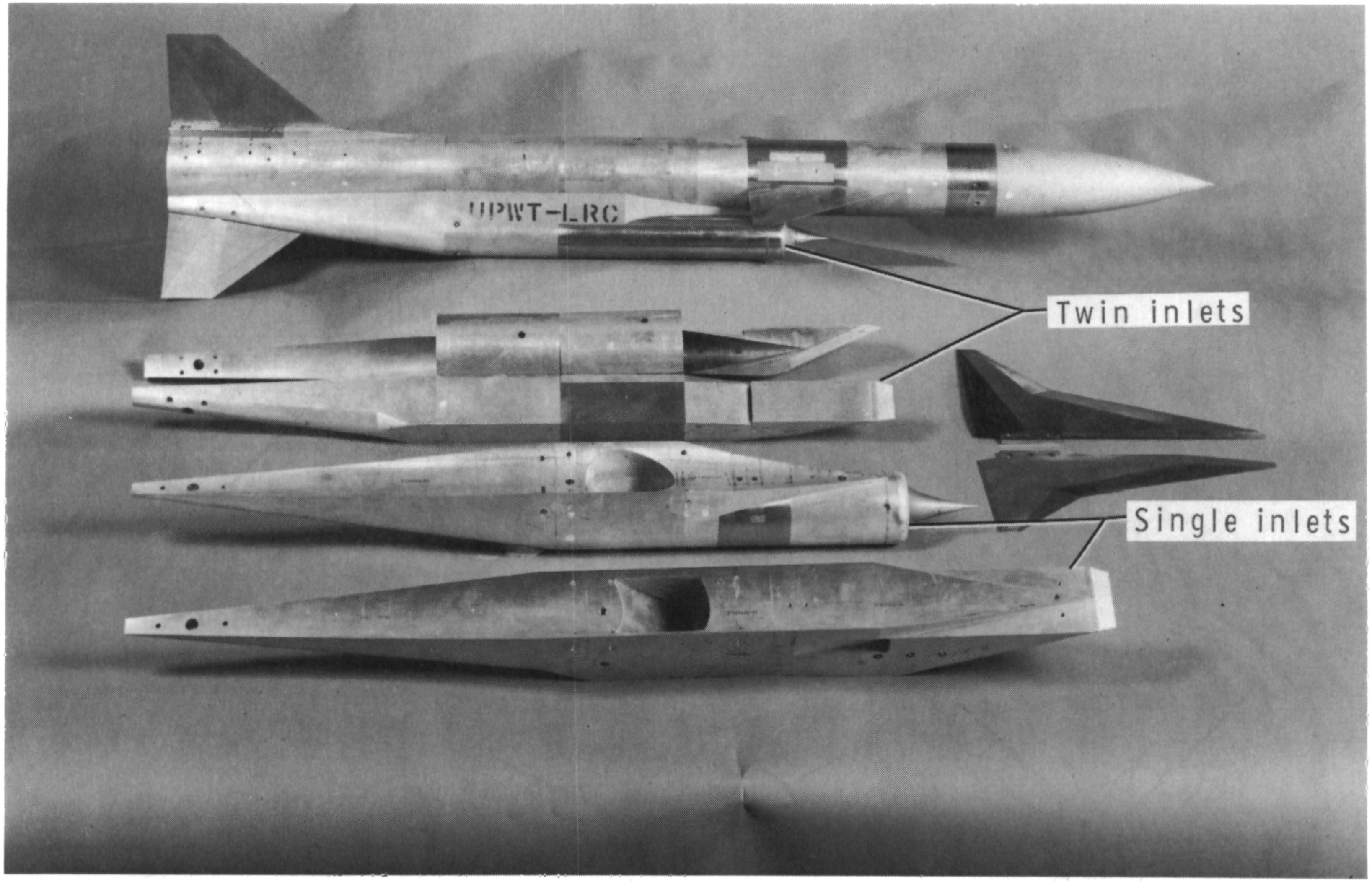

(a) Top view of assembled model plus various parts.

Figure 2.- Photographs of model. Photographs courtesy of David Taylor Naval Ship Research and Development Center.

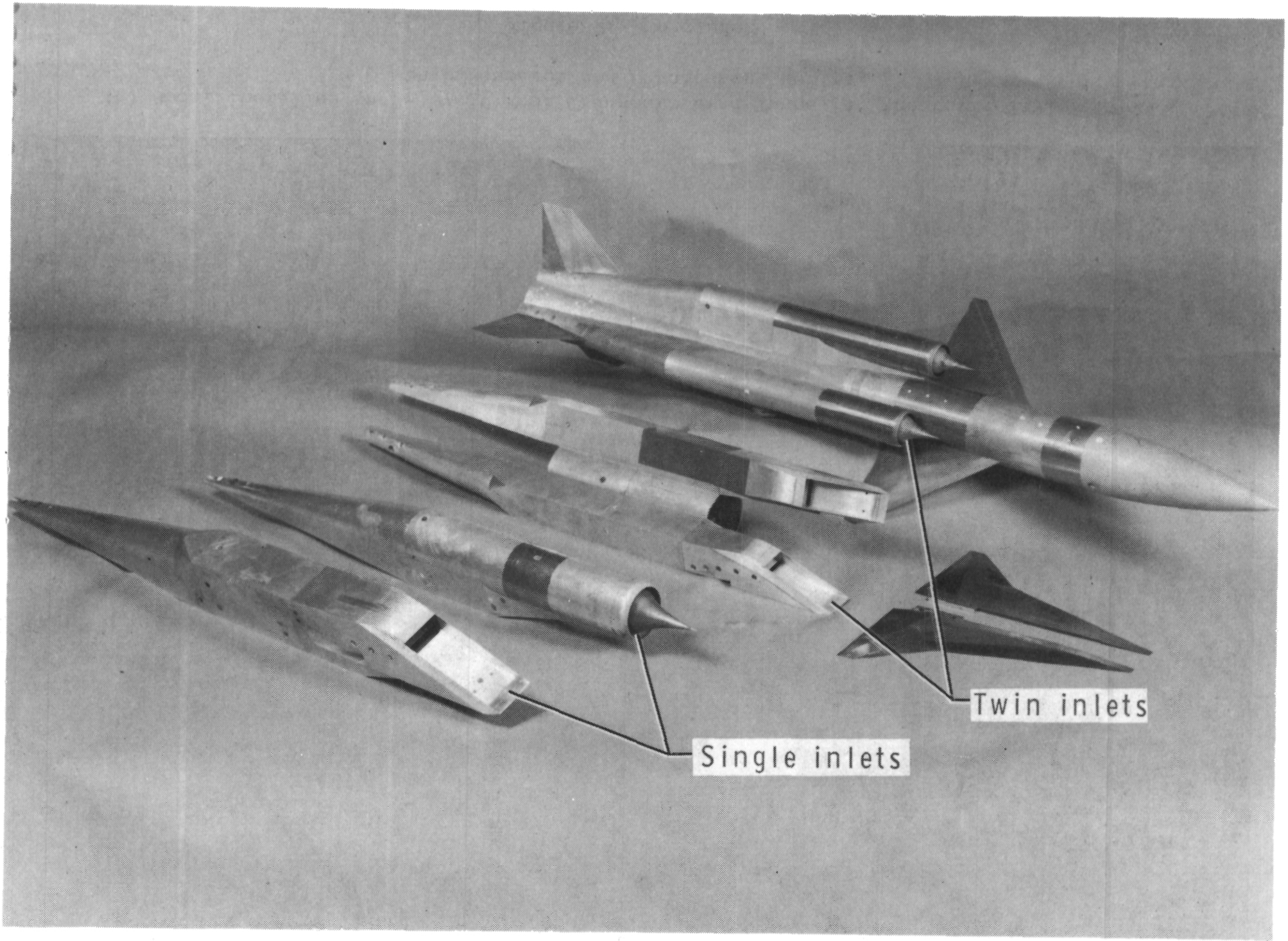

(b) Bottom view of assembled model.

Figure 2.- Continued.

(c) Model installed in 7- by 10-Foot Transonic Wind Tunnel at the David Taylor Naval Ship Research and Development Center.

Figure 2.- Concluded.

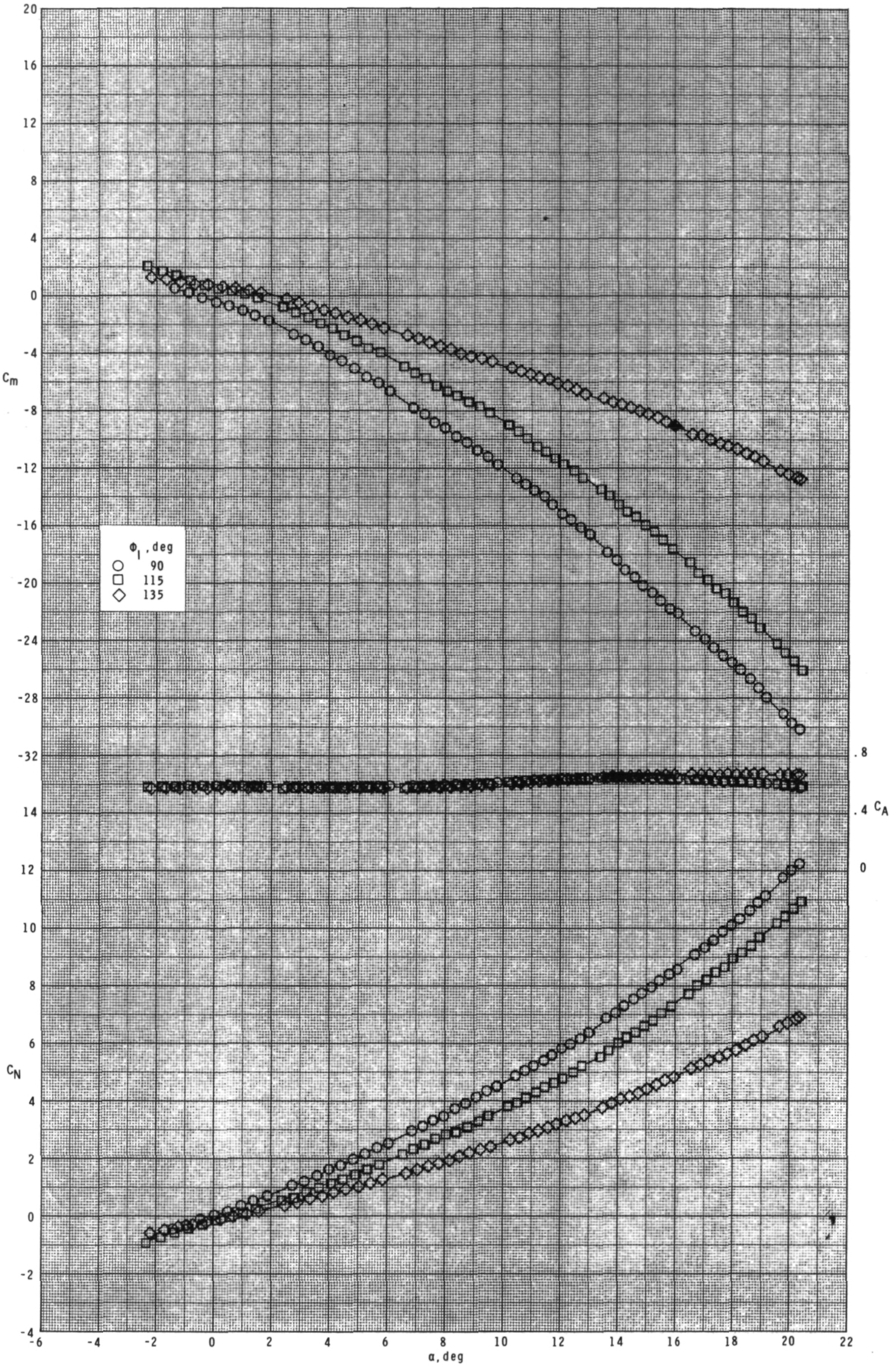

(a) M = 0.60.

Figure 3.- Effect of inlet orientation angle ϕ_I on longitudinal aerodynamic characteristics for configuration $B_1I_1T_1$ with internal ducts closed and $\delta_p = 0°$.

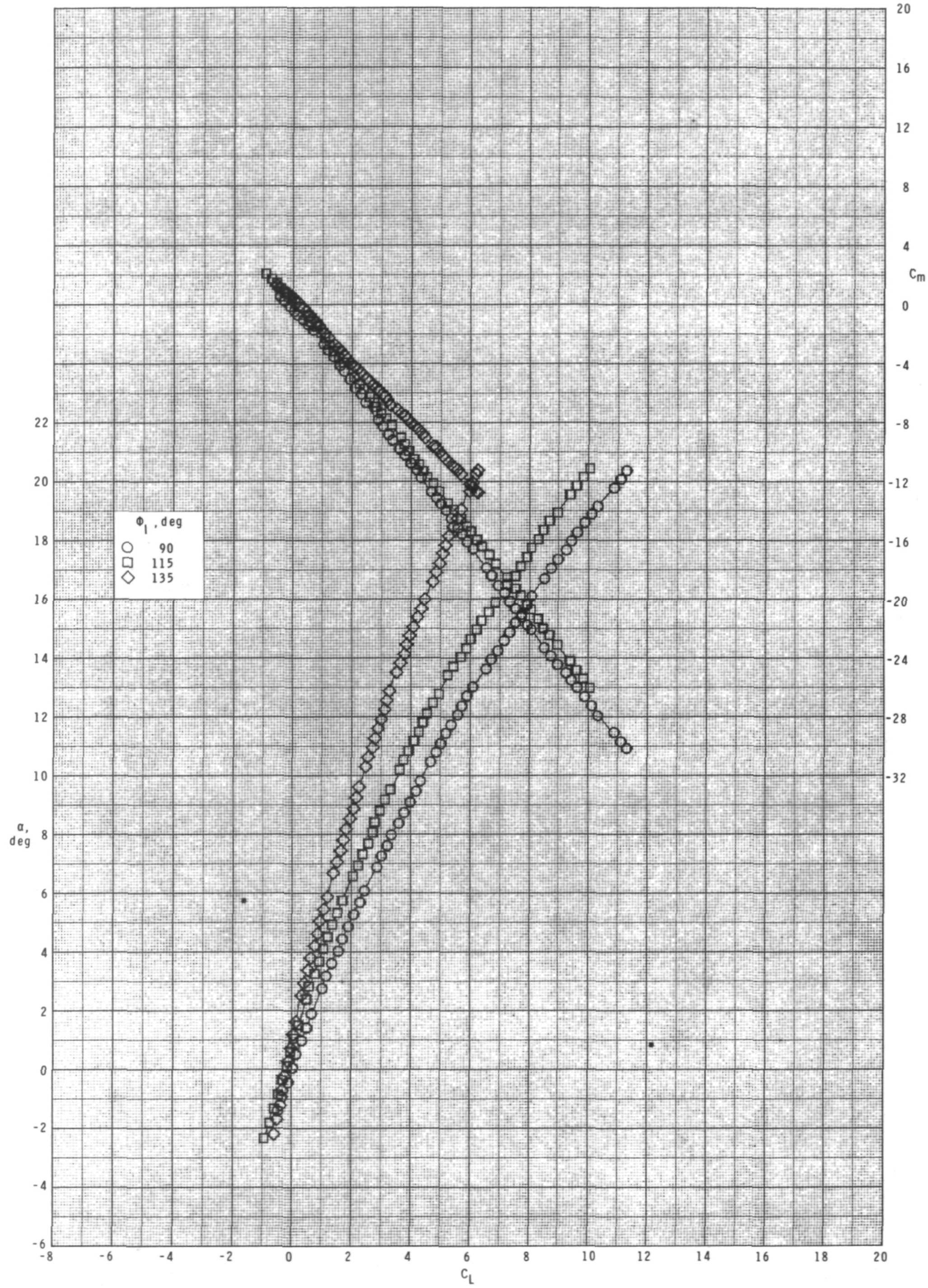

(a) Continued.

Figure 3.- Continued.

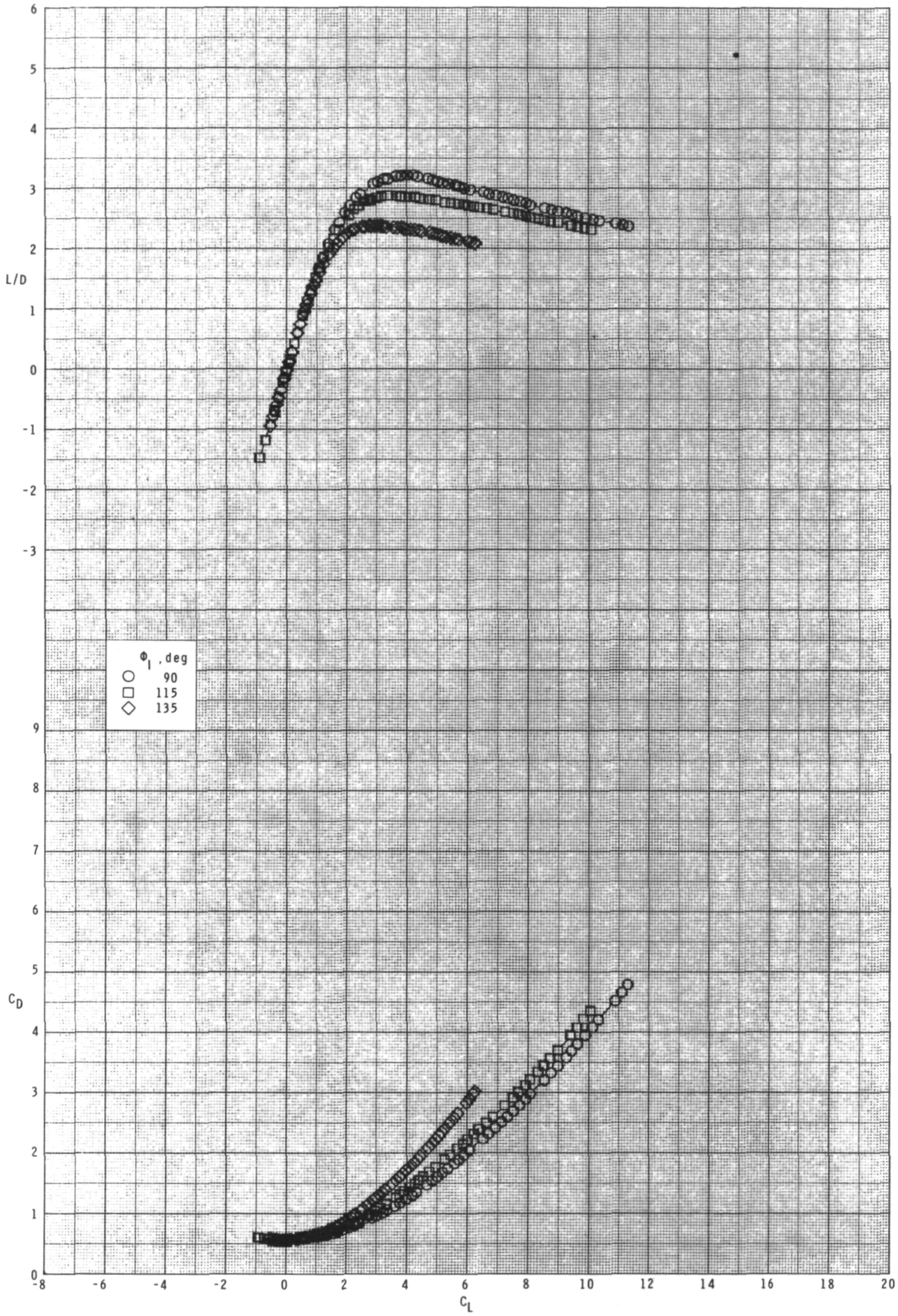

(a) Concluded.

Figure 3.- Continued.

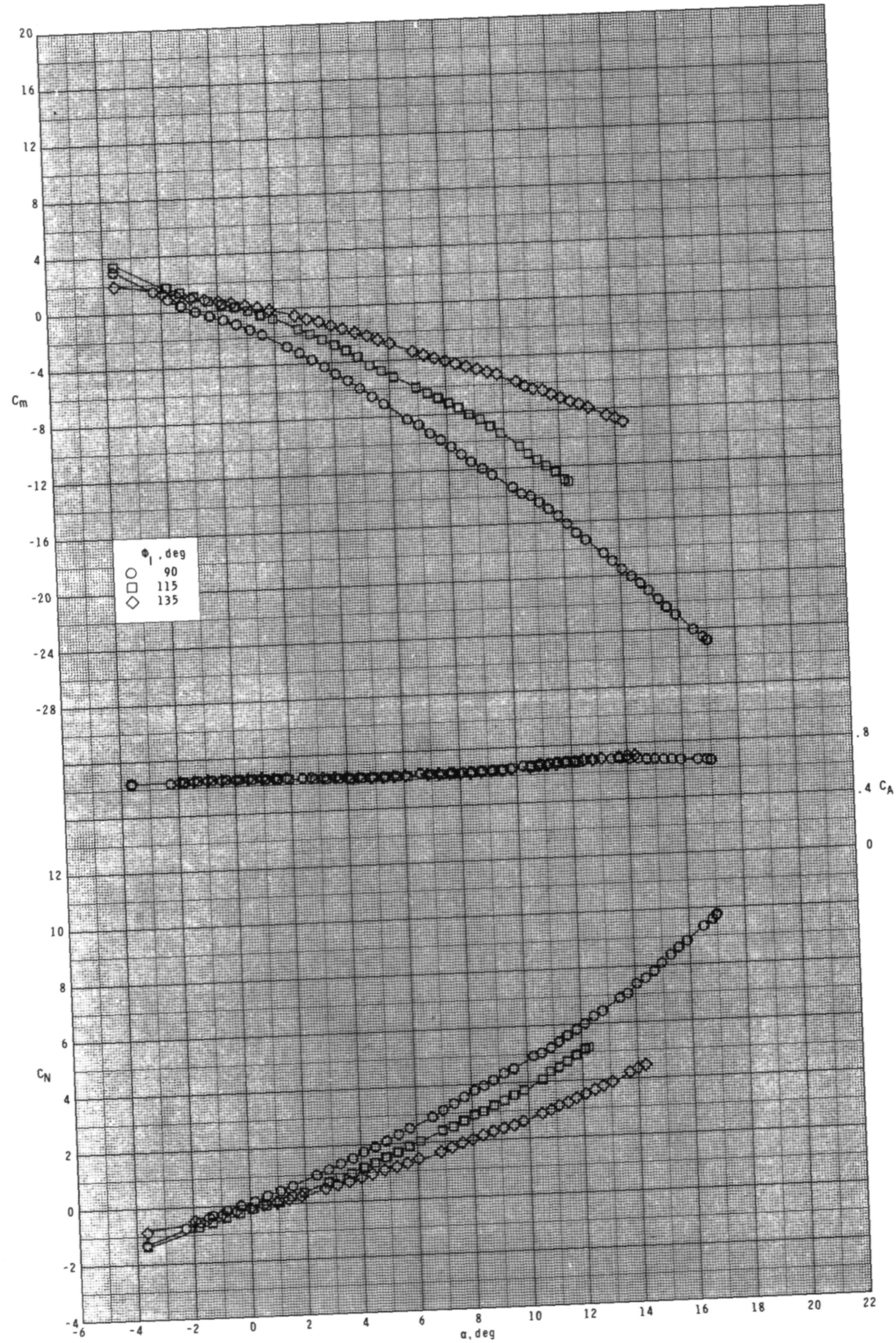

(b) M = 0.80.

Figure 3.- Continued.

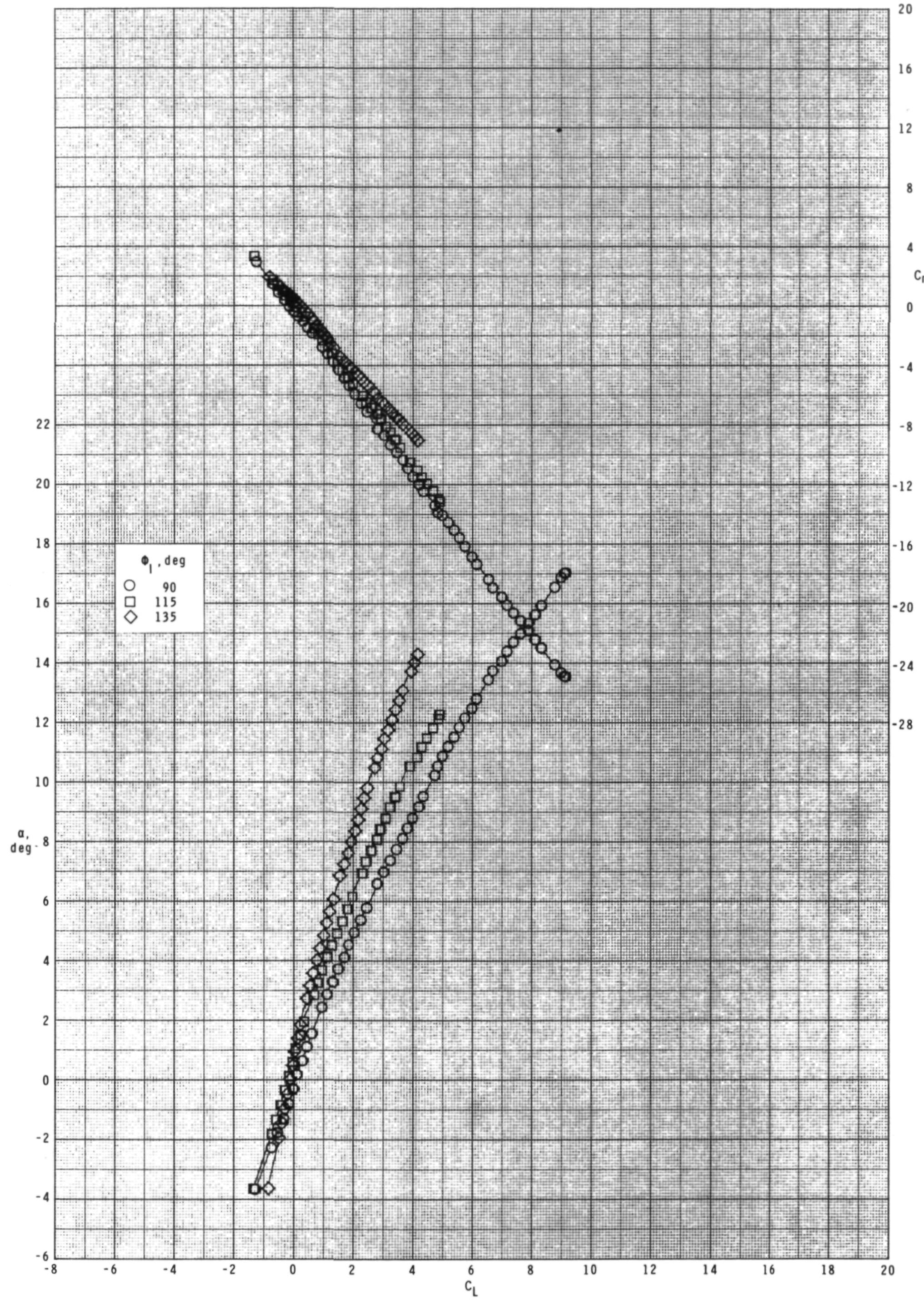

(b) Continued.

Figure 3.- Continued.

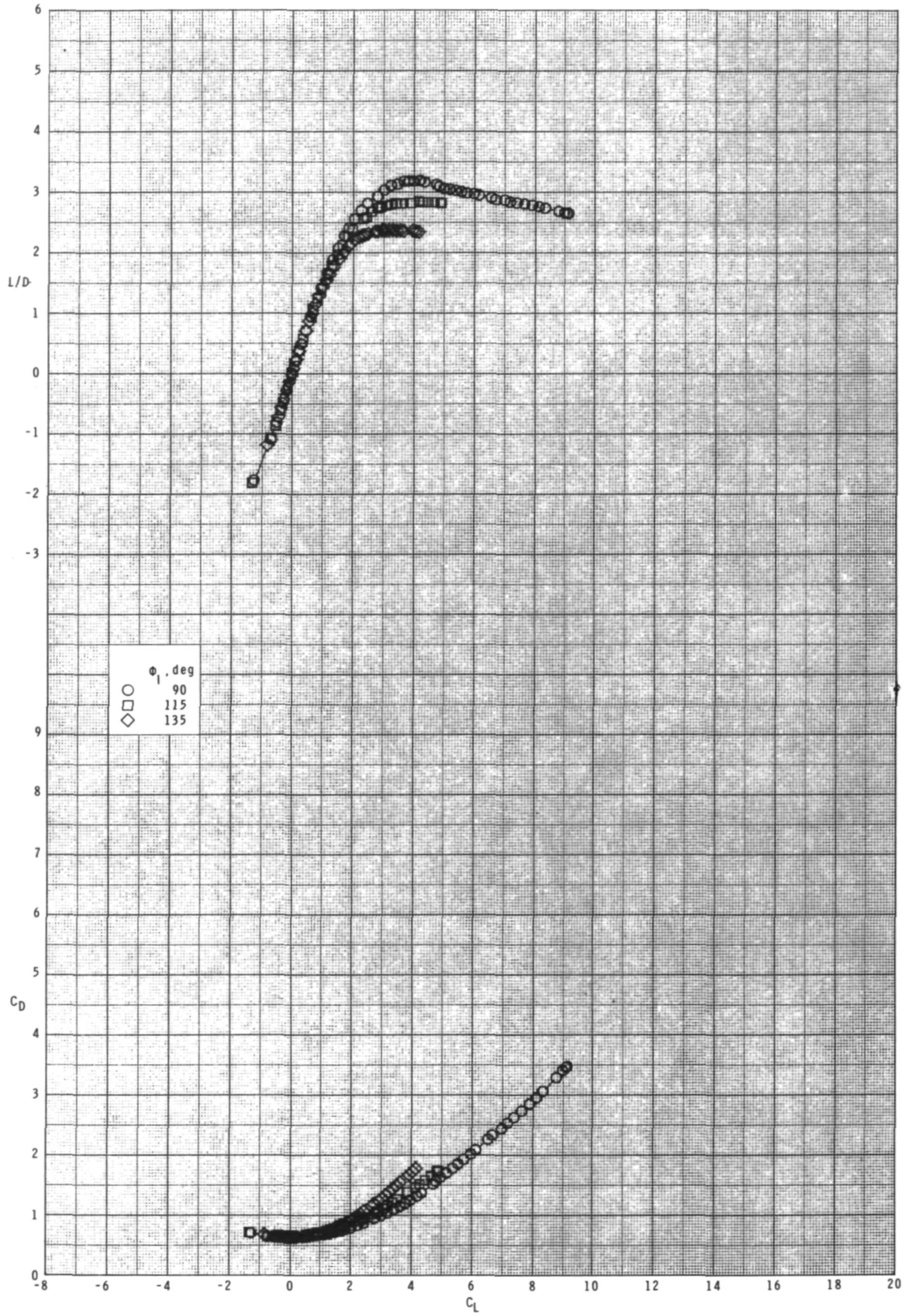

(b) Concluded.

Figure 3.- Continued.

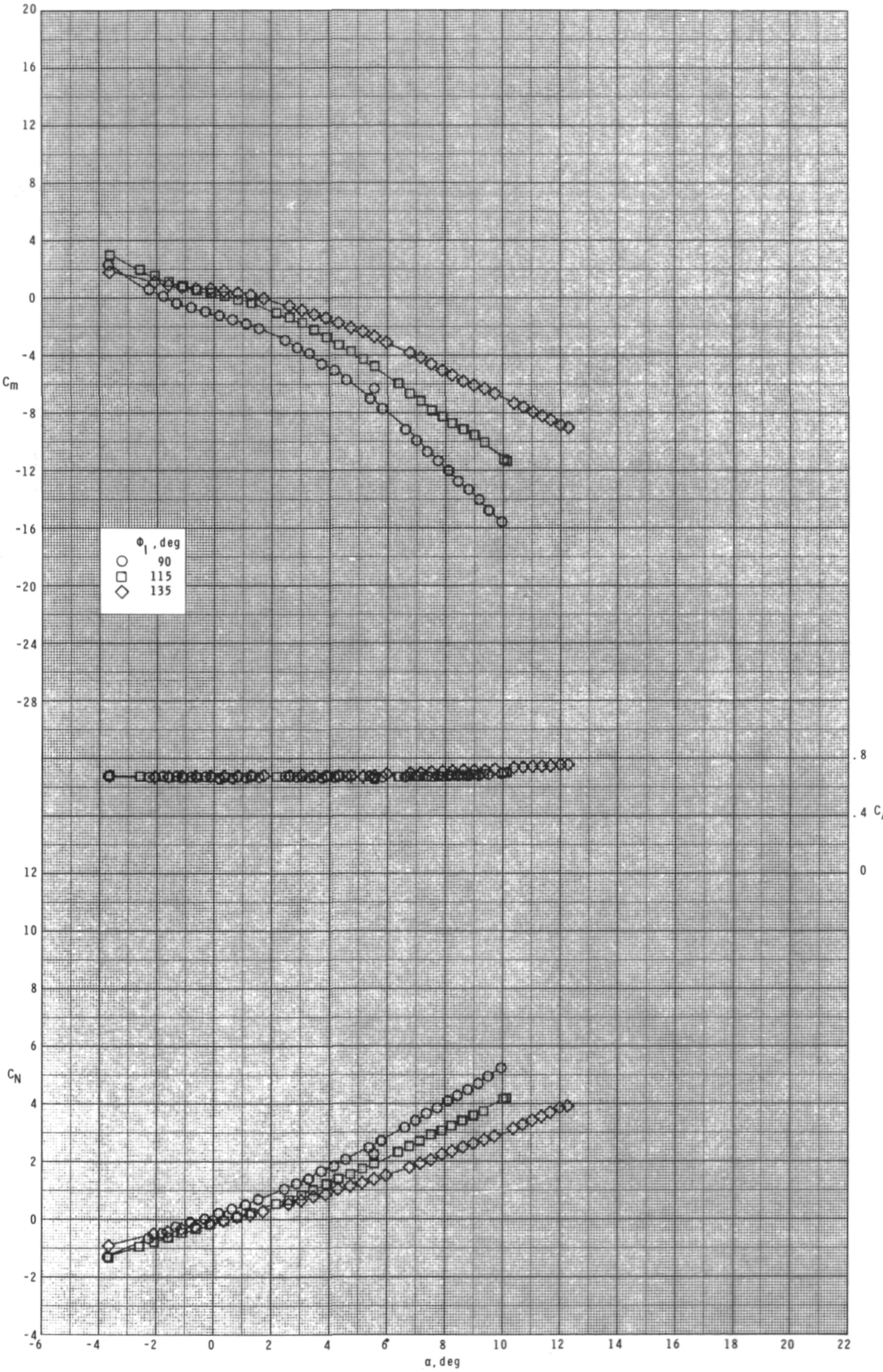

(c) M = 0.95.

Figure 3.- Continued.

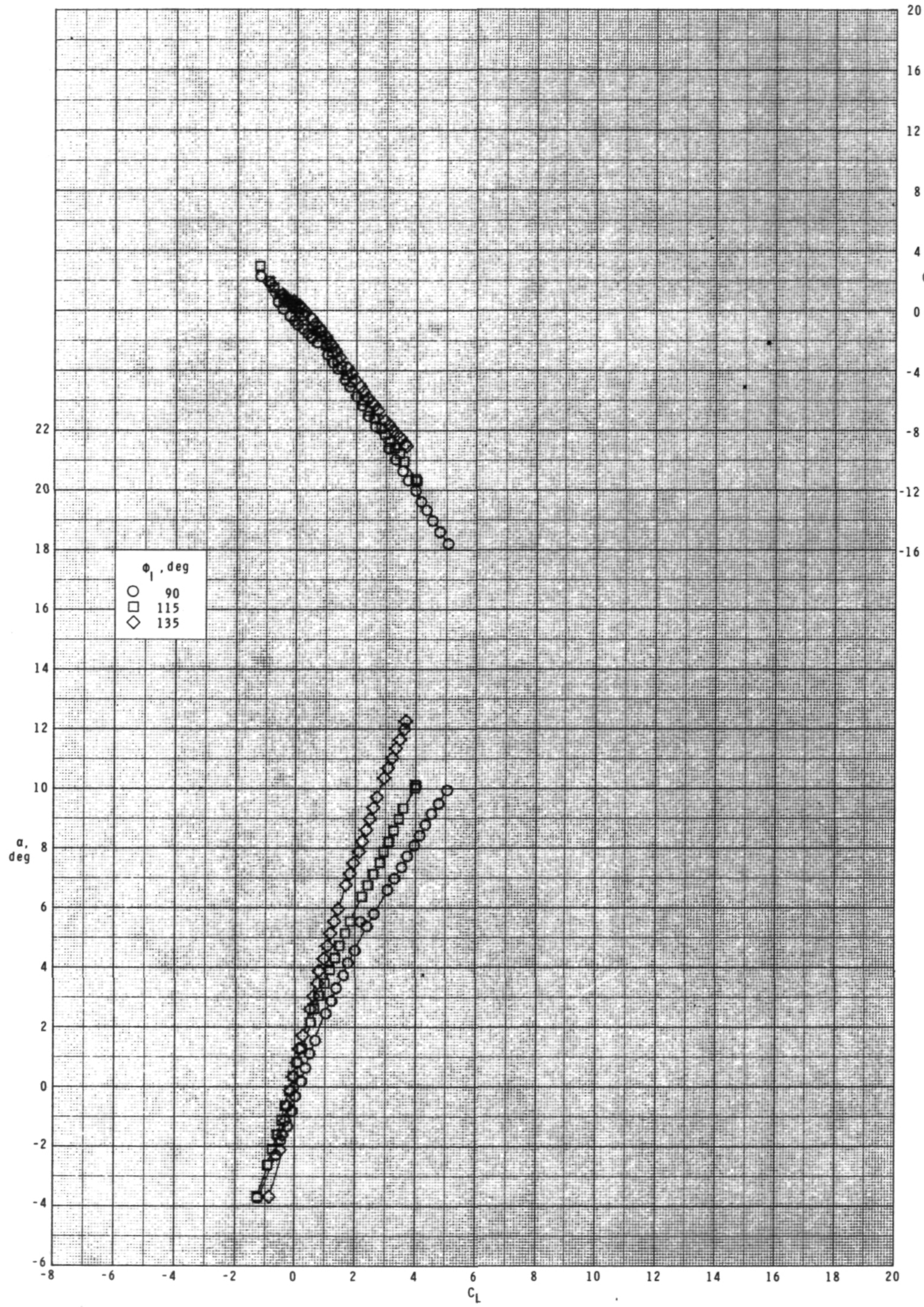

(c) Continued.

Figure 3.- Continued.

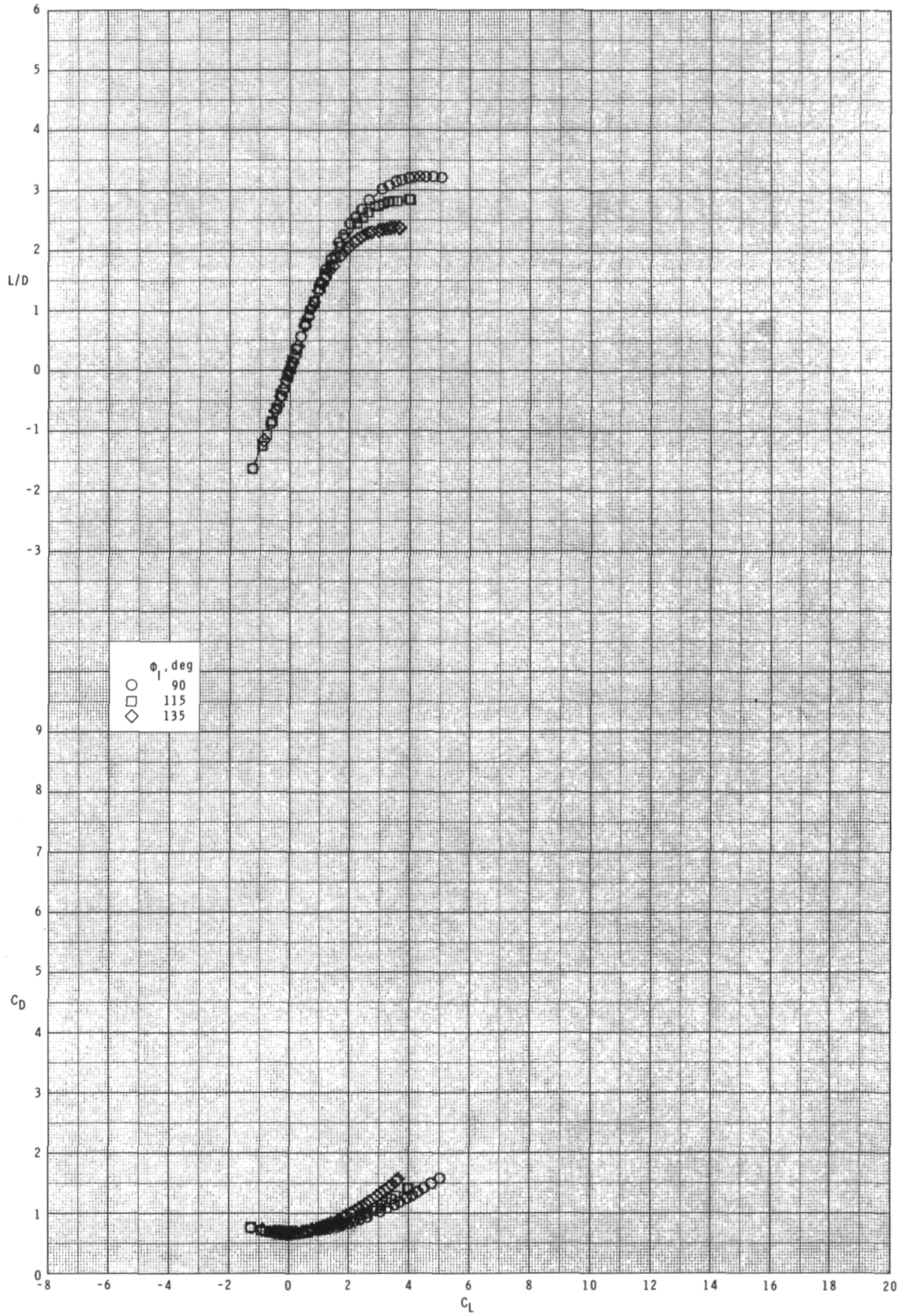

(c) Concluded.

Figure 3.- Concluded.

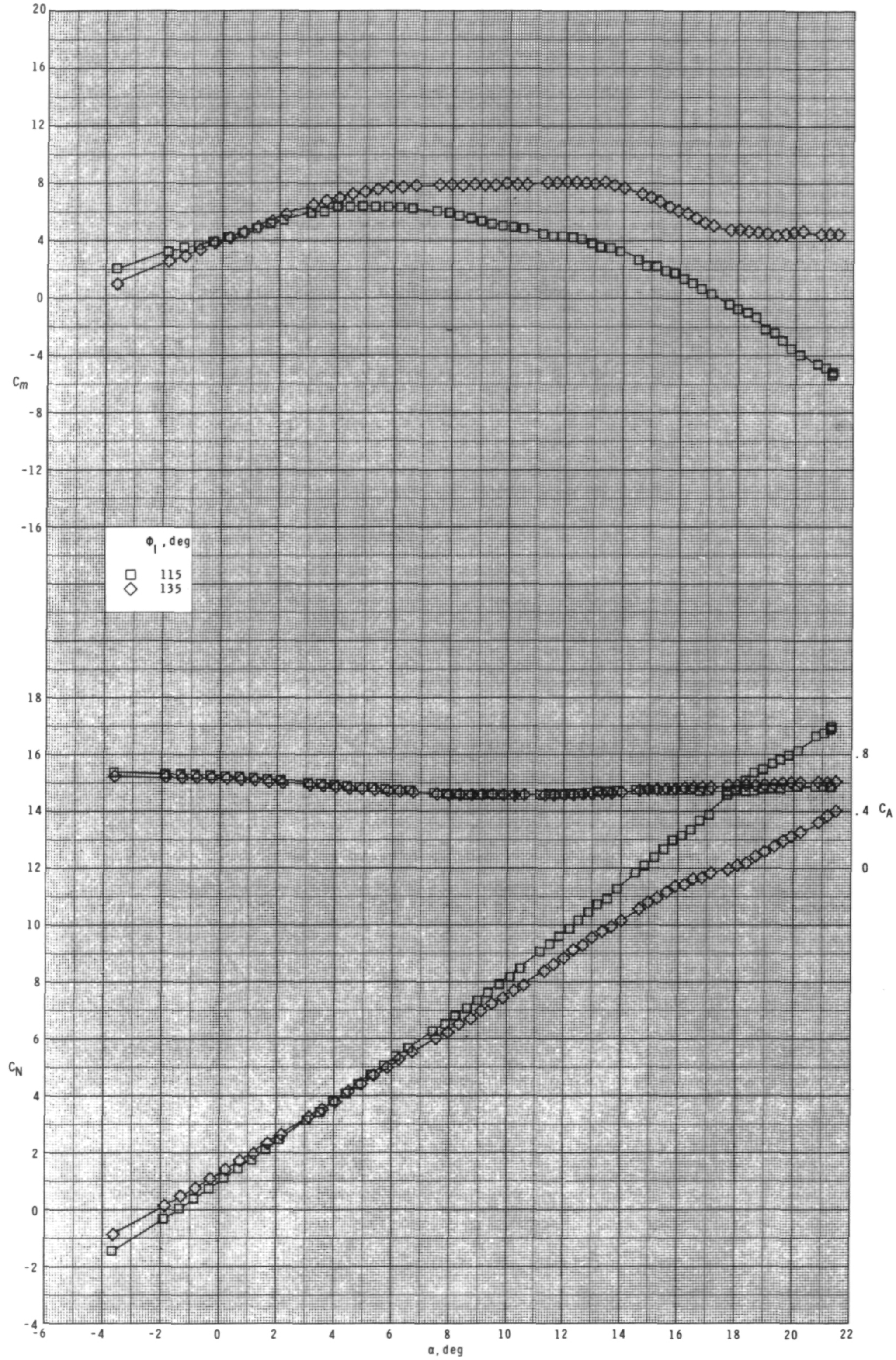

(a) M = 0.60.

Figure 4.- Effect of inlet orientation angle ϕ_I on longitudinal aerodynamic characteristics for configuration $B_1I_1W_1T_1$ with internal ducts closed and $\delta_p = 0°$.

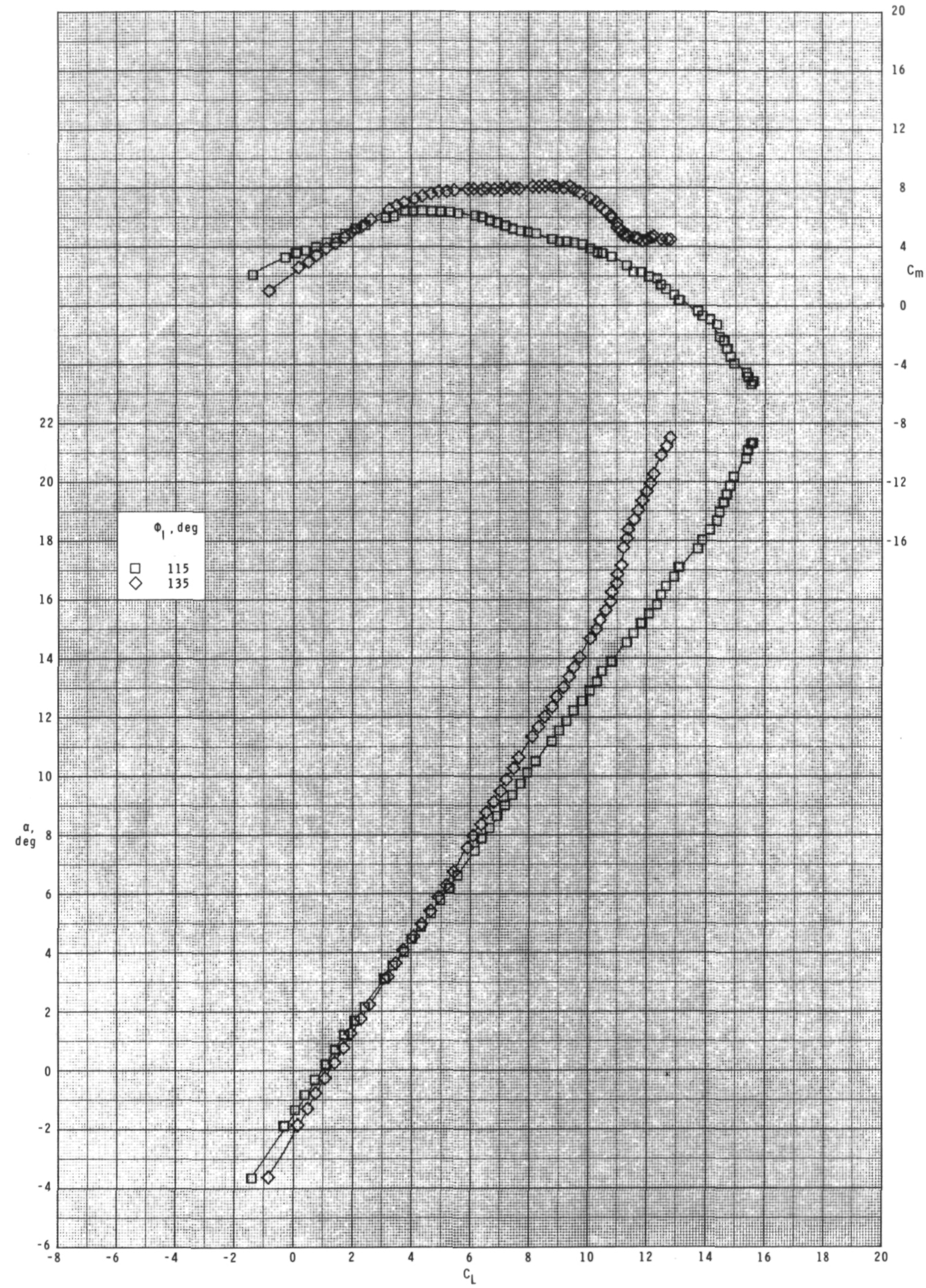

(a) Continued.

Figure 4.- Continued.

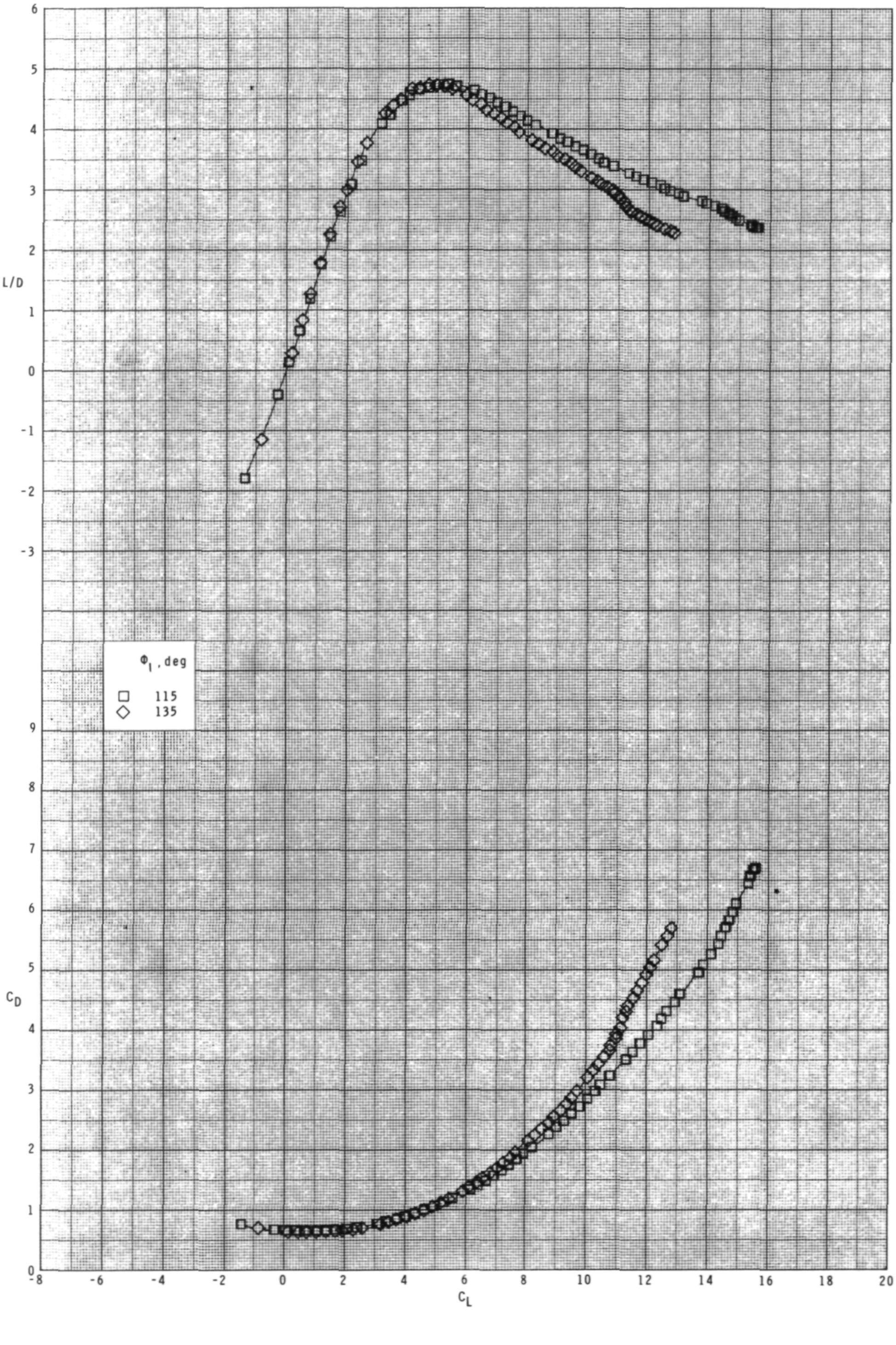

(a) Concluded.

Figure 4.- Continued.

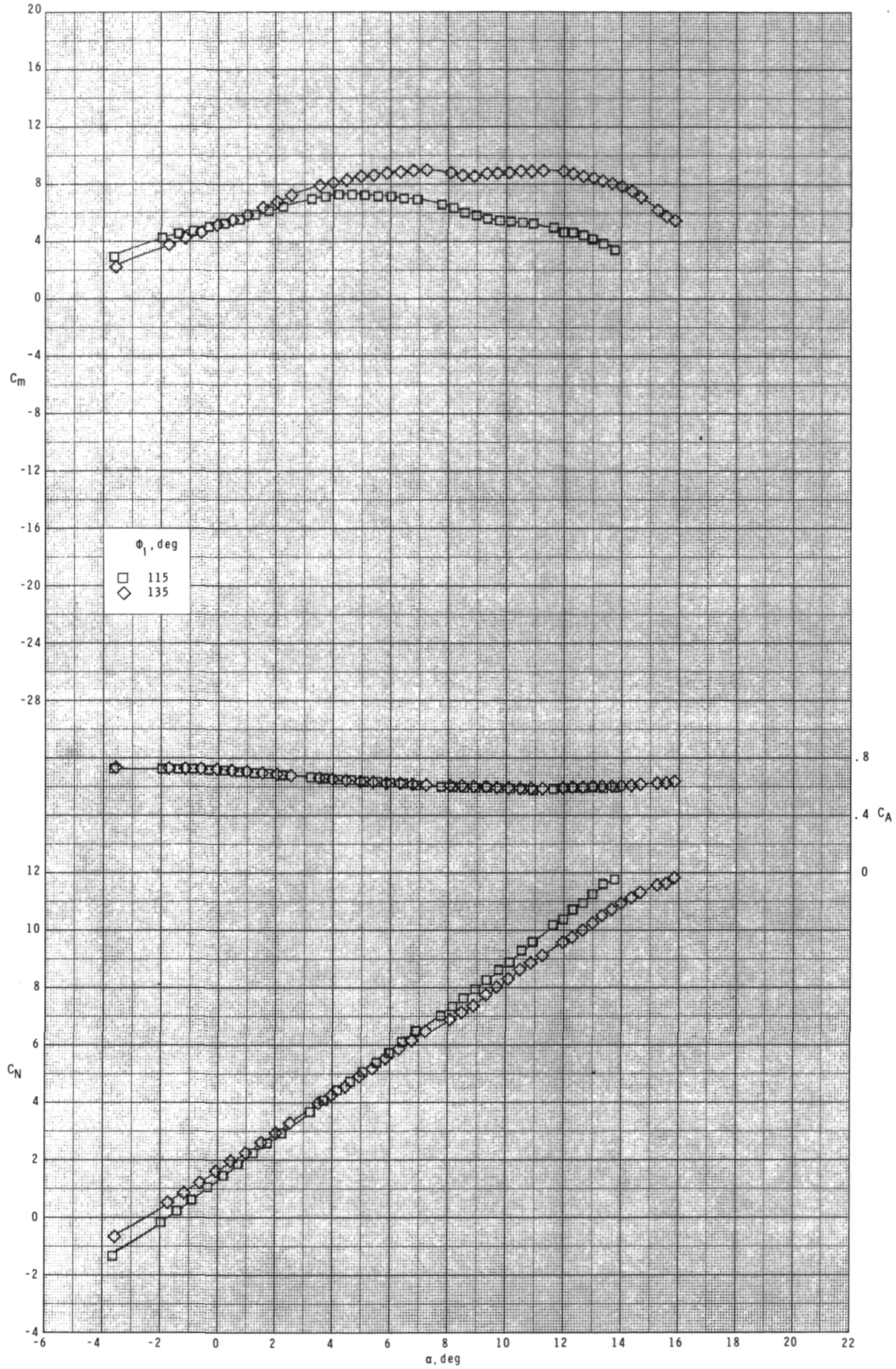

(b) M = 0.80.

Figure 4.- Continued.

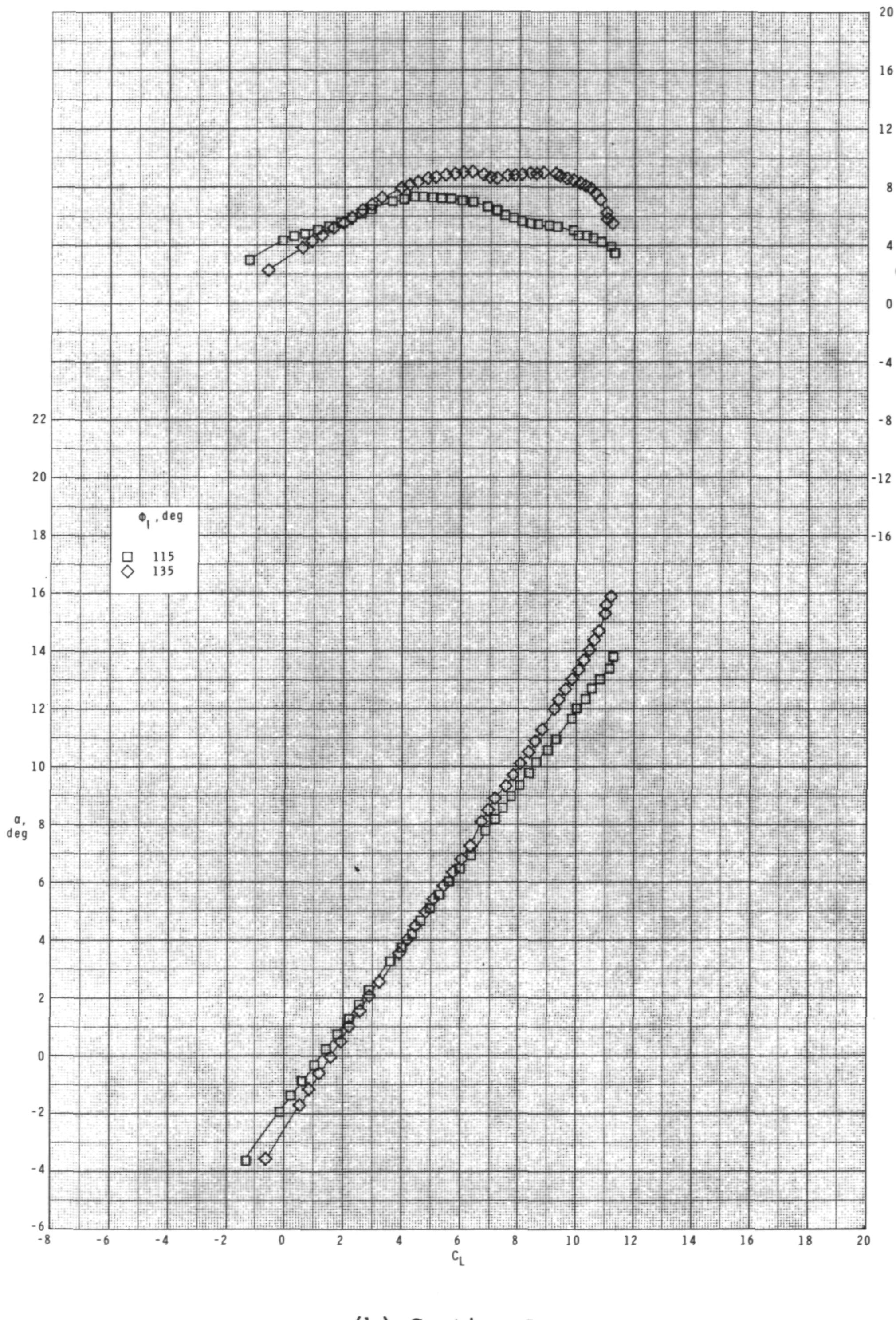

(b) Continued.

Figure 4.- Continued.

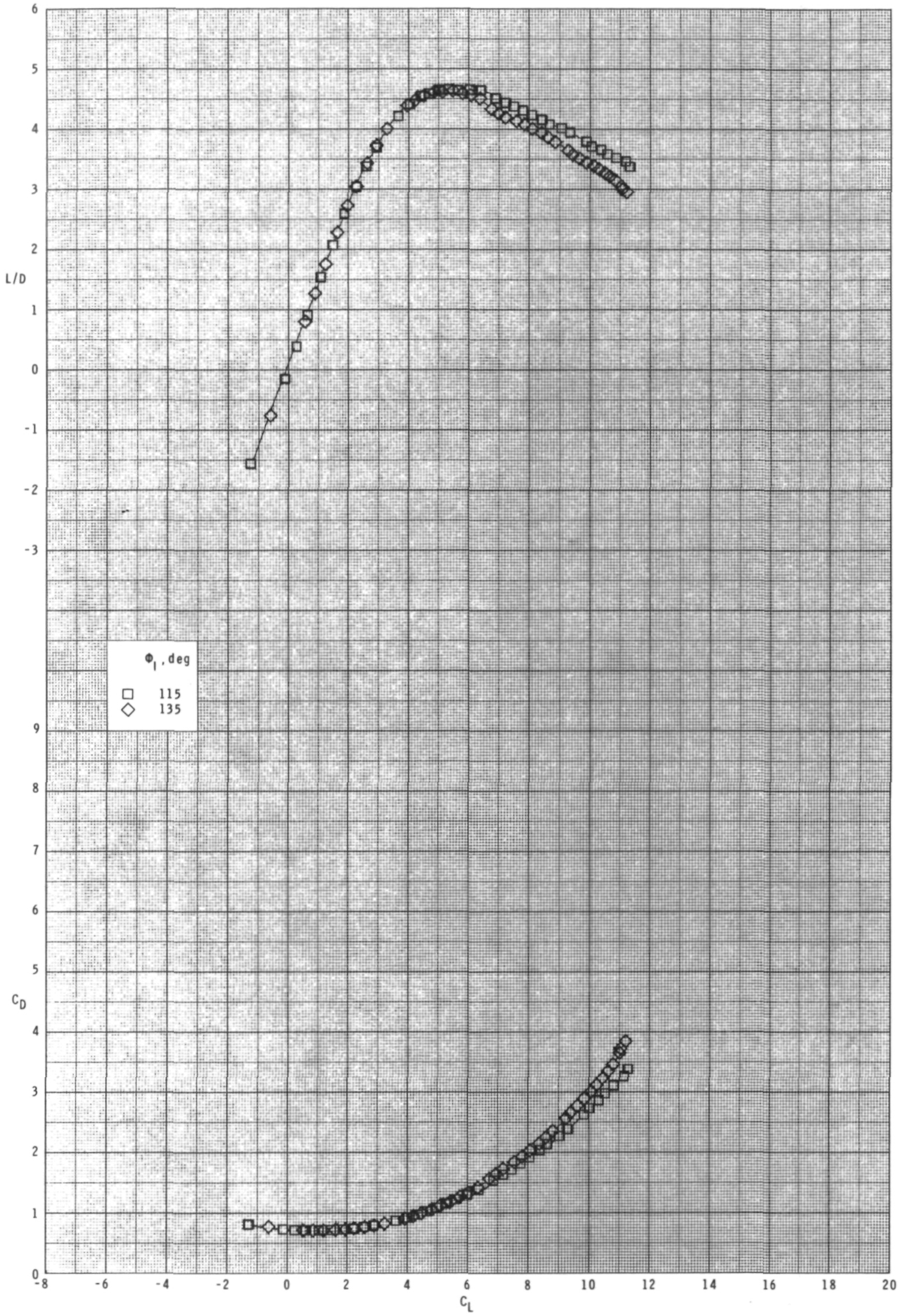

(b) Concluded.

Figure 4.- Continued.

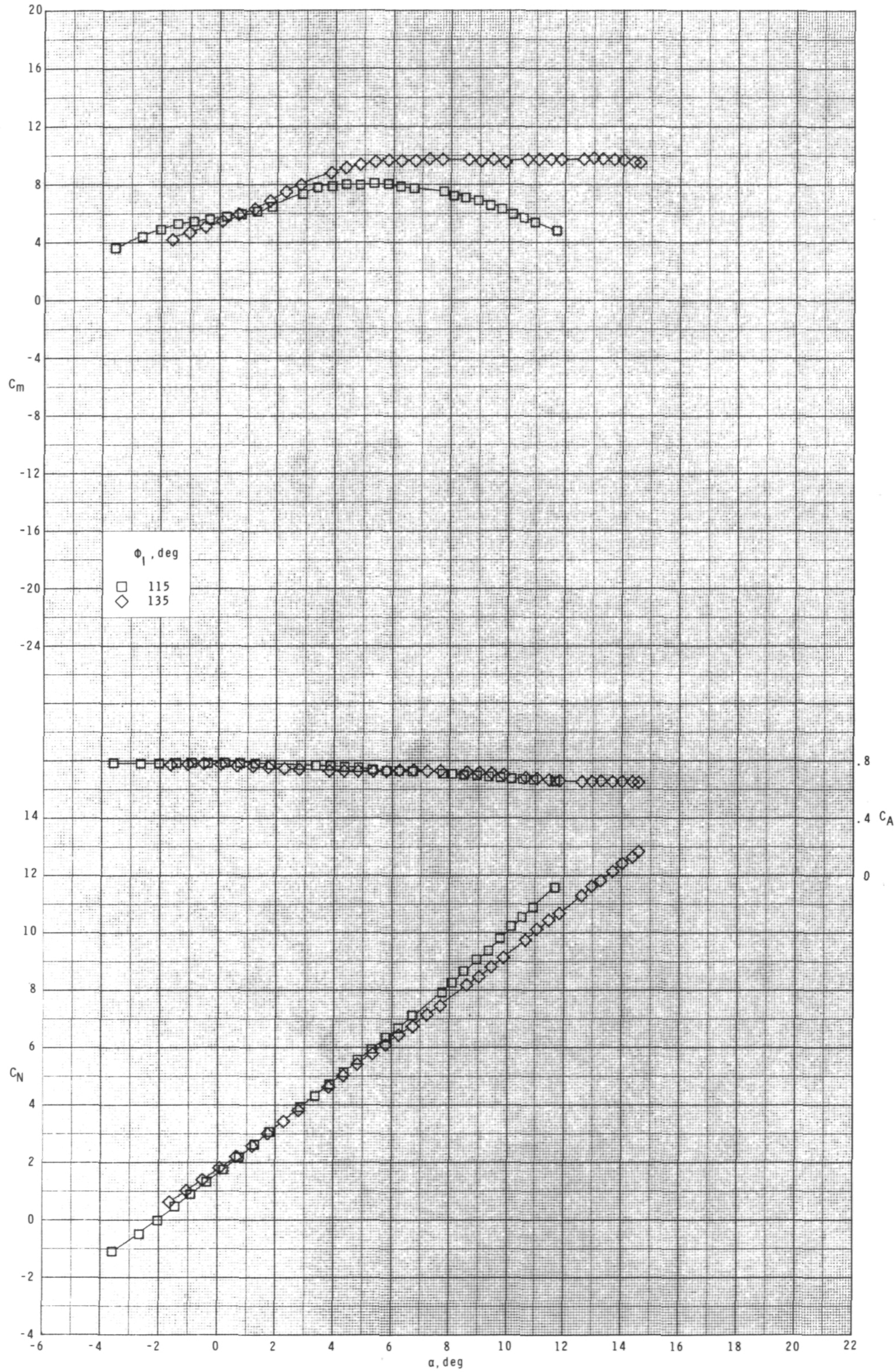

(c) M = 0.95.

Figure 4.- Continued.

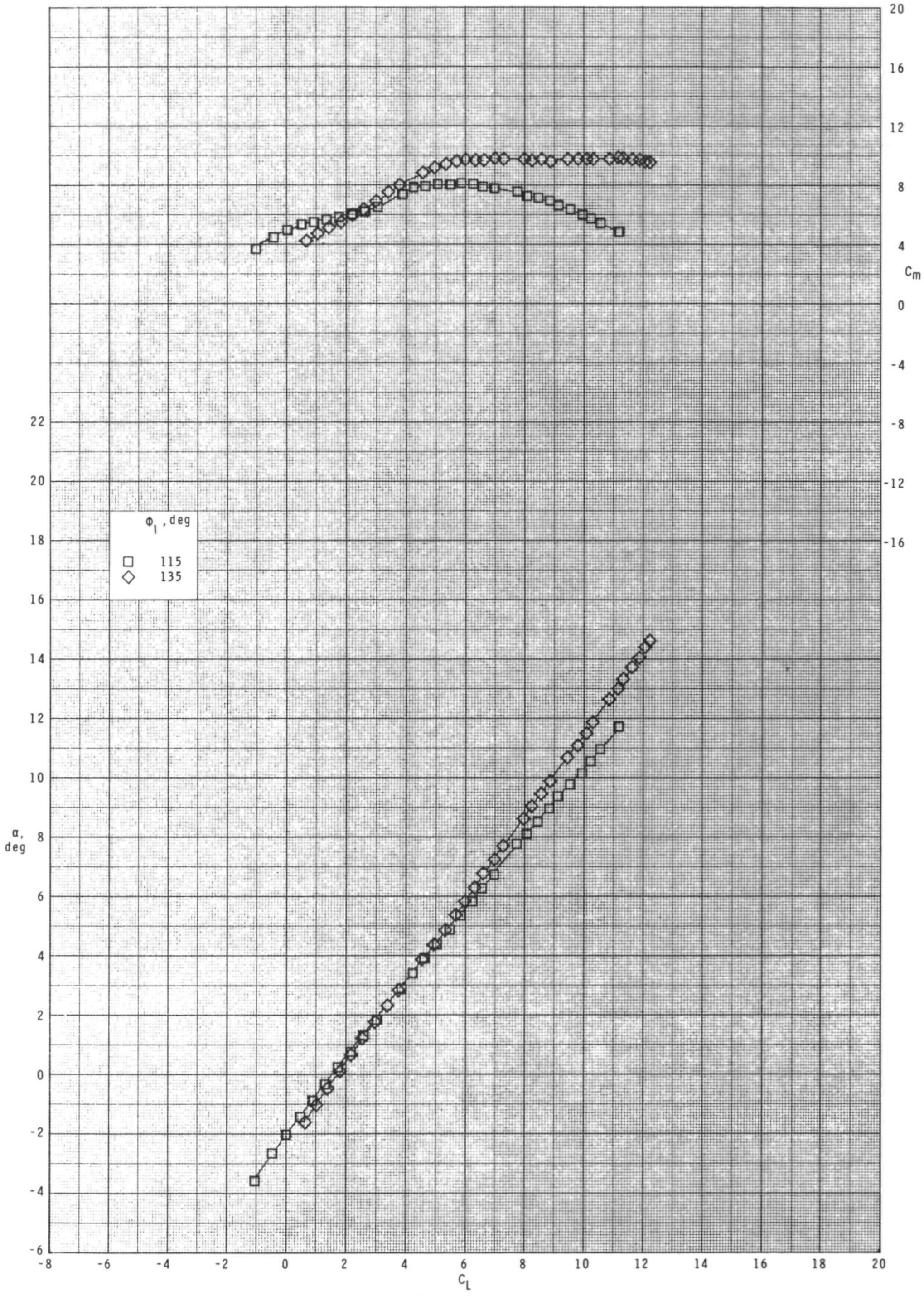

(c) Continued.

Figure 4.- Continued.

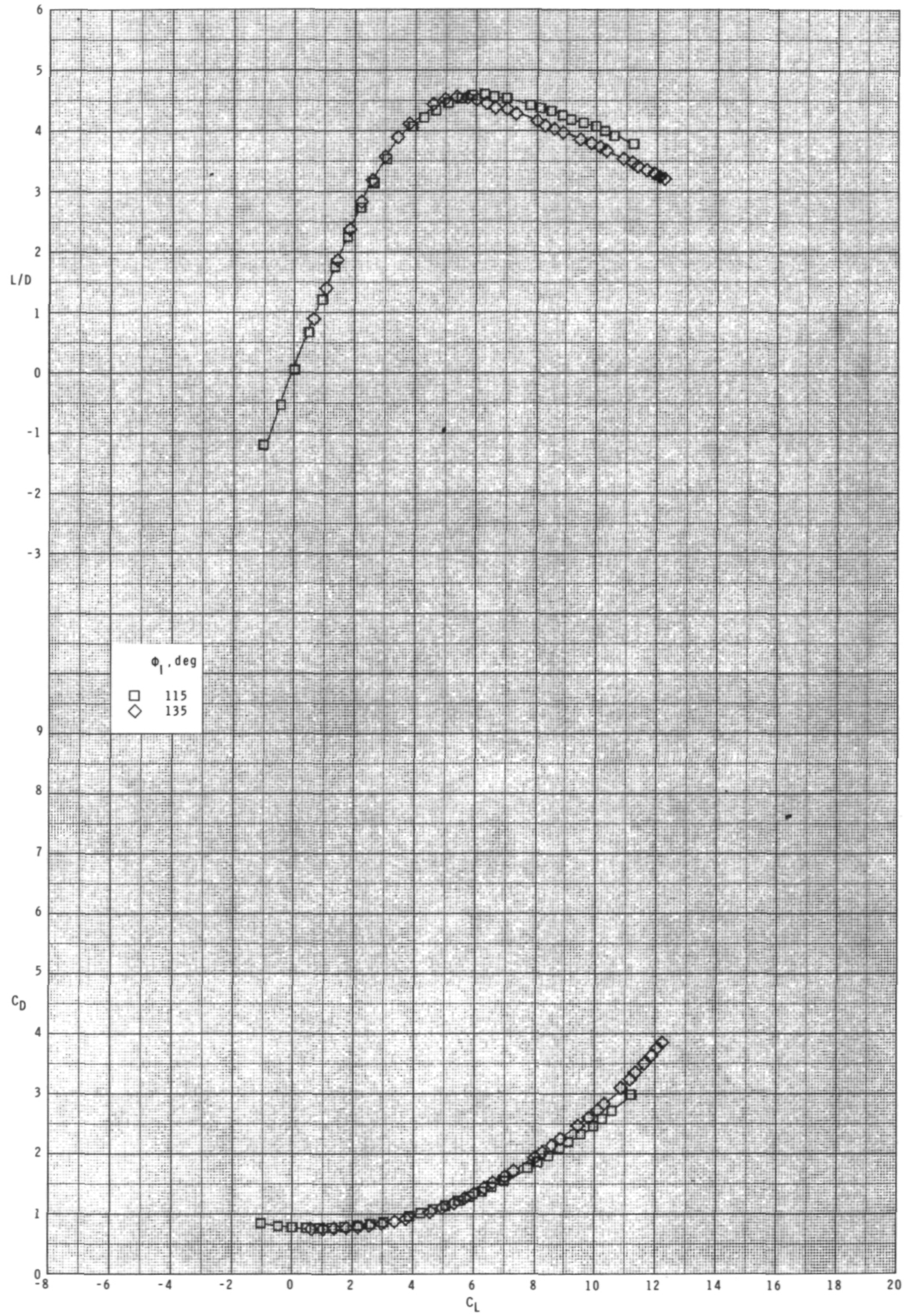

(c) Concluded.

Figure 4.- Concluded.

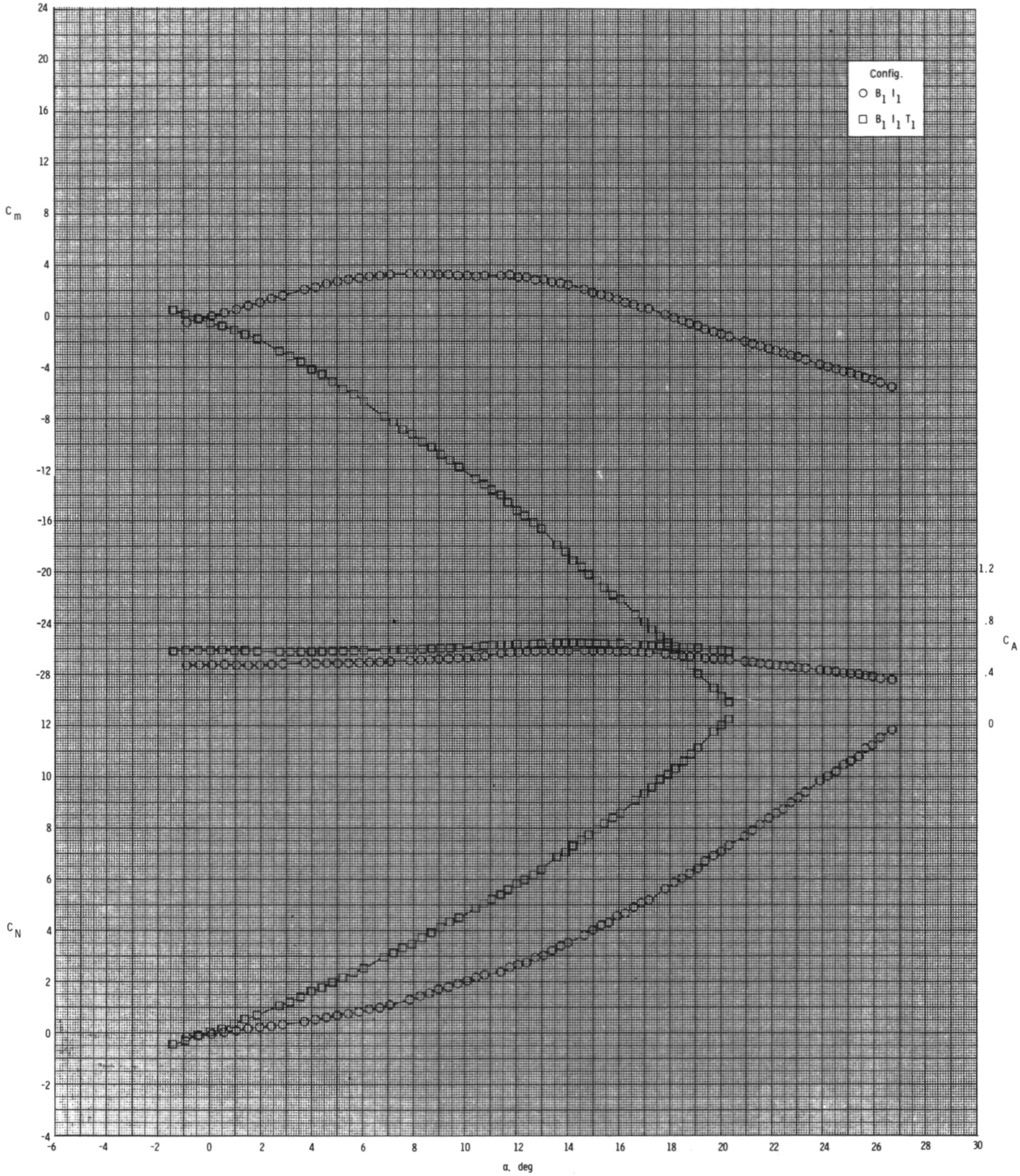

(a) M = 0.60.

Figure 5.- Effect of various model components on longitudinal aerodynamic characteristics for axisymmetric inlets with internal ducts closed, $\phi_I = 90°$, and $\delta_p = 0°$.

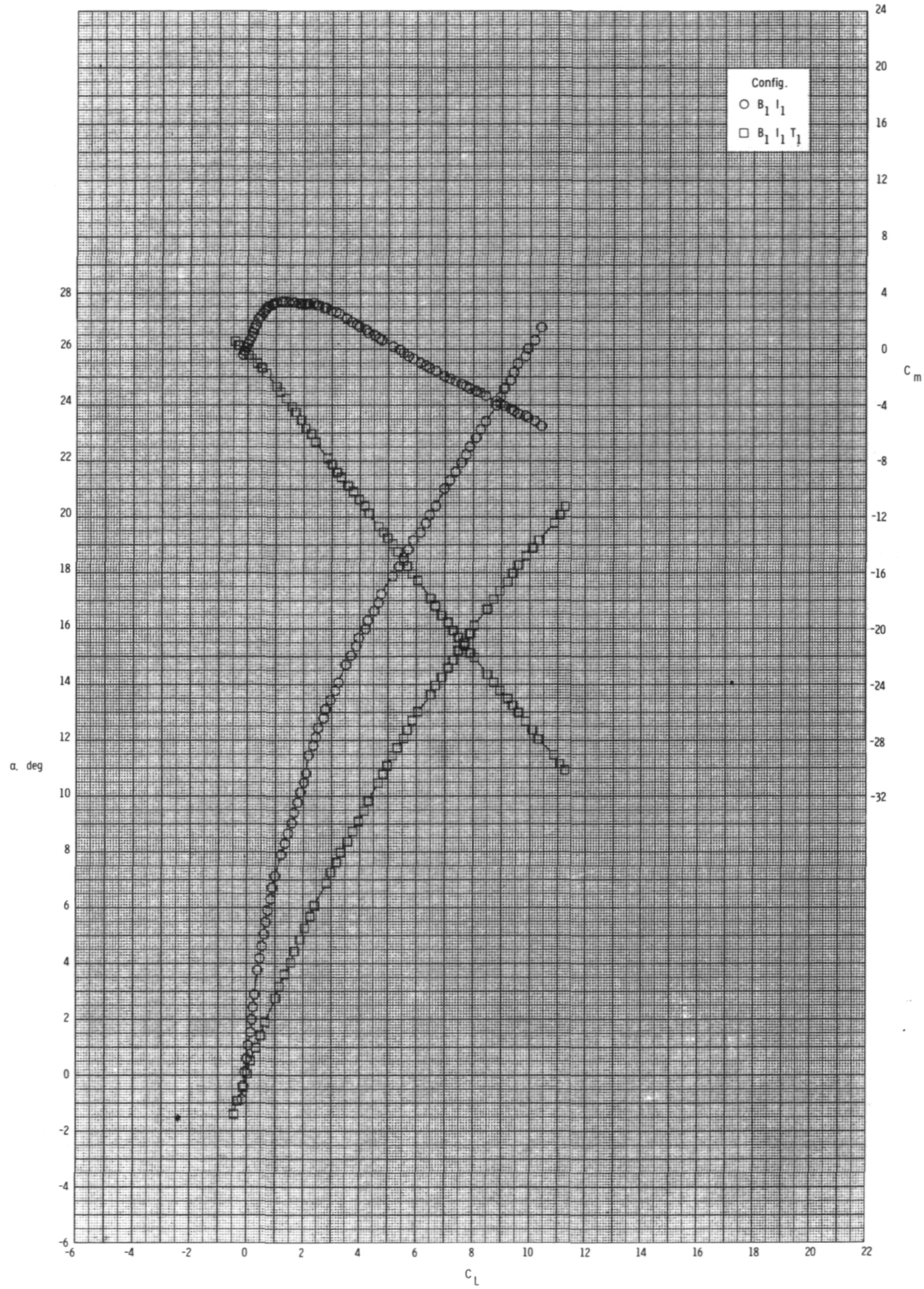

(a) Continued.

Figure 5.- Continued.

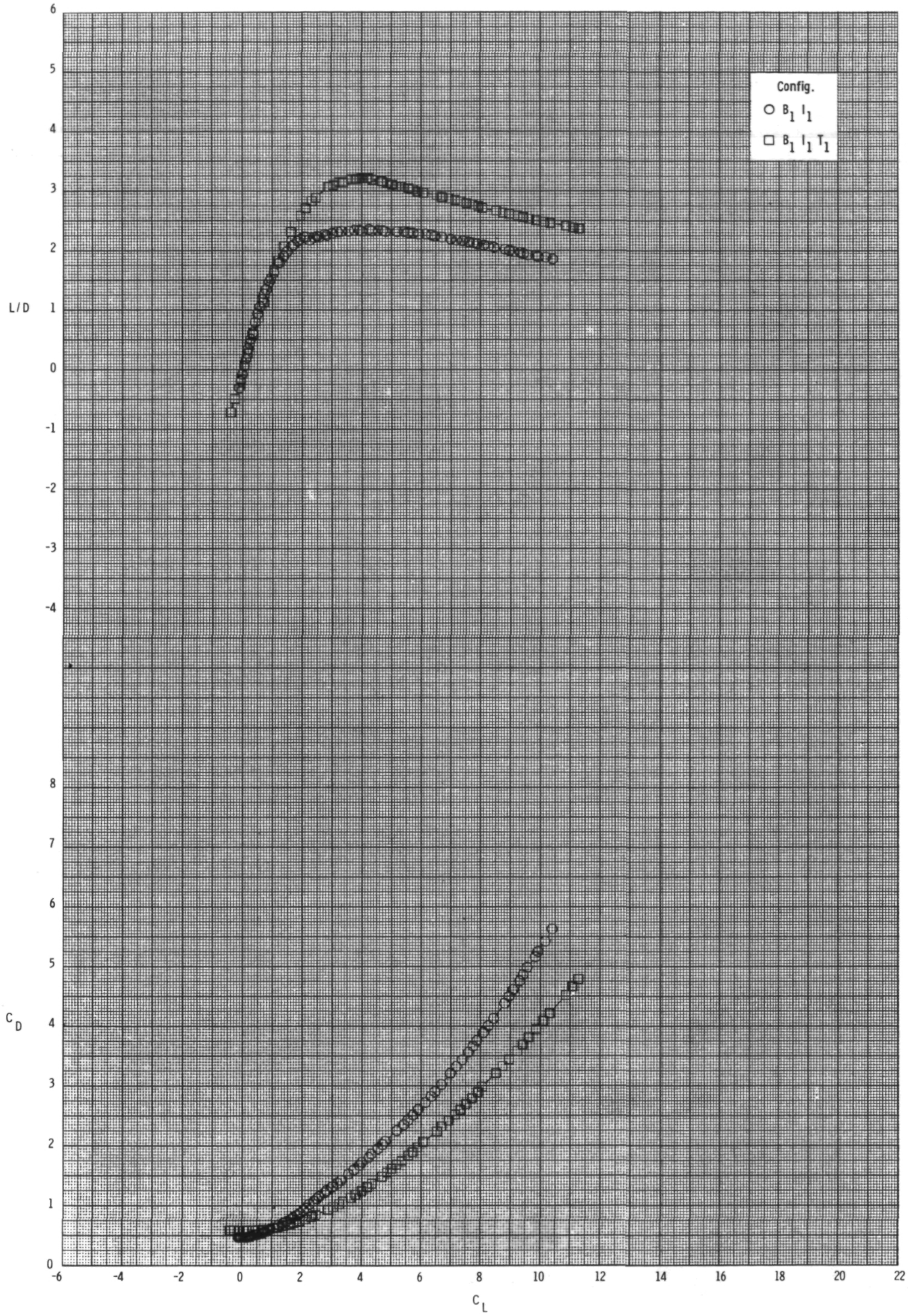

(a) Concluded.

Figure 5.- Continued.

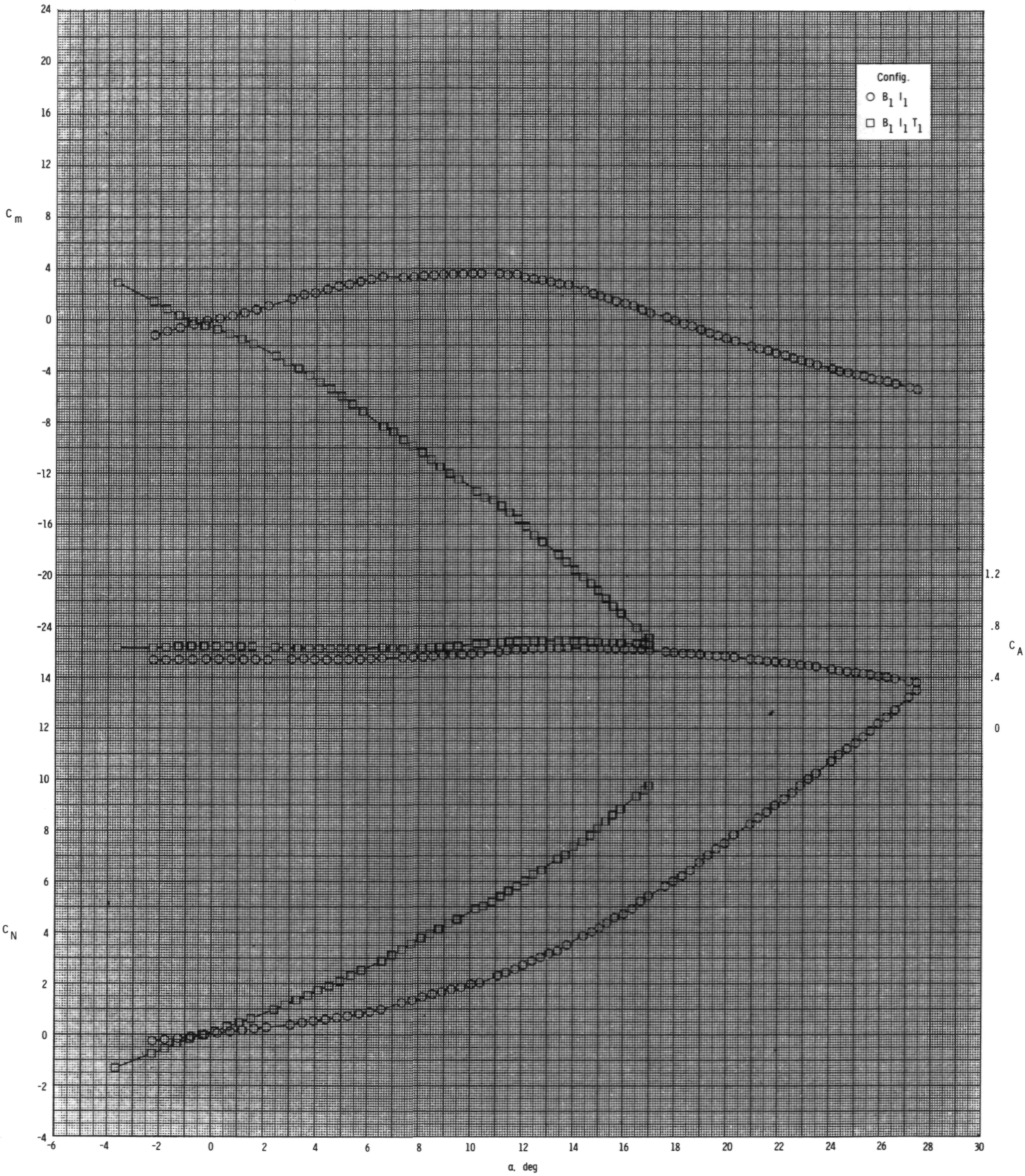

(b) M = 0.80.

Figure 5.- Continued.

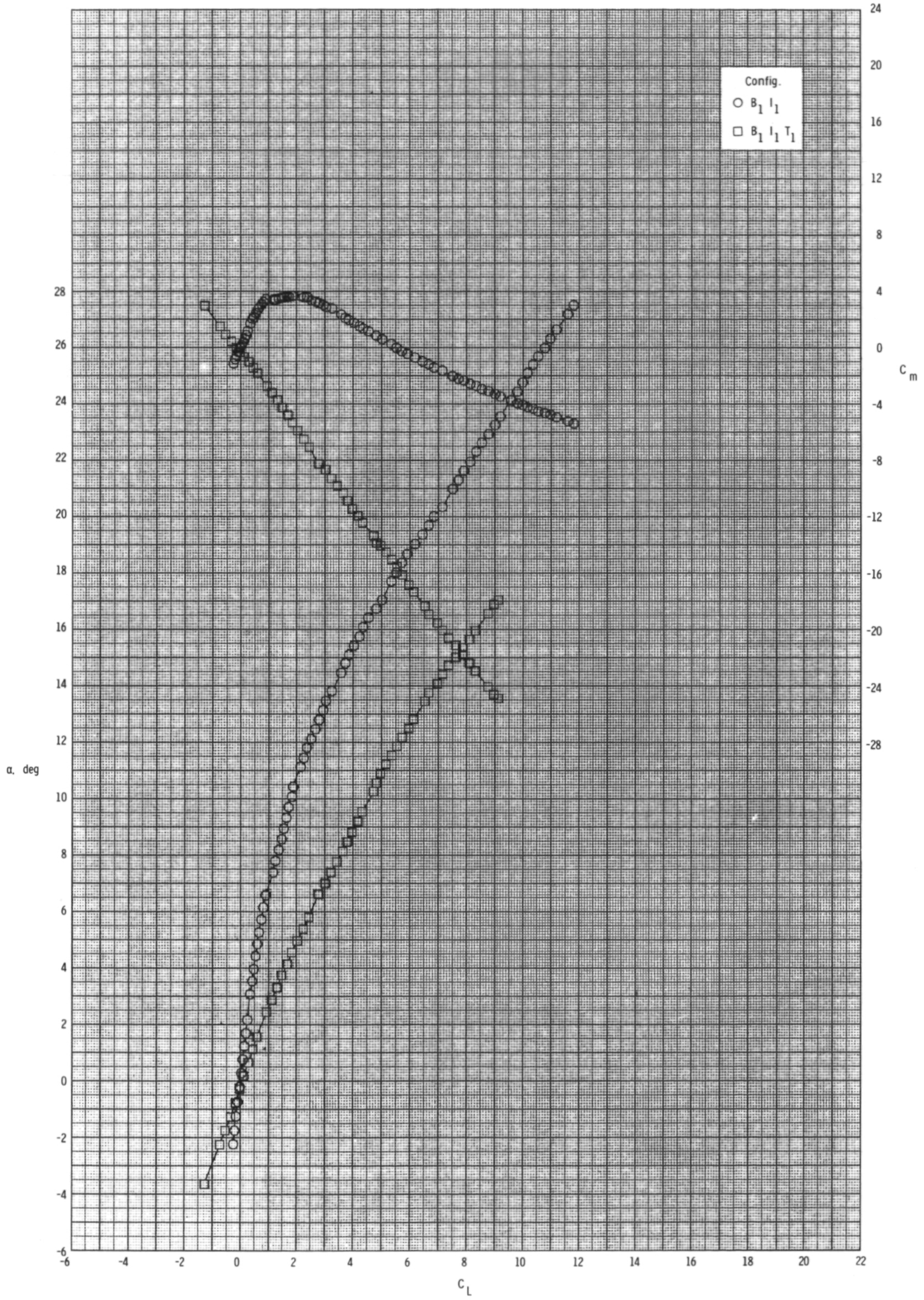

(b) Continued.

Figure 5.- Continued.

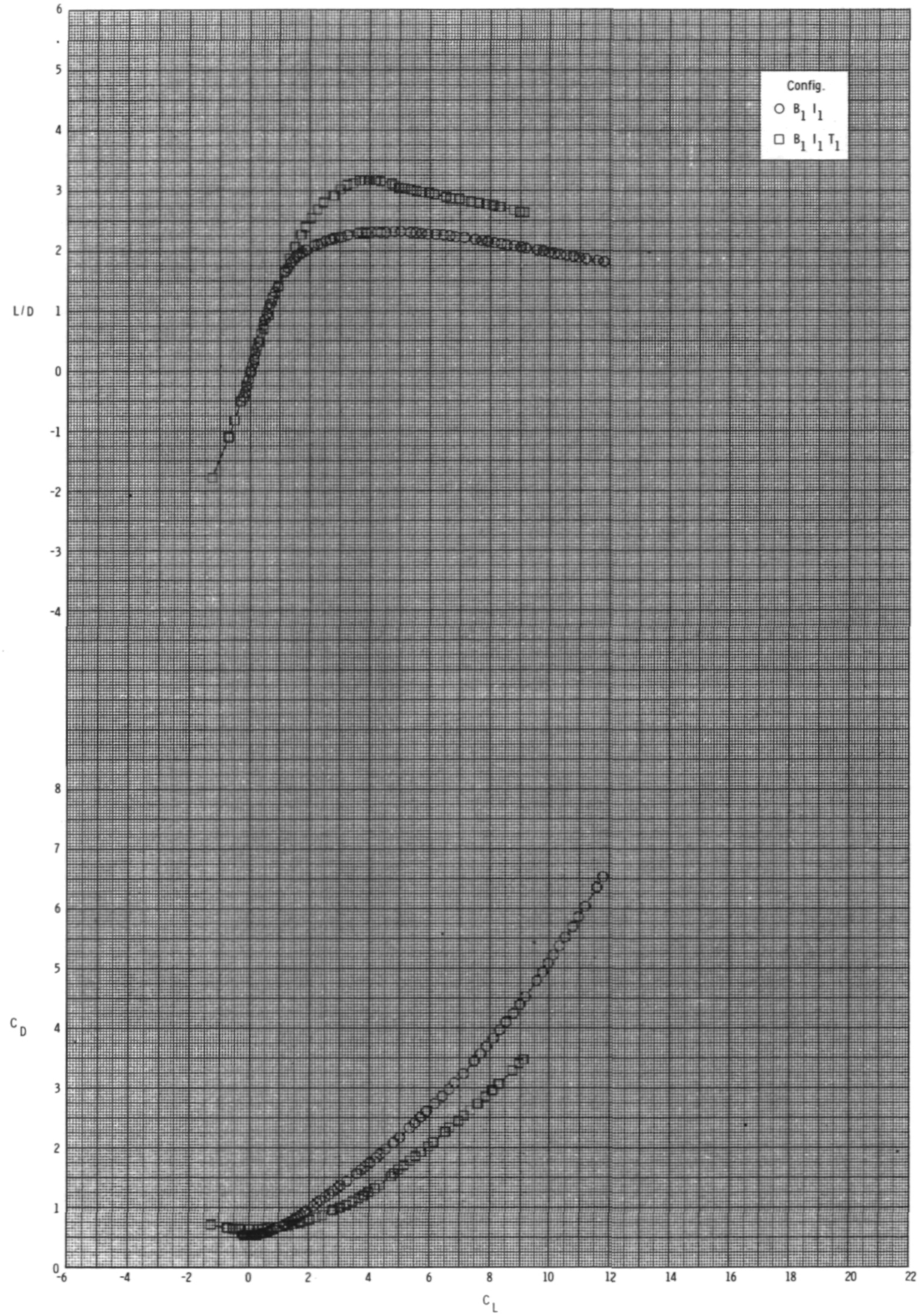

(b) Concluded.

Figure 5.- Continued.

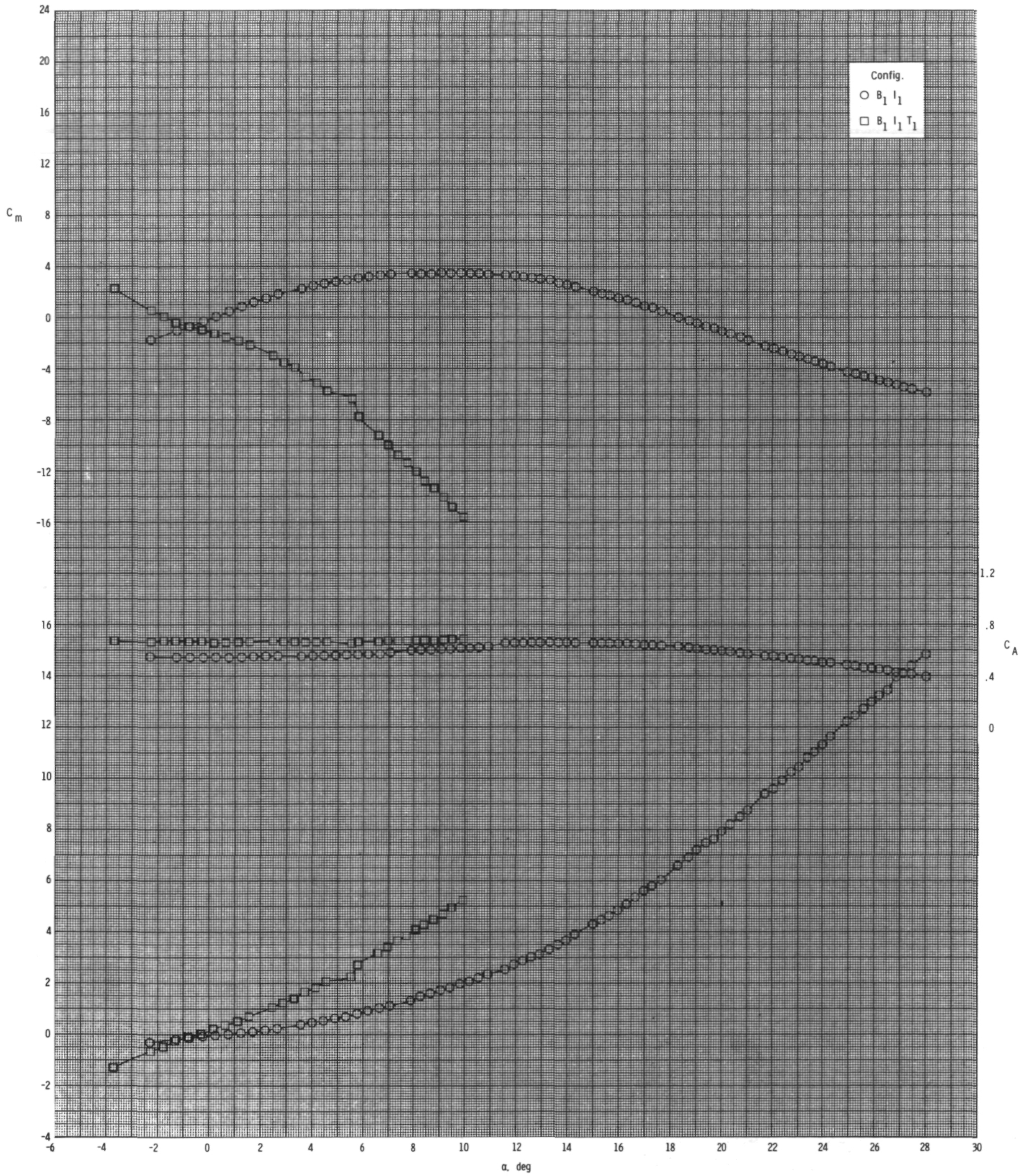

(c) M = 0.95.

Figure 5.- Continued.

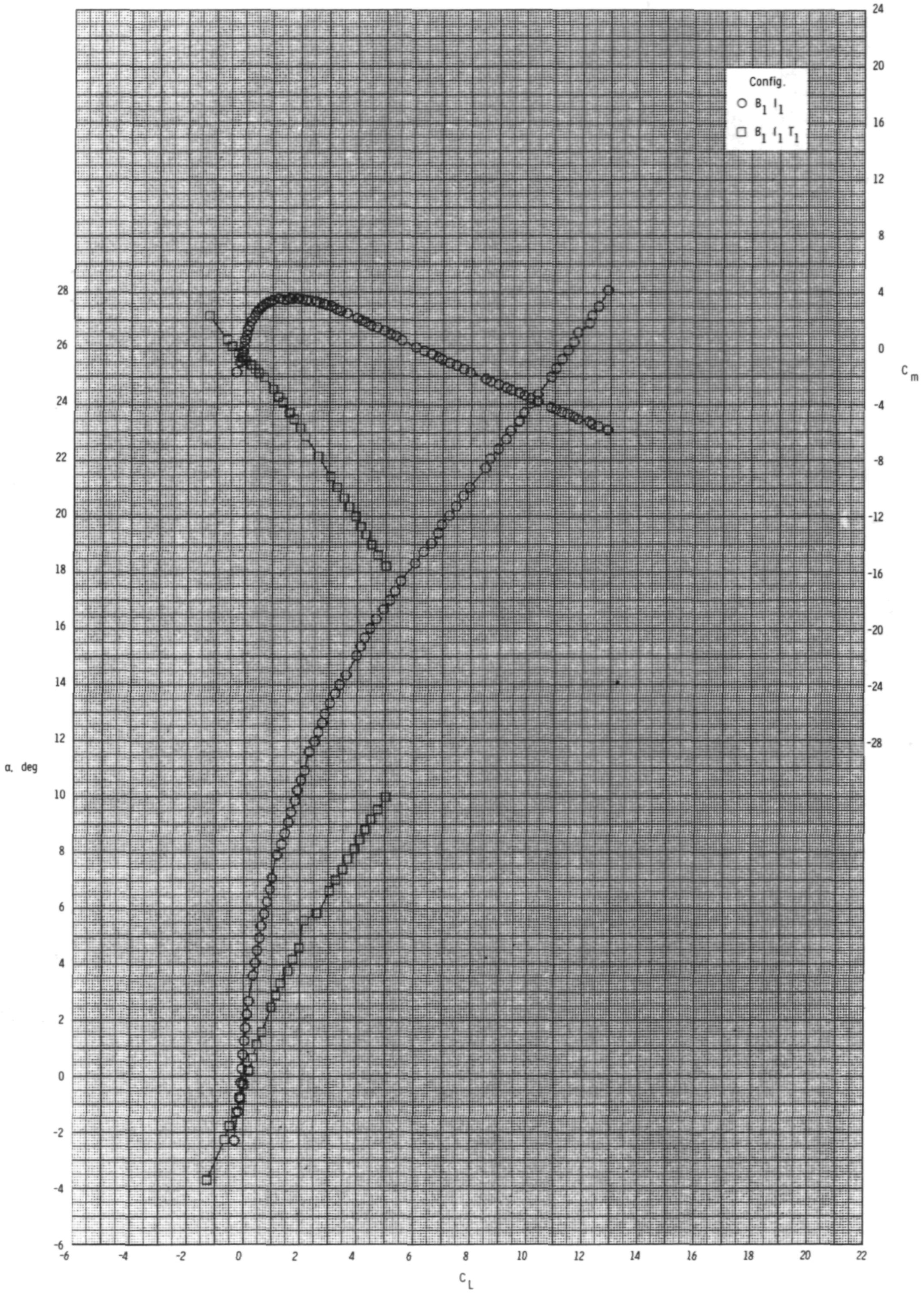

(c) Continued.

Figure 5.- Continued.

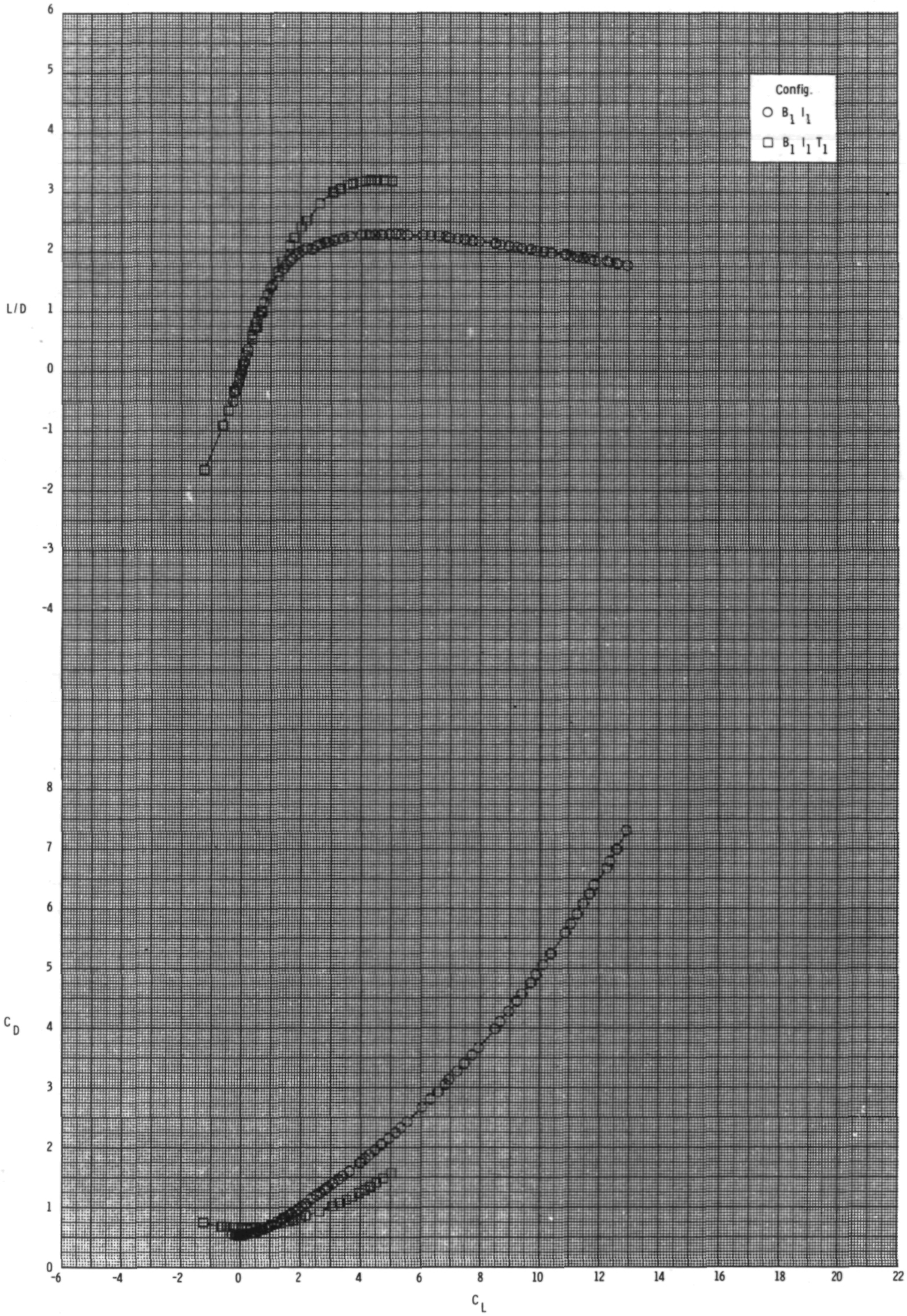

(c) Concluded.

Figure 5.- Concluded.

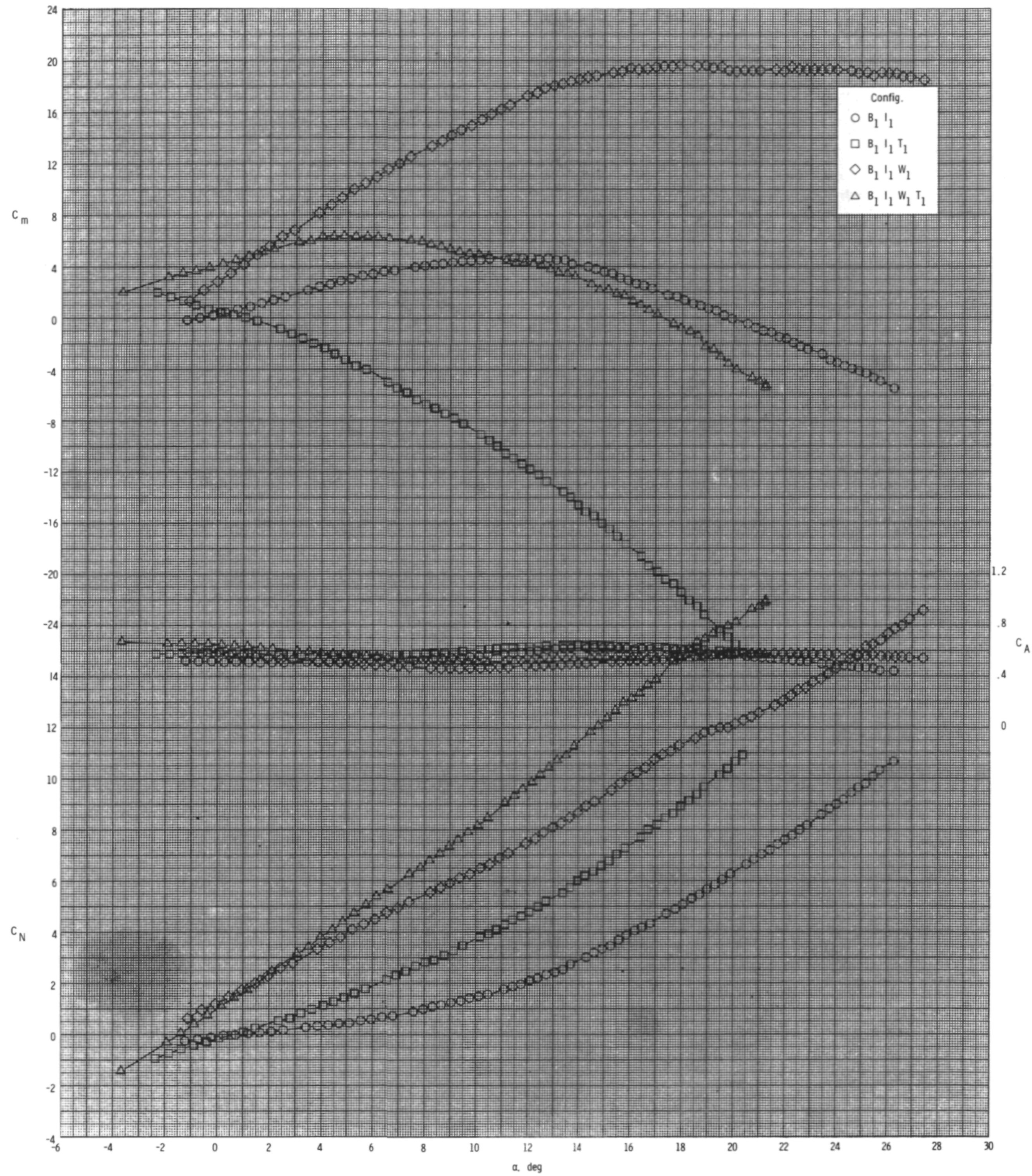

(a) M = 0.60.

Figure 6.- Effect of various model components on longitudinal aerodynamic characteristics for axisymmetric inlets with internal ducts closed, $\phi_I = 115°$, and $\delta_p = 0°$.

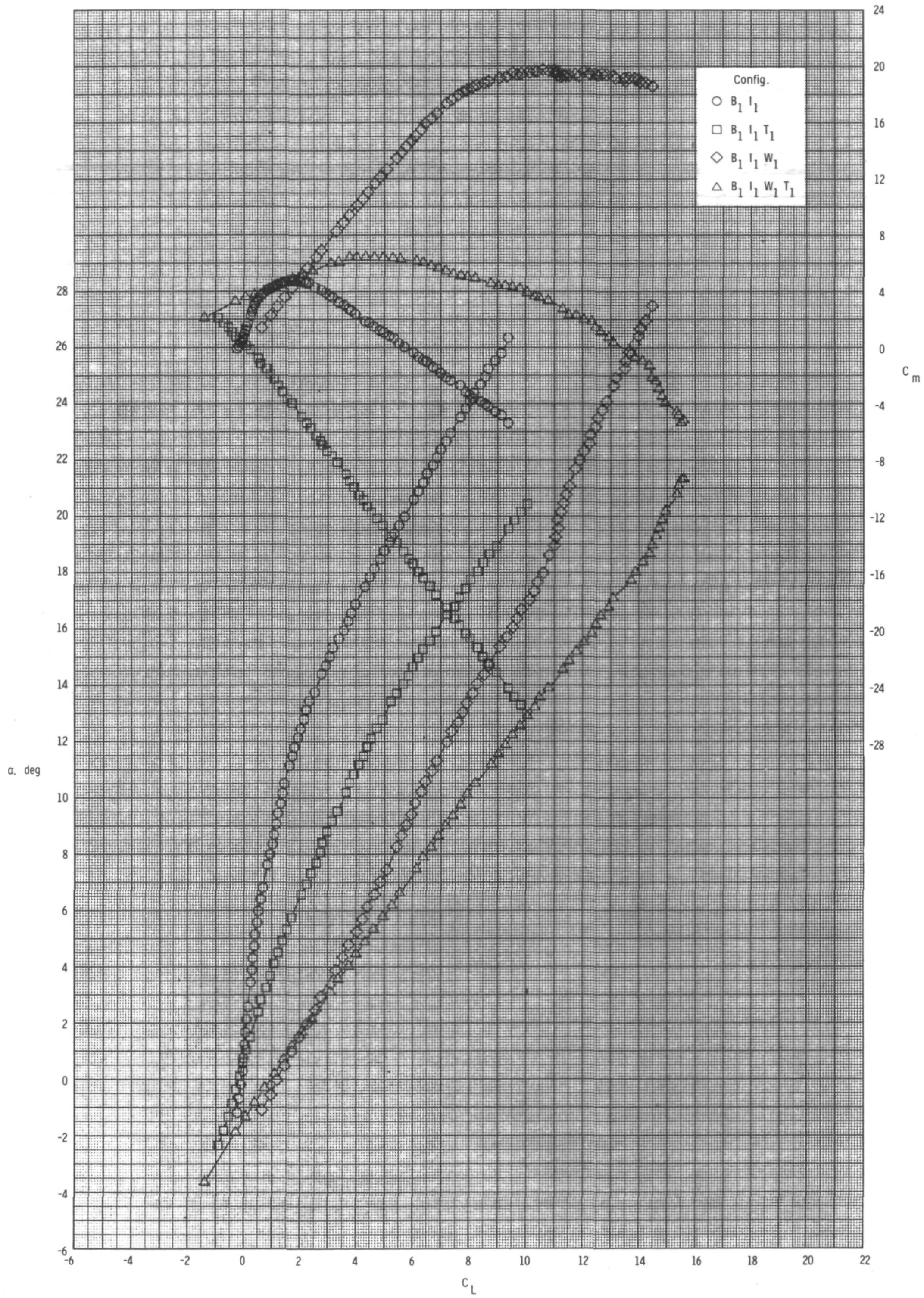

(a) Continued.

Figure 6.- Continued.

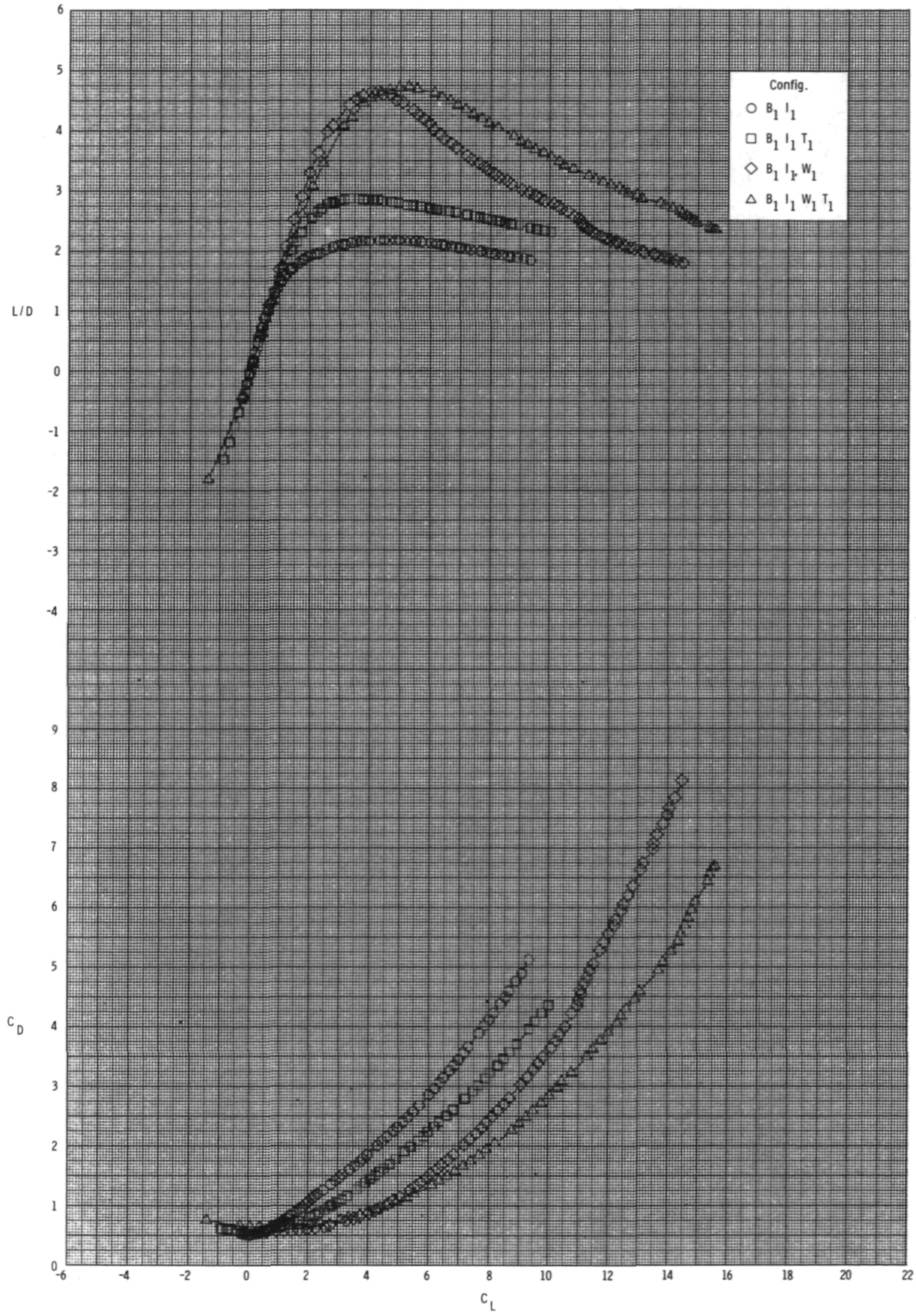

(a) Concluded.

Figure 6.- Continued.

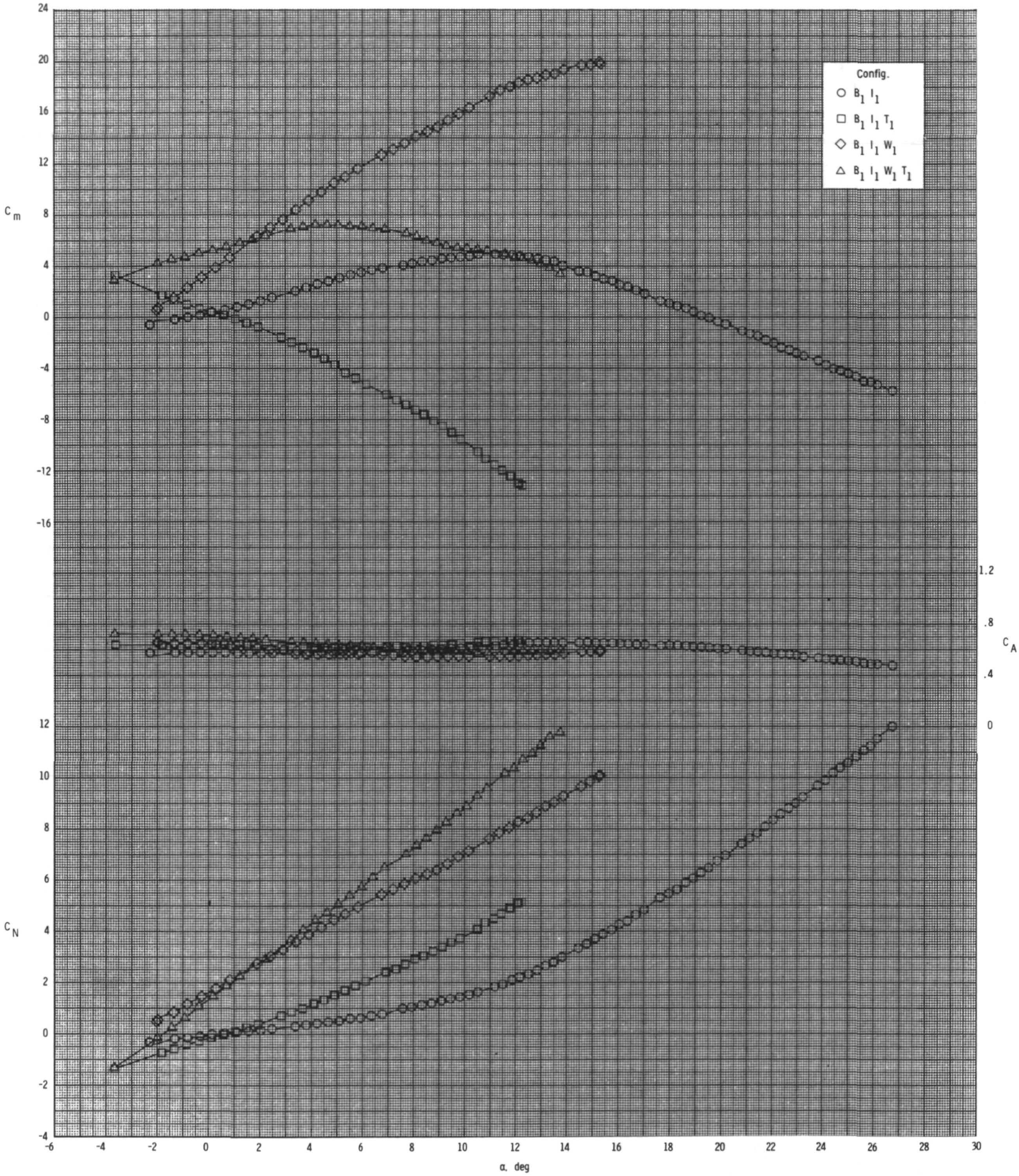

(b) M = 0.80.

Figure 6.- Continued.

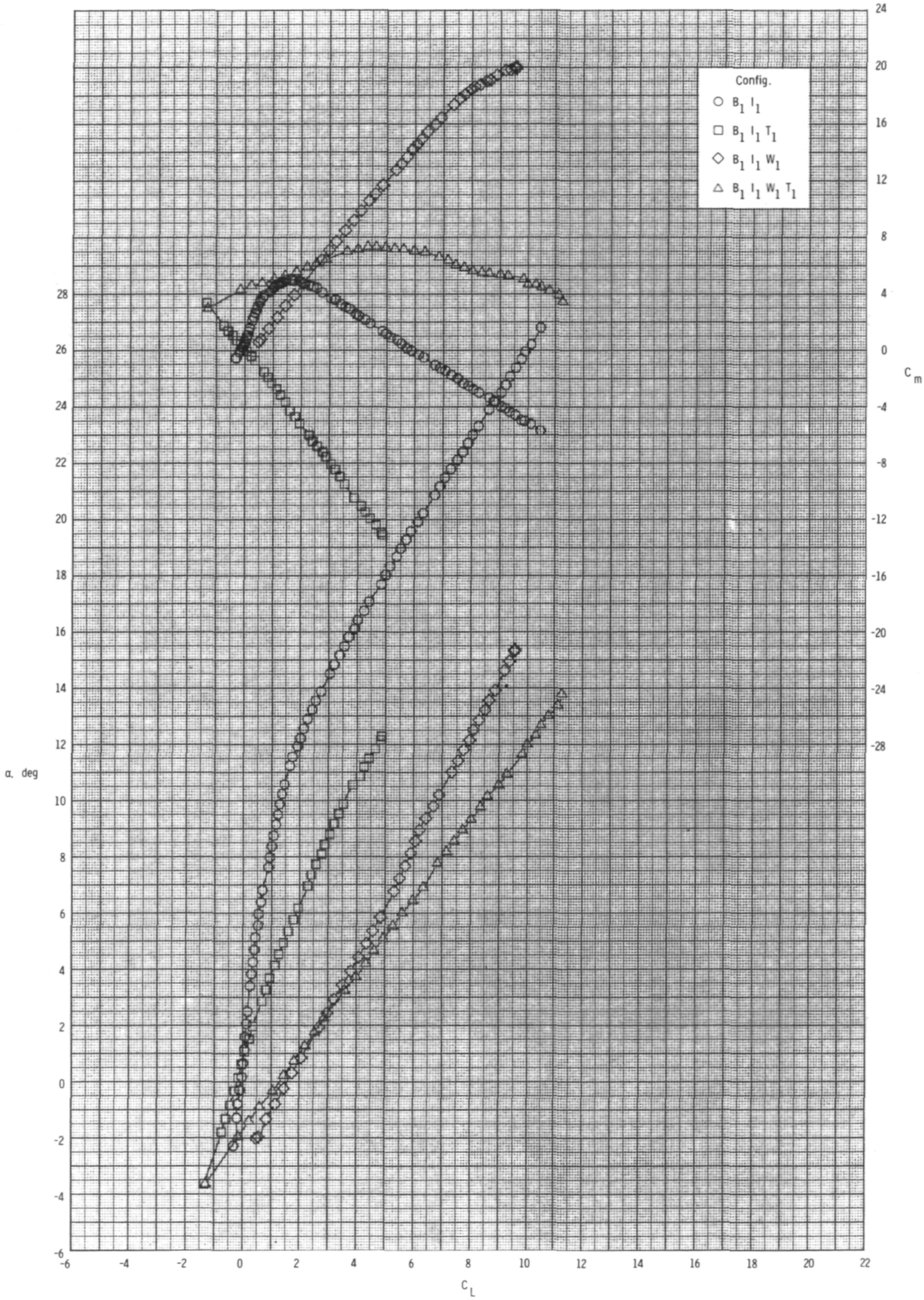

(b) Continued.

Figure 6.- Continued.

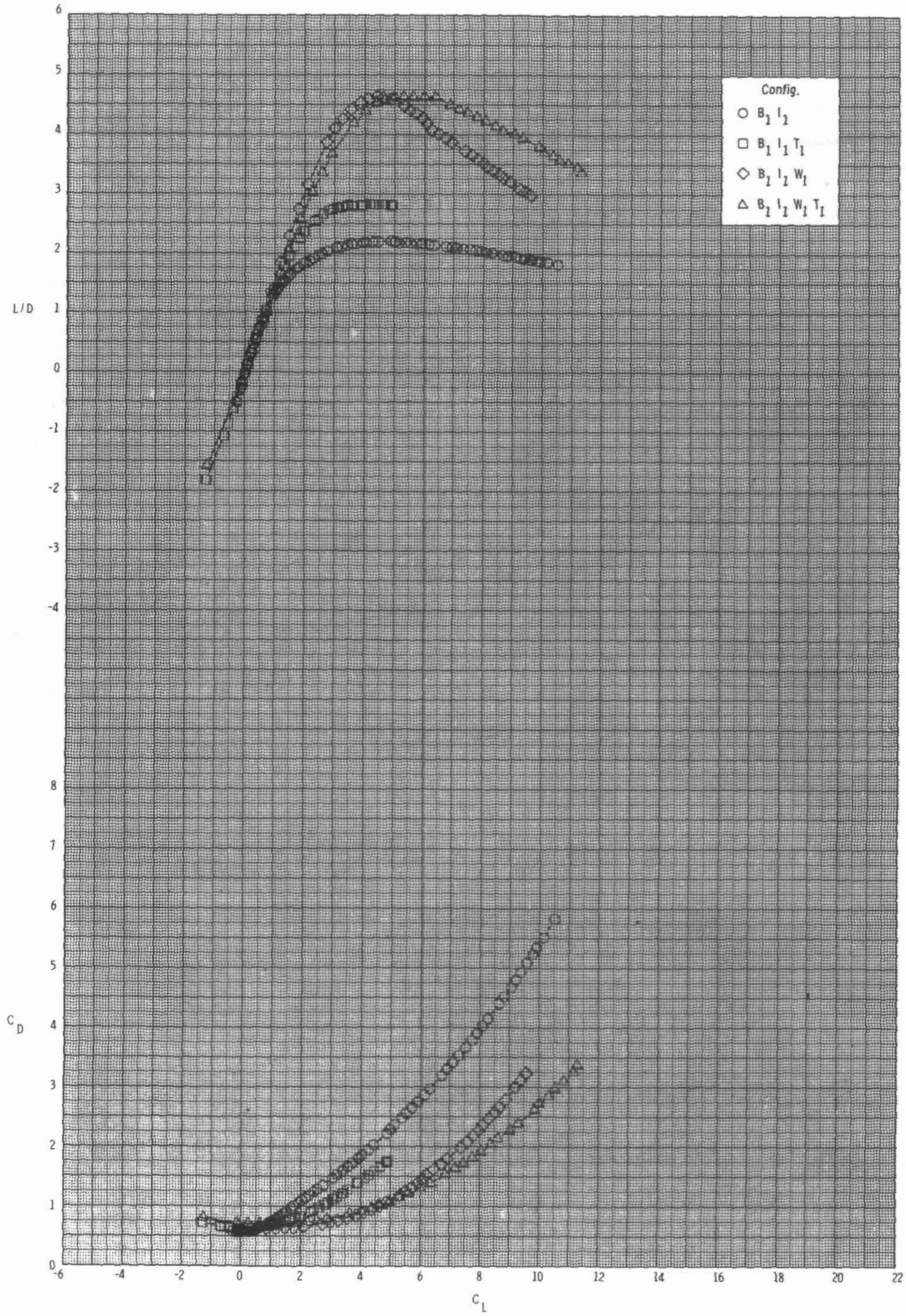

(b) Concluded.

Figure 6.- Continued.

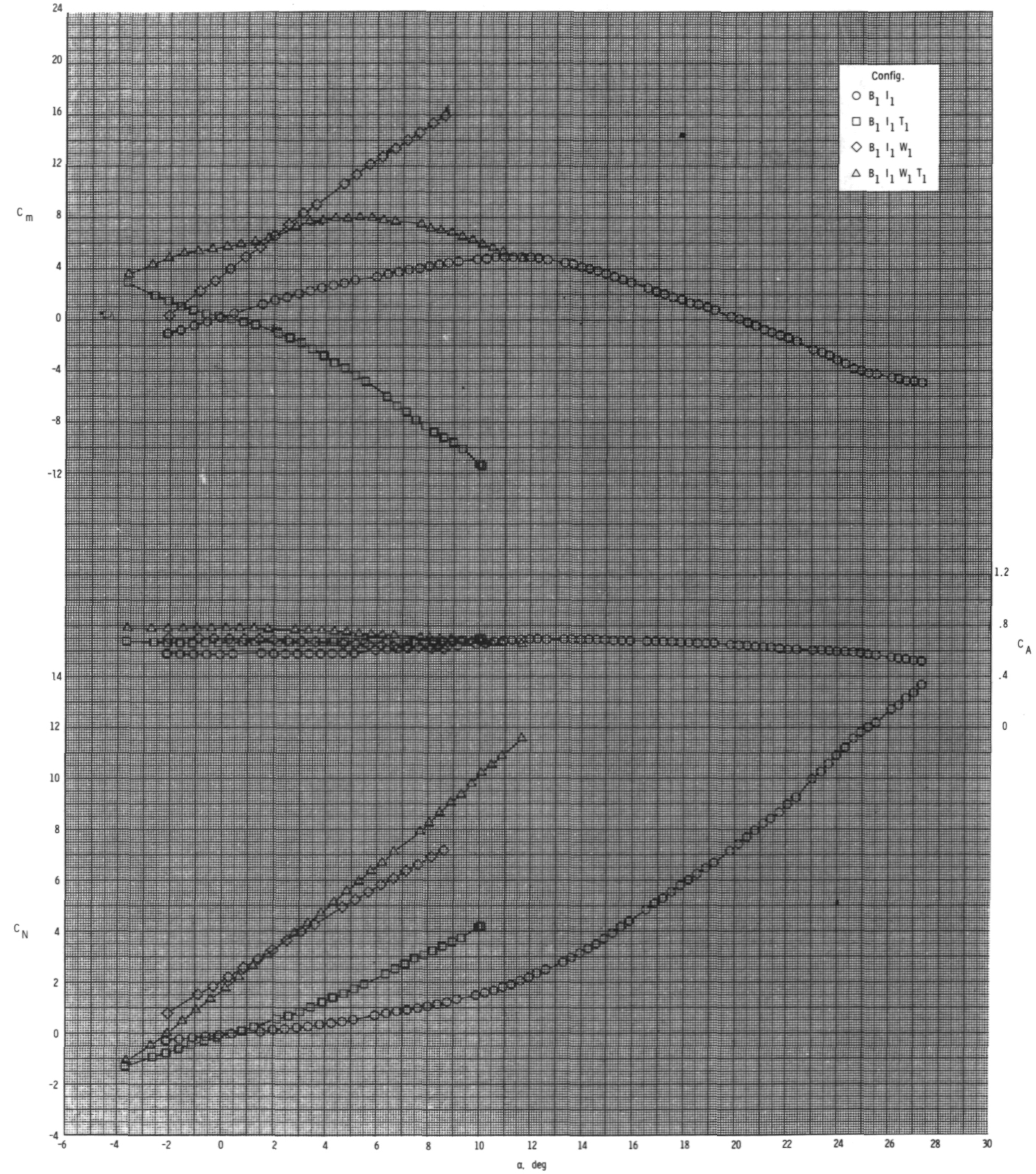

(c) M = 0.95.

Figure 6.- Continued.

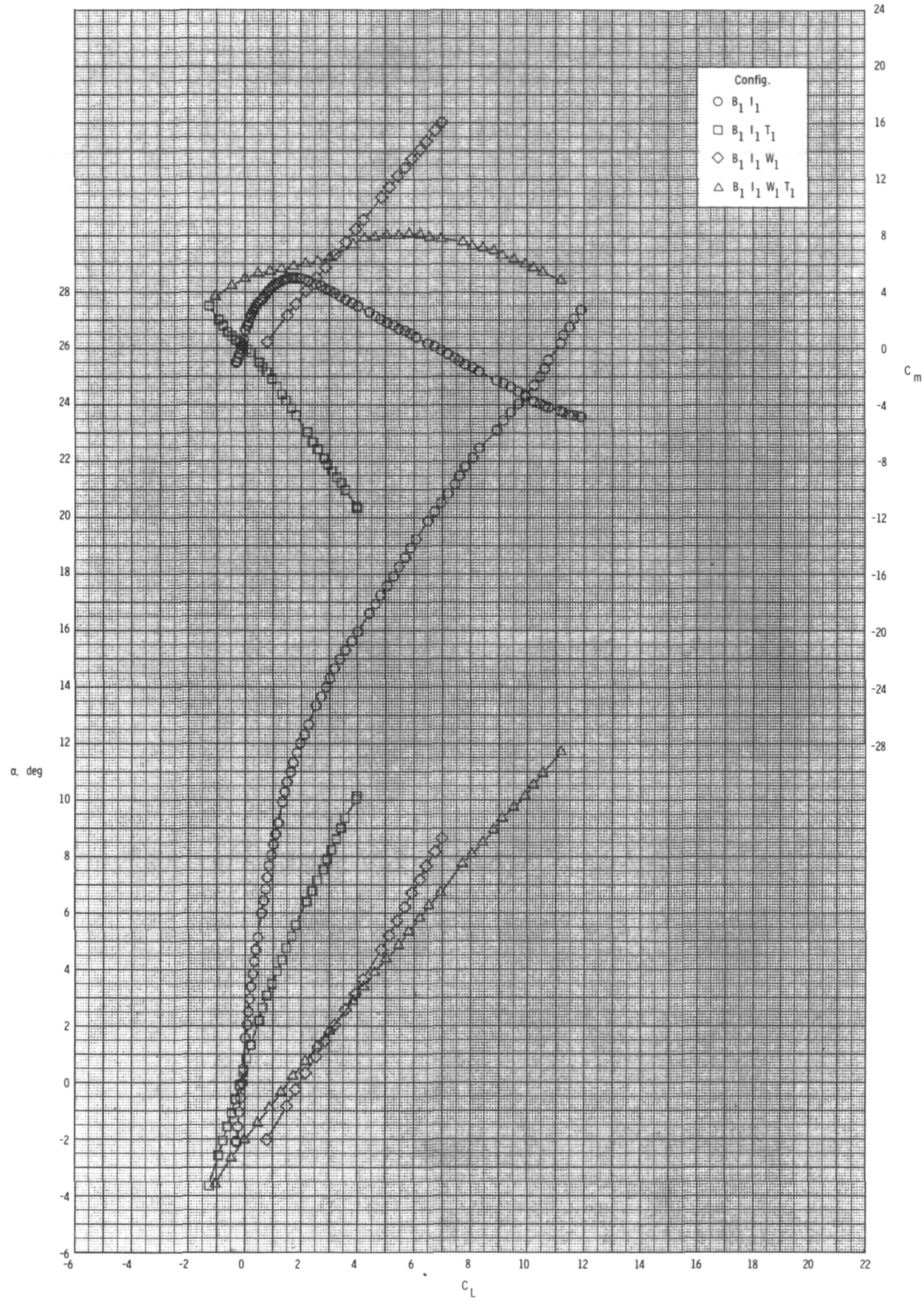

(c) Continued.

Figure 6.- Continued.

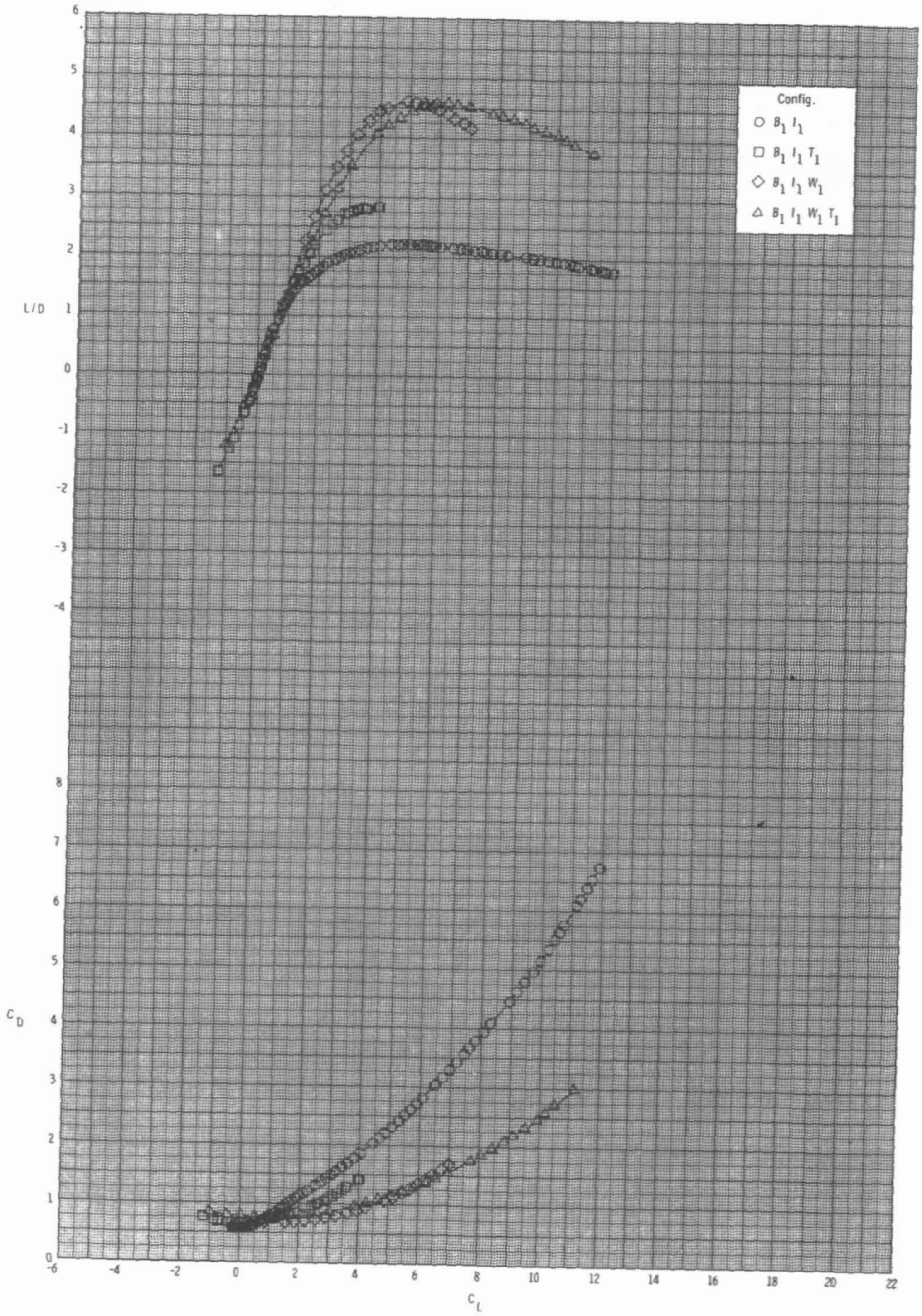

(c) Concluded.

Figure 6.- Concluded.

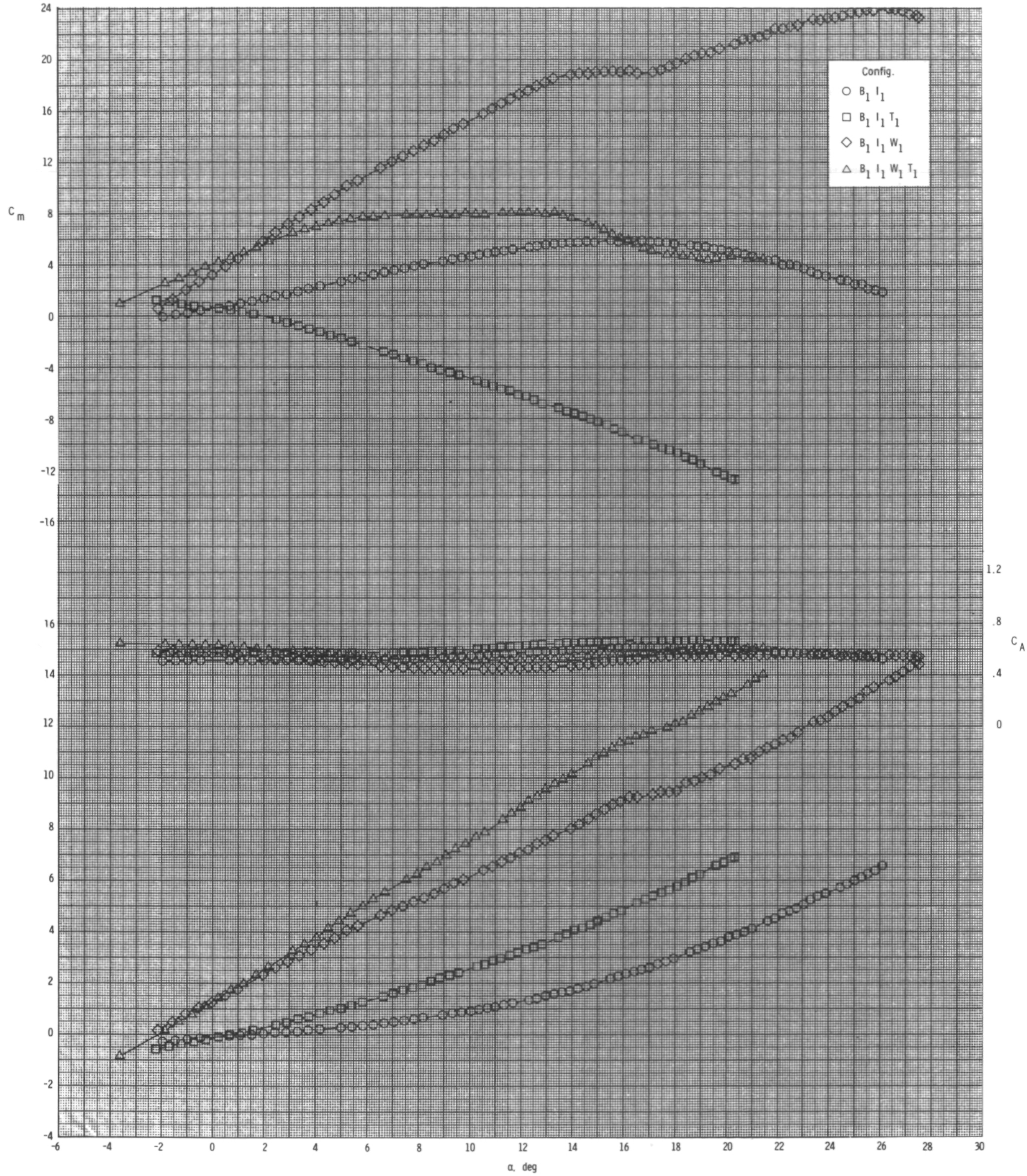

(a) M = 0.60.

Figure 7.- Effect of various model components on longitudinal aerodynamic characteristics for axisymmetric inlets with internal ducts closed, T_1, $\phi_I = 135°$, and $\delta_p = 0°$.

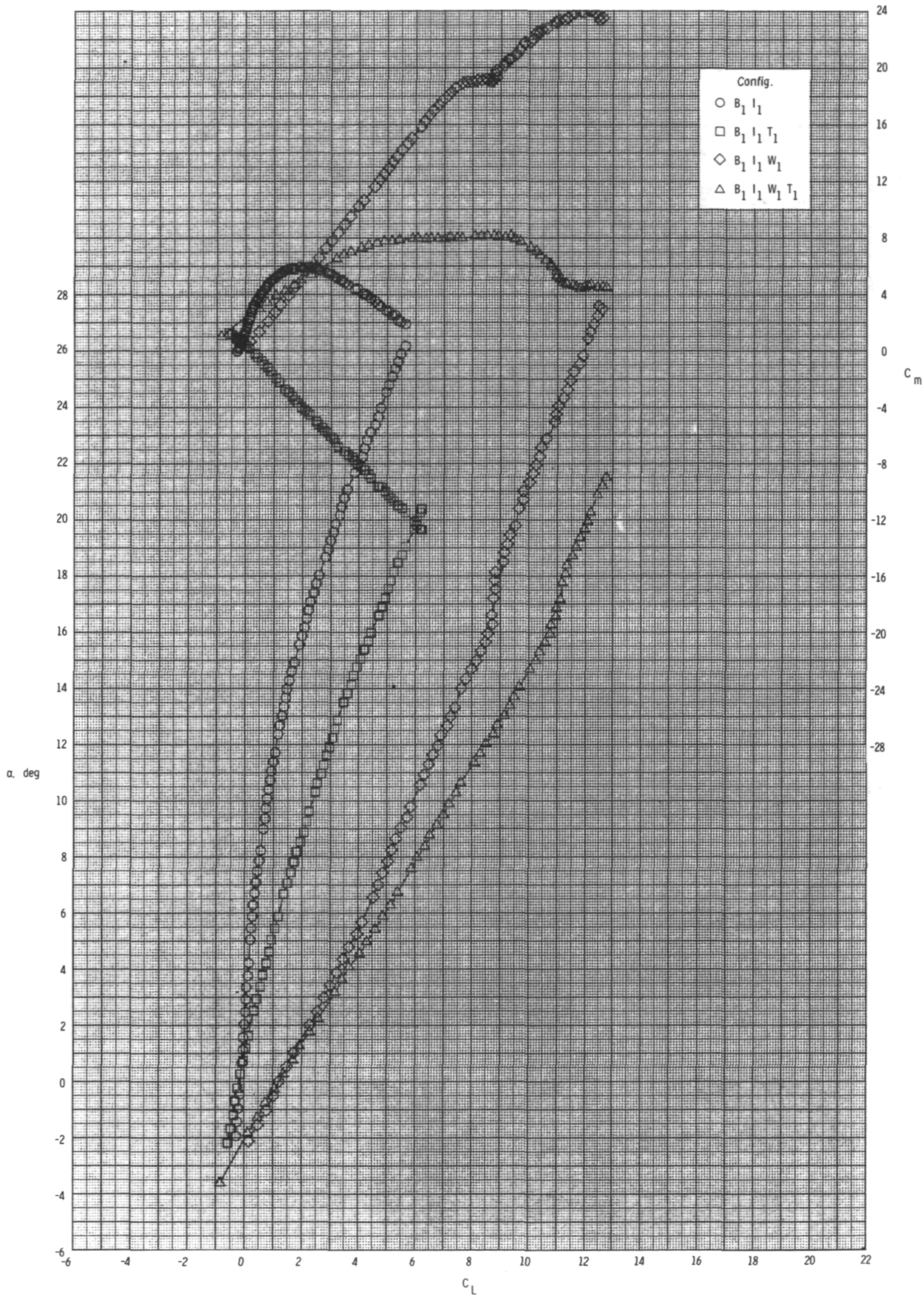

(a) Continued.

Figure 7.- Continued.

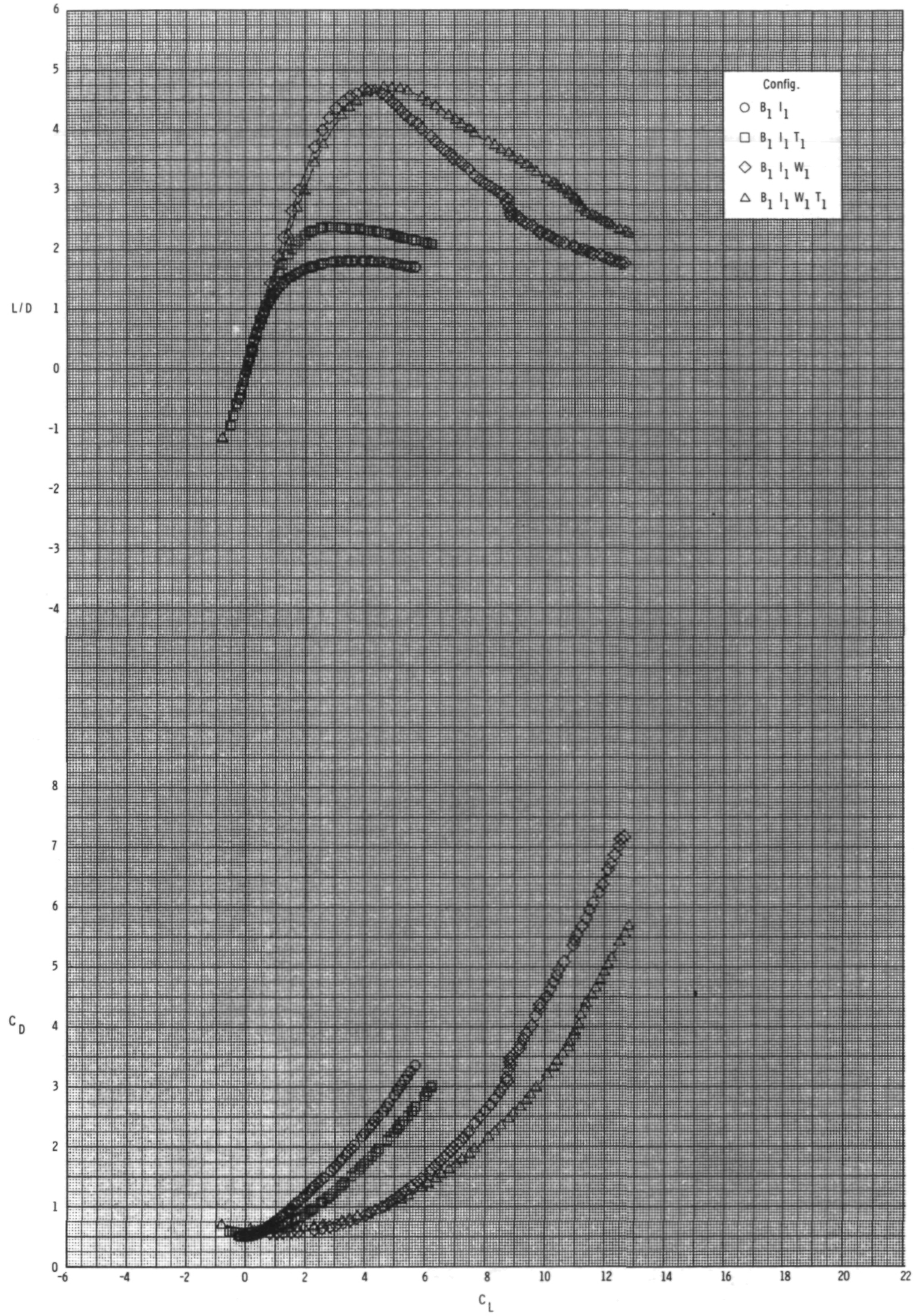

(a) Concluded.

Figure 7.- Continued.

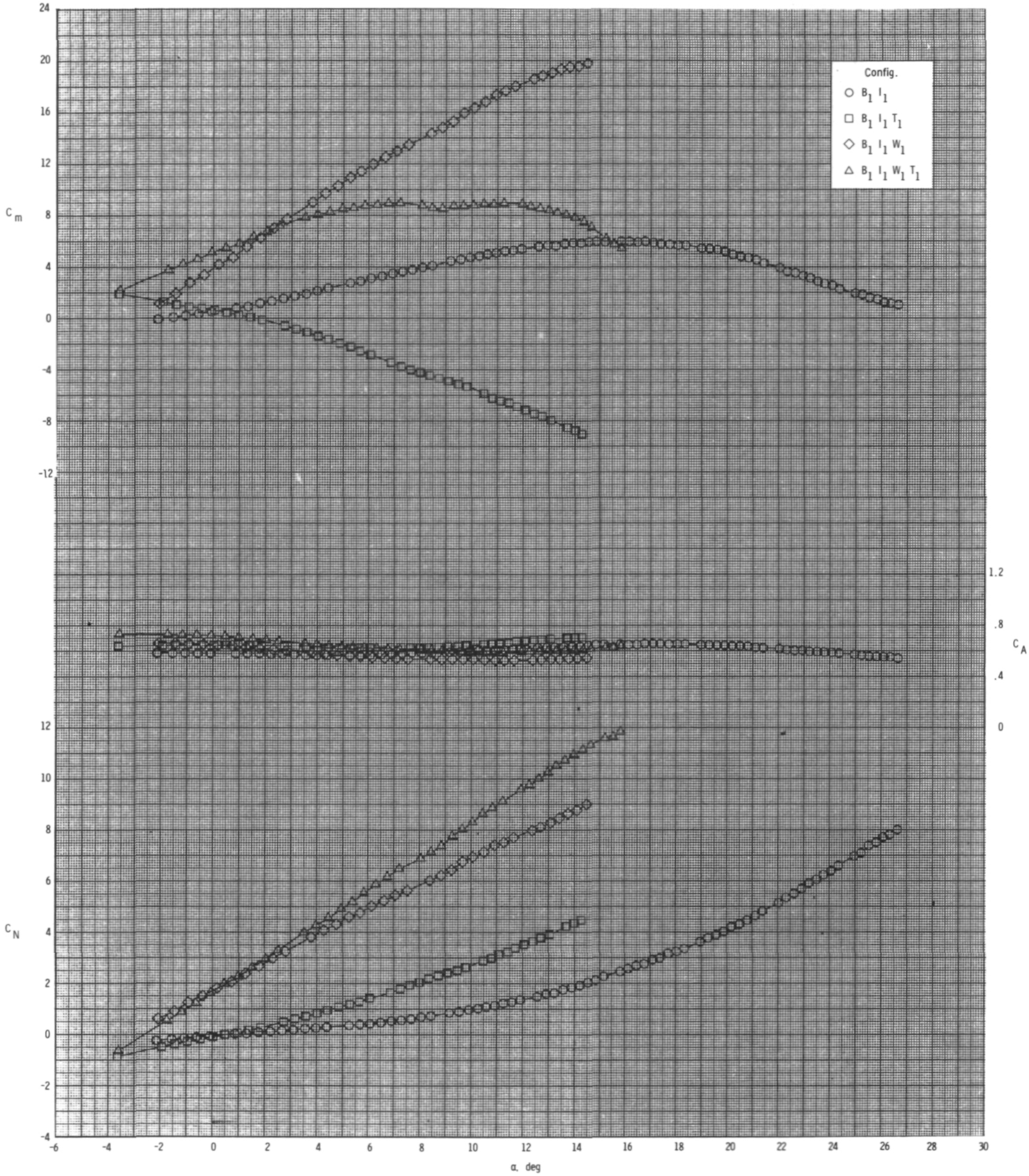

(b) M = 0.80.

Figure 7.- Continued.

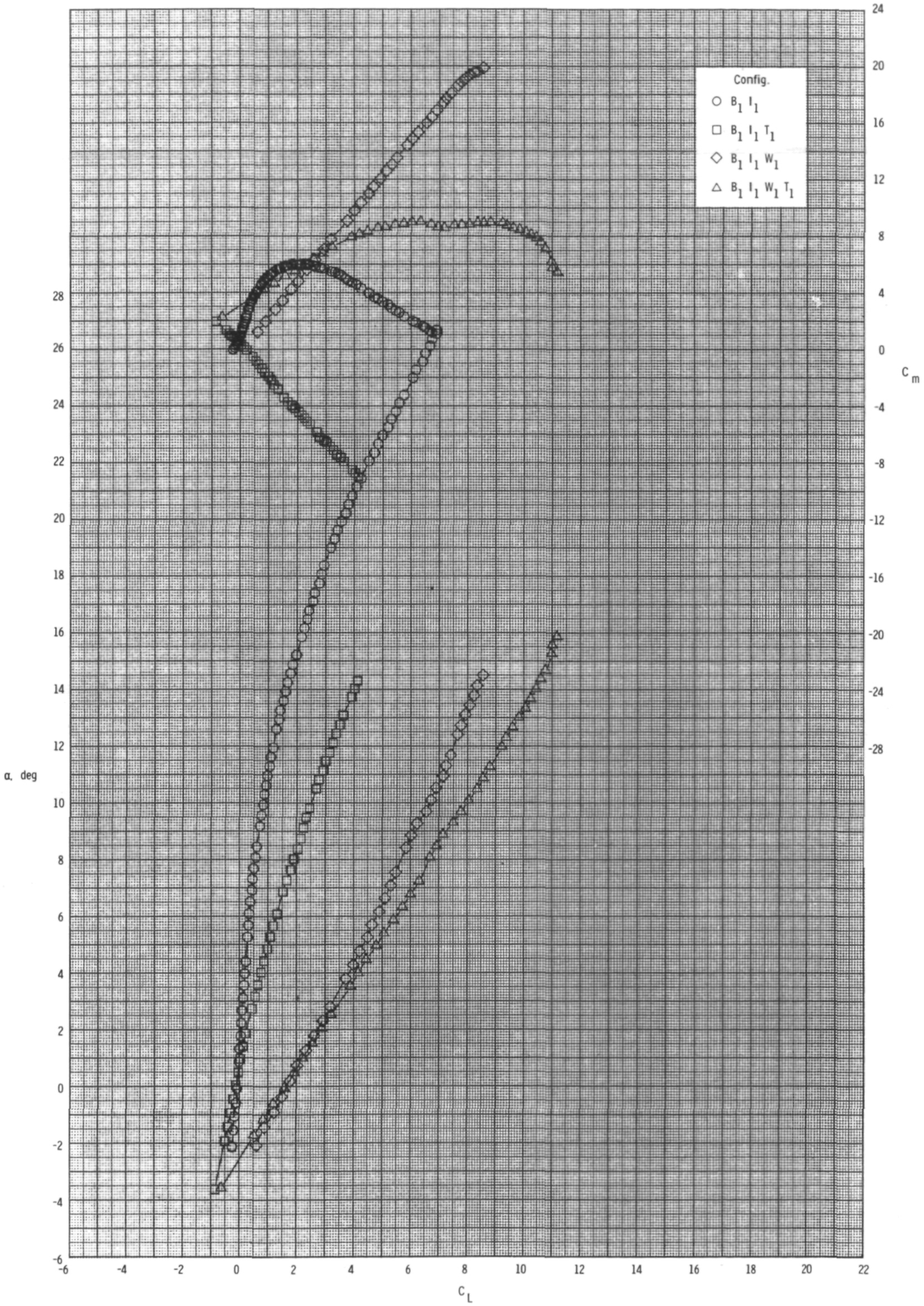

(b) Continued.

Figure 7.- Continued.

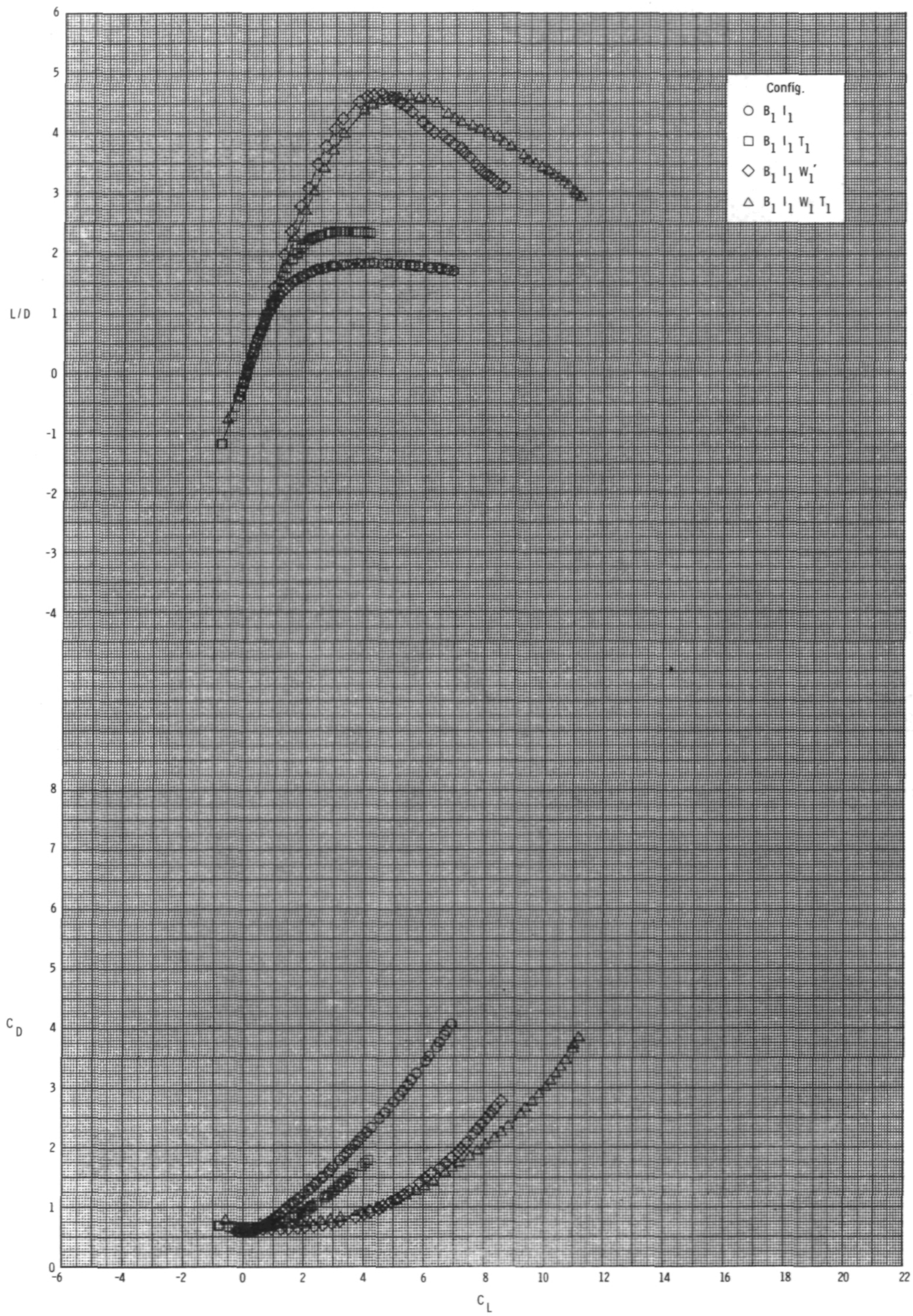

(b) Concluded.

Figure 7.- Continued.

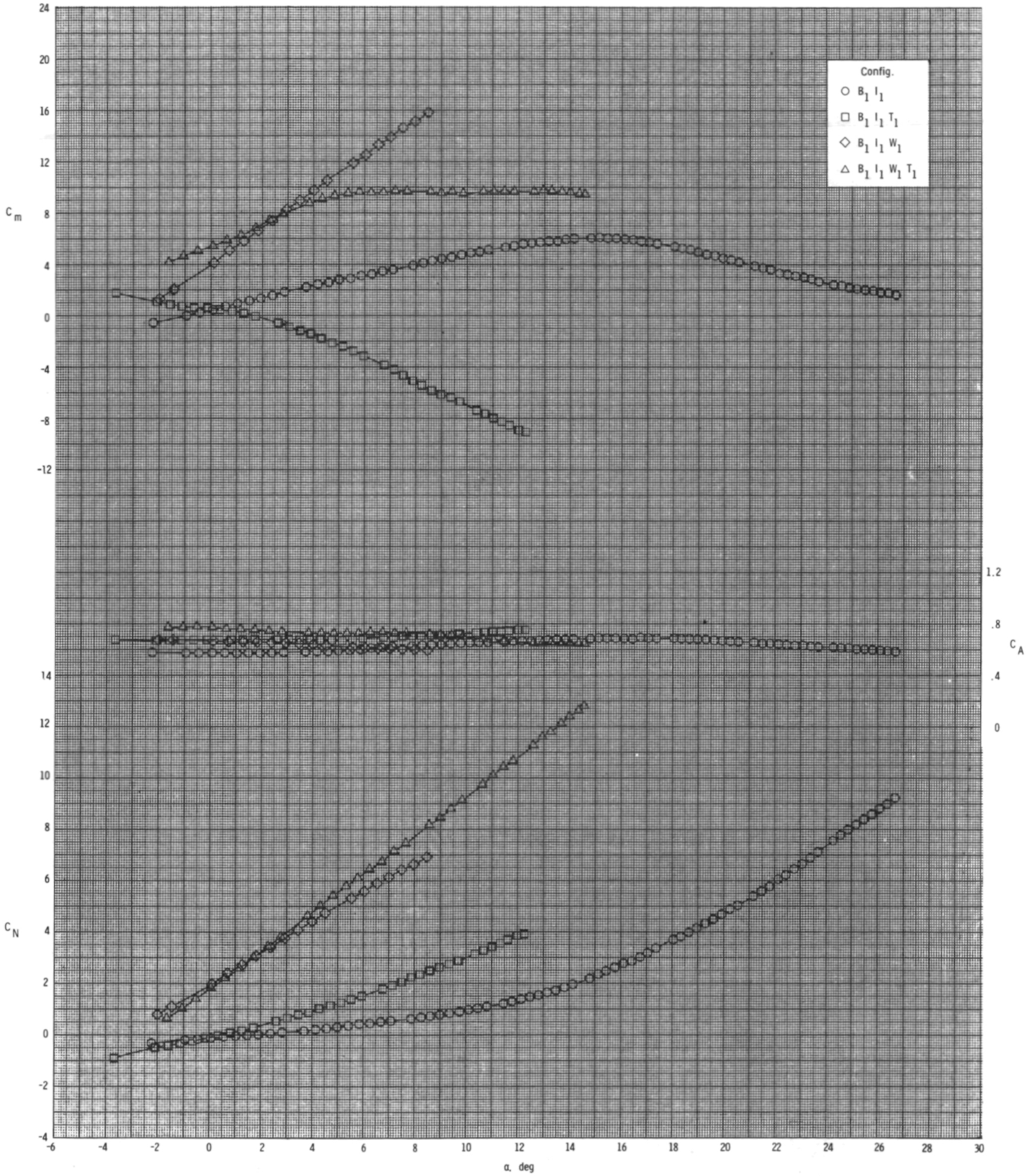

(c) M = 0.95.

Figure 7.- Continued.

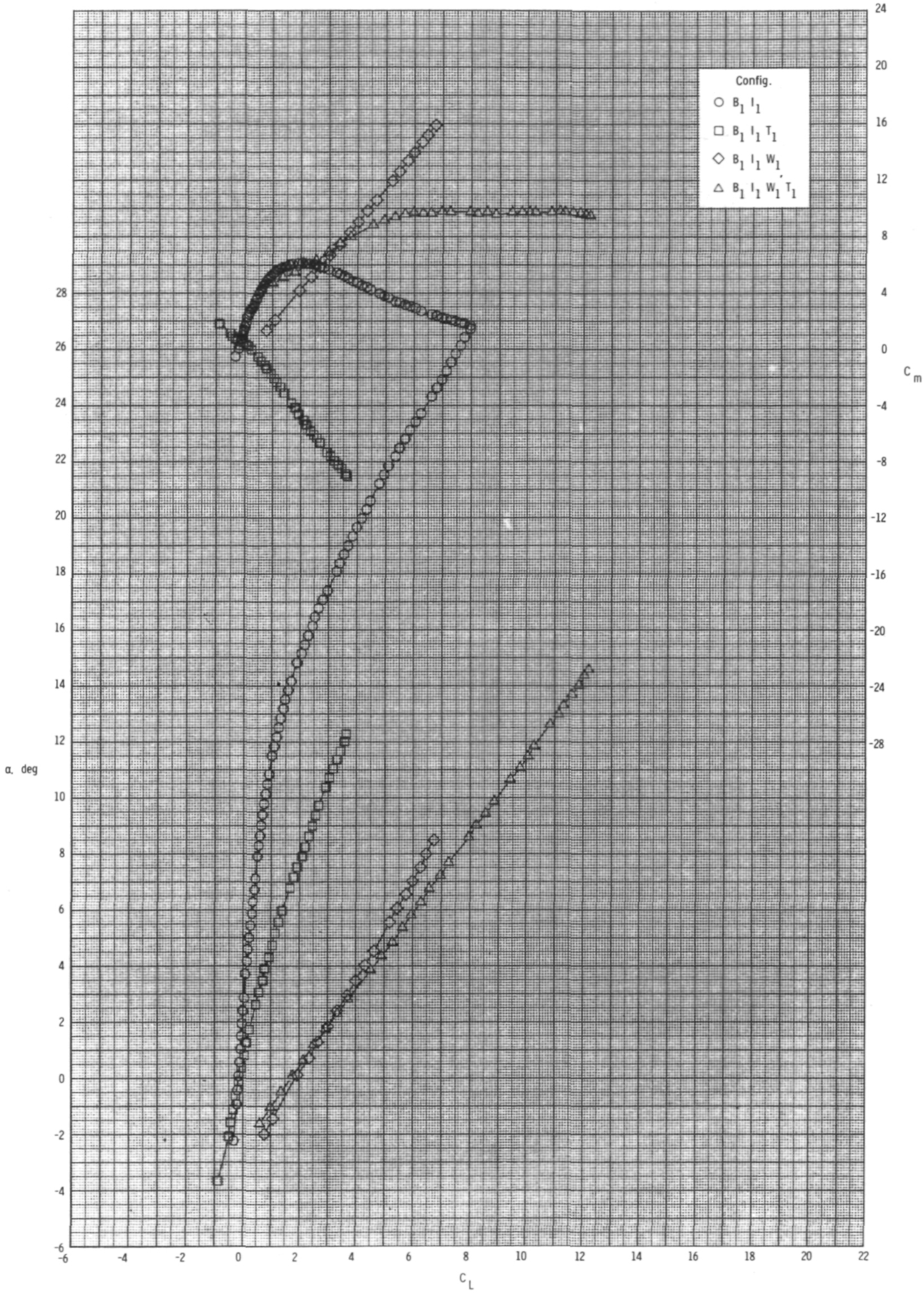

(c) Continued.

Figure 7.- Continued.

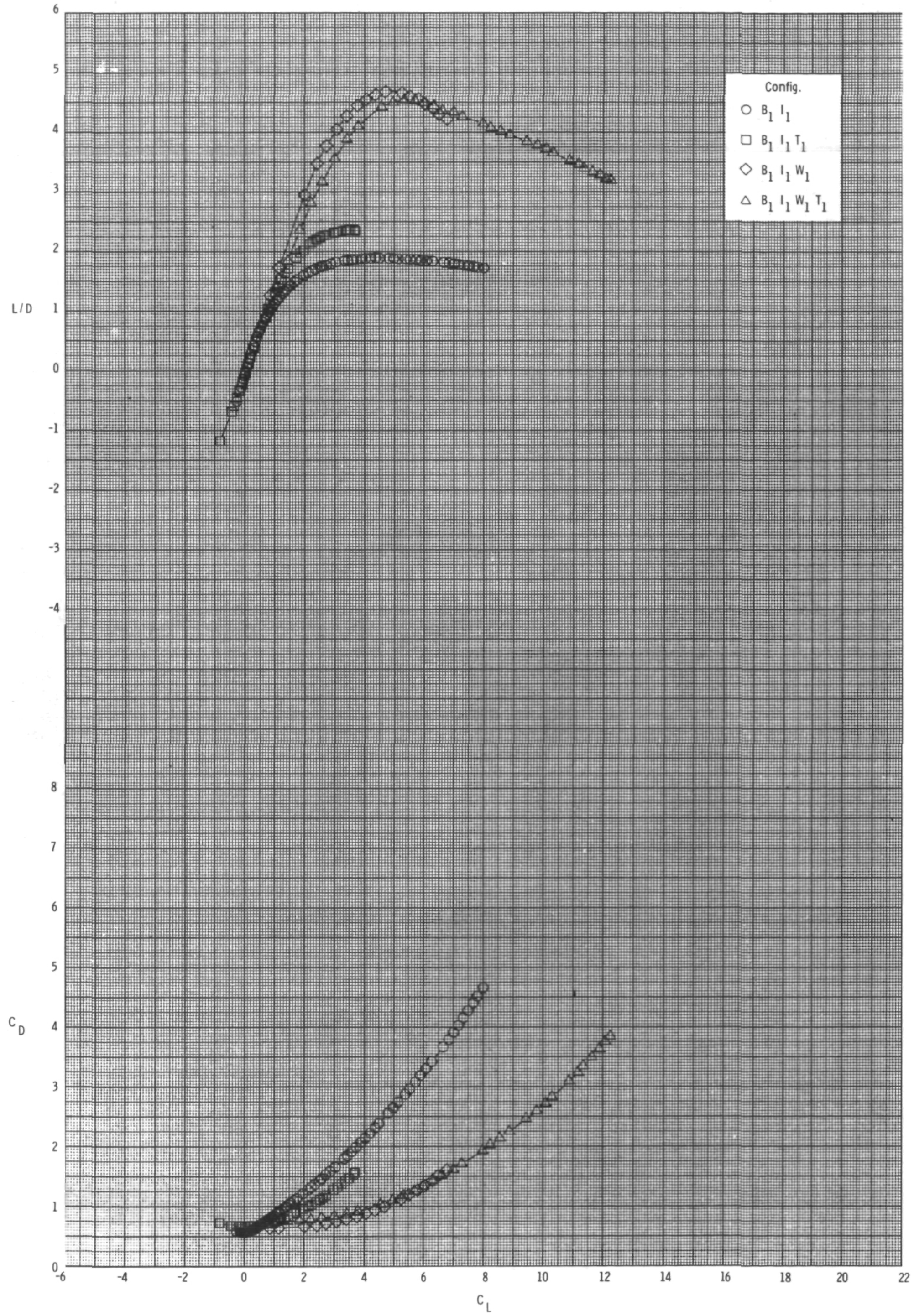

(c) Concluded.

Figure 7.- Concluded.

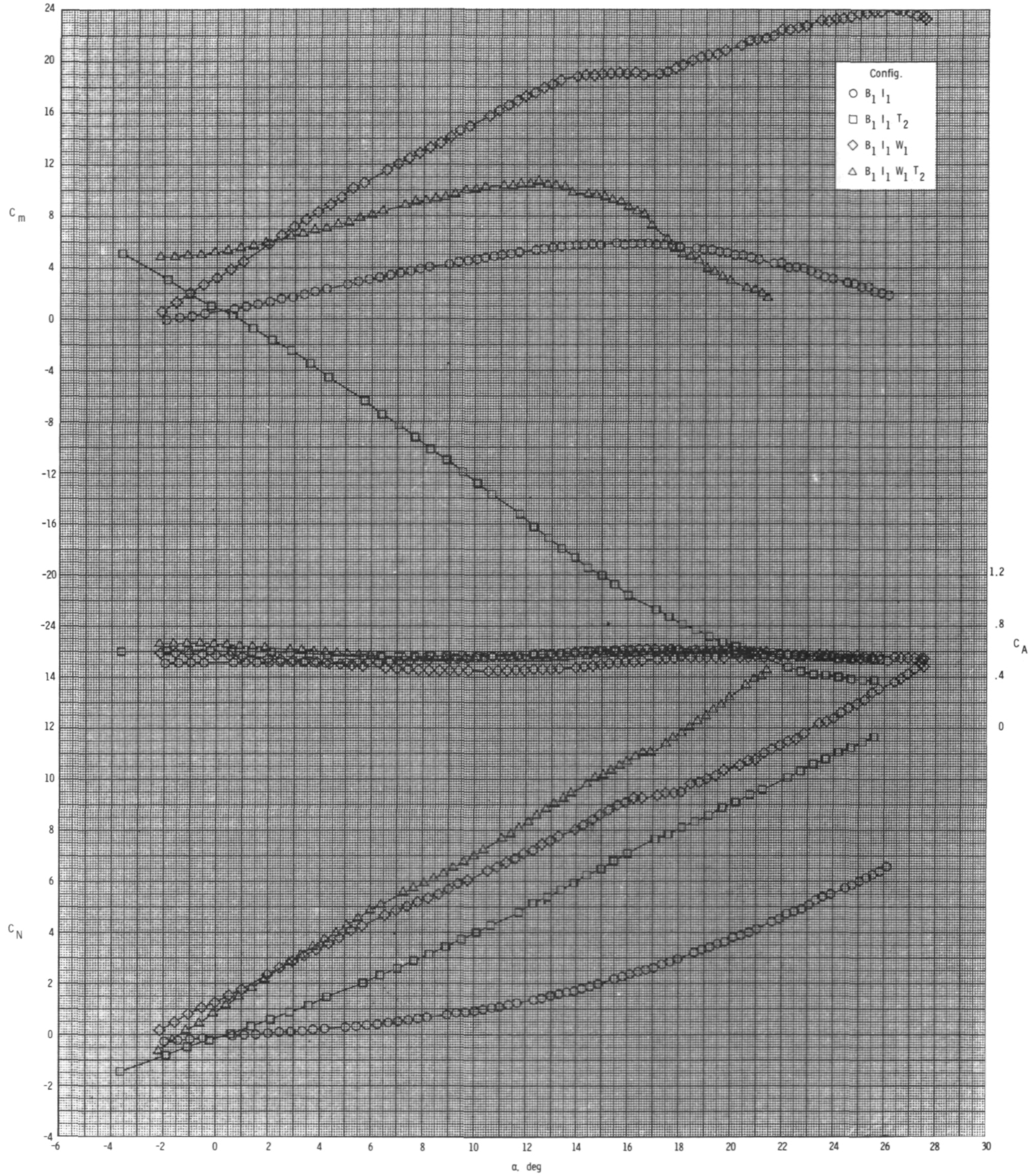

(a) M = 0.60.

Figure 8.- Effect of various model components on longitudinal aerodynamic characteristics for axisymmetric inlets with internal ducts closed, T_2, $\phi_I = 135°$, and $\delta_p = 0°$.

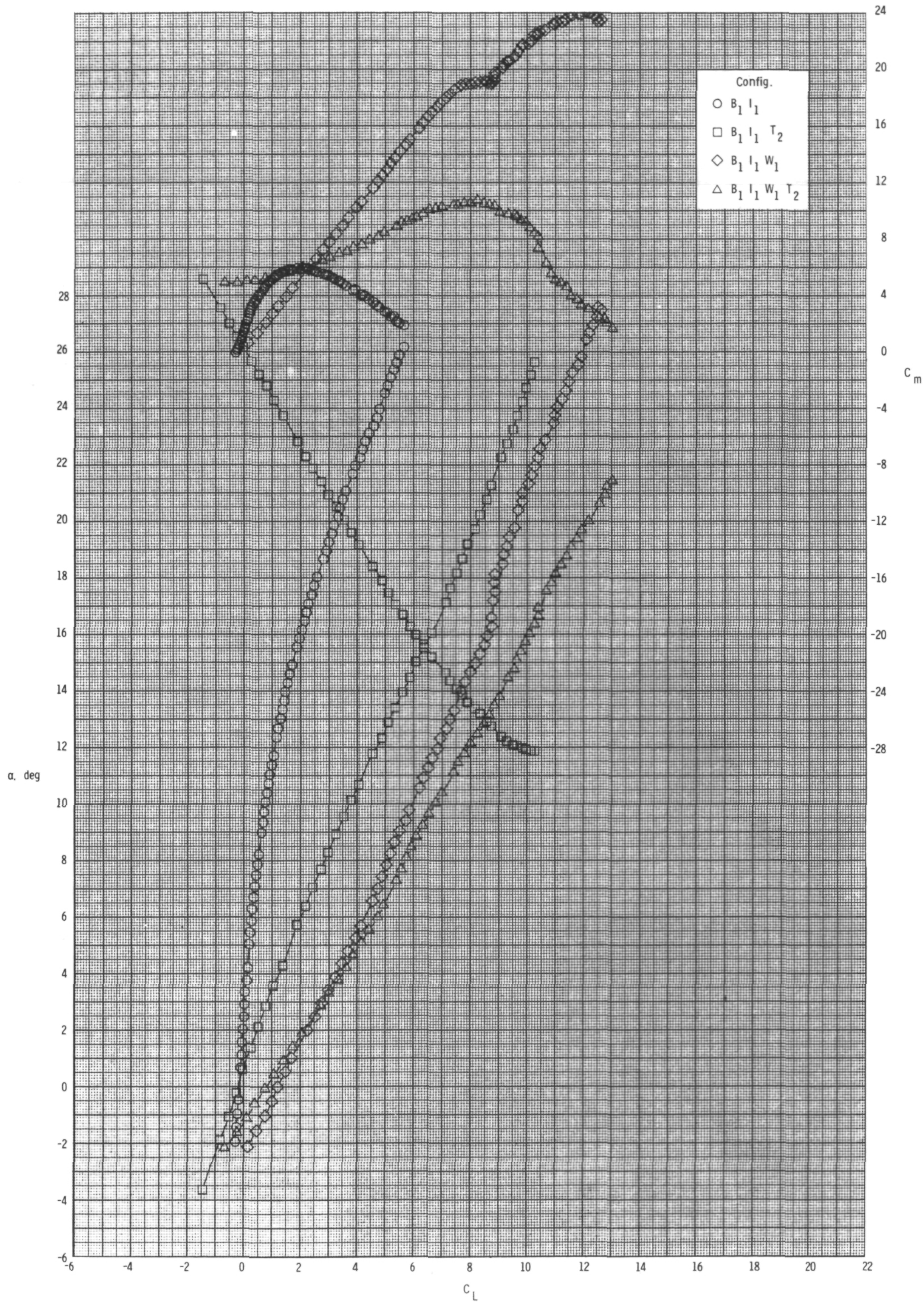

(a) Continued.

Figure 8.- Continued.

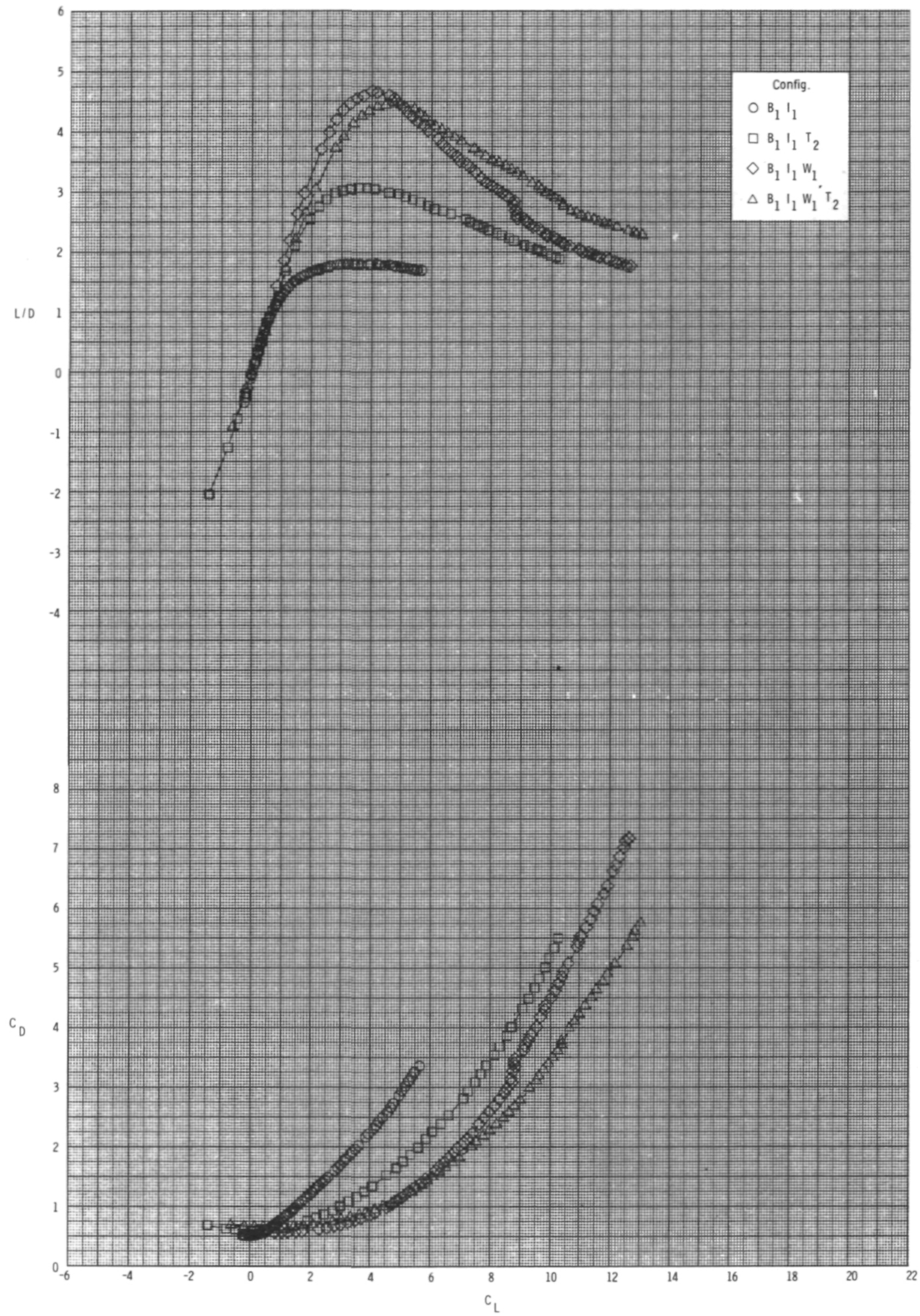

(a) Concluded.

Figure 8.- Continued.

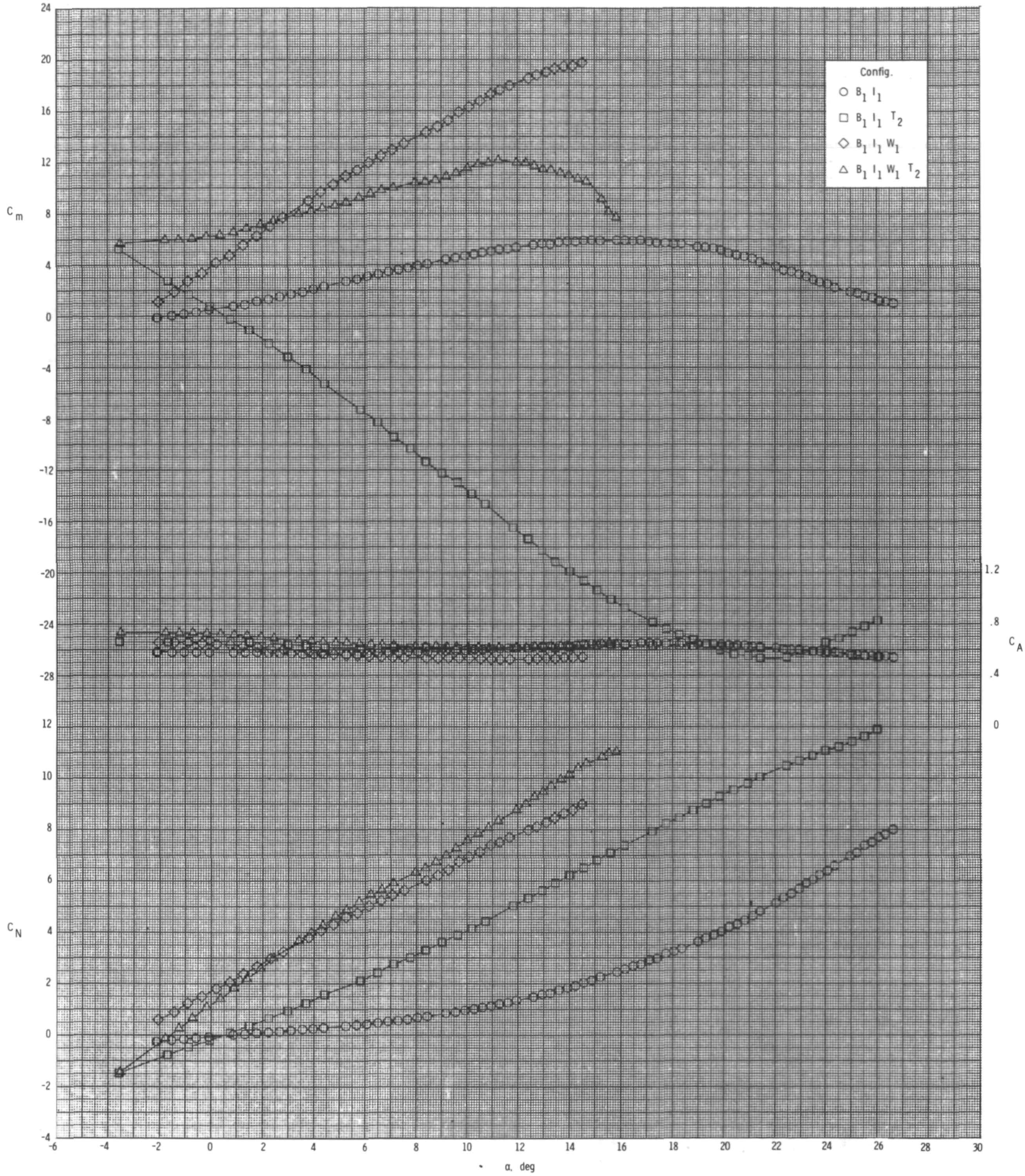

(b) M = 0.80.

Figure 8.- Continued.

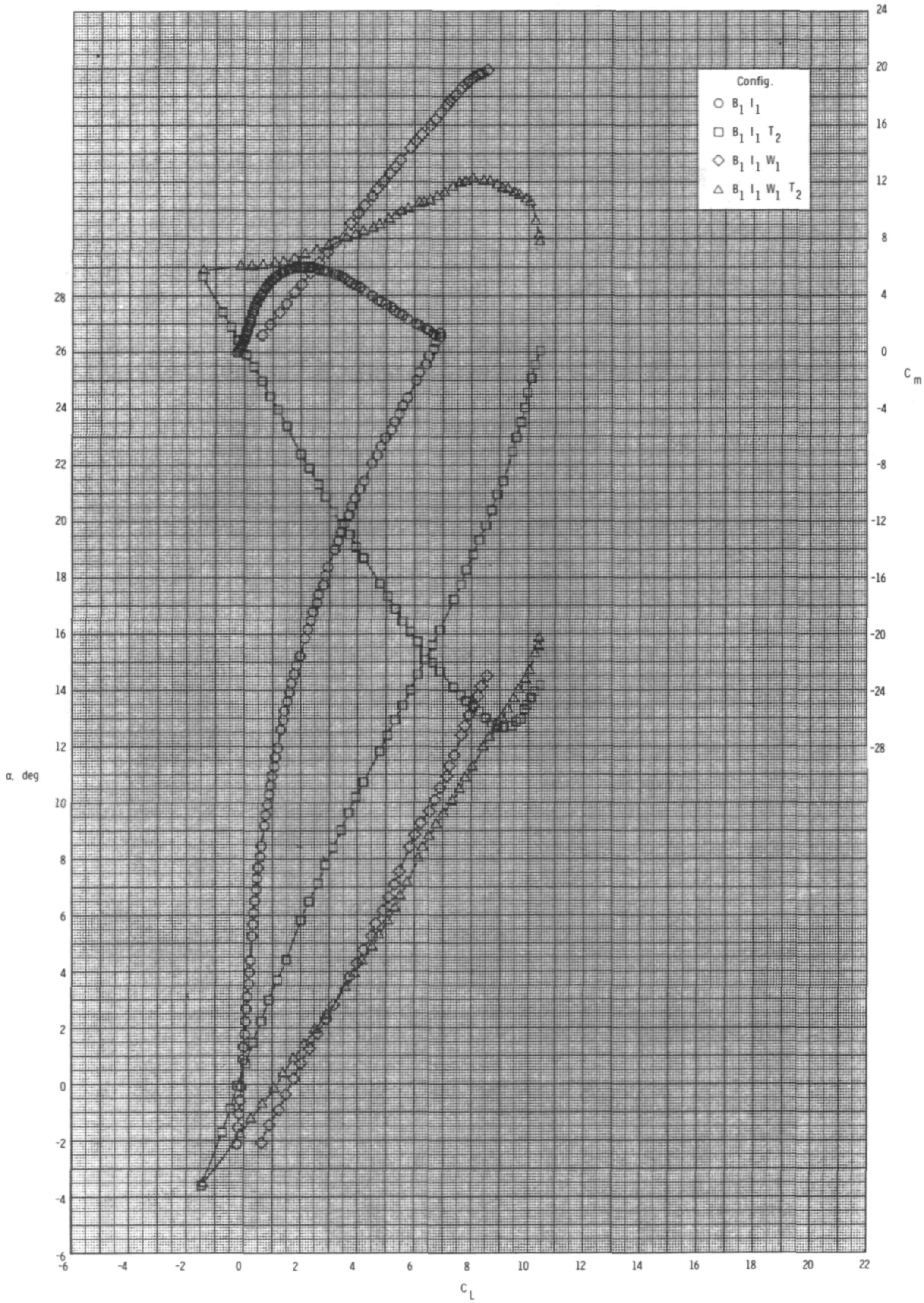

(b) Continued.

Figure 8.- Continued.

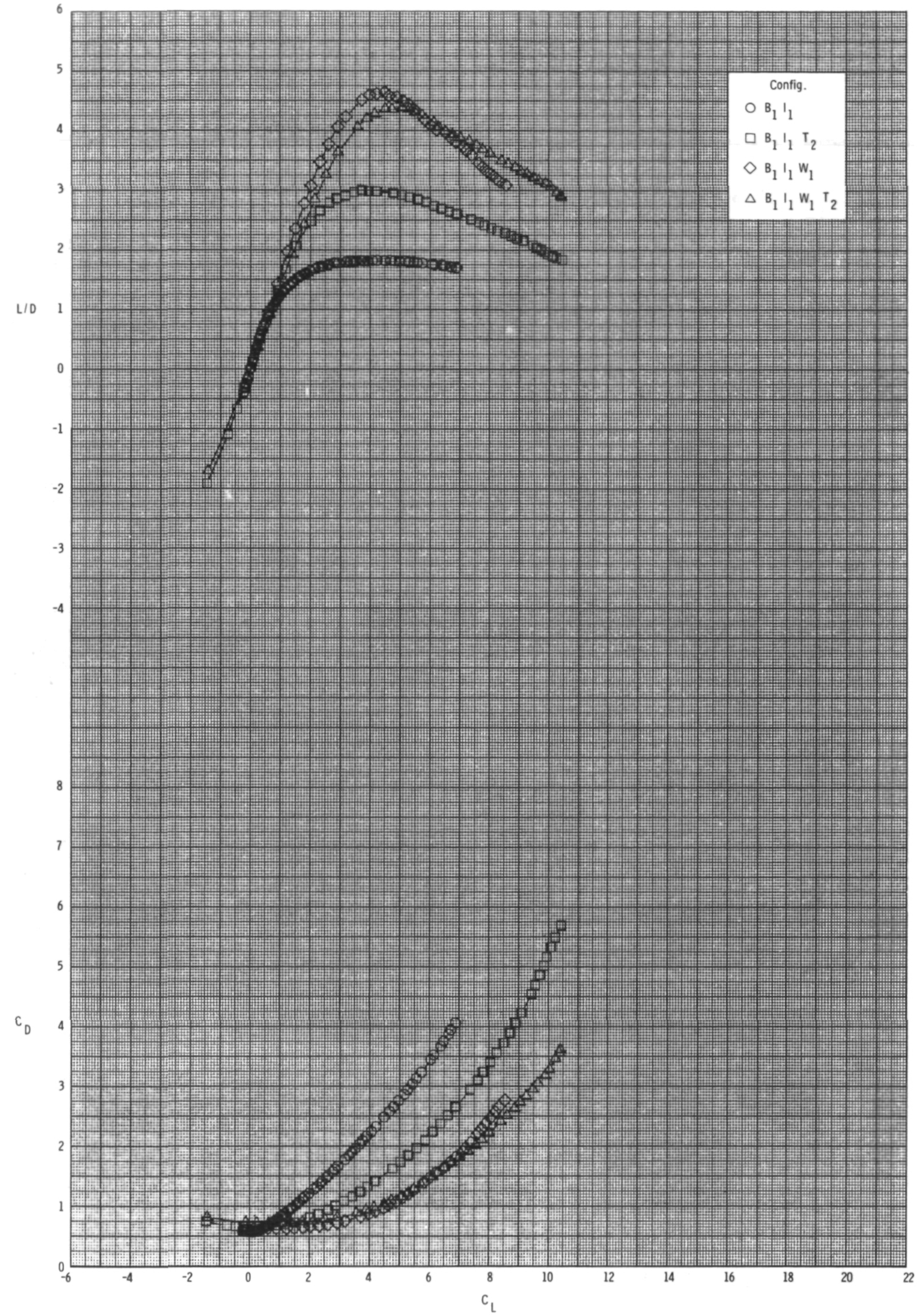

(b) Concluded.

Figure 8.- Continued.

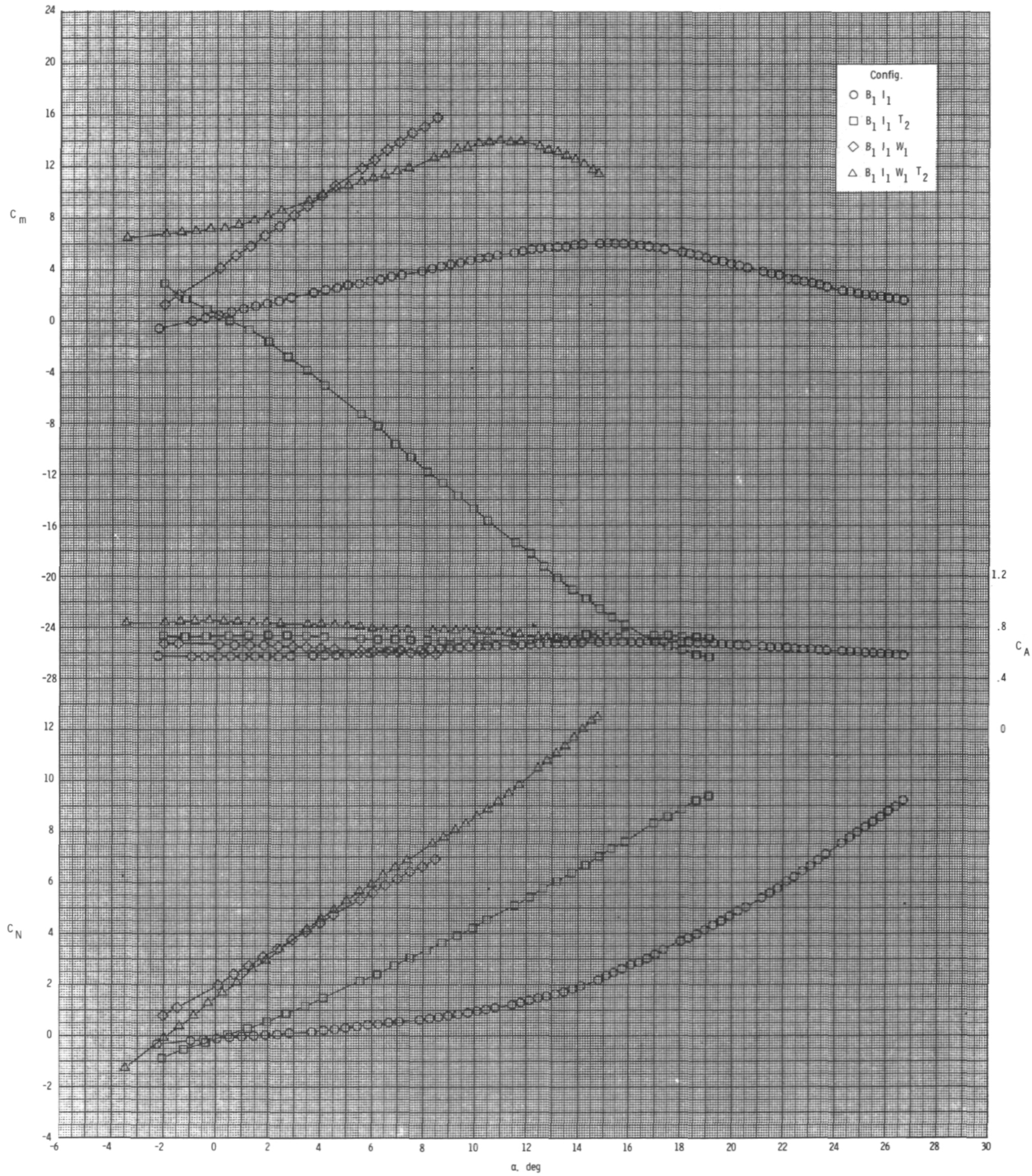

(c) M = 0.95.

Figure 8.- Continued.

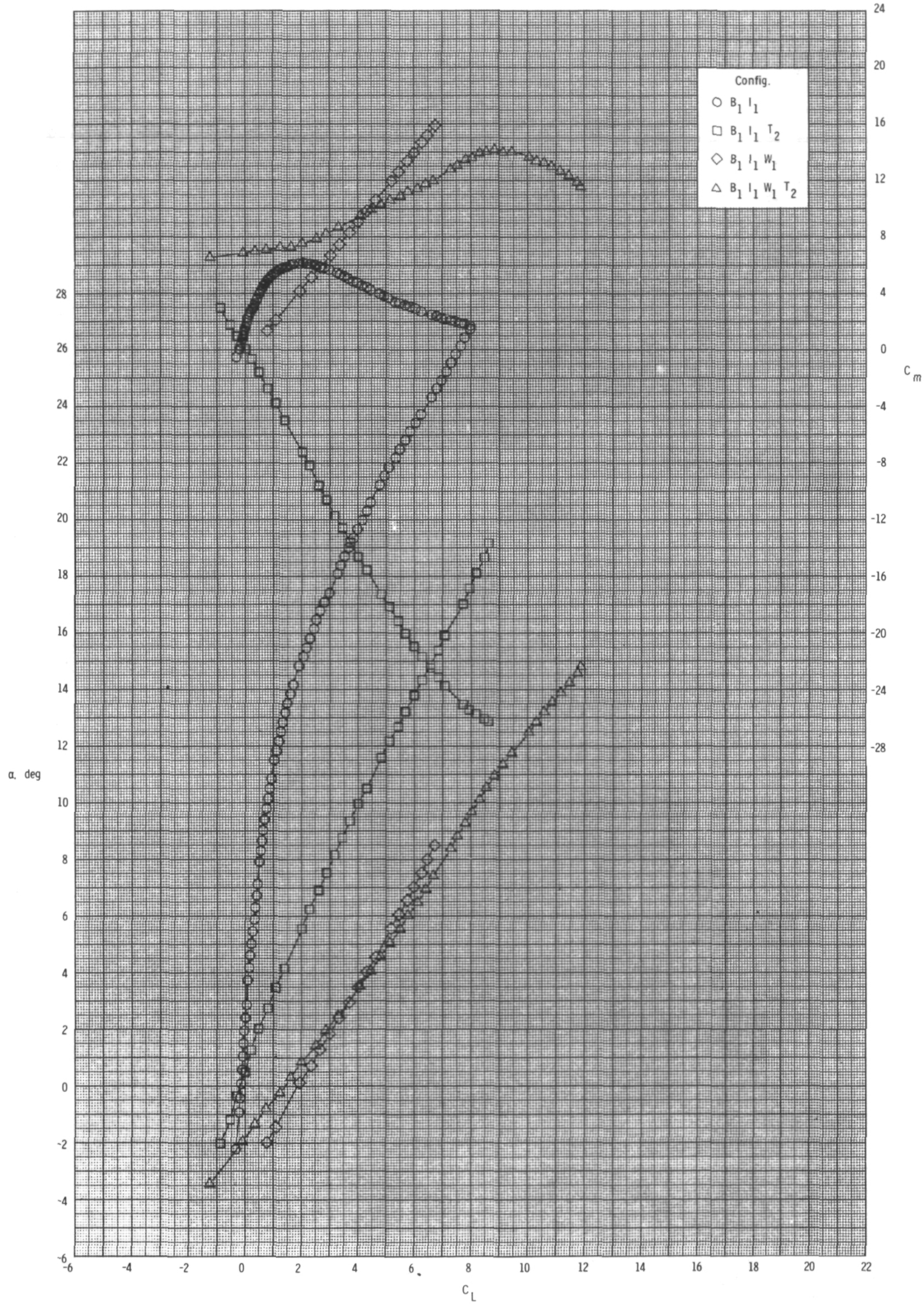

(c) Continued.

Figure 8.- Continued.

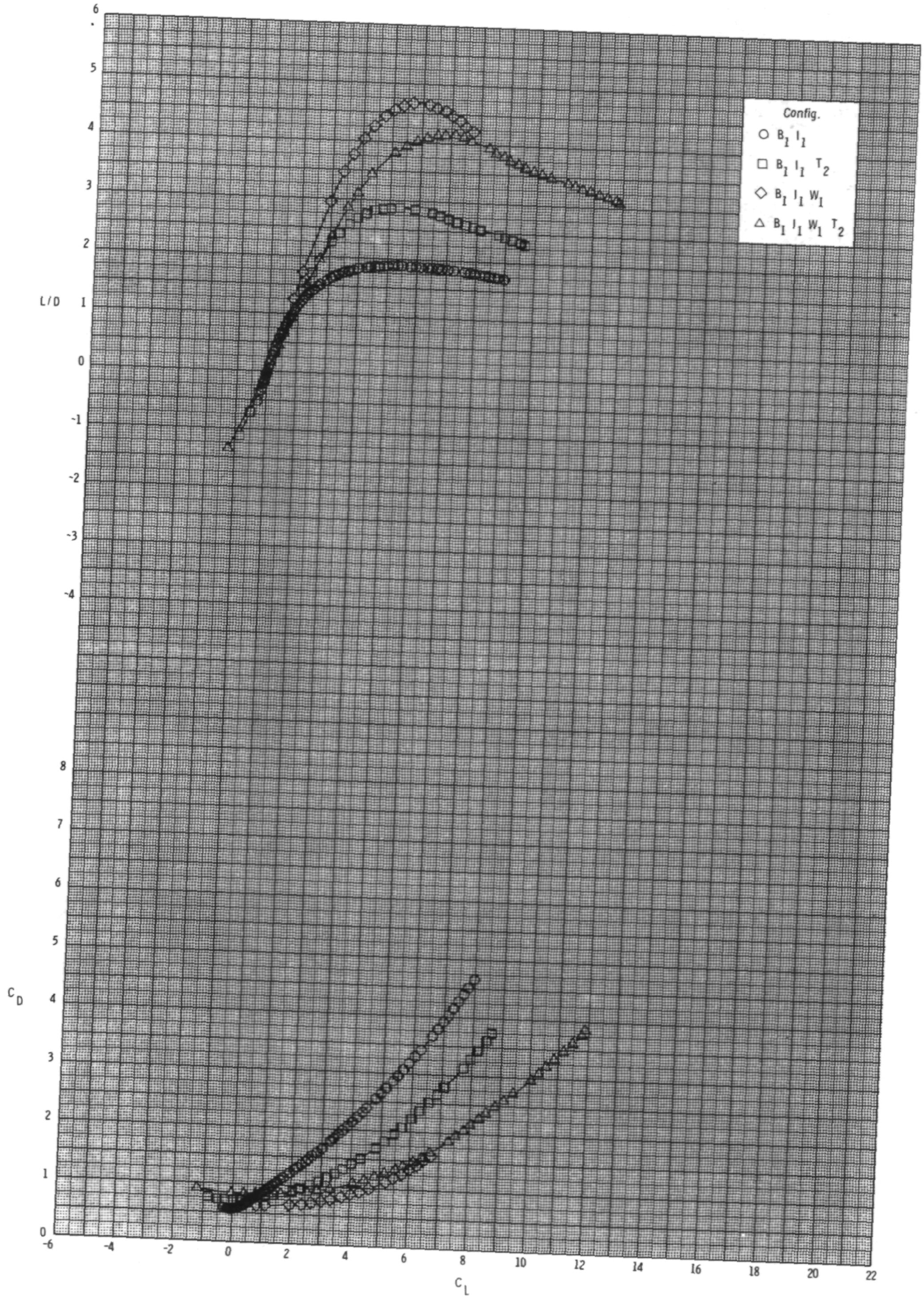

(c) Concluded.

Figure 8.- Concluded.

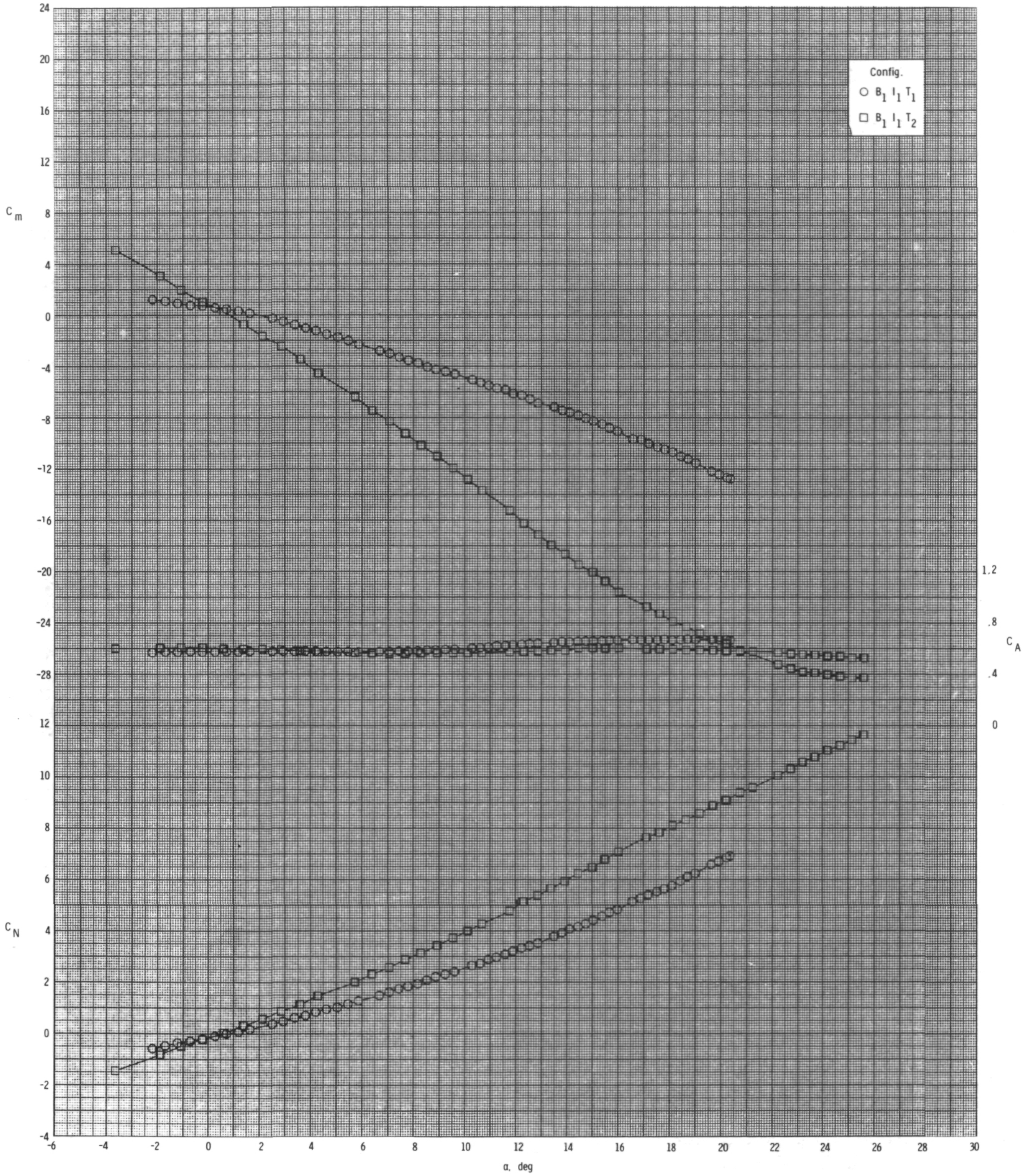

(a) M = 0.60.

Figure 9.- Effect of tail configuration on longitudinal aerodynamic characteristics for configuration B_1I_1T with internal ducts closed, $\phi_I = 135°$, and $\delta_p = 0°$.

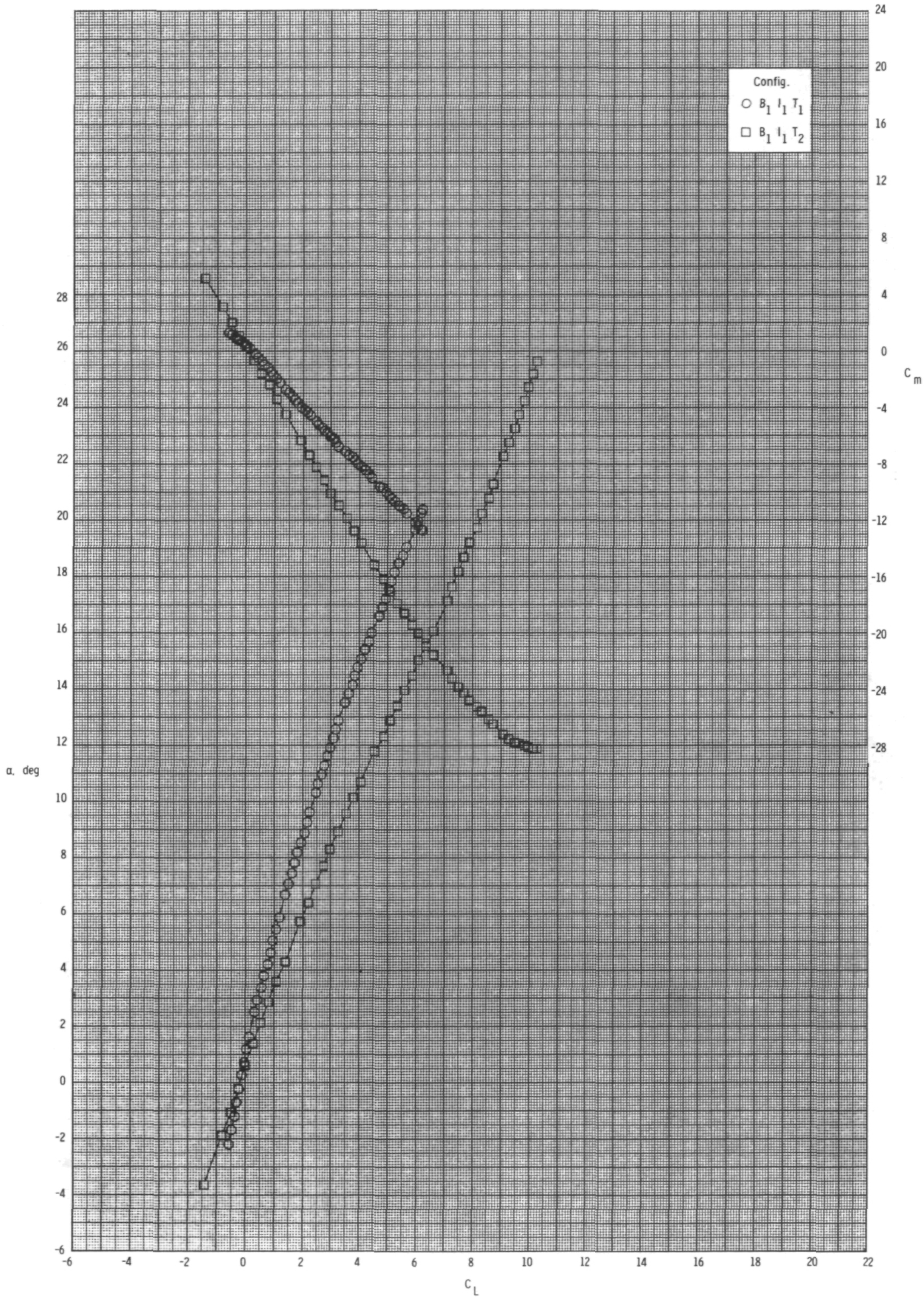

(a) Continued.

Figure 9.- Continued.

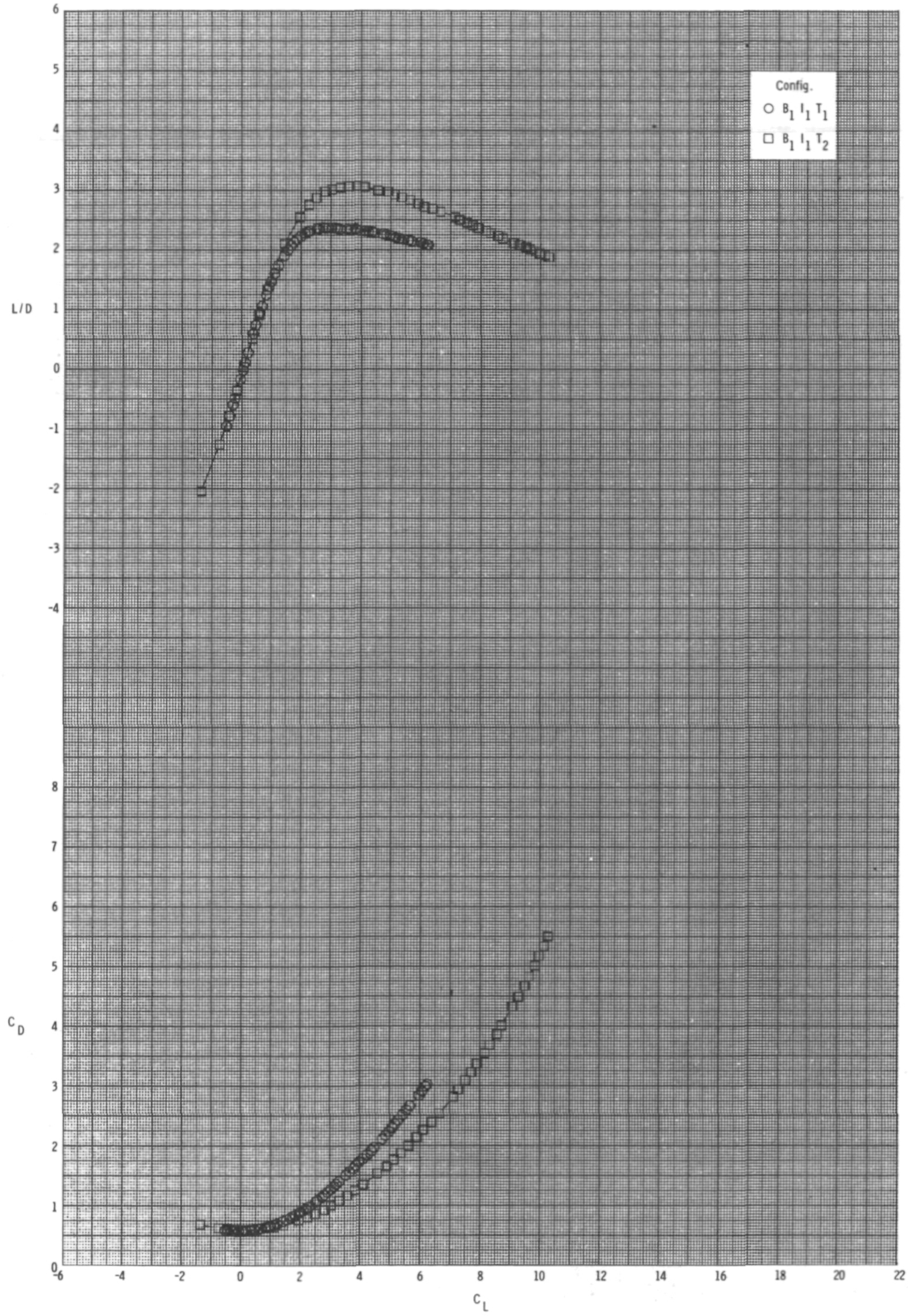

(a) Concluded.

Figure 9.- Continued.

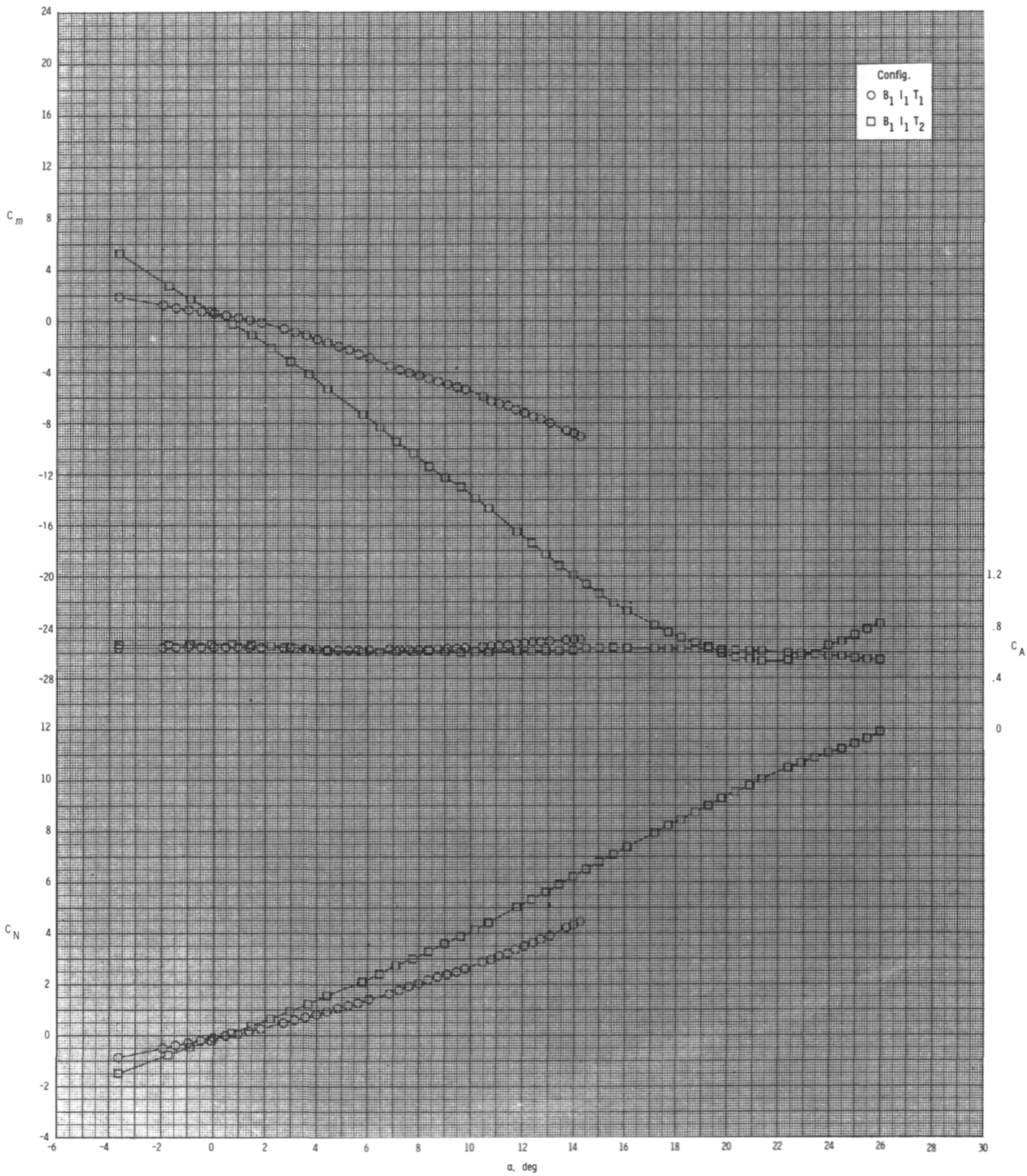

(b) M = 0.80.

Figure 9.- Continued.

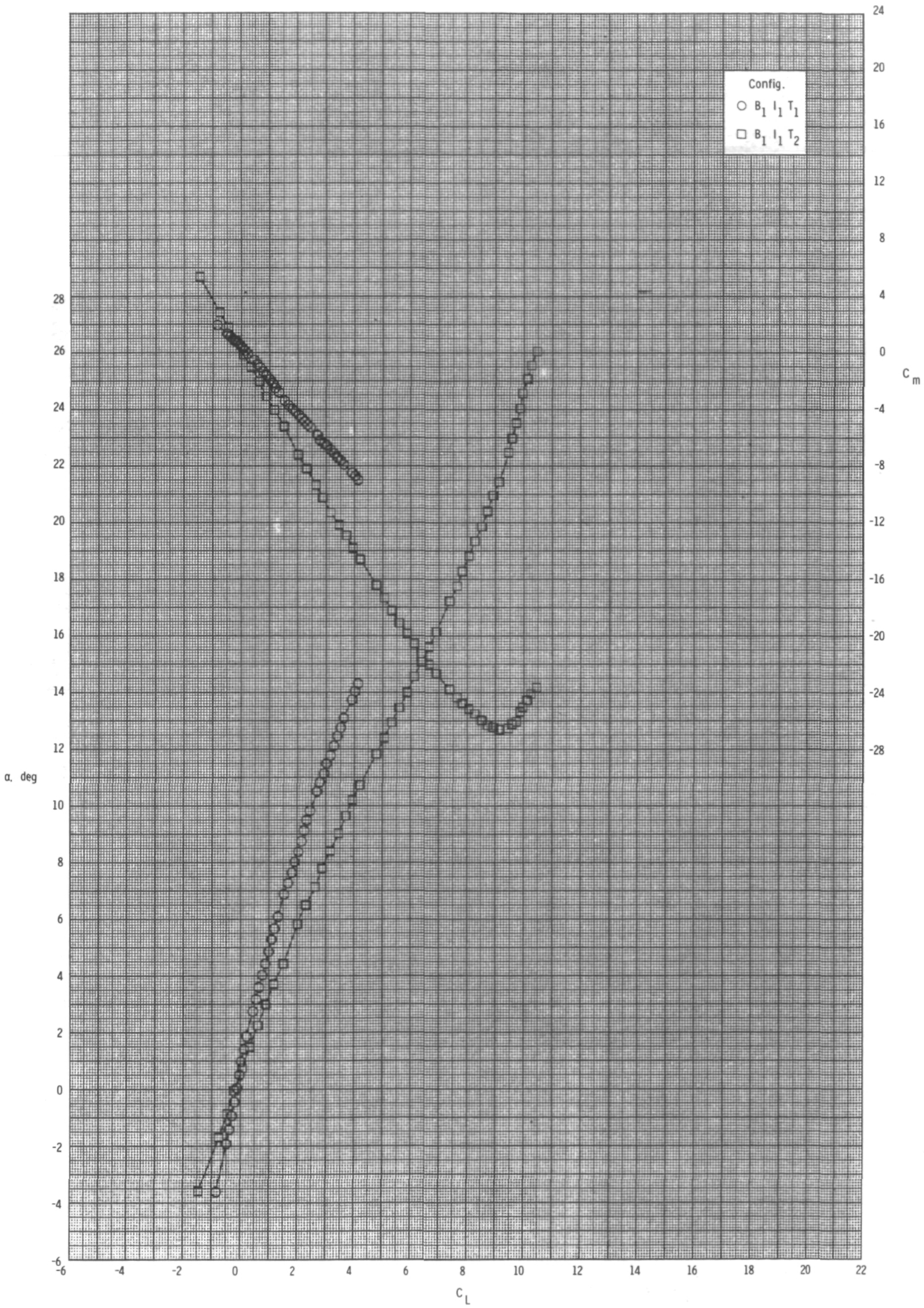

(b) Continued.

Figure 9.- Continued.

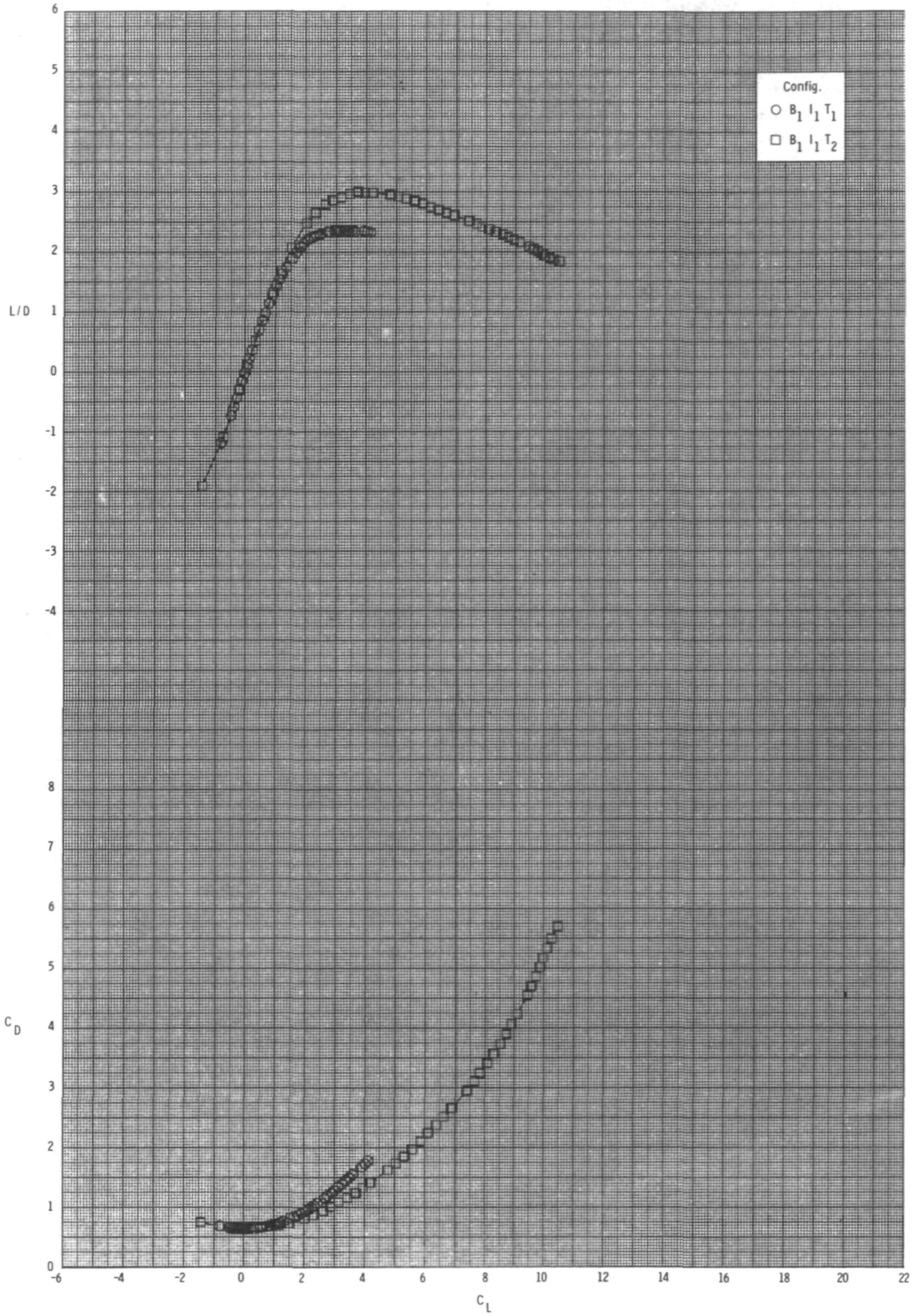

(b) Concluded.

Figure 9.- Continued.

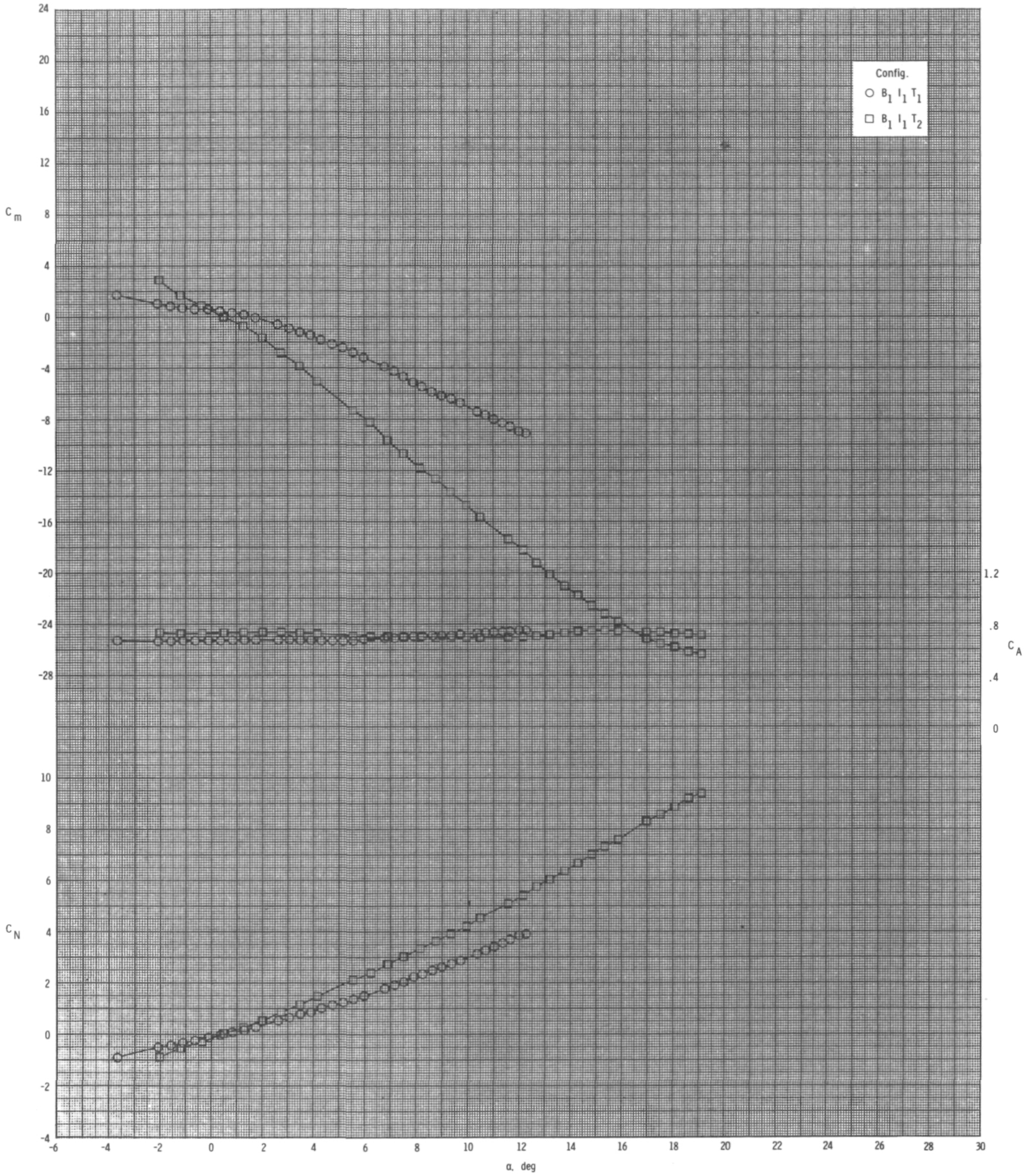

(c) M = 0.95.

Figure 9.- Continued.

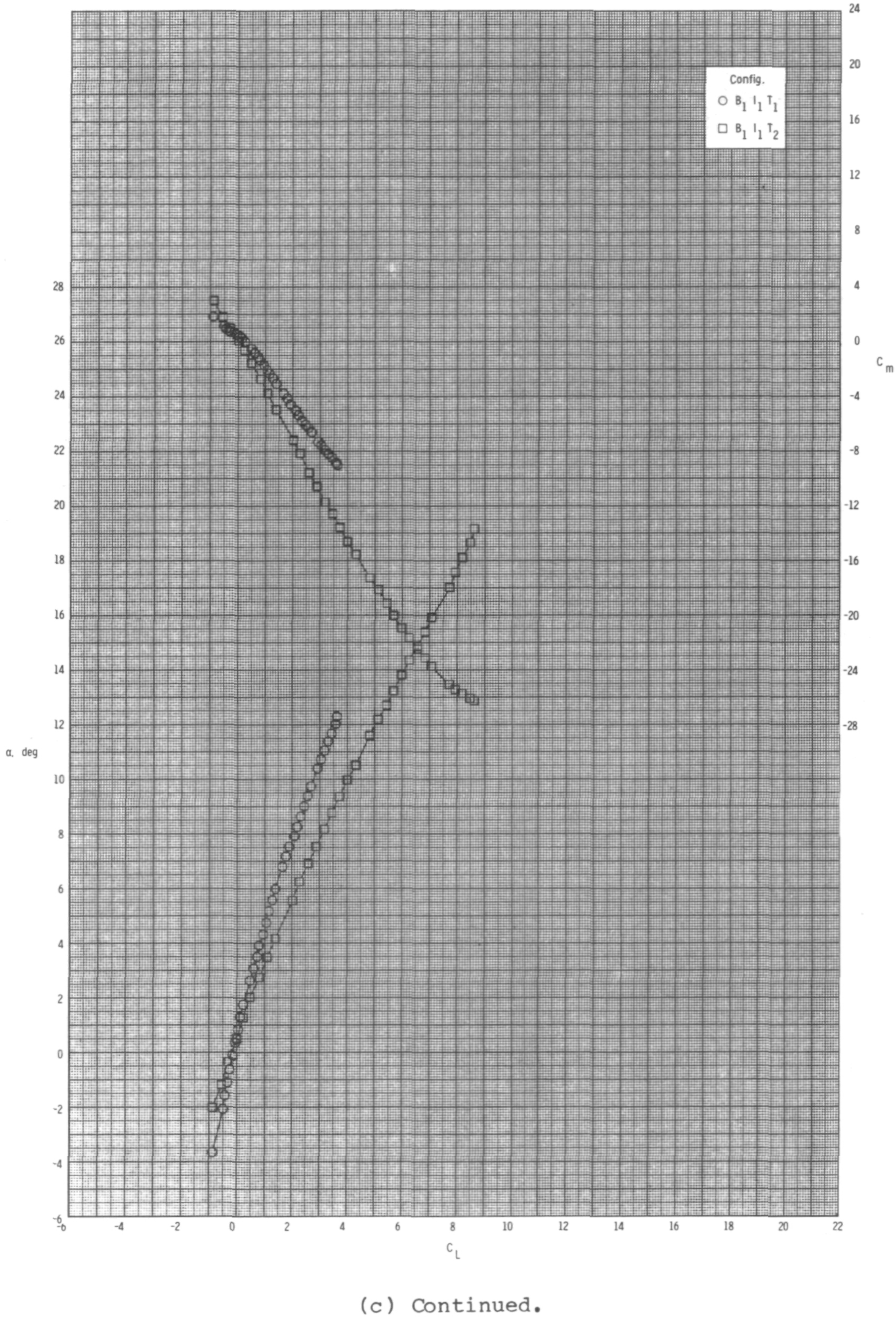

(c) Continued.

Figure 9.- Continued.

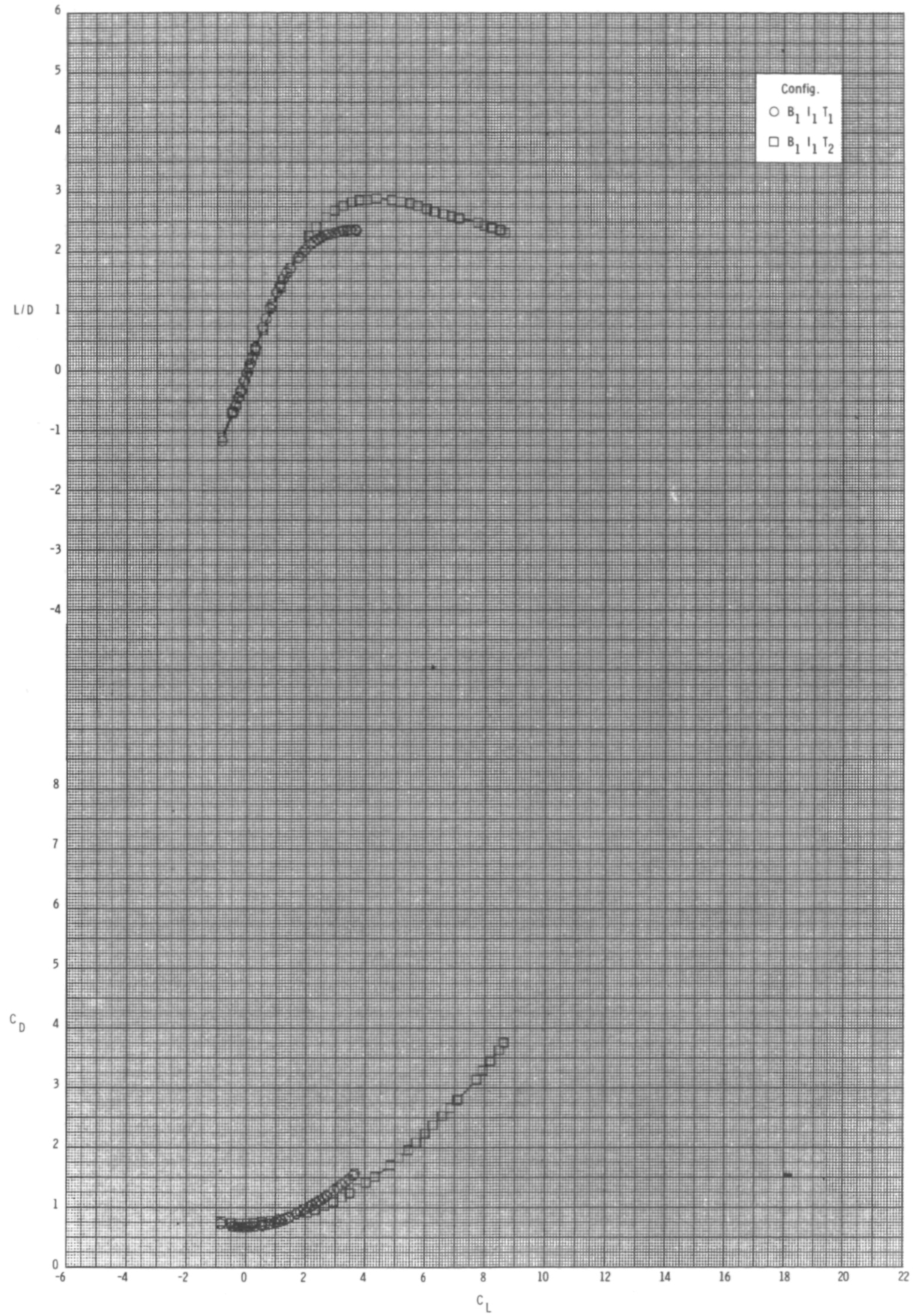

(c) Concluded.

Figure 9.- Concluded.

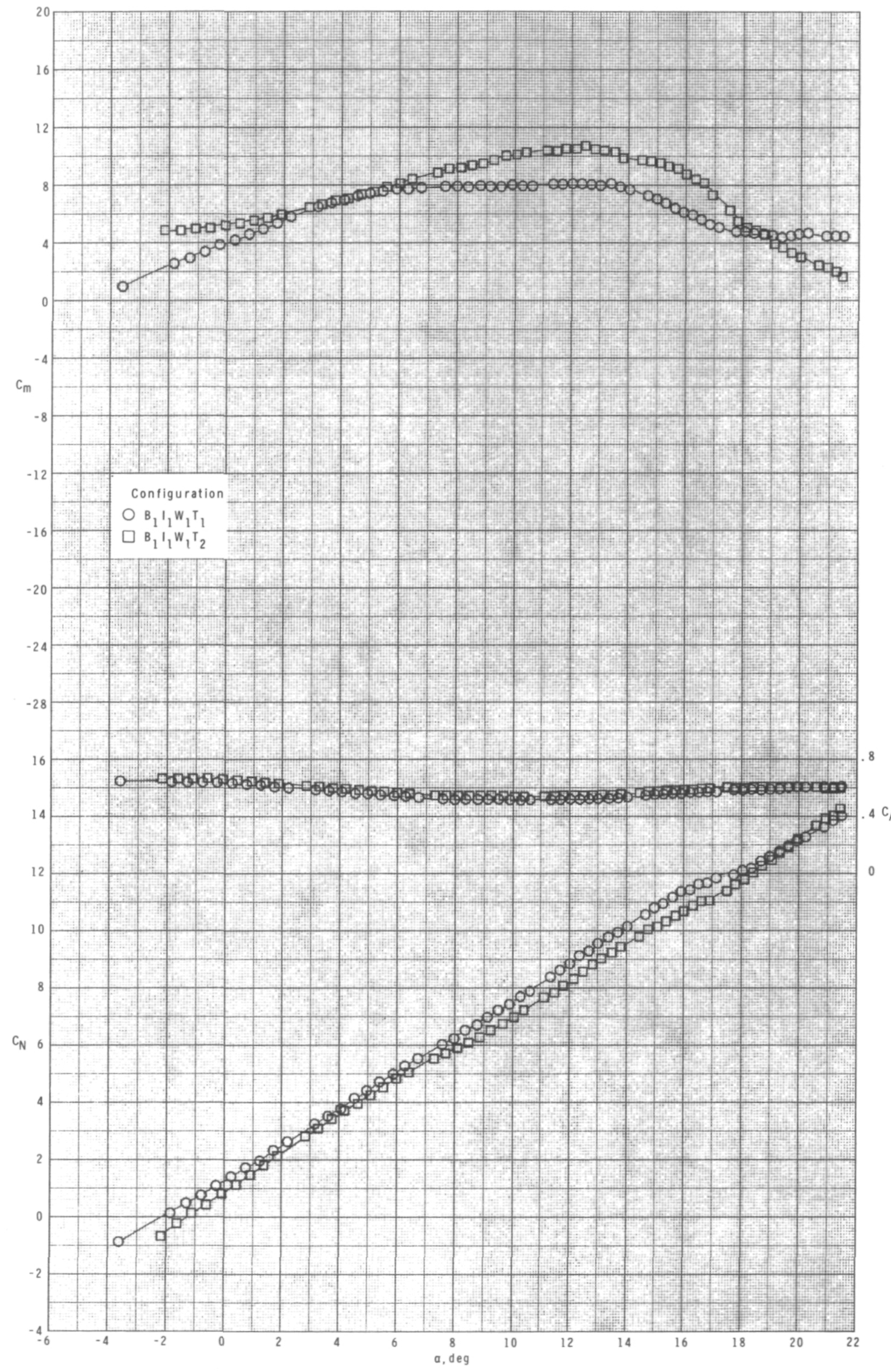

(a) M = 0.60.

Figure 10.- Effect of tail configuration on longitudinal aerodynamic characteristics for configuration $B_1I_1W_1T$ with internal ducts closed, $\delta_I = 135°$, and $\delta_p = 0°$.

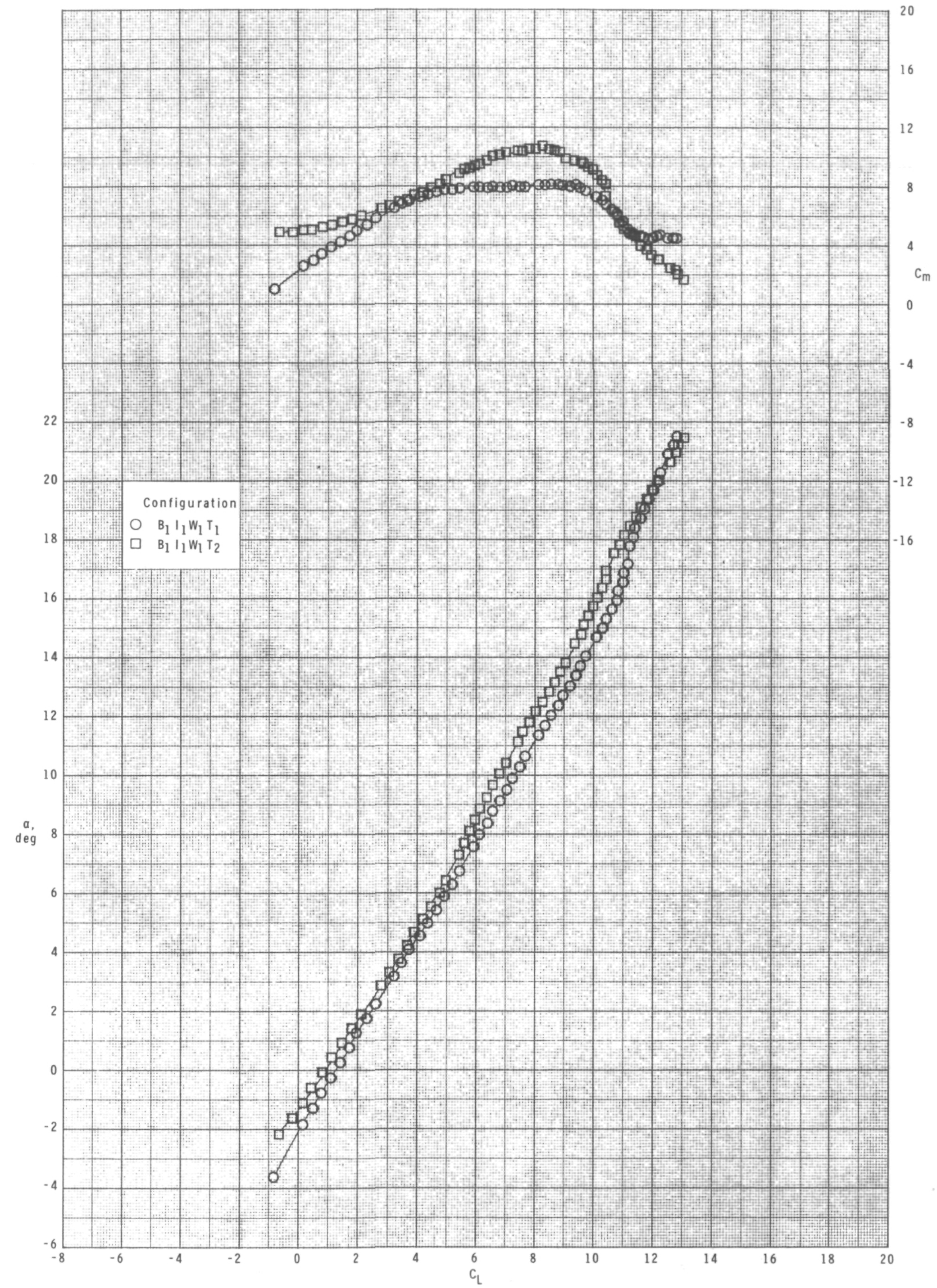

(a) Continued.

Figure 10.- Continued.

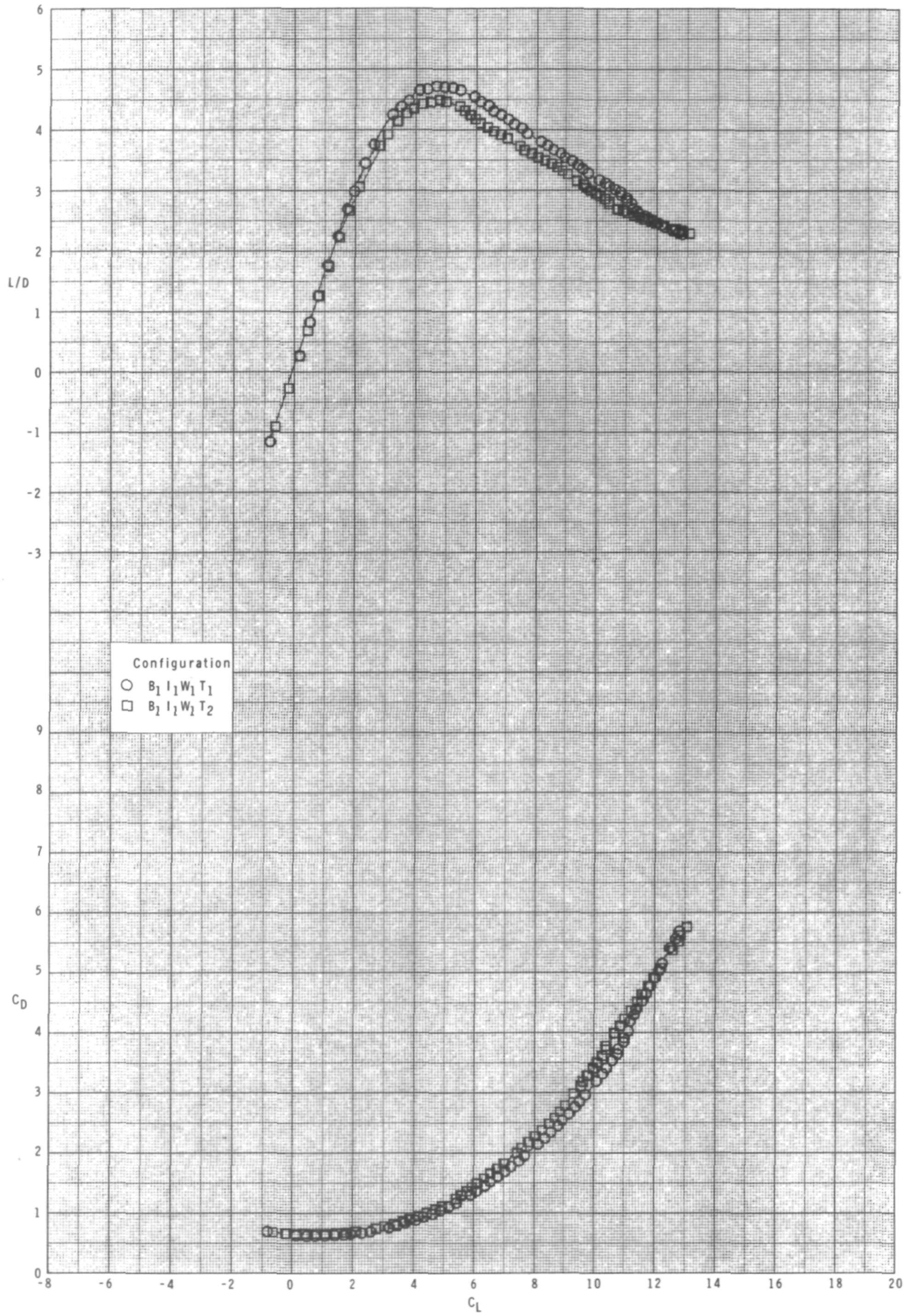

(a) Concluded.

Figure 10.- Continued.

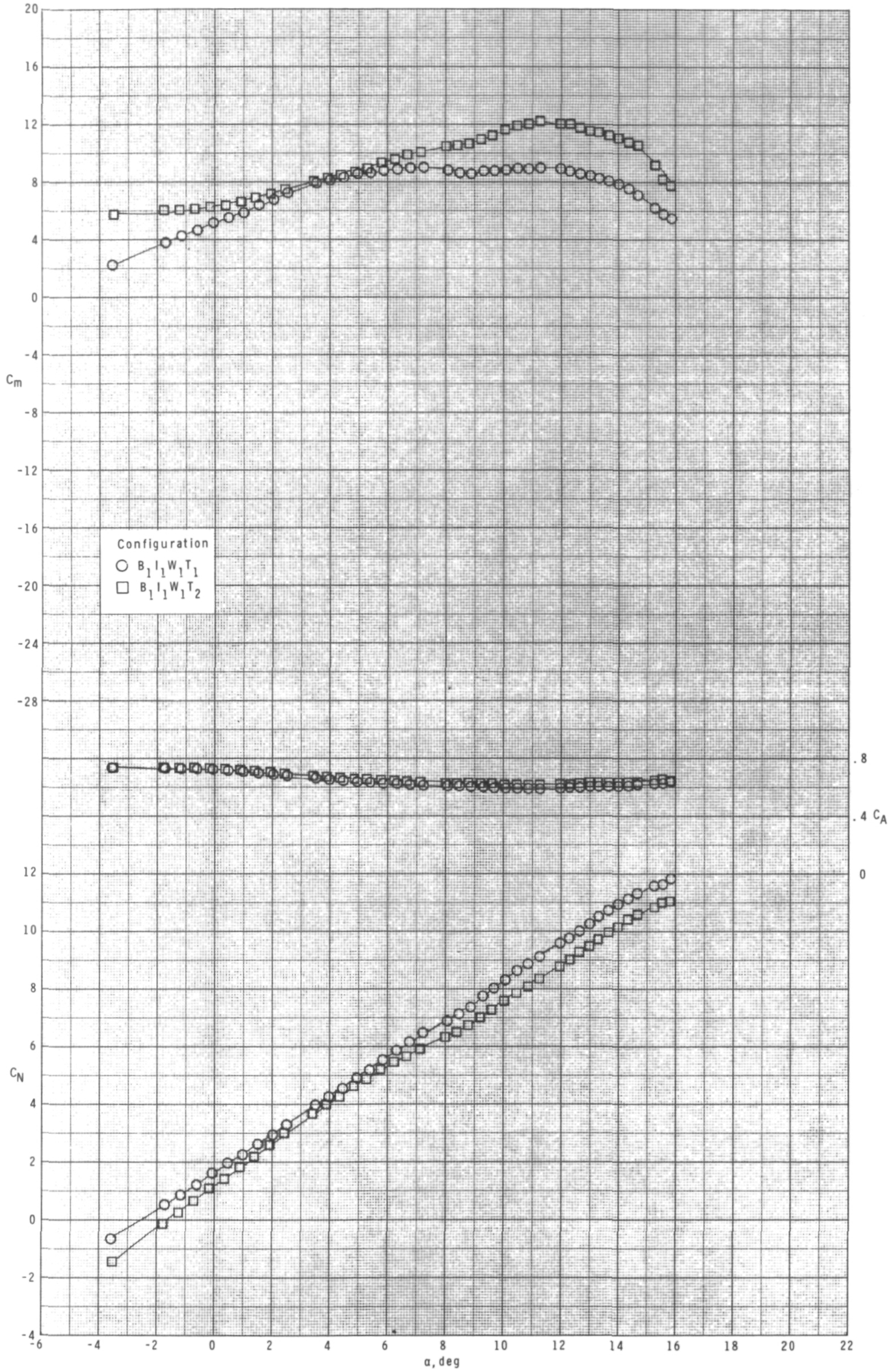

(b) M = 0.80.

Figure 10.- Continued.

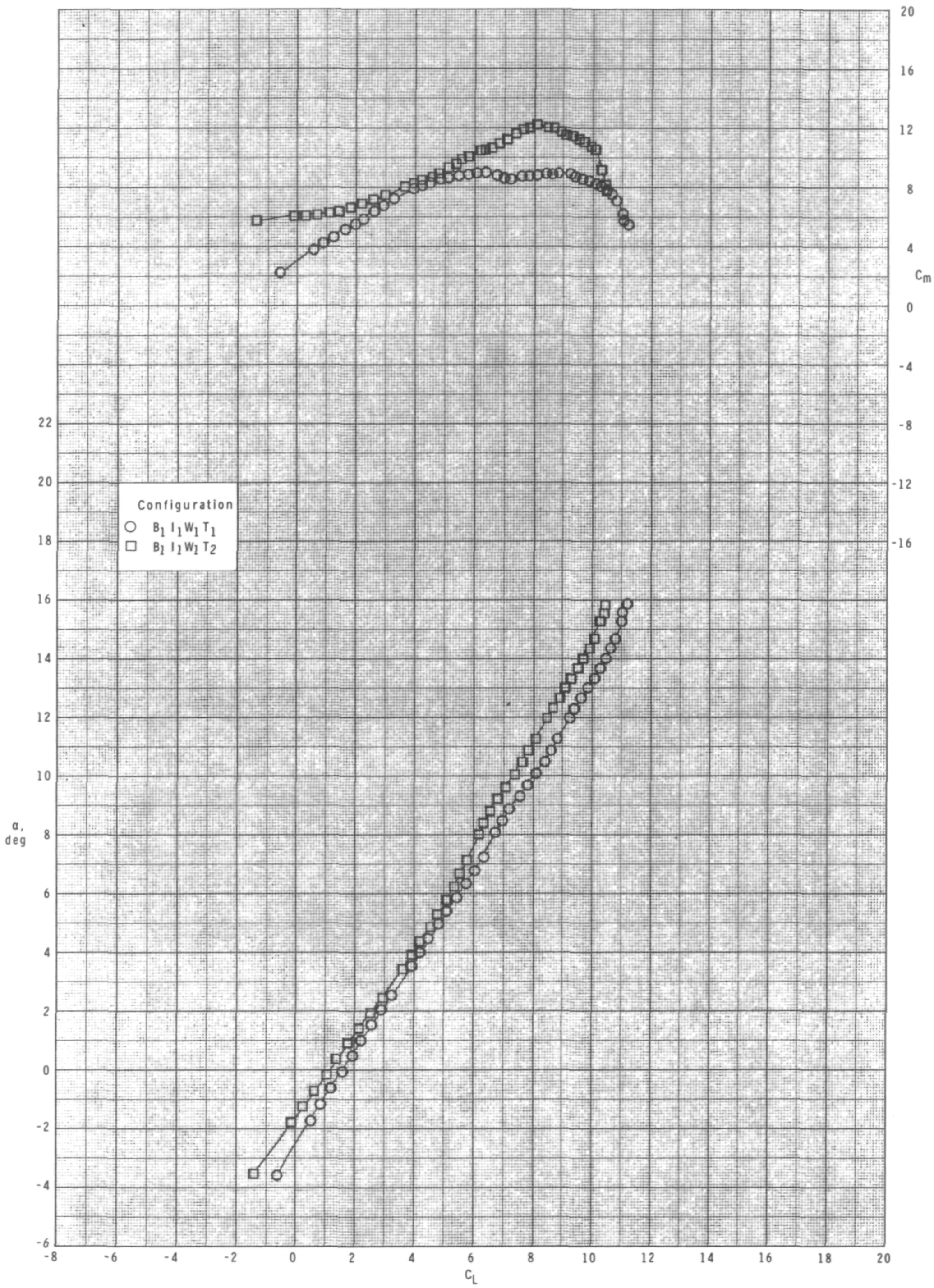

(b) Continued.

Figure 10.- Continued.

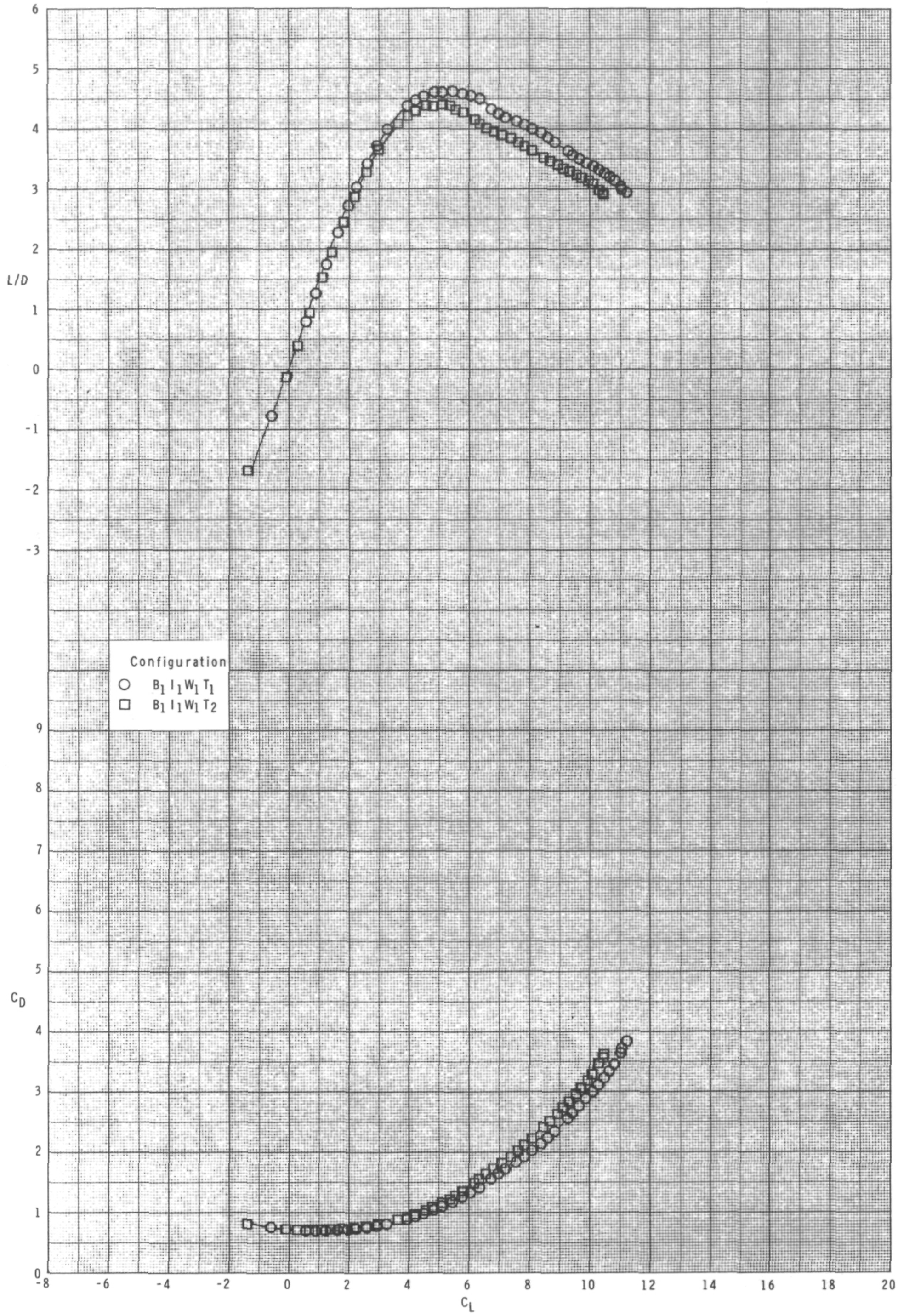

(b) Concluded.

Figure 10.- Continued.

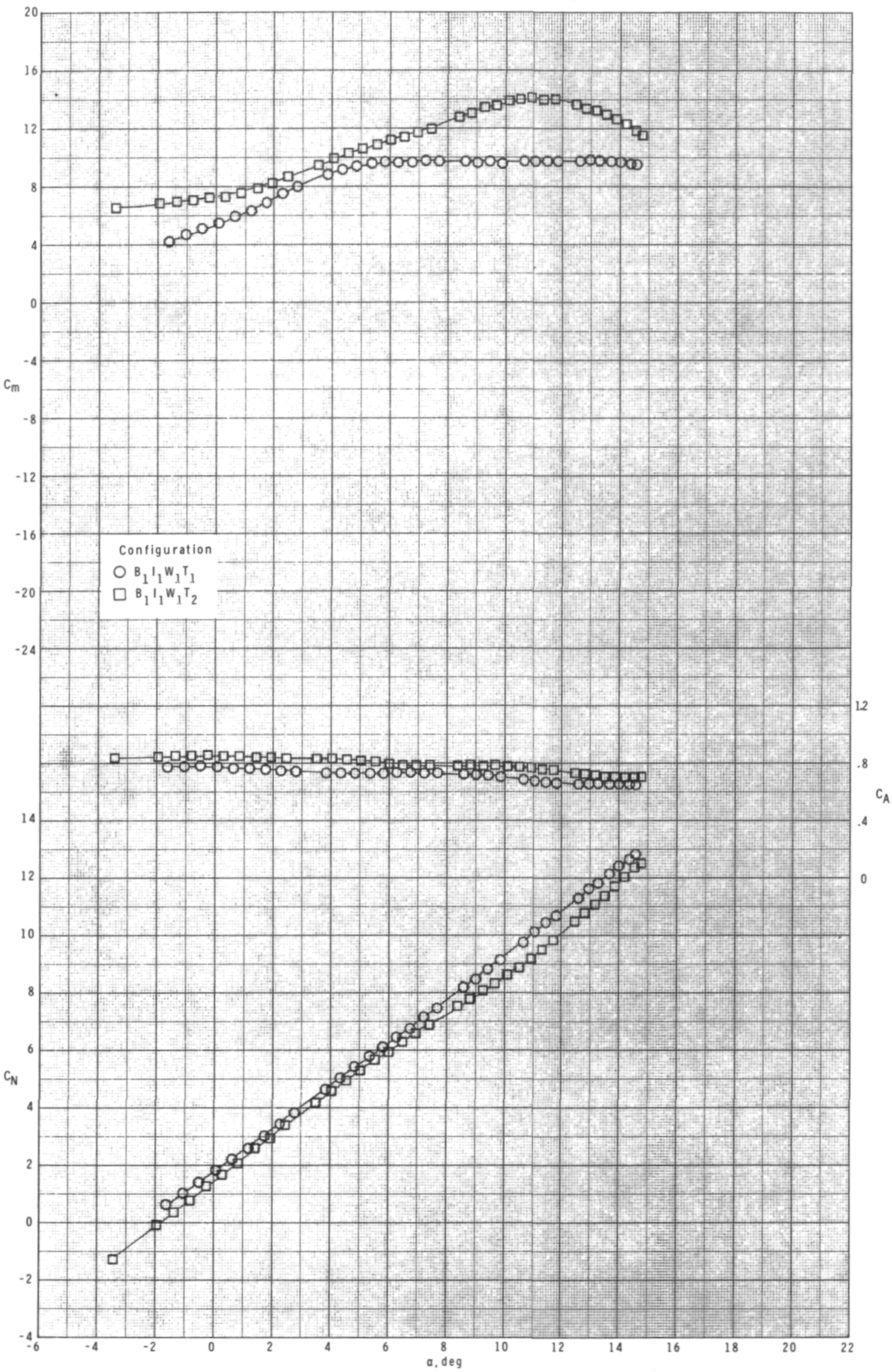

(c) M = 0.95.

Figure 10.- Continued.

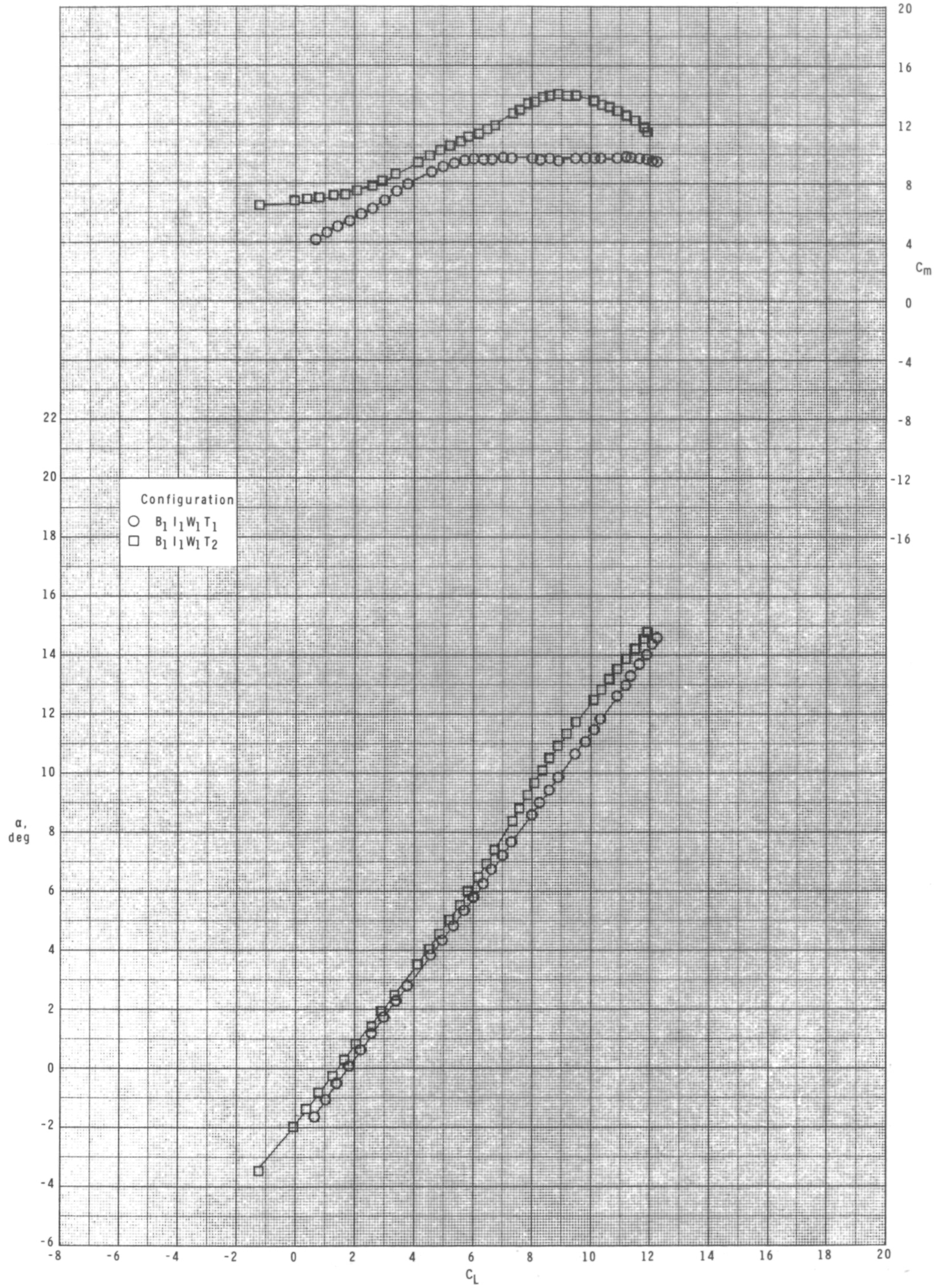

(c) Continued.

Figure 10.- Continued.

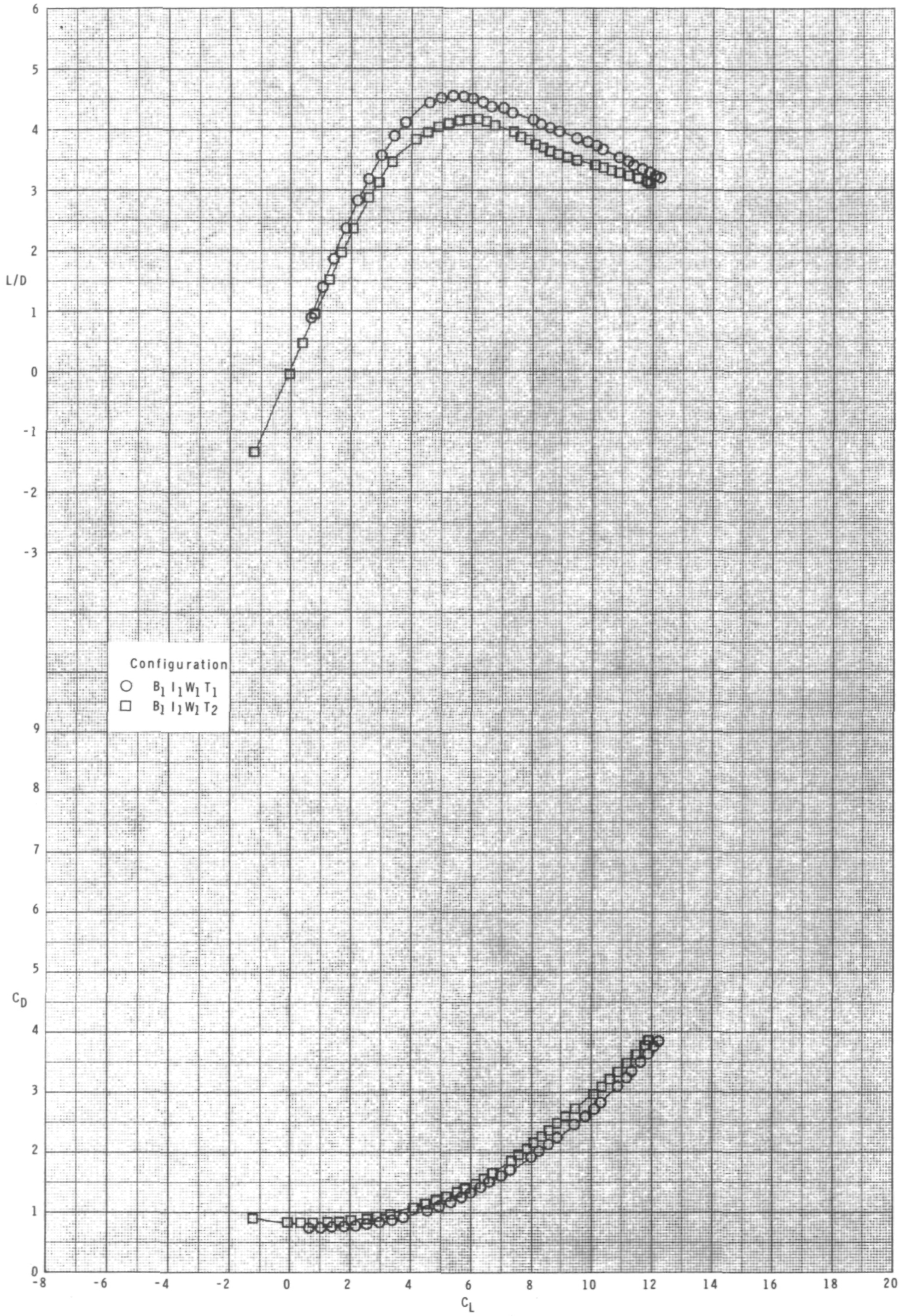

(c) Concluded.

Figure 10.- Concluded.

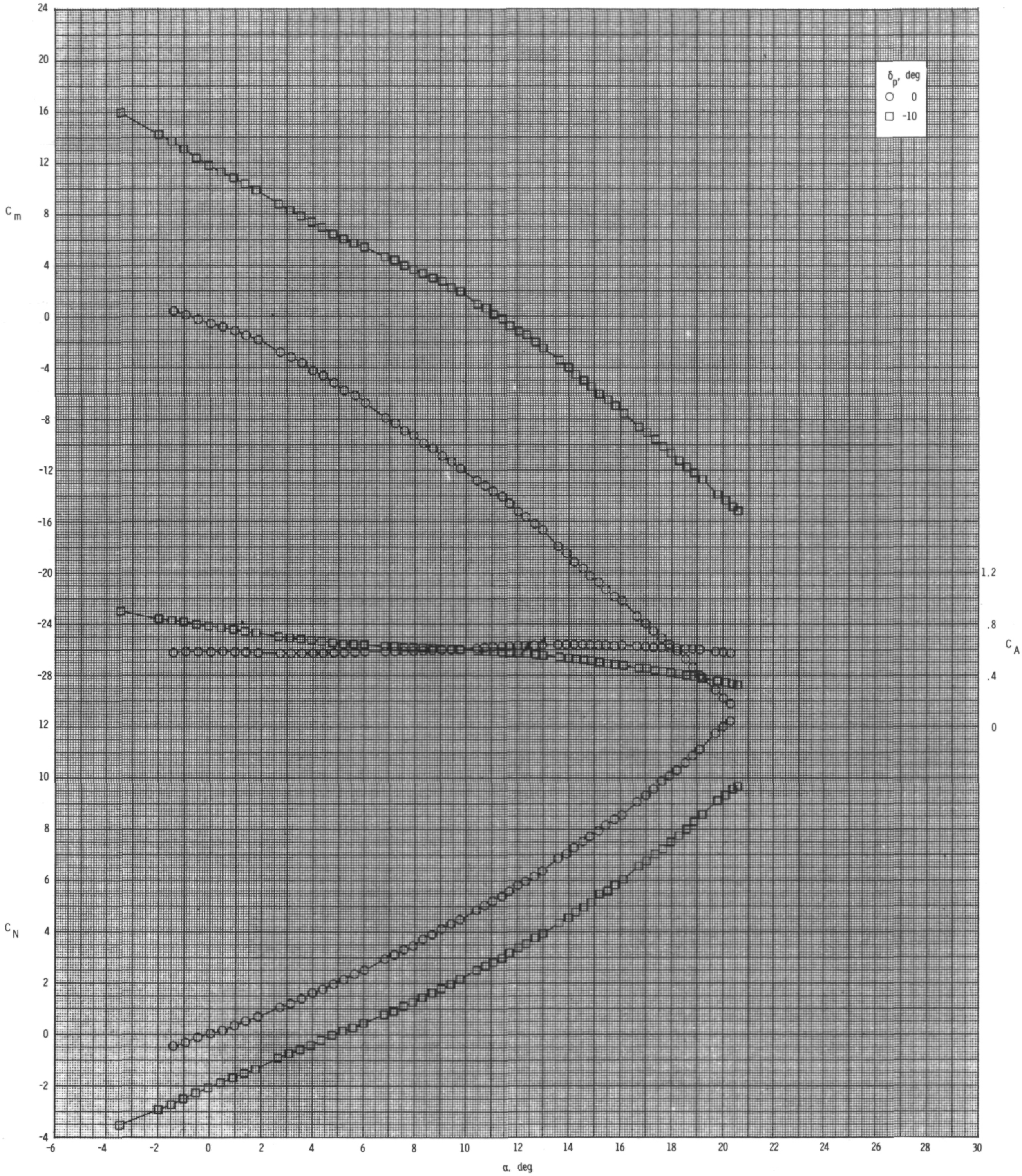

(a) M = 0.60.

Figure 11.- Pitch-control effectiveness for configuration $B_1I_1T_1$ with internal ducts closed and $\phi_I = 90°$.

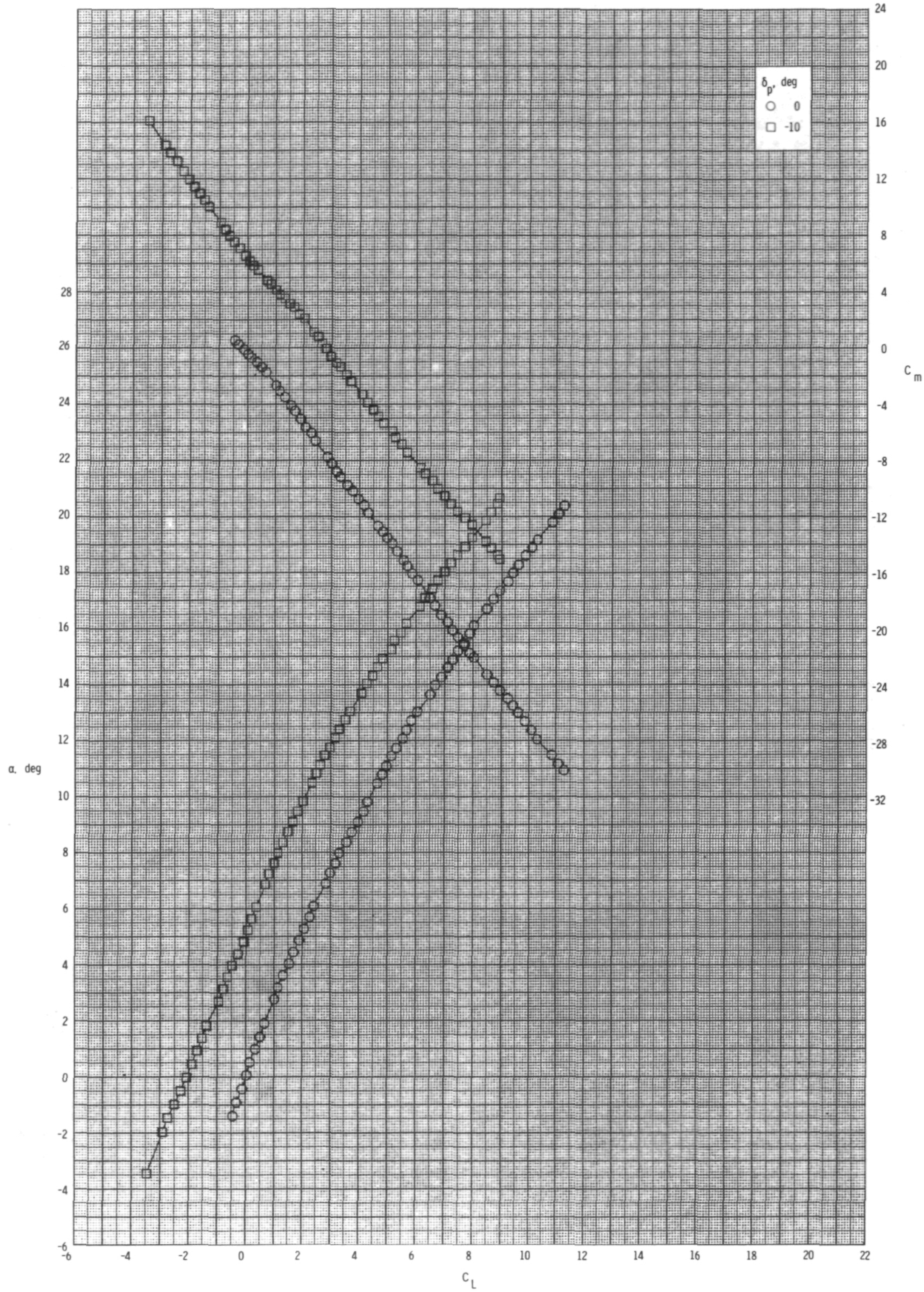

(a) Continued.

Figure 11.- Continued.

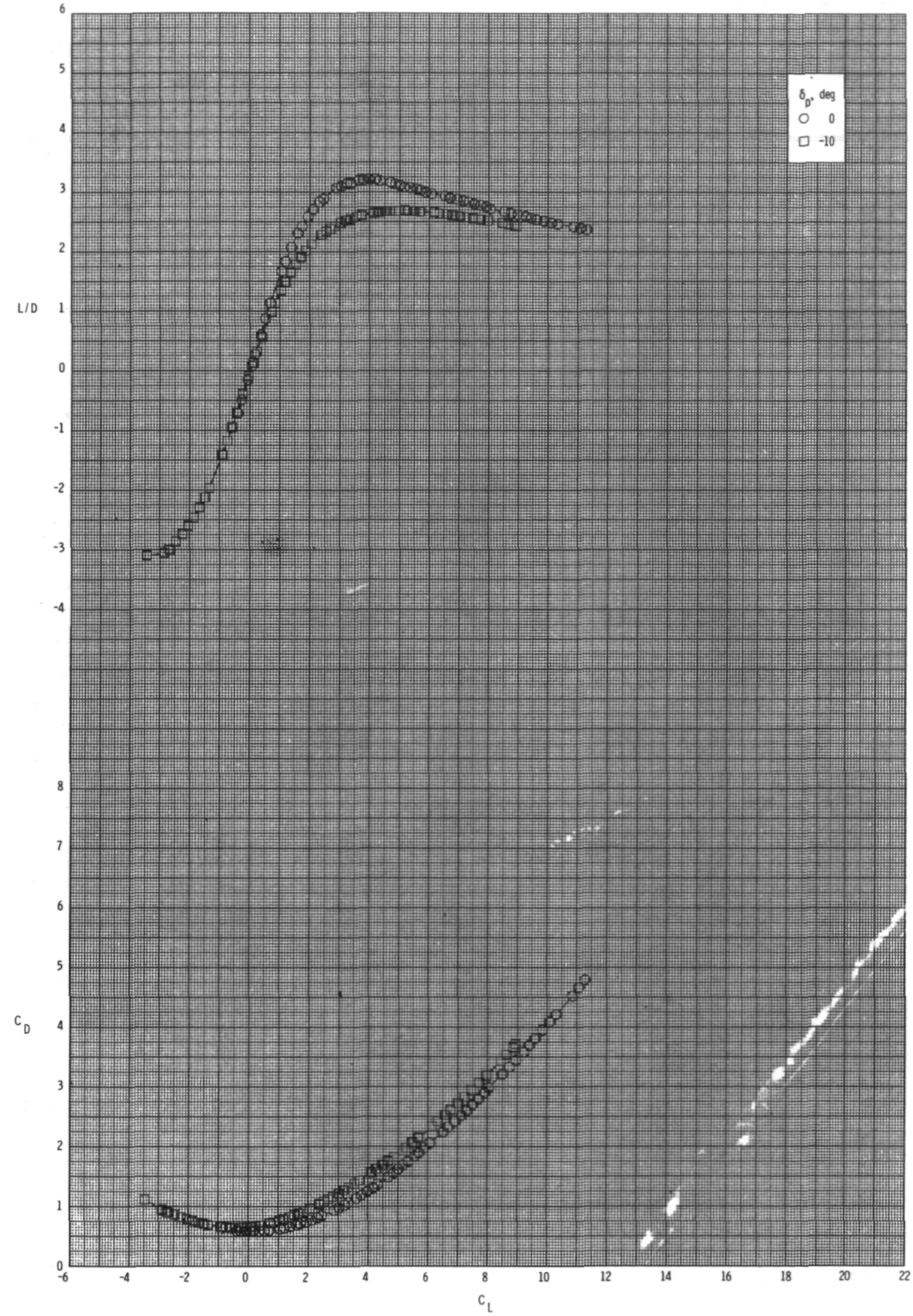

(a) Concluded.

Figure 11.- Continued.

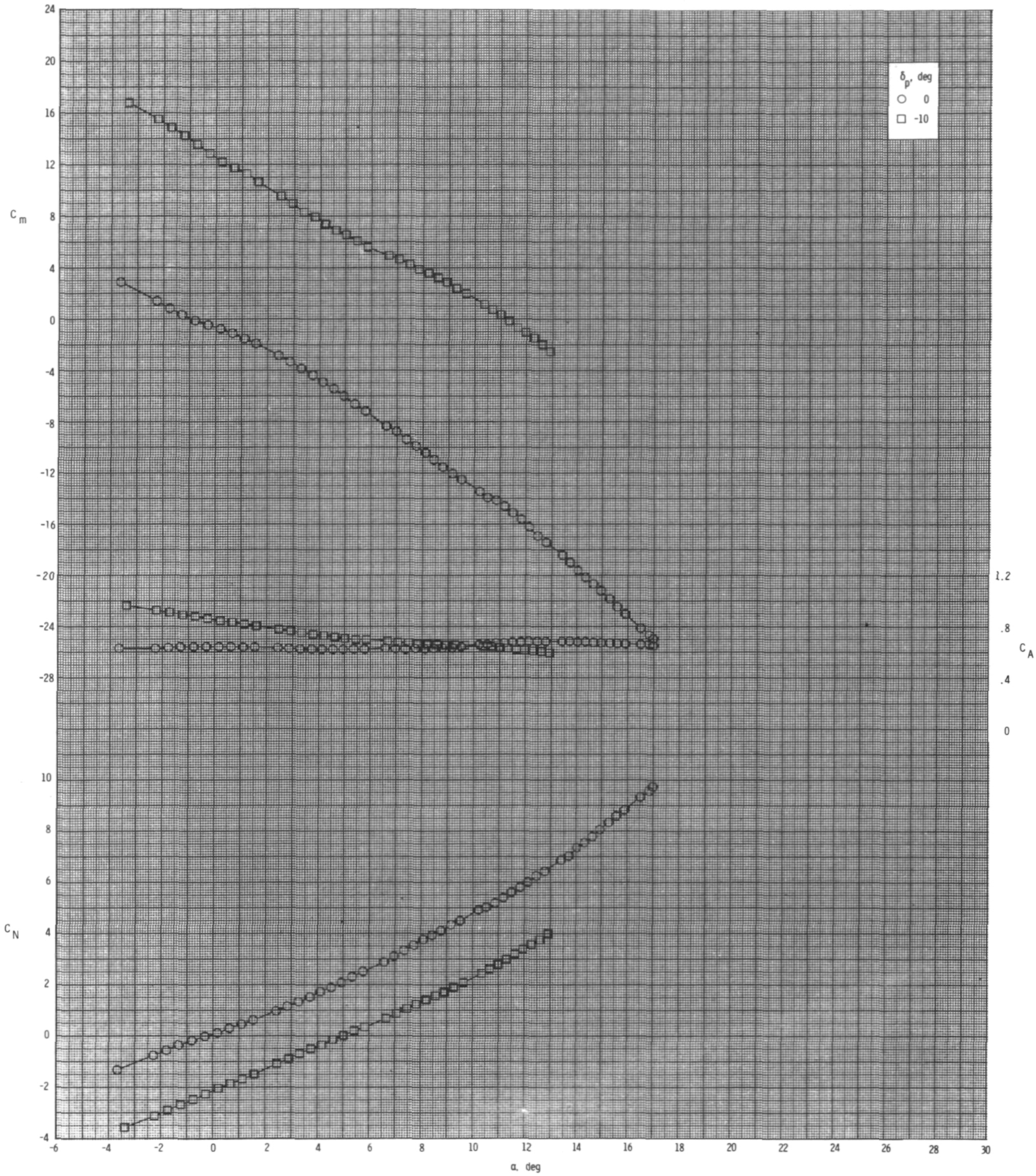

(b) M = 0.80.

Figure 11.- Continued.

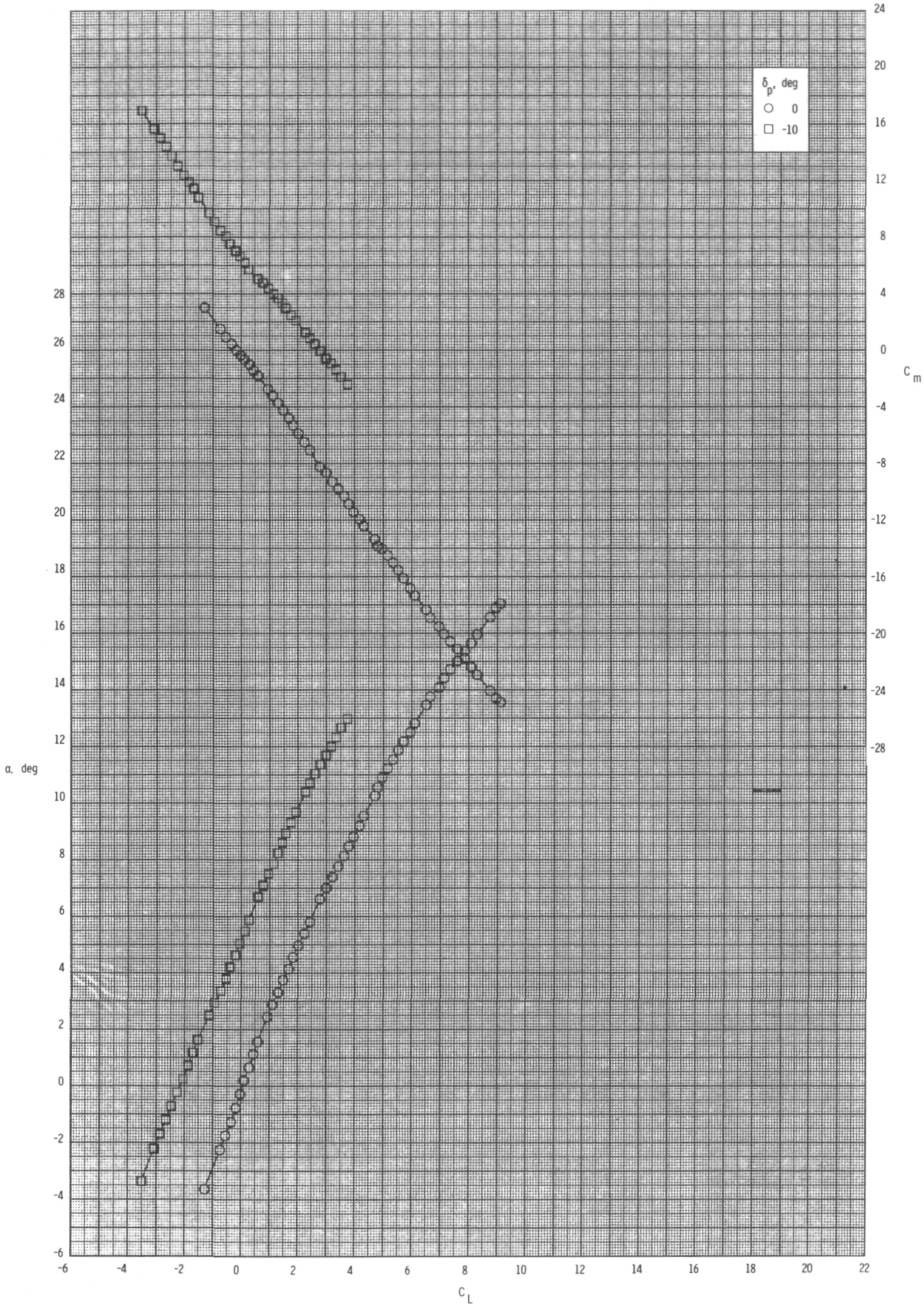

(b) Continued.

Figure 11.- Continued.

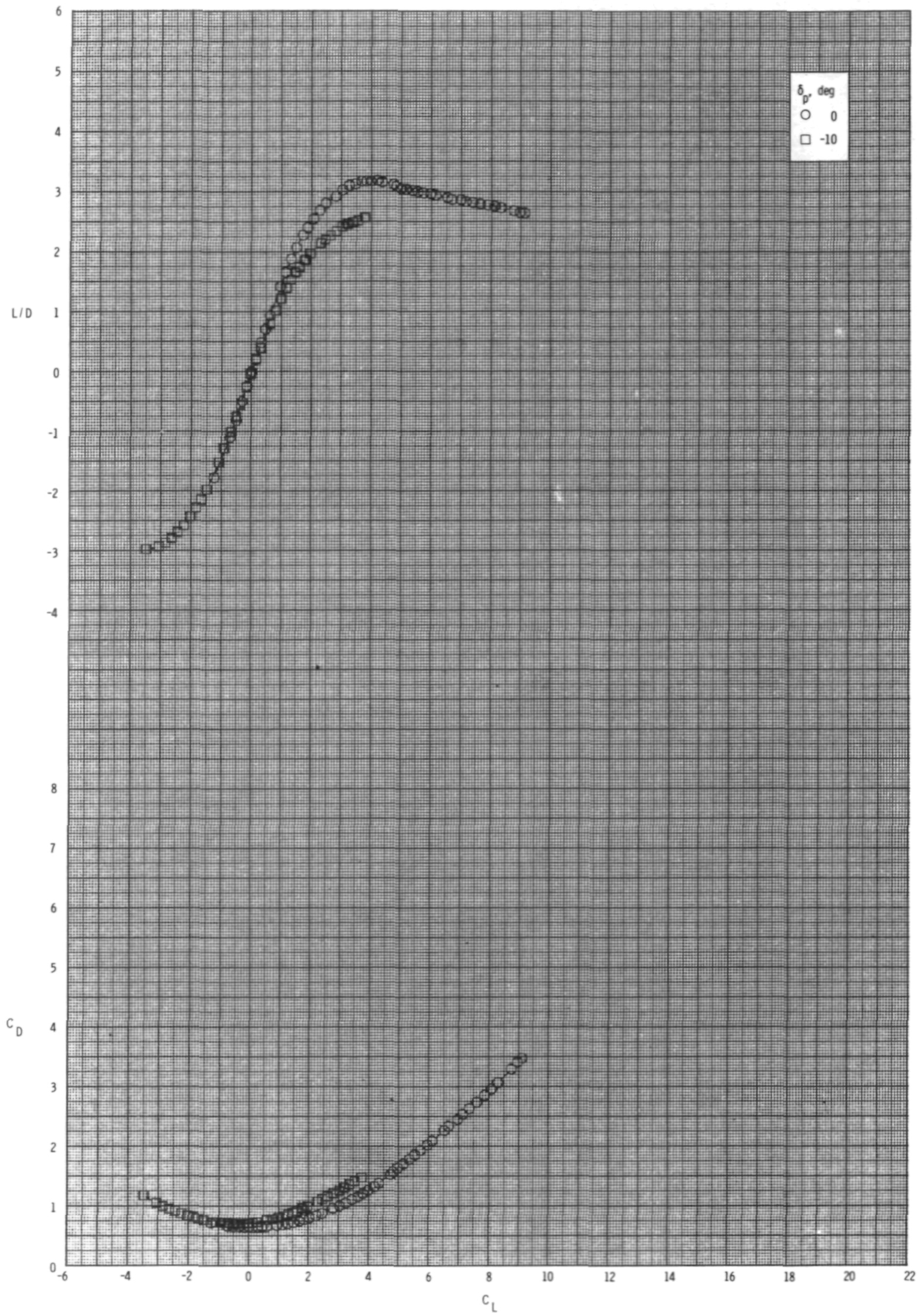

(b) Concluded.

Figure 11.- Continued.

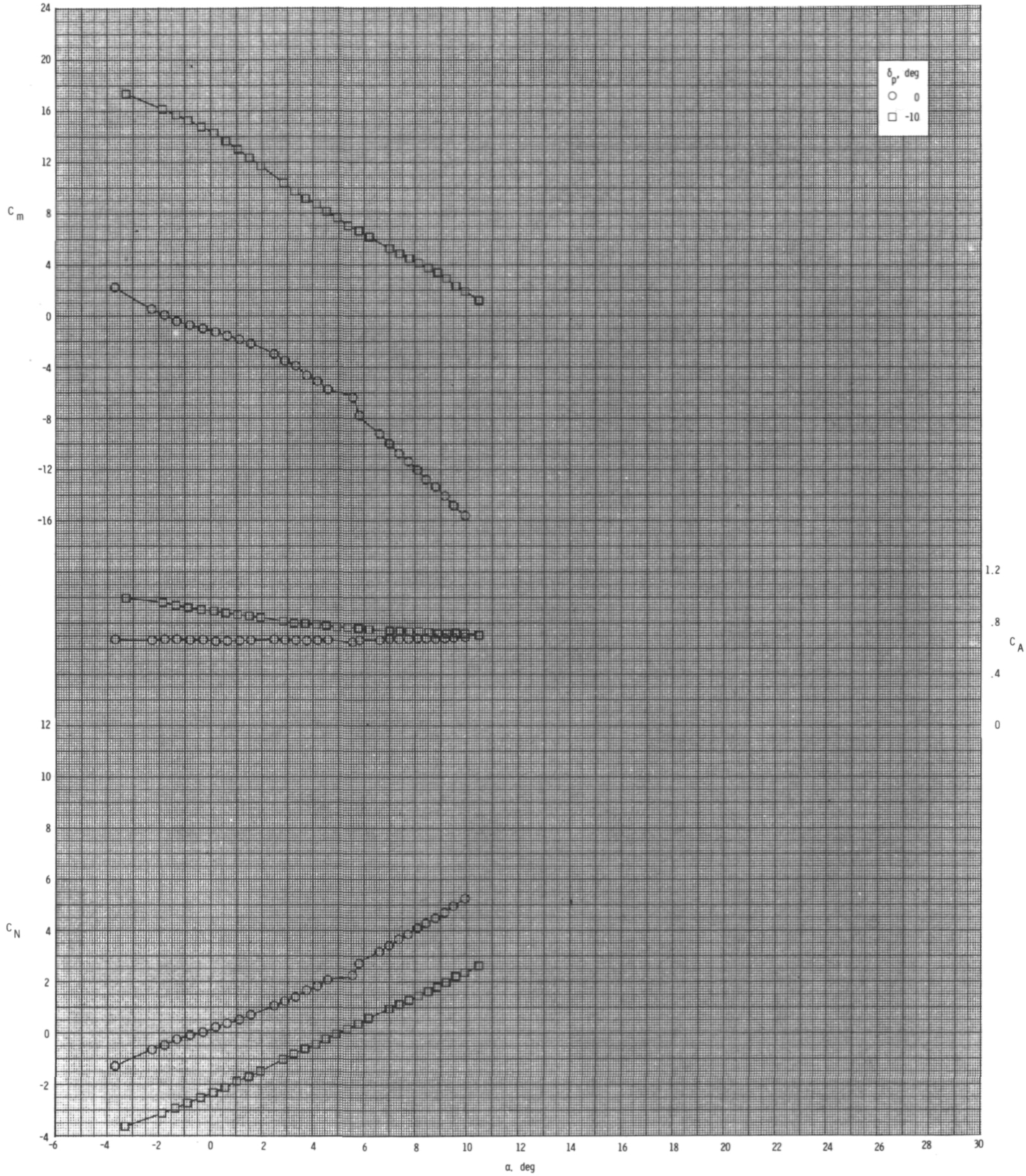

(c) M = 0.95.

Figure 11.- Continued.

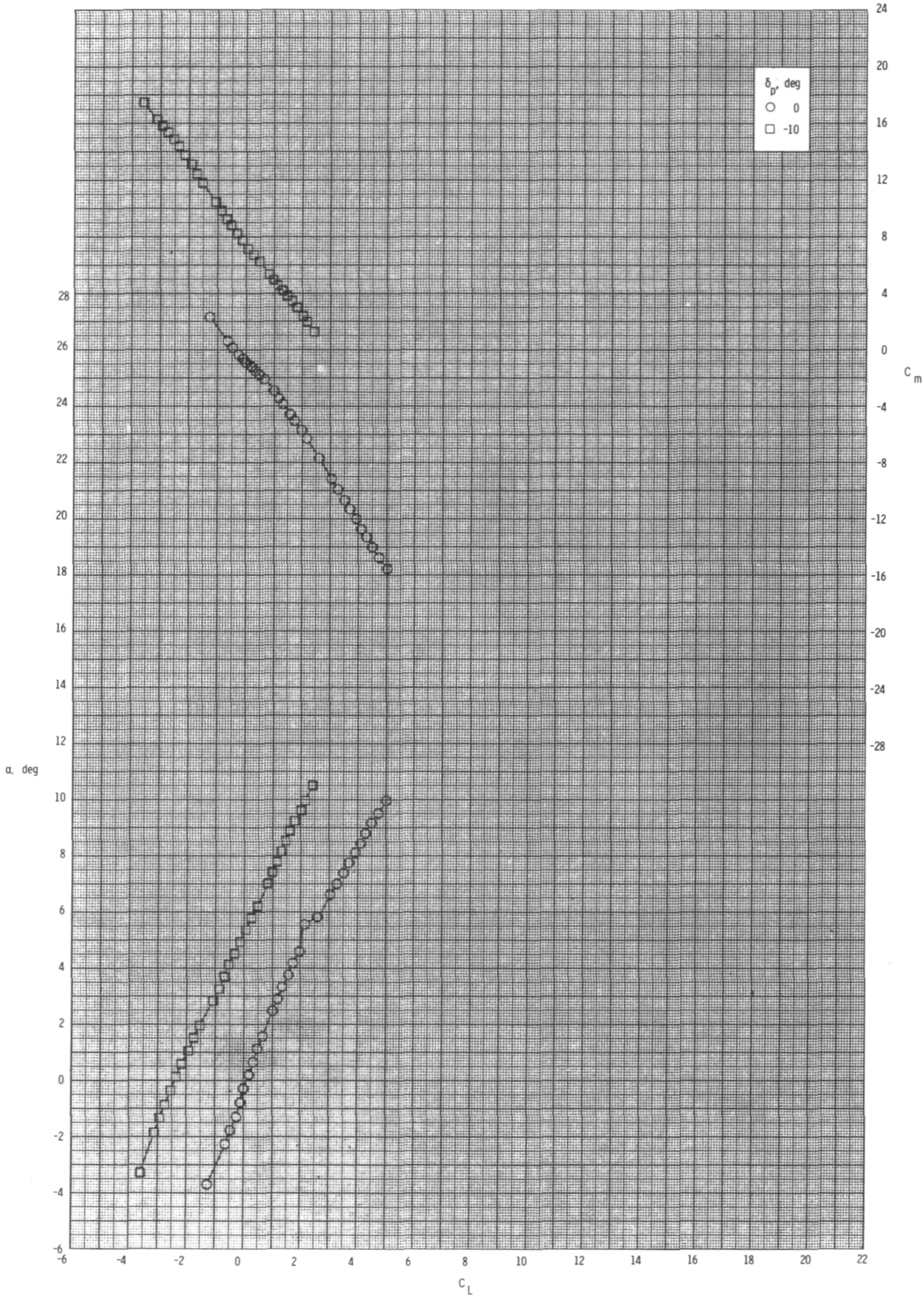

(c) Continued.

Figure 11.- Continued.

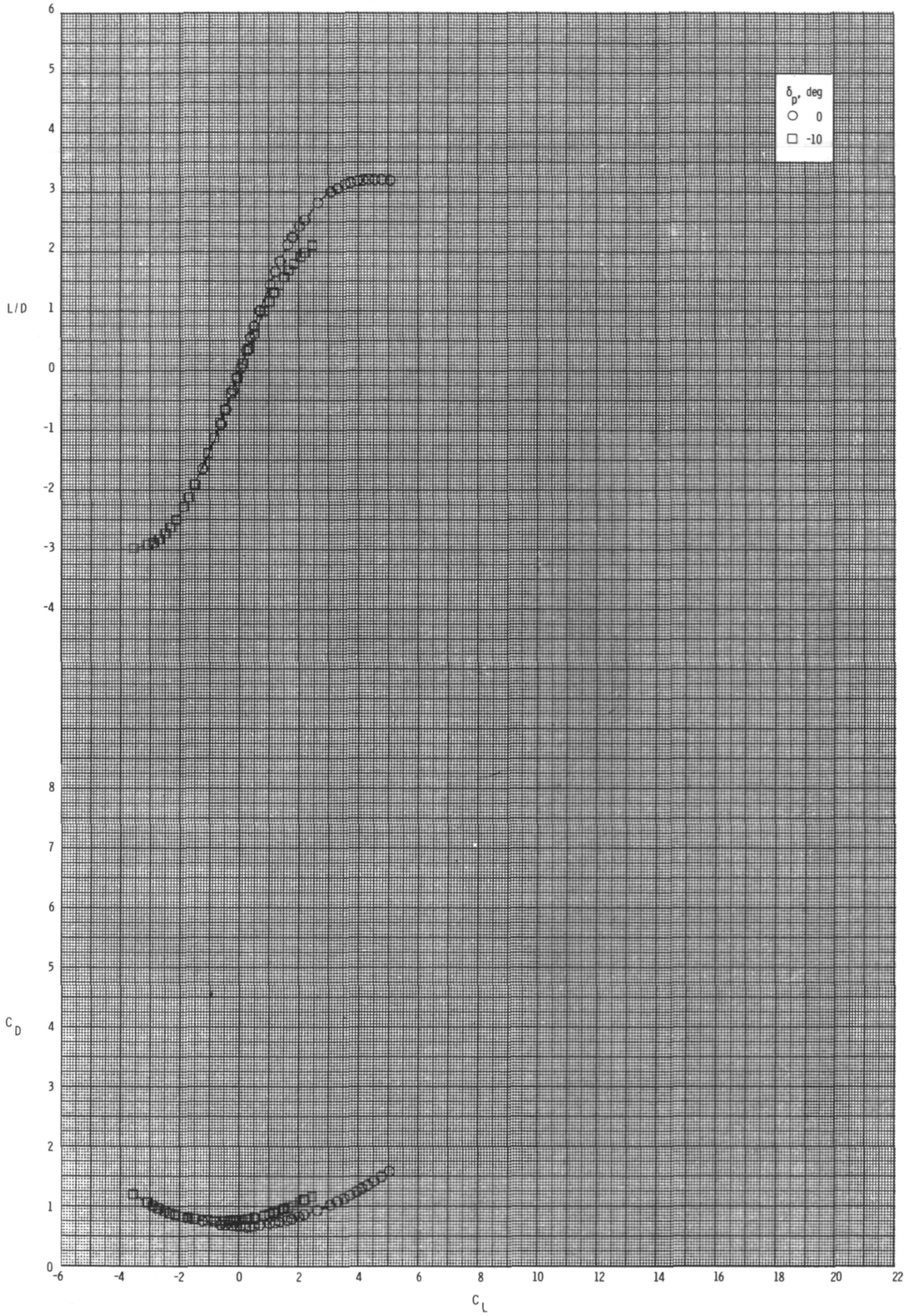

(c) Concluded.

Figure 11.- Concluded.

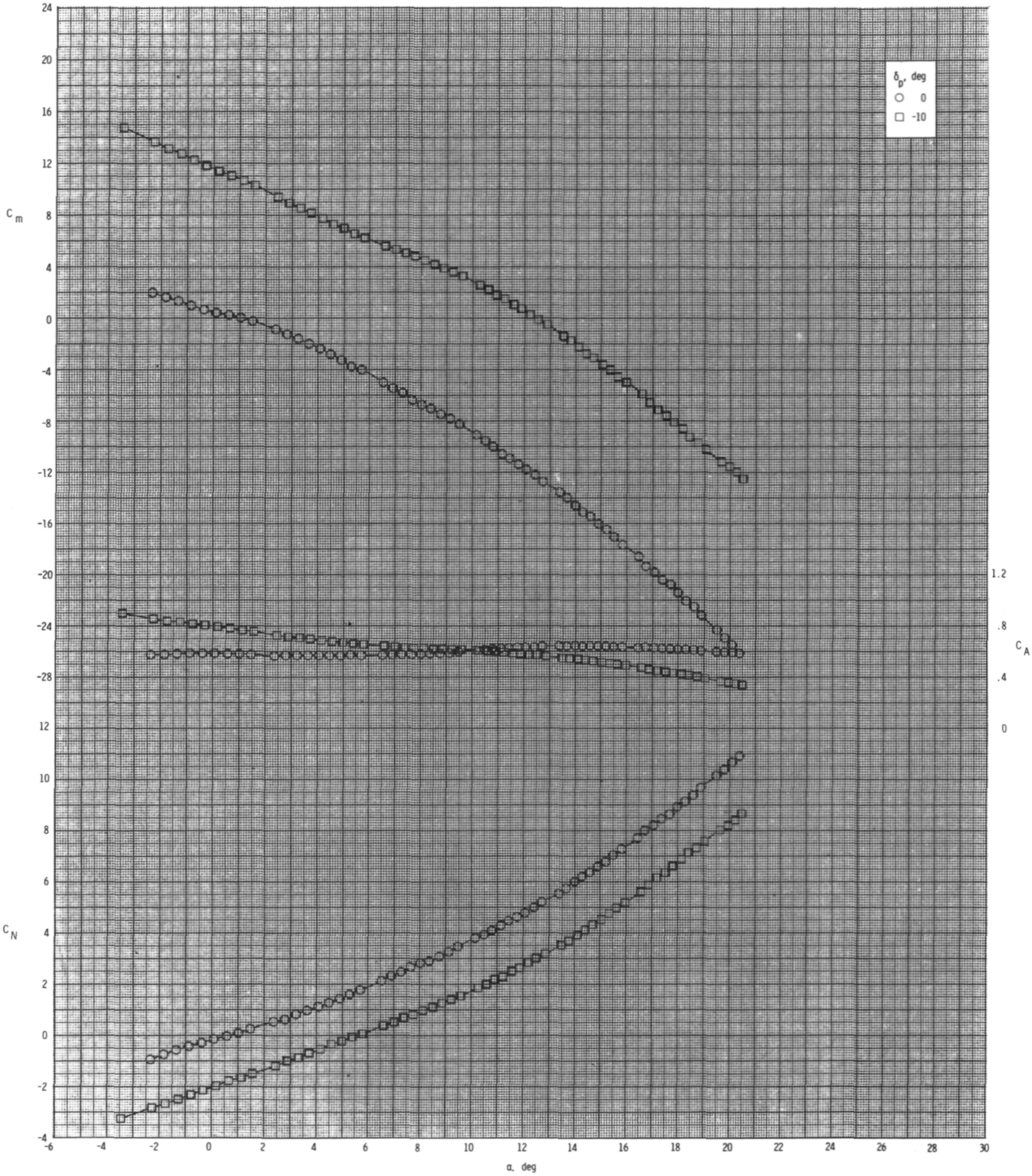

(a) M = 0.60.

Figure 12.- Pitch-control effectiveness for configuration $B_1I_1T_1$ with internal ducts closed and $\phi_I = 115°$.

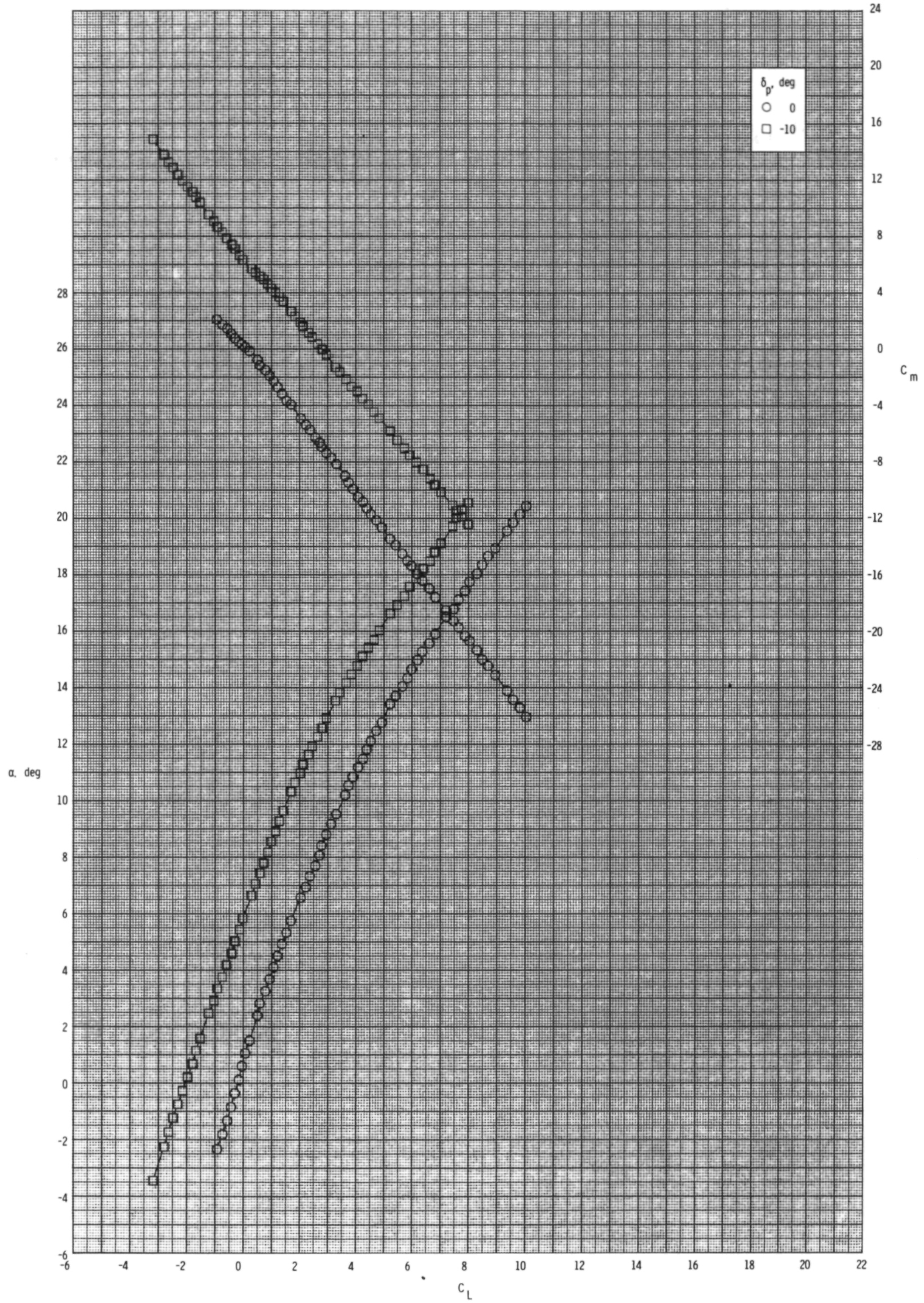

(a) Continued.

Figure 12.- Continued.

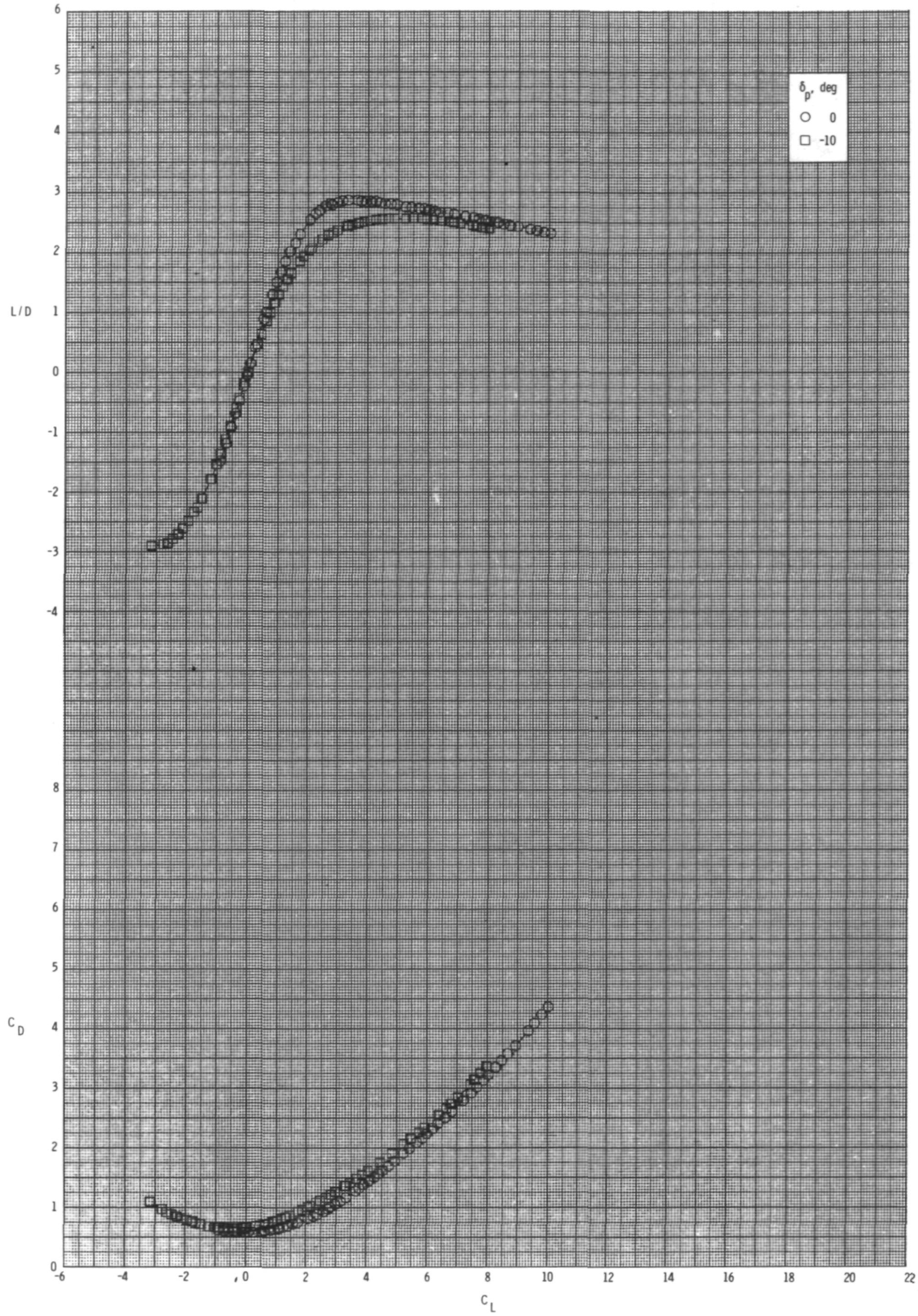

(a) Concluded.

Figure 12.- Continued.

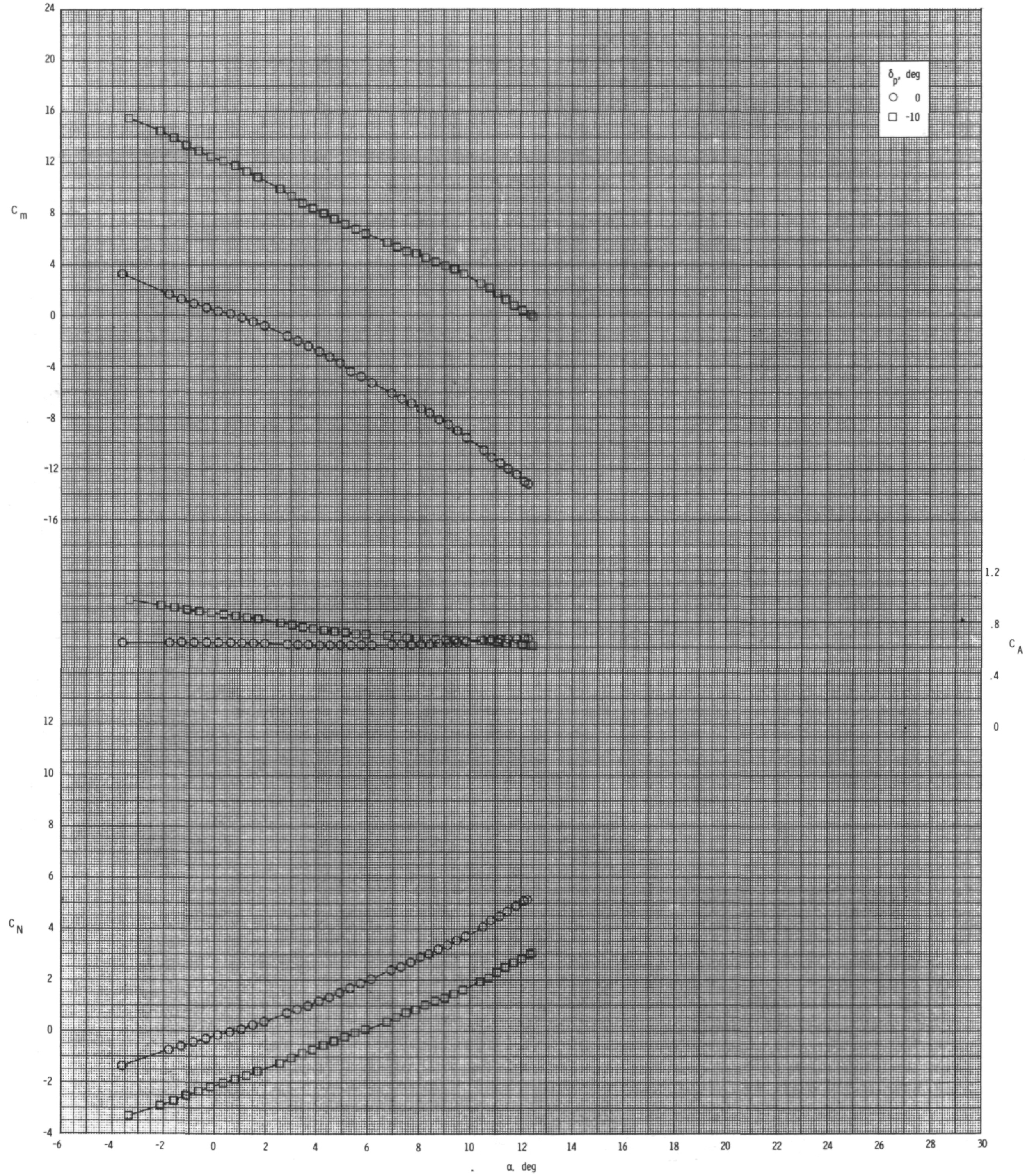

(b) M = 0.80.

Figure 12.- Continued.

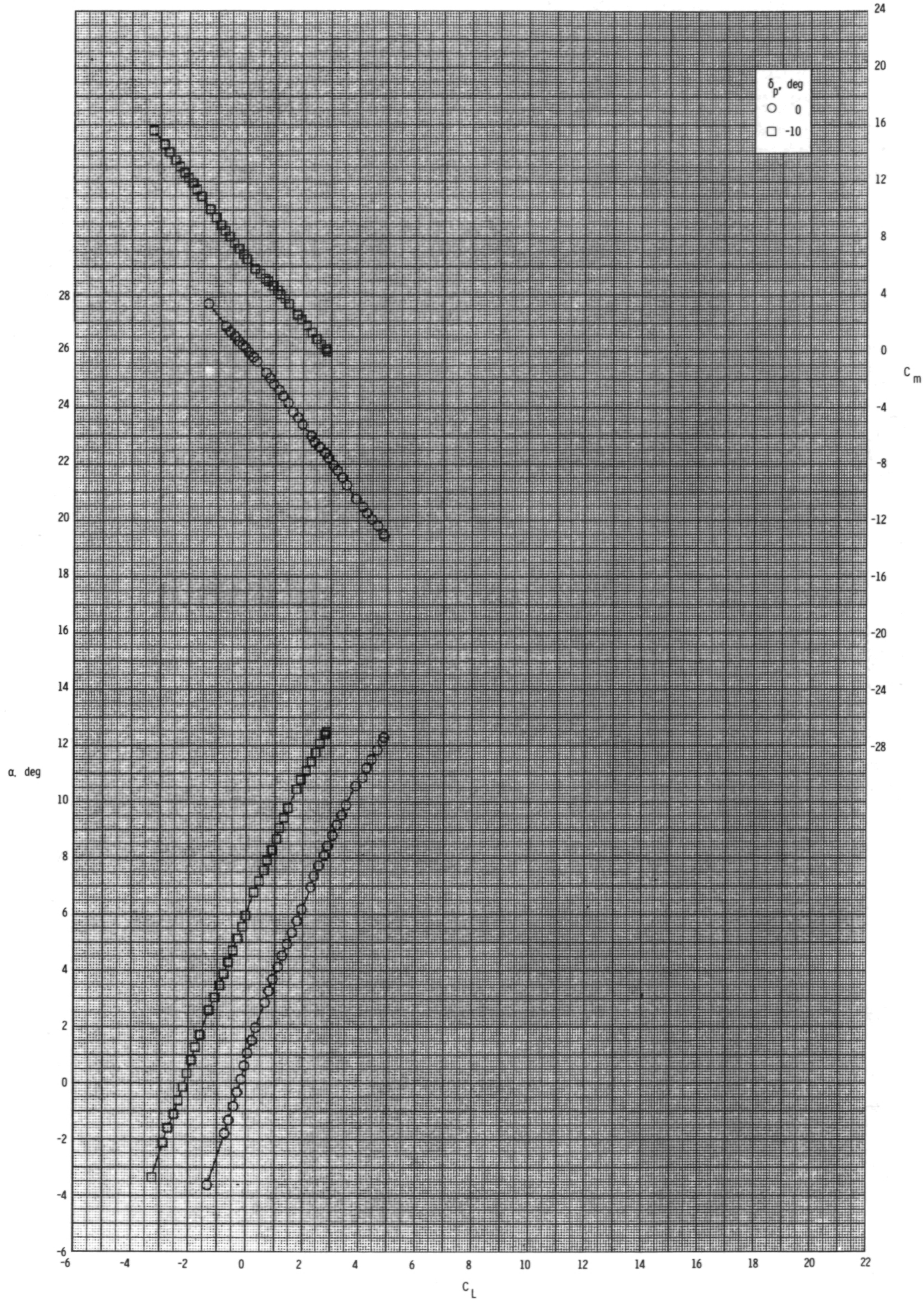

(b) Continued.

Figure 12.- Continued.

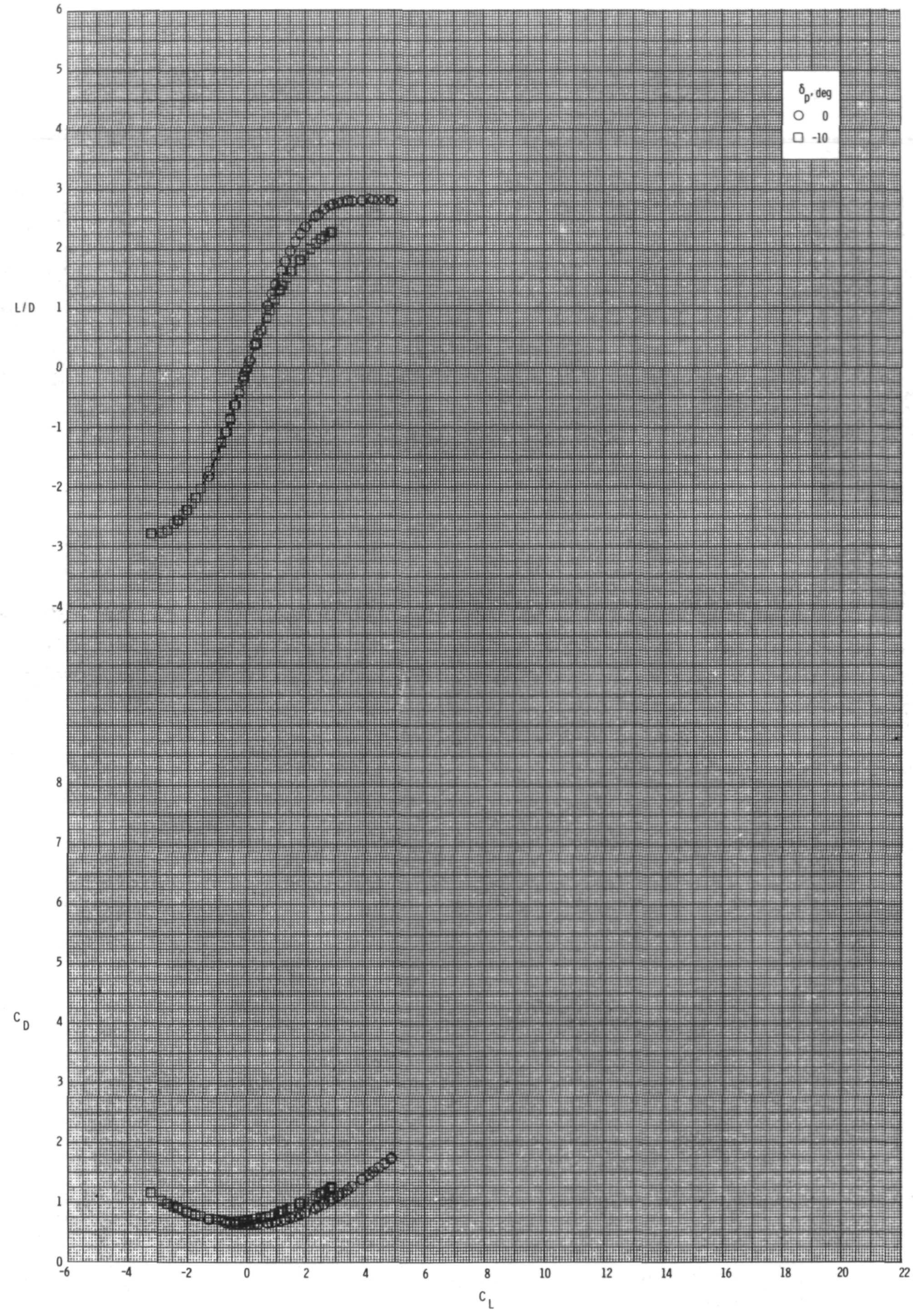

(b) Concluded.

Figure 12.- Continued.

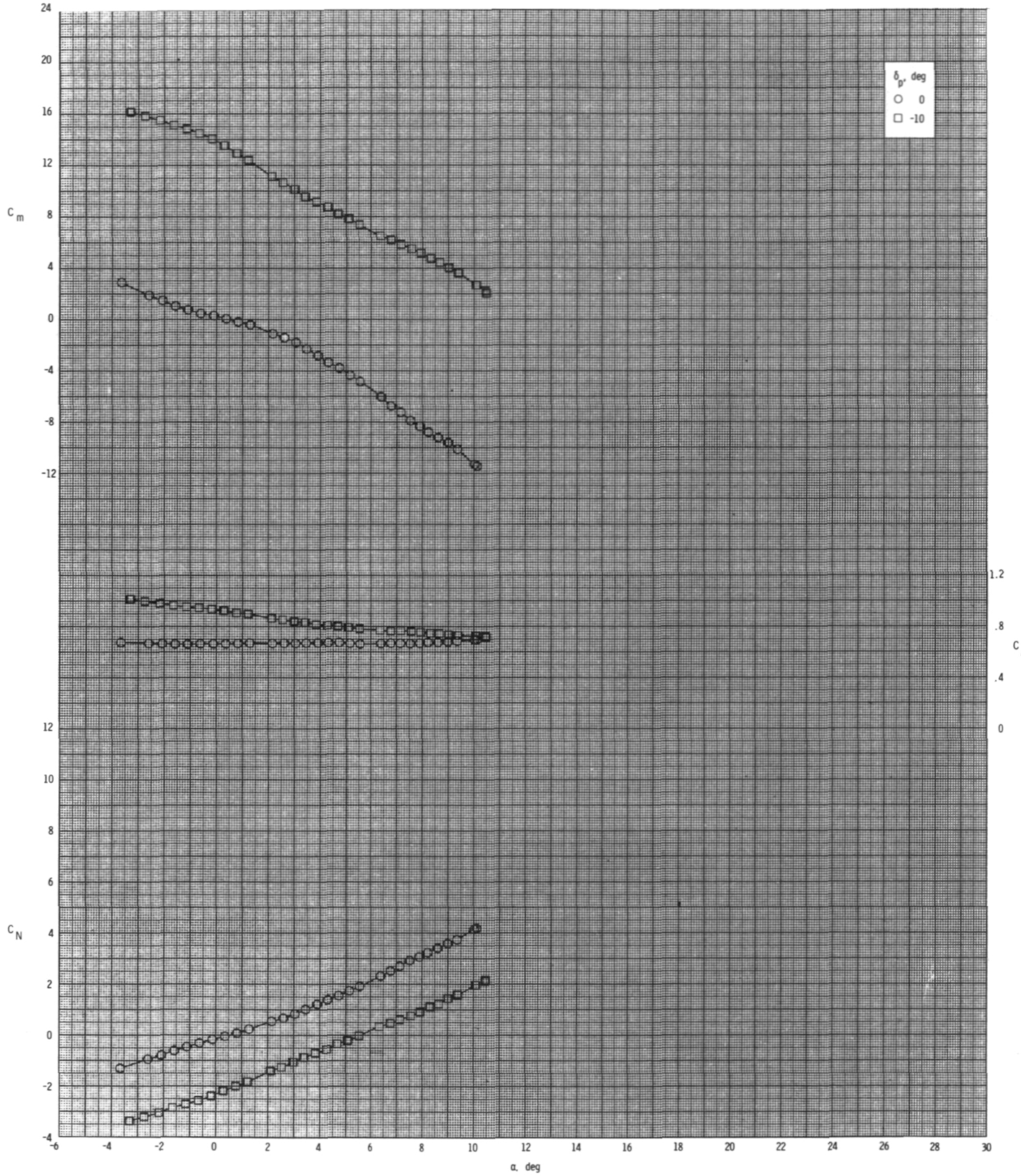

(c) M = 0.95.

Figure 12.- Continued.

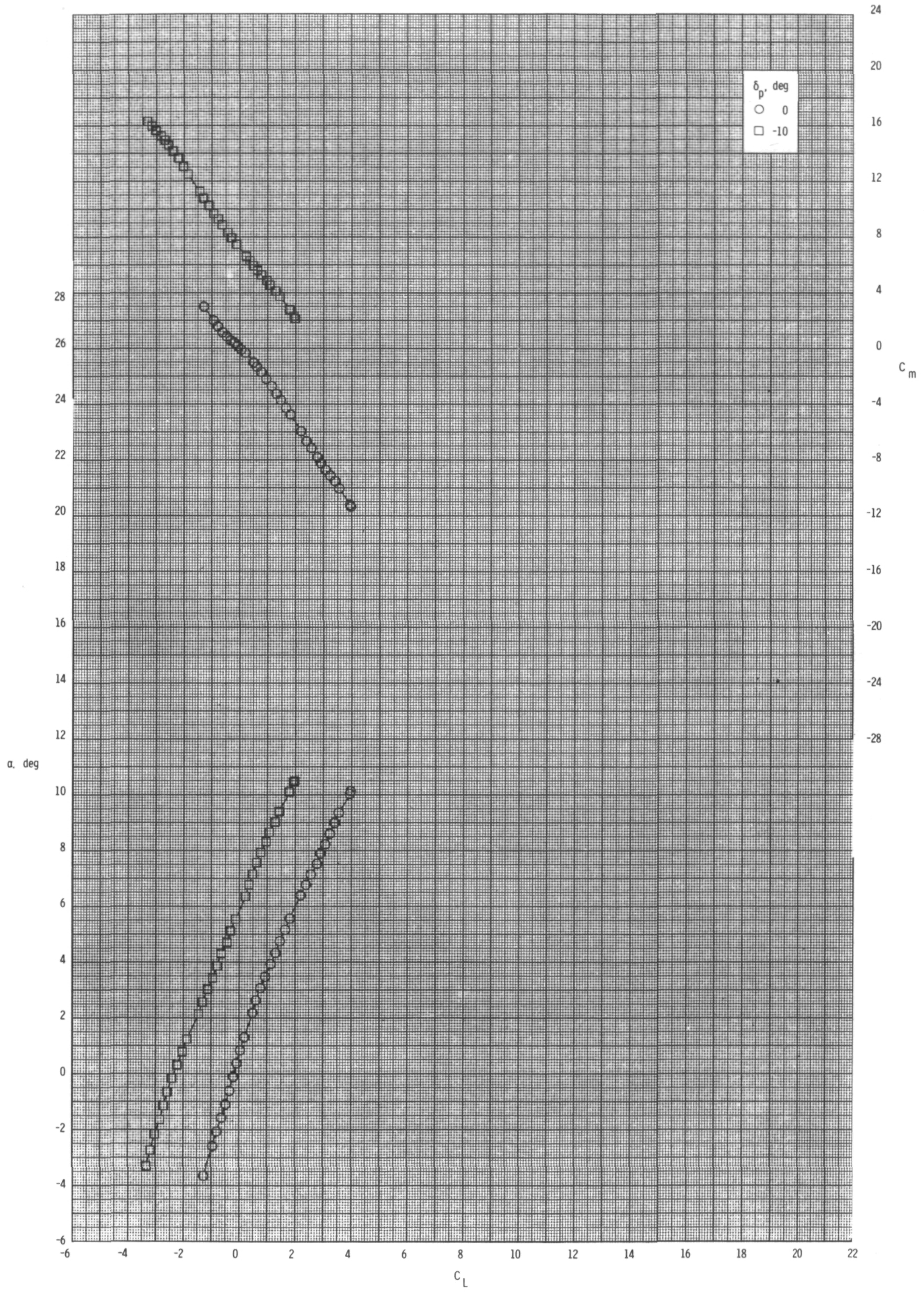

(c) Continued.

Figure 12.- Continued.

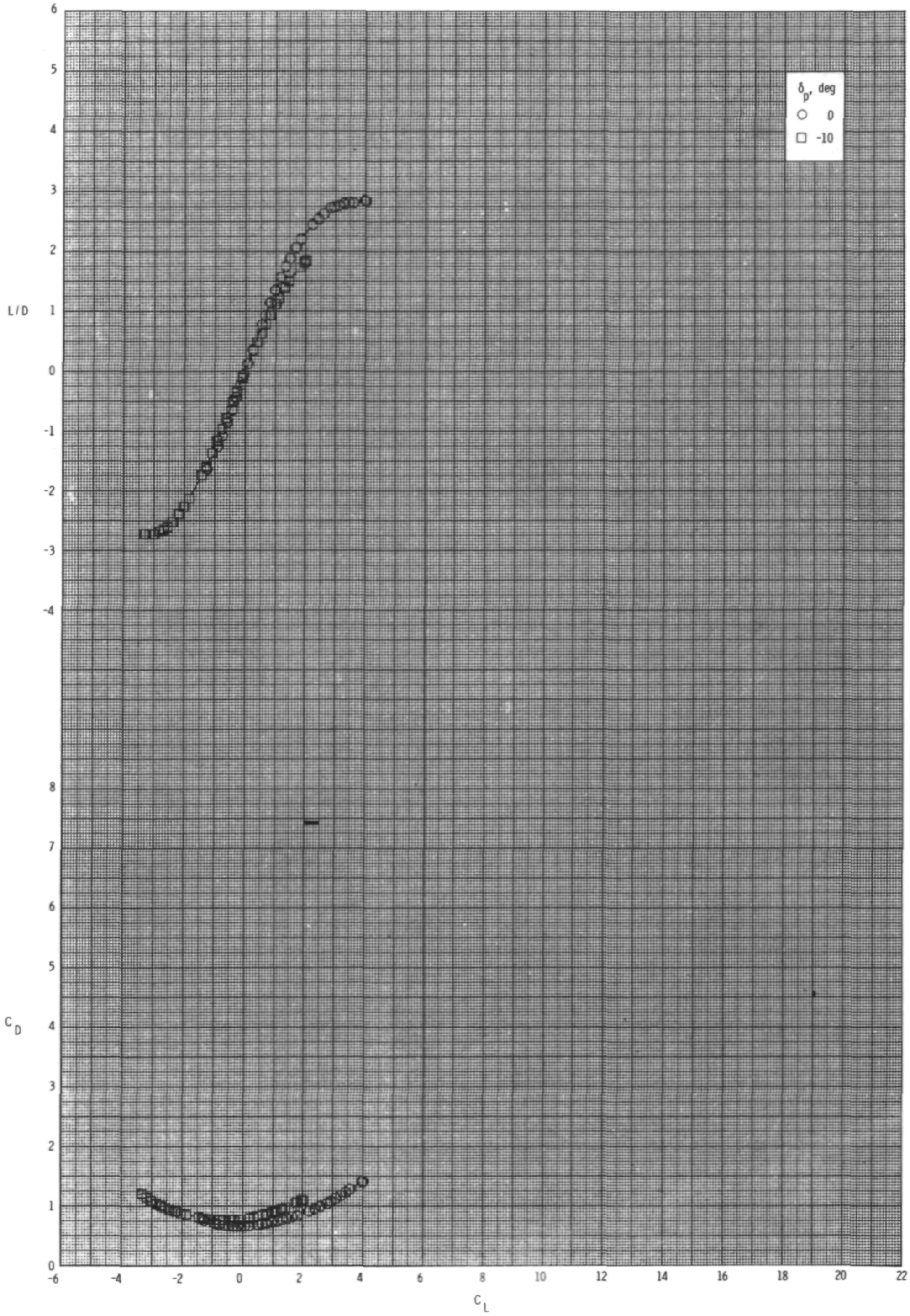

(c) Concluded.

Figure 12.- Concluded.

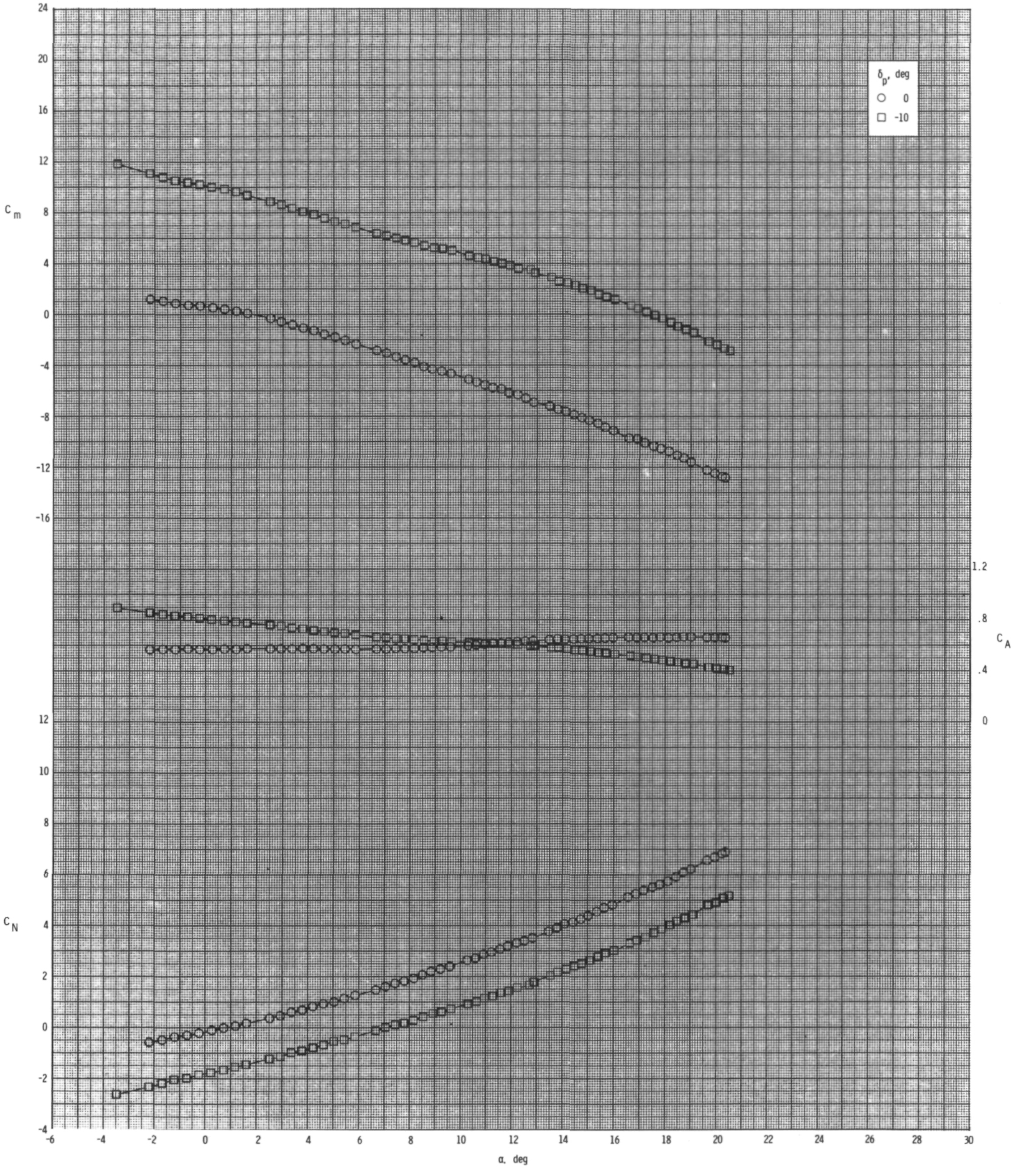

(a) M = 0.60.

Figure 13.- Pitch-control effectiveness for configuration $B_1I_1T_1$ with internal ducts closed and $\phi_I = 135°$.

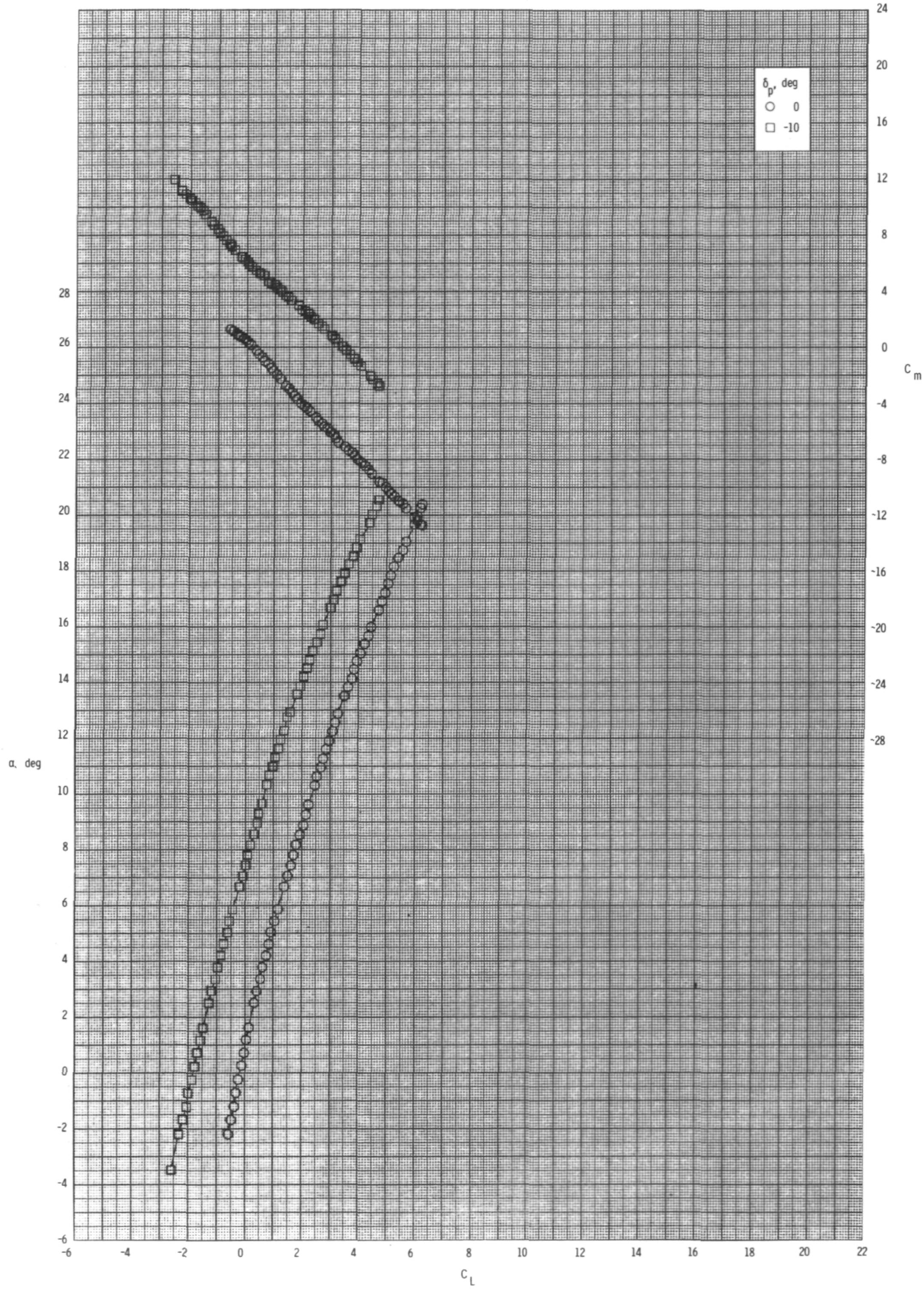

(a) Continued.

Figure 13.- Continued.

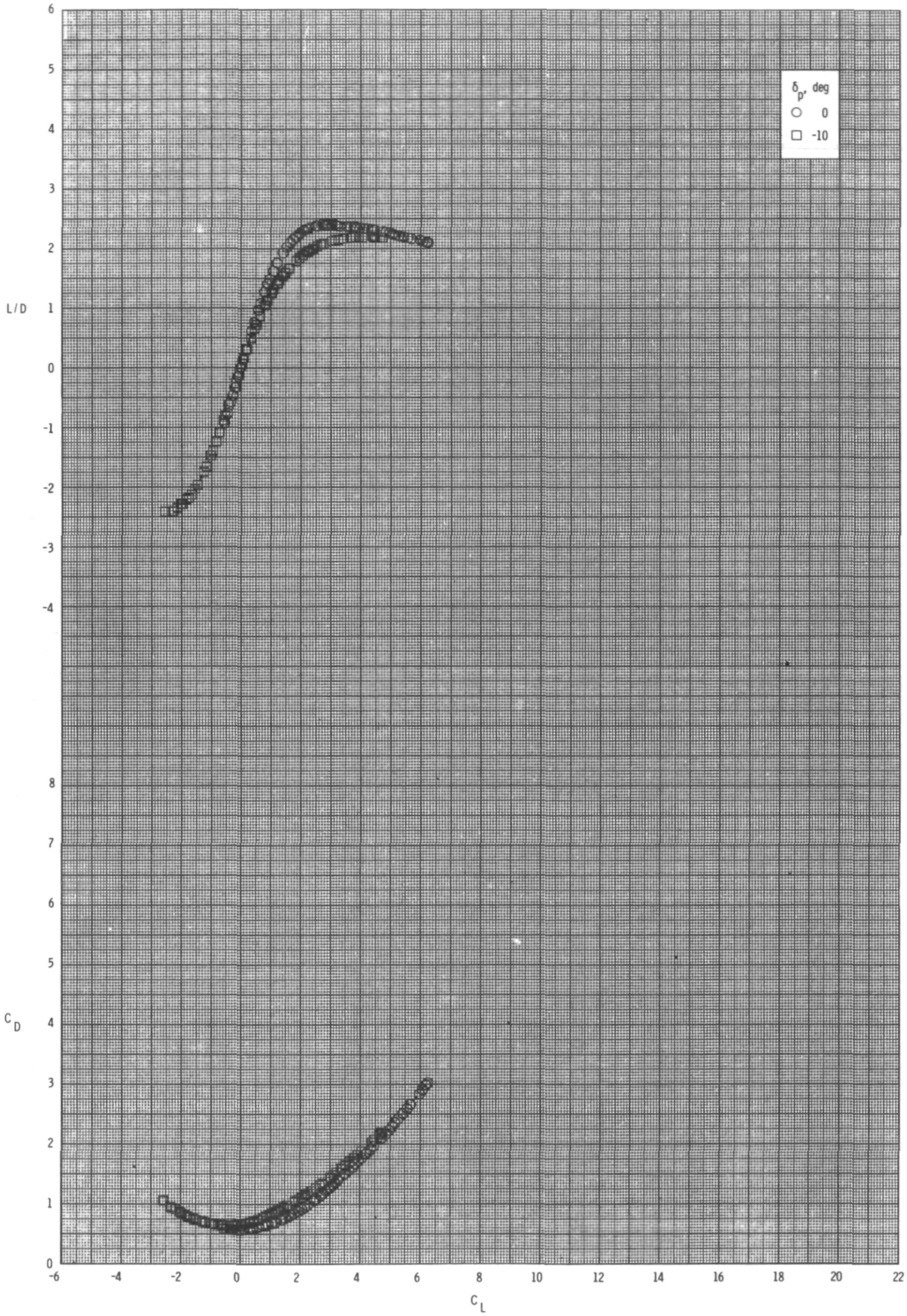

(a) Concluded.

Figure 13.- Continued.

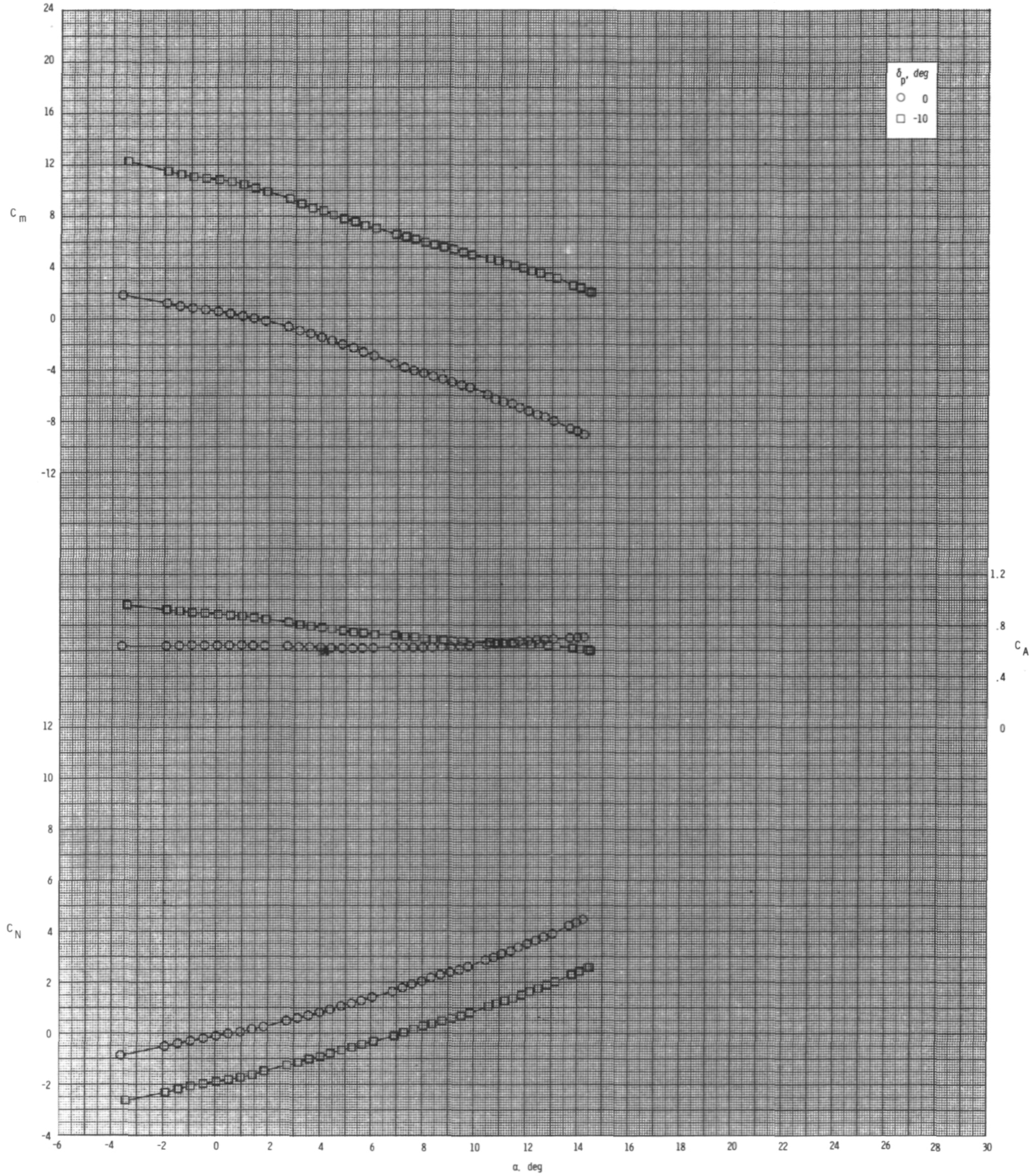

(b) M = 0.80.

Figure 13.- Continued.

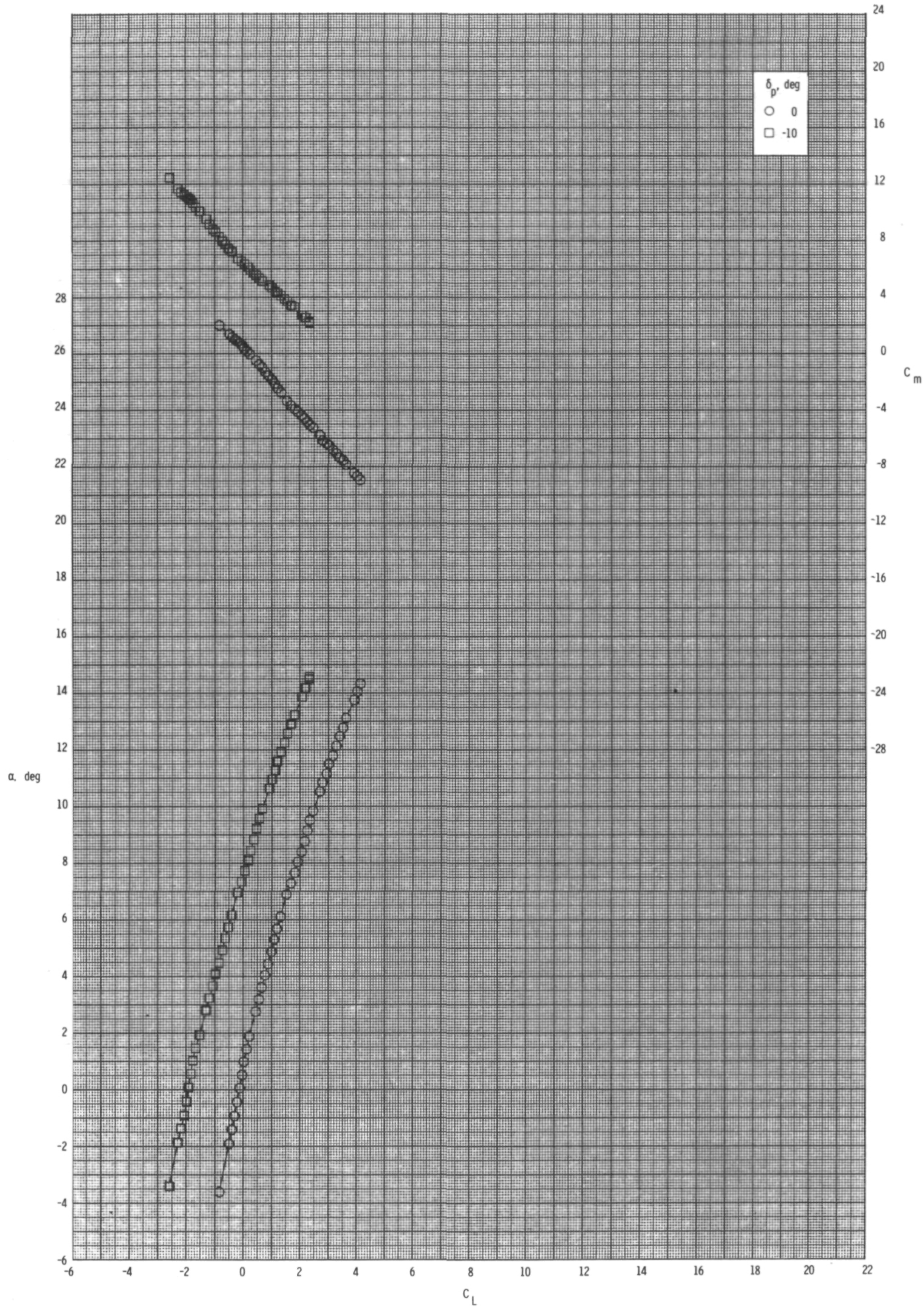

(b) Continued.

Figure 13.- Continued.

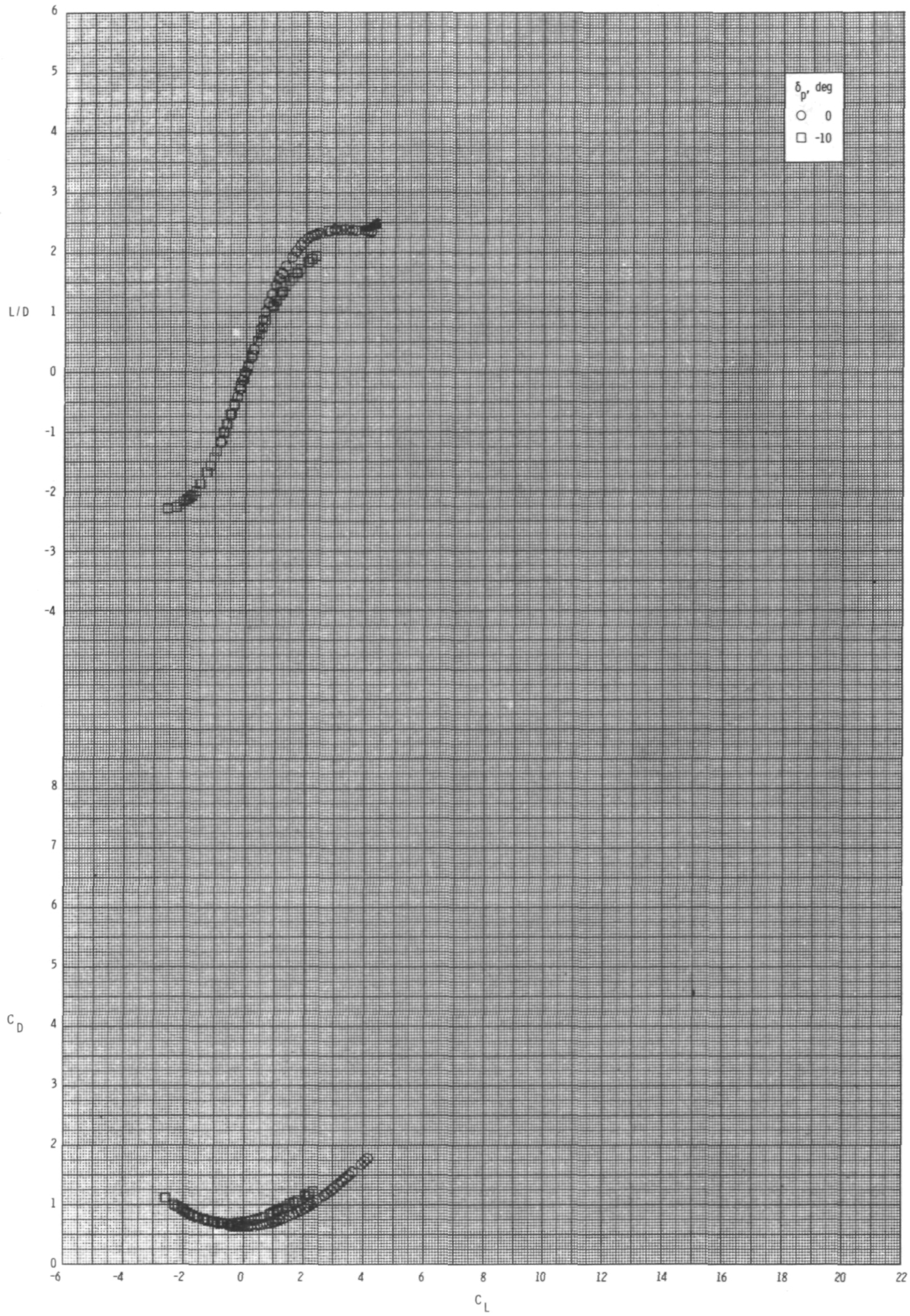

(b) Concluded.

Figure 13.- Continued.

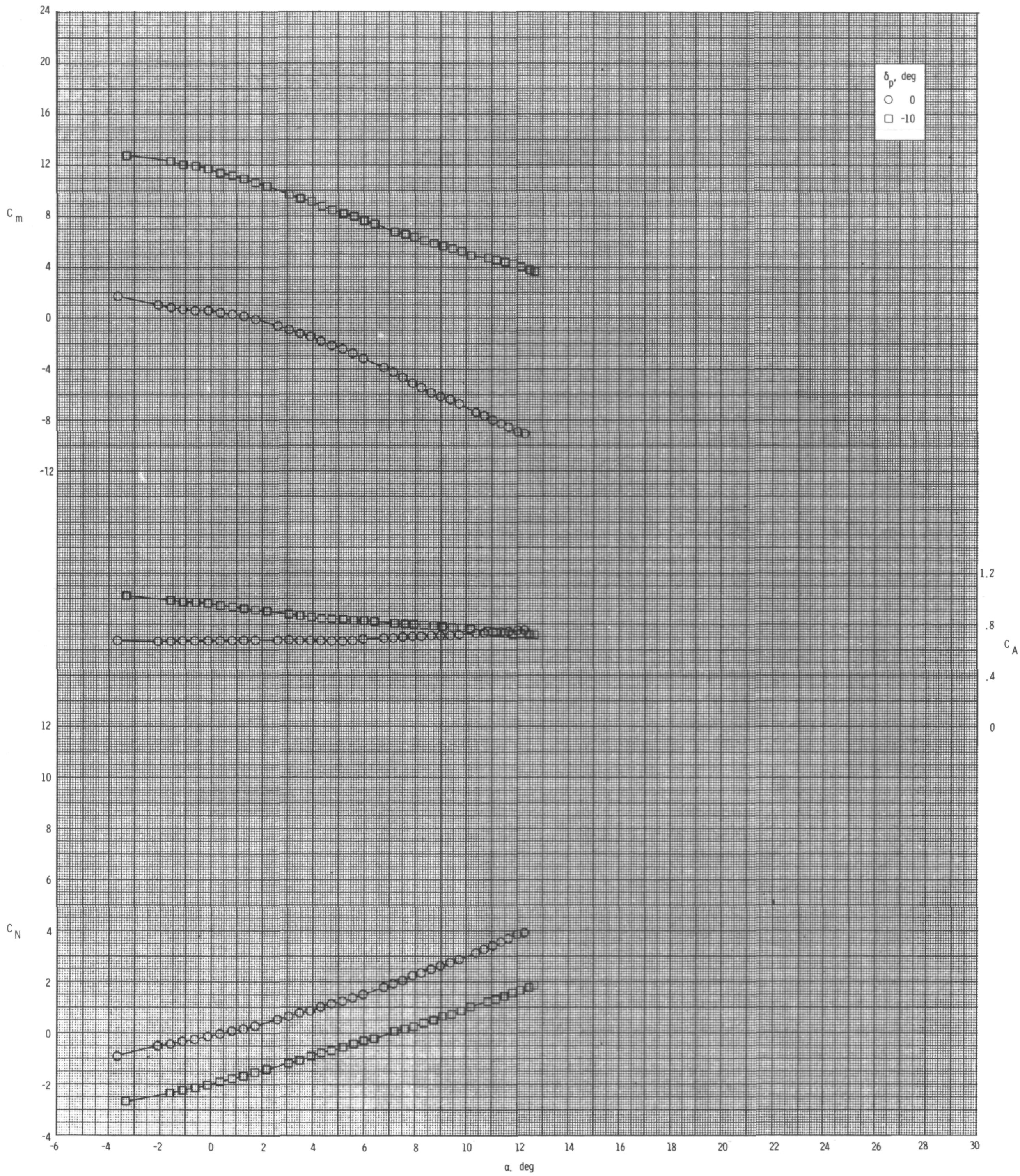

(c) M = 0.95.

Figure 13.- Continued.

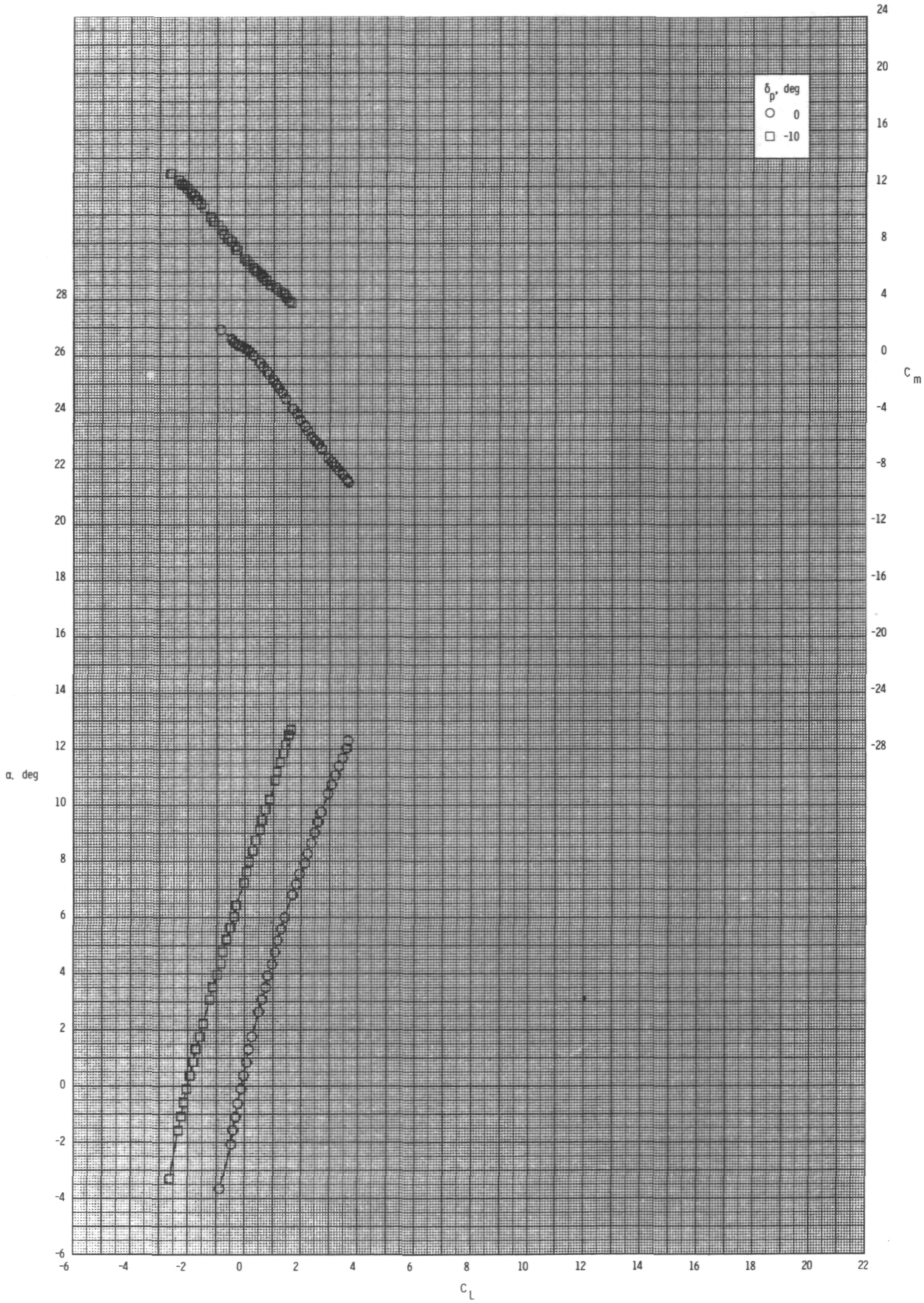

(c) Continued.

Figure 13.- Continued.

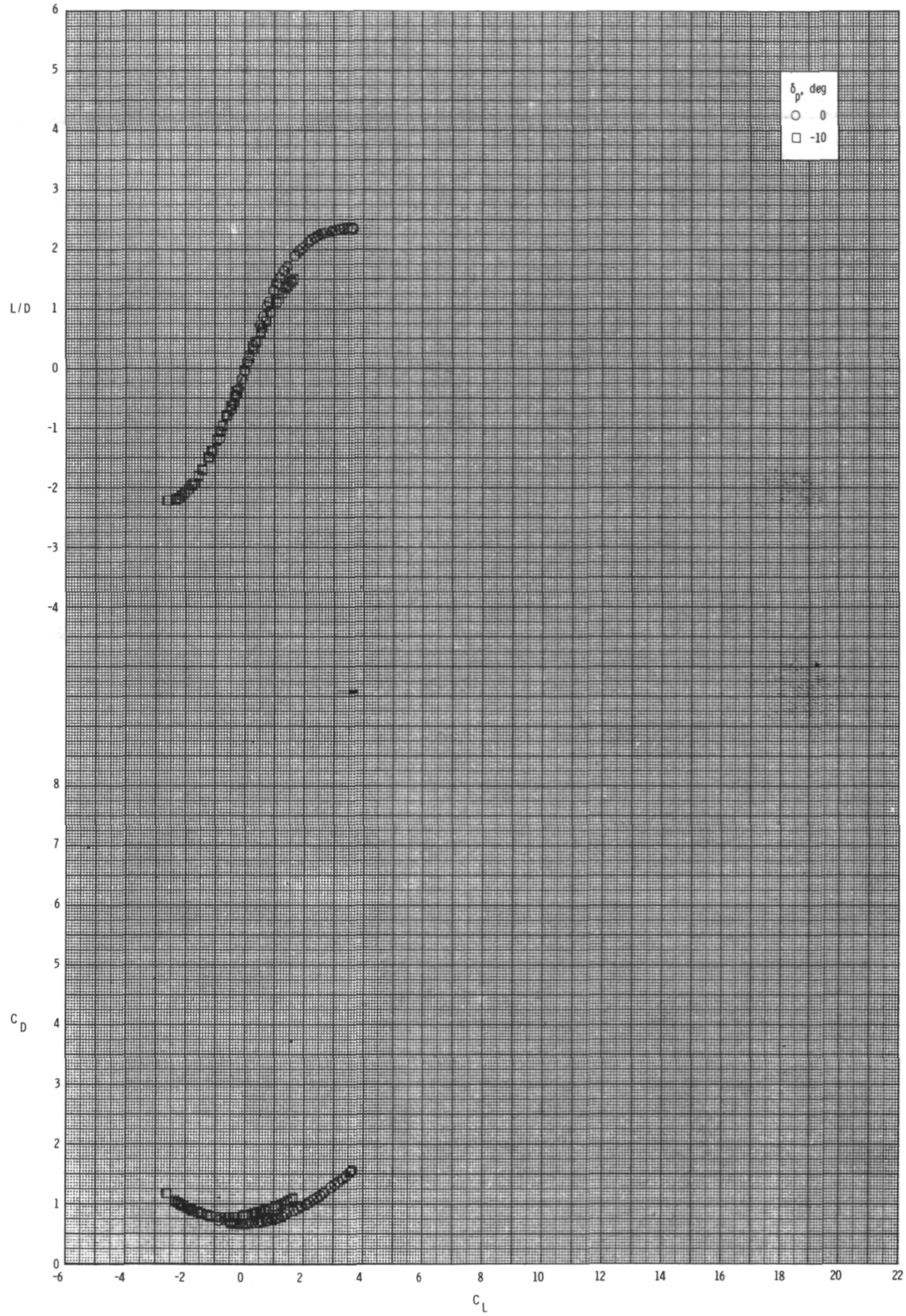

(c) Concluded.

Figure 13.- Concluded.

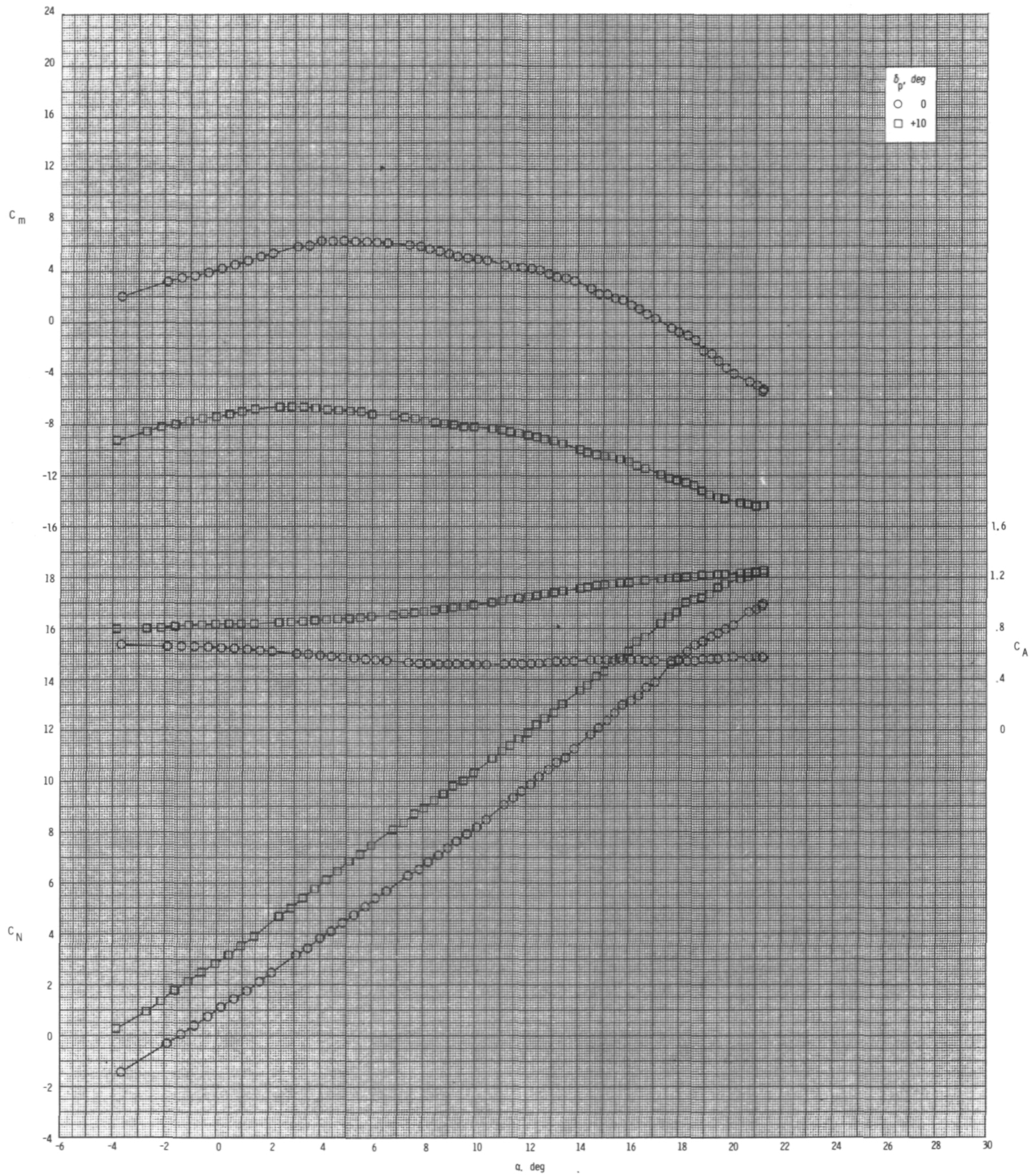

(a) M = 0.60.

Figure 14.- Pitch-control effectiveness for configuration $B_1I_1W_1T_1$ with internal ducts closed and ϕ_I = 115°.

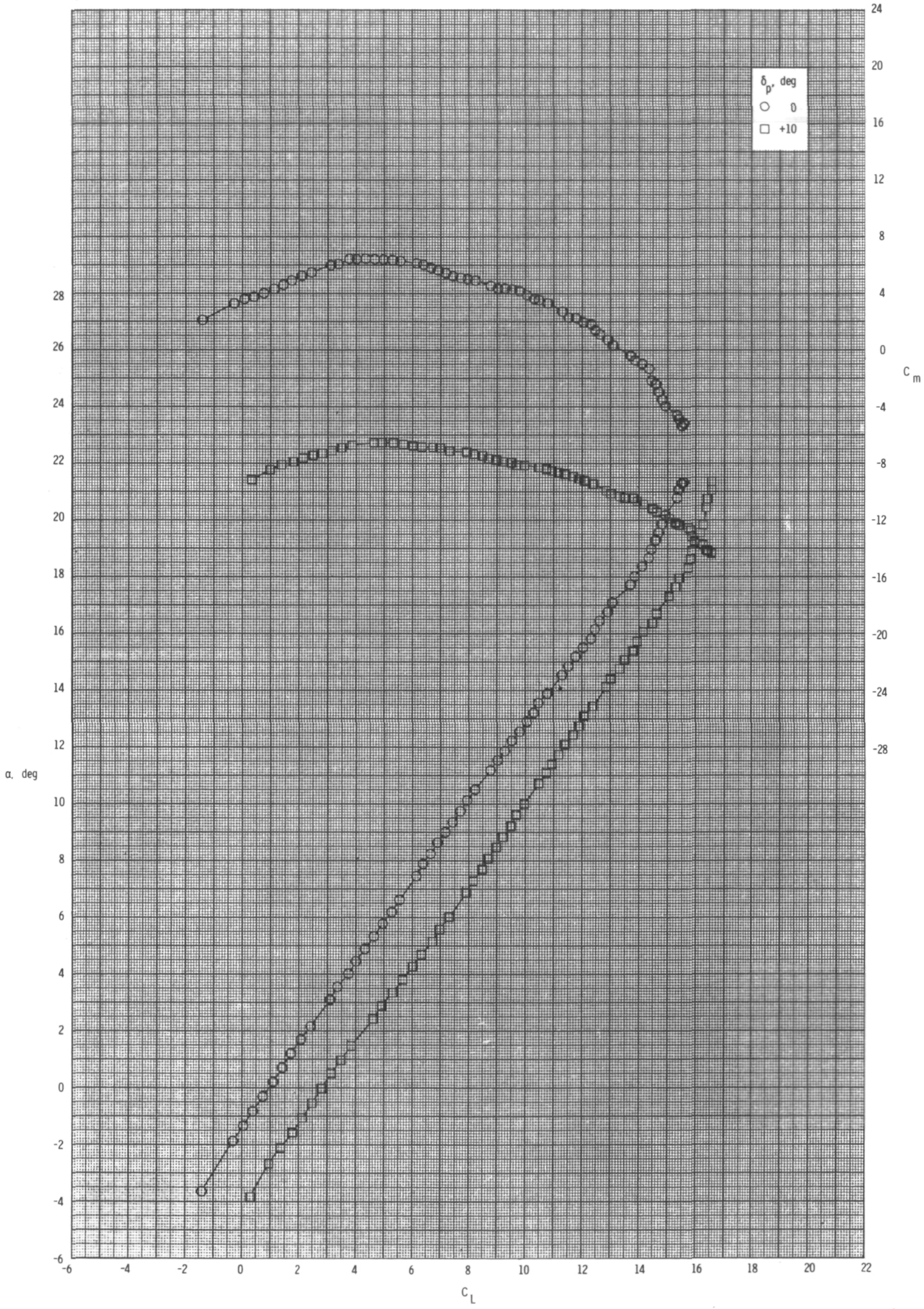

(a) Continued.

Figure 14.- Continued.

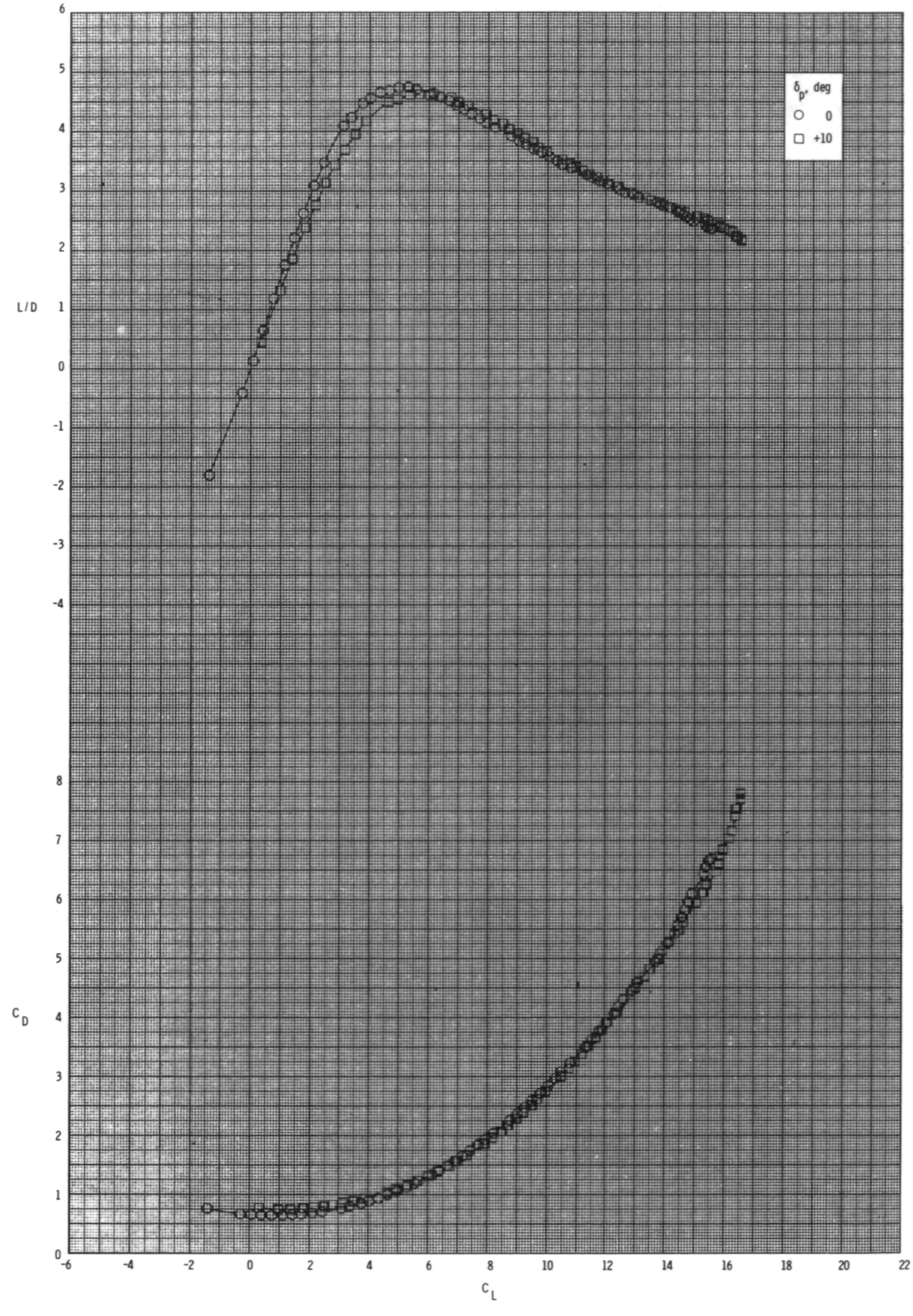

(a) Concluded.

Figure 14.- Continued.

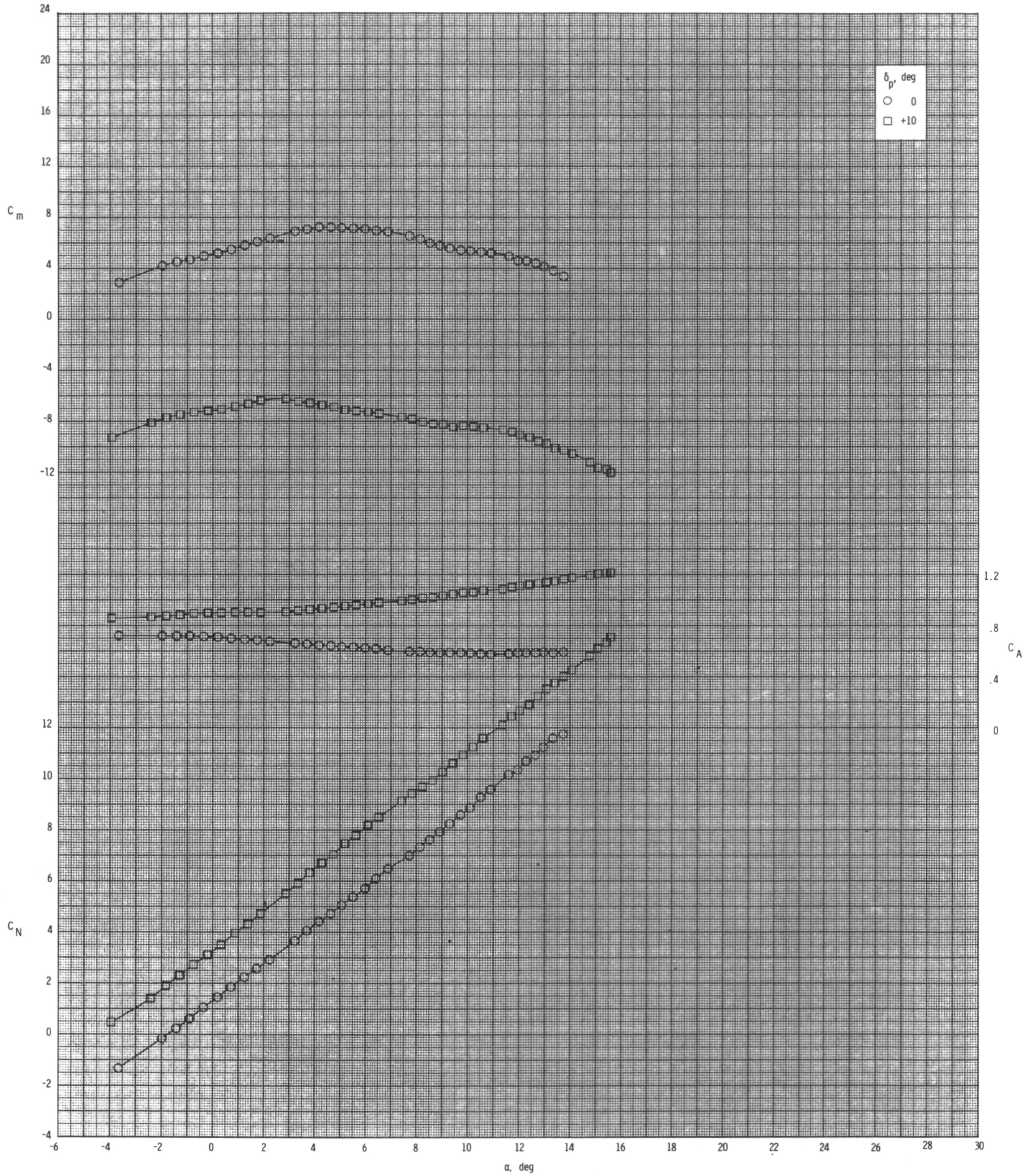

(b) M = 0.80.

Figure 14.- Continued.

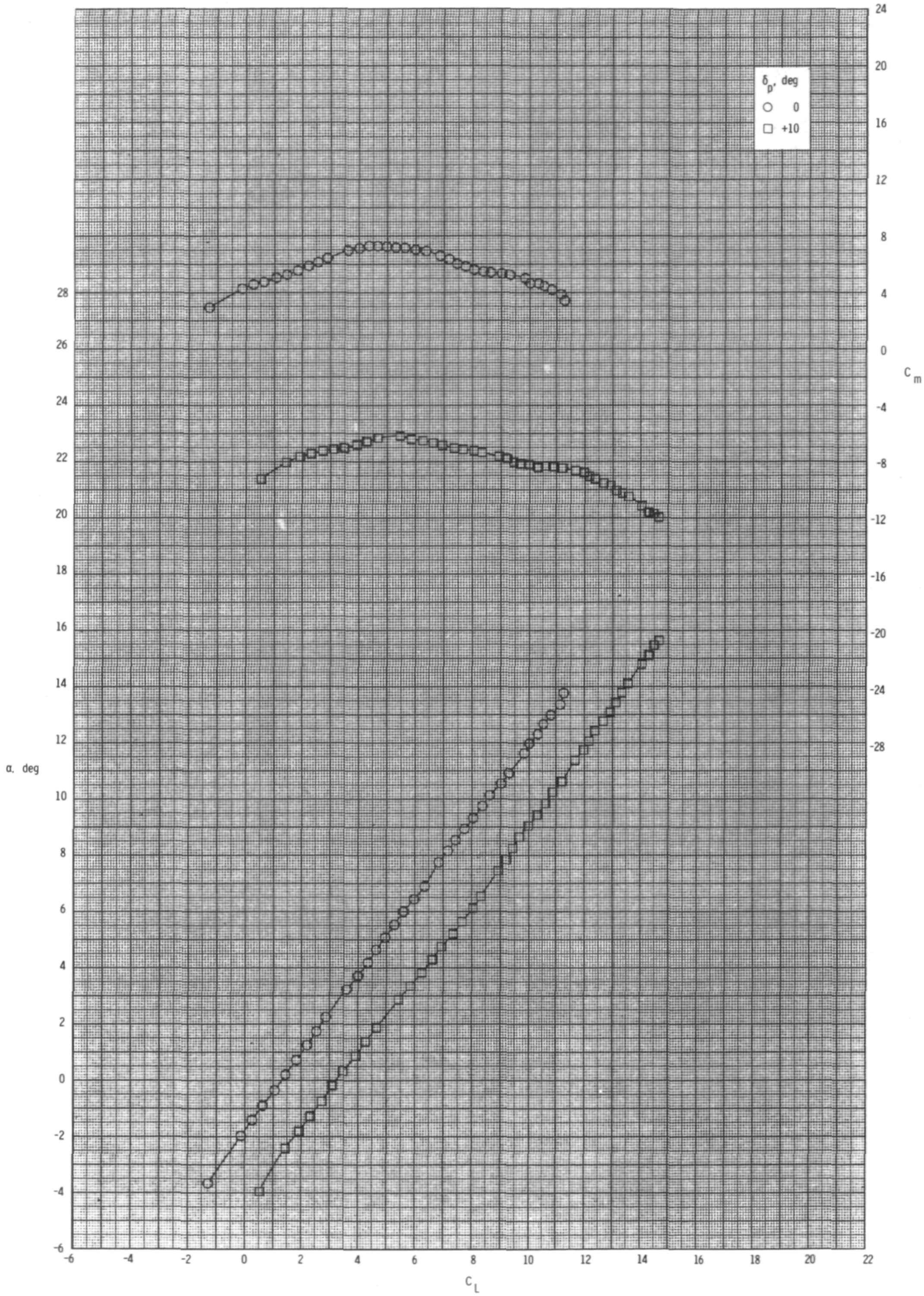

(b) Continued.

Figure 14.- Continued.

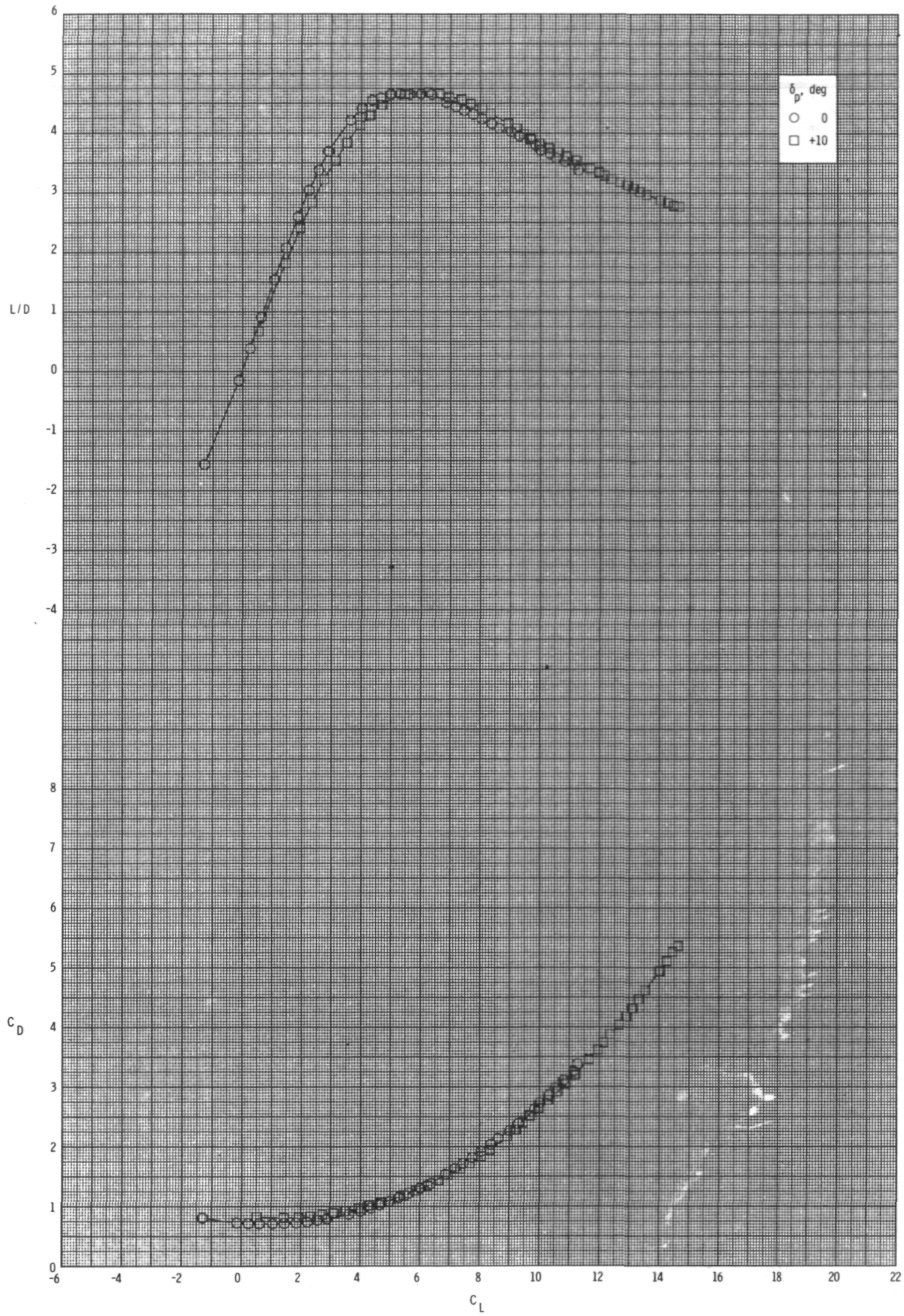

(b) Concluded.

Figure 14.- Continued.

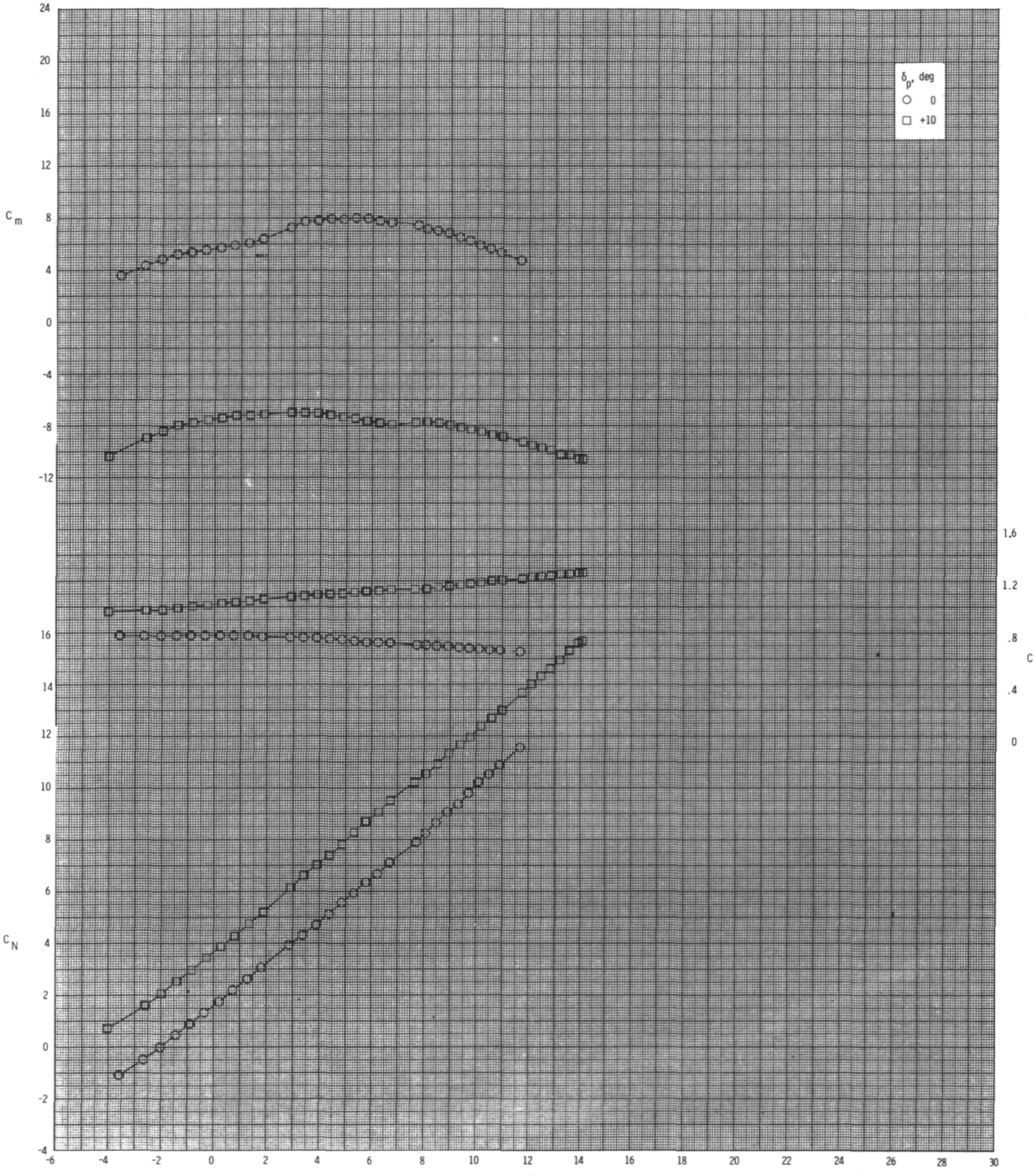

(c) M = 0.95.

Figure 14.- Continued.

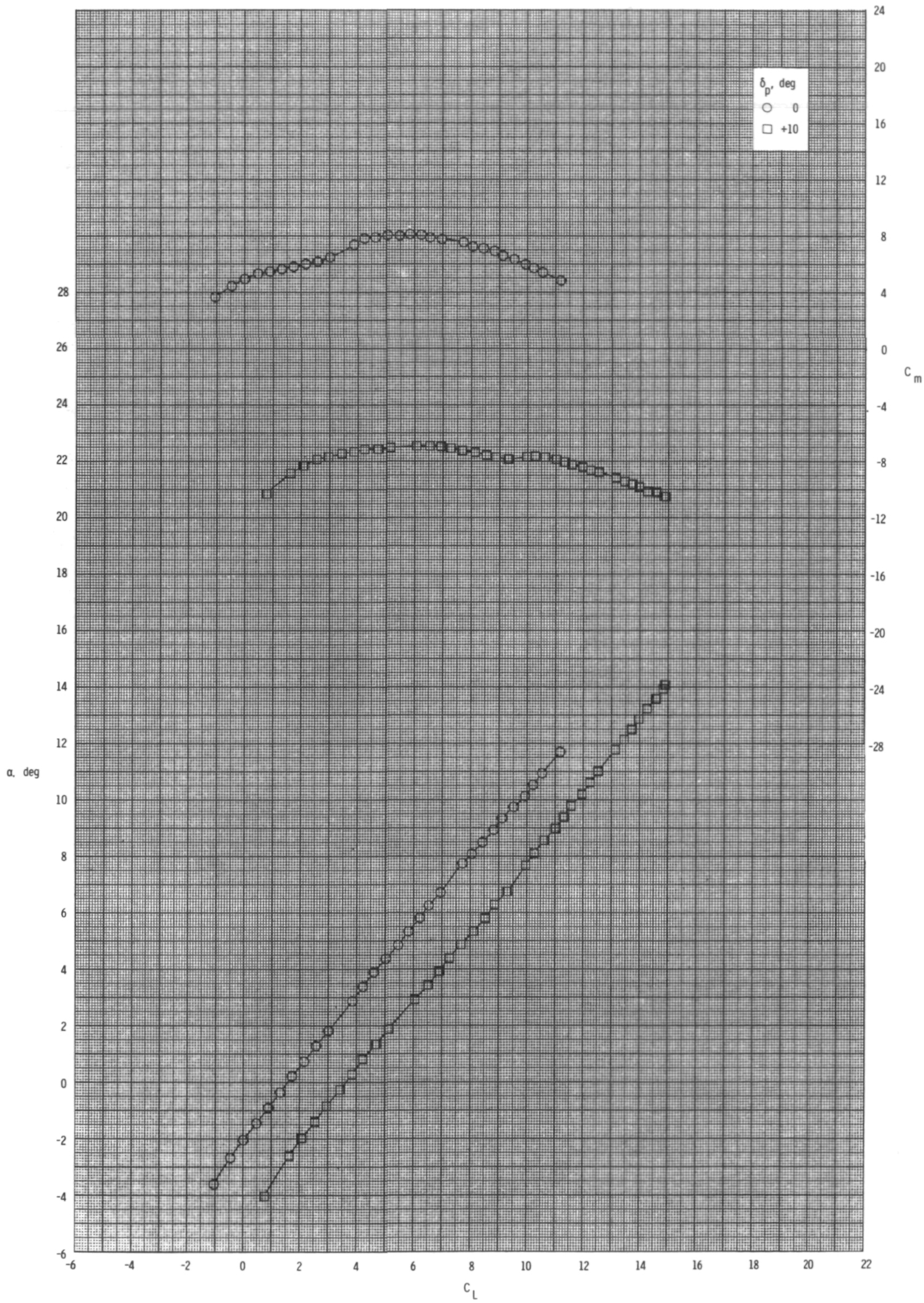

(c) Continued.

Figure 14.- Continued.

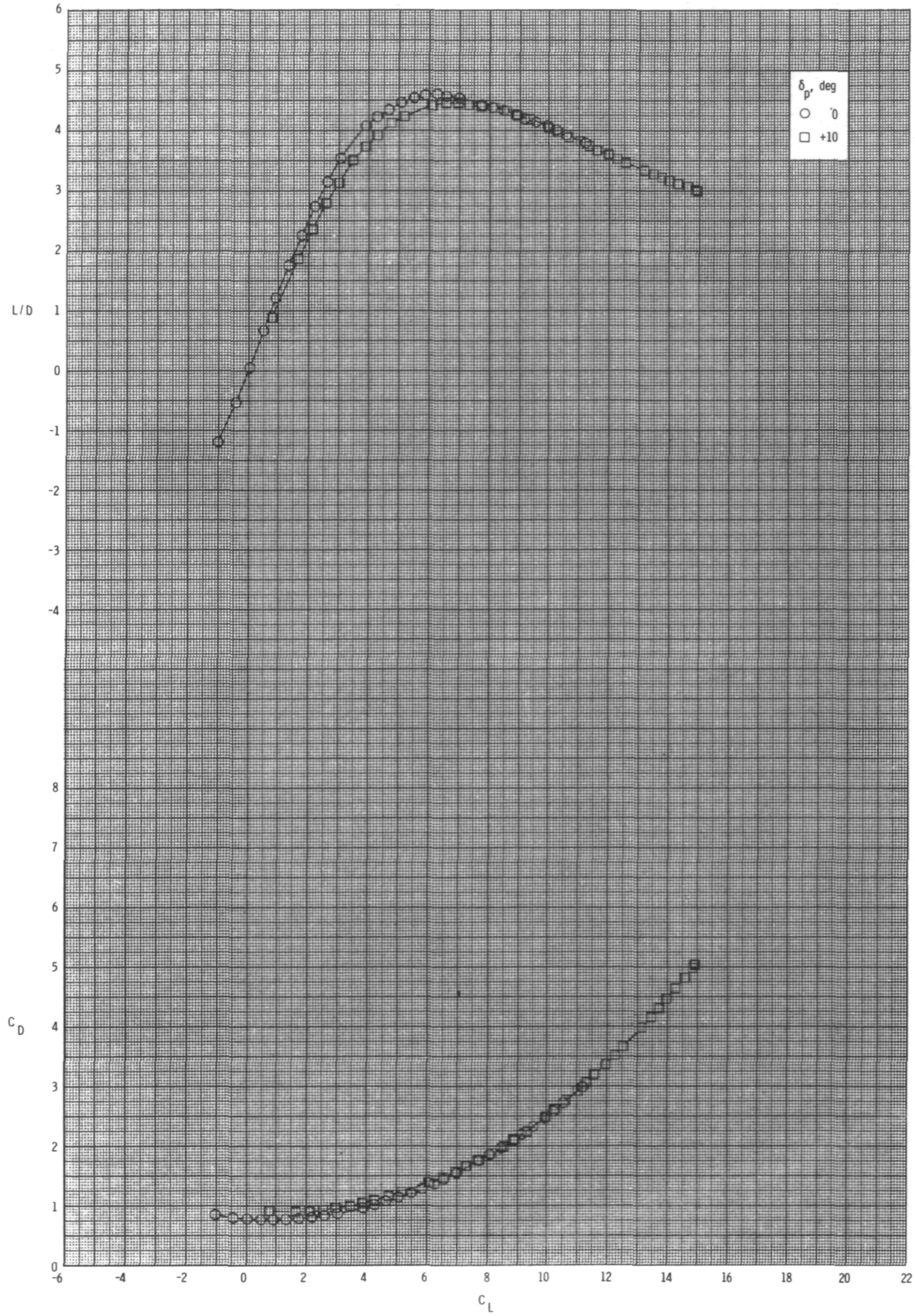

(c) Concluded.

Figure 14.- Concluded.

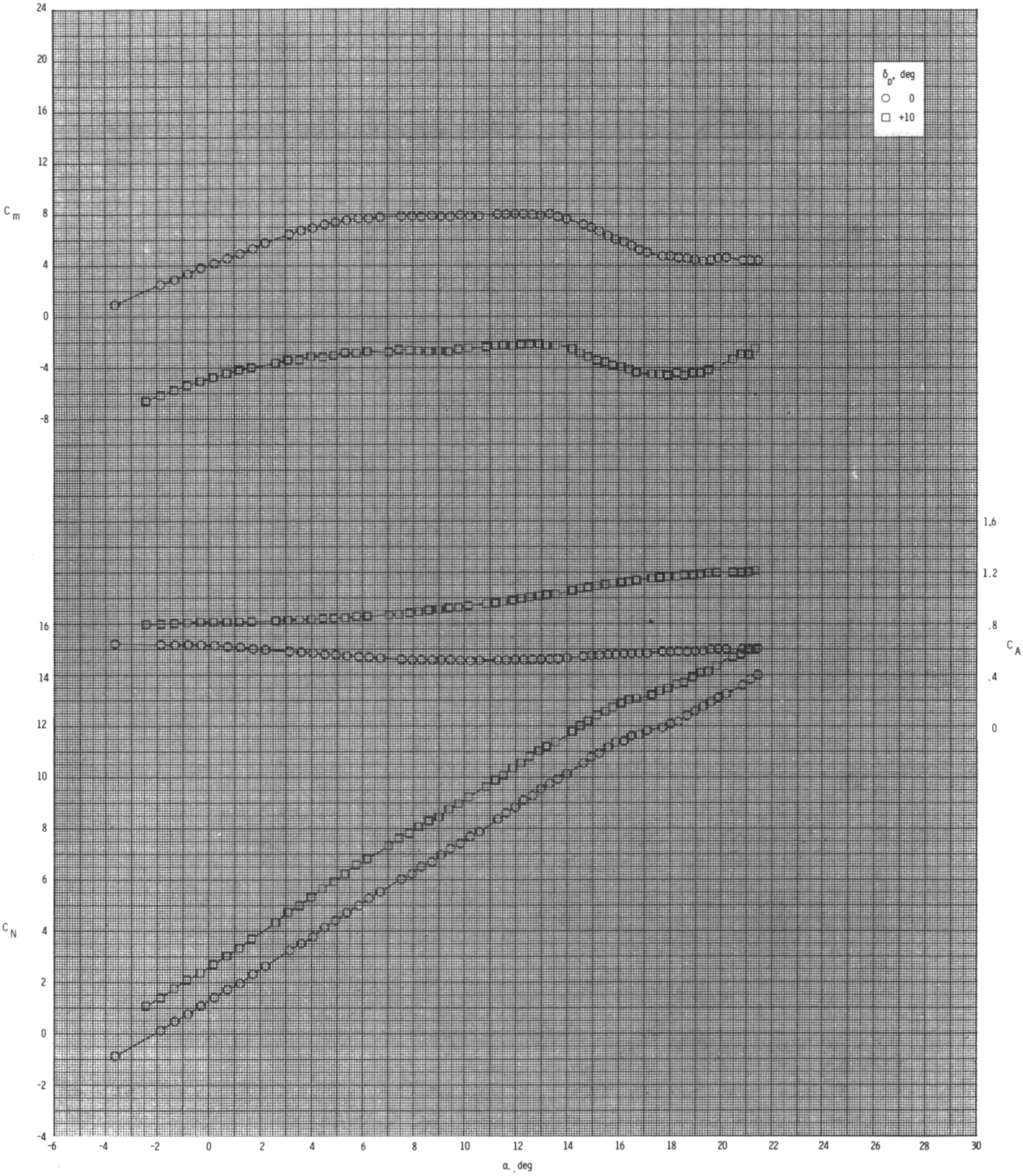

(a) M = 0.60.

Figure 15.- Pitch-control effectiveness for configuration $B_1I_1W_1T_1$ with internal ducts closed and ϕ_I = 135°.

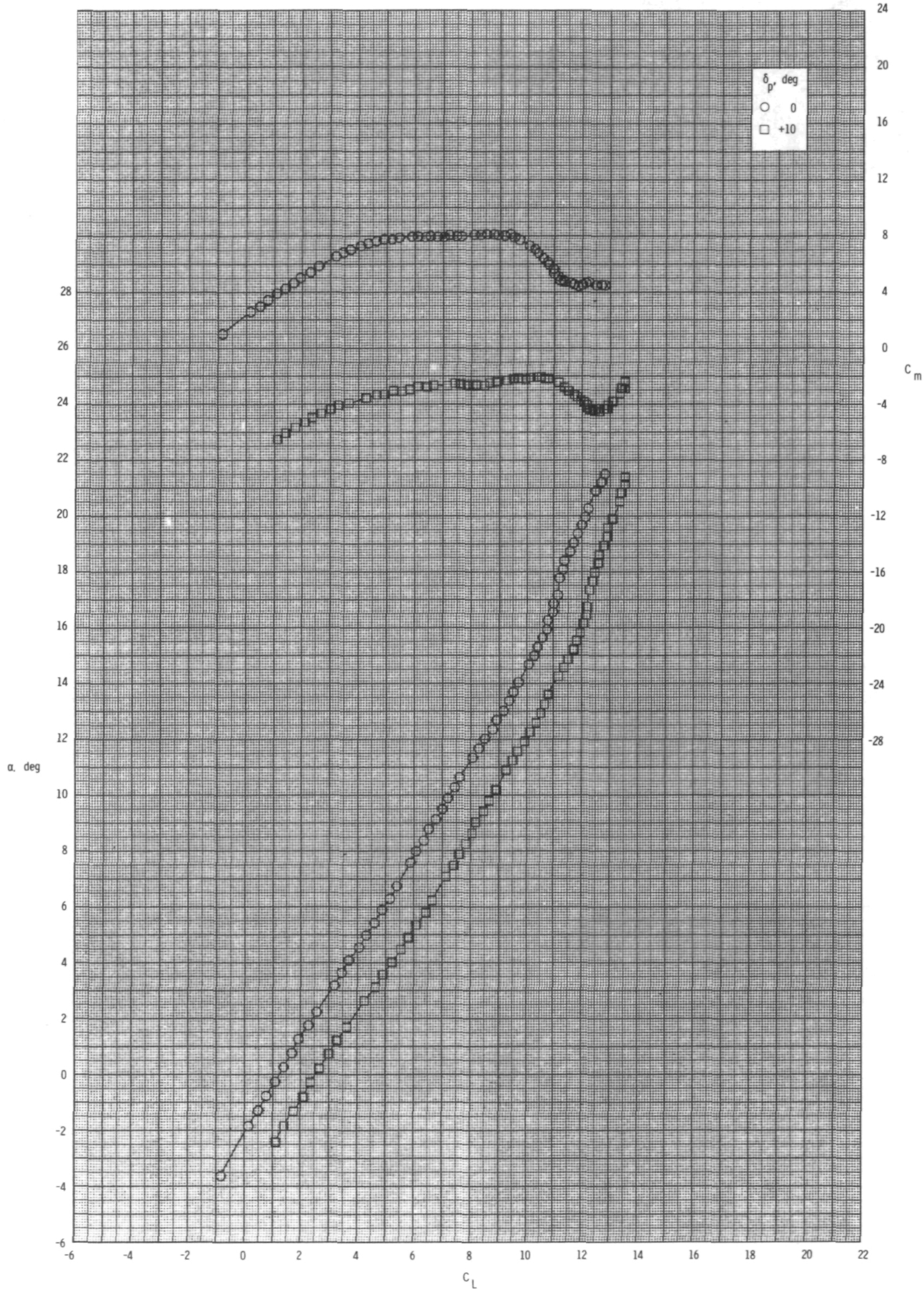

(a) Continued.

Figure 15.- Continued.

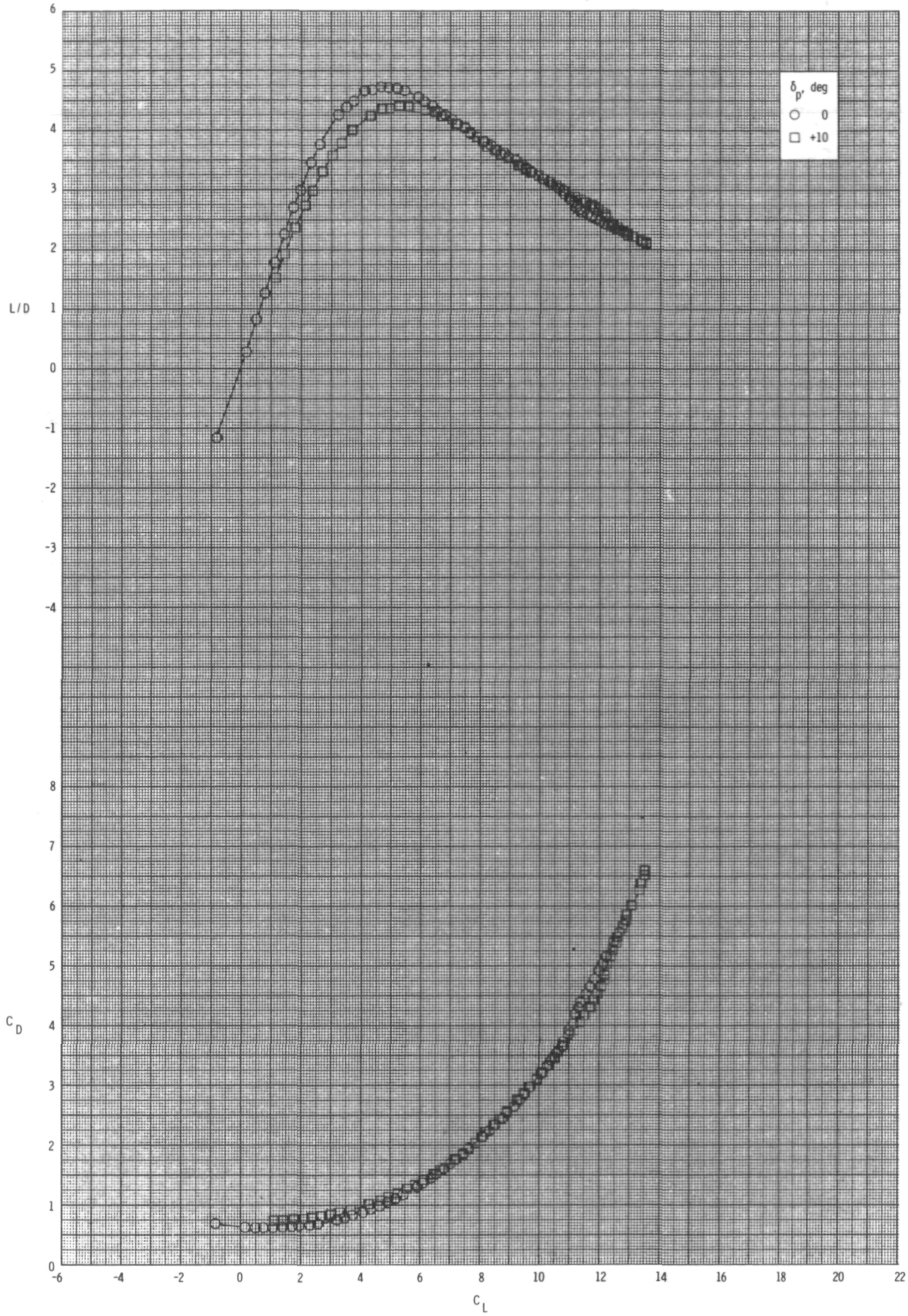

(a) Concluded.

Figure 15.- Continued.

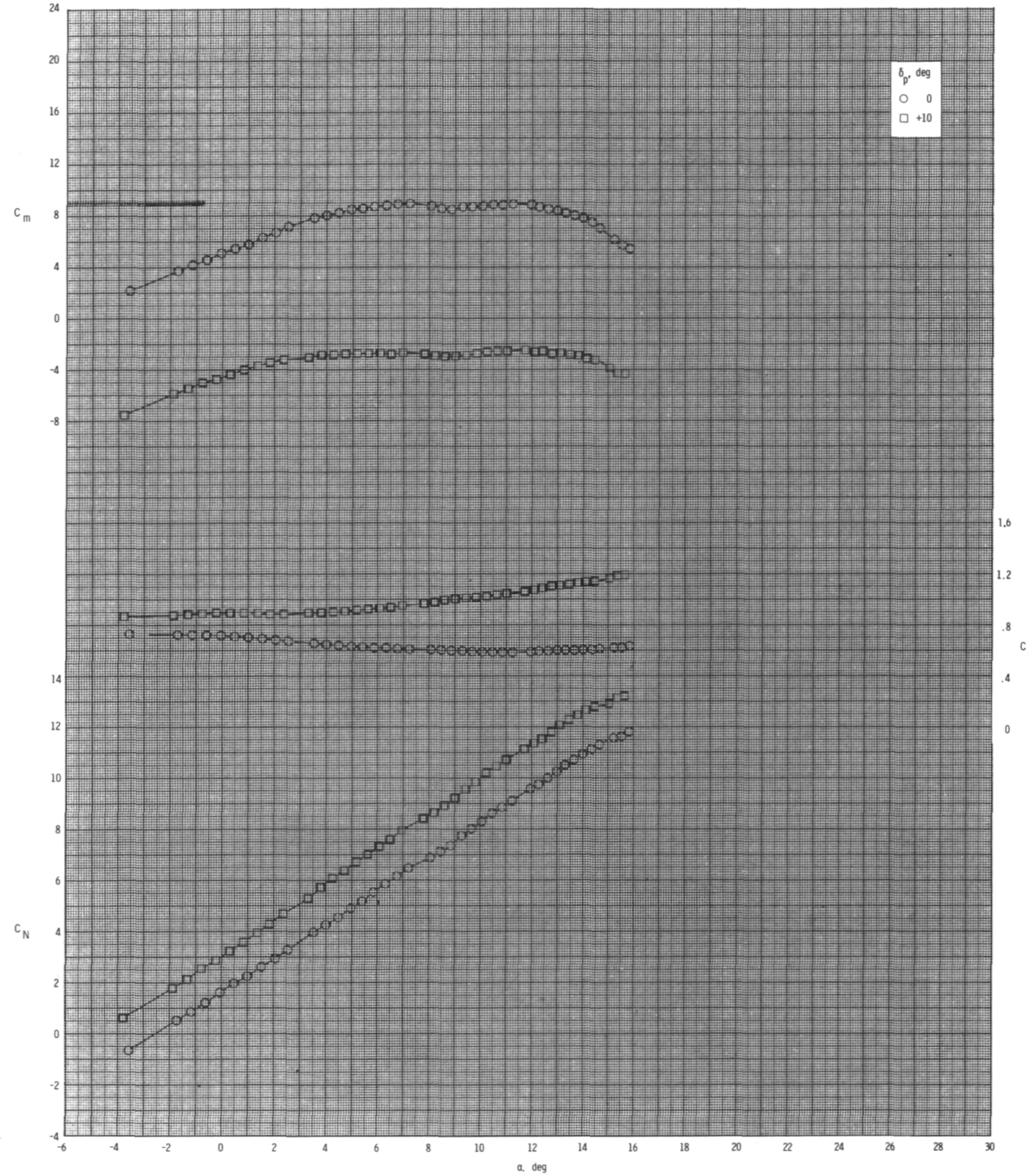

(b) M = 0.80.

Figure 15.- Continued.

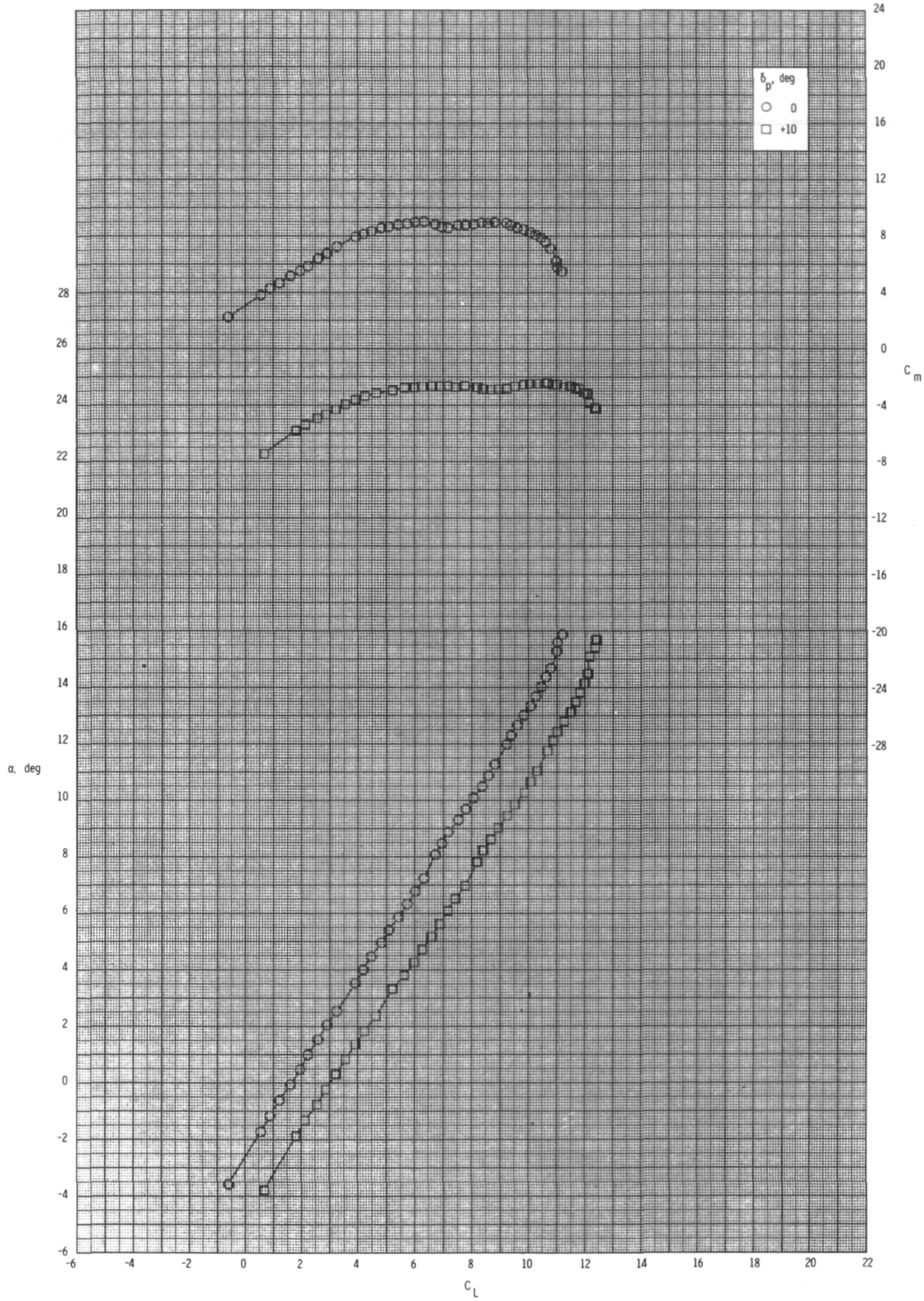

(b) Continued.

Figure 15.- Continued.

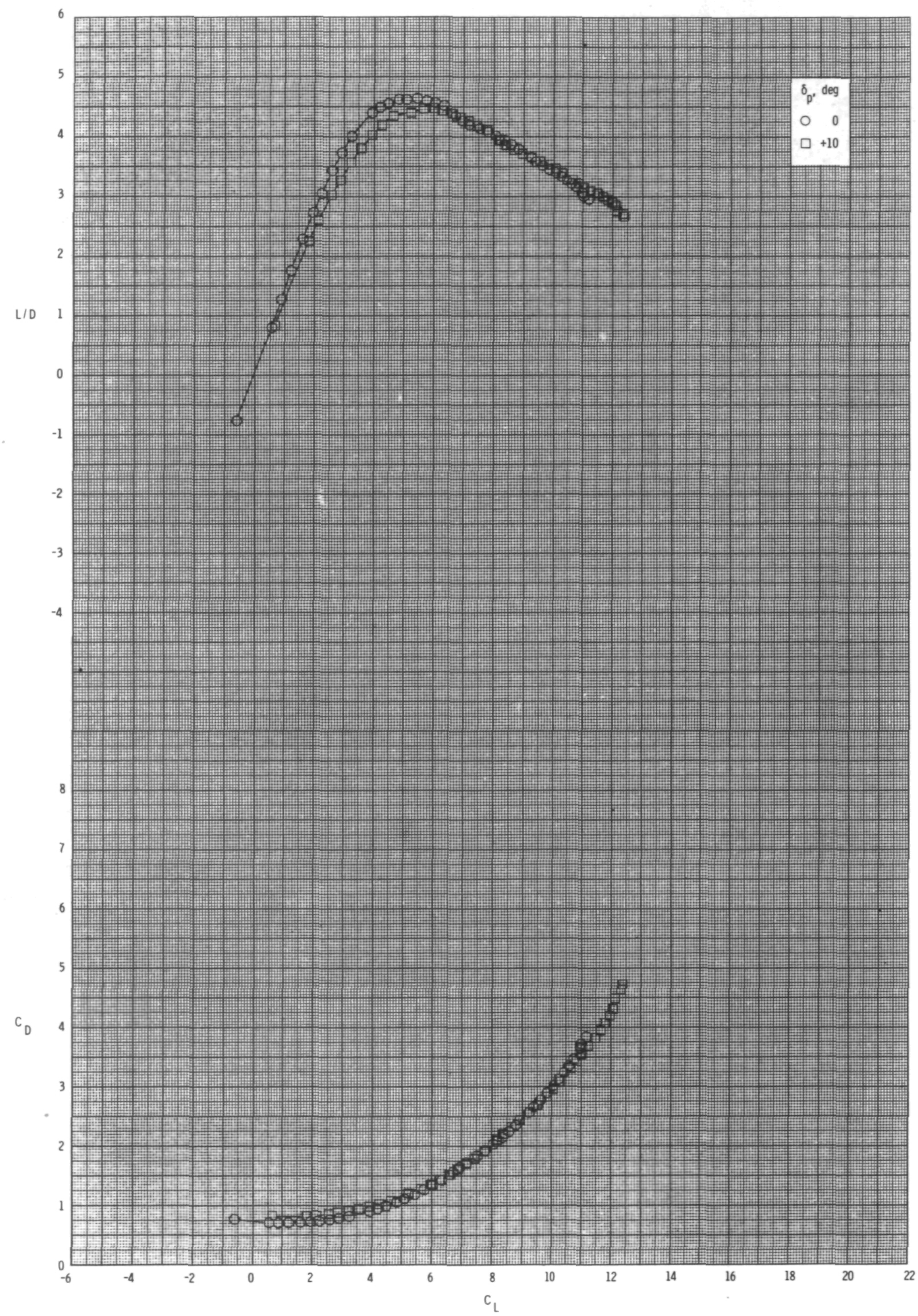

(b) Concluded.

Figure 15.- Continued.

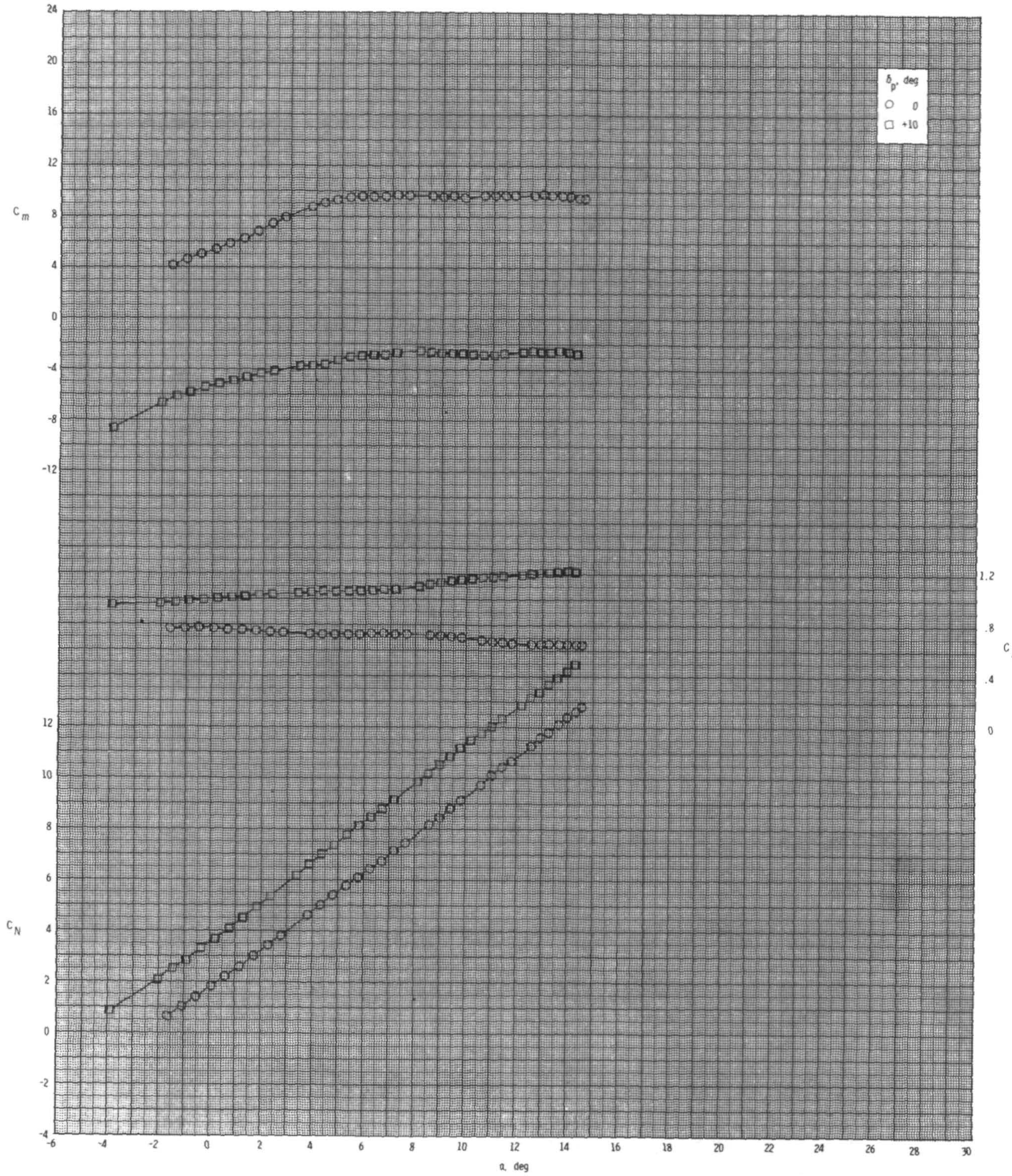

(c) M = 0.95.

Figure 15.- Continued.

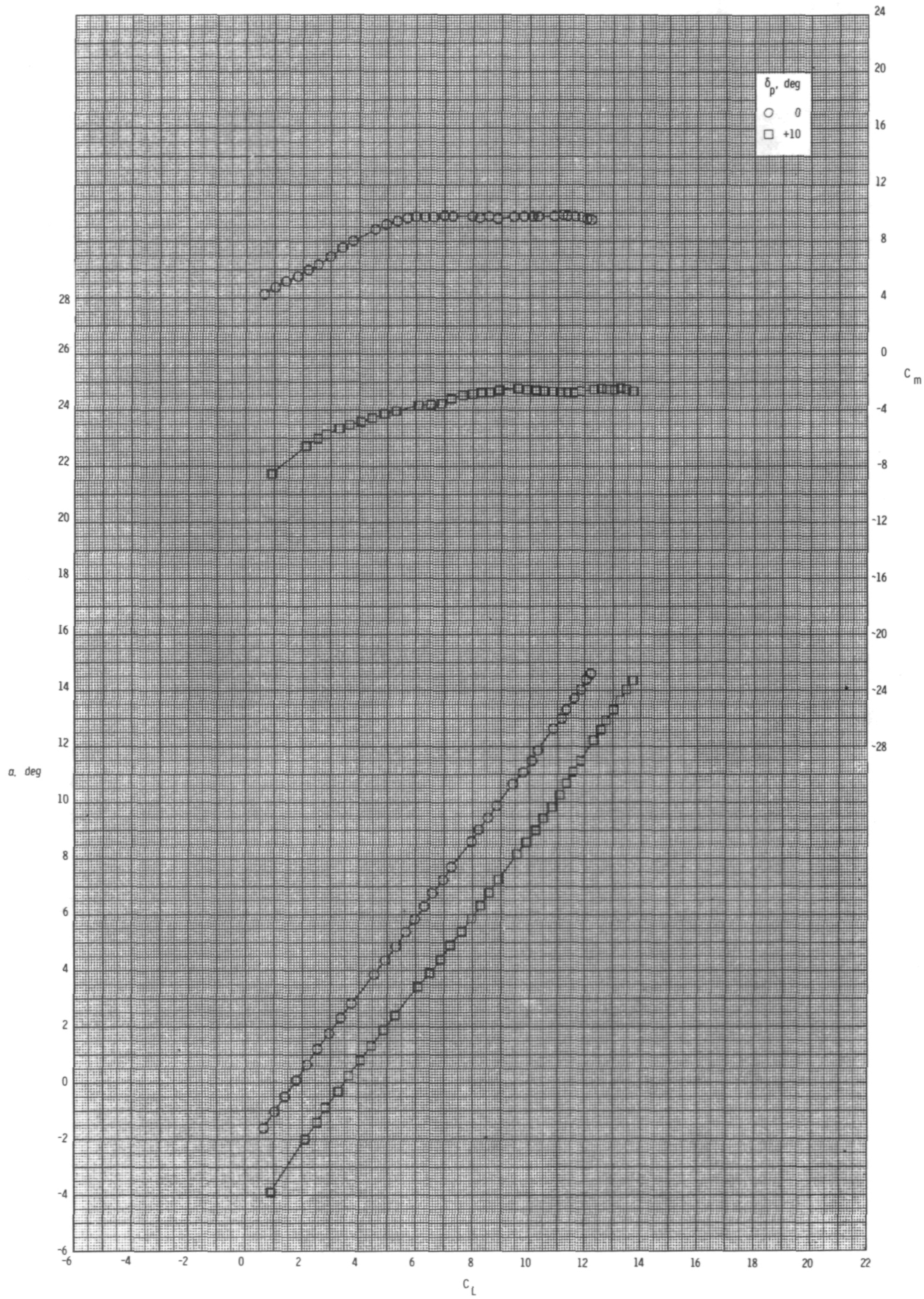

(c) Continued.

Figure 15.- Continued.

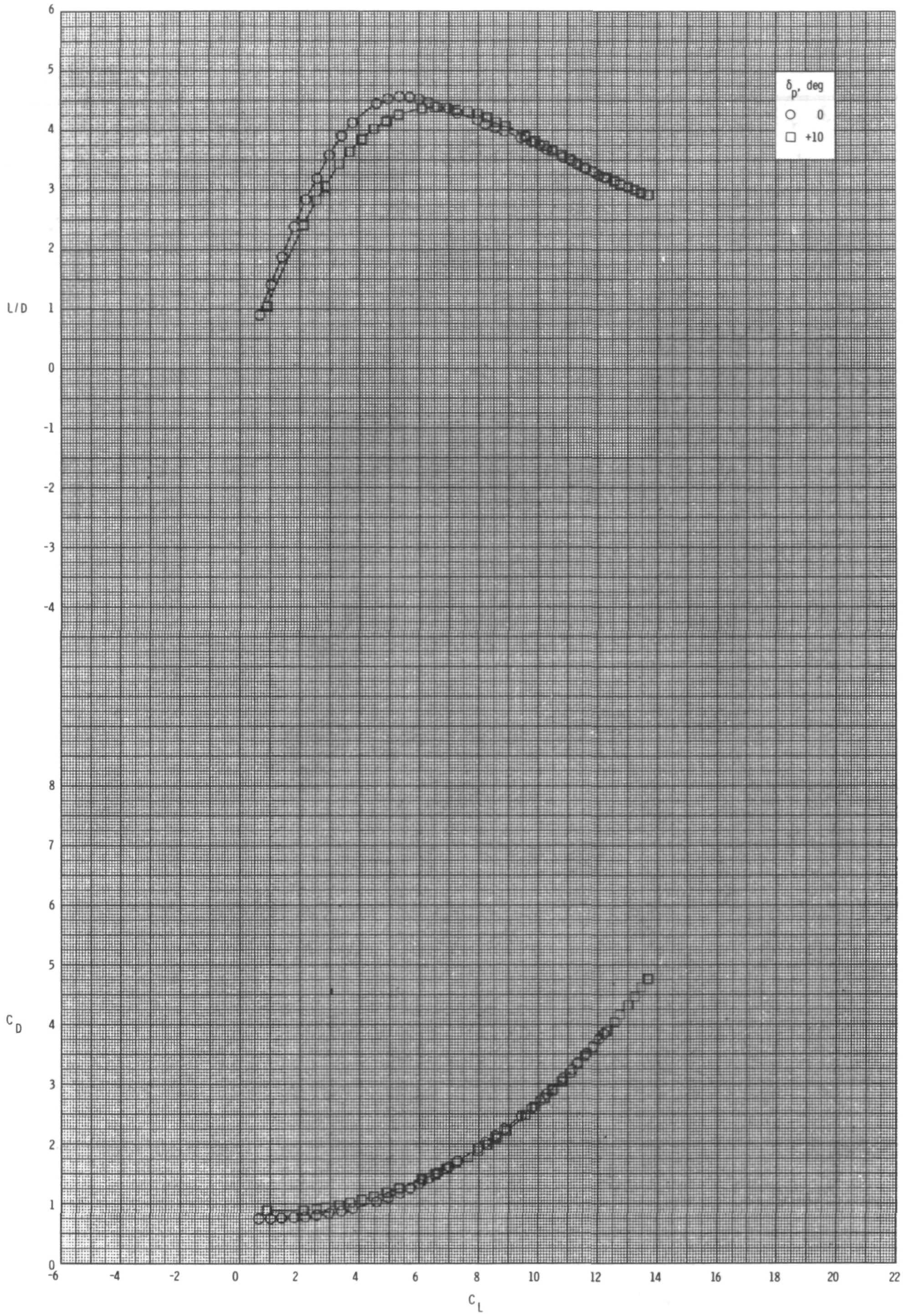

(c) Concluded.

Figure 15.- Concluded.

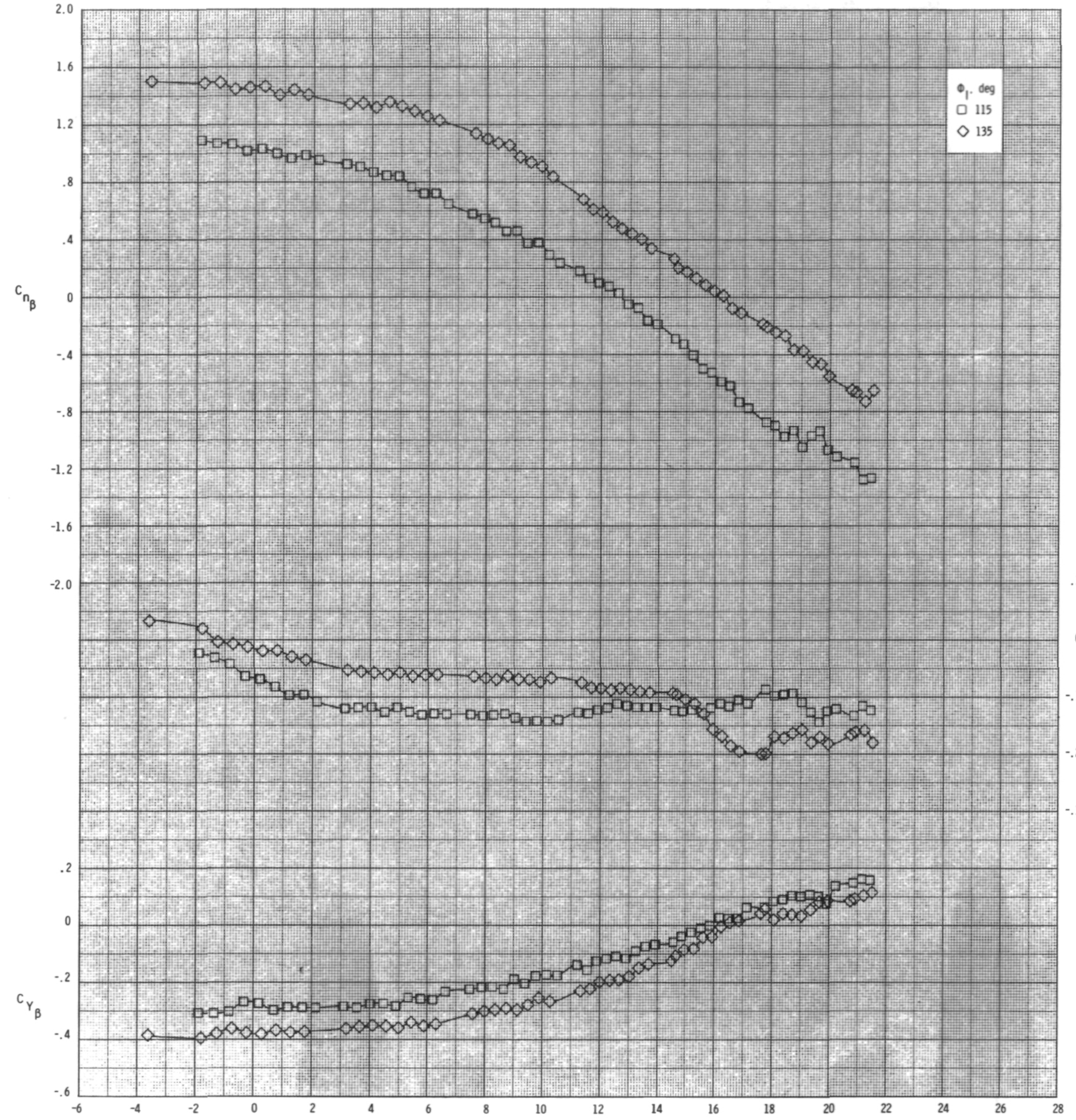

(a) M = 0.60.

Figure 16.- Effect of inlet orientation angle ϕ_I on lateral-directional stability for configuration $B_1I_1W_1T_1$ with internal ducts closed and $\delta_p = 0°$.

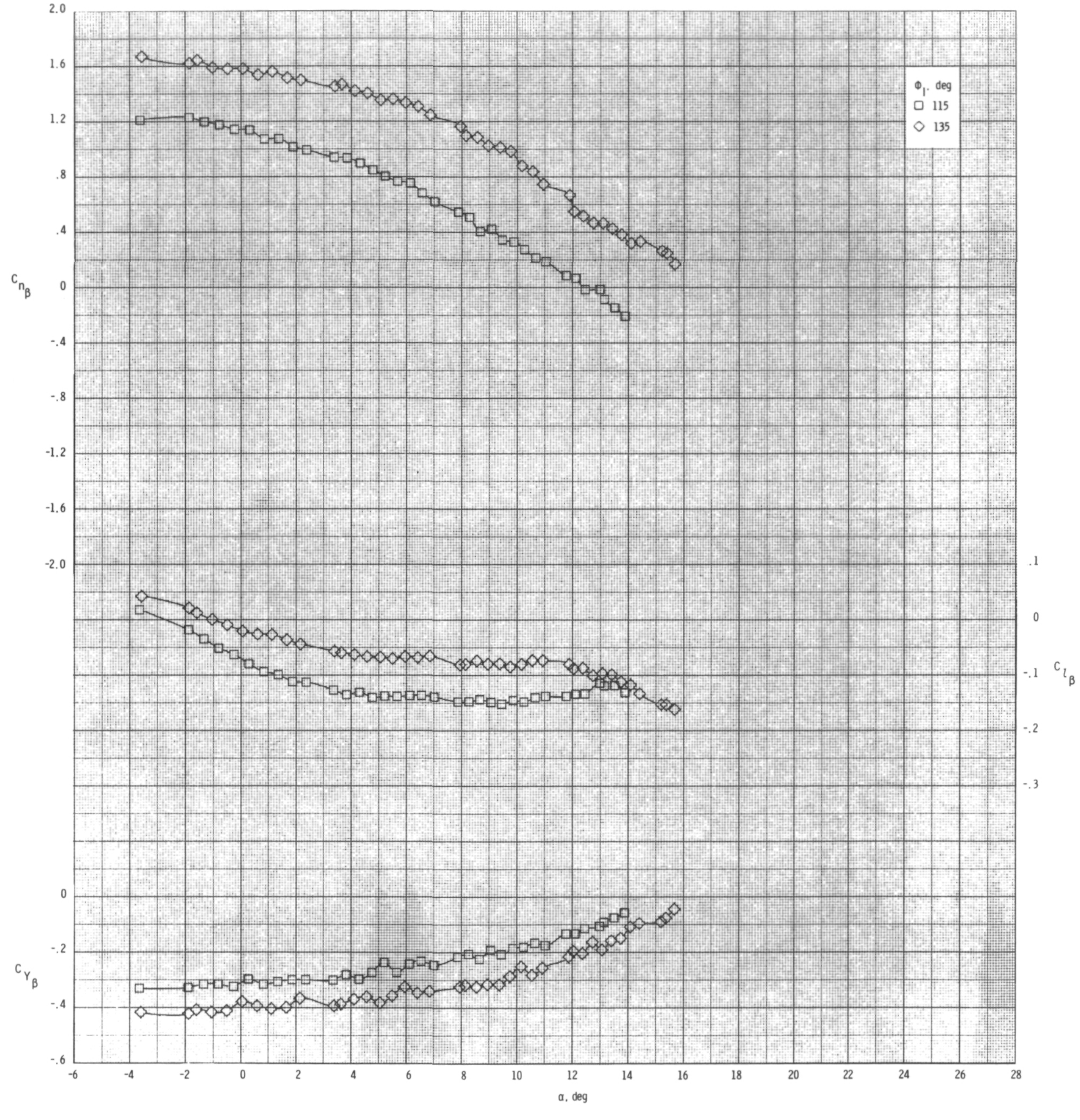

(b) M = 0.80.

Figure 16.- Continued.

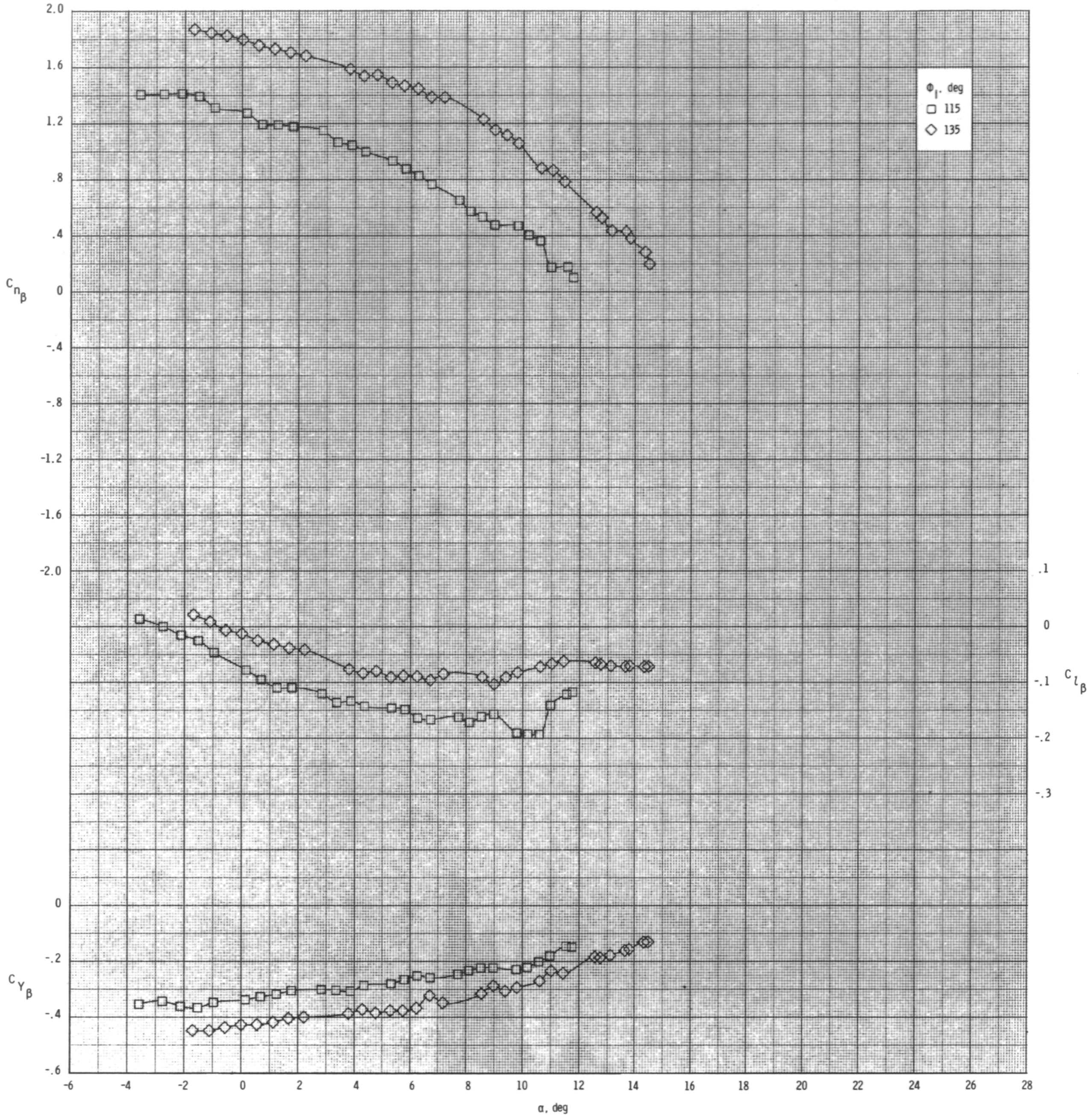

(c) M = 0.95.

Figure 16.- Concluded.

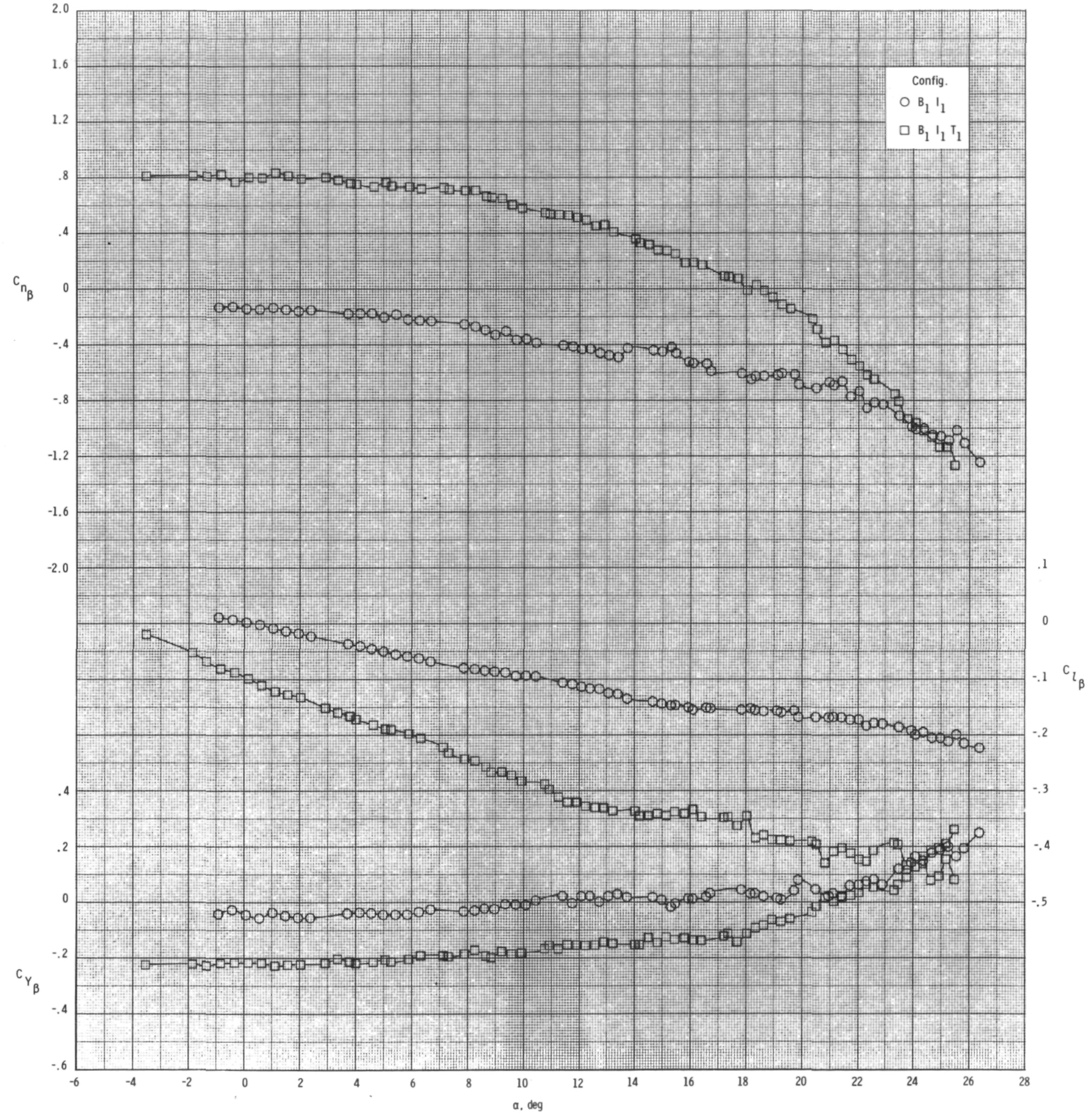

(a) M = 0.60.

Figure 17.- Effect of various model components on lateral-directional stability for axisymmetric inlets with internal ducts closed, $\phi_I = 90°$, and $\delta_p = 0°$.

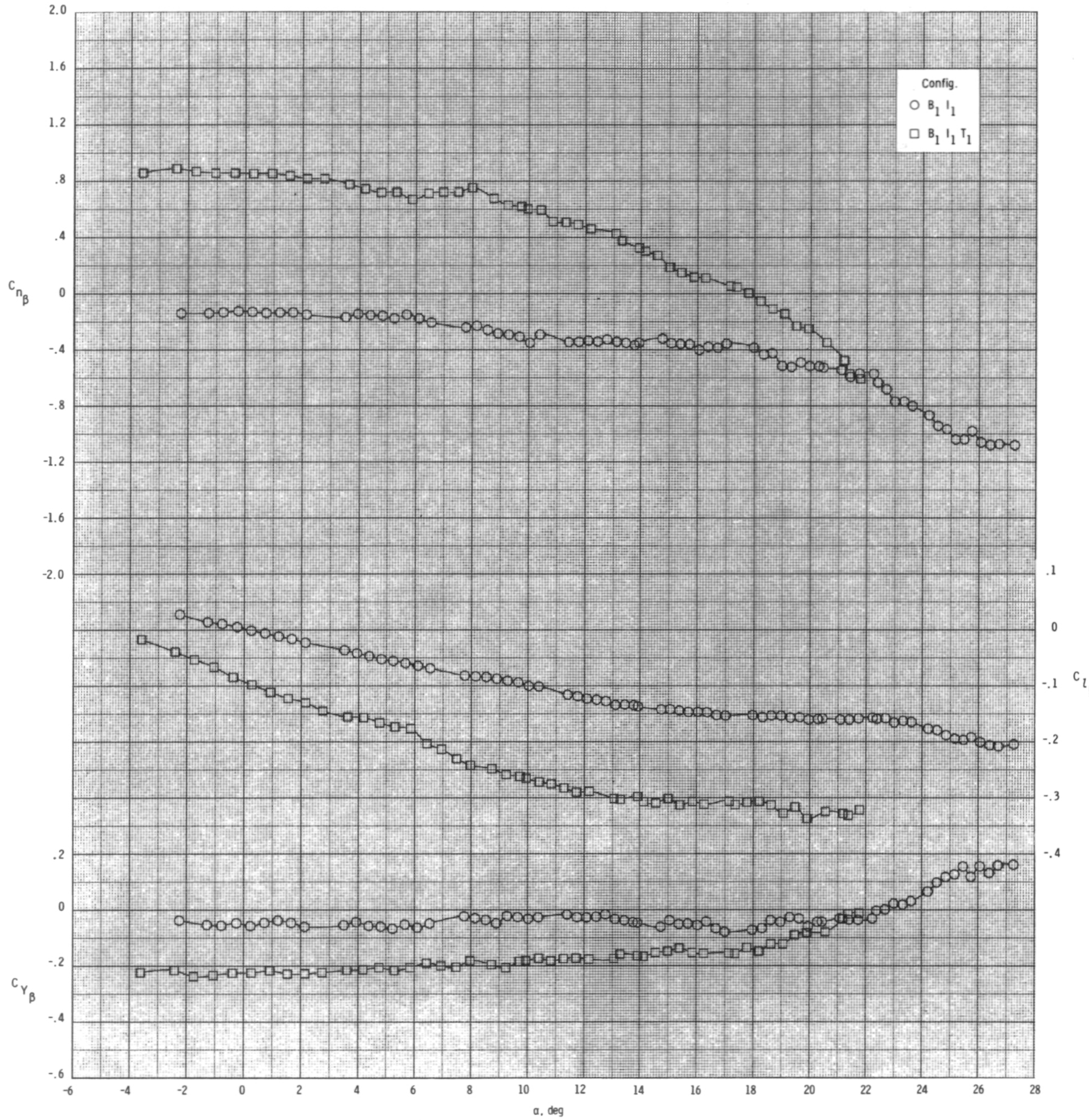

(b) M = 0.80.

Figure 17.- Continued.

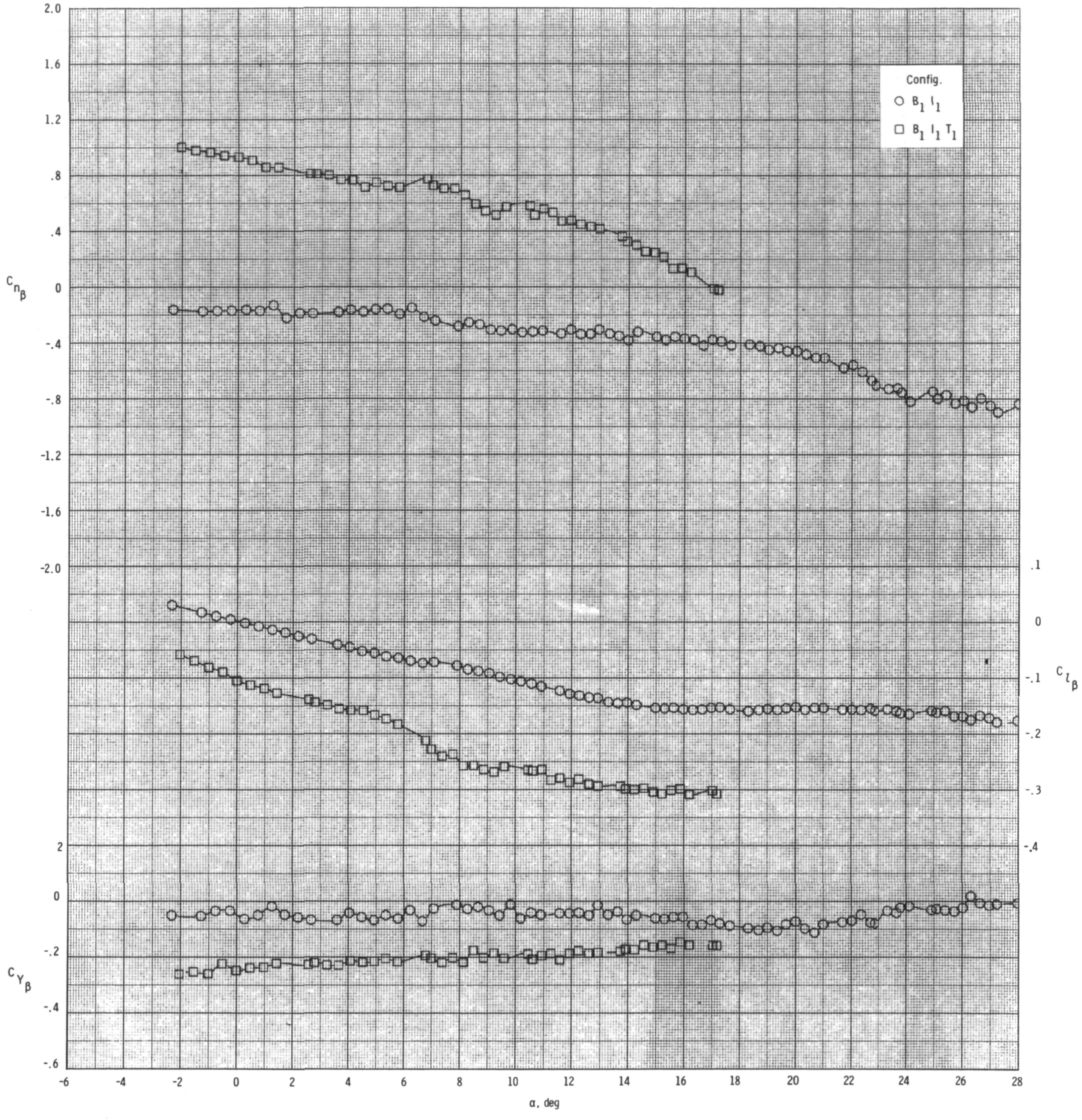

(c) M = 0.95.

Figure 17.- Concluded.

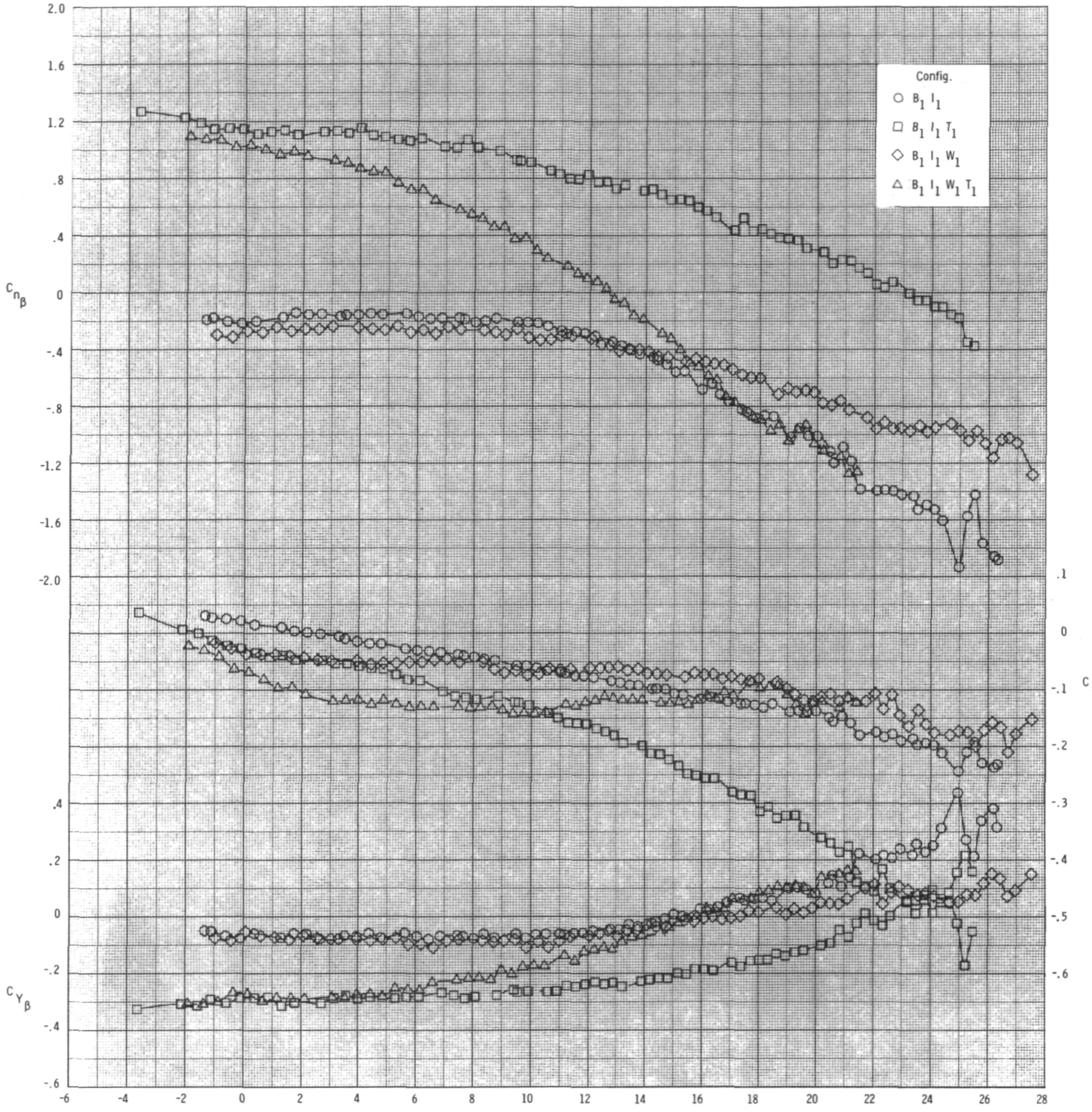

(a) M = 0.60.

Figure 18.- Effect of various model components on lateral-directional stability for axisymmetric inlets with internal ducts closed, $\phi_I = 115°$, and $\delta_p = 0°$.

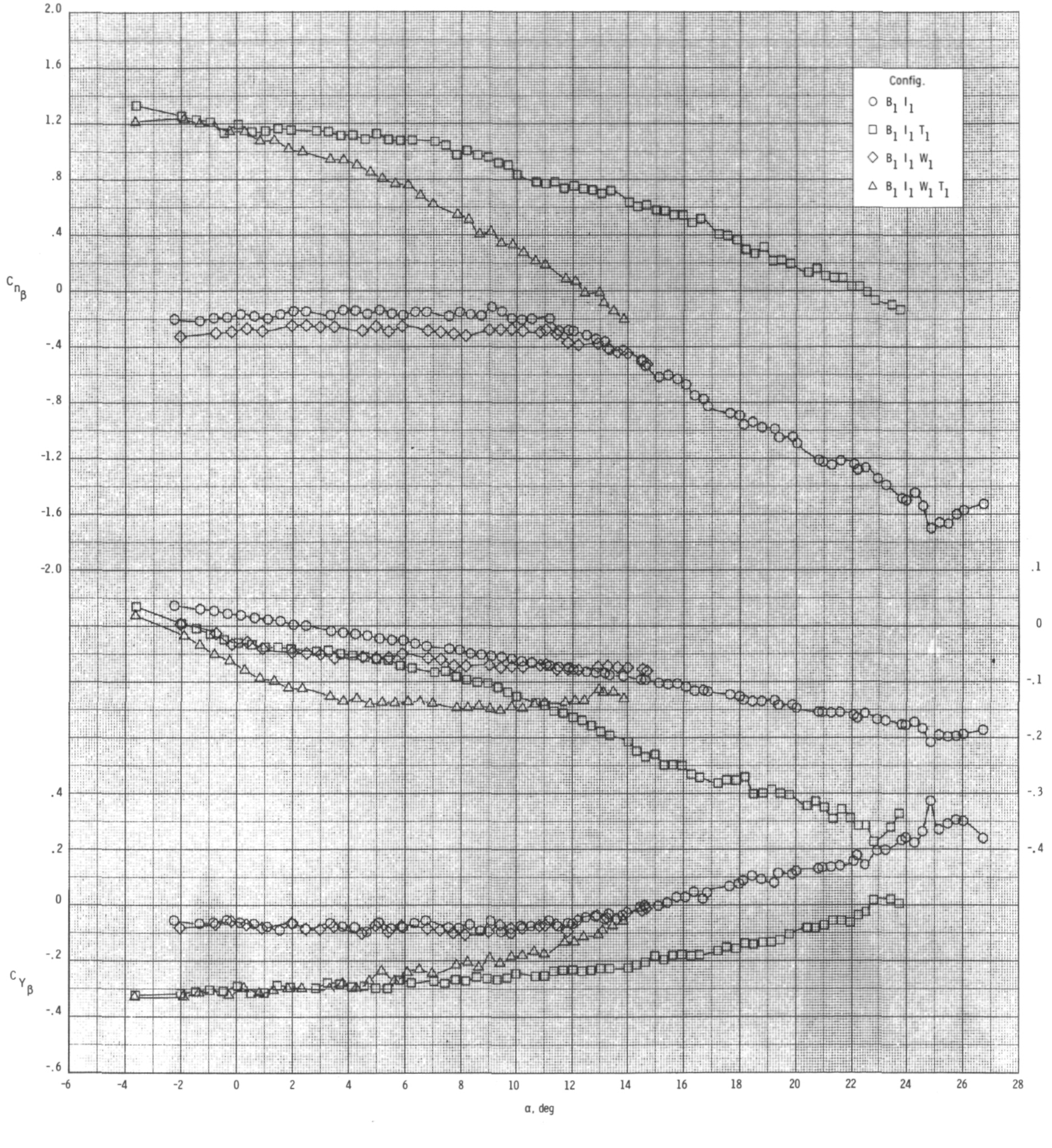

(b) M = 0.80.

Figure 18.- Continued.

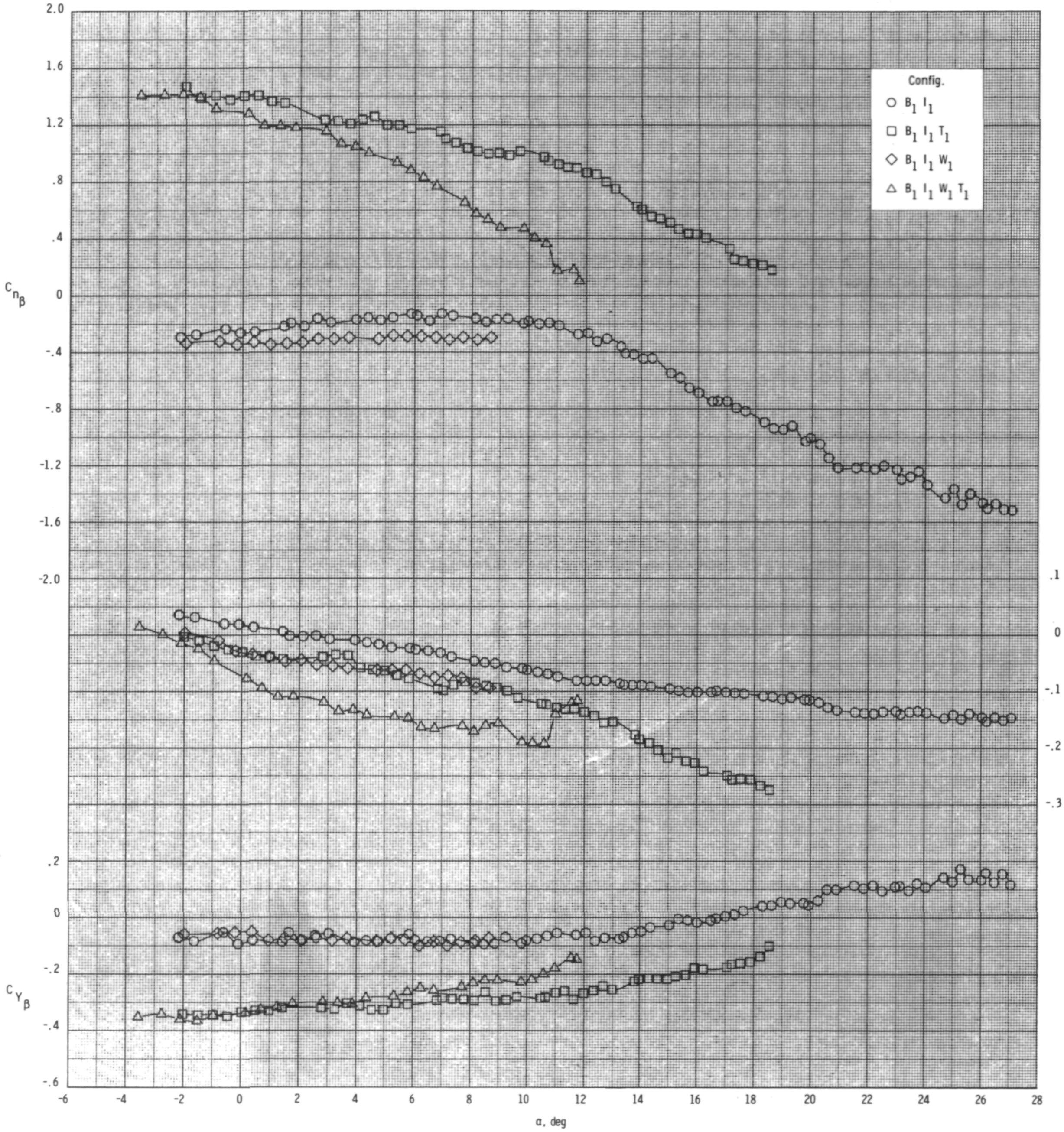

(c) M = 0.95.

Figure 18.- Concluded.

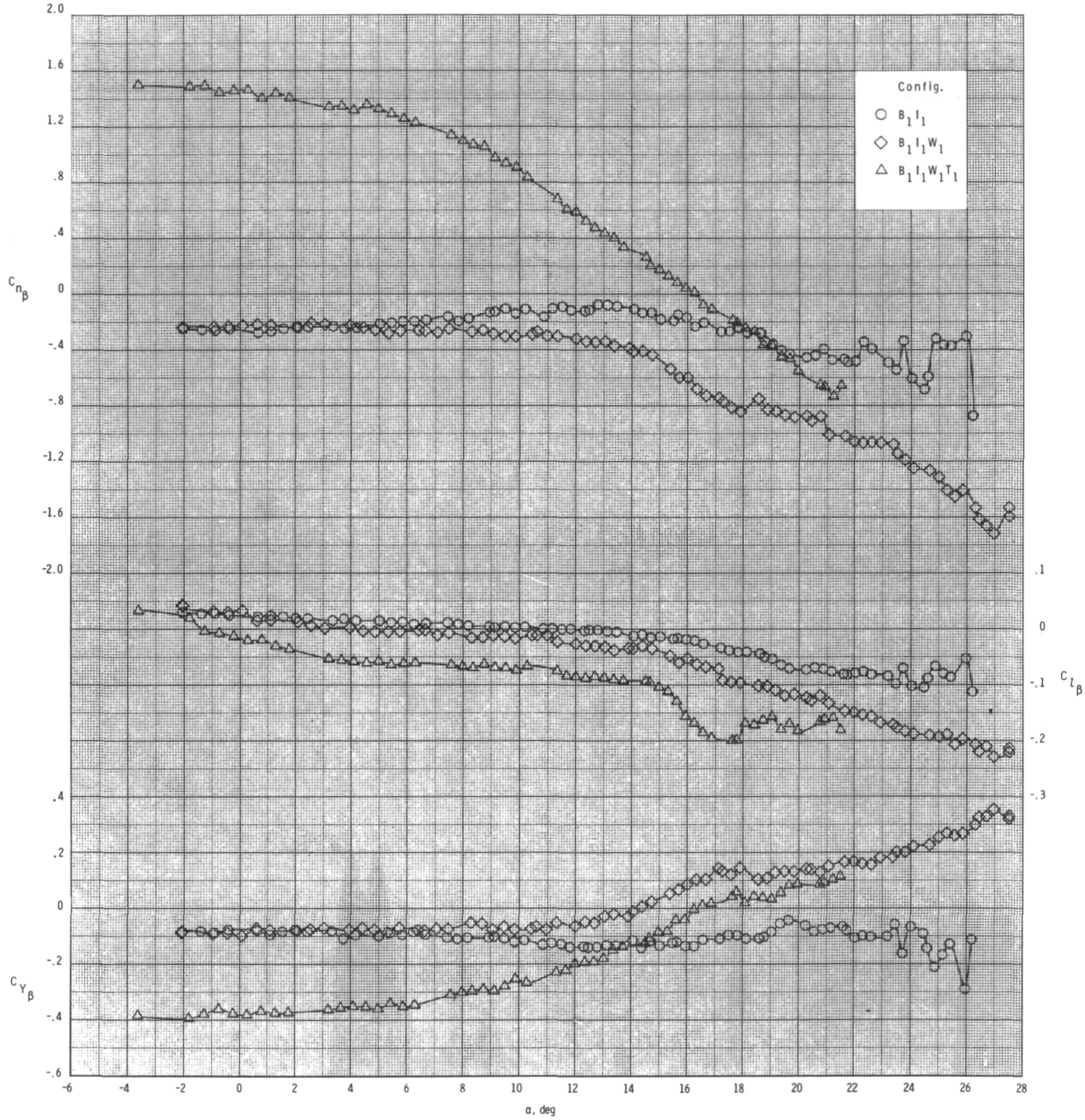

(a) M = 0.60.

Figure 19.- Effect of various model components on lateral-directional stability for axisymmetric inlets with internal ducts closed, T_1, $\phi_I = 135°$, and $\delta_p = 0°$.

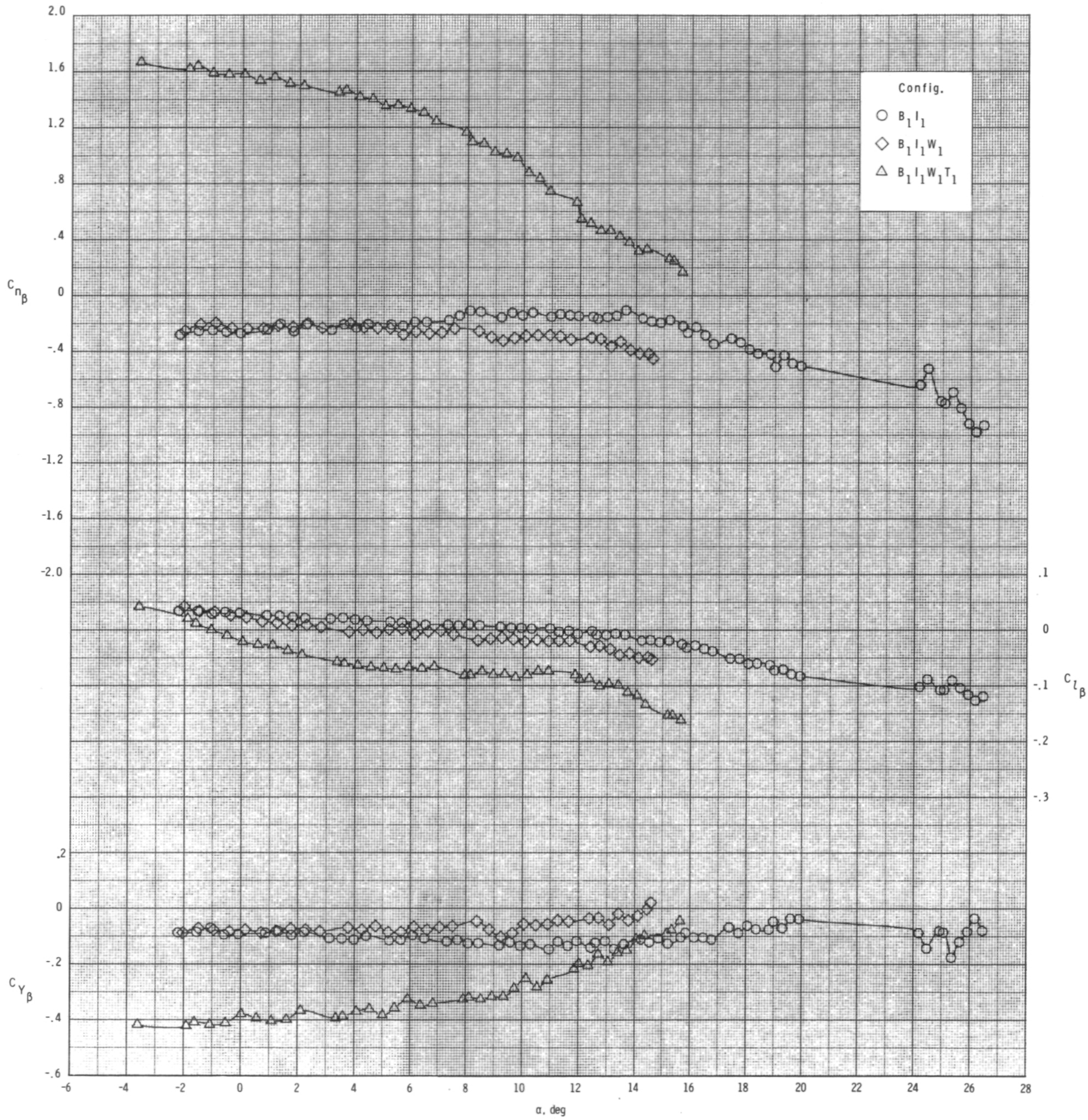

(b) M = 0.80.

Figure 19.- Continued.

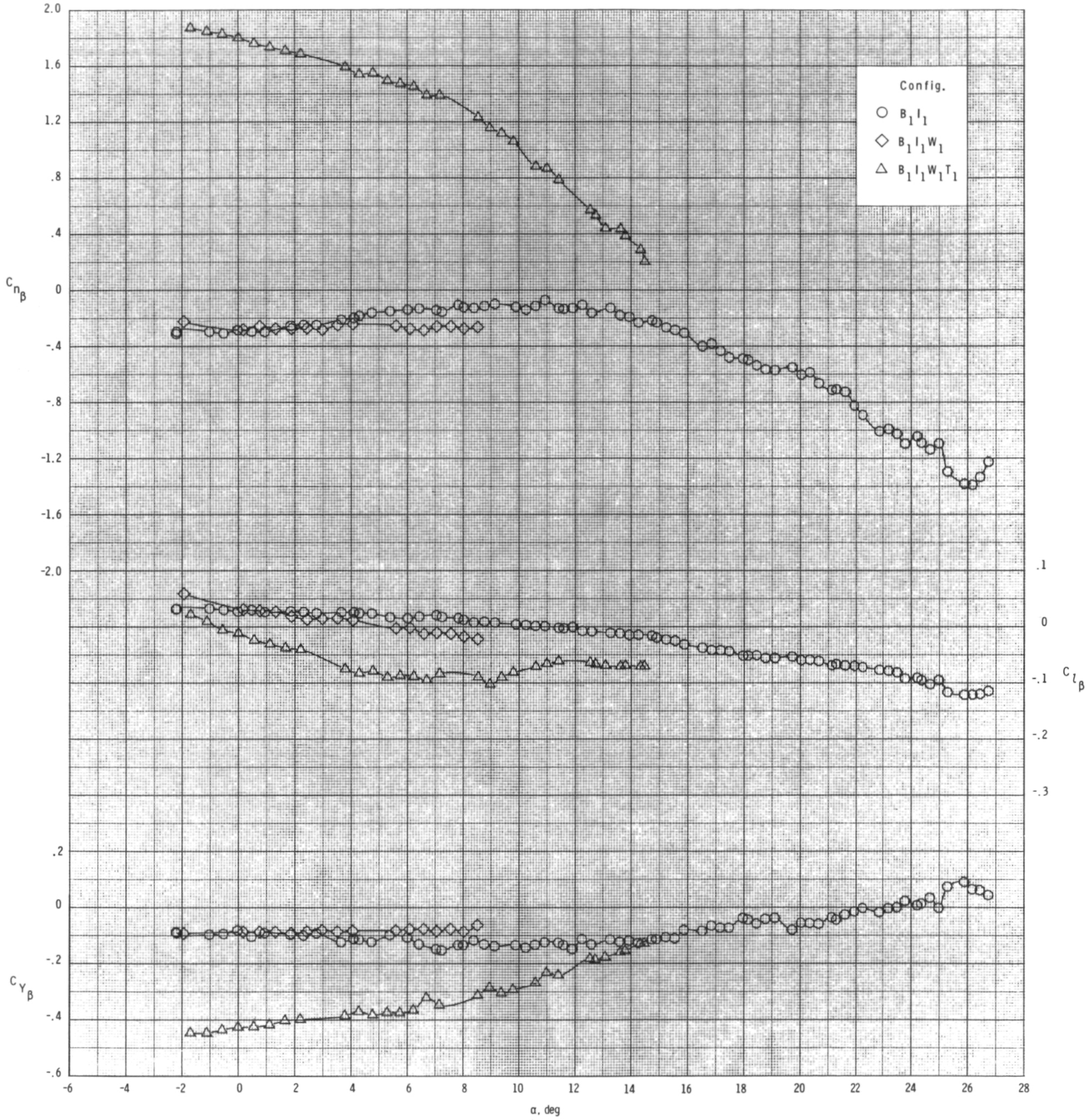

(c) M = 0.95.

Figure 19.- Concluded.

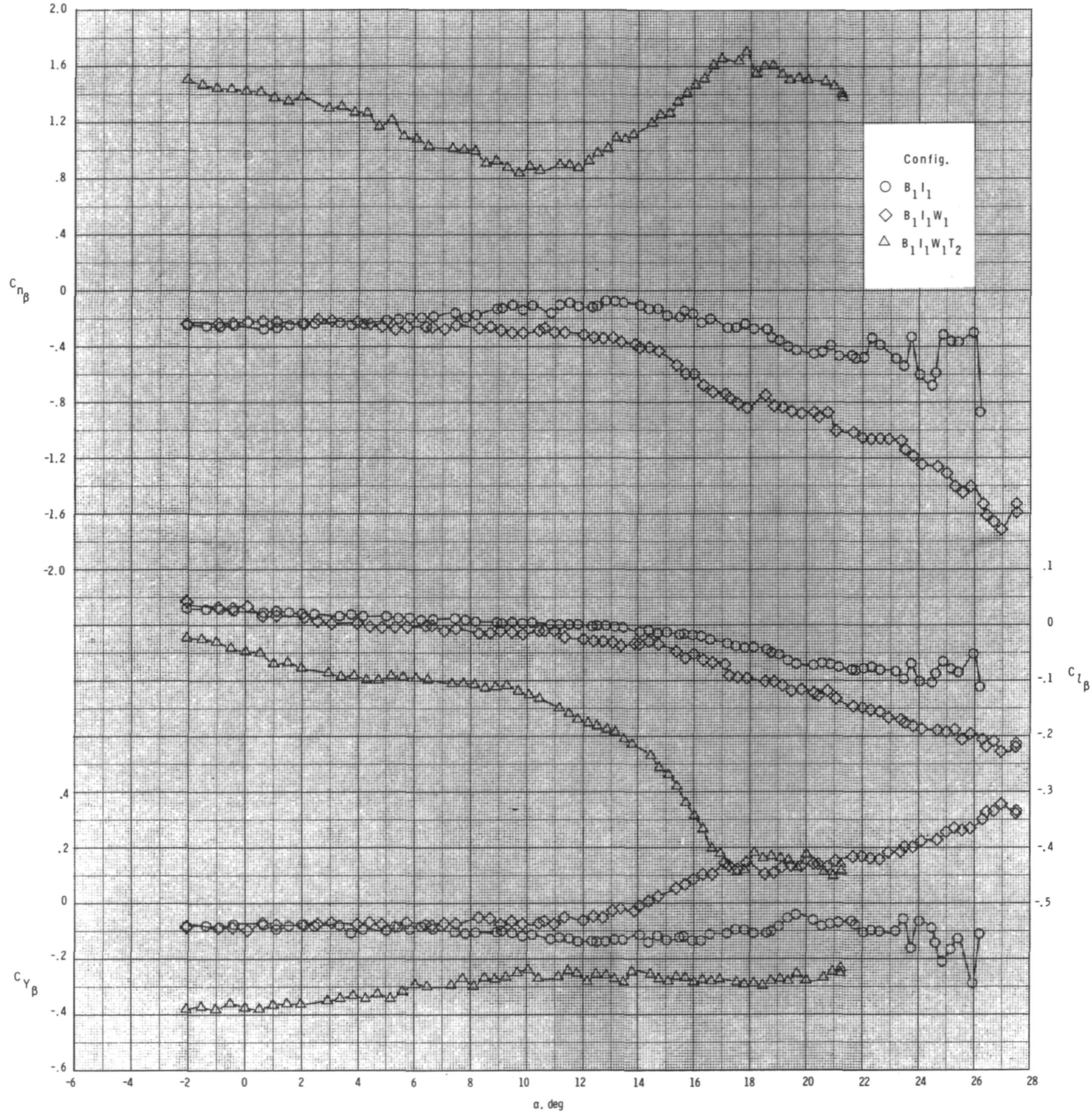

(a) M = 0.60.

Figure 20.- Effect of various model components on lateral-directional stability for axisymmetric inlets with internal ducts closed, T_2, $\phi_I = 135°$, and $\delta_p = 0°$.

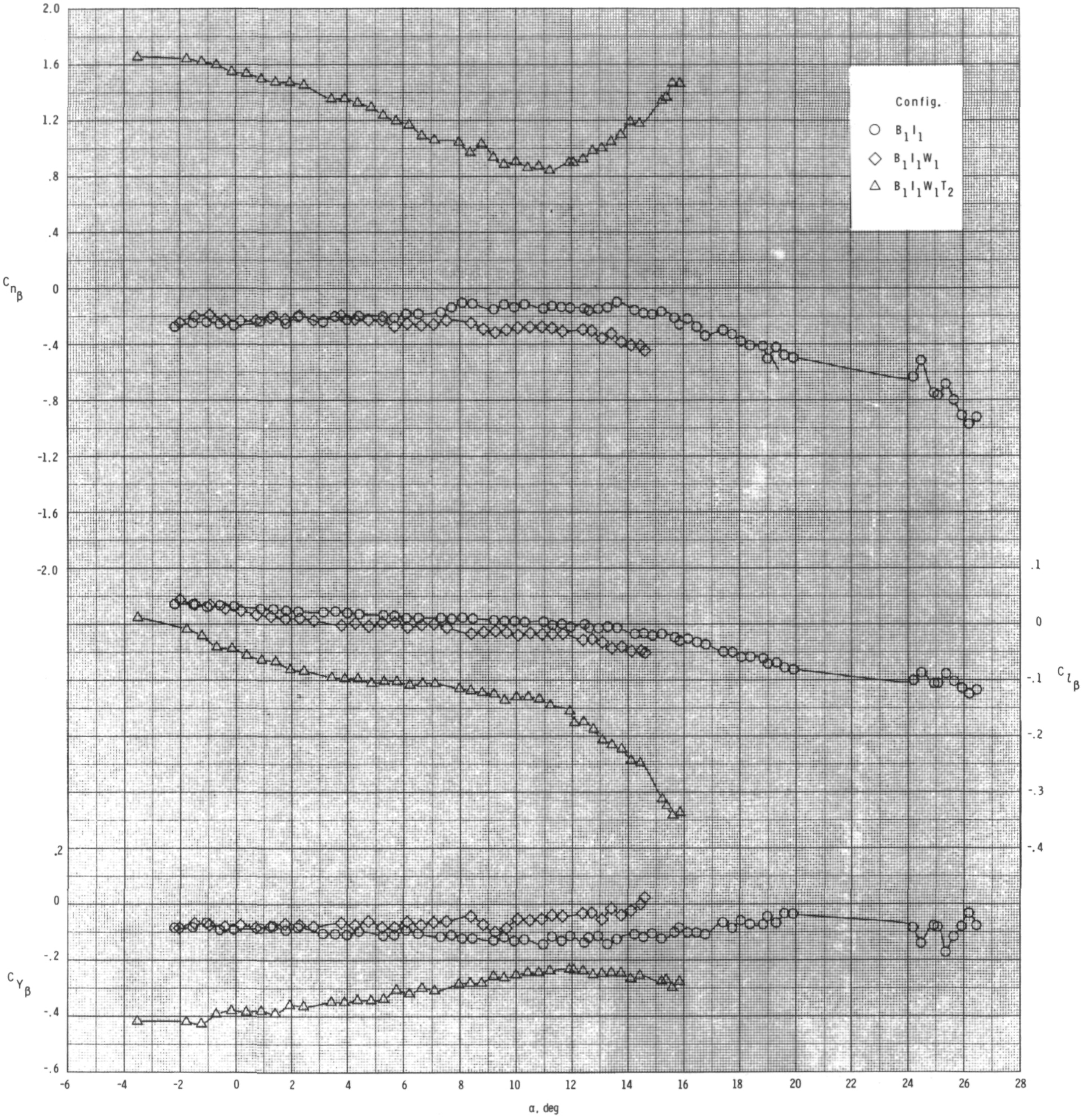

(b) M = 0.80.

Figure 20.- Continued.

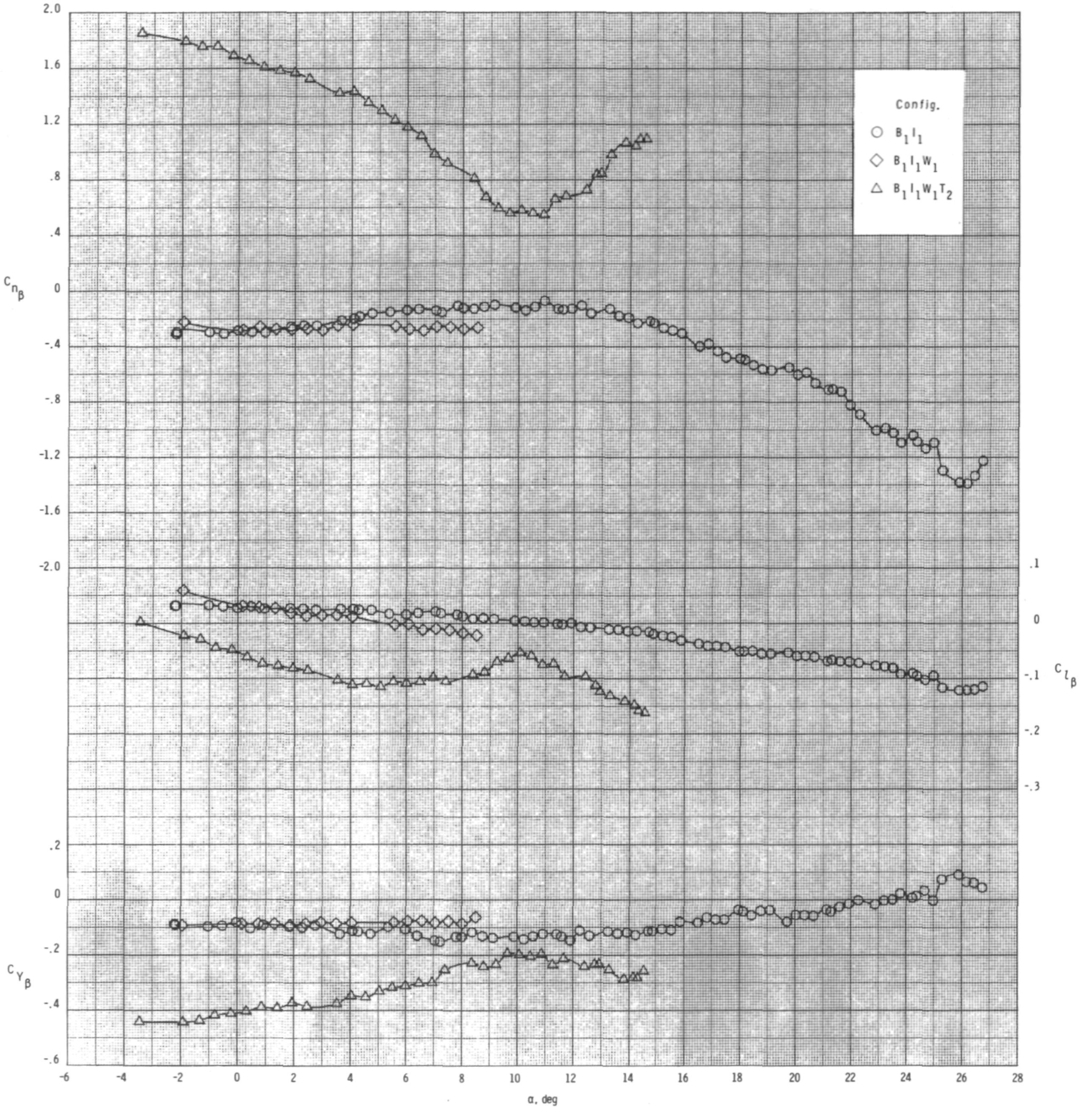

(c) M = 0.95.

Figure 20.- Concluded.

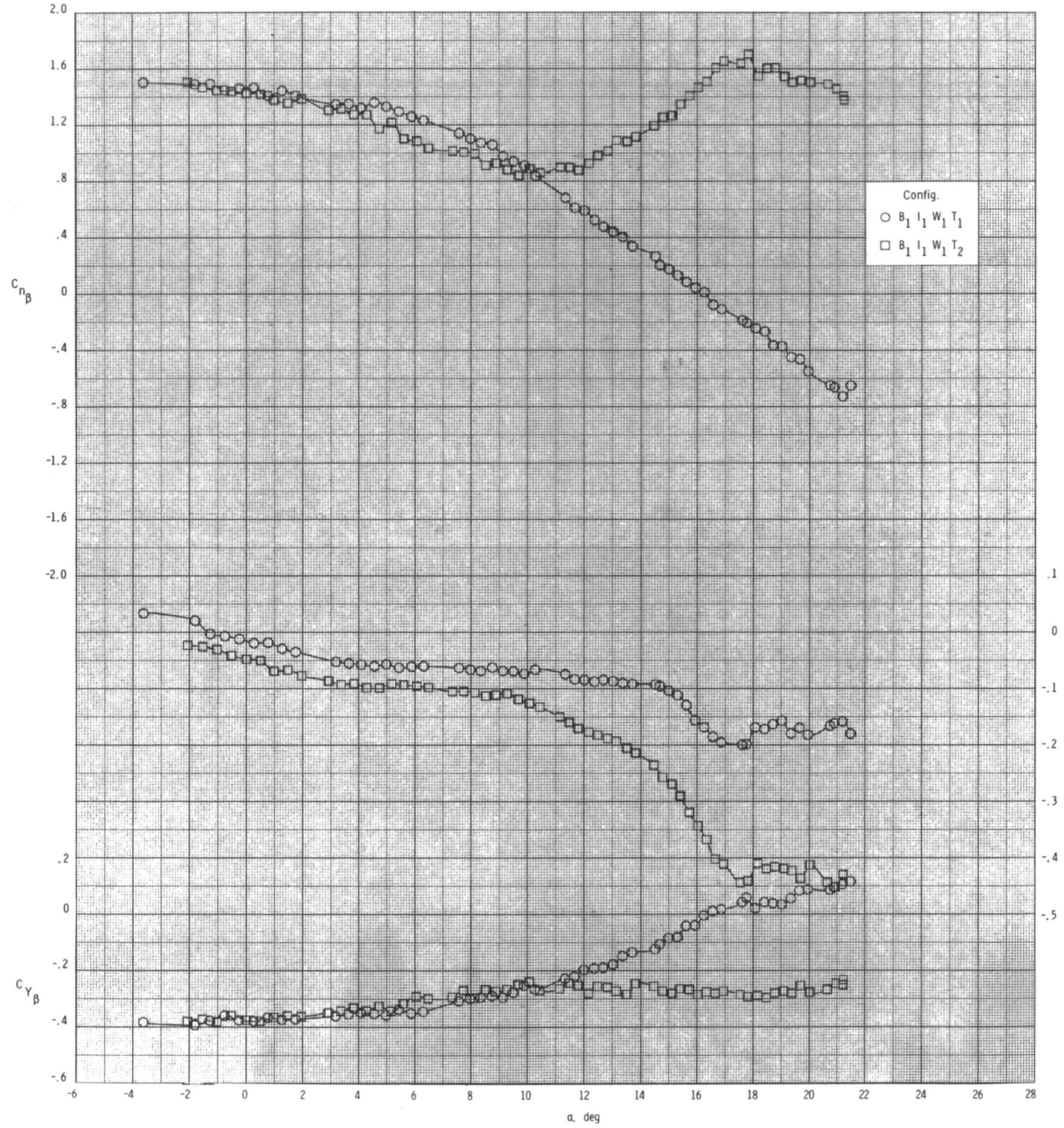

(a) M = 0.60.

Figure 21.- Effect of tail configuration on lateral-directional stability for configuration $B_1I_1W_1T$ with internal ducts closed, ϕ_I = 135°, and δ_p = 0°.

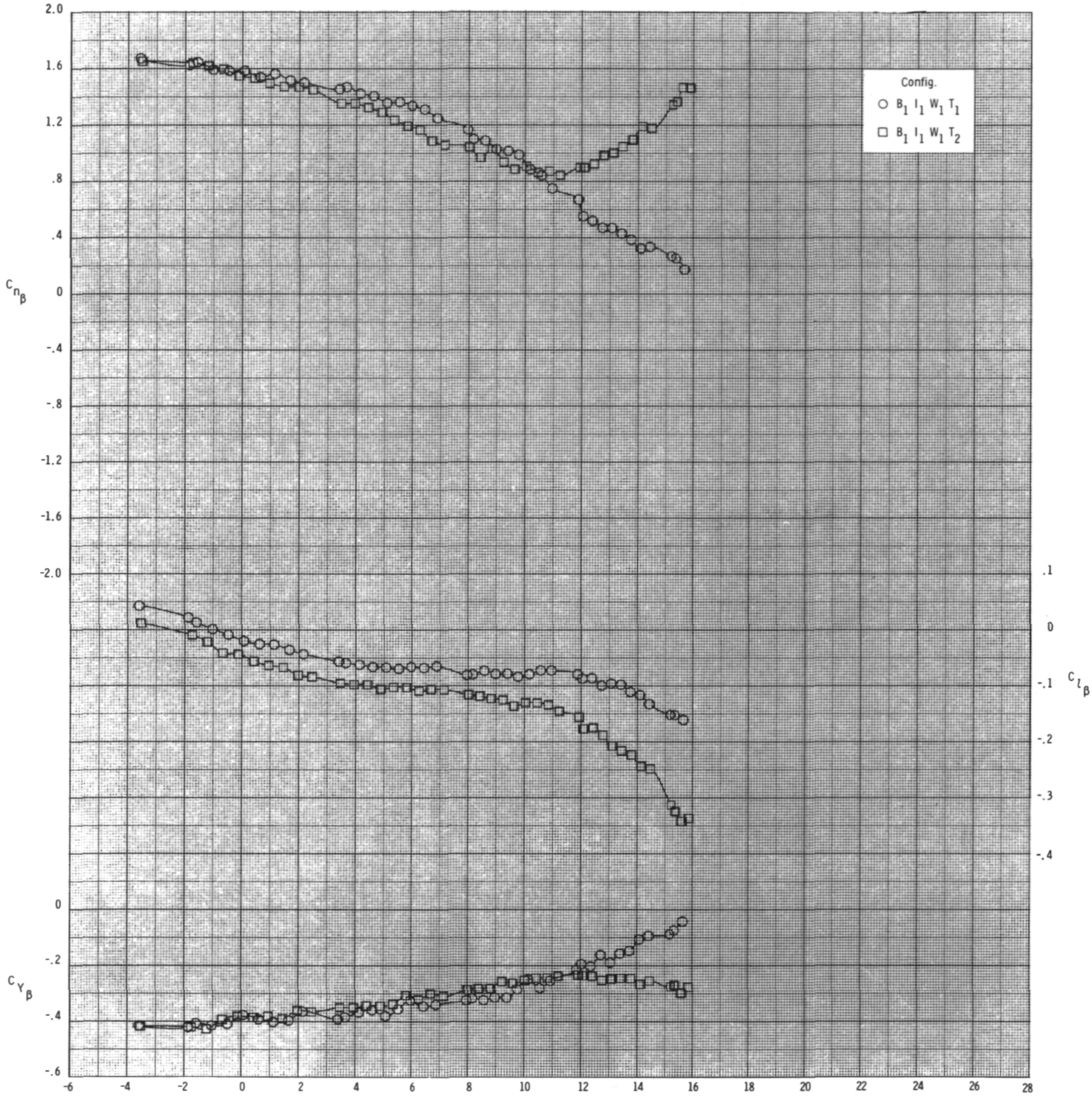

(b) M = 0.80.

Figure 21.- Continued.

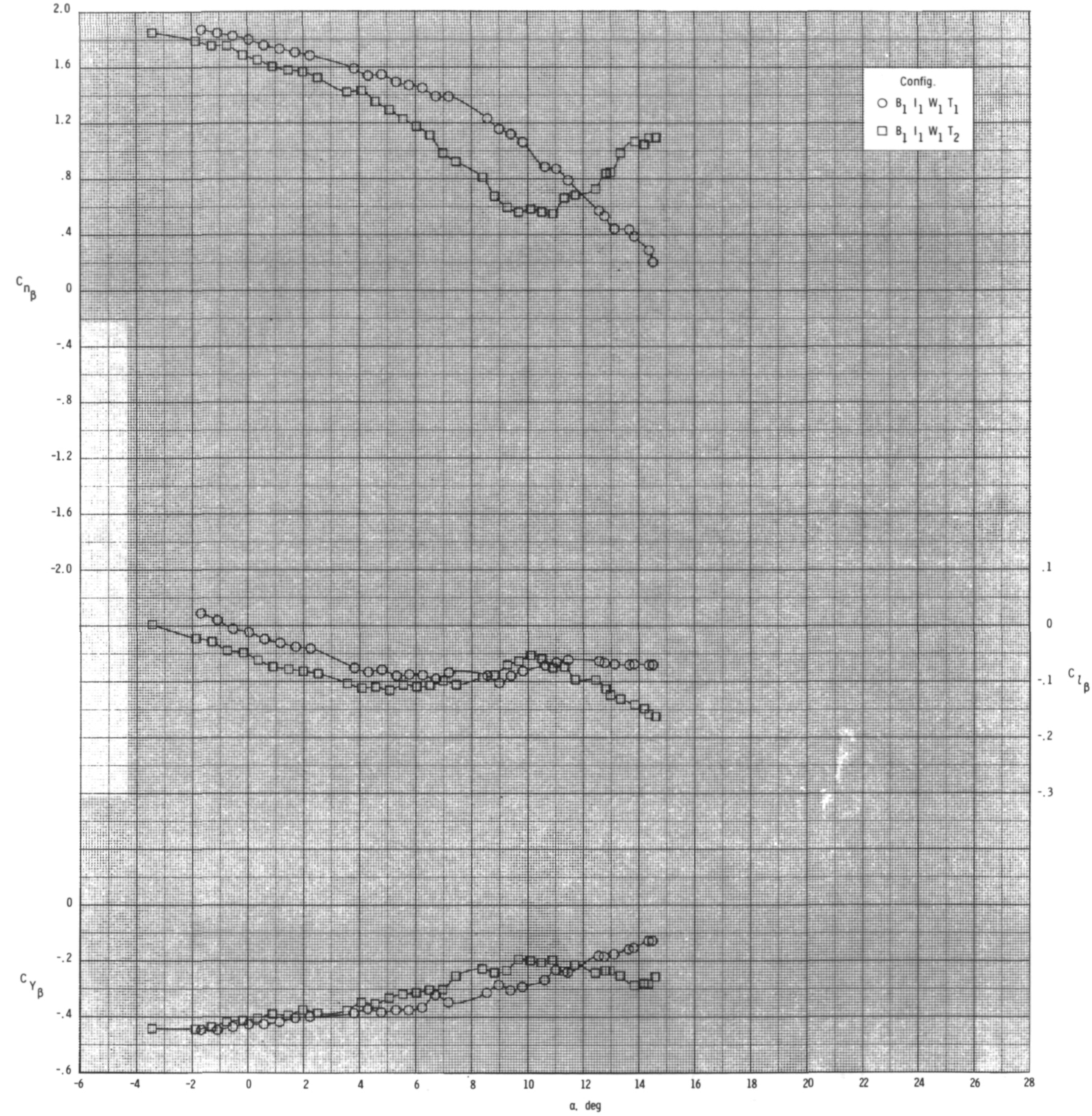

(c) M = 0.95.

Figure 21.- Concluded.

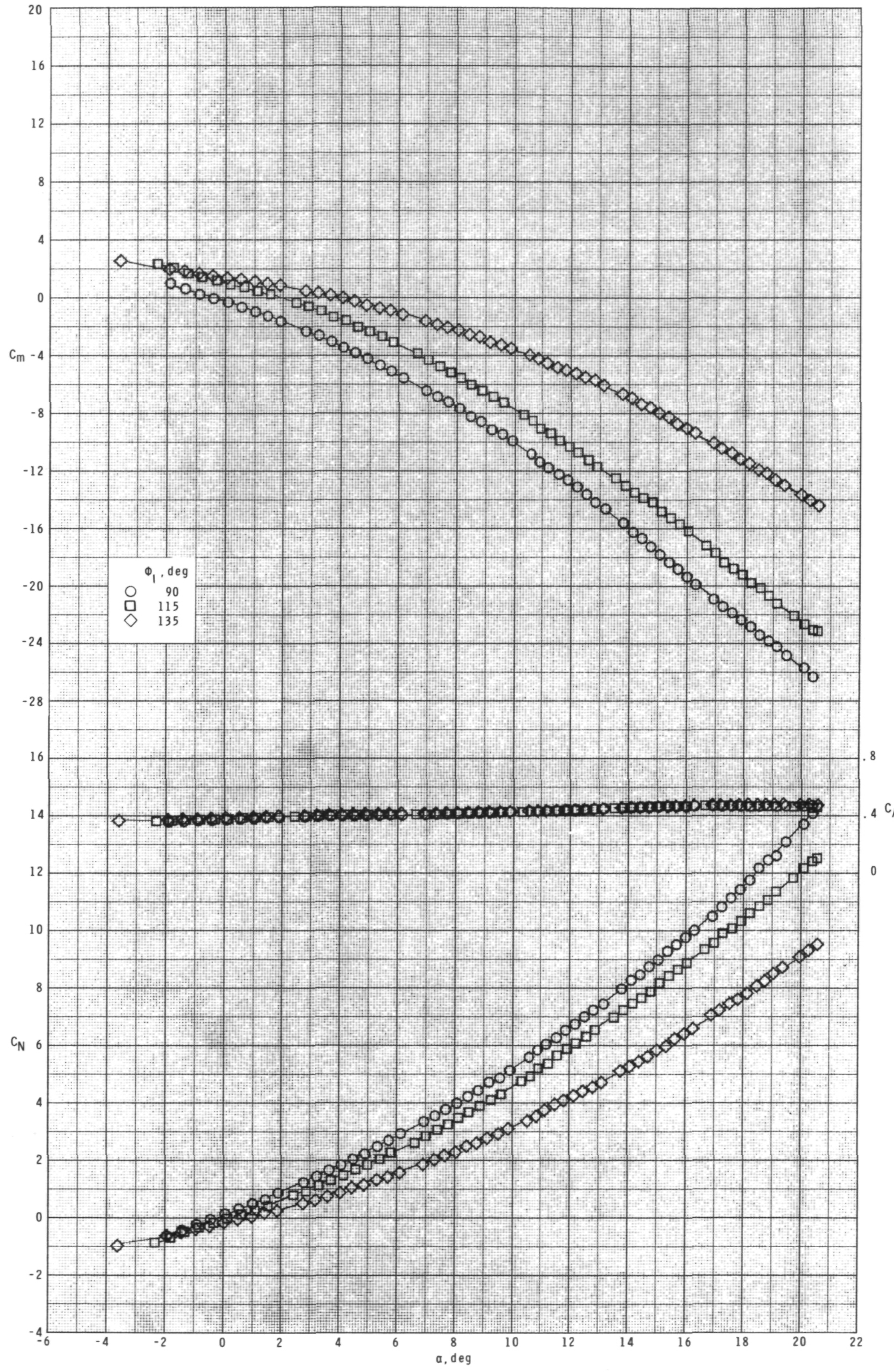

(a) M = 0.60.

Figure 22.- Effect of inlet orientation angle ϕ_I on longitudinal aerodynamic characteristics for configuration $B_1 I_{2c} T_1$ with internal ducts closed and $\delta_p = 0°$.

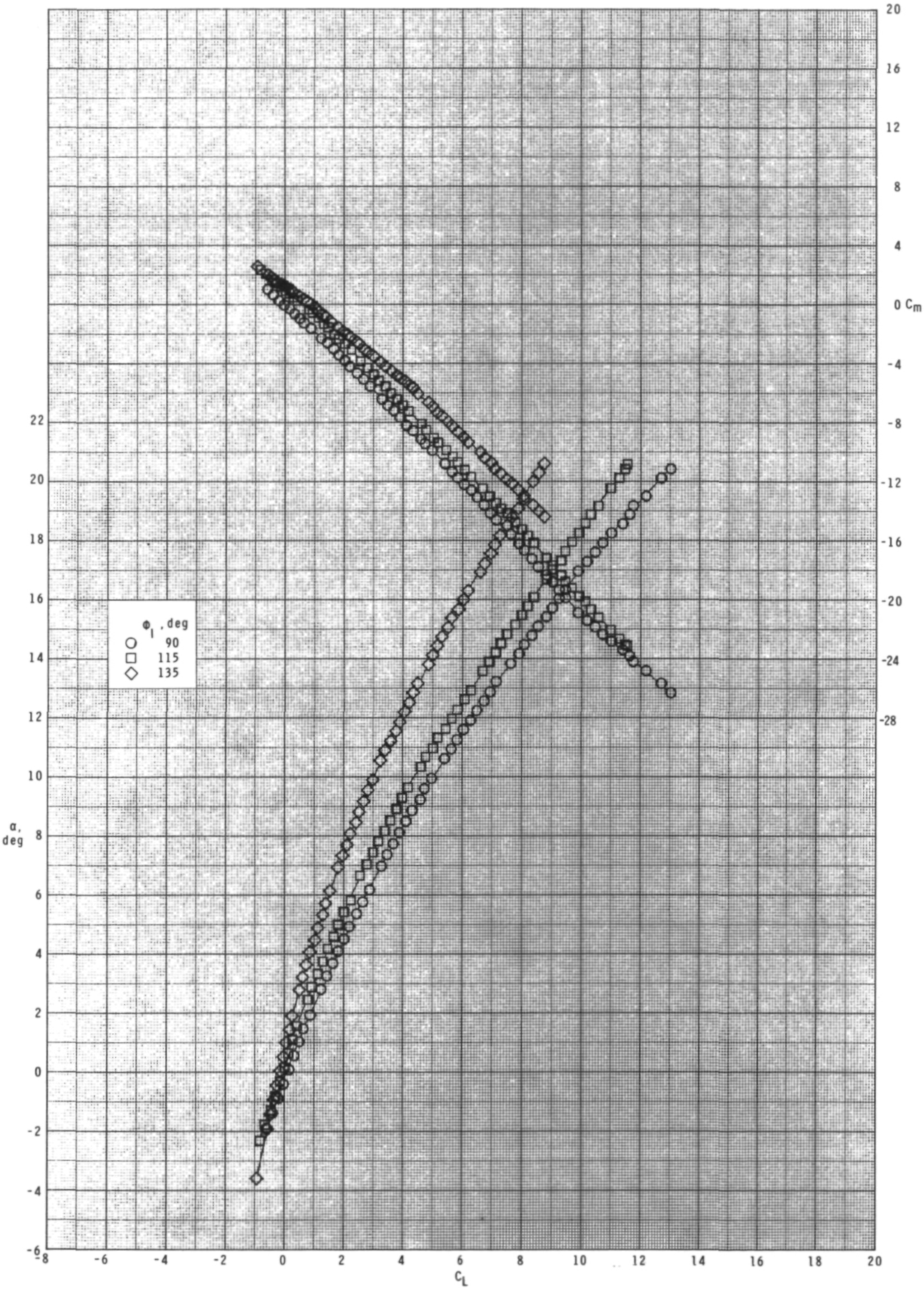

(a) Continued.

Figure 22.- Continued.

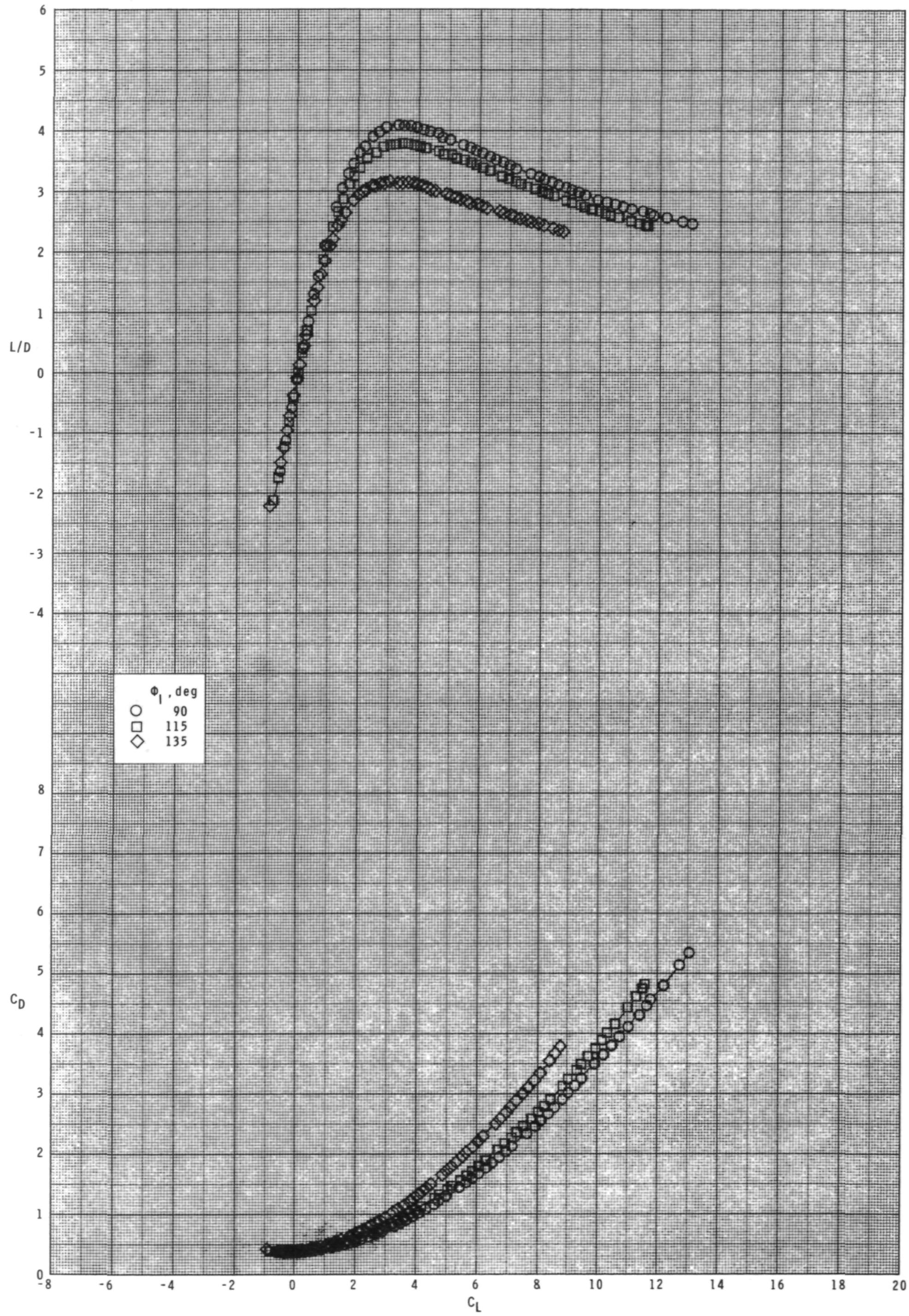

(a) Concluded.

Figure 22.- Continued.

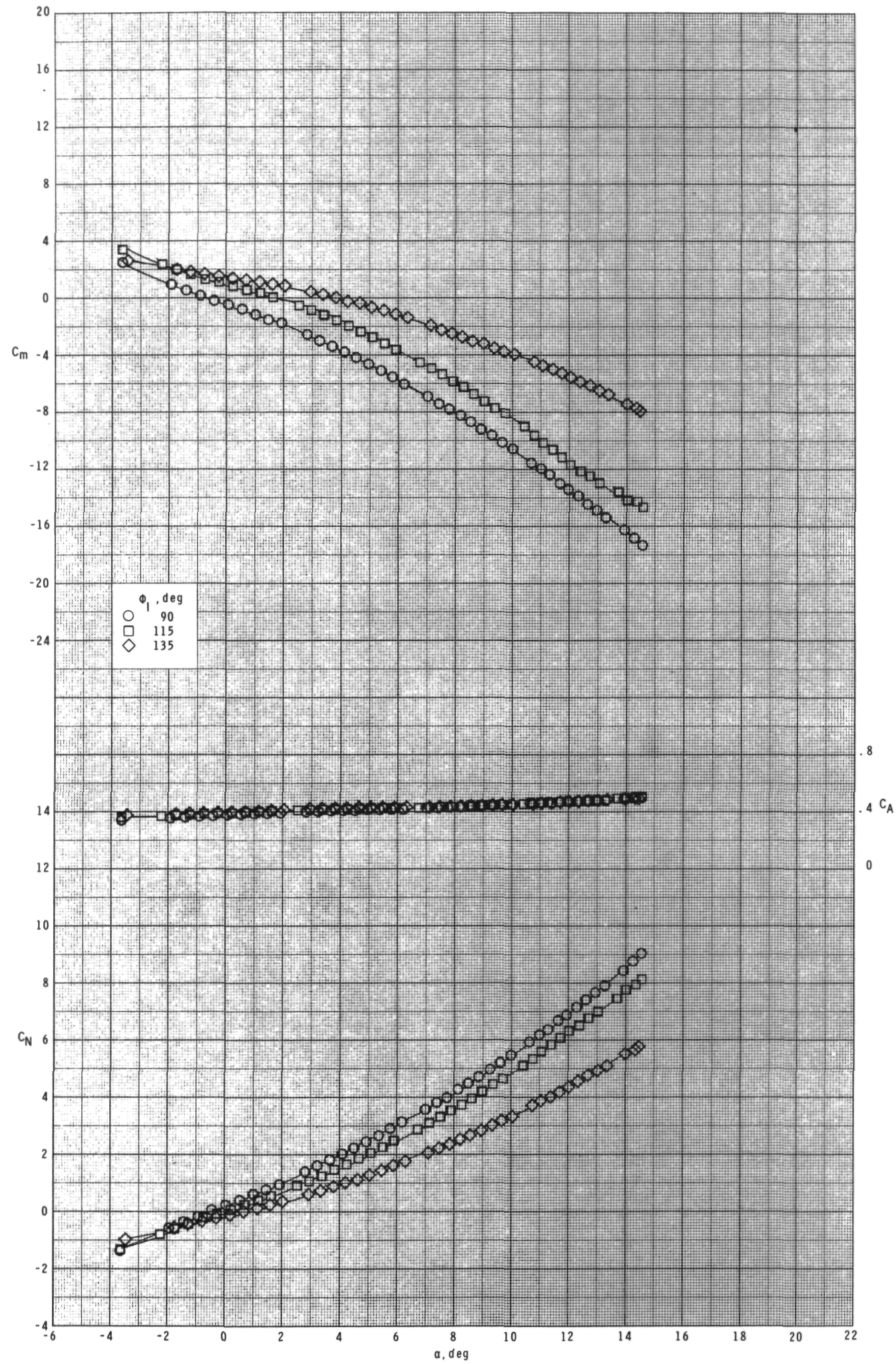

(b) M = 0.80.

Figure 22.- Continued.

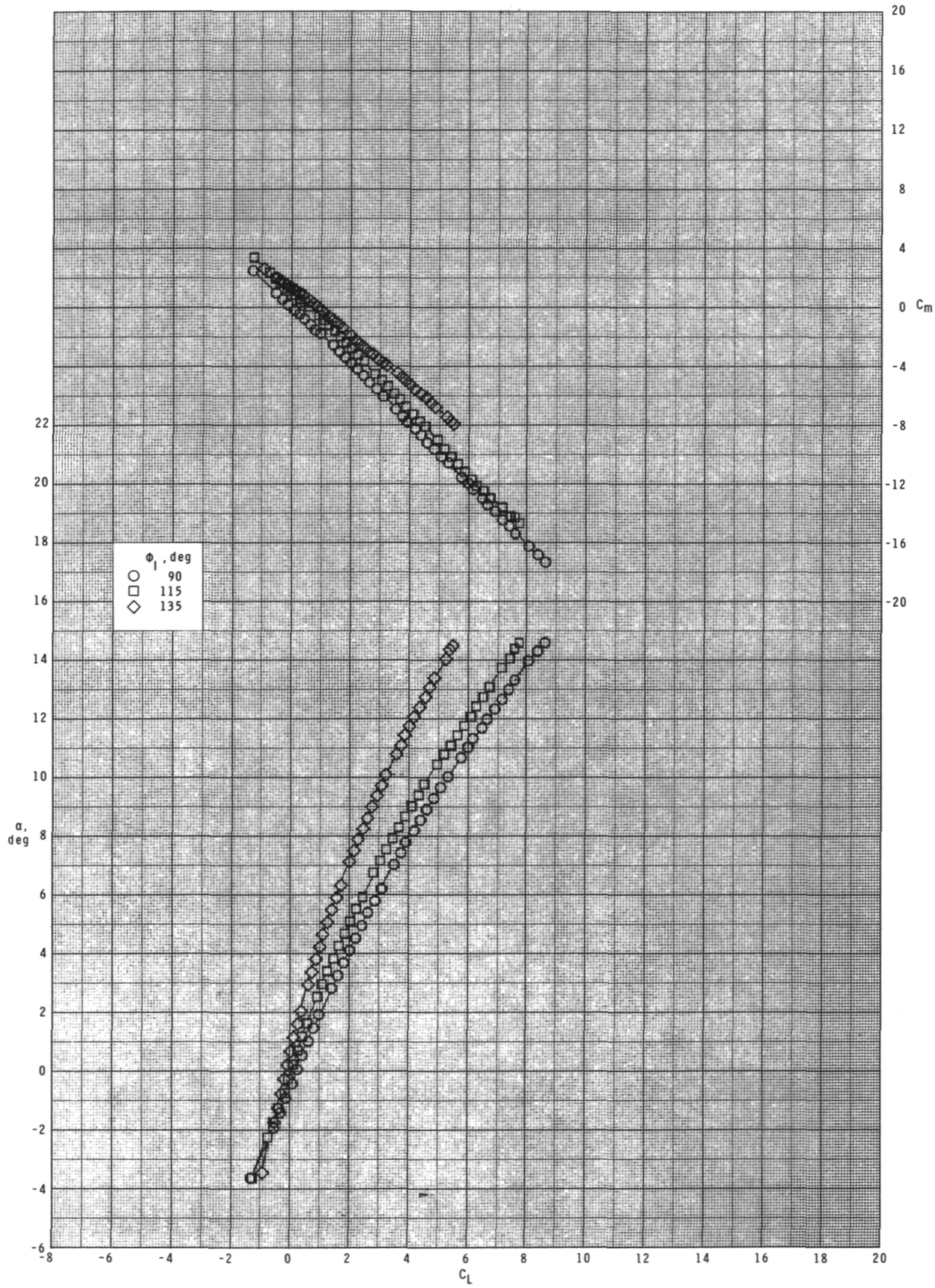

(b) Continued.

Figure 22.- Continued.

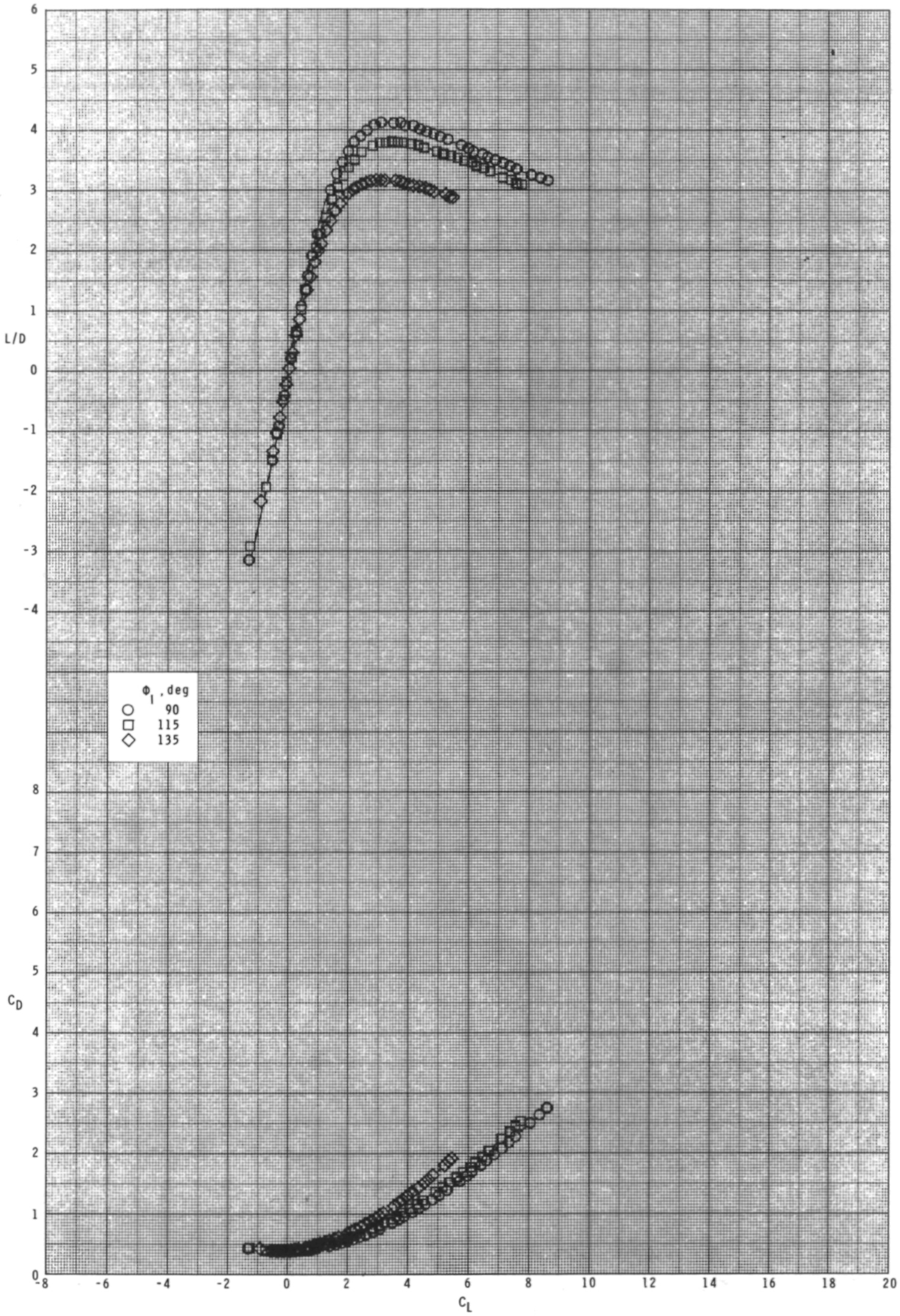

(b) Concluded.

Figure 22.- Continued.

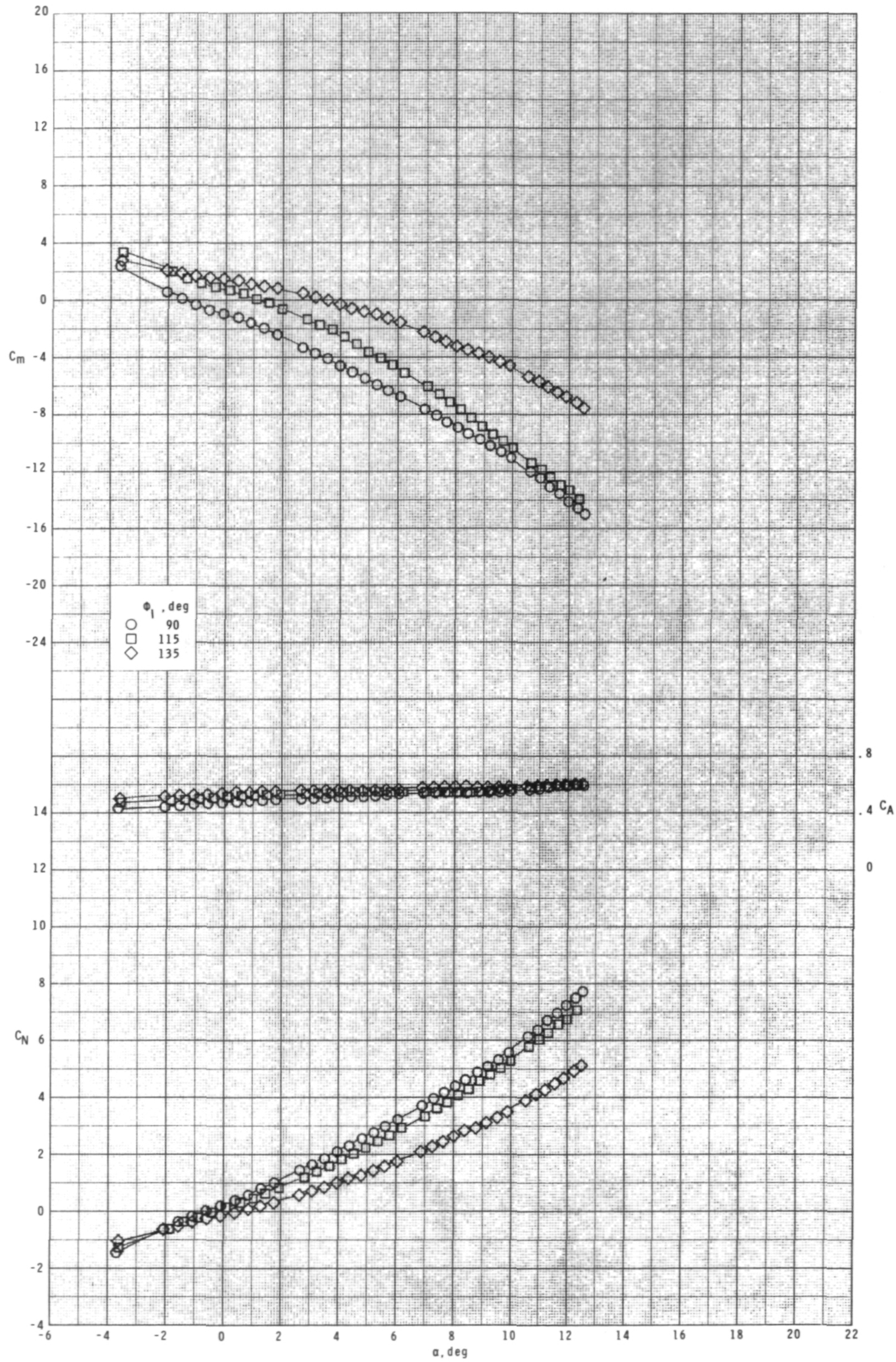

(c) M = 0.95.

Figure 22.- Continued.

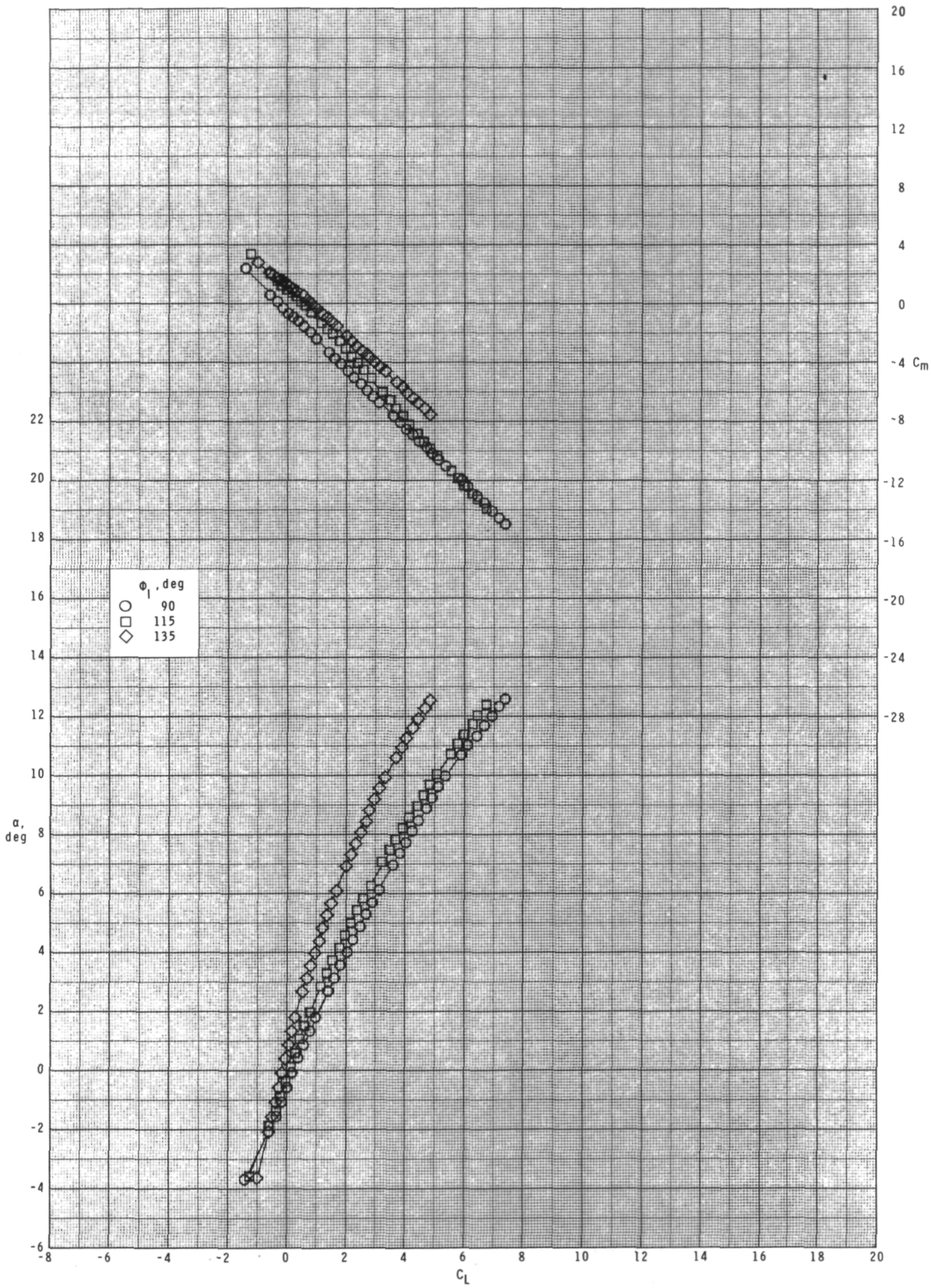

(c) Continued.

Figure 22.- Continued.

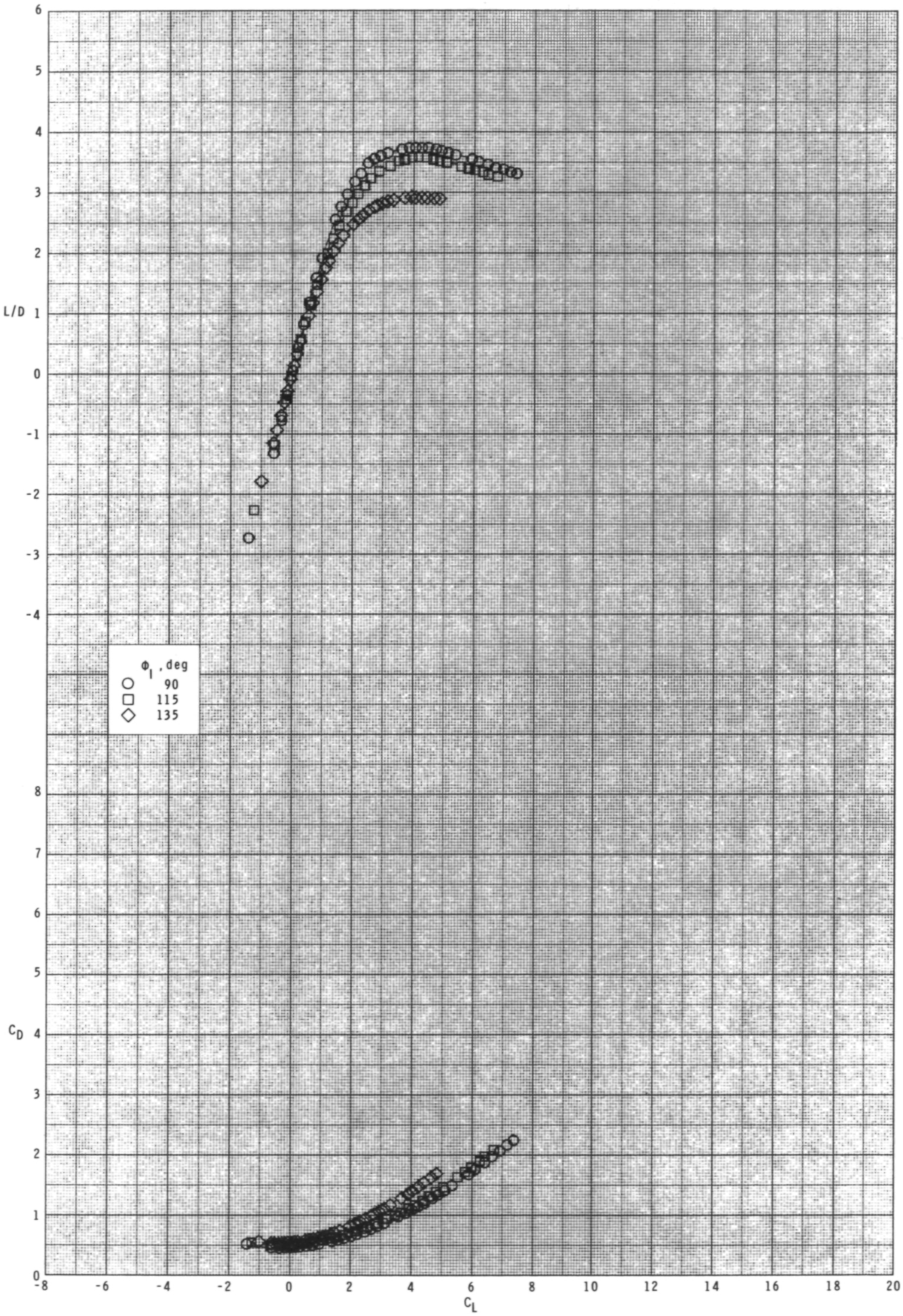

(c) Concluded.

Figure 22.- Concluded.

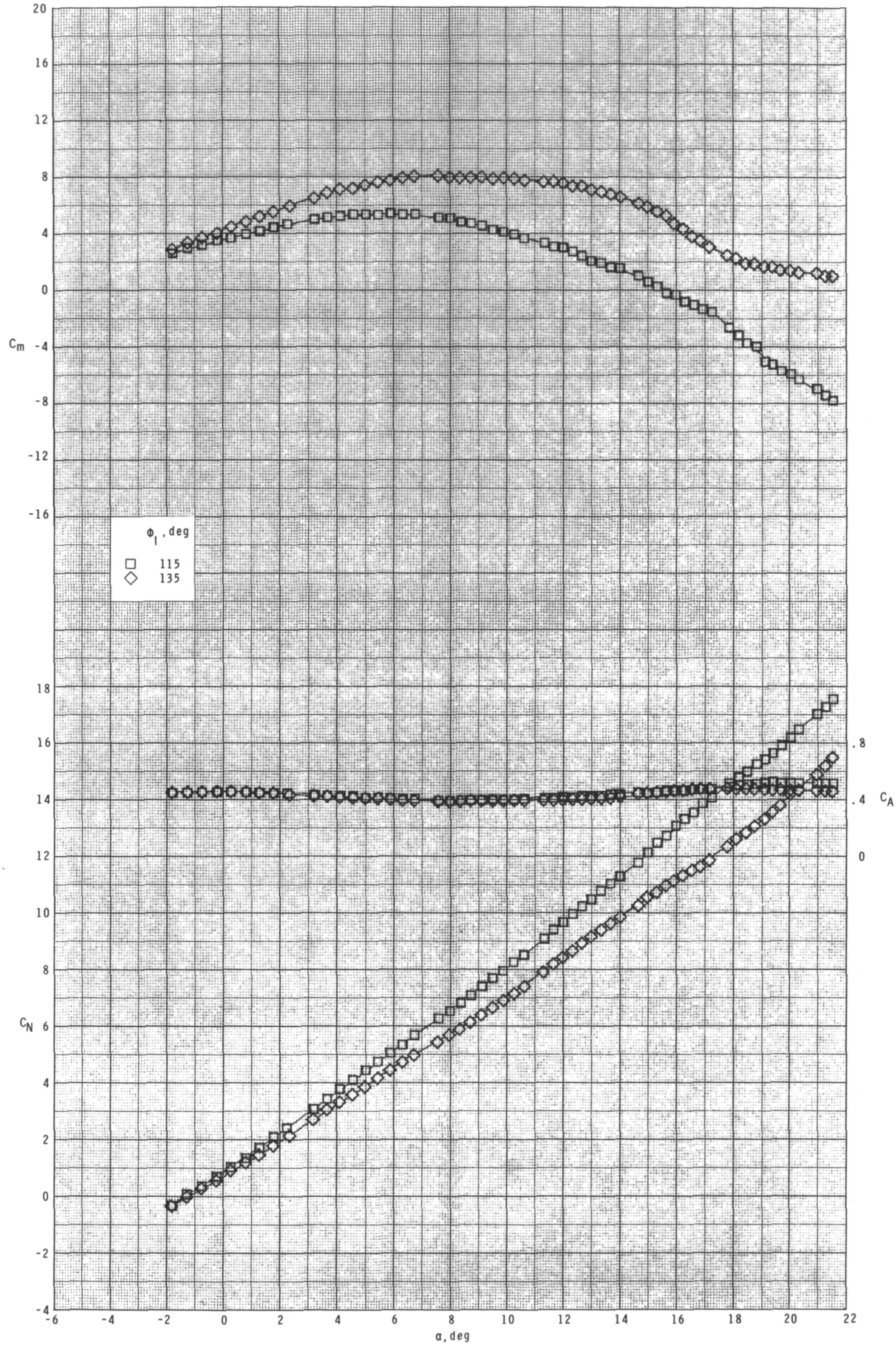

(a) M = 0.60.

Figure 23.- Effect of inlet orientation angle ϕ_I on longitudinal aerodynamic characteristics for configuration $B_1 I_{2c} W_1 T_1$ with internal ducts closed and $\delta_p = 0°$.

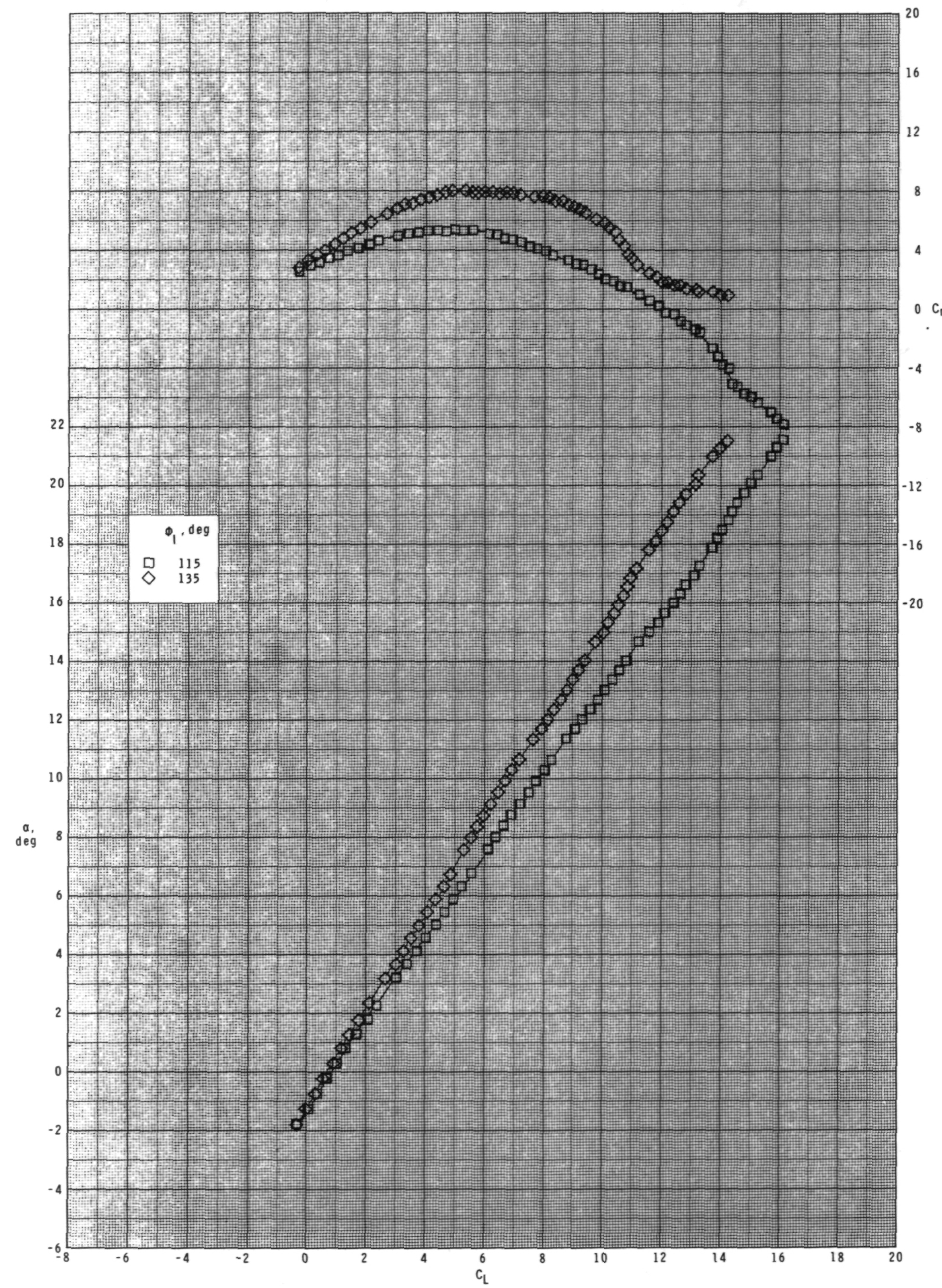

(a) Continued.

Figure 23.- Continued.

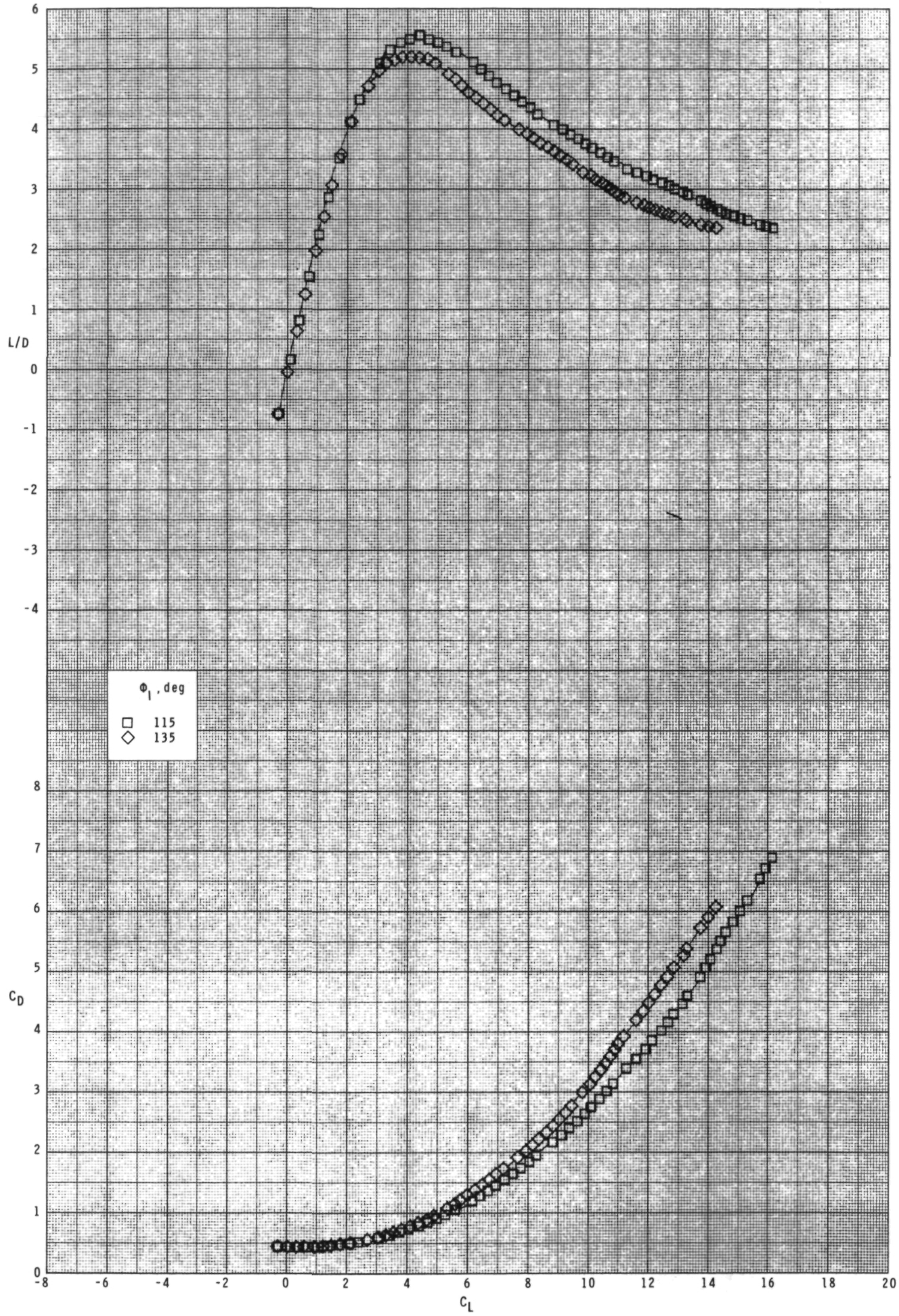

(a) Concluded.

Figure 23.- Continued.

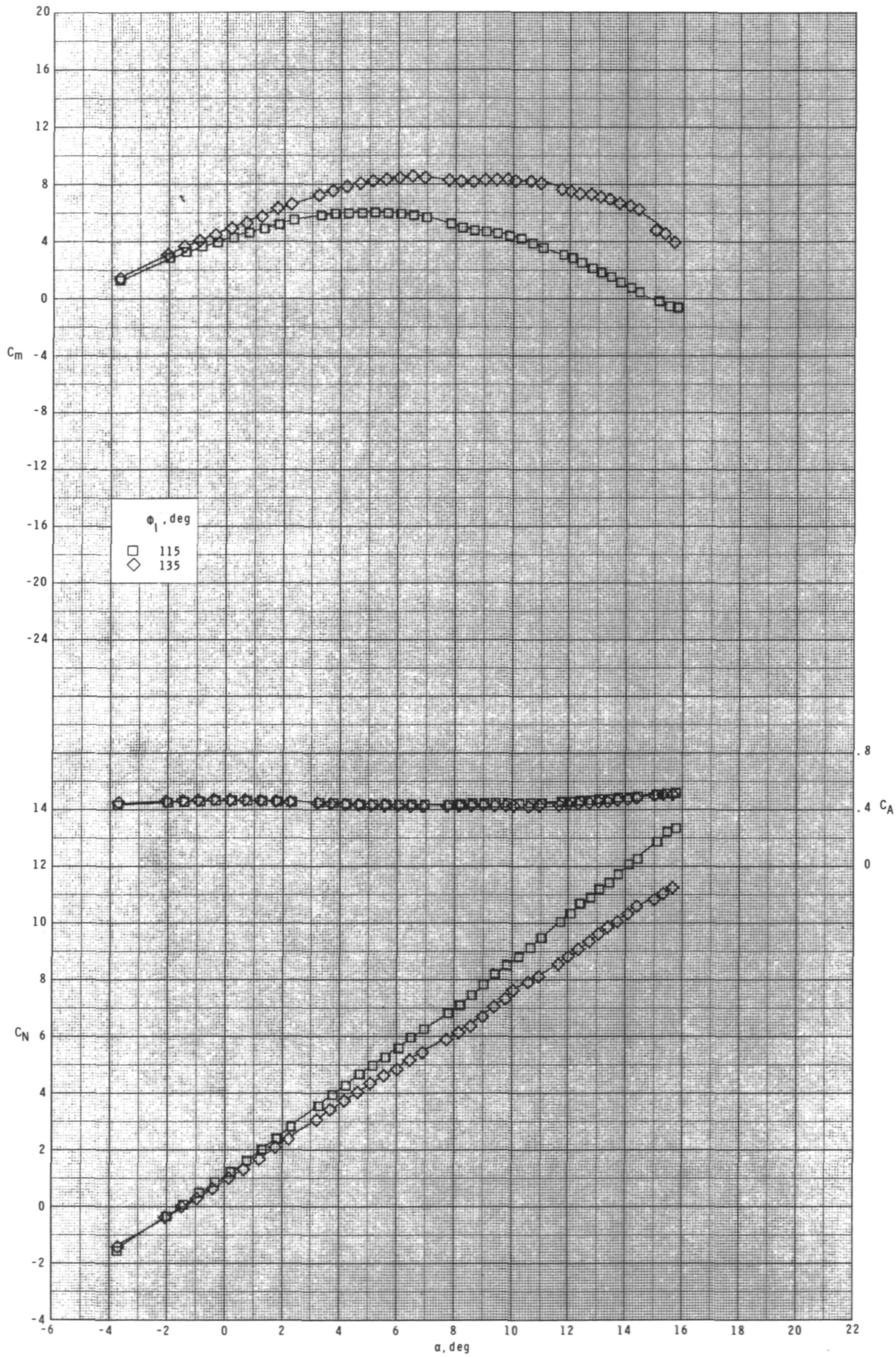

(b) M = 0.80.

Figure 23.- Continued.

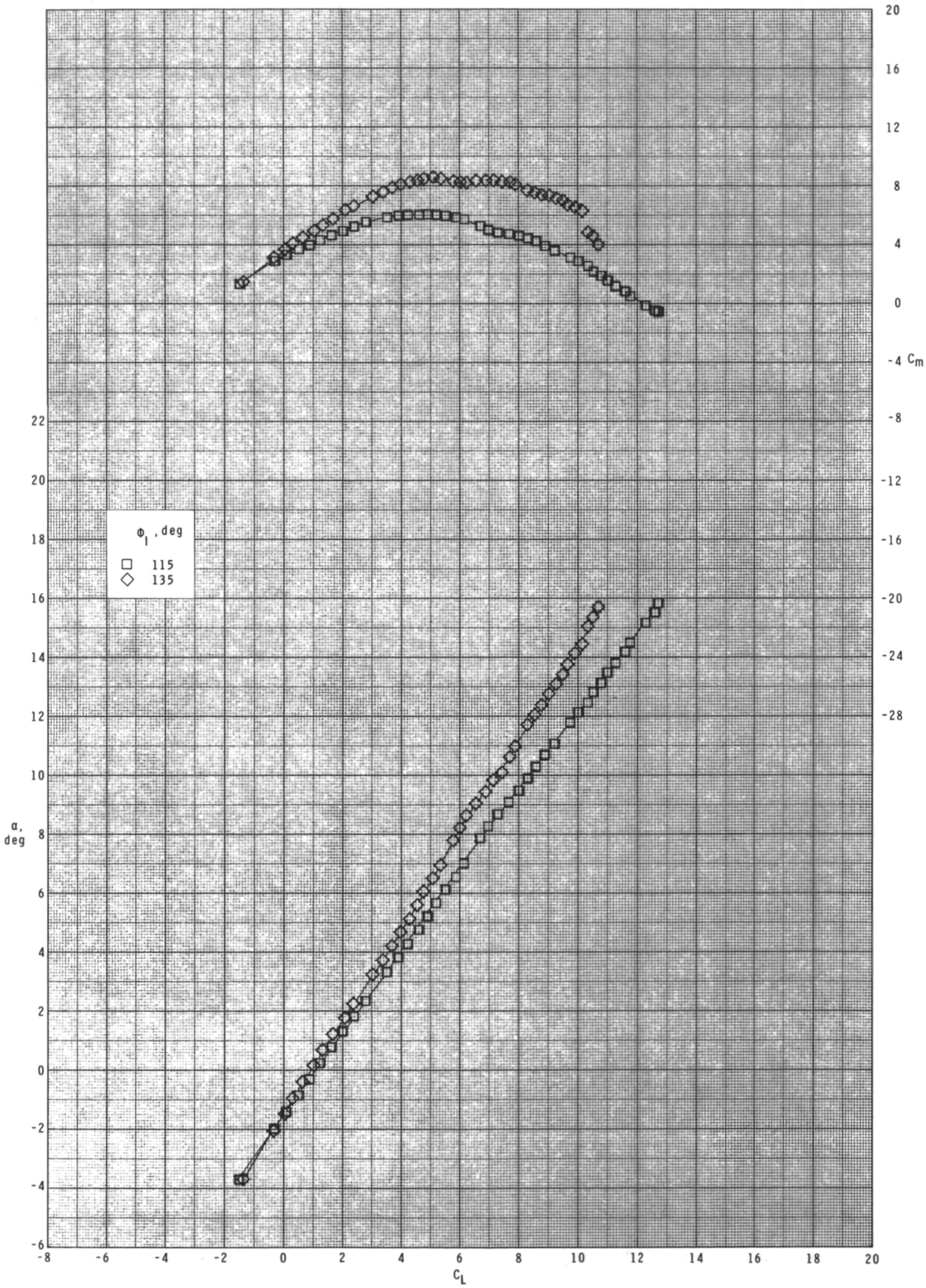

(b) Continued.

Figure 23.- Continued.

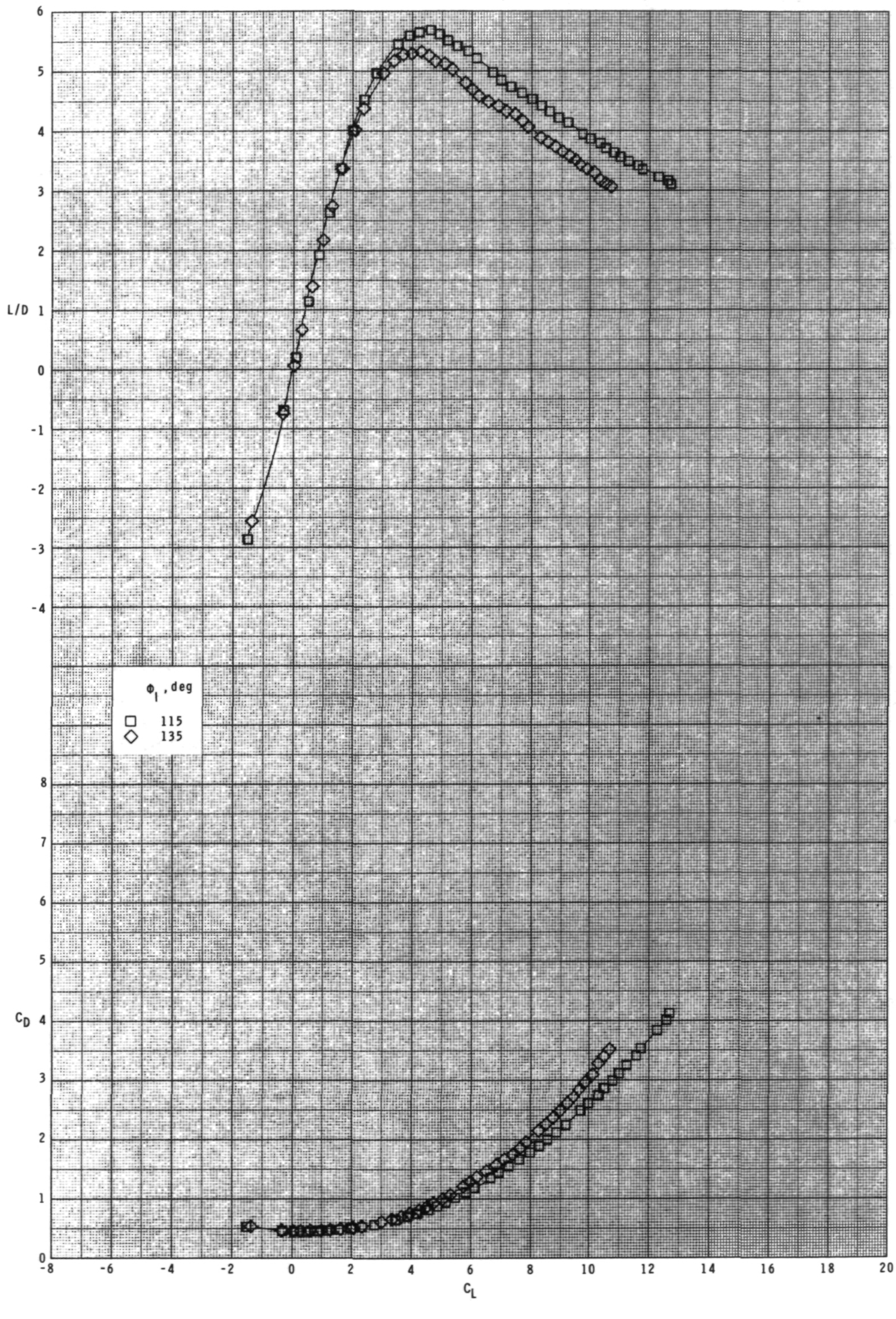

(b) Concluded.

Figure 23.- Continued.

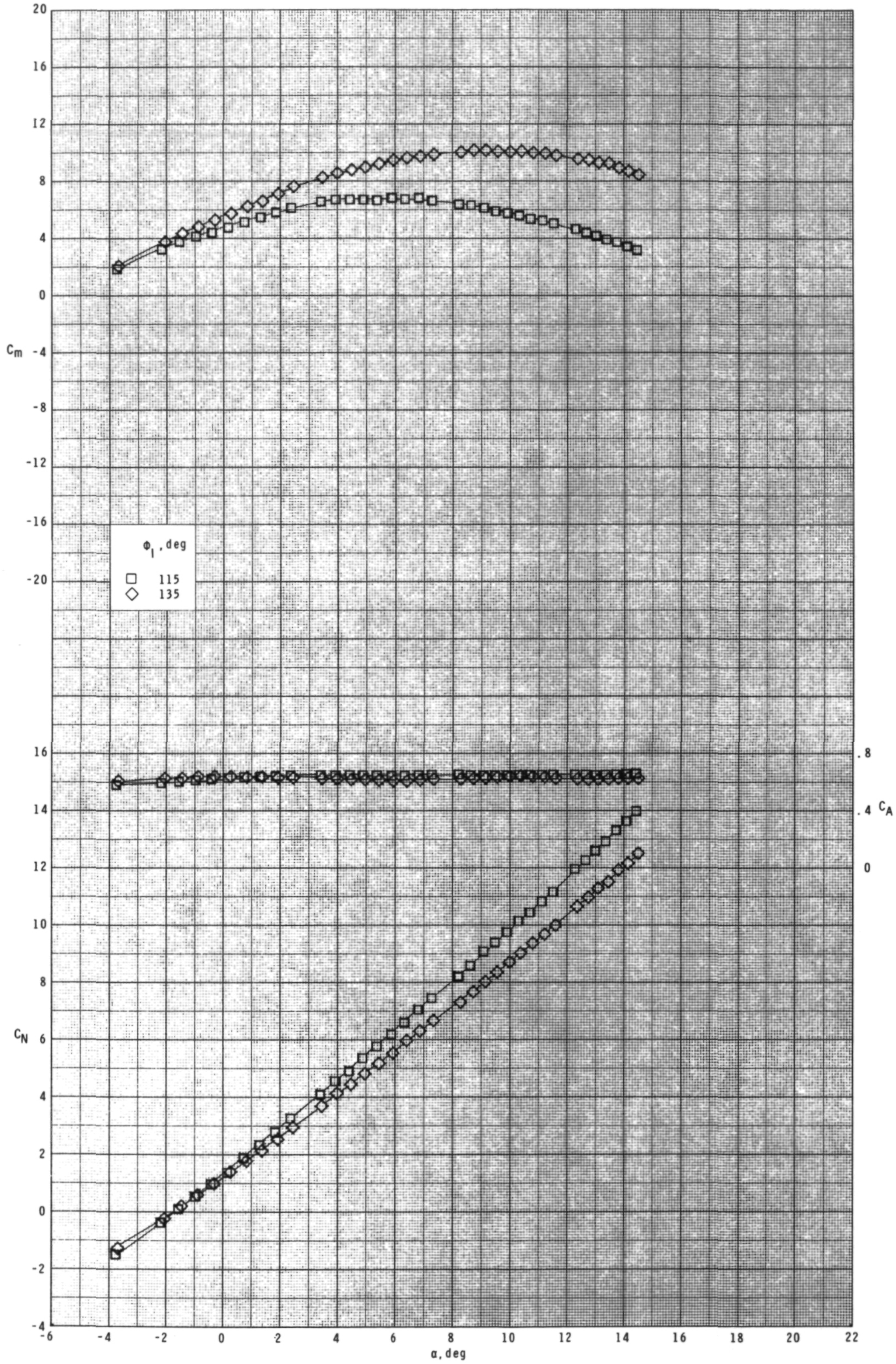

(c) M = 0.95.

Figure 23.- Continued.

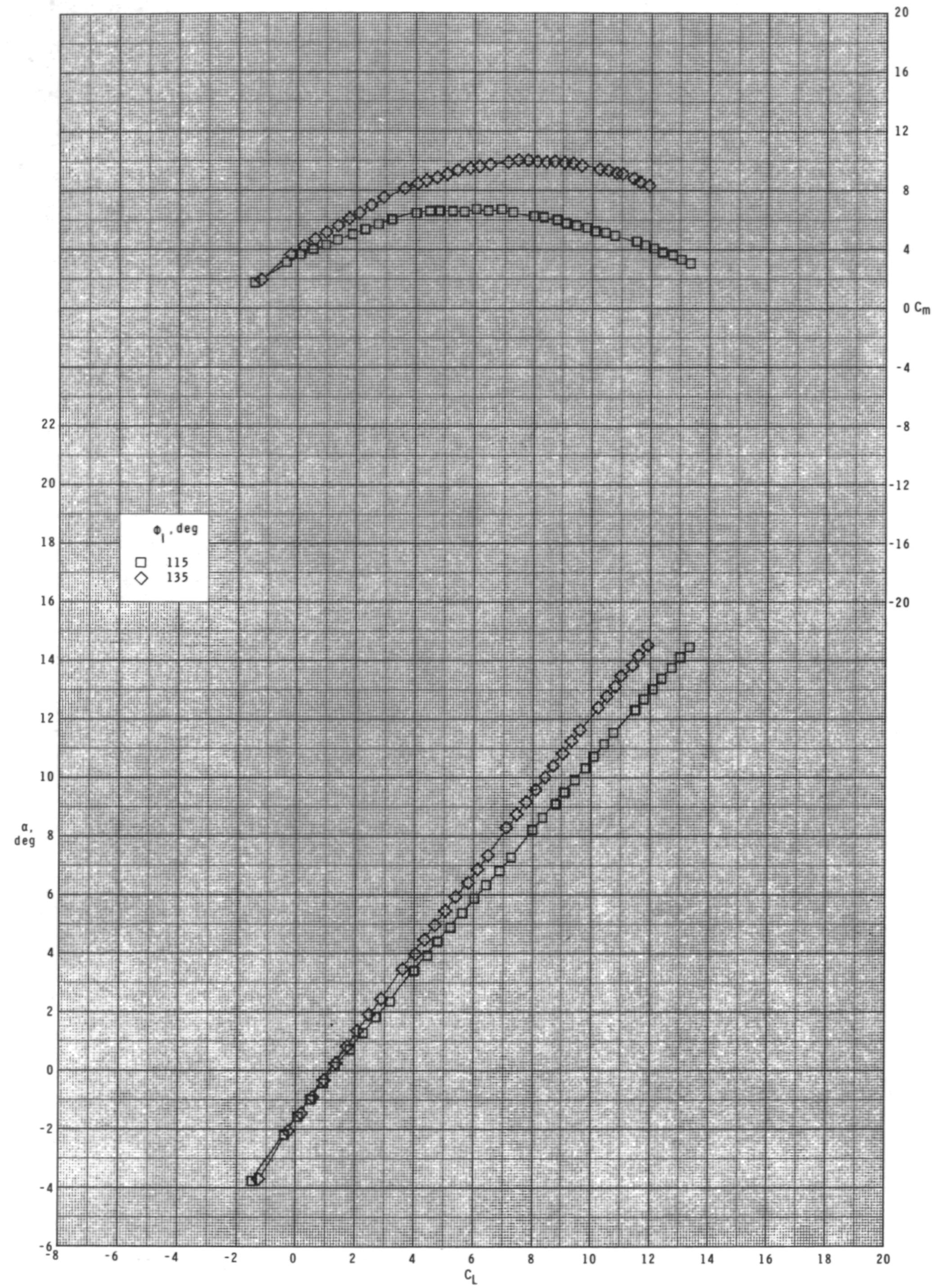

(c) Continued.

Figure 23.- Continued.

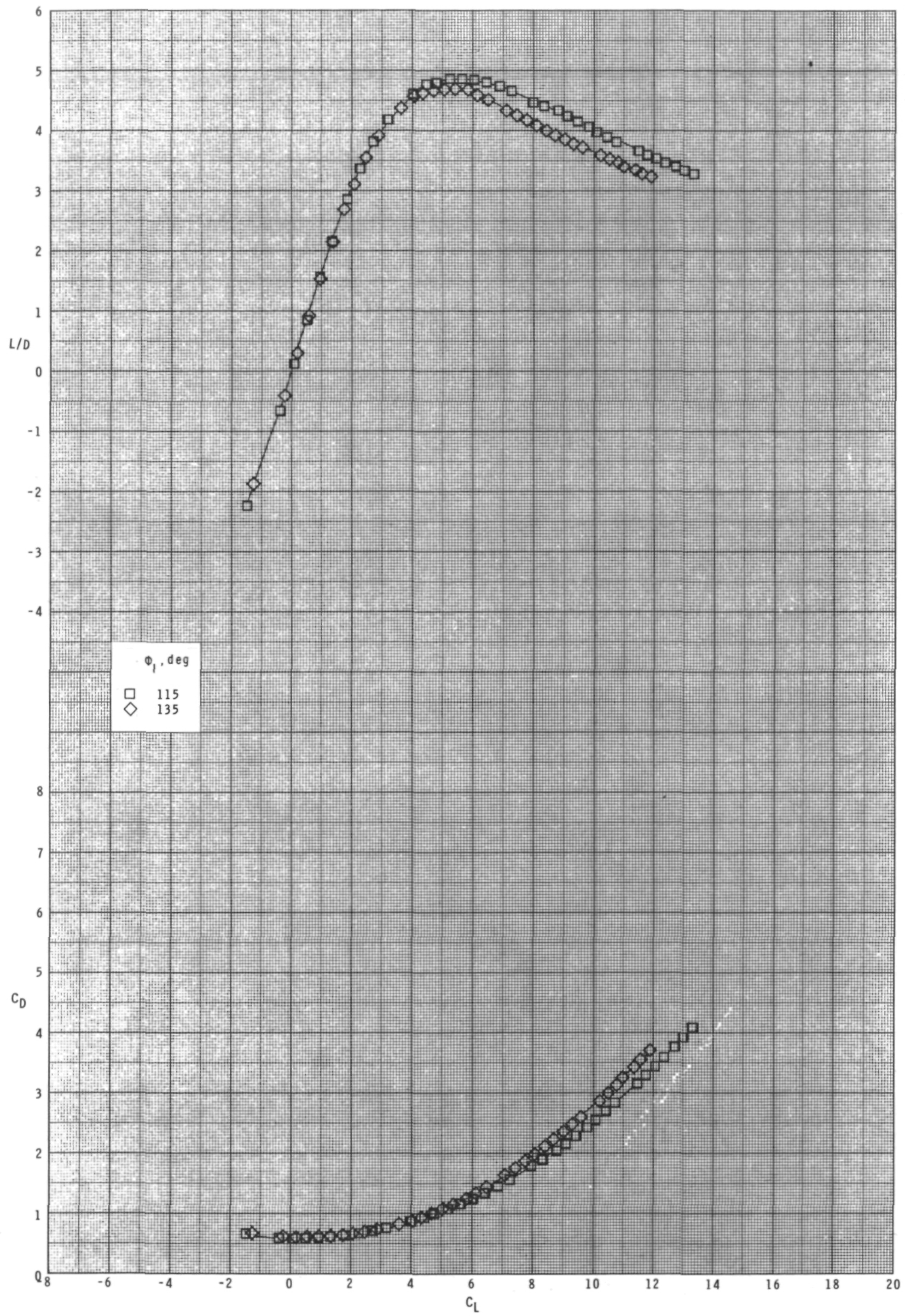

(c) Concluded.

Figure 23.- Concluded.

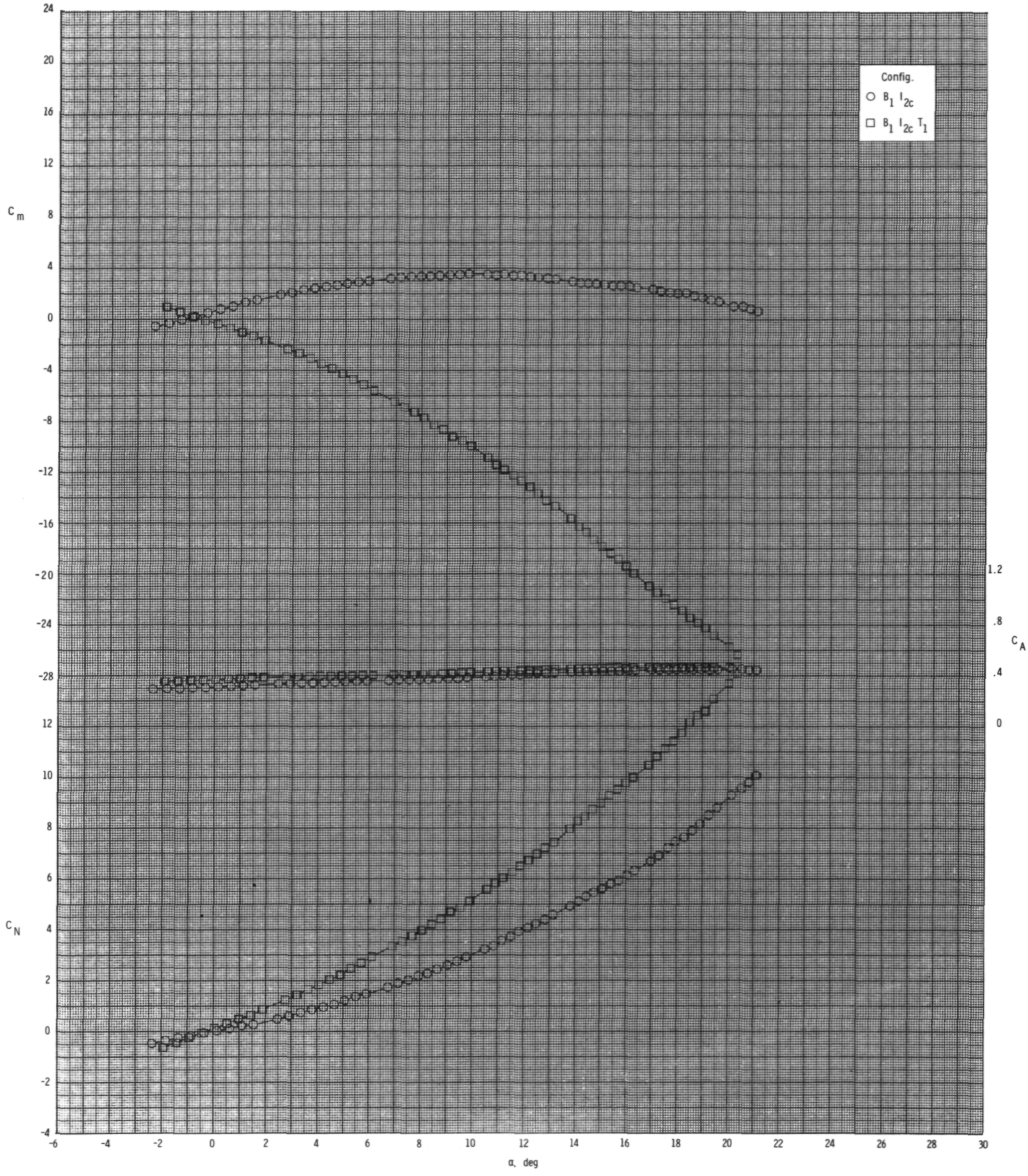

(a) M = 0.60.

Figure 24.- Effect of various model components on longitudinal aerodynamic characteristics for 2-D inlets with internal ducts closed, inlet covers installed, $\phi_I = 90°$, and $\delta_p = 0°$.

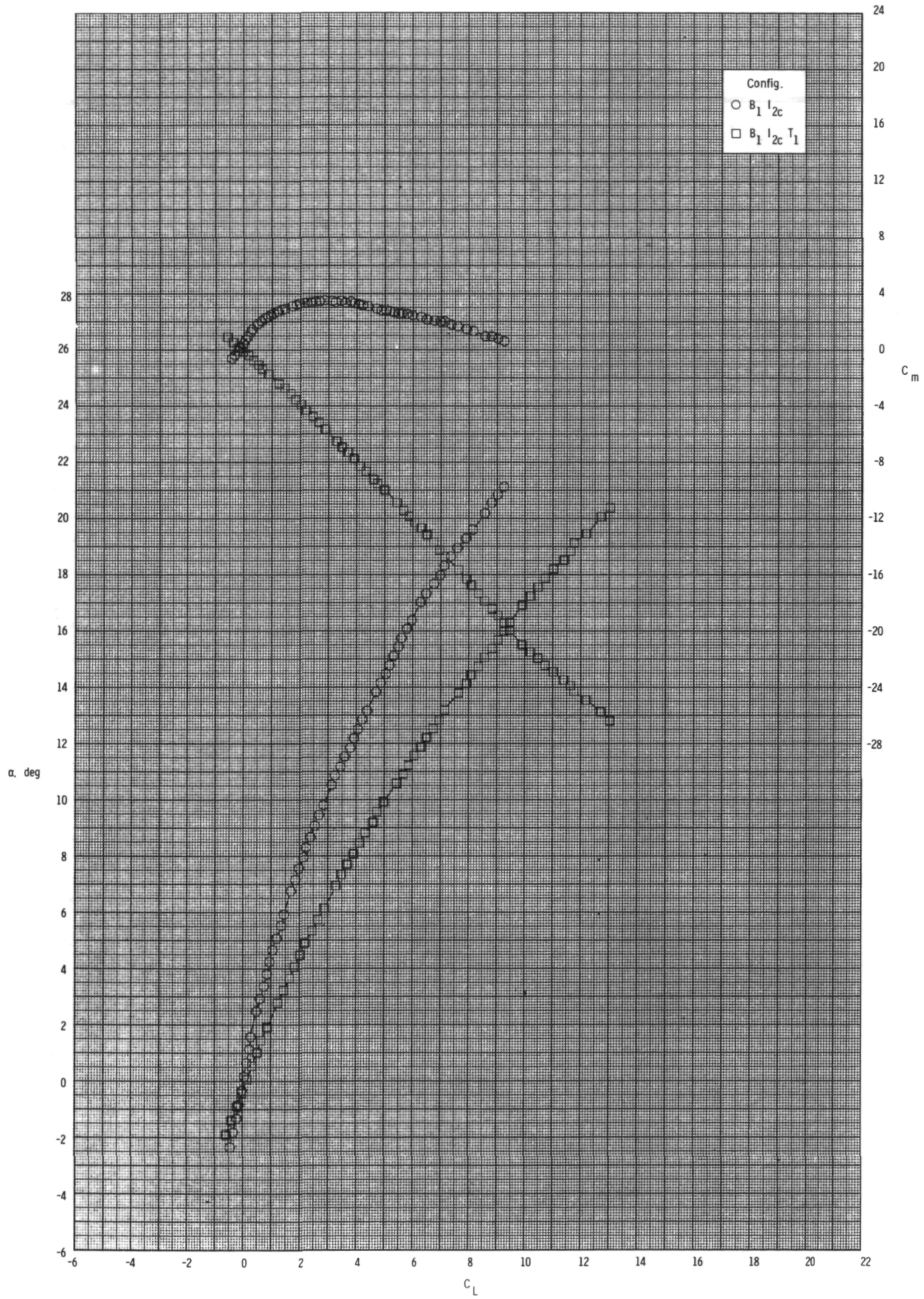

(a) Continued.

Figure 24.- Continued.

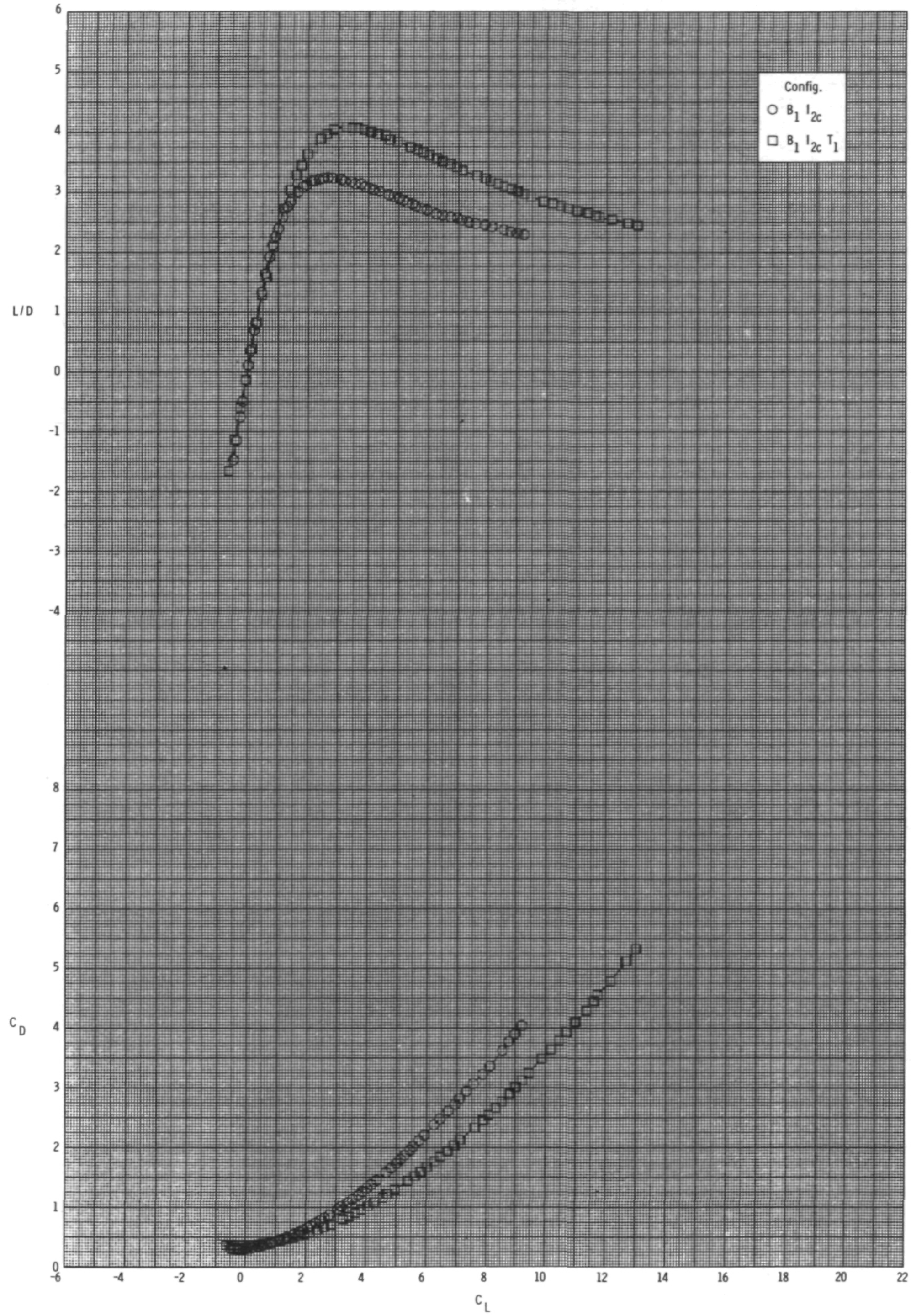

(a) Concluded.

Figure 24.- Continued.

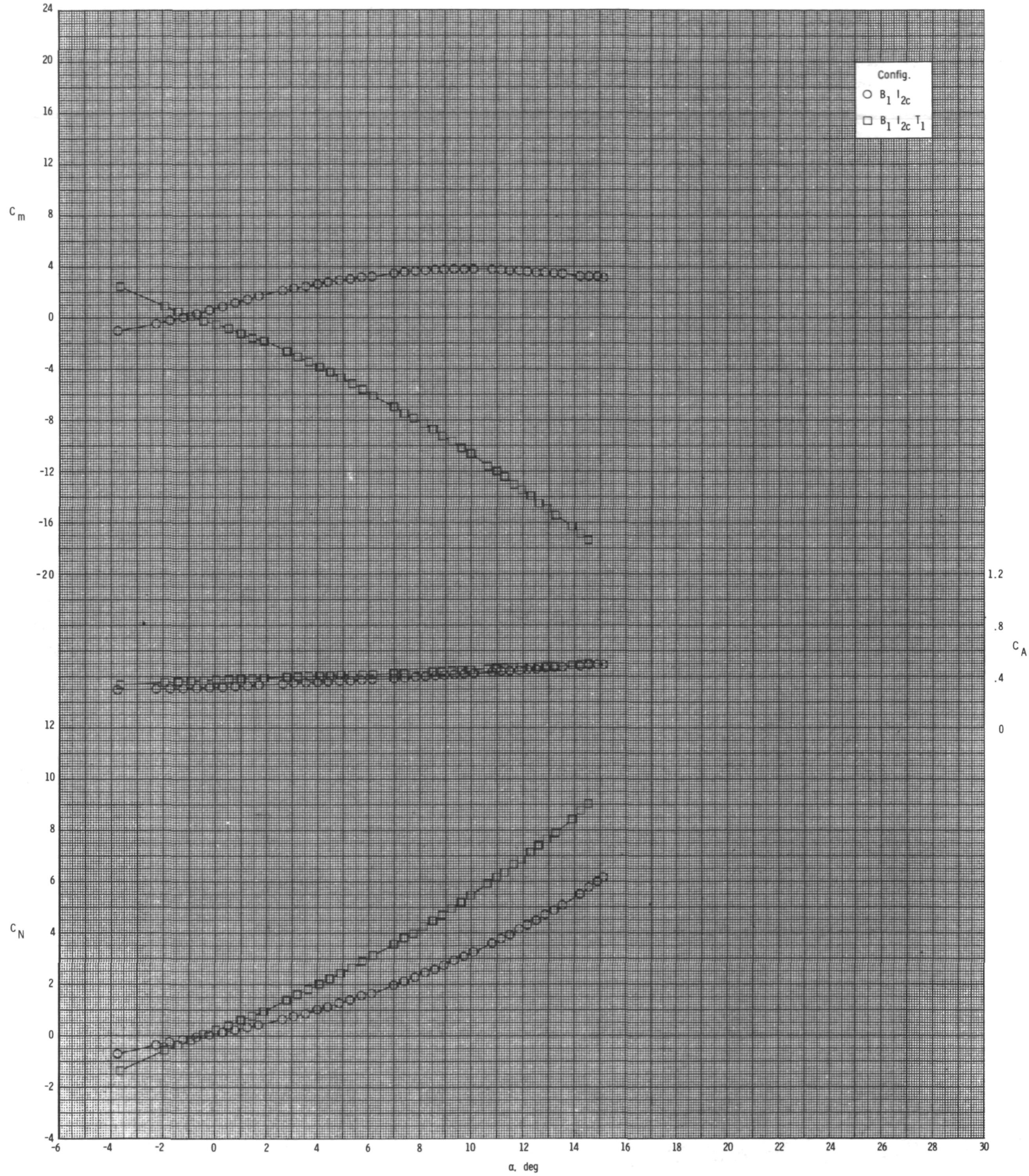

(b) M = 0.80.

Figure 24.- Continued.

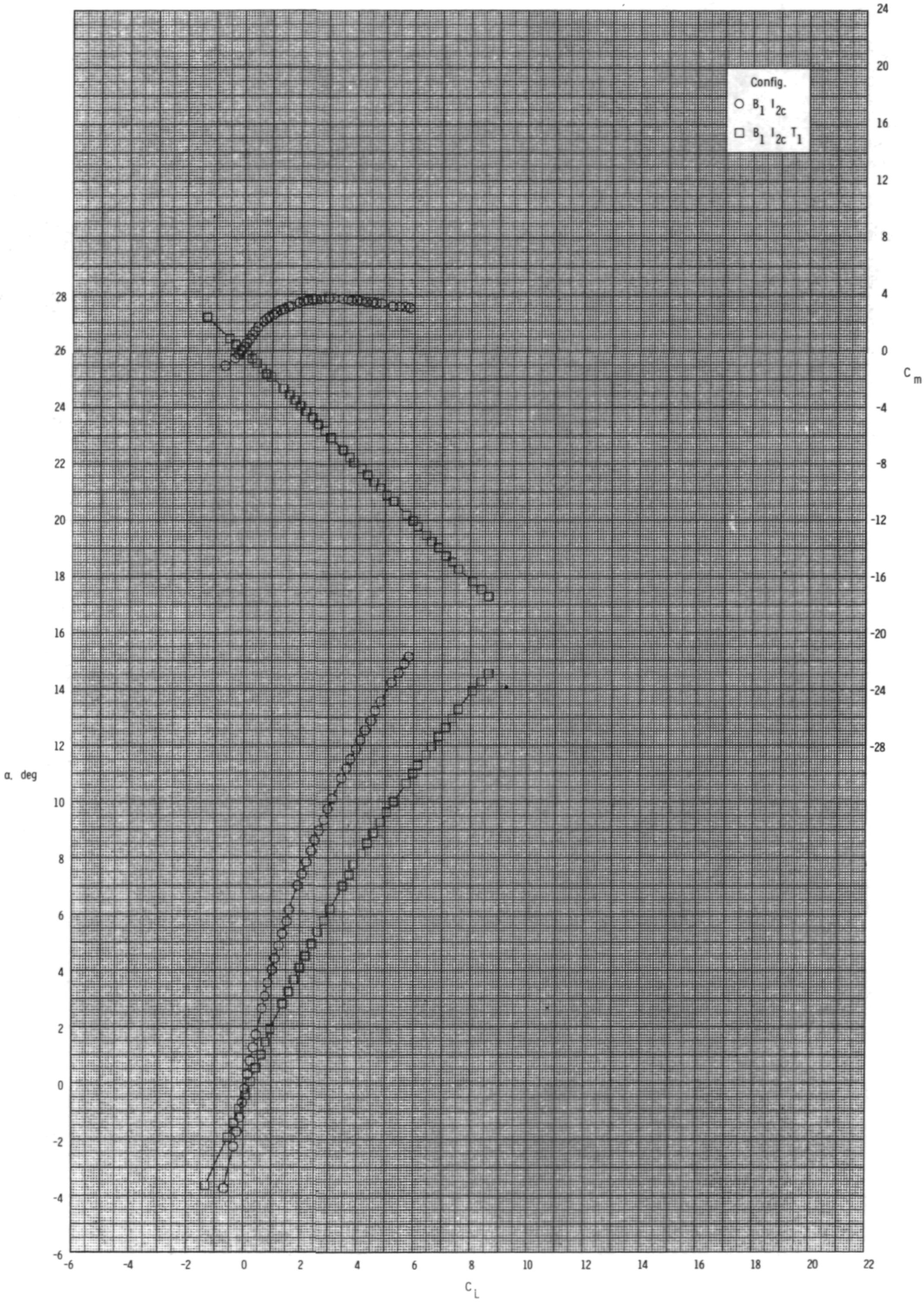

(b) Continued.

Figure 24.- Continued.

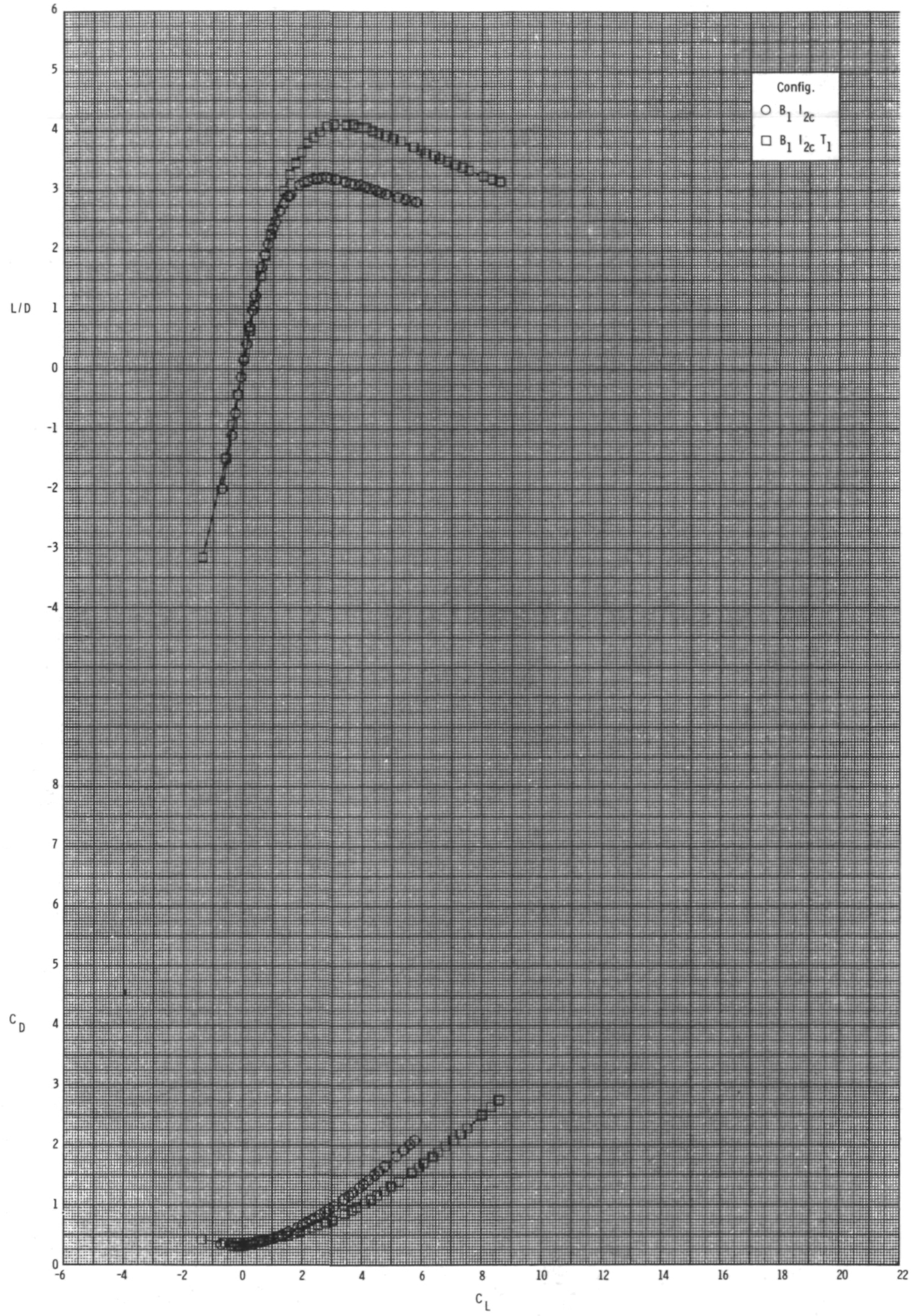

(b) Concluded.

Figure 24.- Continued.

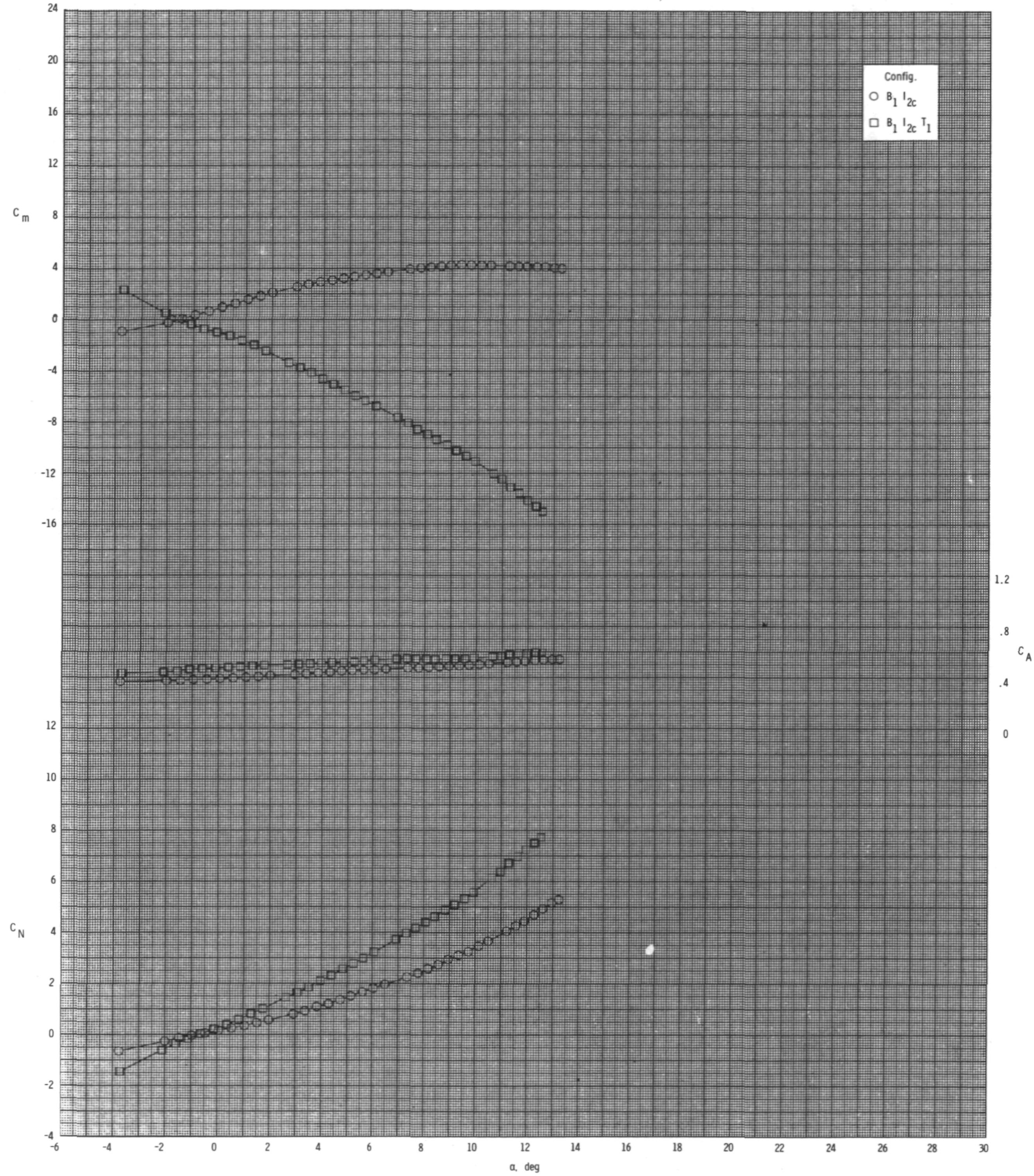

(c) M = 0.95.

Figure 24.- Continued.

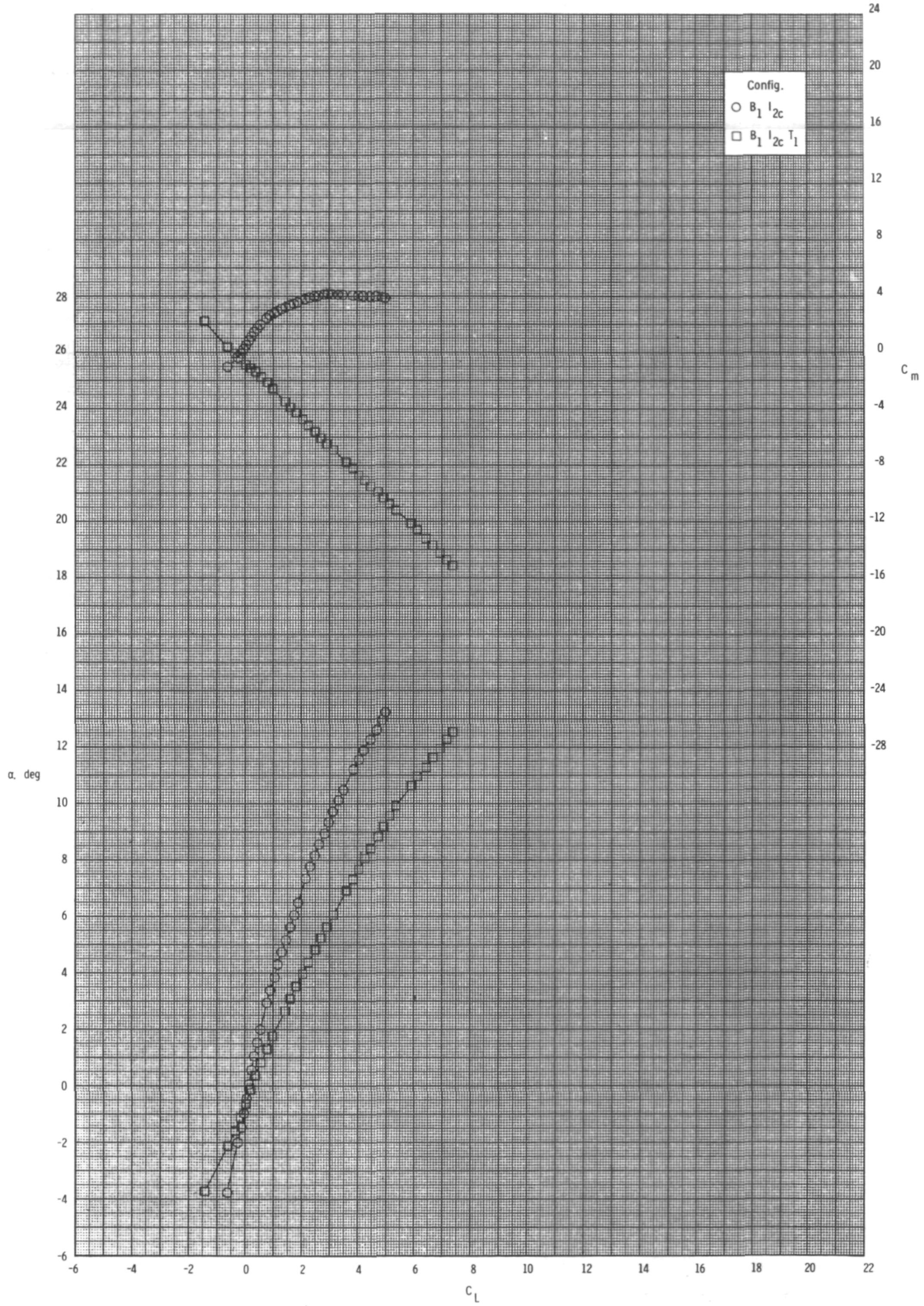

(c) Continued.

Figure 24.- Continued.

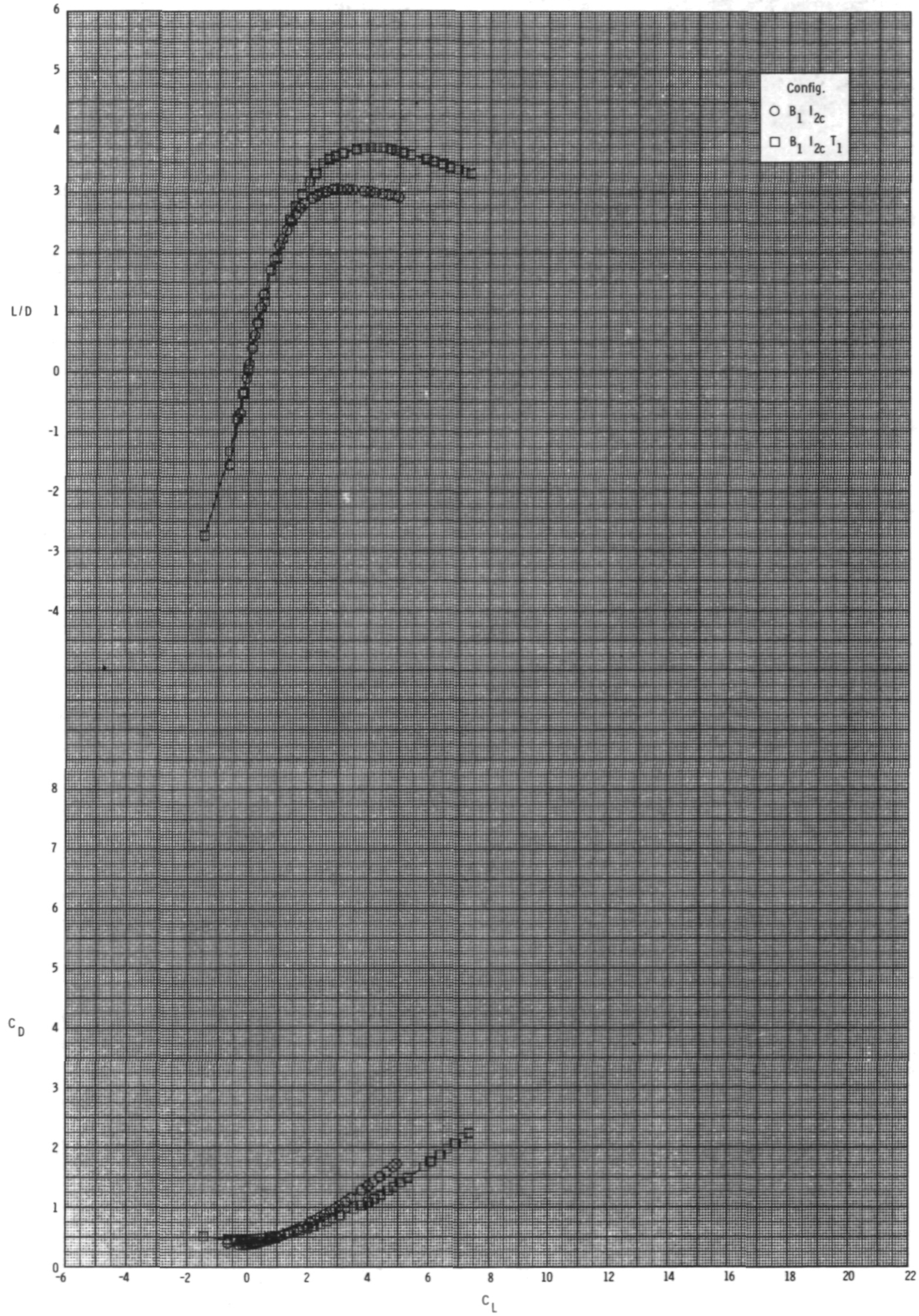

(c) Concluded.

Figure 24.- Concluded.

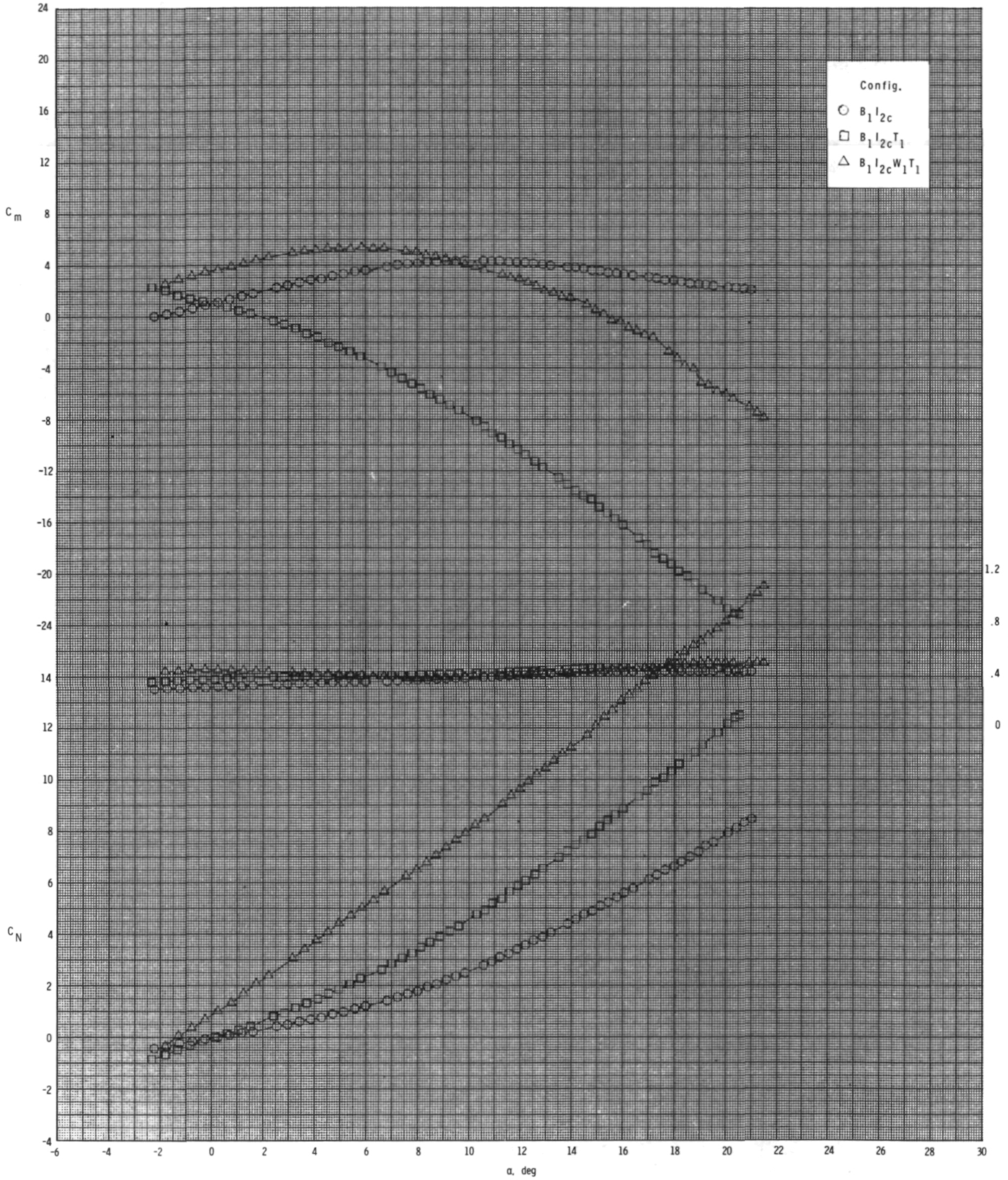

(a) M = 0.60.

Figure 25.- Effect of various model components on longitudinal aerodynamic characteristics for 2-D inlets with internal ducts closed, inlet covers installed, $\phi_I = 115°$, and $\delta_p = 0°$.

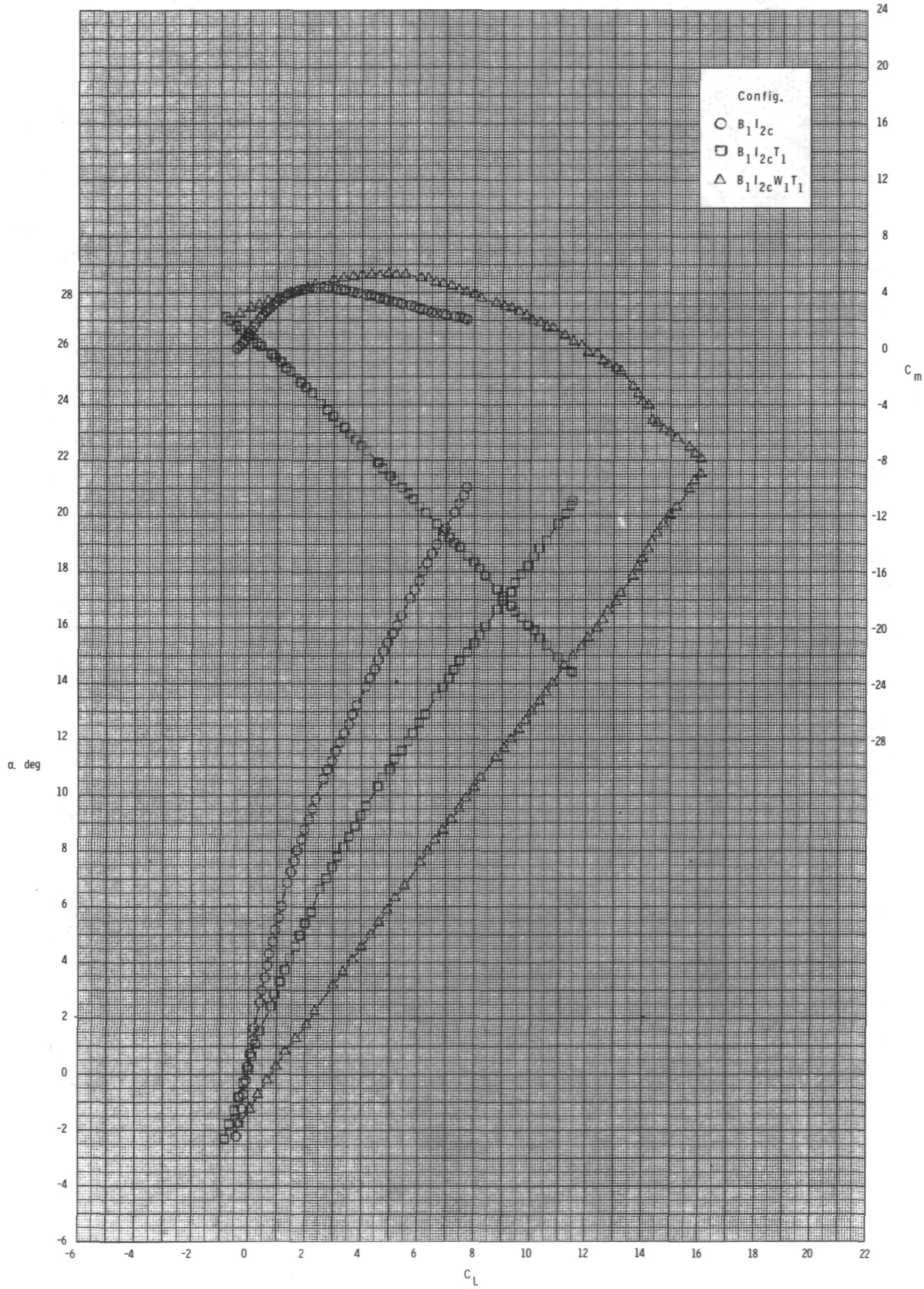

(a) Continued.

Figure 25.- Continued.

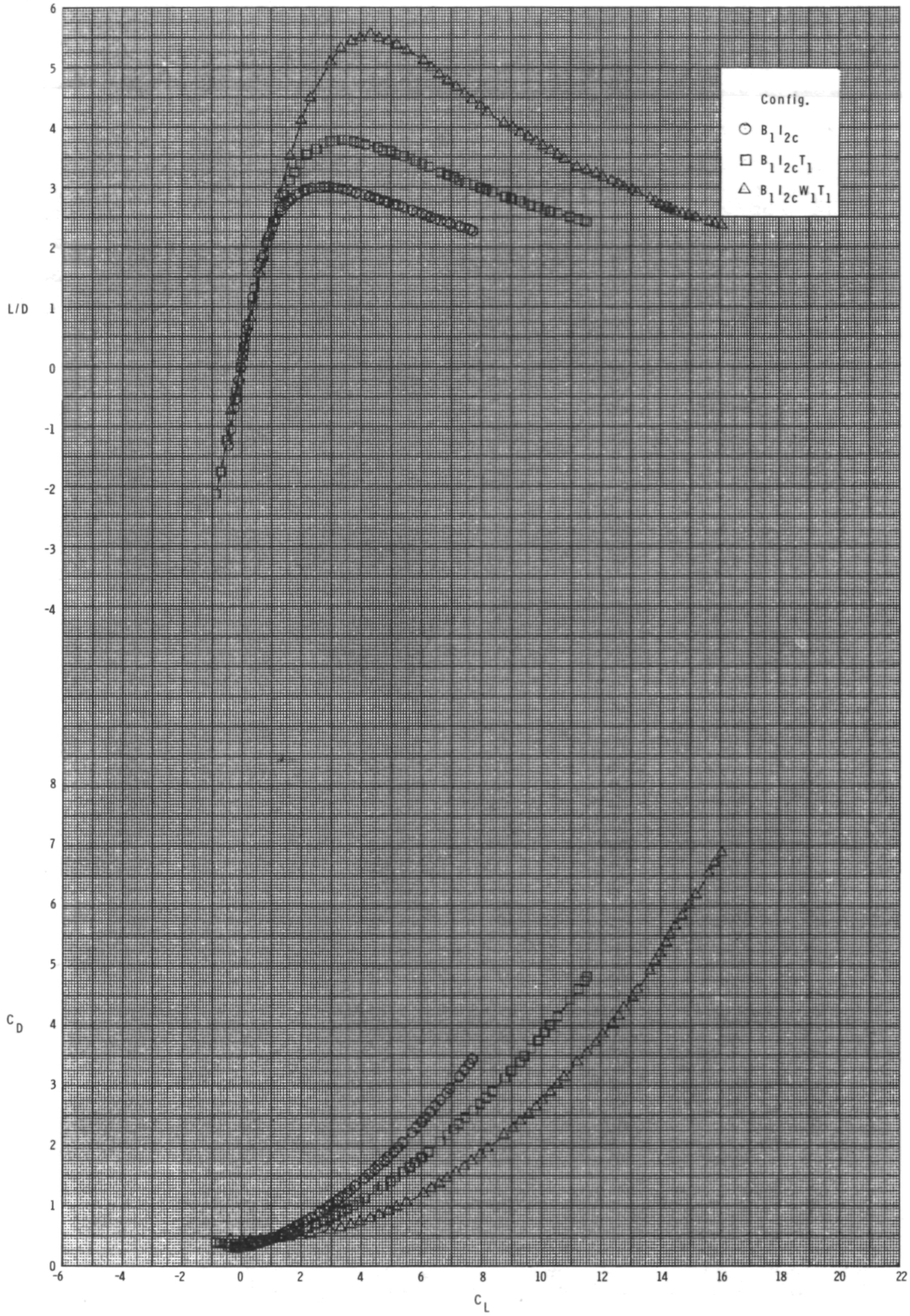

(a) Concluded.

Figure 25.- Continued.

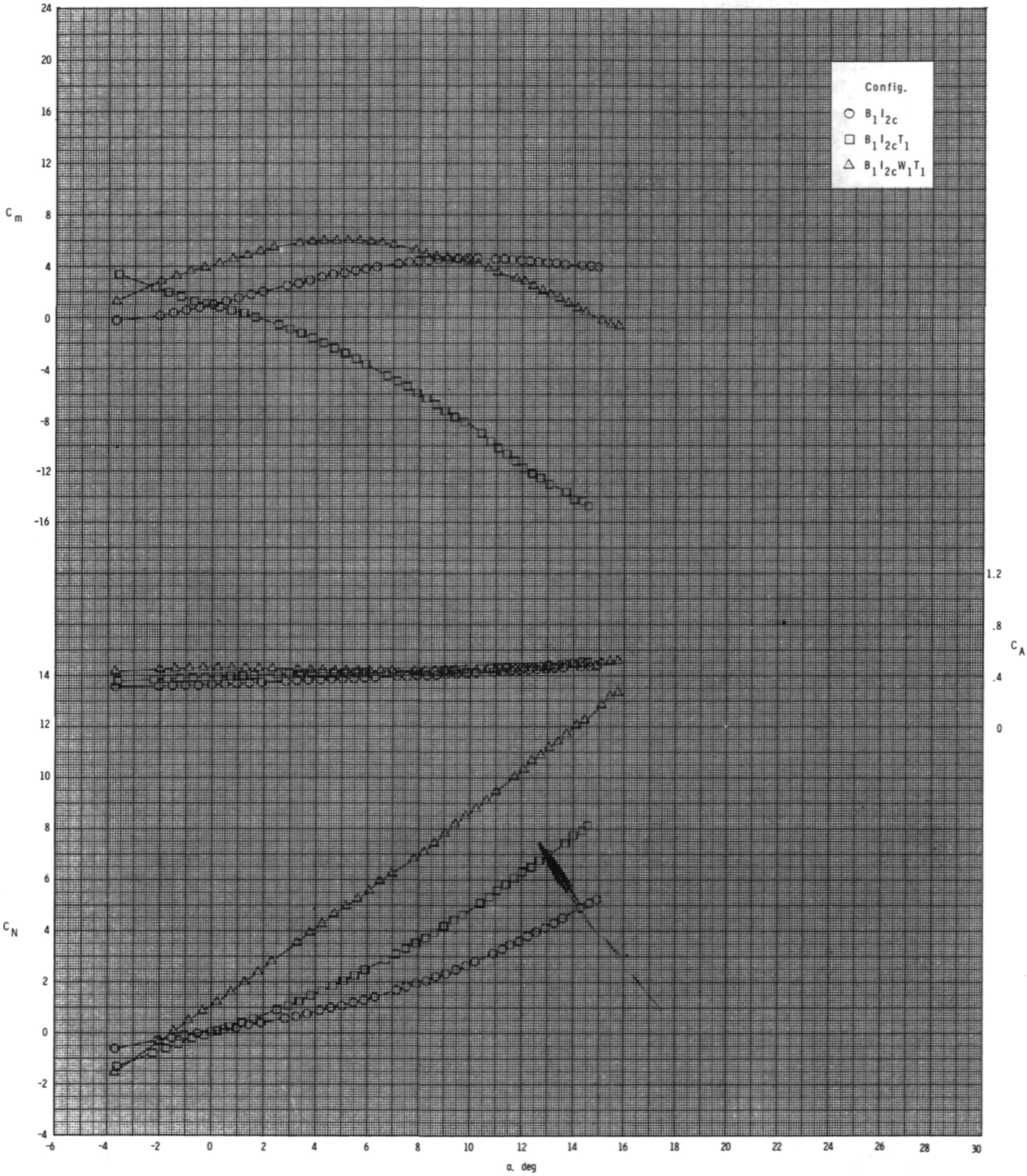

(b) M = 0.80.

Figure 25.- Continued.

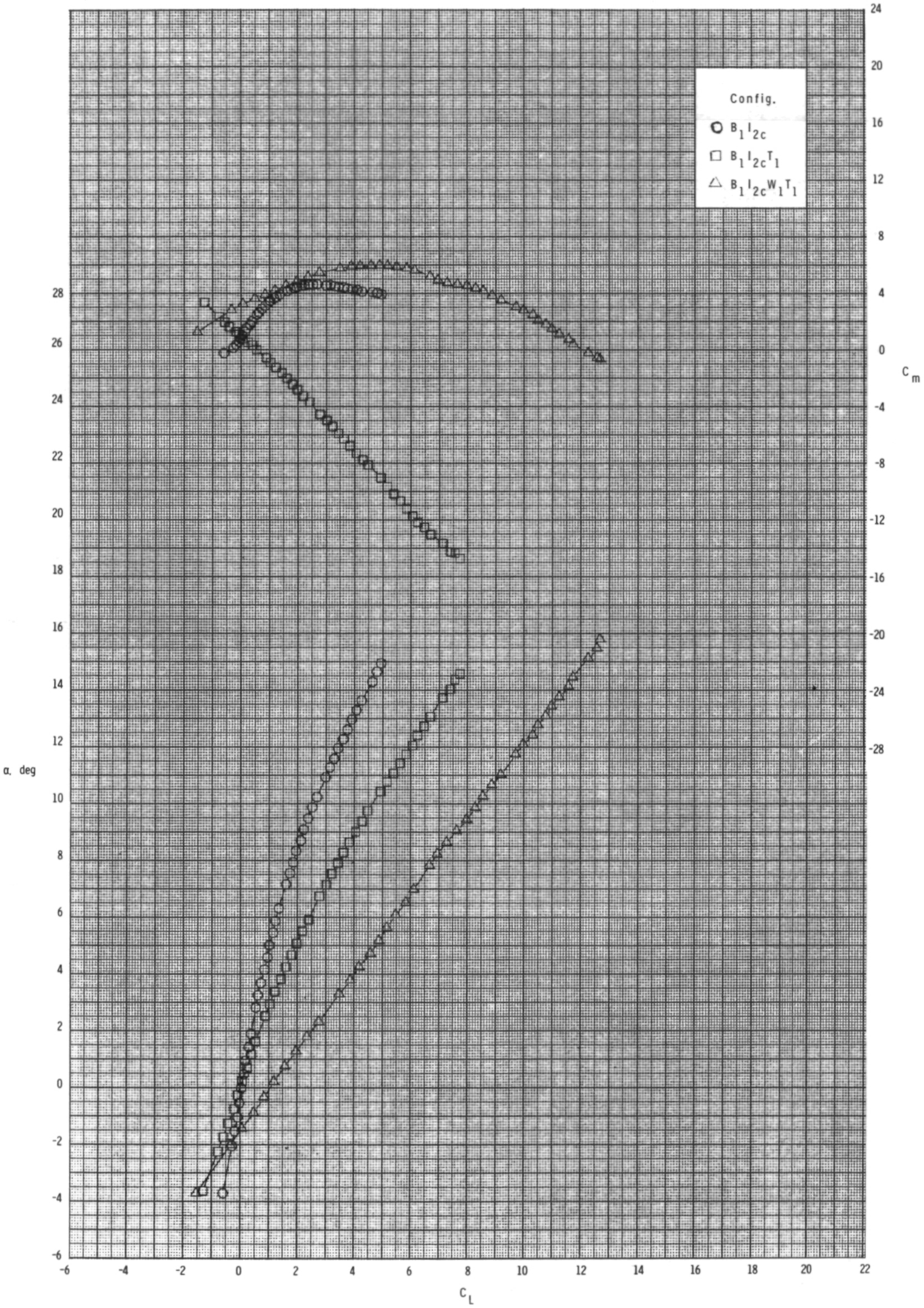

(b) Continued.

Figure 25.- Continued.

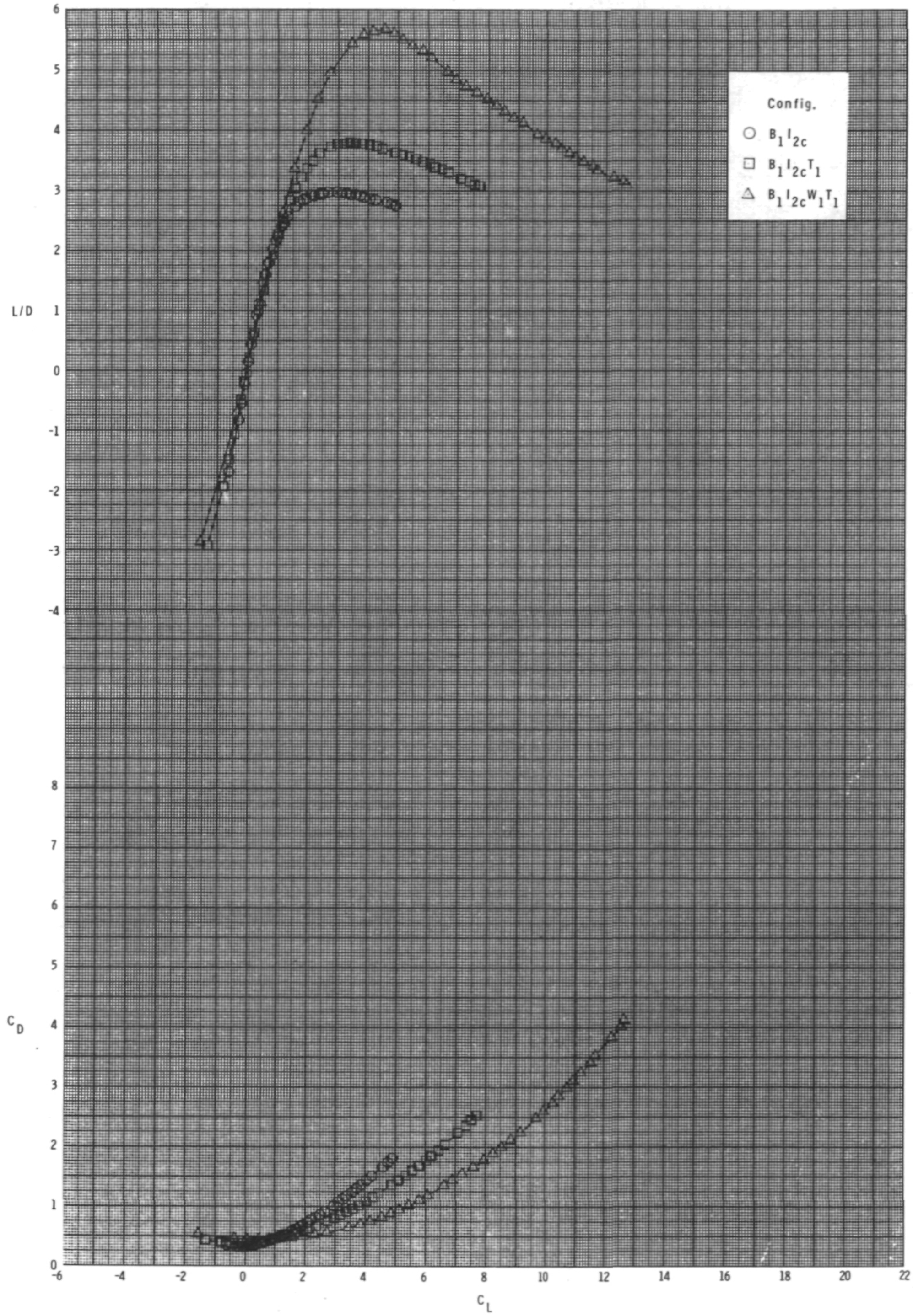

(b) Concluded.

Figure 25.- Continued.

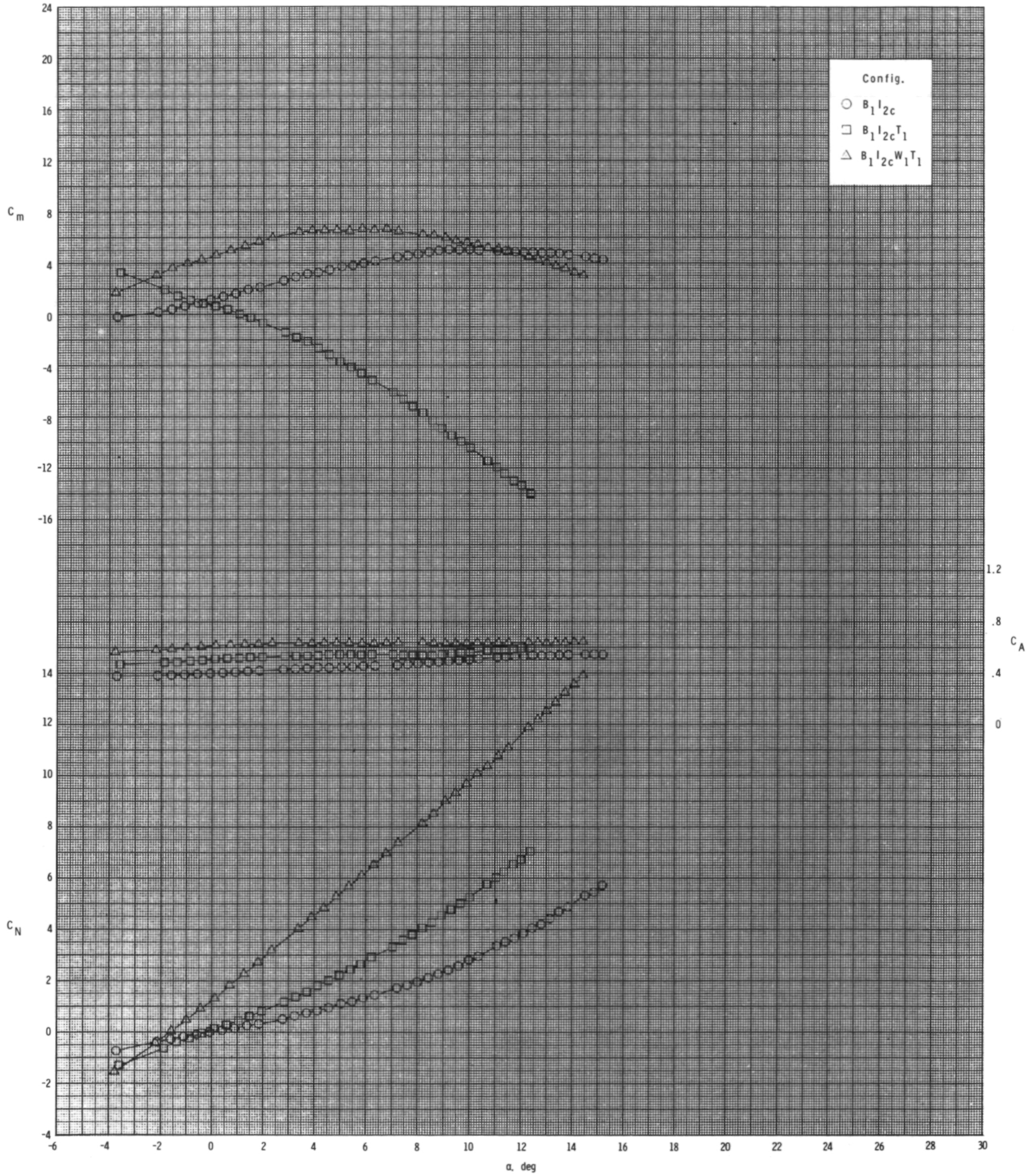

(c) M = 0.95.

Figure 25.- Continued.

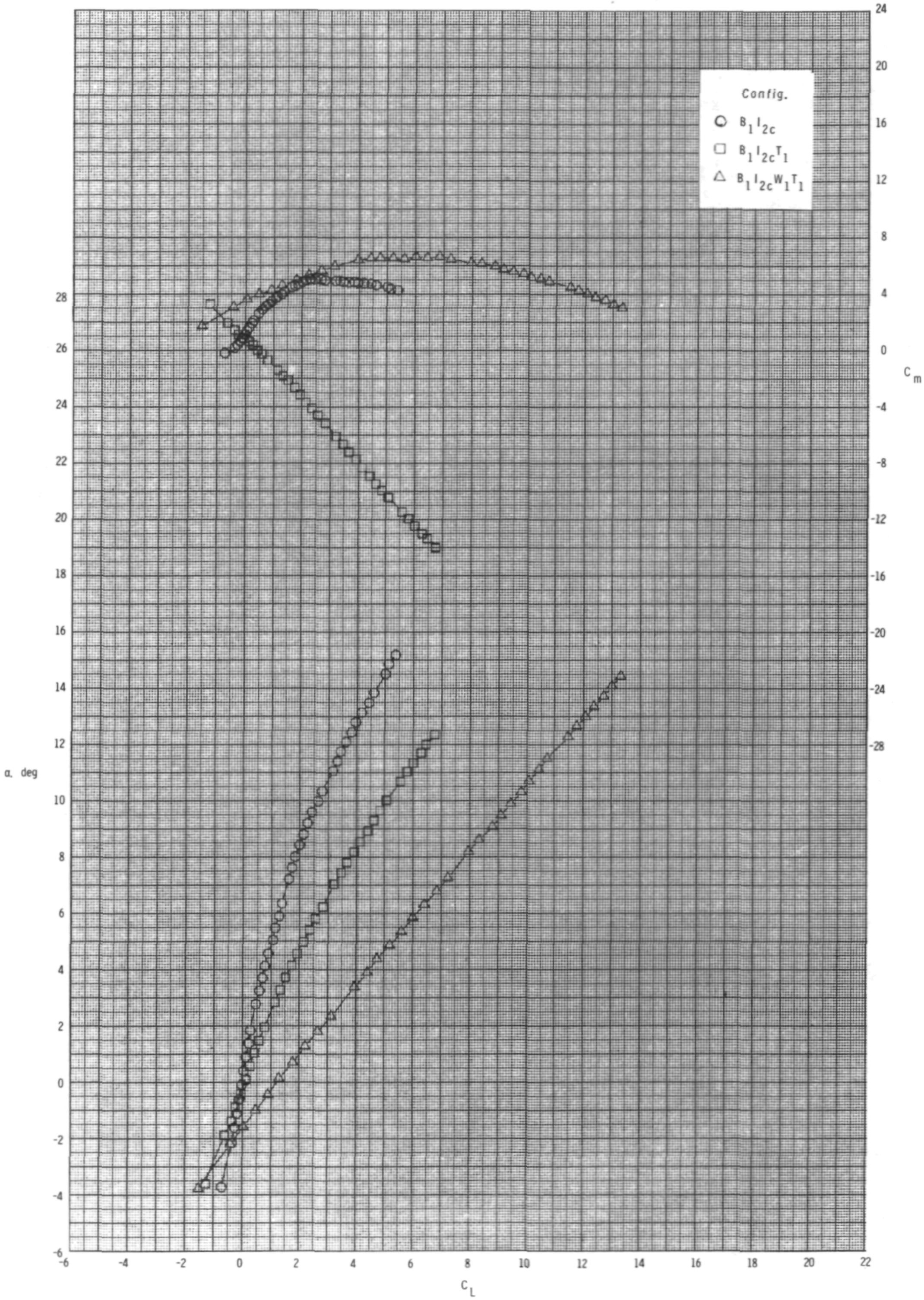

(c) Continued.

Figure 25.- Continued.

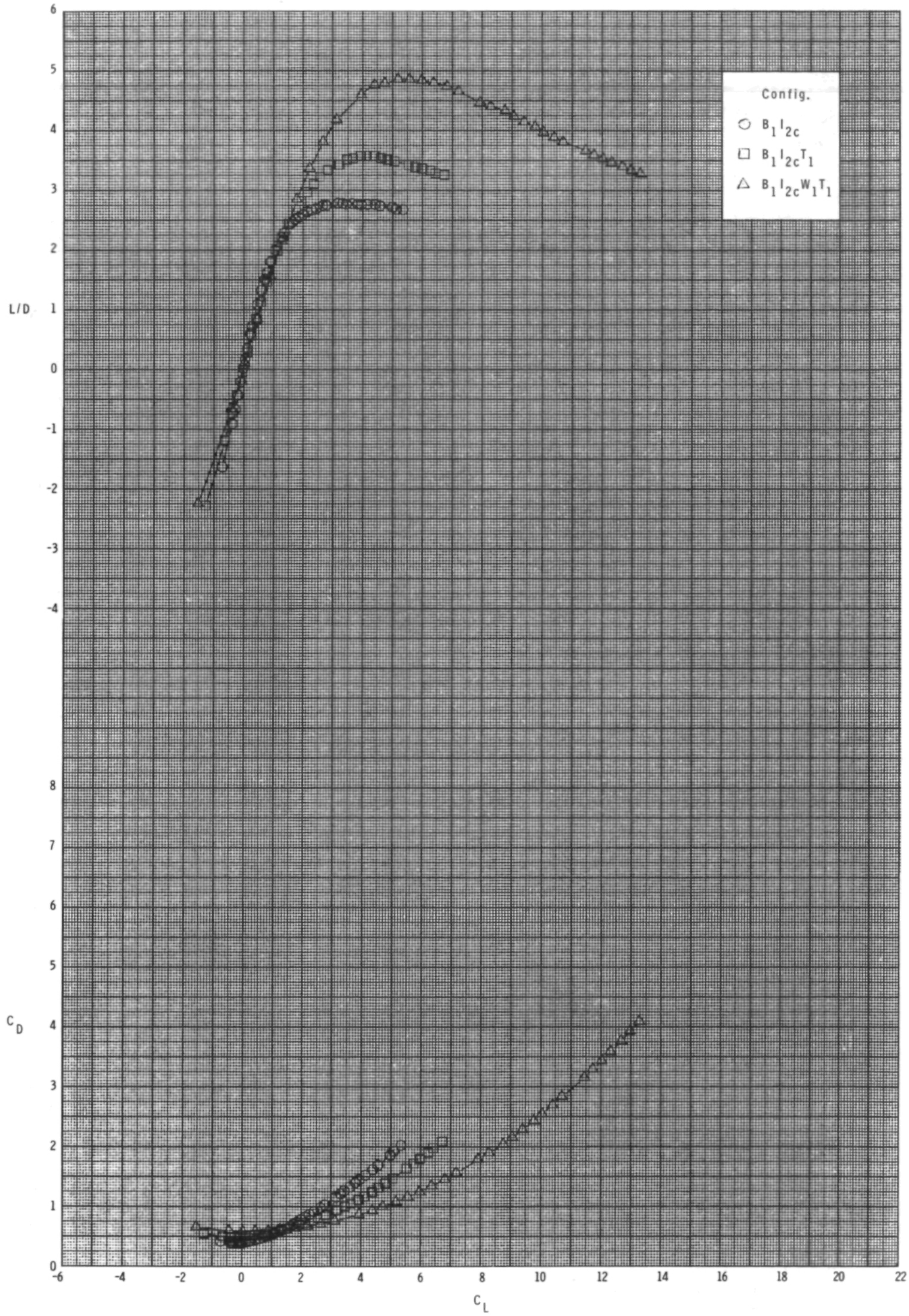

(c) Concluded.

Figure 25.- Concluded.

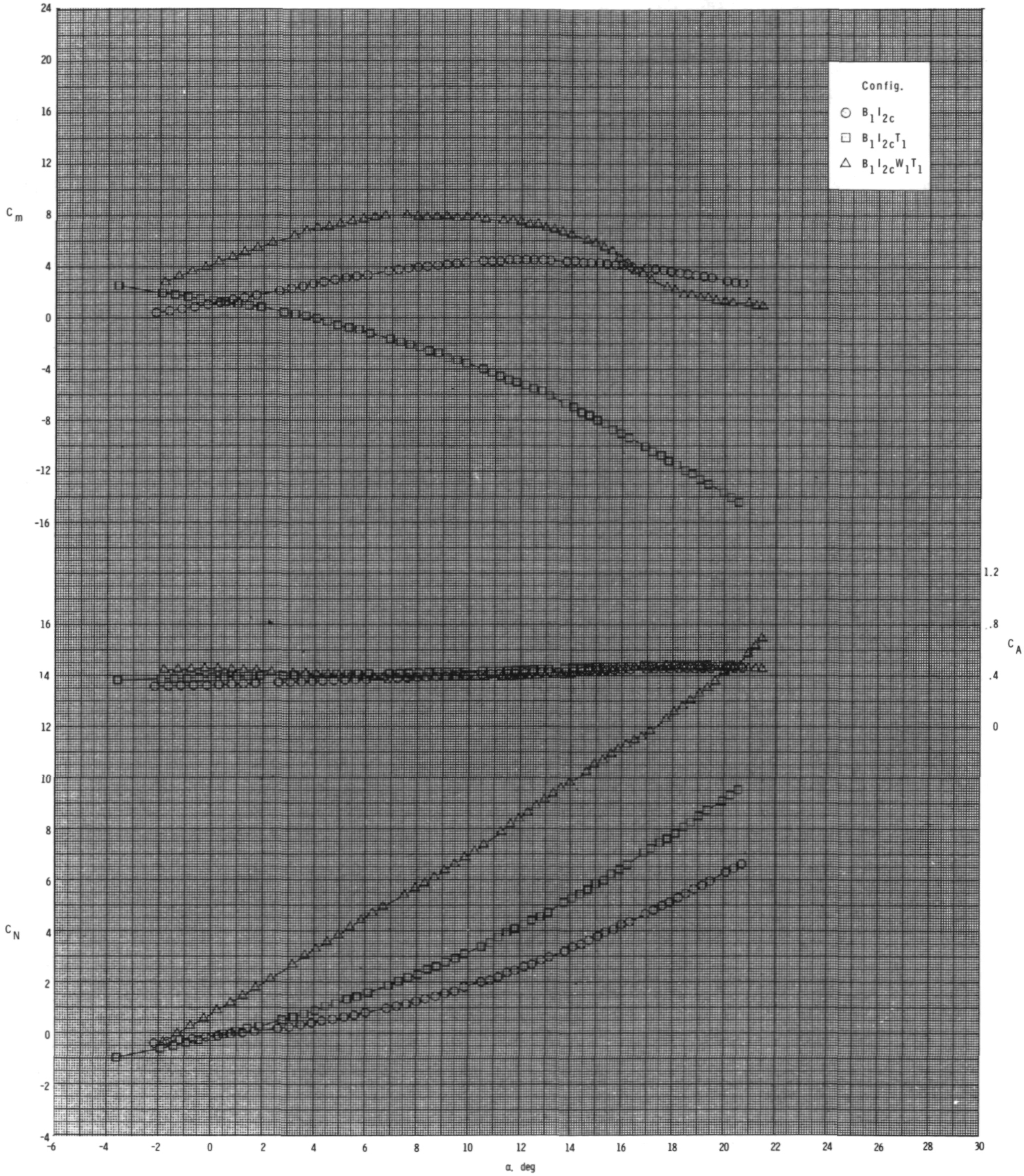

(a) M = 0.60.

Figure 26.- Effect of various model components on longitudinal aerodynamic characteristics for 2-D inlets with internal ducts closed, inlet covers installed, T_1, $\phi_I = 135°$, and $\delta_p = 0°$.

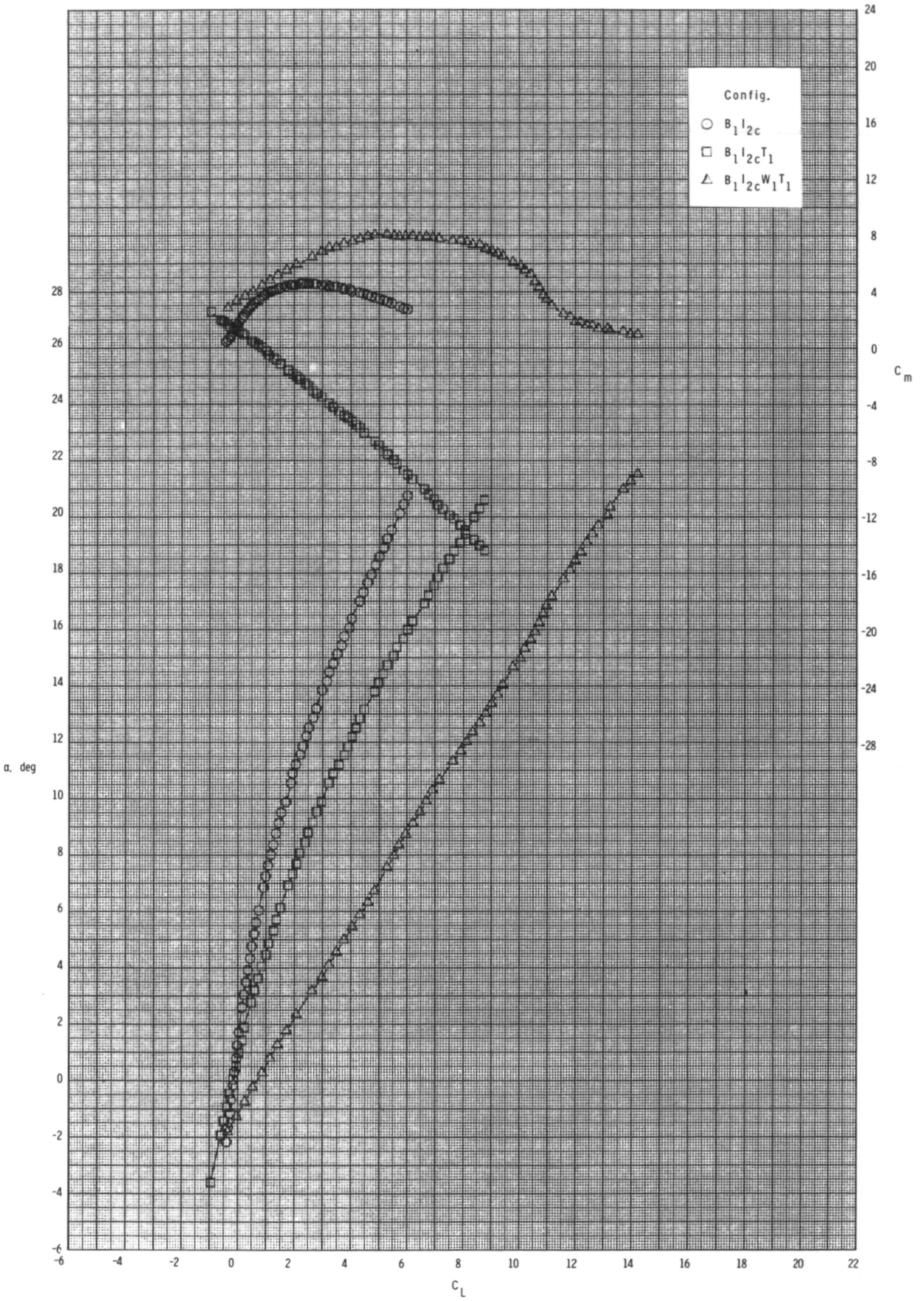

(a) Continued.

Figure 26.- Continued.

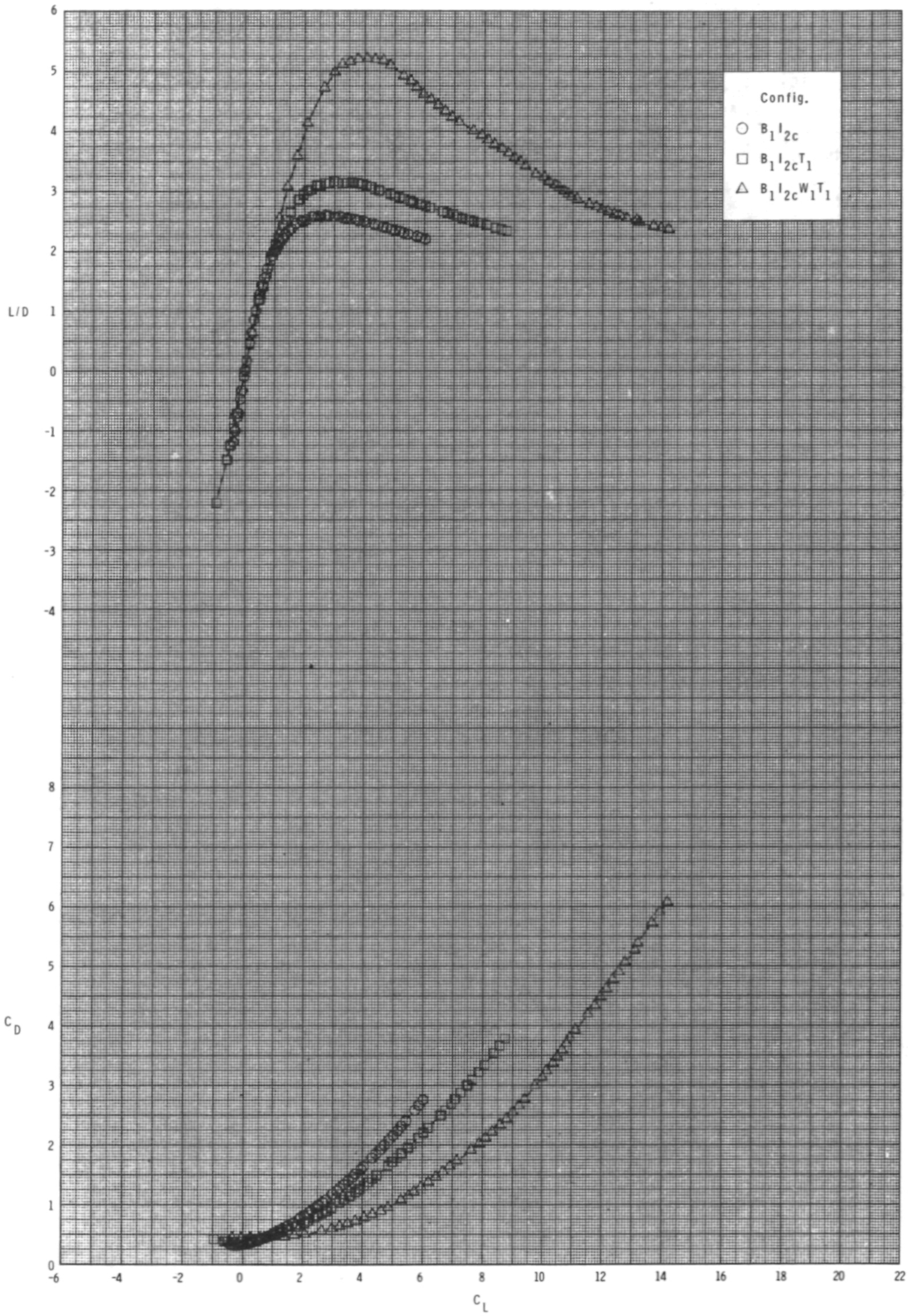

(a) Concluded.

Figure 26.- Continued.

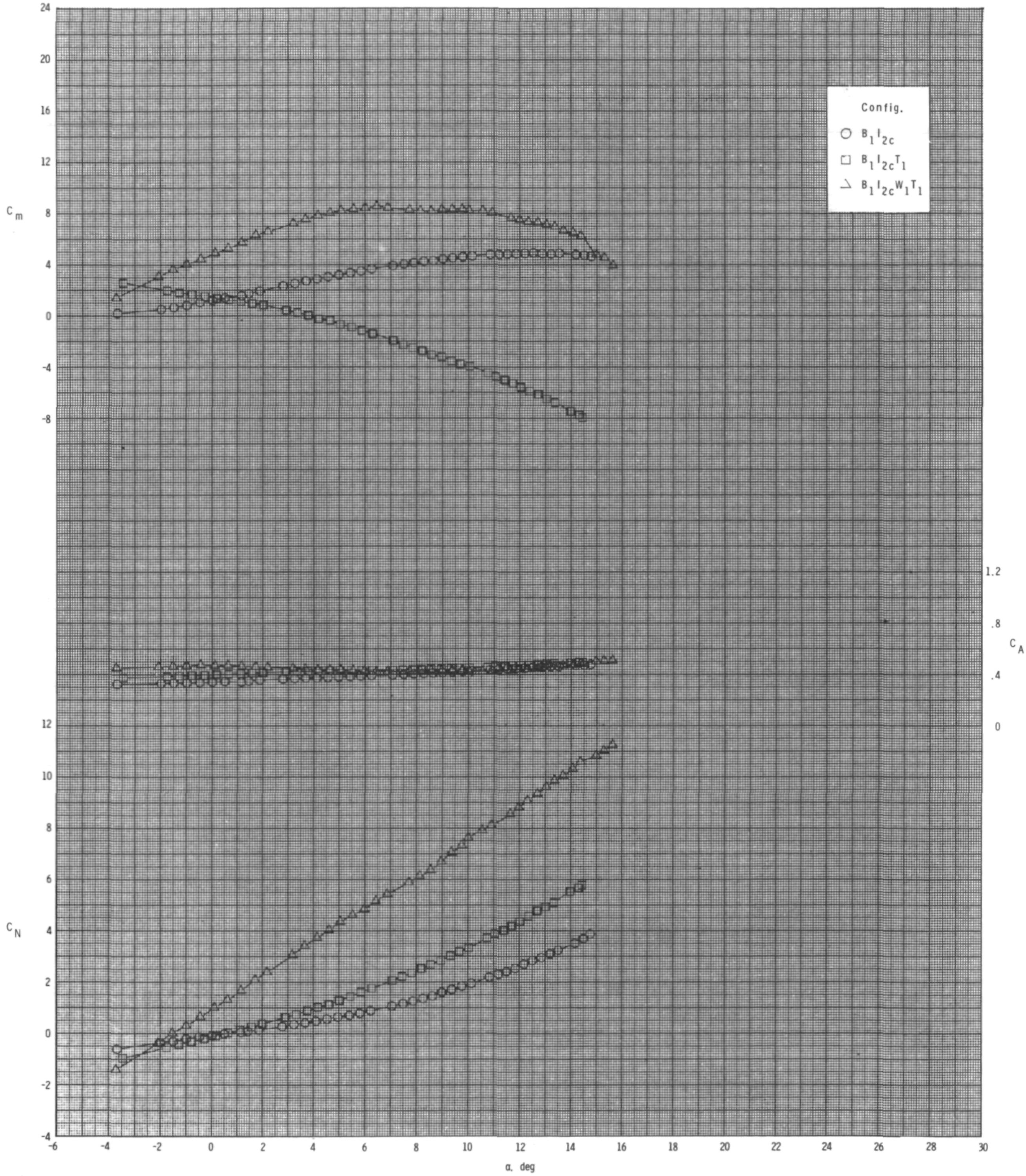

(b) M = 0.80.

Figure 26.- Continued.

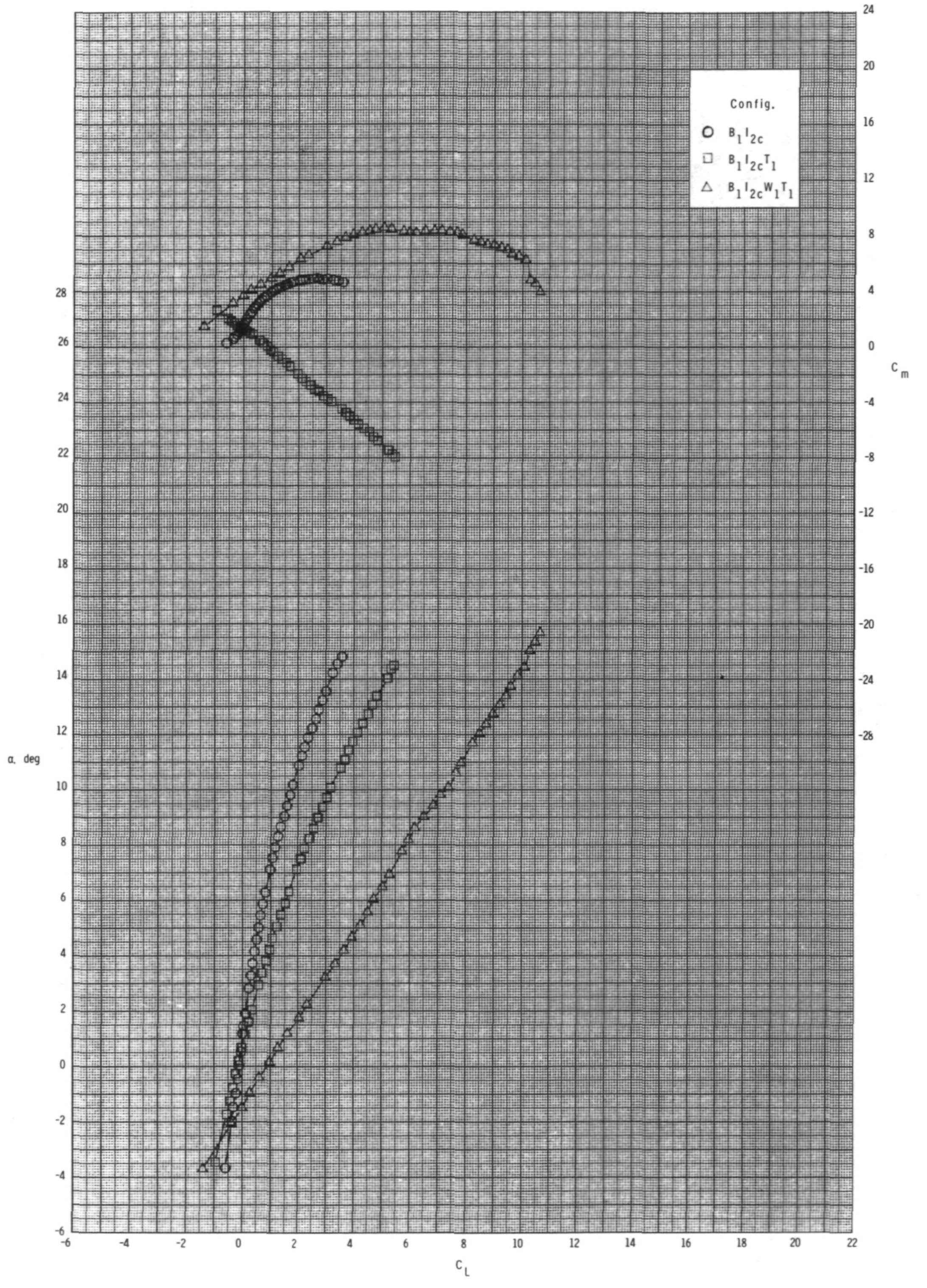

(b) Continued.

Figure 26.- Continued.

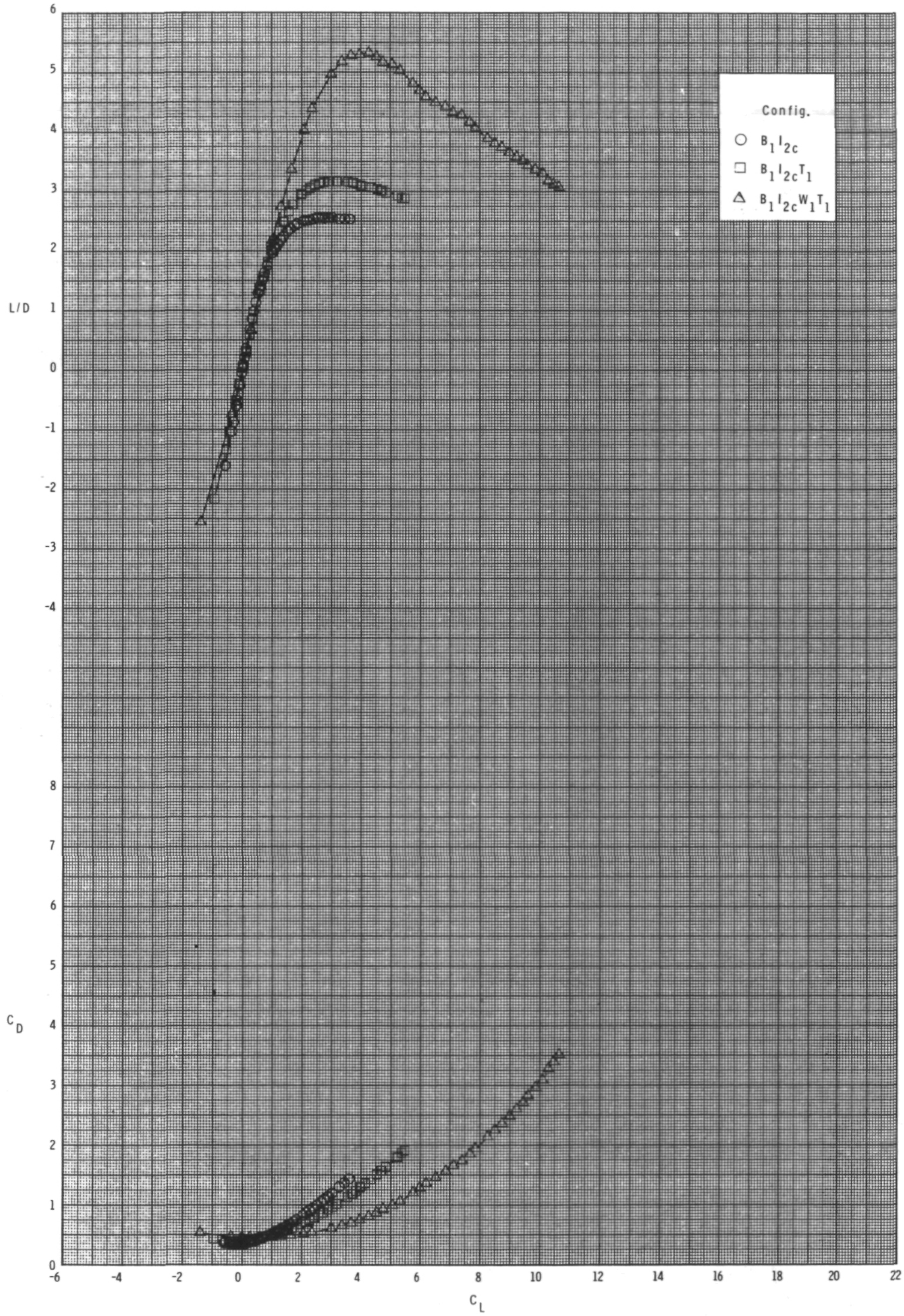

(b) Concluded.

Figure 26.- Continued.

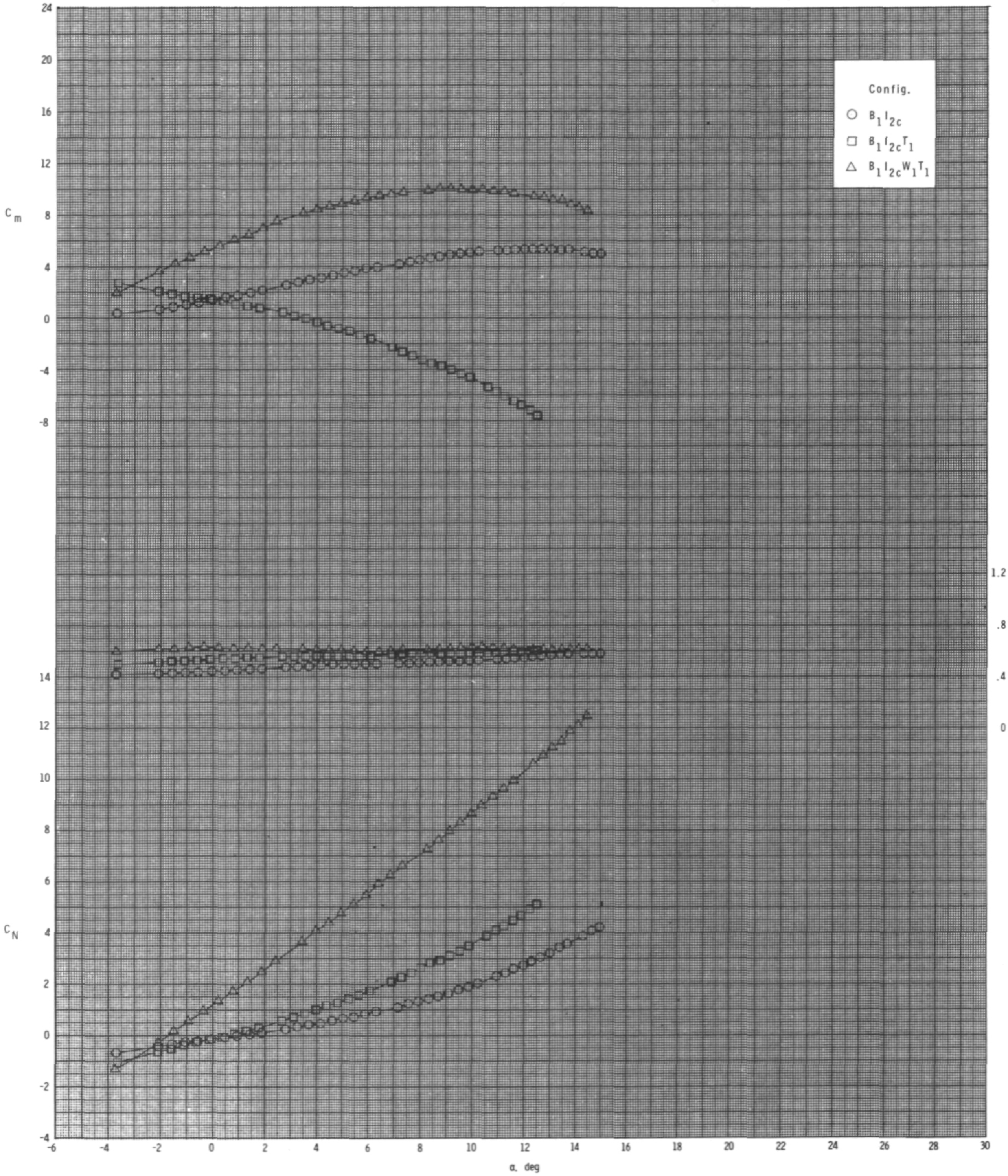

(c) M = 0.95.

Figure 26.- Continued.

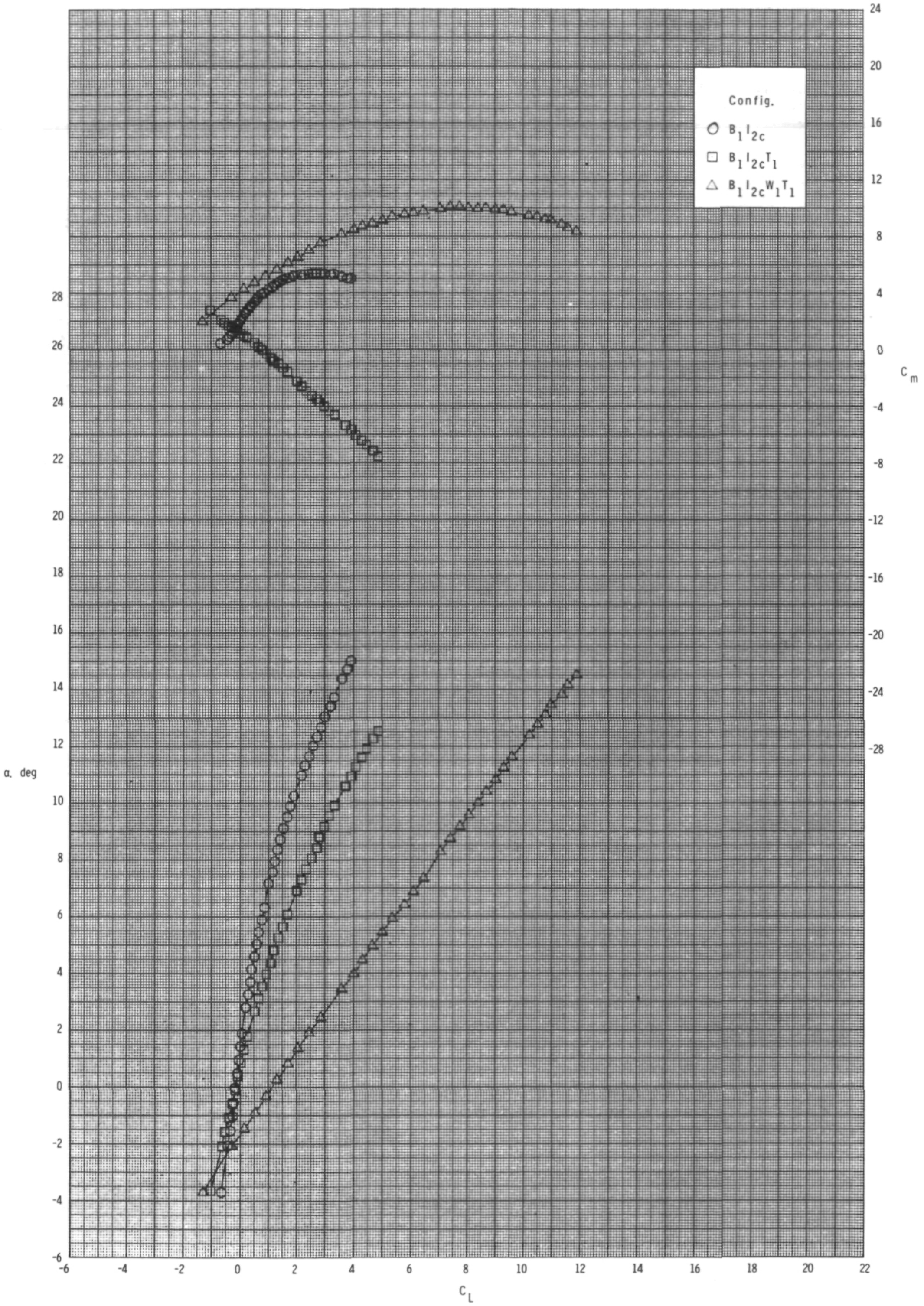

(c) Continued.

Figure 26.- Continued.

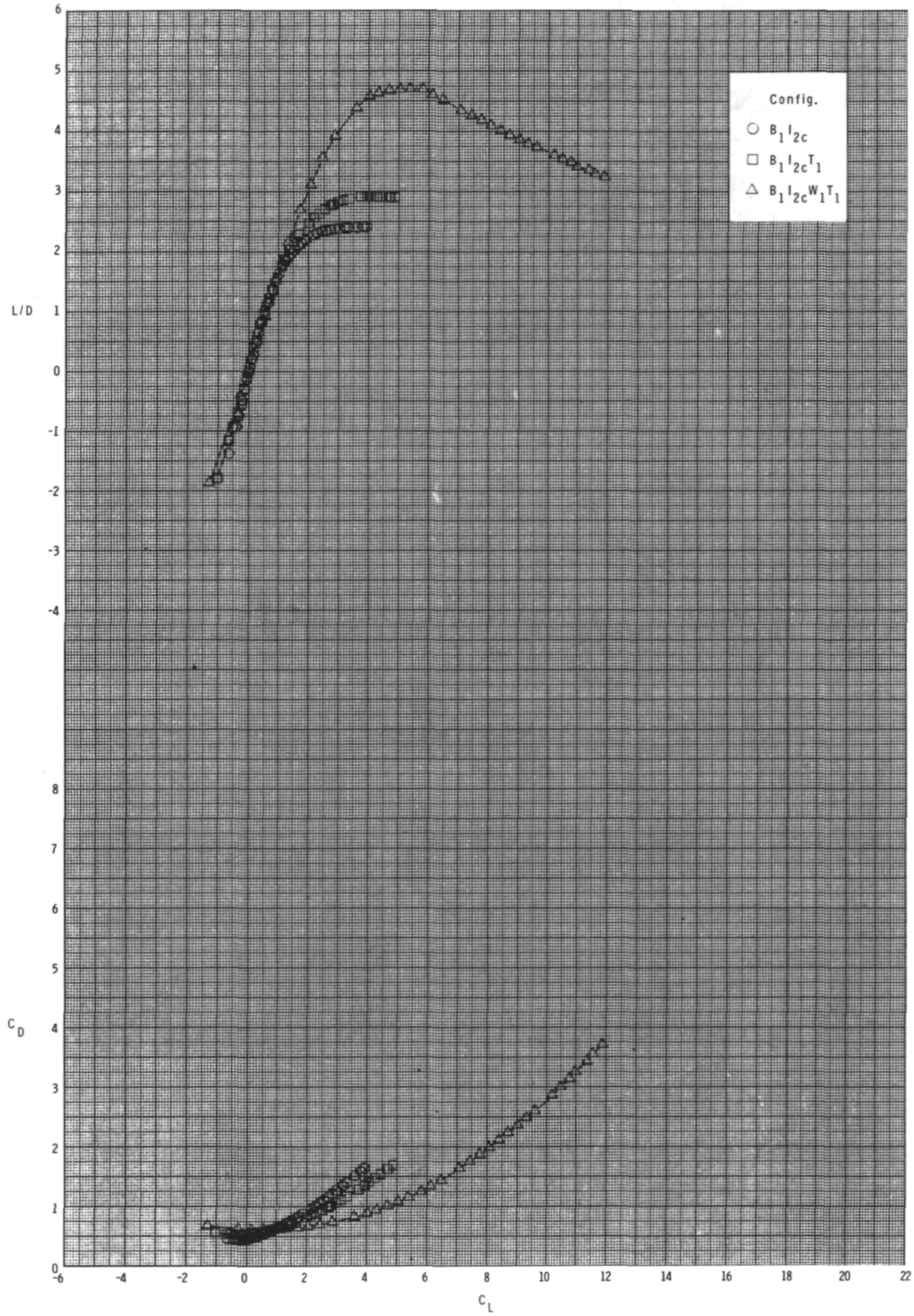

(c) Concluded.

Figure 26.- Concluded.

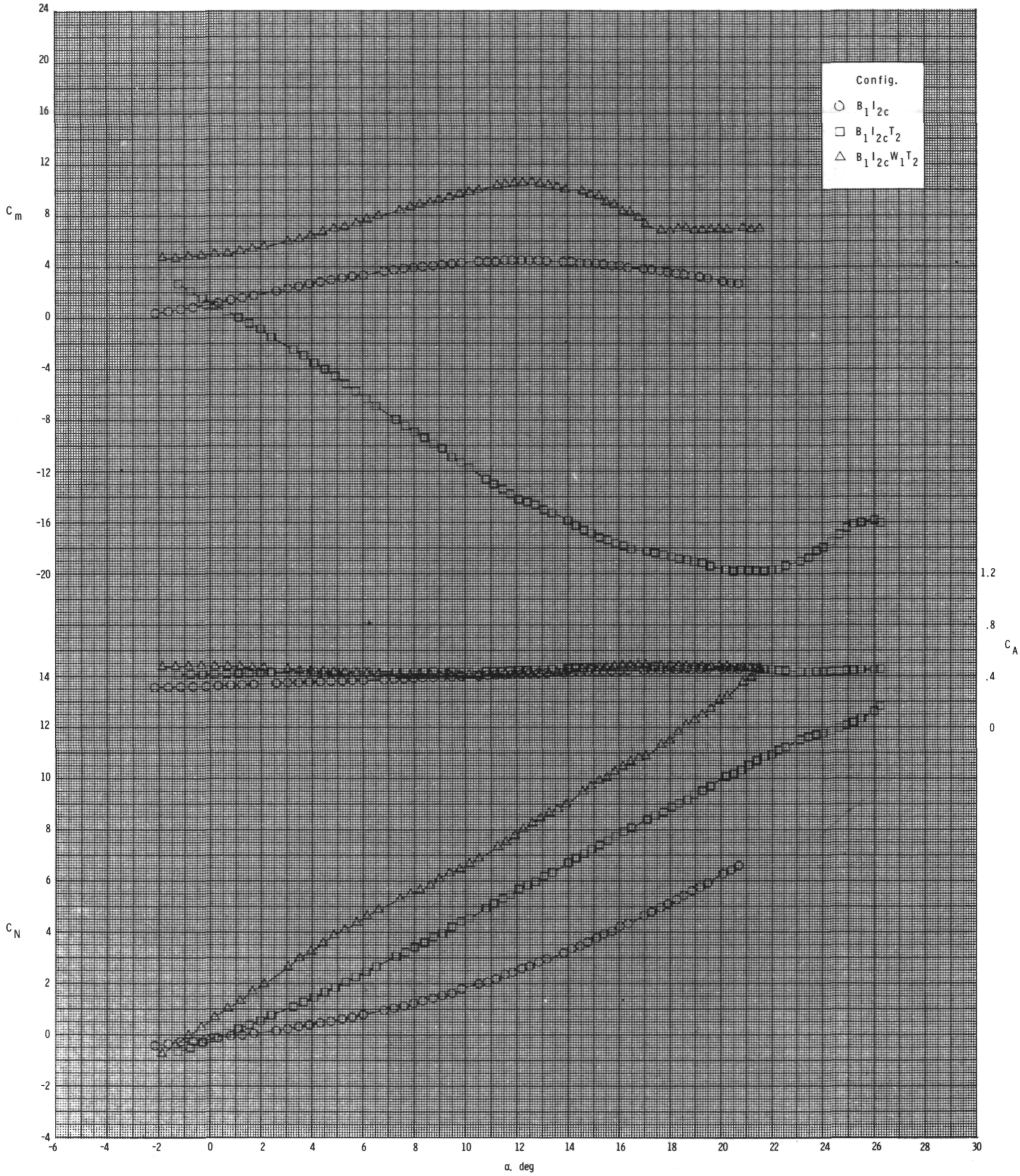

(a) M = 0.60.

Figure 27.- Effect of various model components on longitudinal aerodynamic characteristics for 2-D inlets with internal ducts closed, inlet covers installed, T_2, $\phi_I = 135°$, and $\delta_p = 0°$.

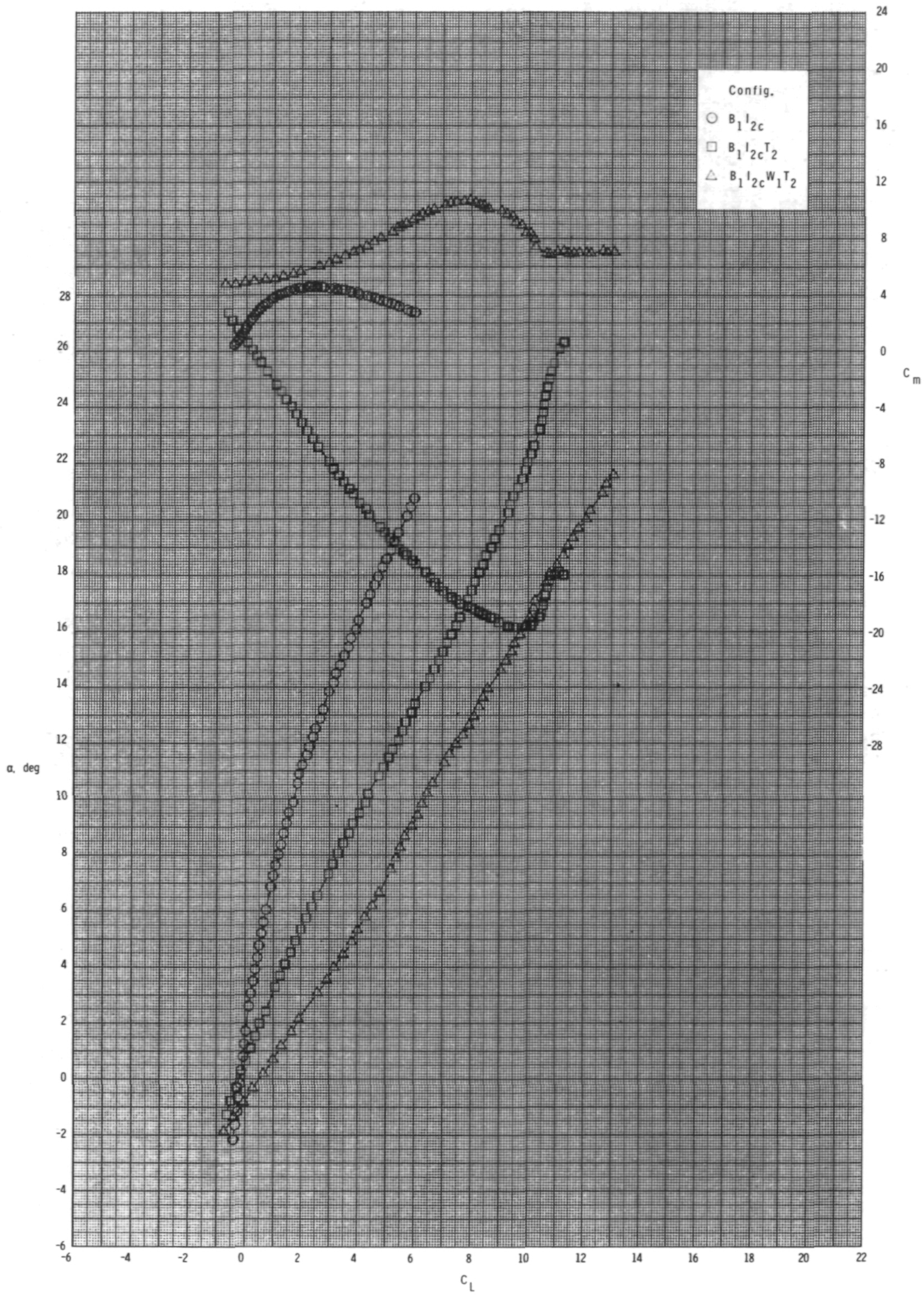

(a) Continued.

Figure 27.- Continued.

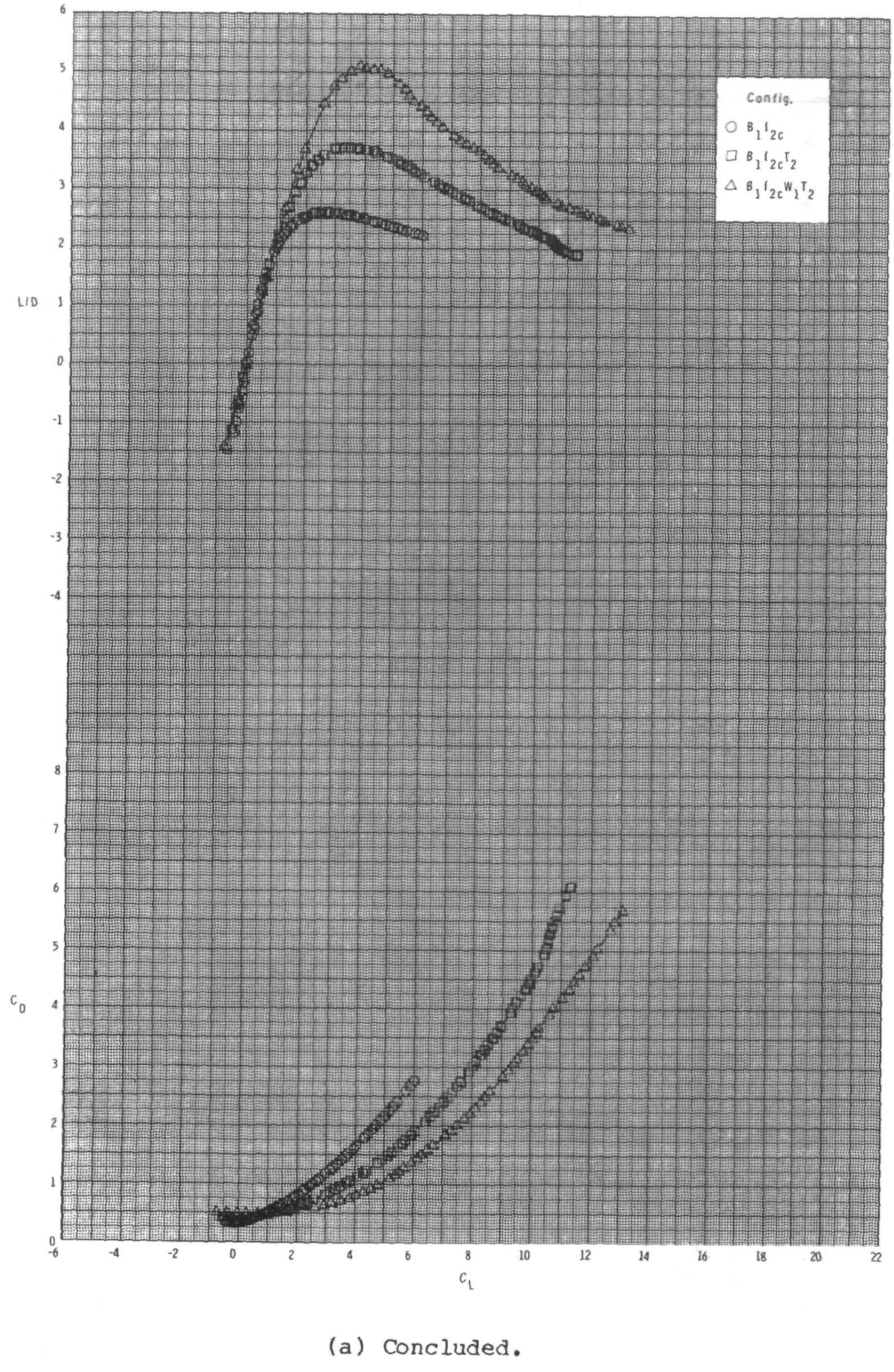

(a) Concluded.

Figure 27.- Continued.

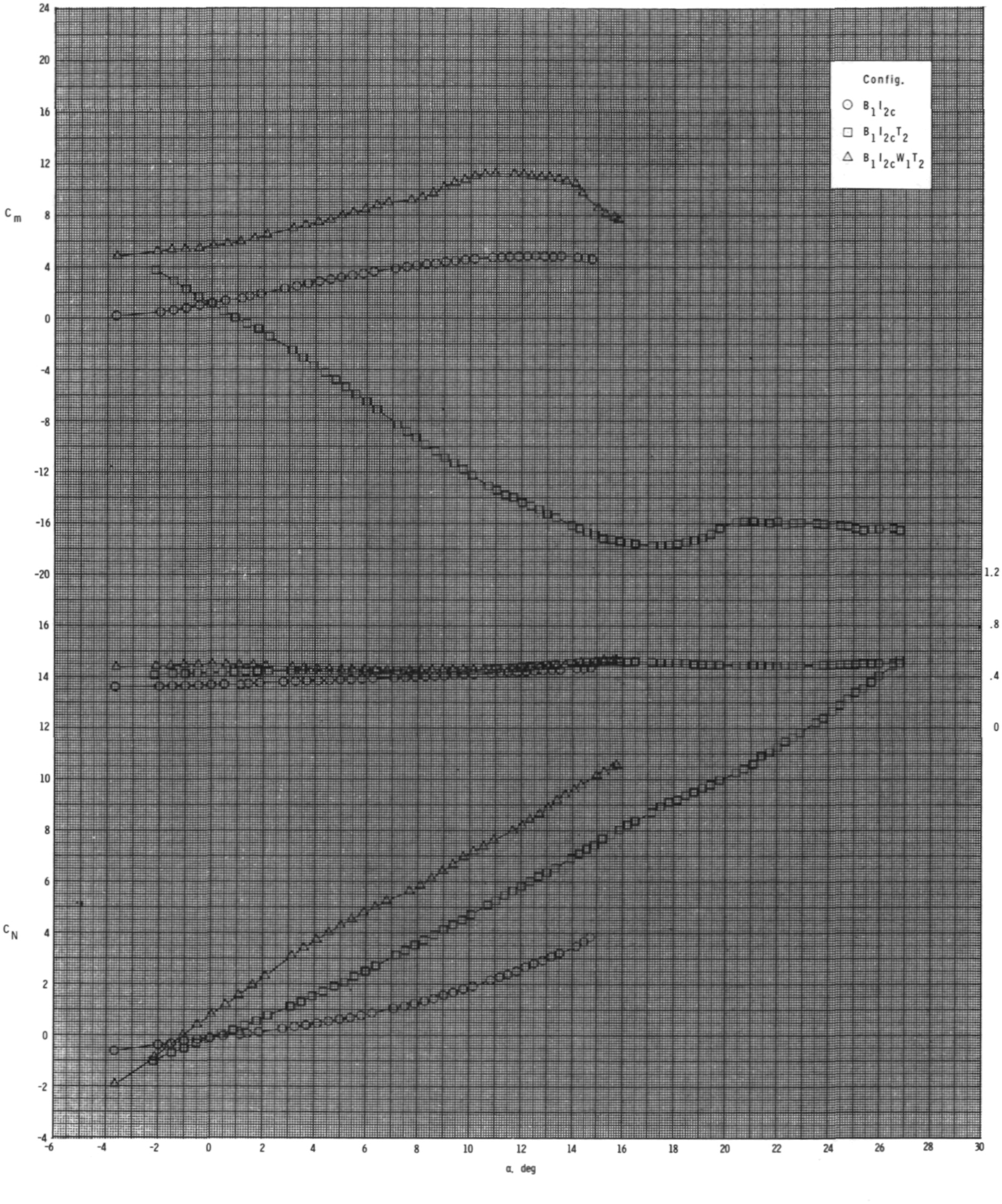

(b) M = 0.80.

Figure 27.- Continued.

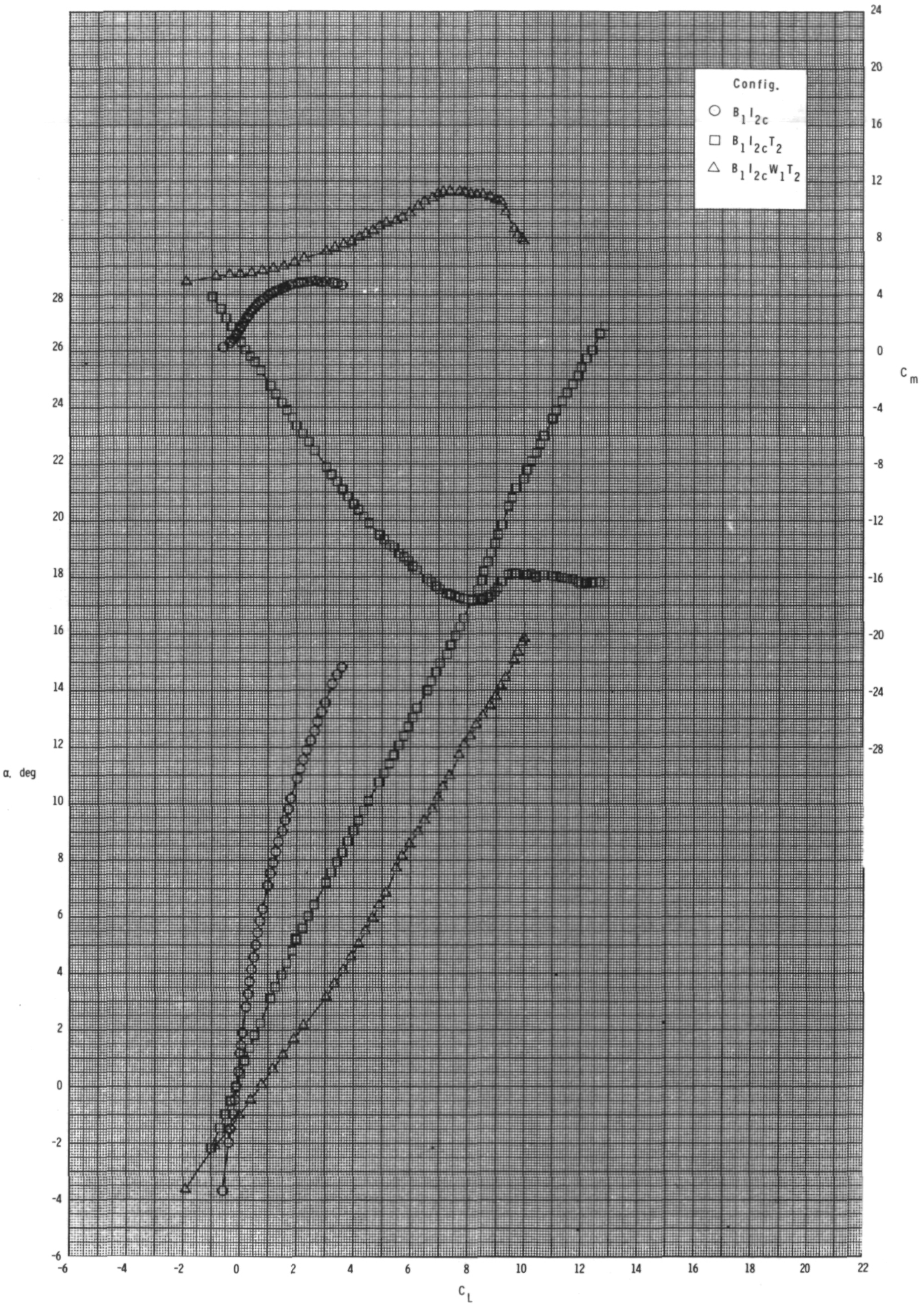

(b) Continued.

Figure 27.- Continued.

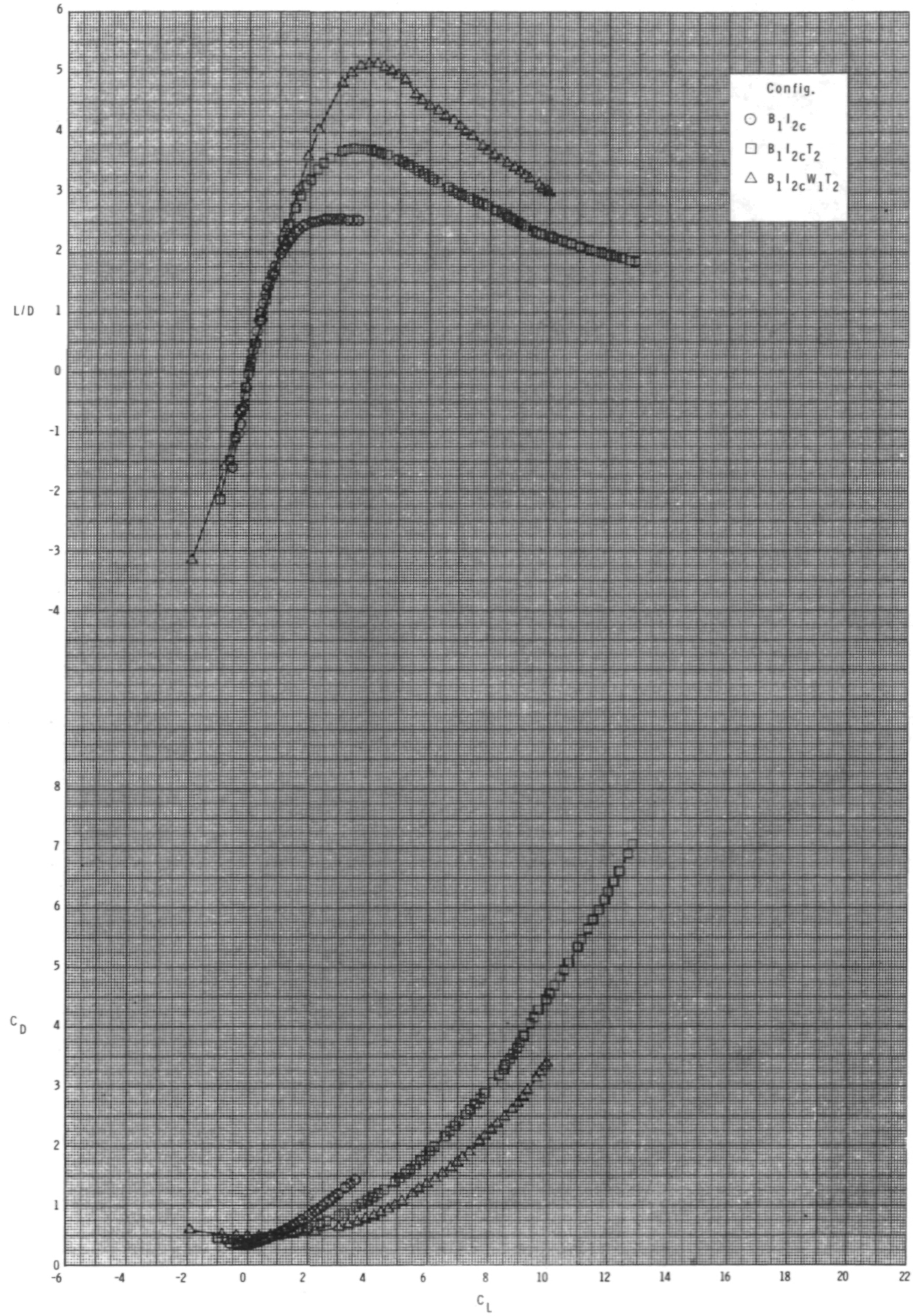

(b) Concluded.

Figure 27.- Continued.

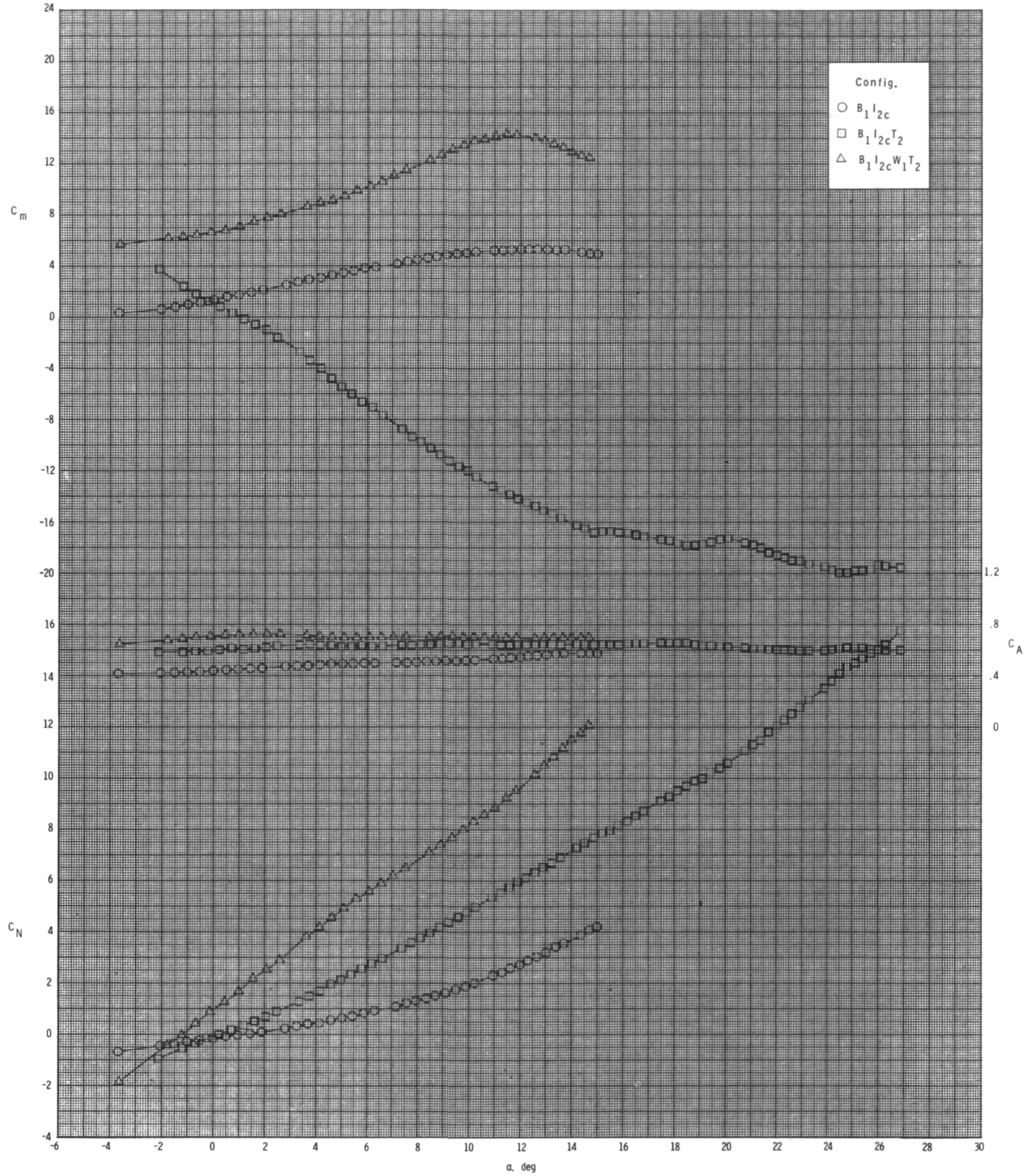

(c) M = 0.95.

Figure 27.- Continued.

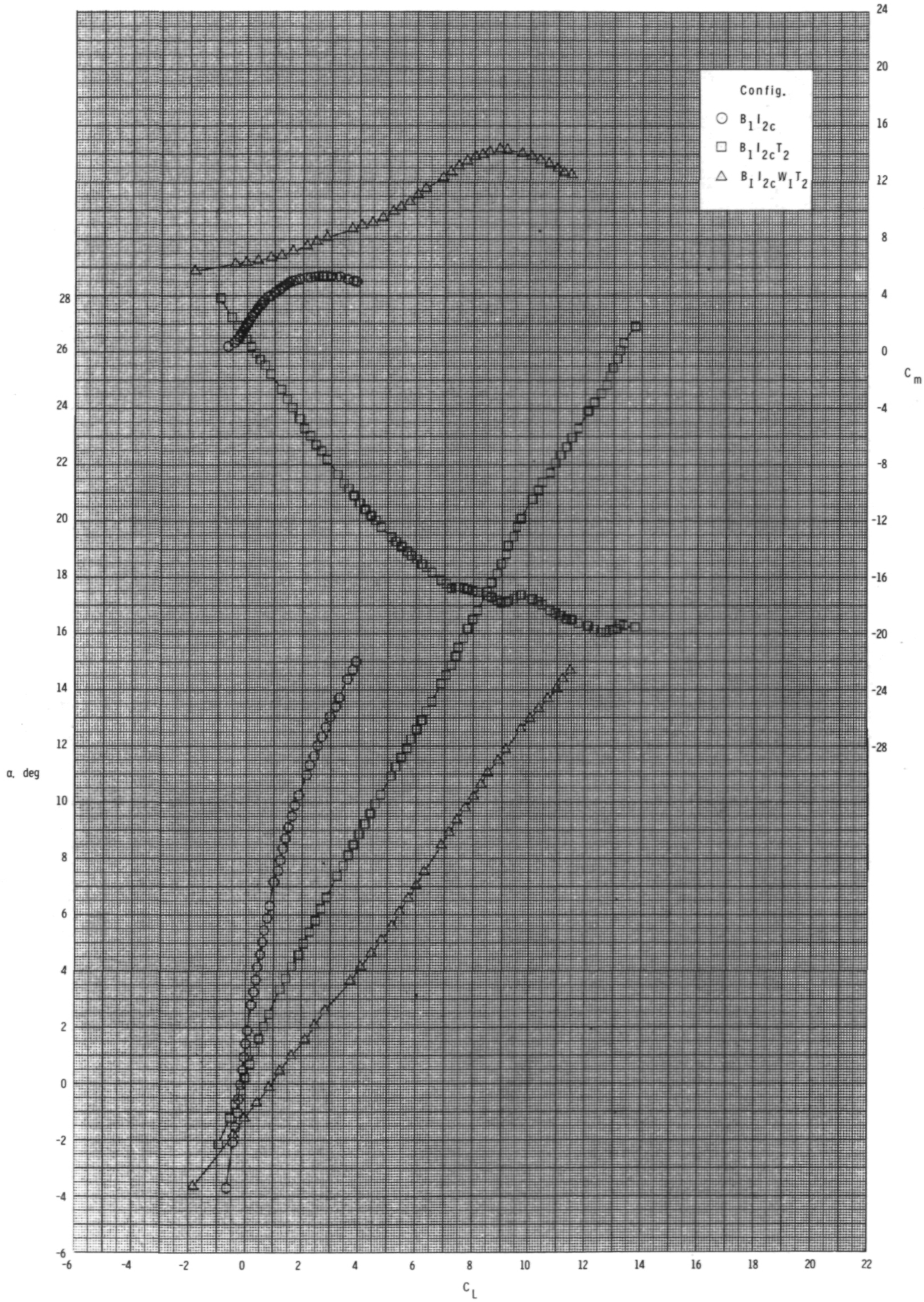

(c) Continued.

Figure 27.- Continued.

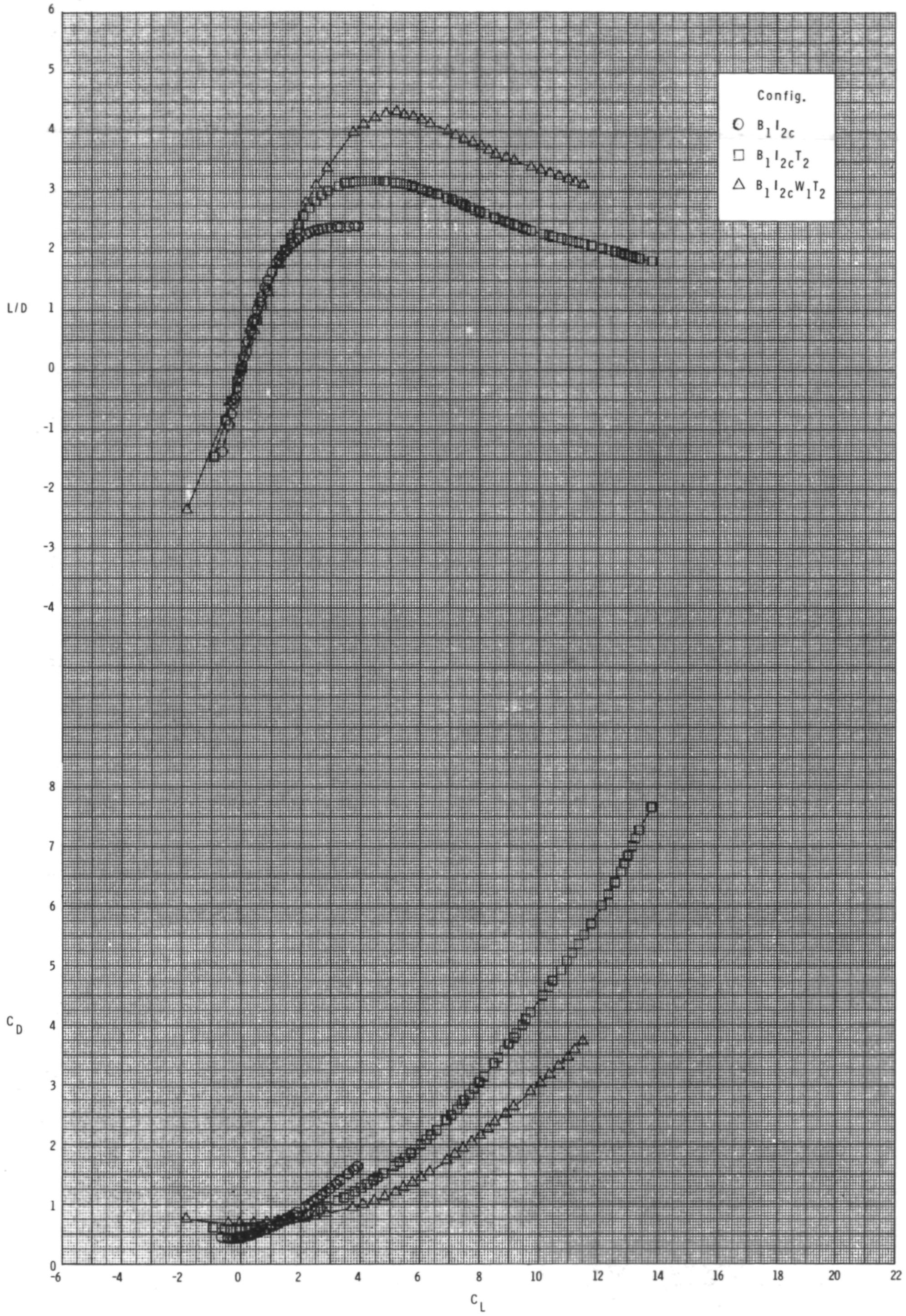

(c) Concluded.

Figure 27.- Concluded.

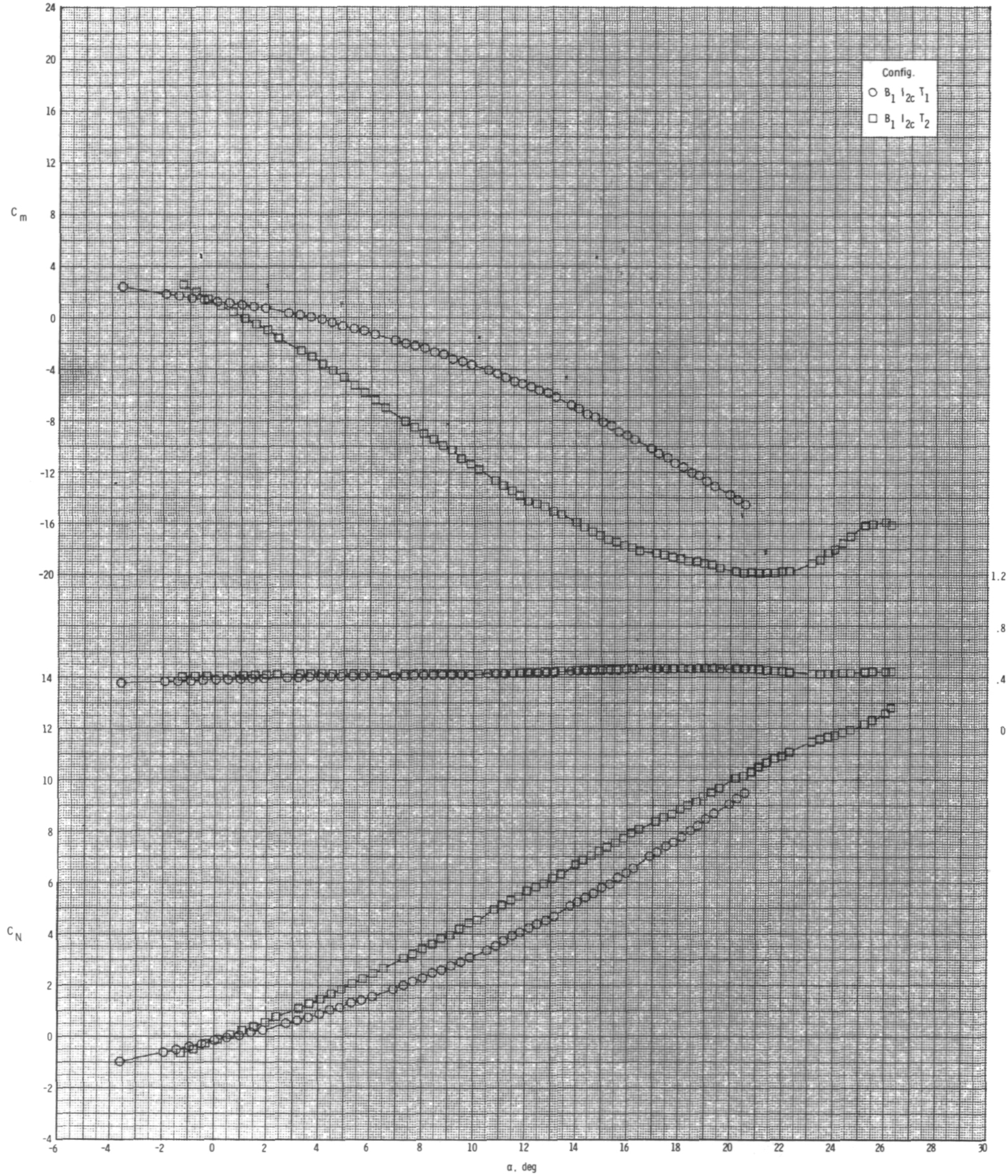

(a) M = 0.60.

Figure 28.- Effect of tail configuration on longitudinal aerodynamic characteristics for configuration $B_1I_{2c}T$ with internal ducts closed, $\phi_I = 135°$, and $\delta_p = 0°$.

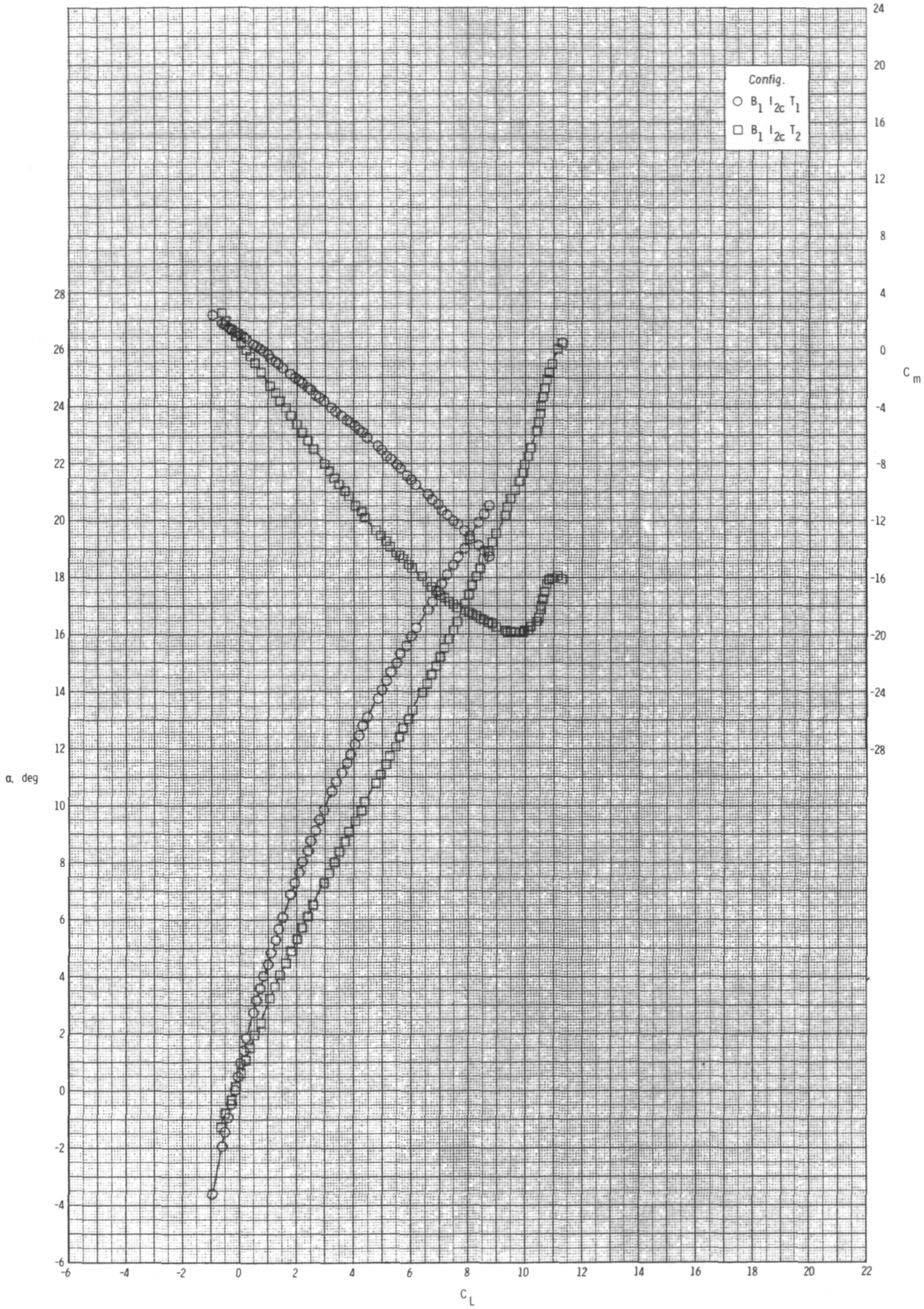

(a) Continued.

Figure 28.- Continued.

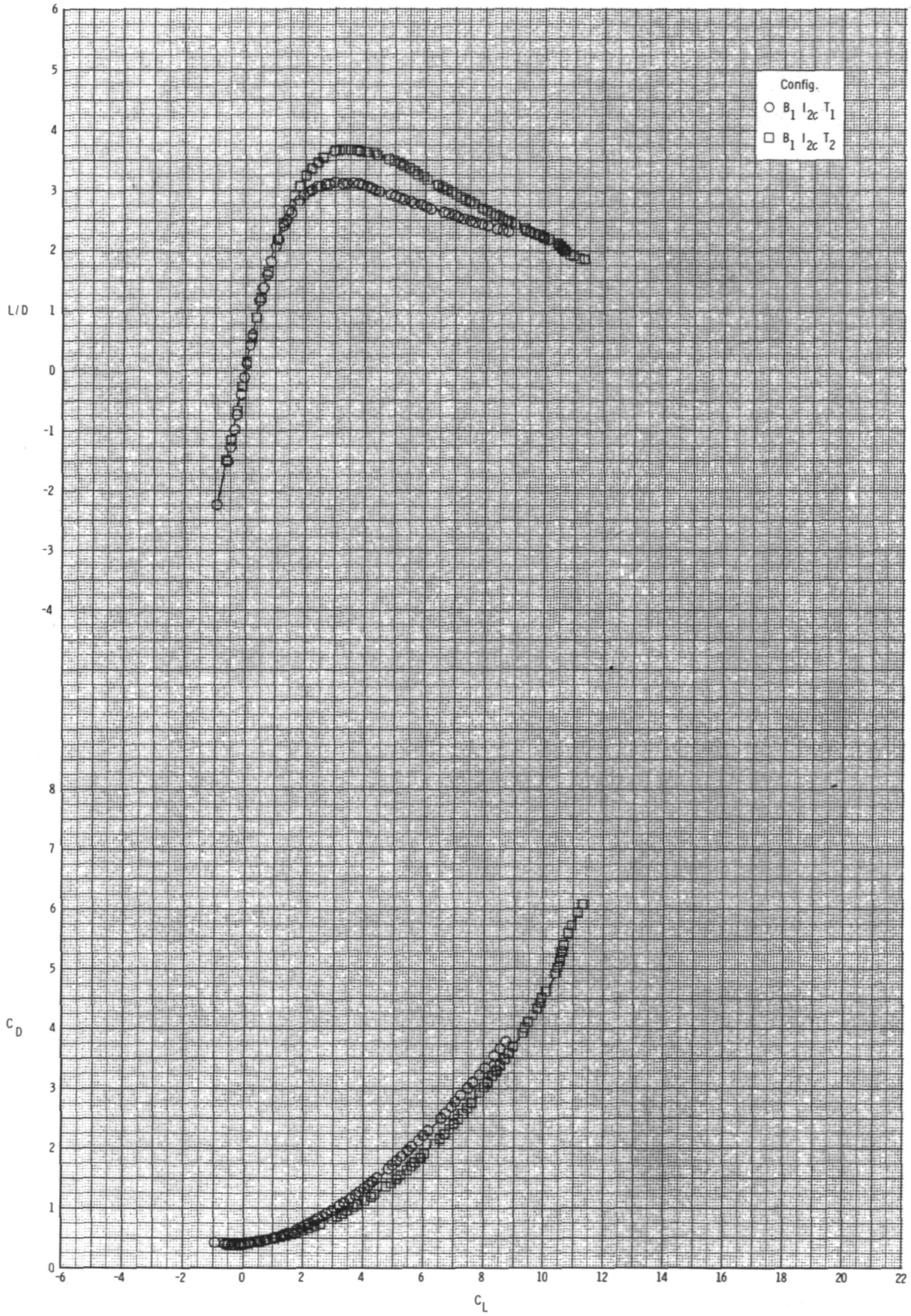

(a) Concluded.

Figure 28.- Continued.

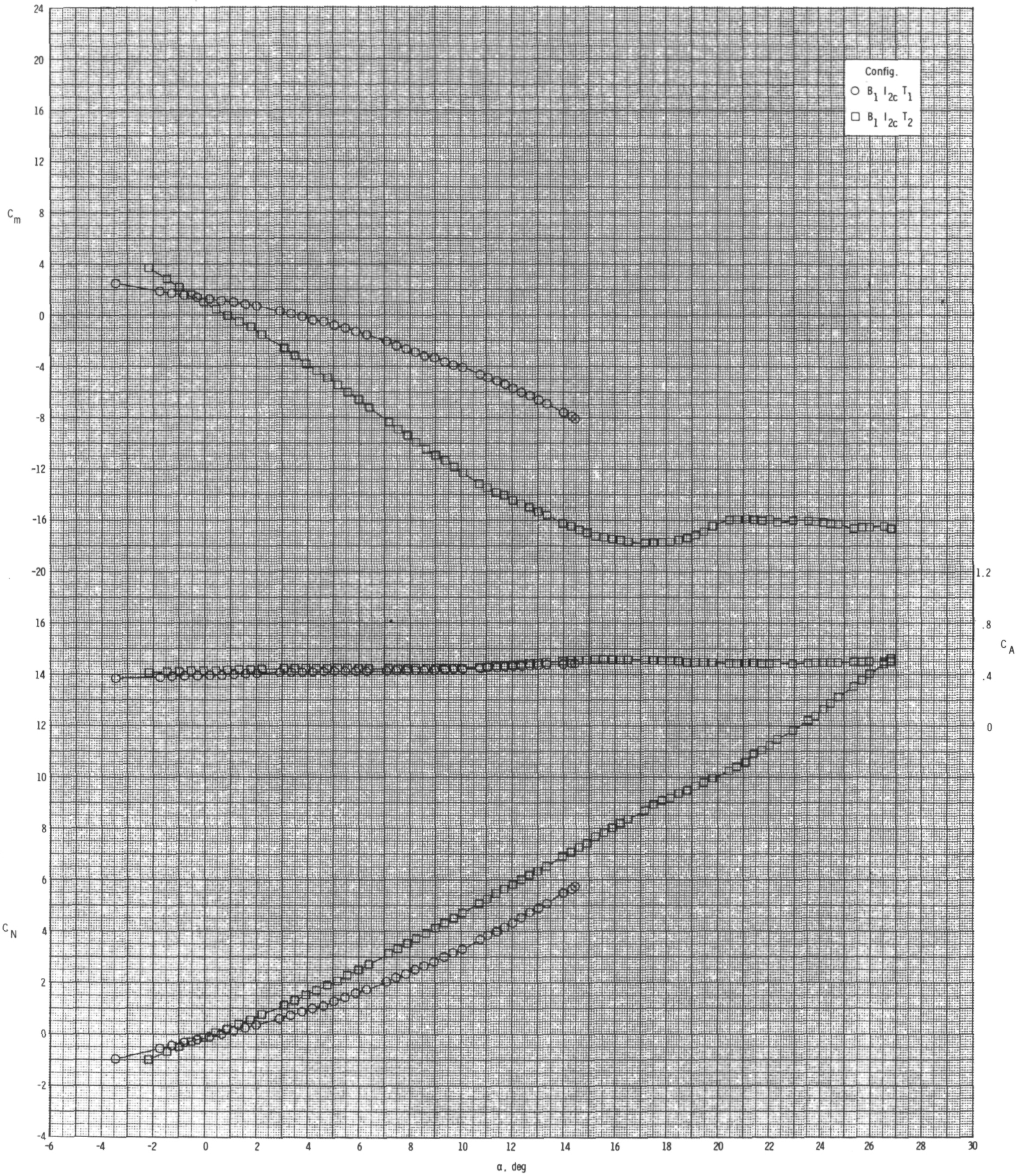

(b) M = 0.80.

Figure 28.- Continued.

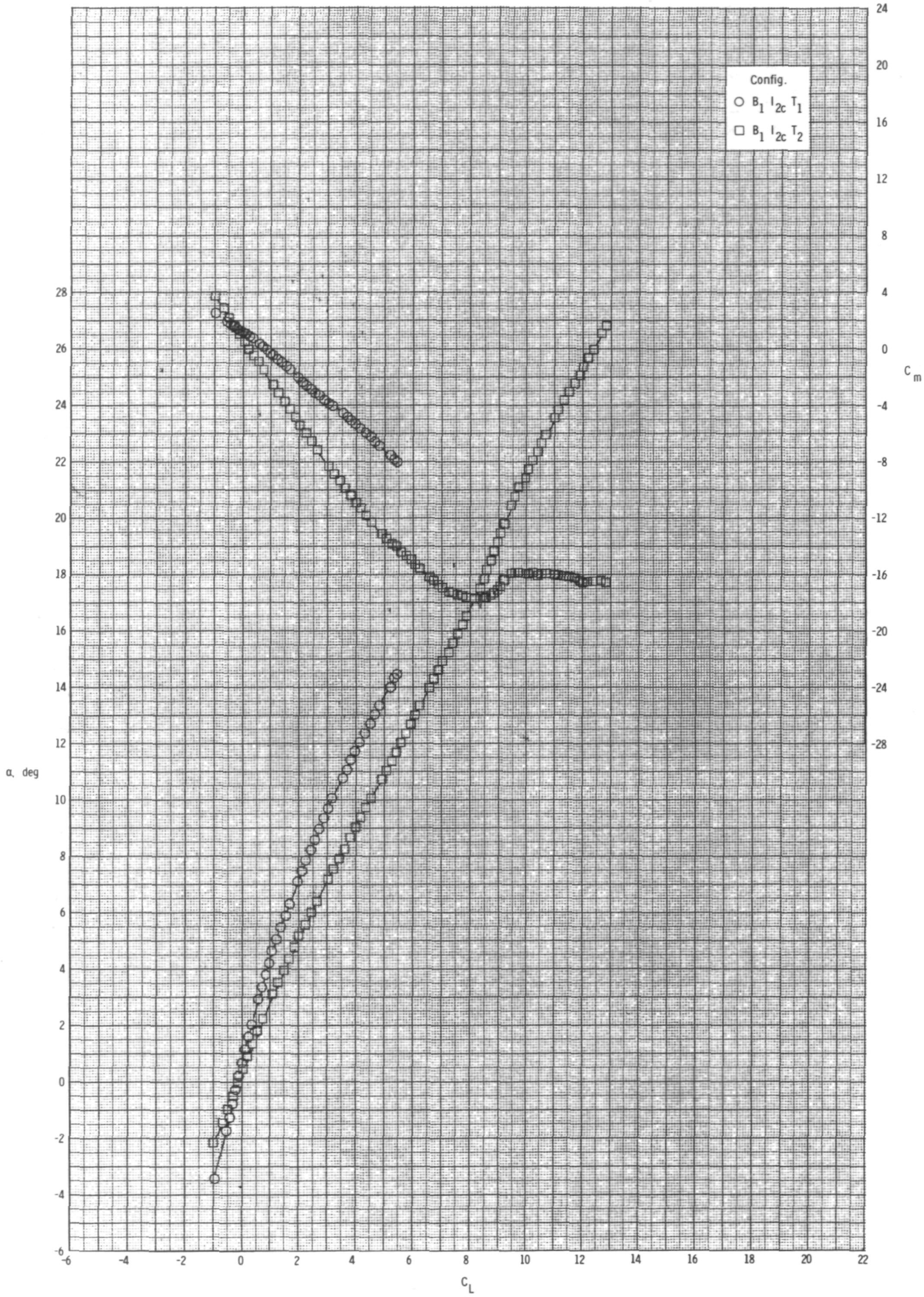

(b) Continued.

Figure 28.- Continued.

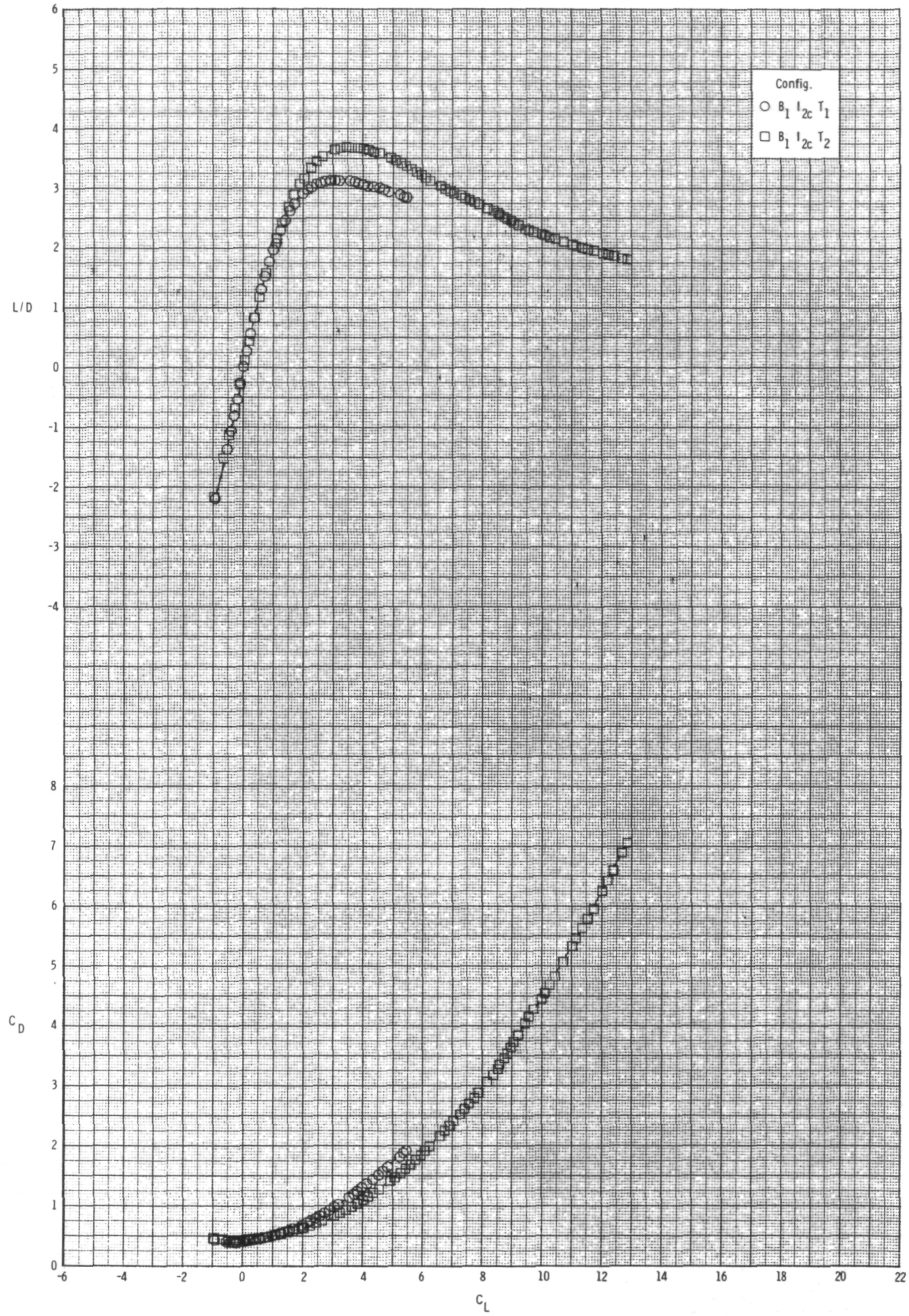

(b) Concluded.

Figure 28.- Continued.

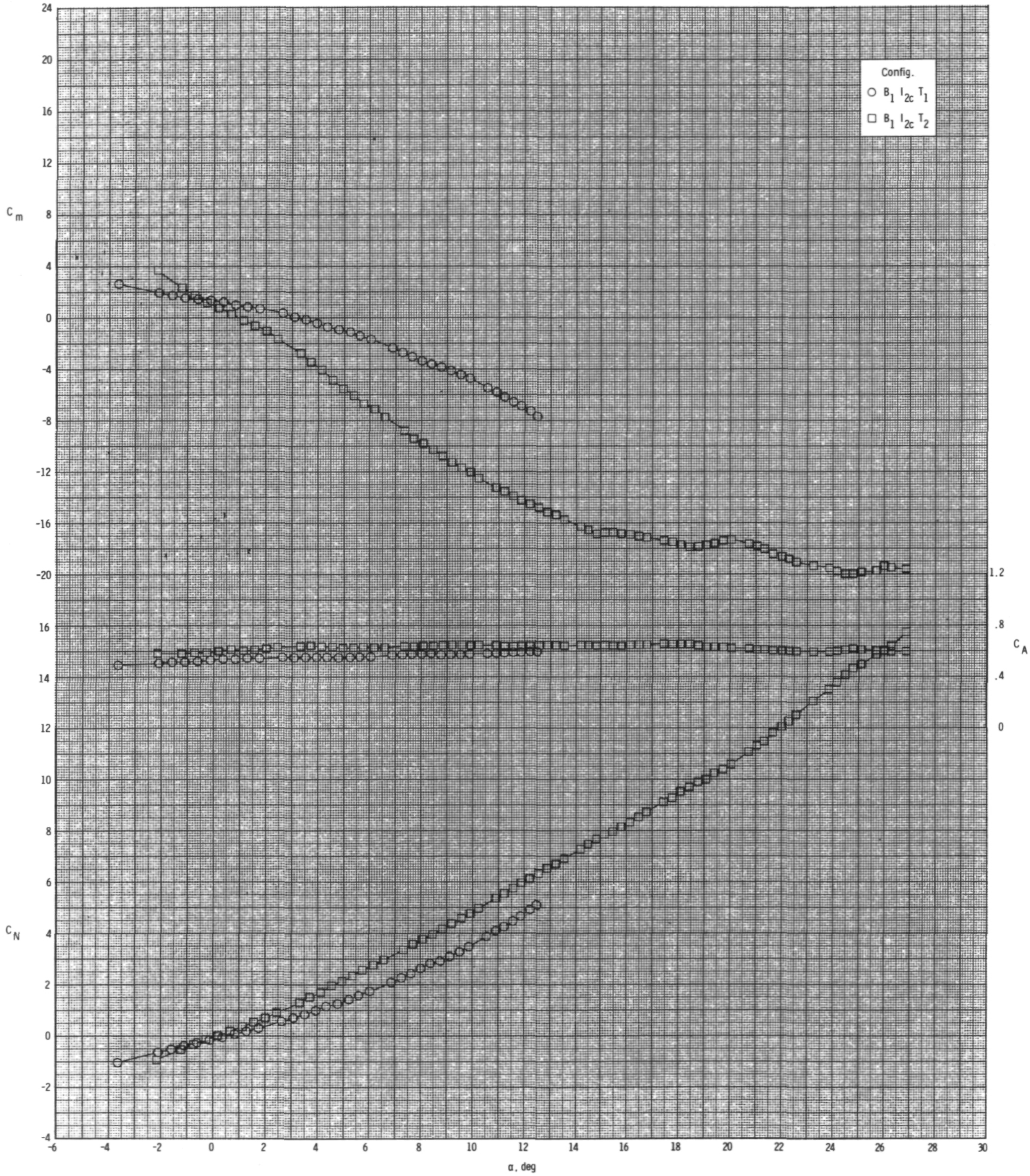

(c) M = 0.95.

Figure 28.- Continued.

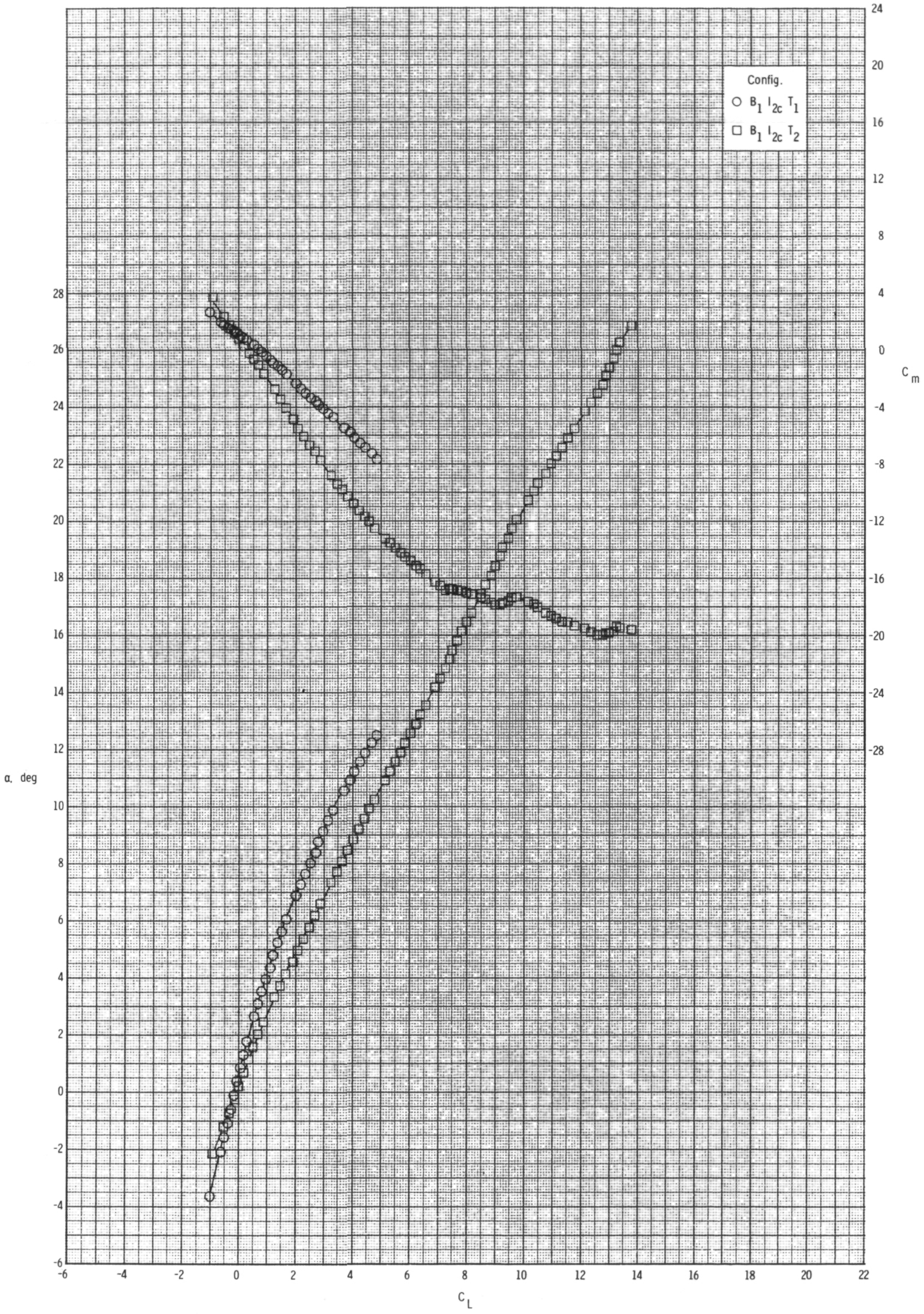

(c) Continued.

Figure 28.- Continued.

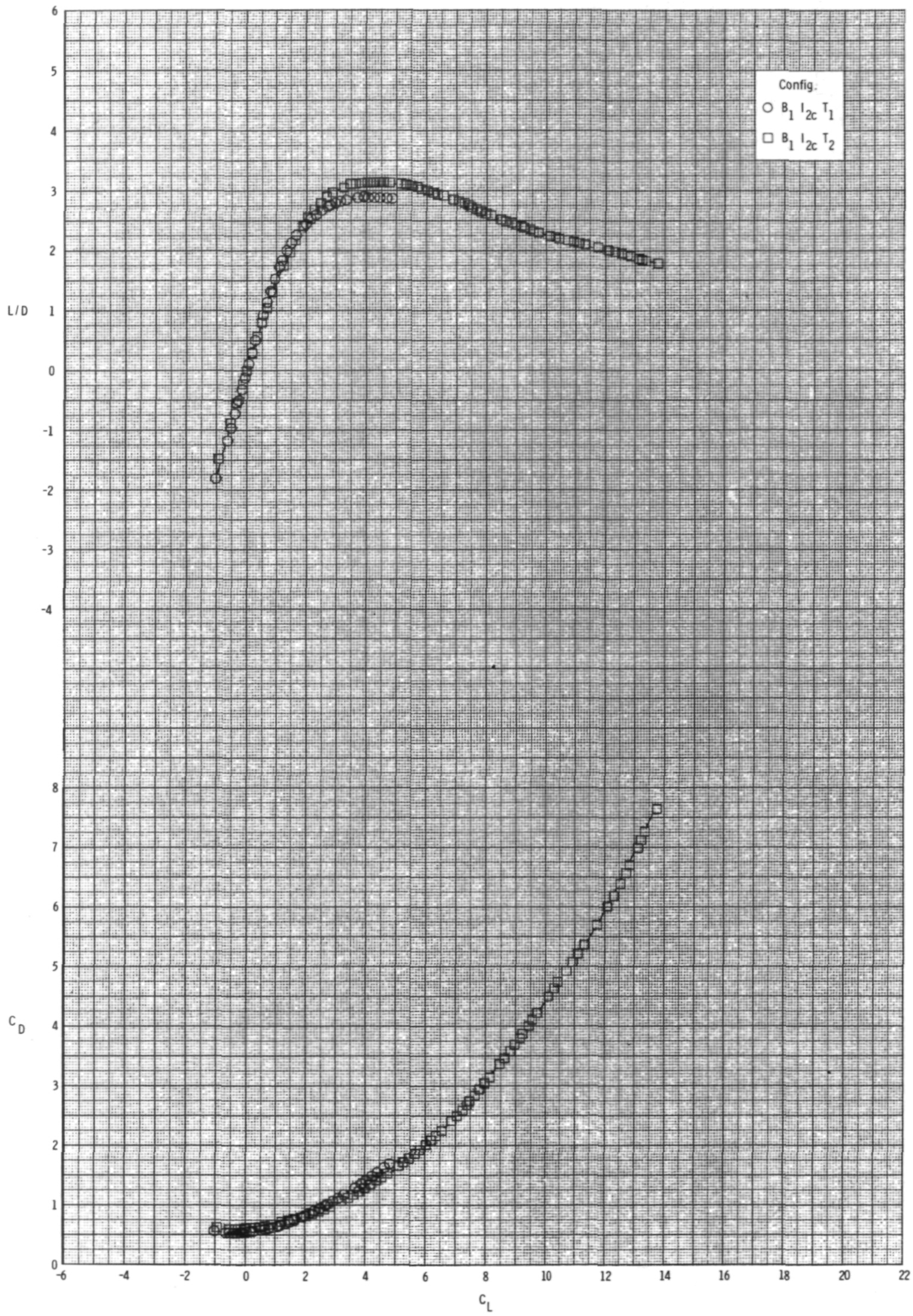

(c) Concluded.

Figure 28.- Concluded.

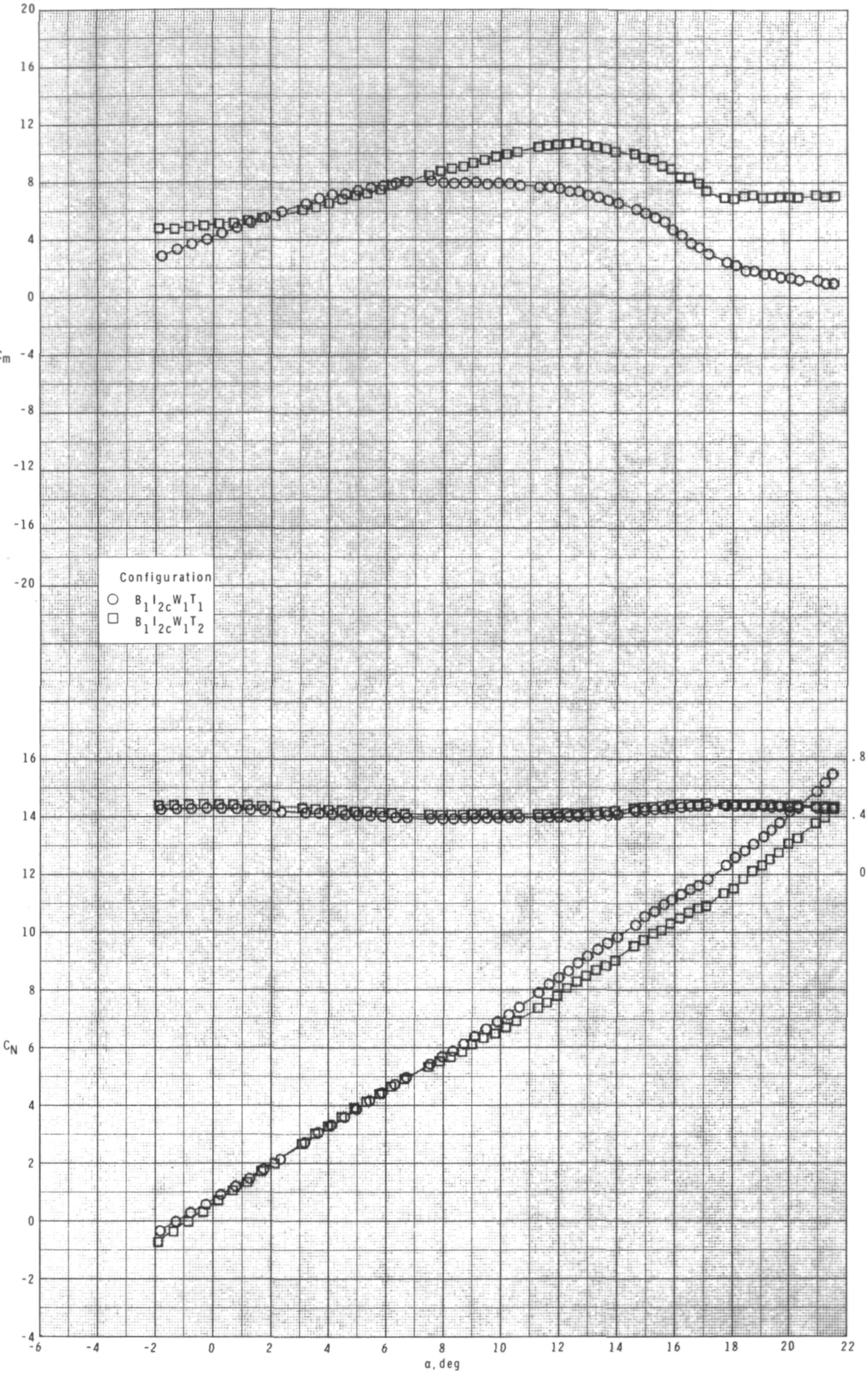

(a) M = 0.60.

Figure 29.- Effect of tail configuration of longitudinal aerodynamic characteristics for configuration $B_1I_{2c}W_1T$ with internal ducts closed, $\phi_I = 135°$, and $\delta_p = 0°$.

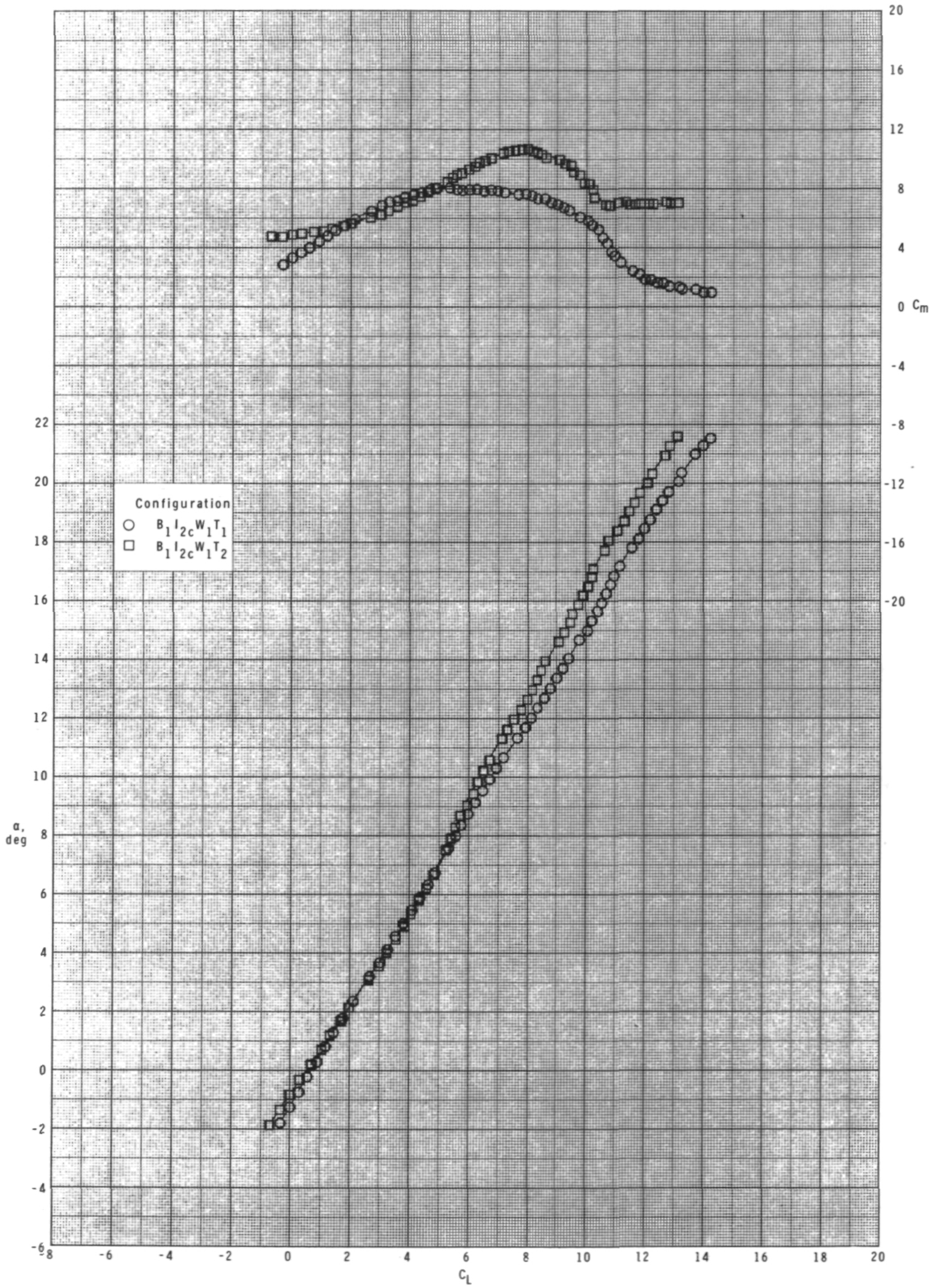

(a) Continued.

Figure 29.- Continued.

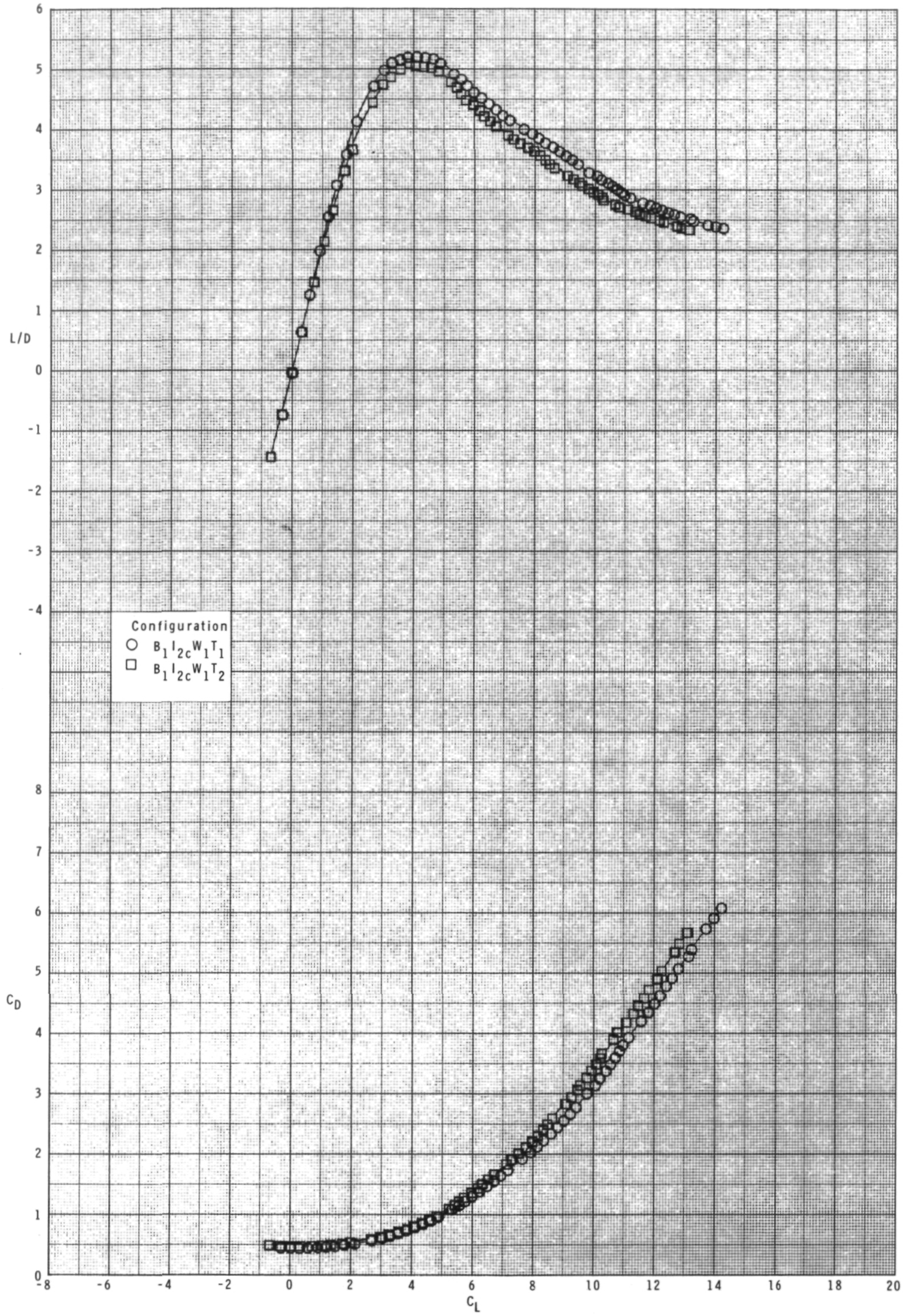

(a) Concluded.

Figure 29.- Continued.

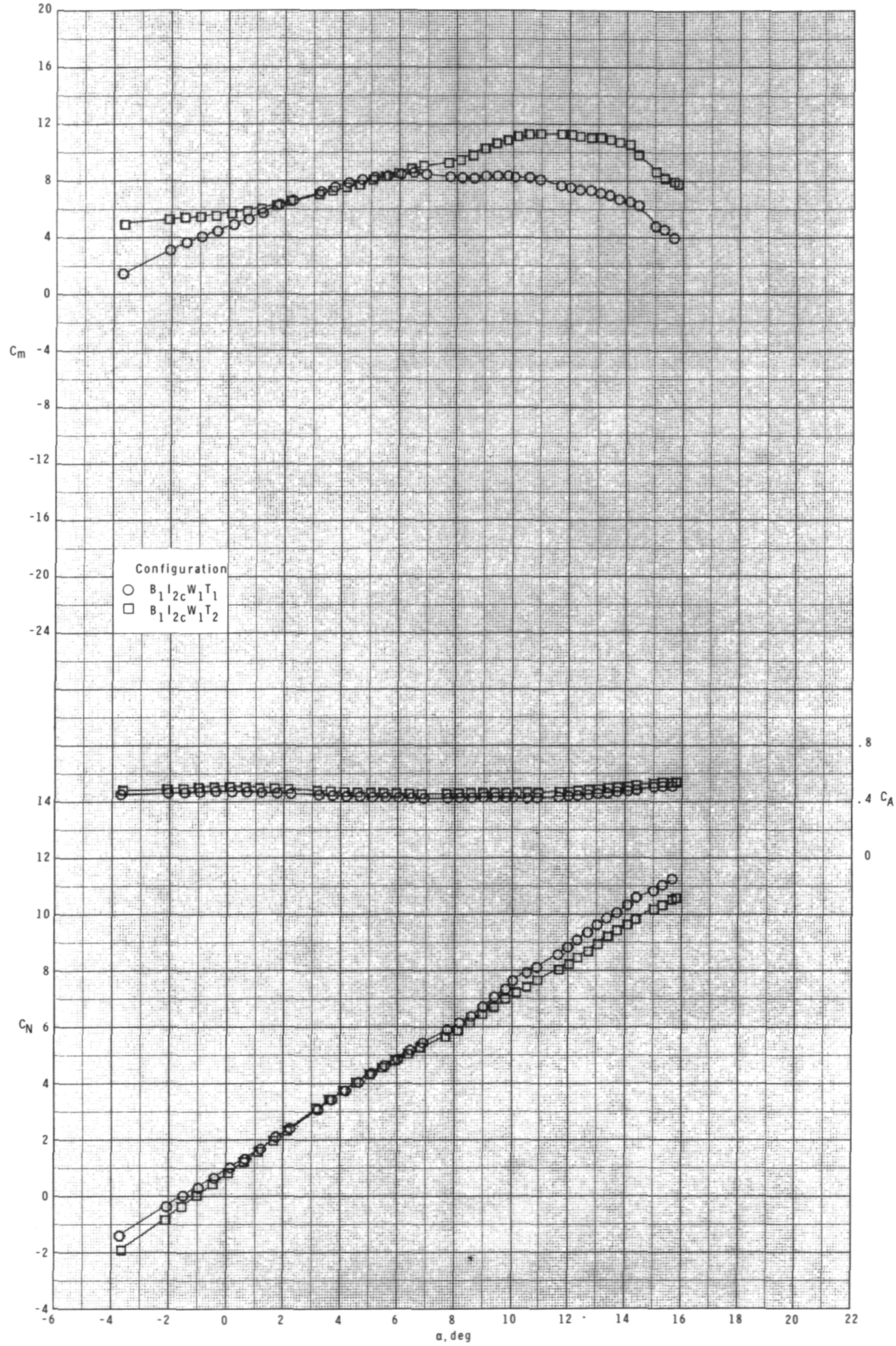

(b) M = 0.80.

Figure 29.- Continued.

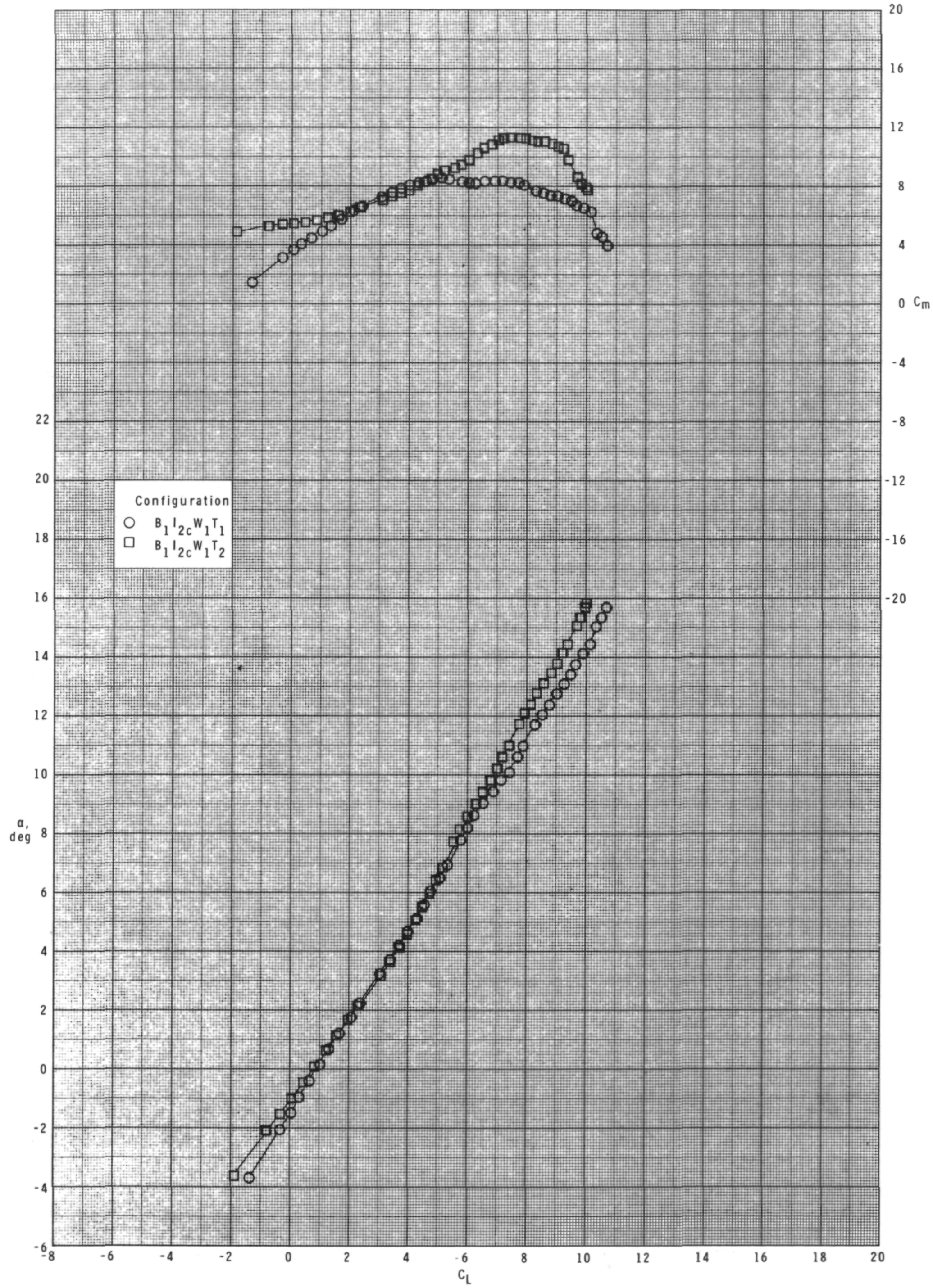

(b) Continued.

Figure 29.- Continued.

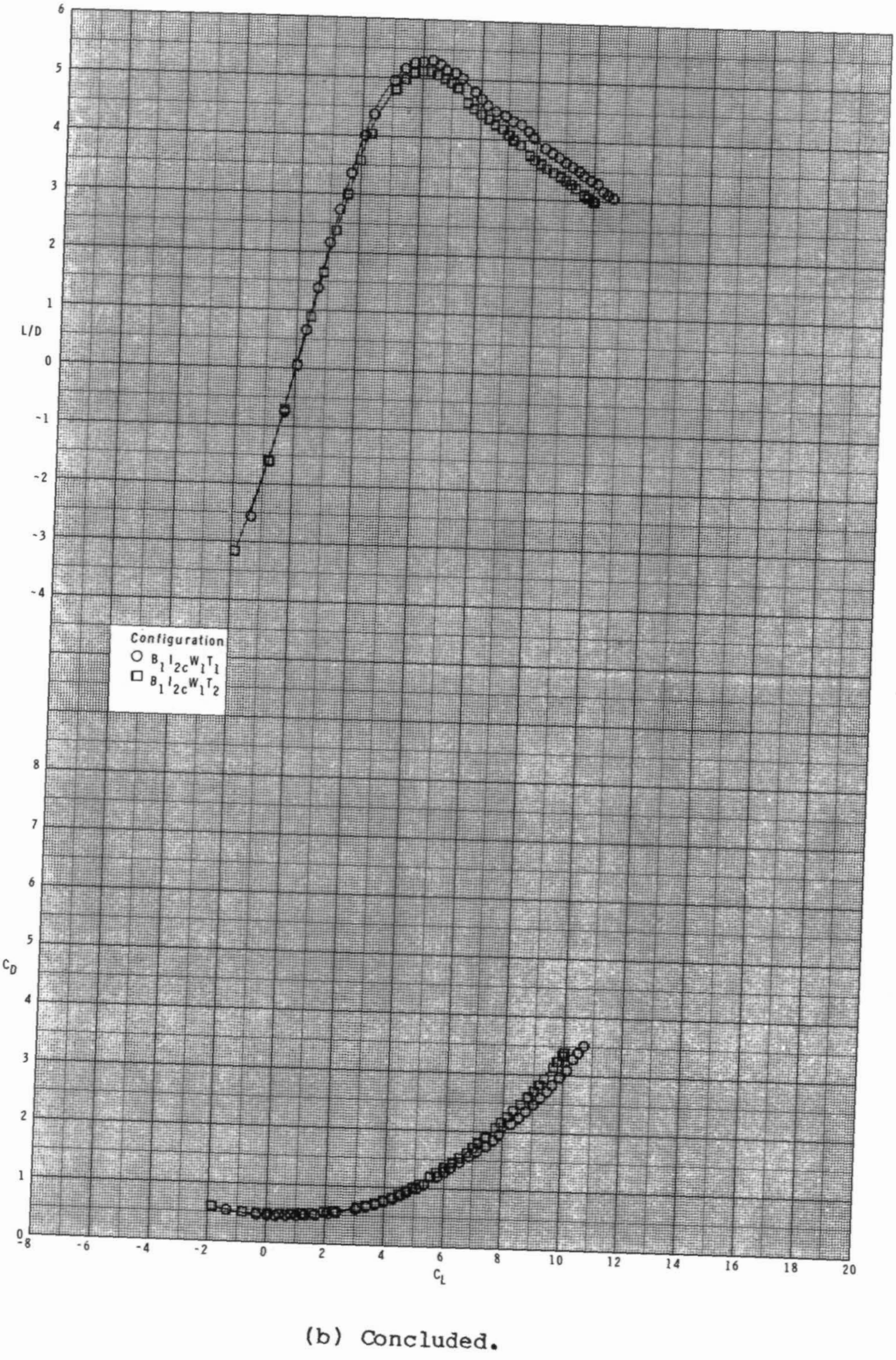

(b) Concluded.

Figure 29.- Continued.

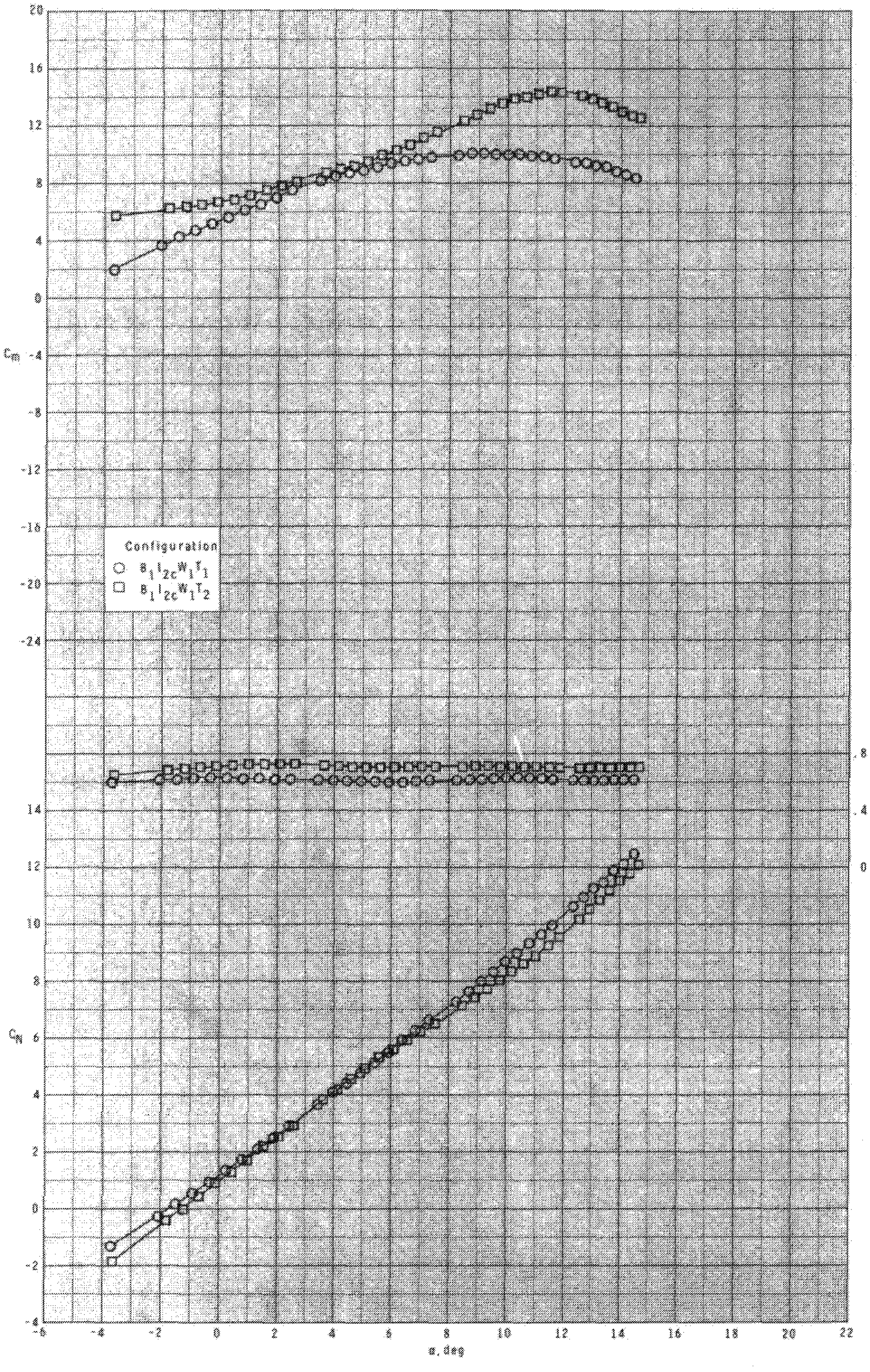

(c) M = 0.95.

Figure 29.- Continued.

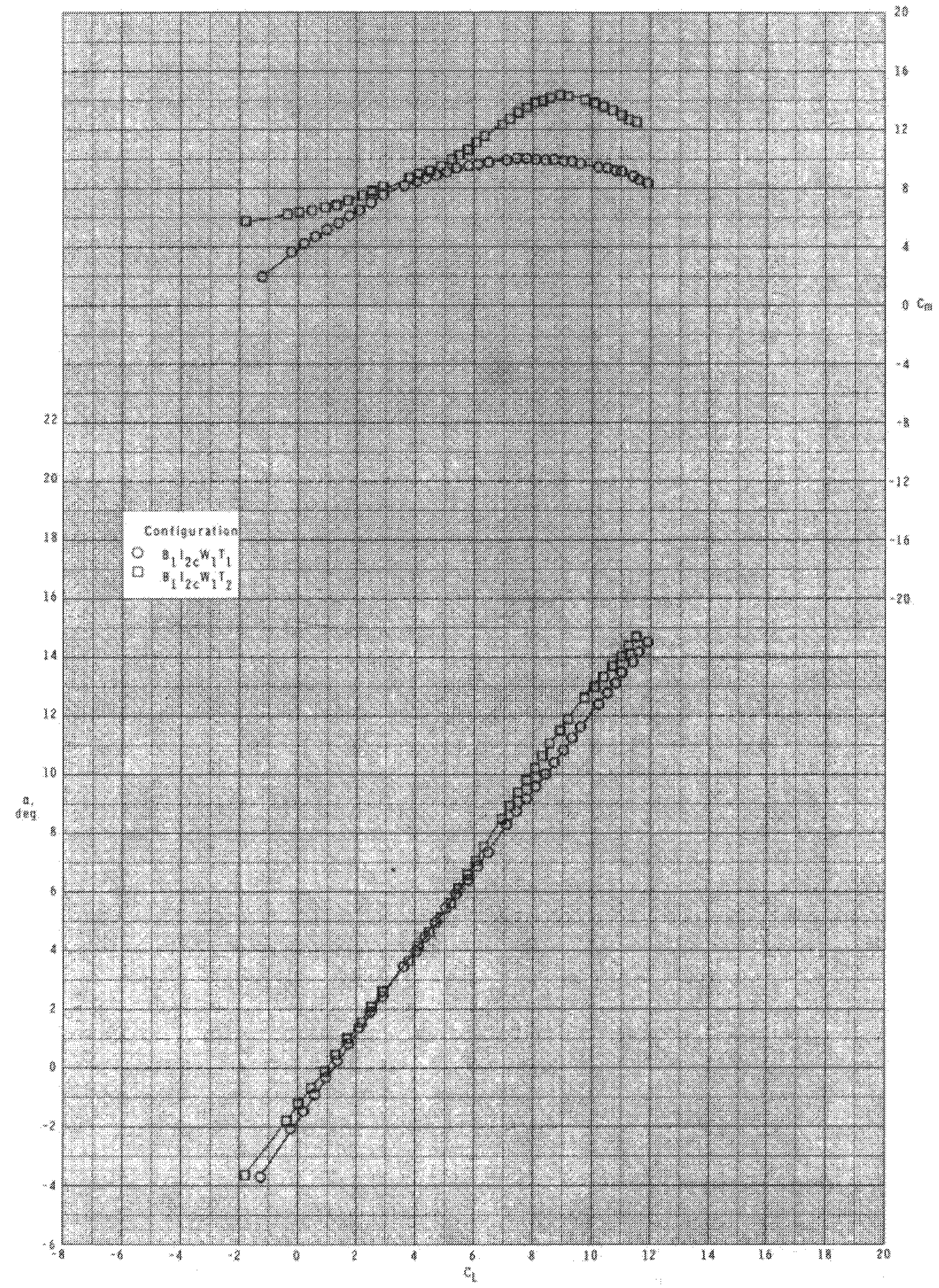

(c) Continued.

Figure 29.- Continued.

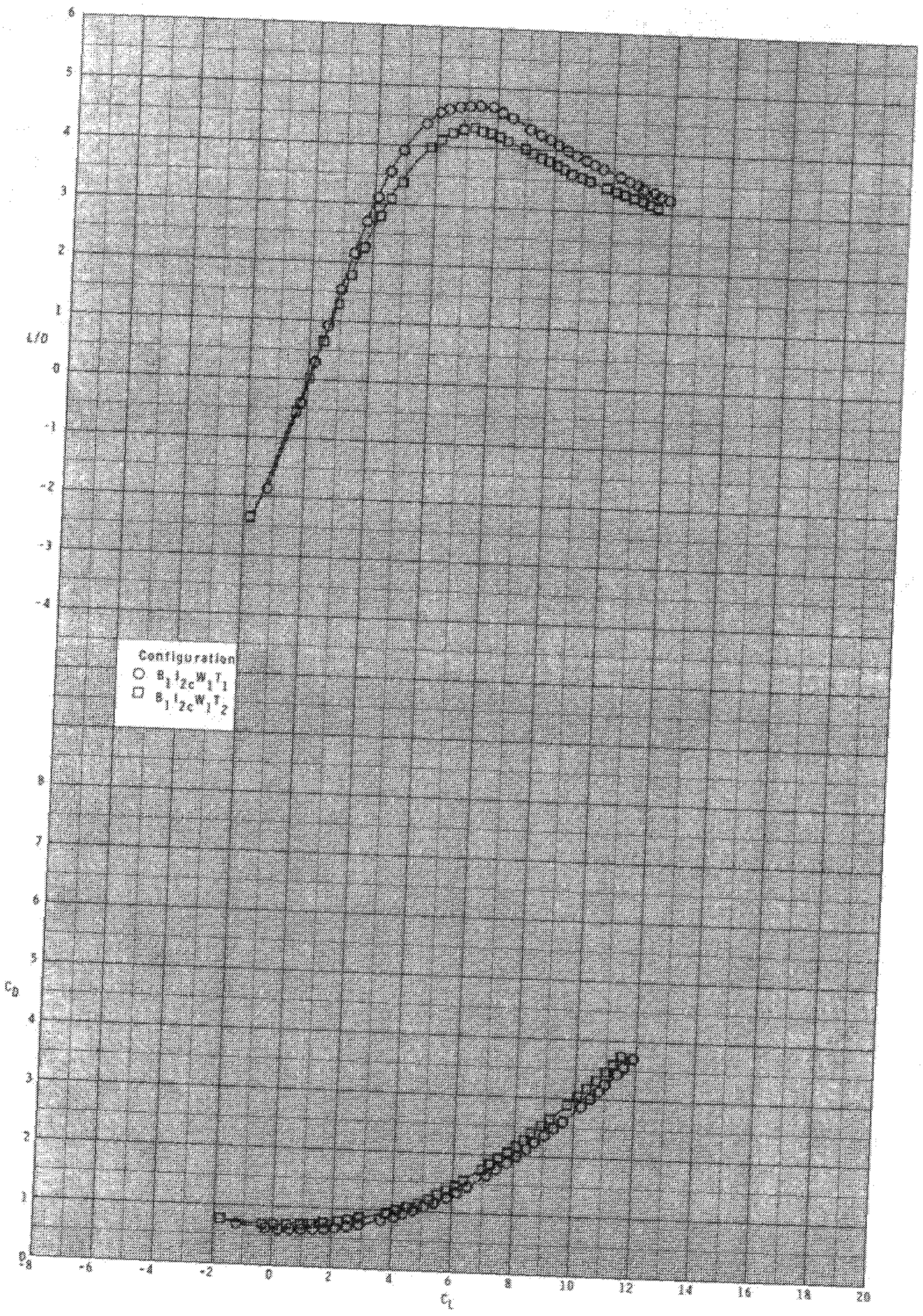

(c) Concluded.

Figure 29.- Concluded.

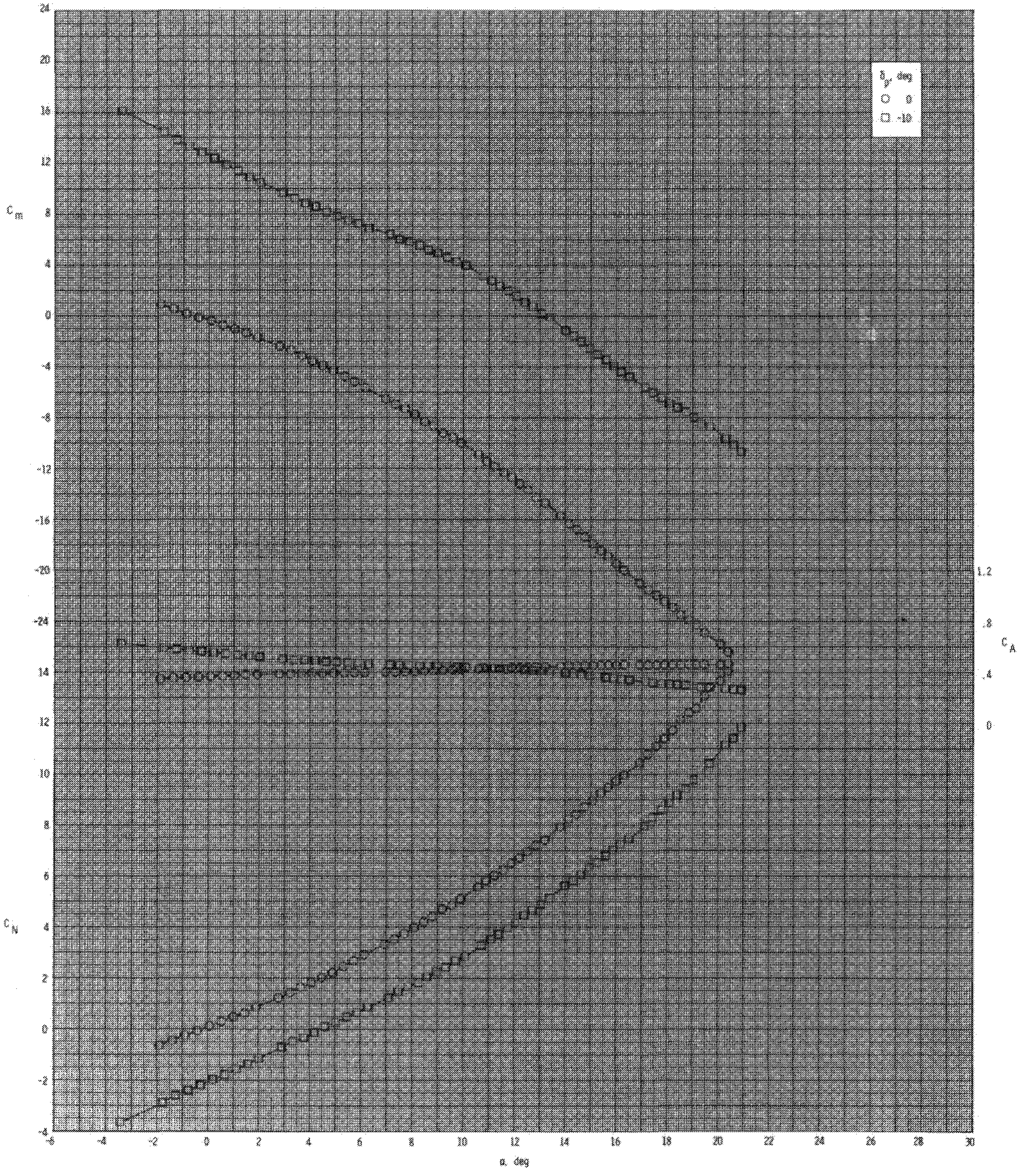

(a) M = 0.60.

Figure 30.- Pitch-control effectiveness for configuration $B_1I_{2c}T_1$ with internal ducts closed and $\phi_I = 90°$.

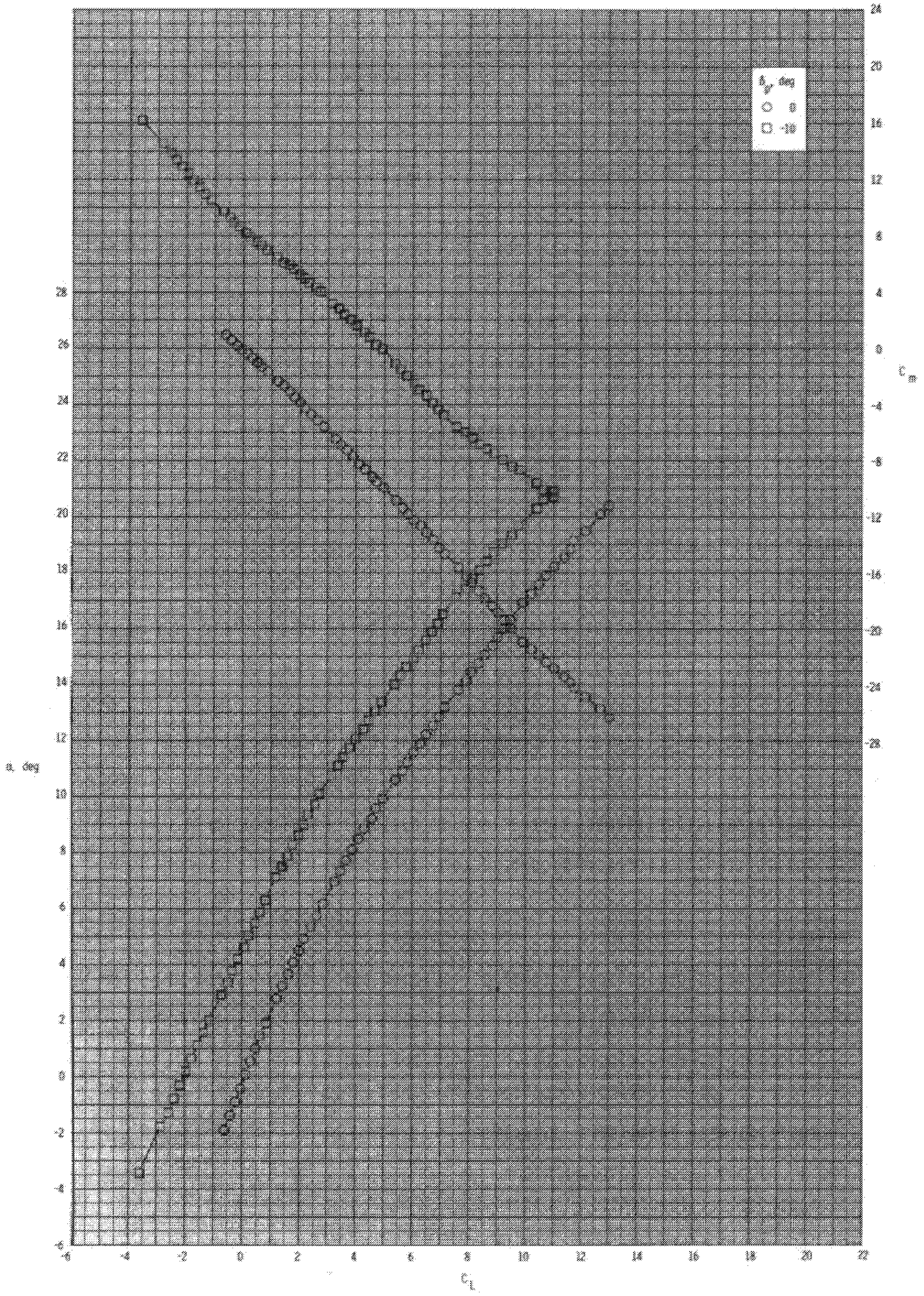

(a) Continued.

Figure 30.- Continued.

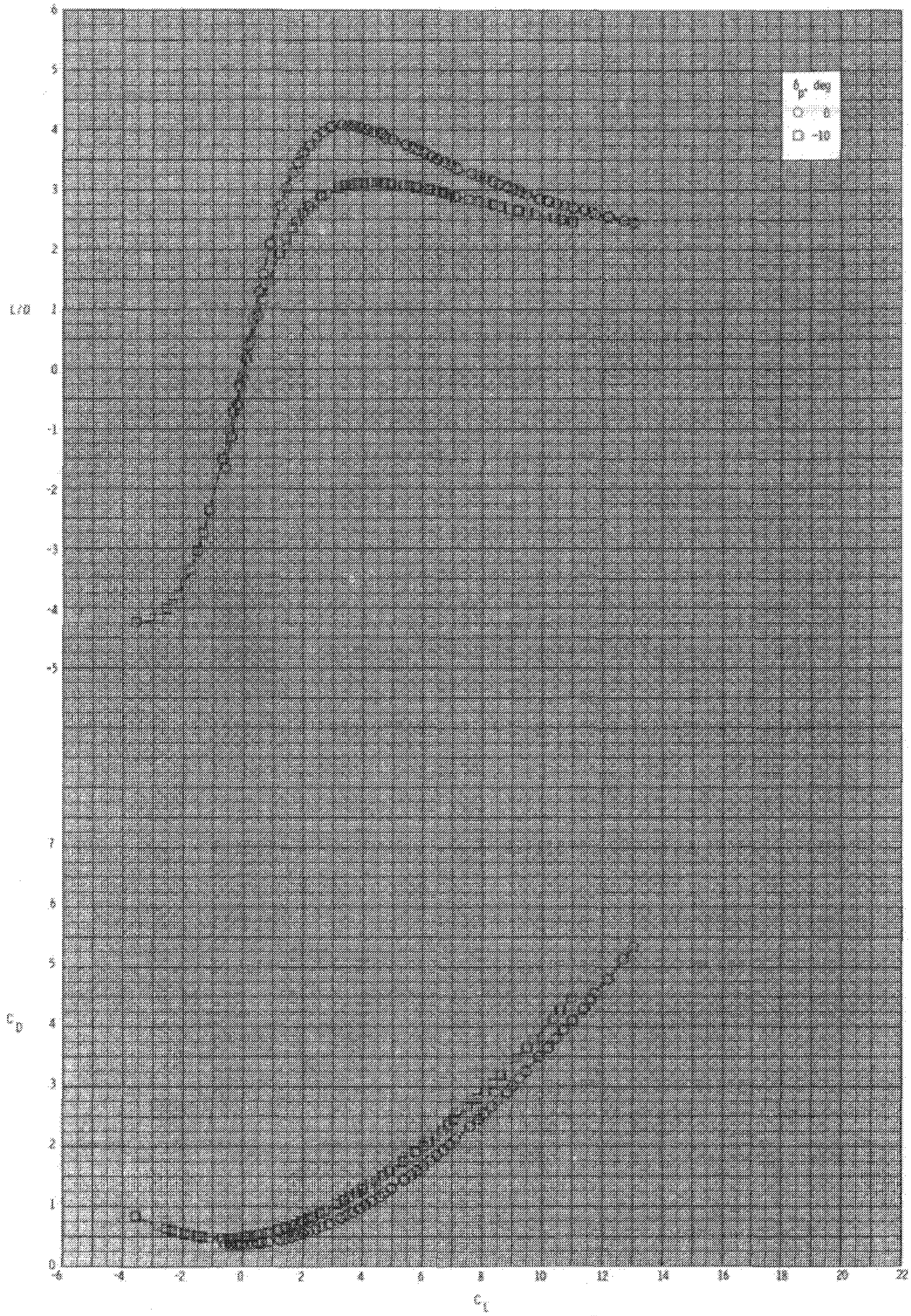

(a) Concluded.

Figure 30.- Continued.

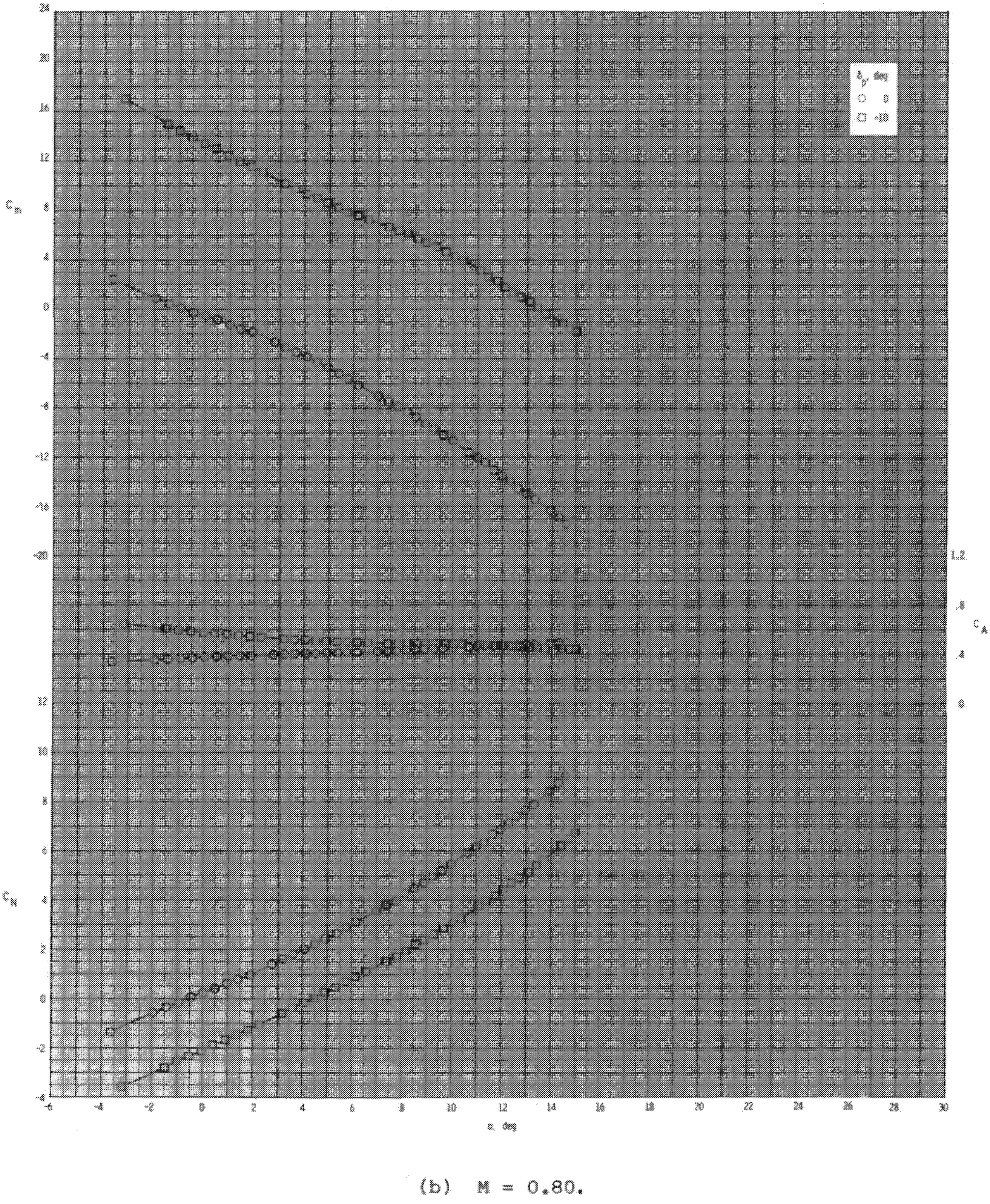

(b) M = 0.80.

Figure 30.- Continued.

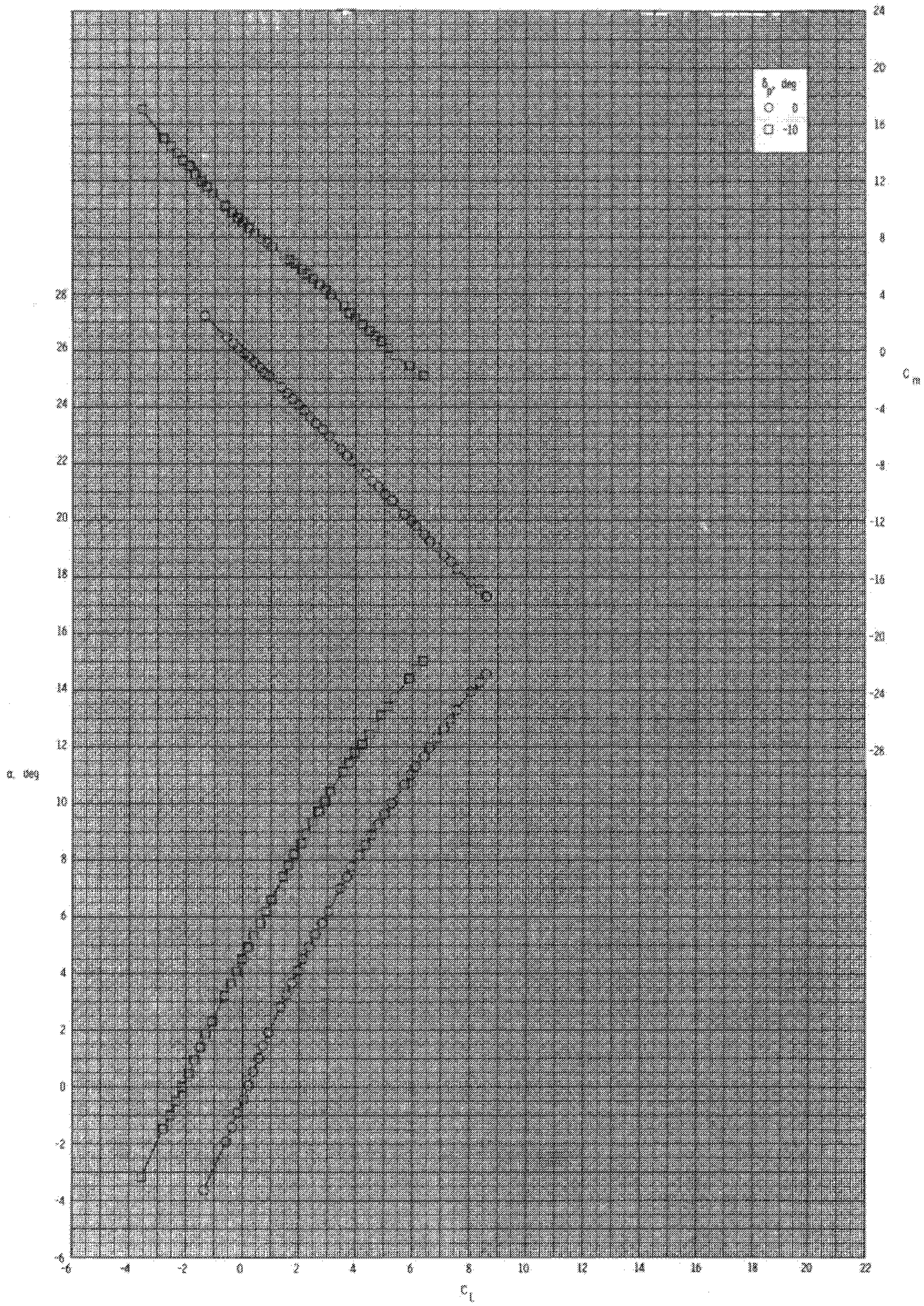

(b) Continued.

Figure 30.- Continued.

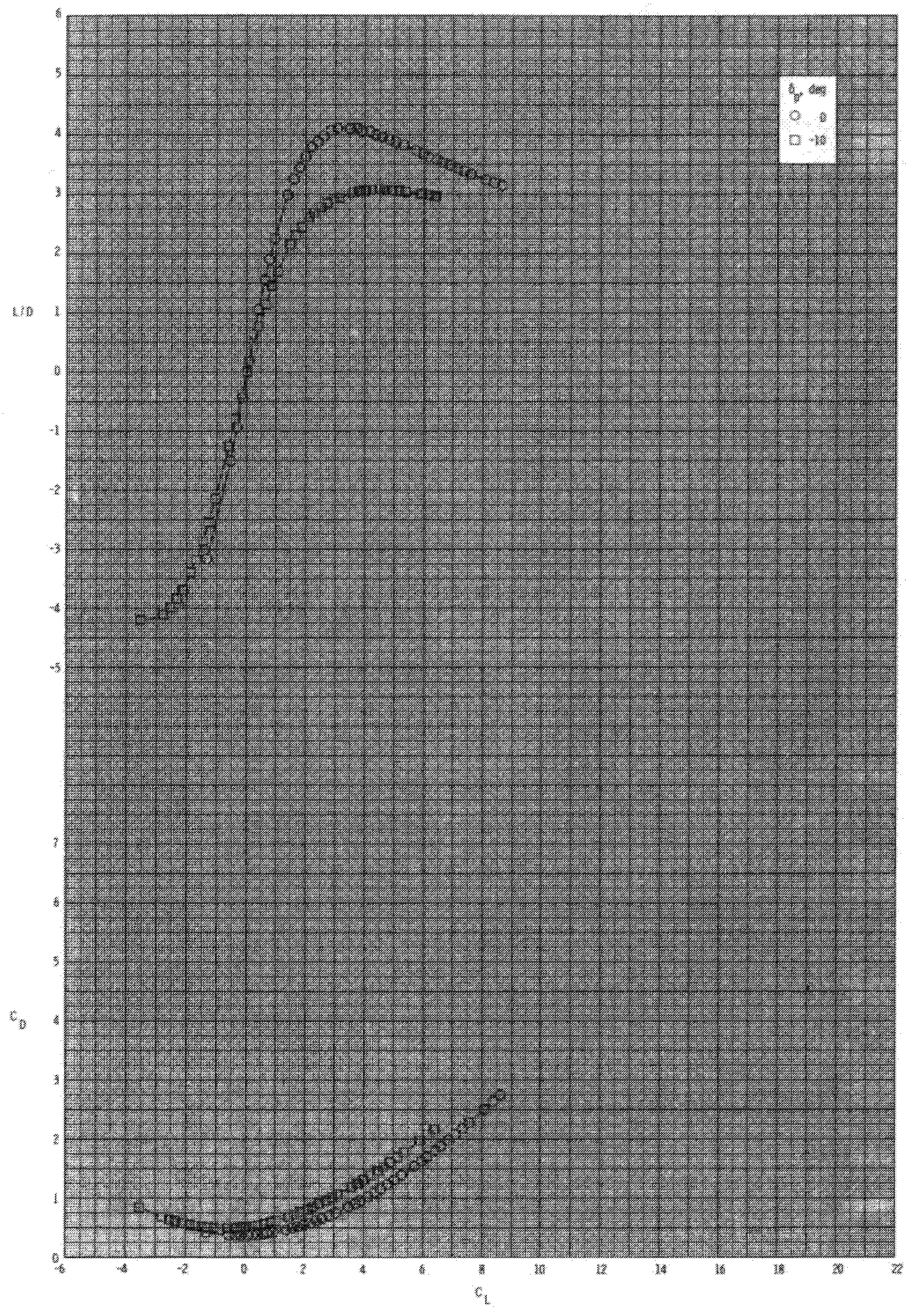

(b) Concluded.

Figure 30.- Continued.

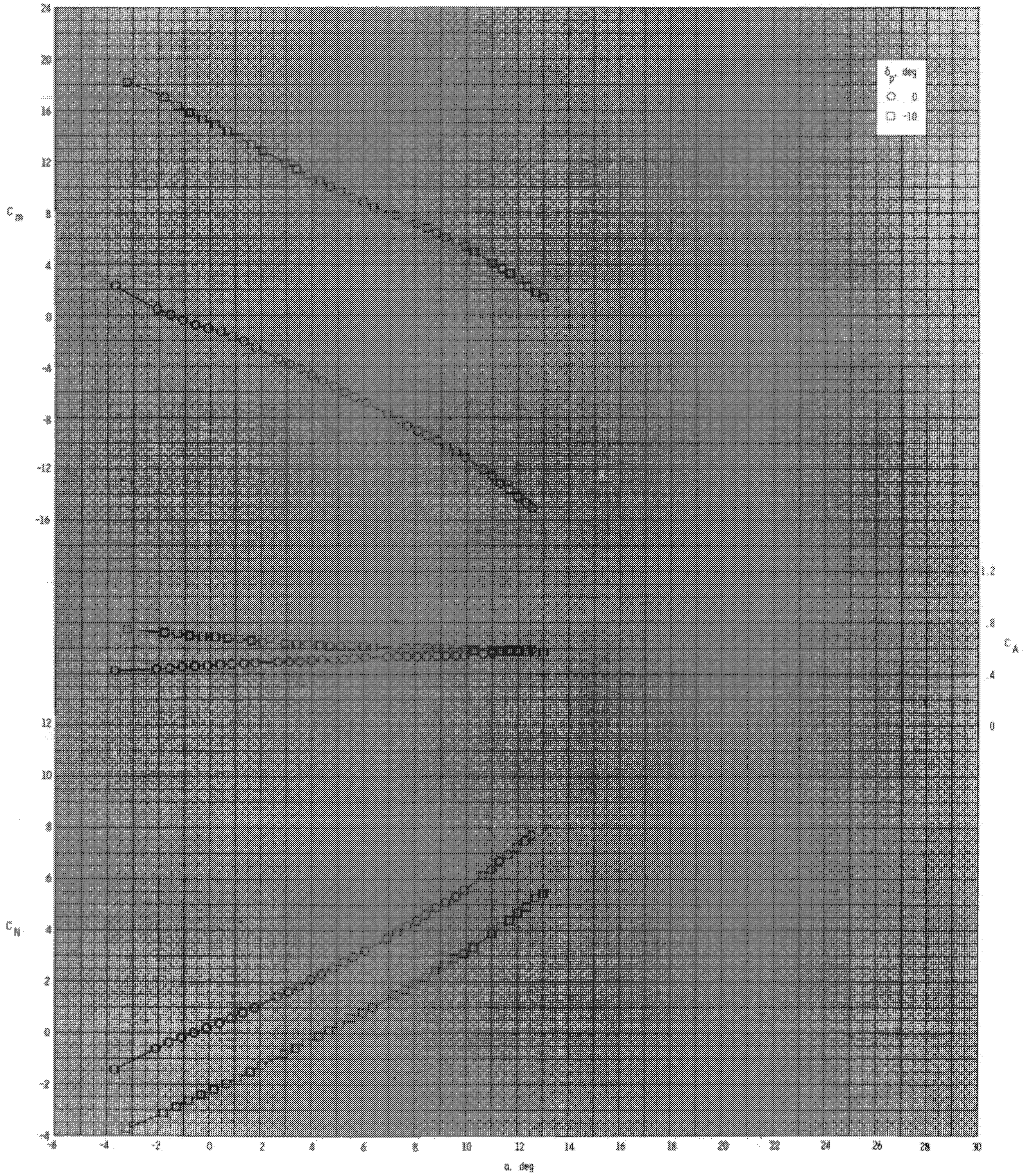

(c) M = 0.95.

Figure 30.- Continued.

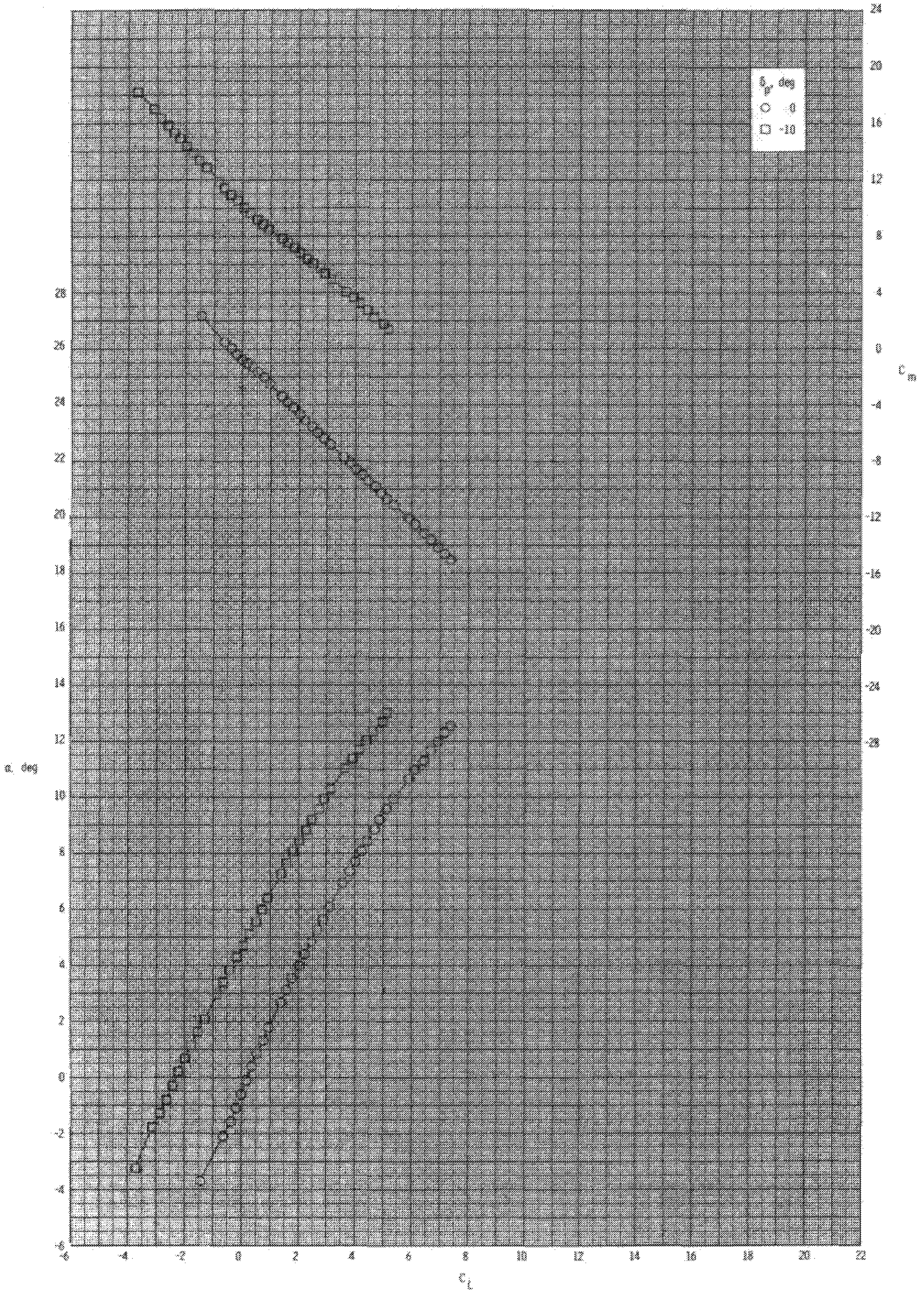

(c) Continued.

Figure 30.- Continued.

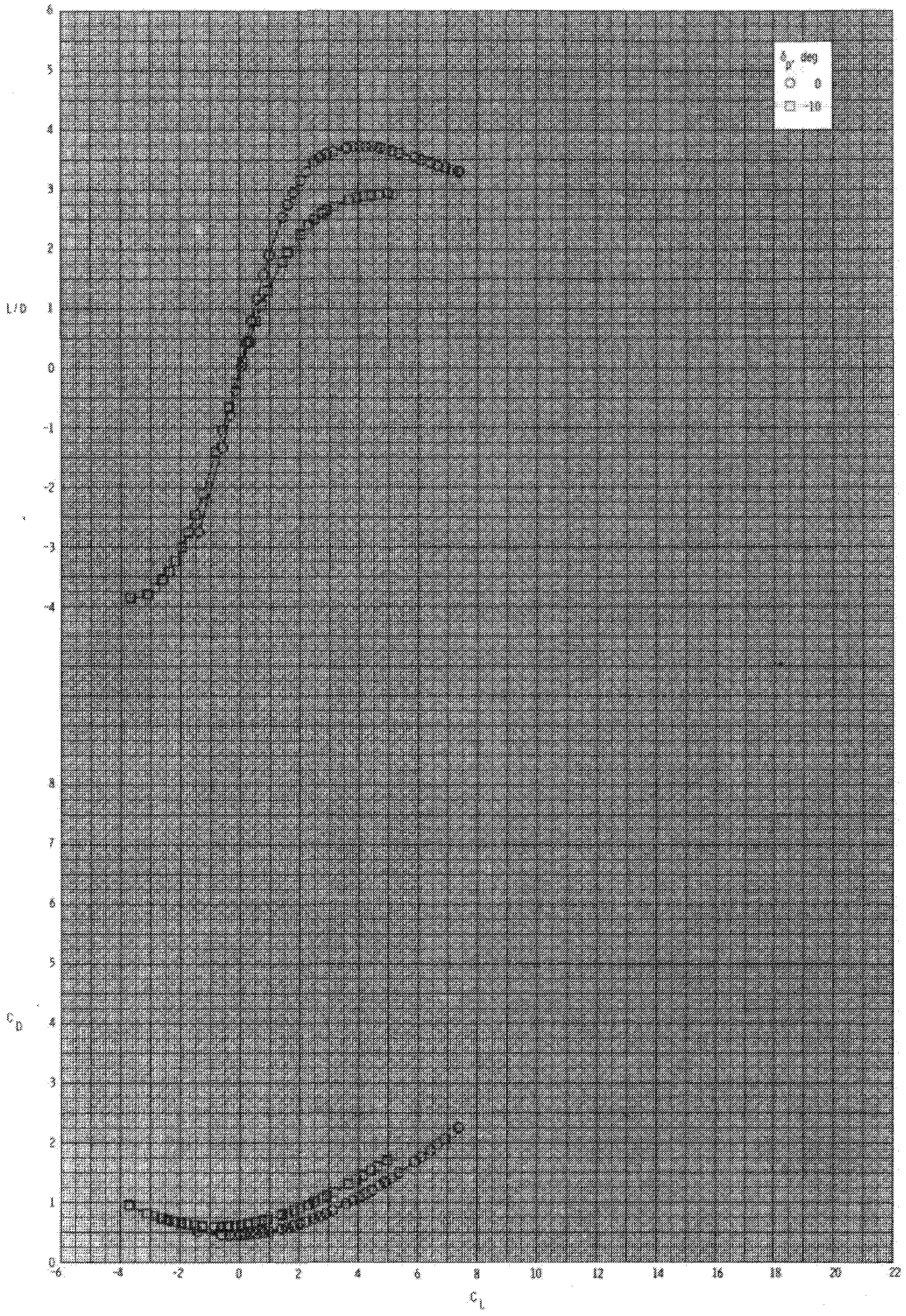

(c) Concluded.

Figure 30.- Concluded.

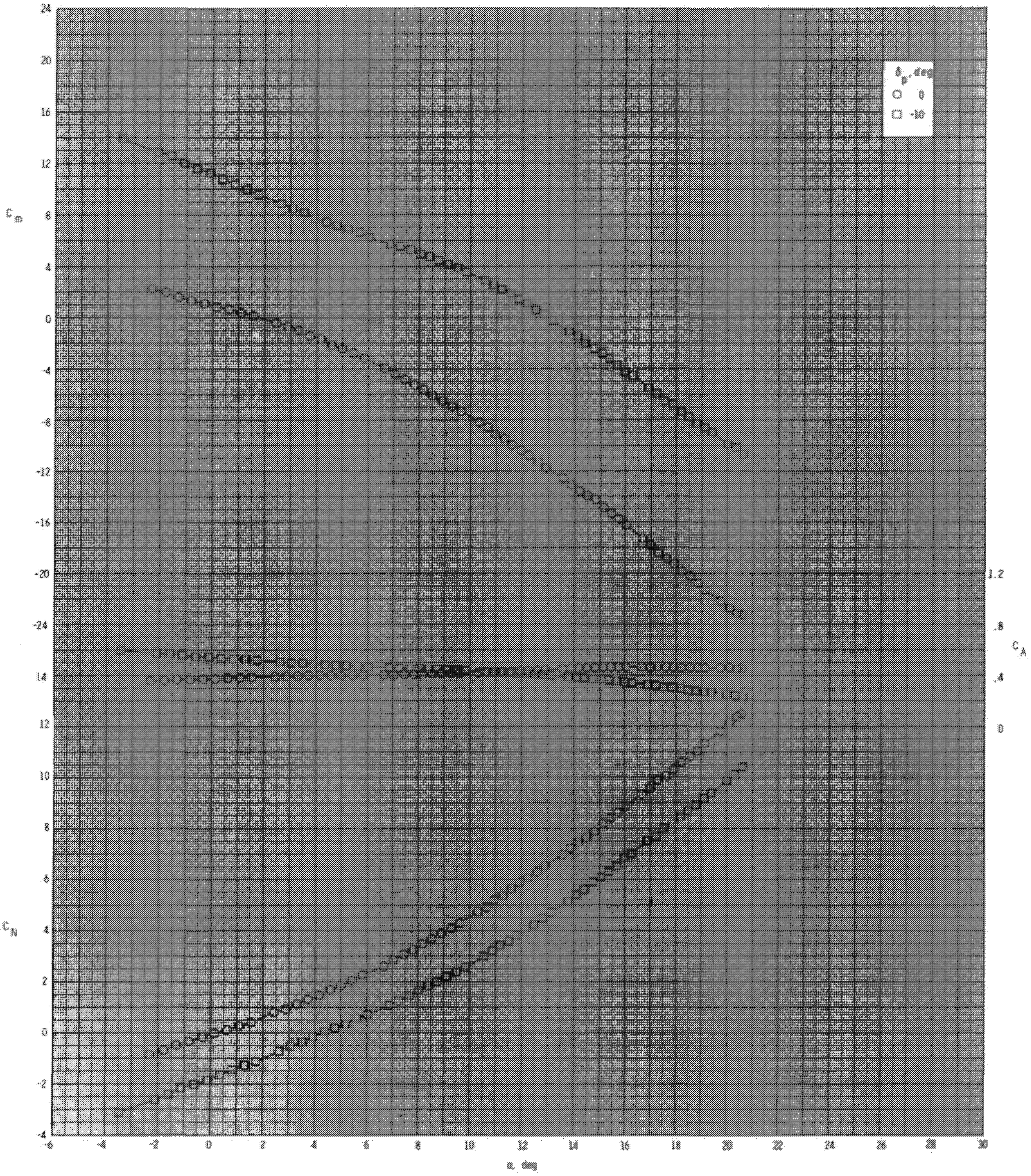

(a) M = 0.60.

Figure 31.- Pitch-control effectiveness for configuration $B_1I_{2C}T_1$ with internal ducts closed and ϕ_I = 115°.

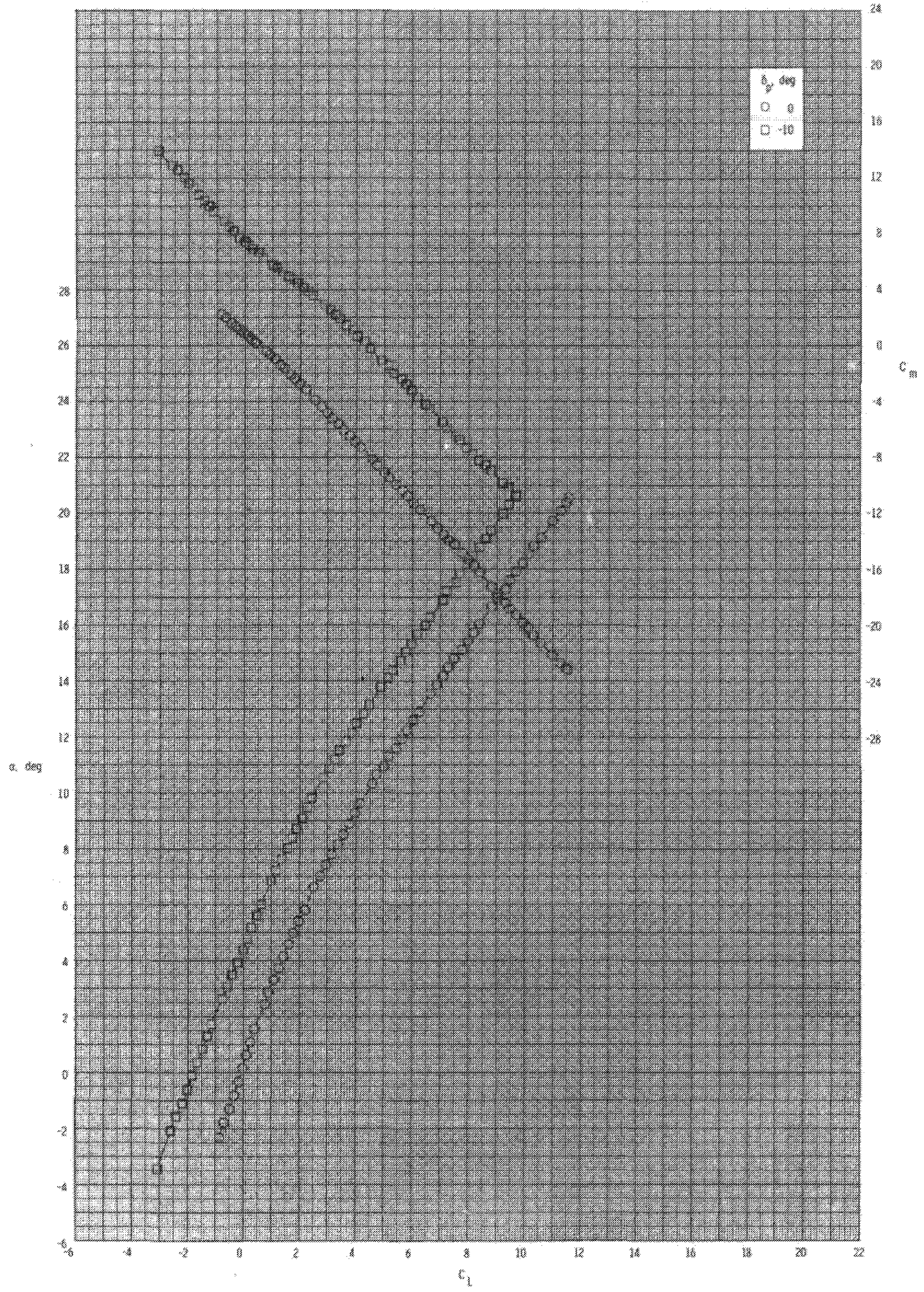

(a) Continued.

Figure 31.- Continued.

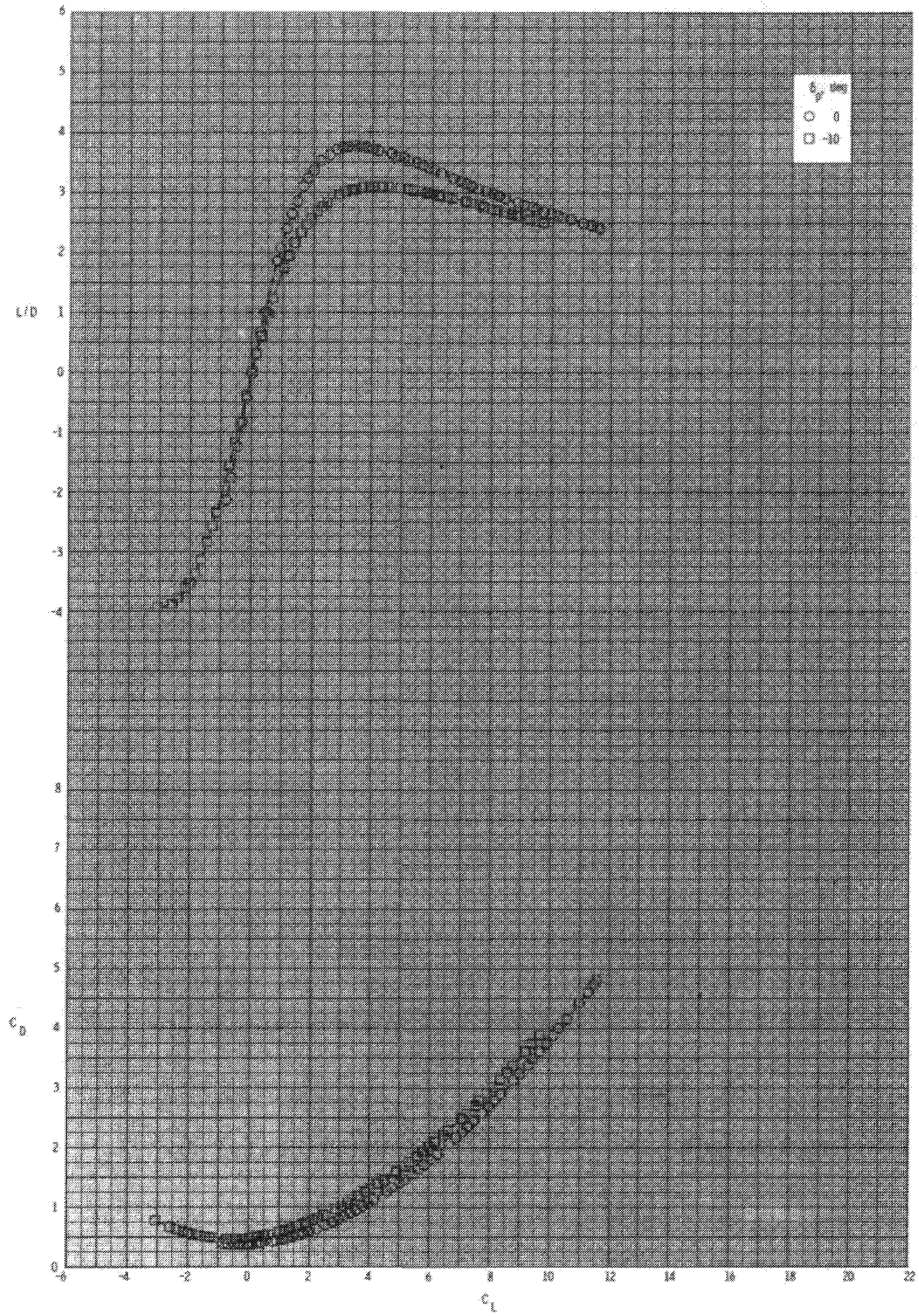

(a) Concluded.

Figure 31.- Continued.

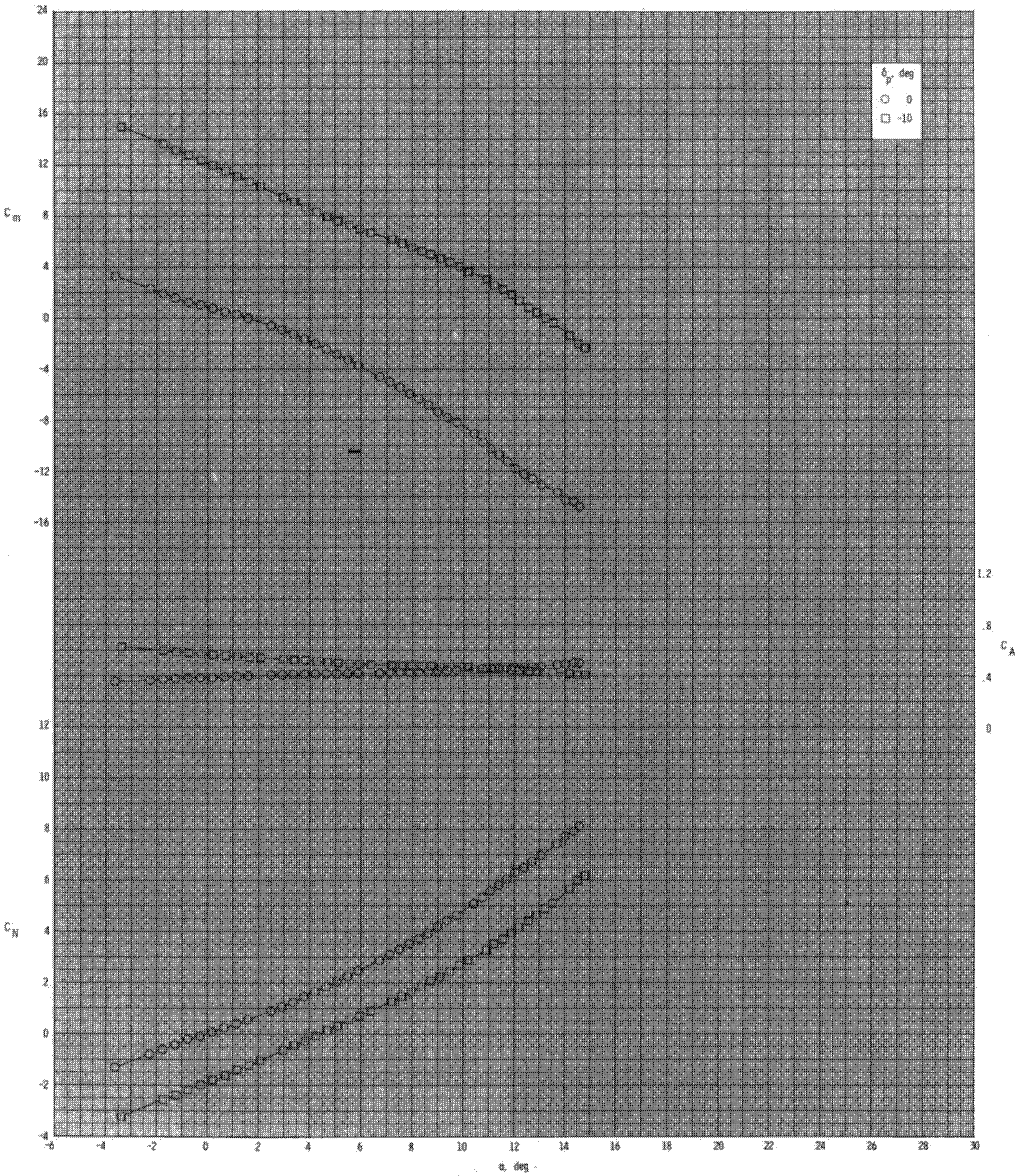

(b) M = 0.80.

Figure 31.- Continued.

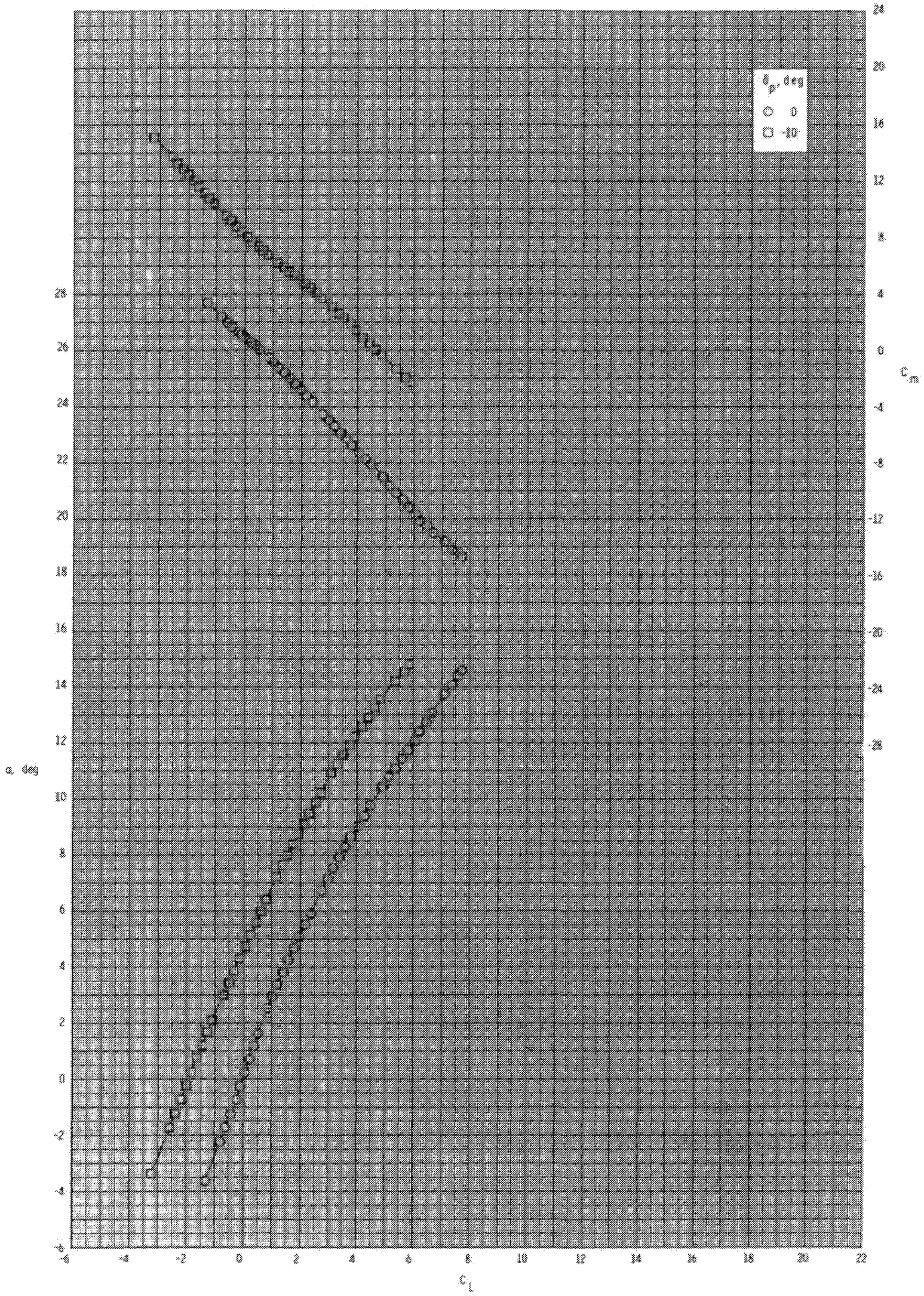

(b) Continued.

Figure 31.- Continued.

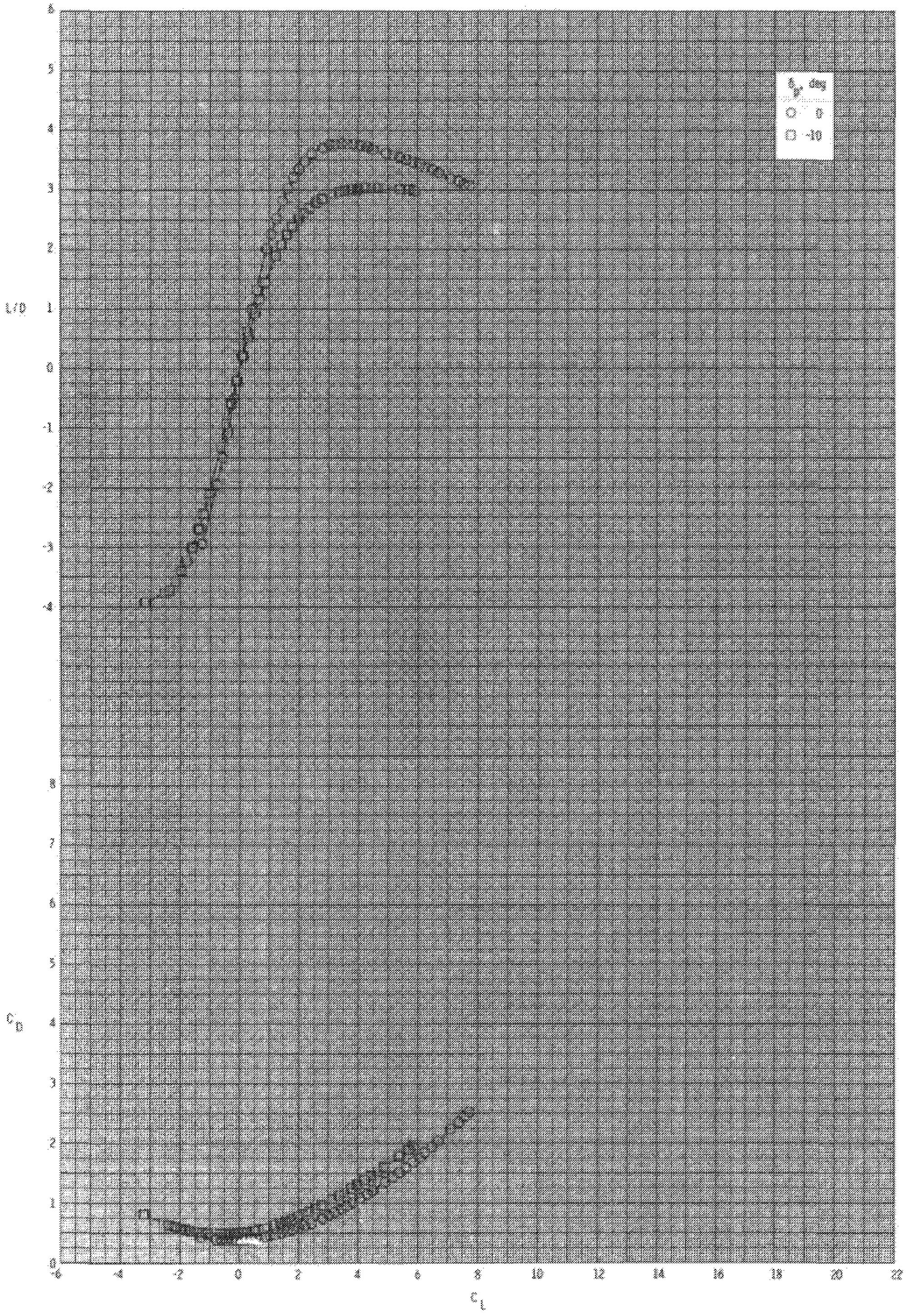

(b) Concluded.

Figure 31.- Continued.

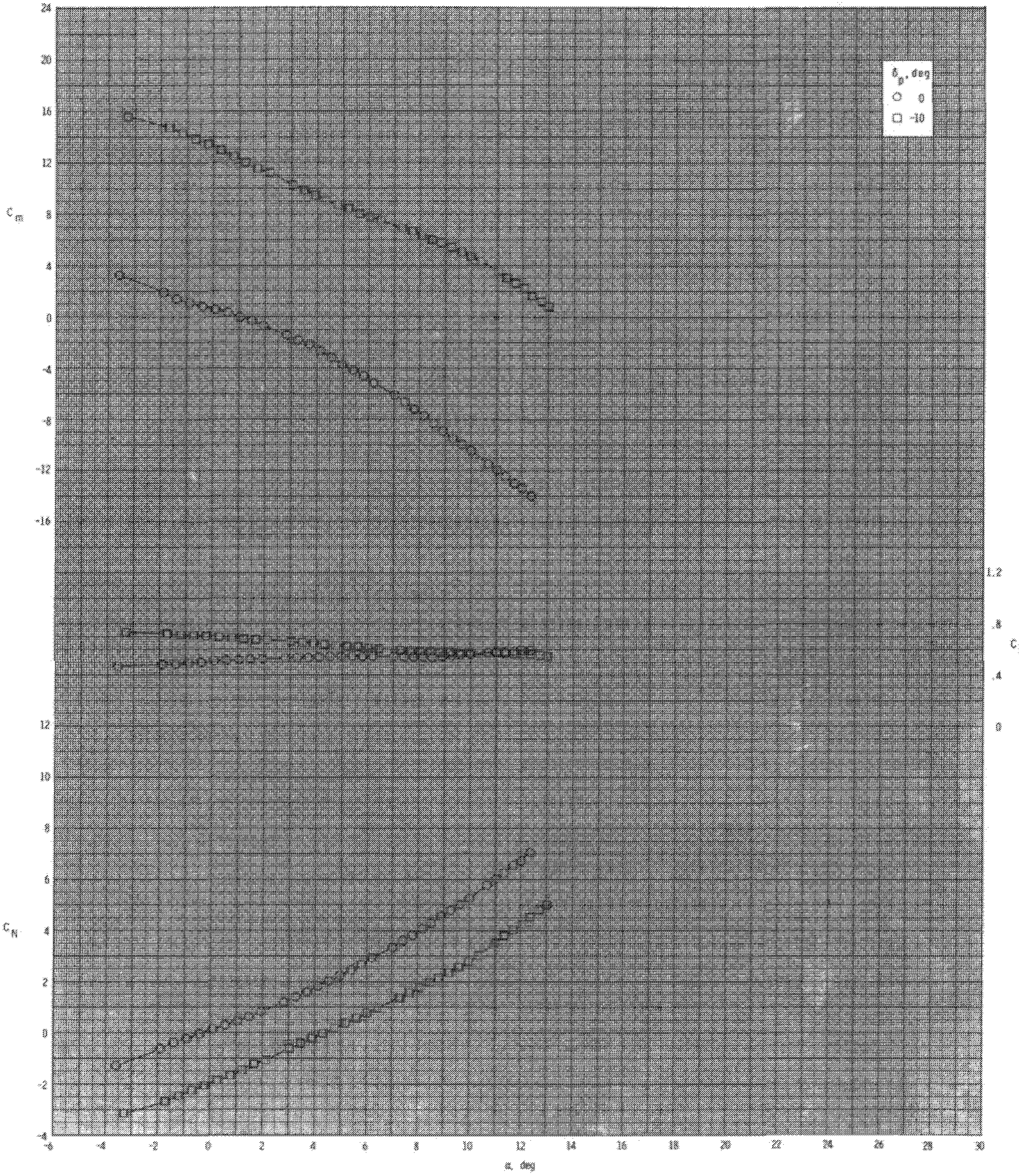

(c) M = 0.95.

Figure 31.- Continued.

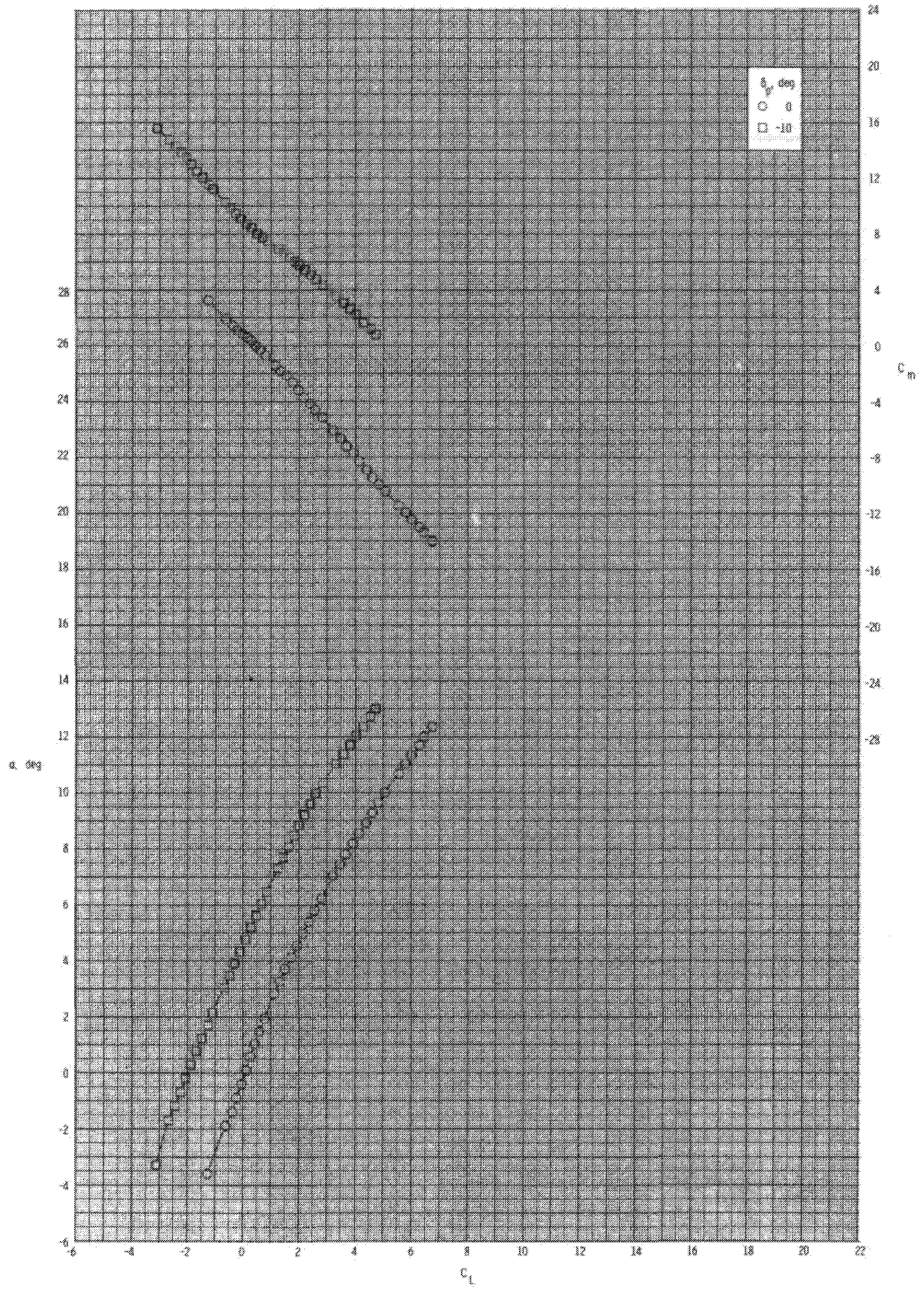

(c) Continued.

Figure 31.- Continued.

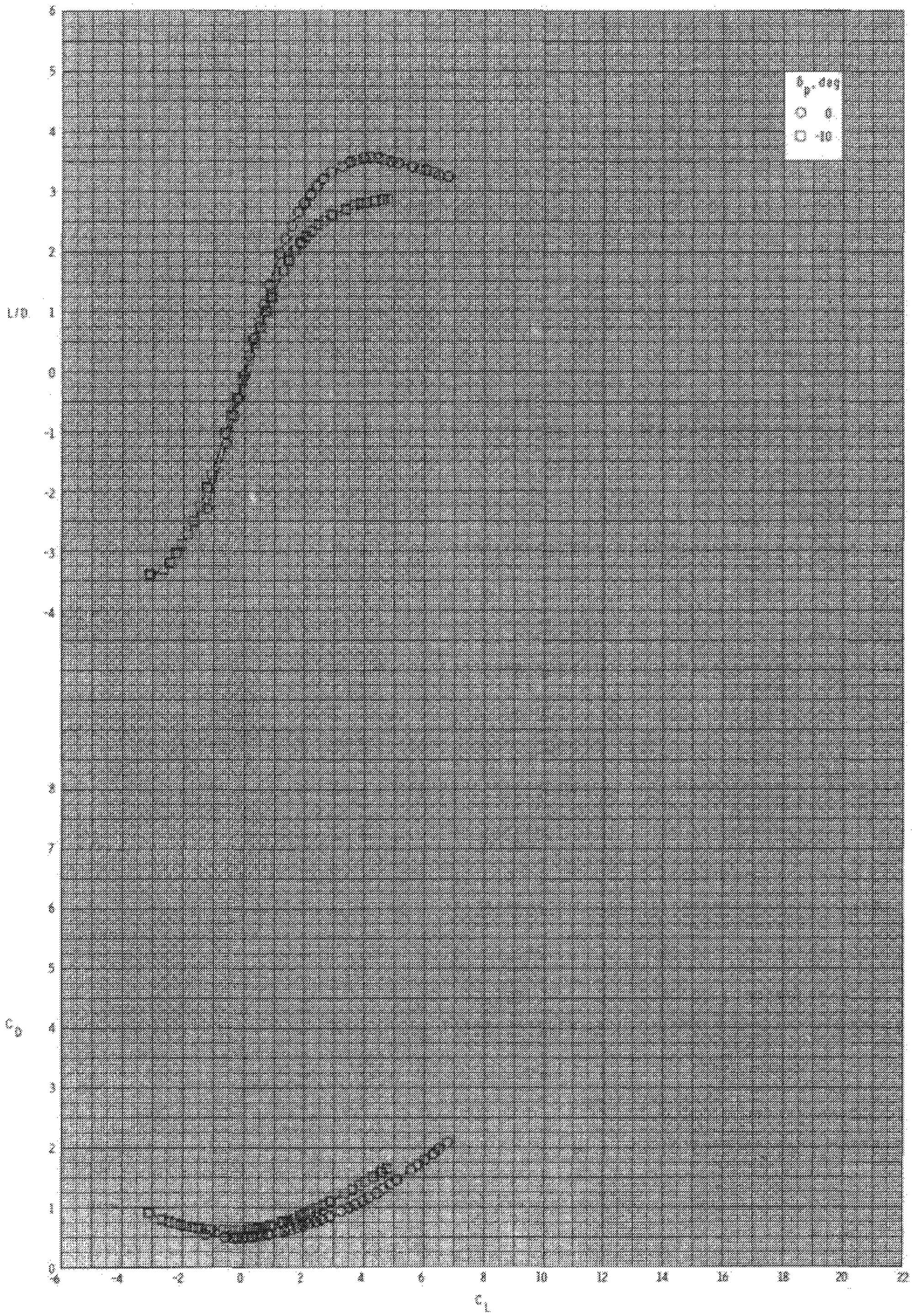

(c) Concluded.

Figure 31.- Concluded.

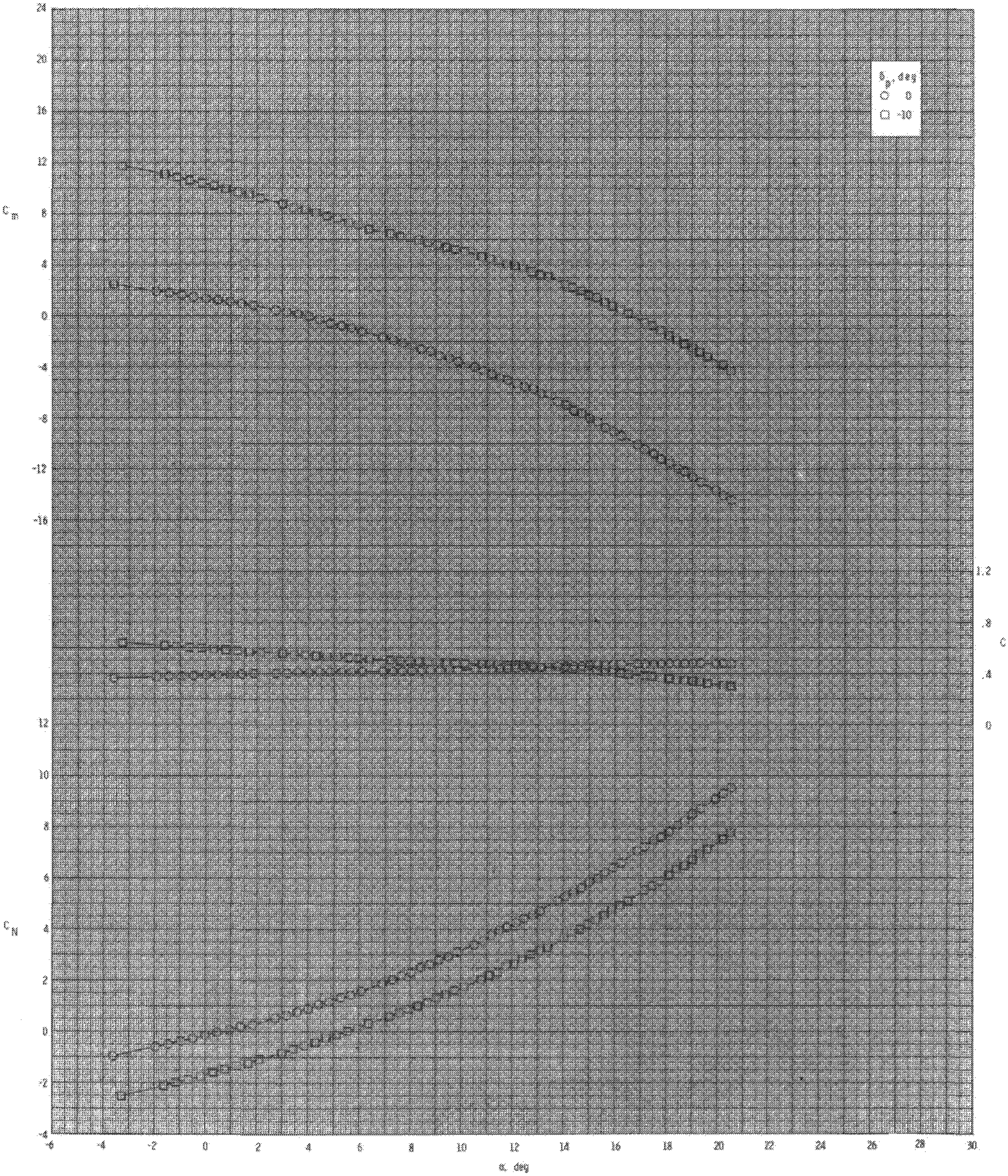

(a) M = 0.60.

Figure 32.- Pitch-control effectiveness for configuration $B_1I_{2c}T_1$ with internal ducts closed and $\phi_I = 135°$.

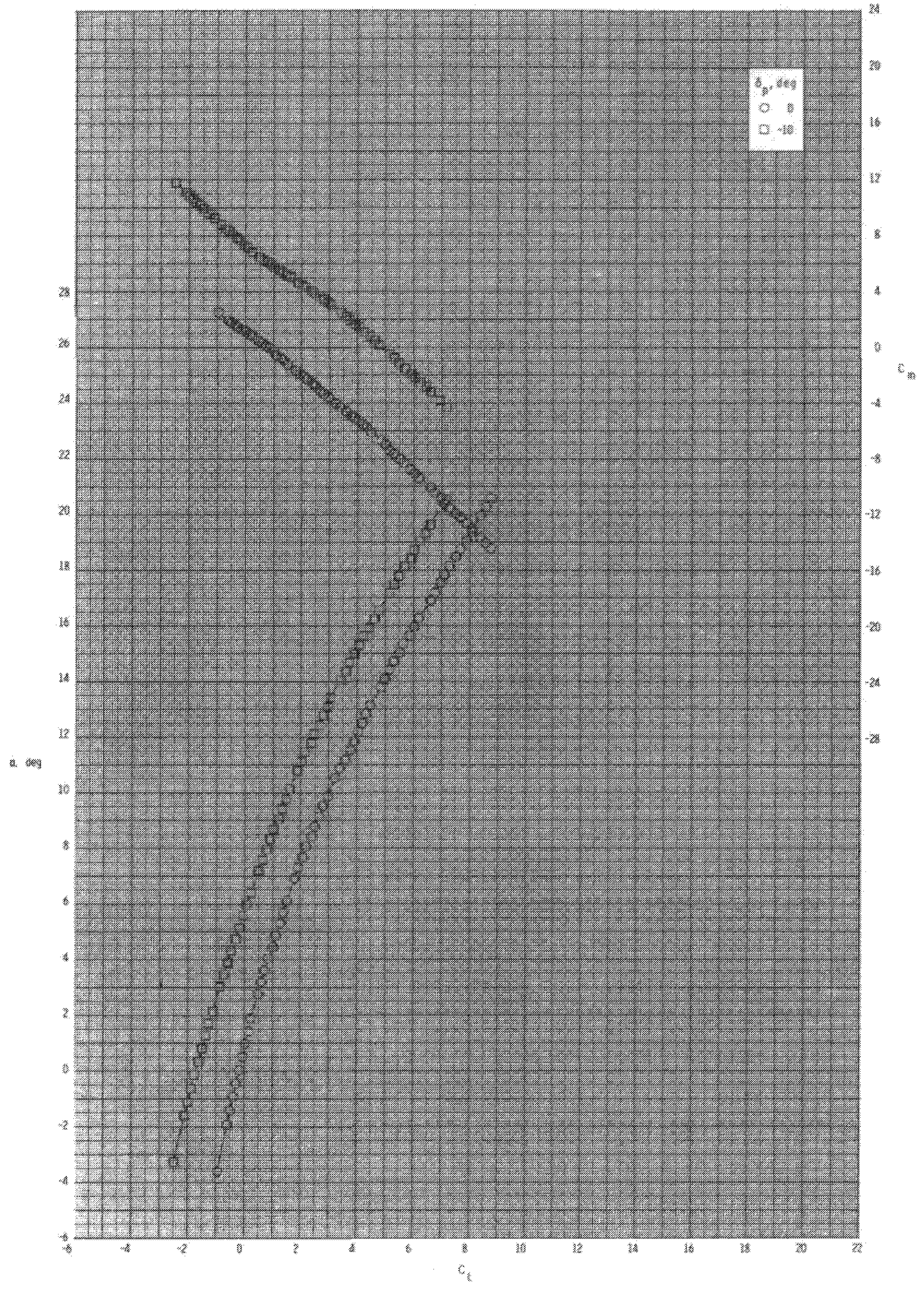

(a) Continued.

Figure 32.- Continued.

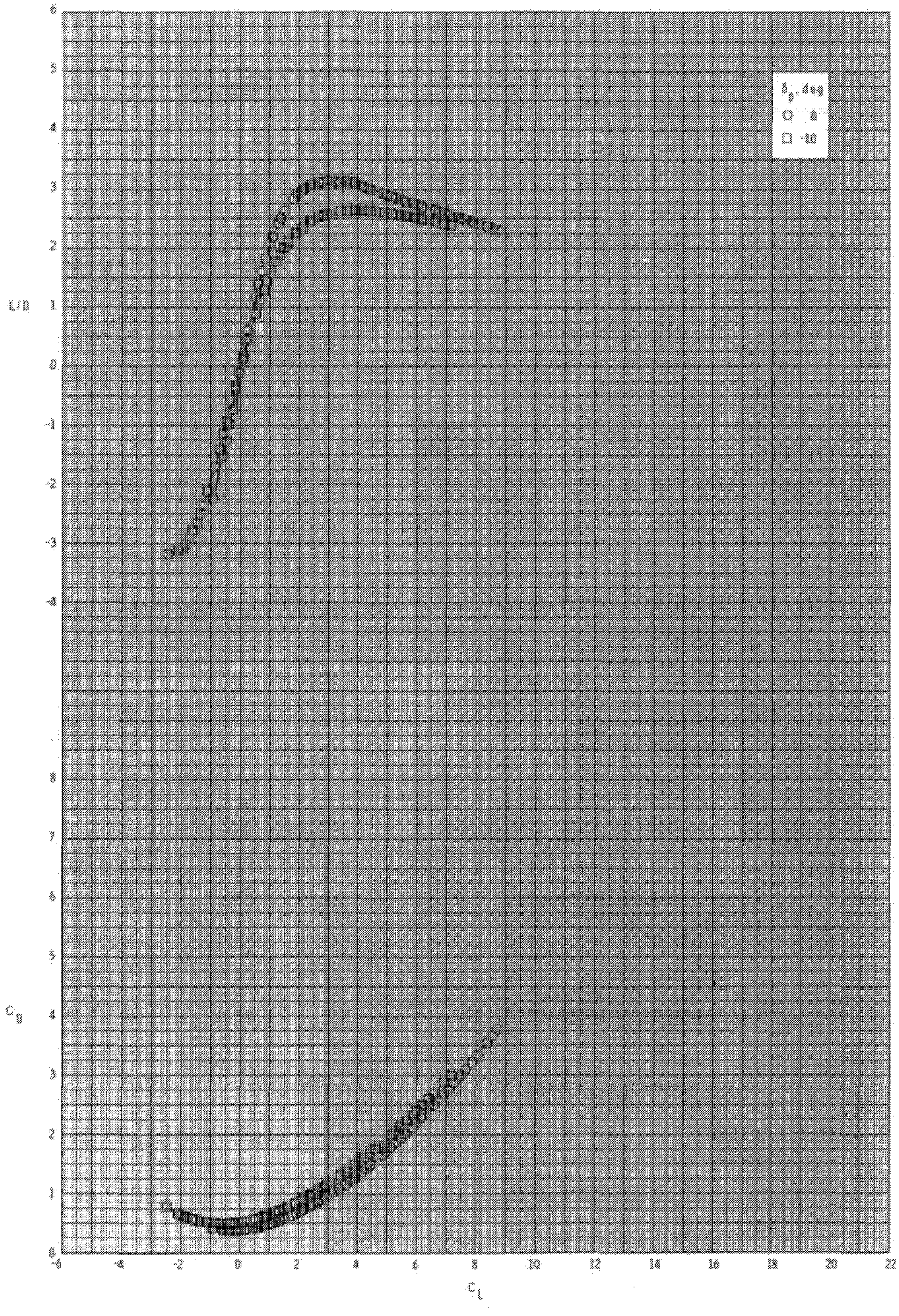

(a) Concluded.

Figure 32.- Continued.

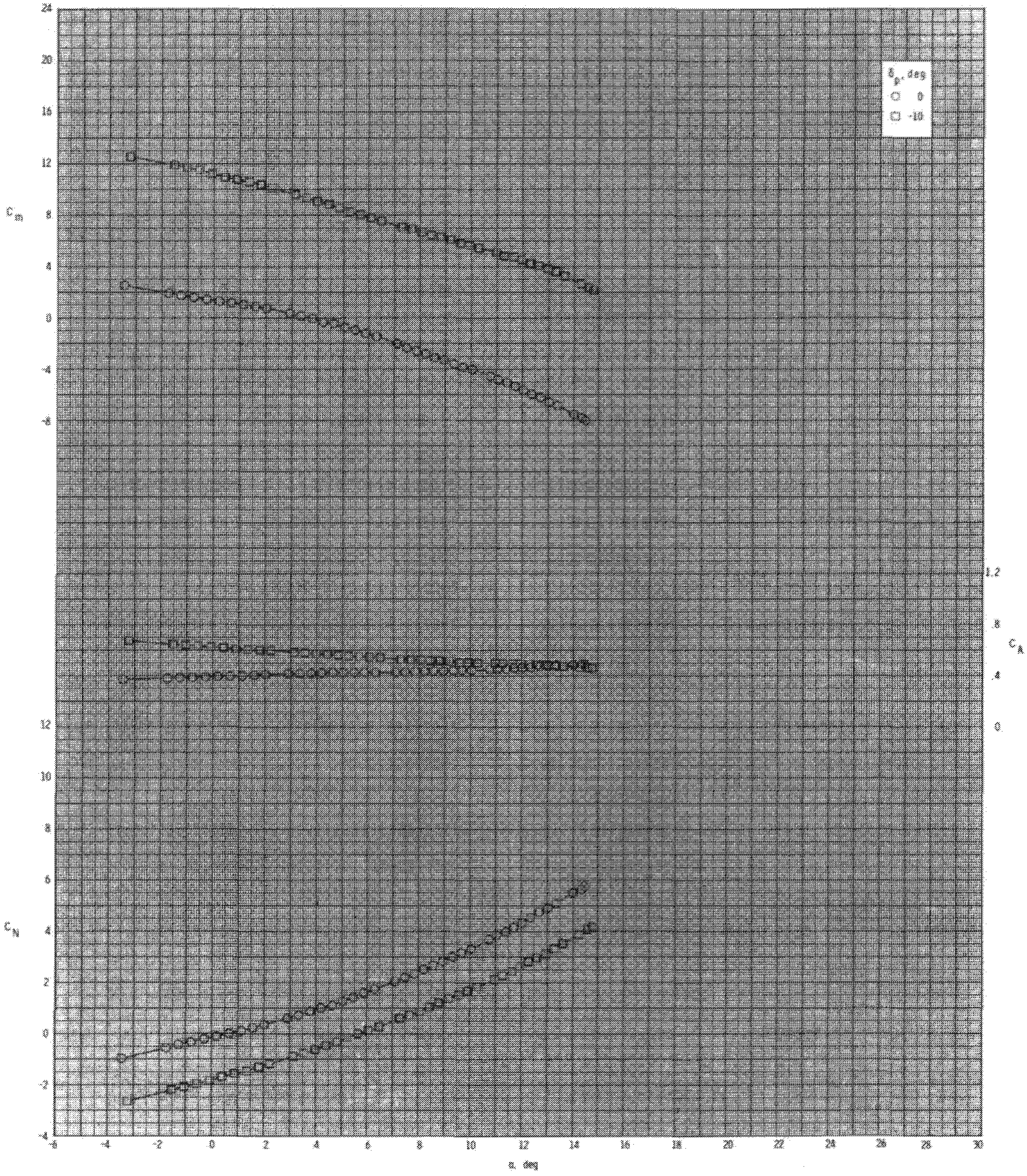

(b) M = 0.80.

Figure 32. Continued.

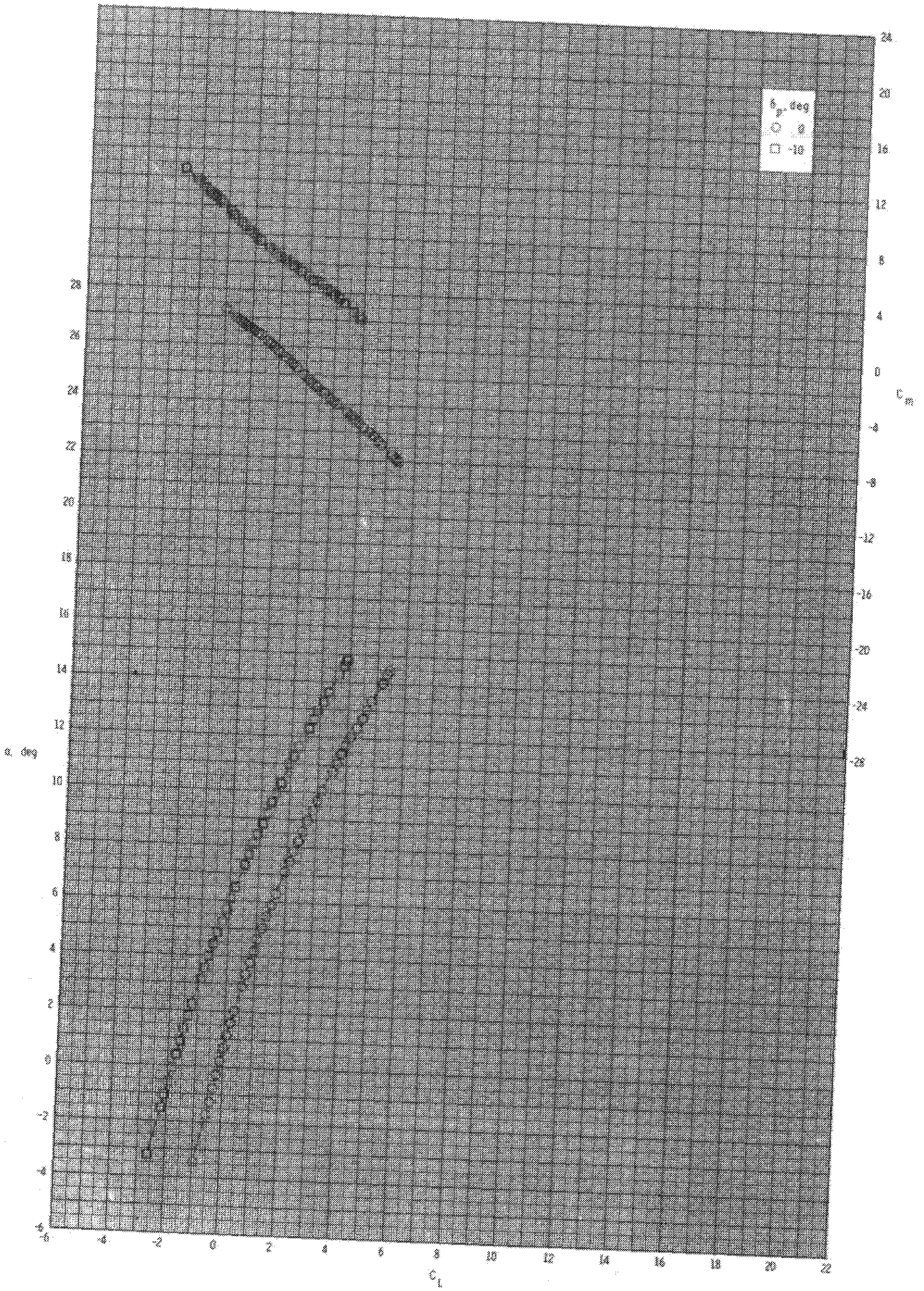

(b) Continued.

Figure 32.- Continued.

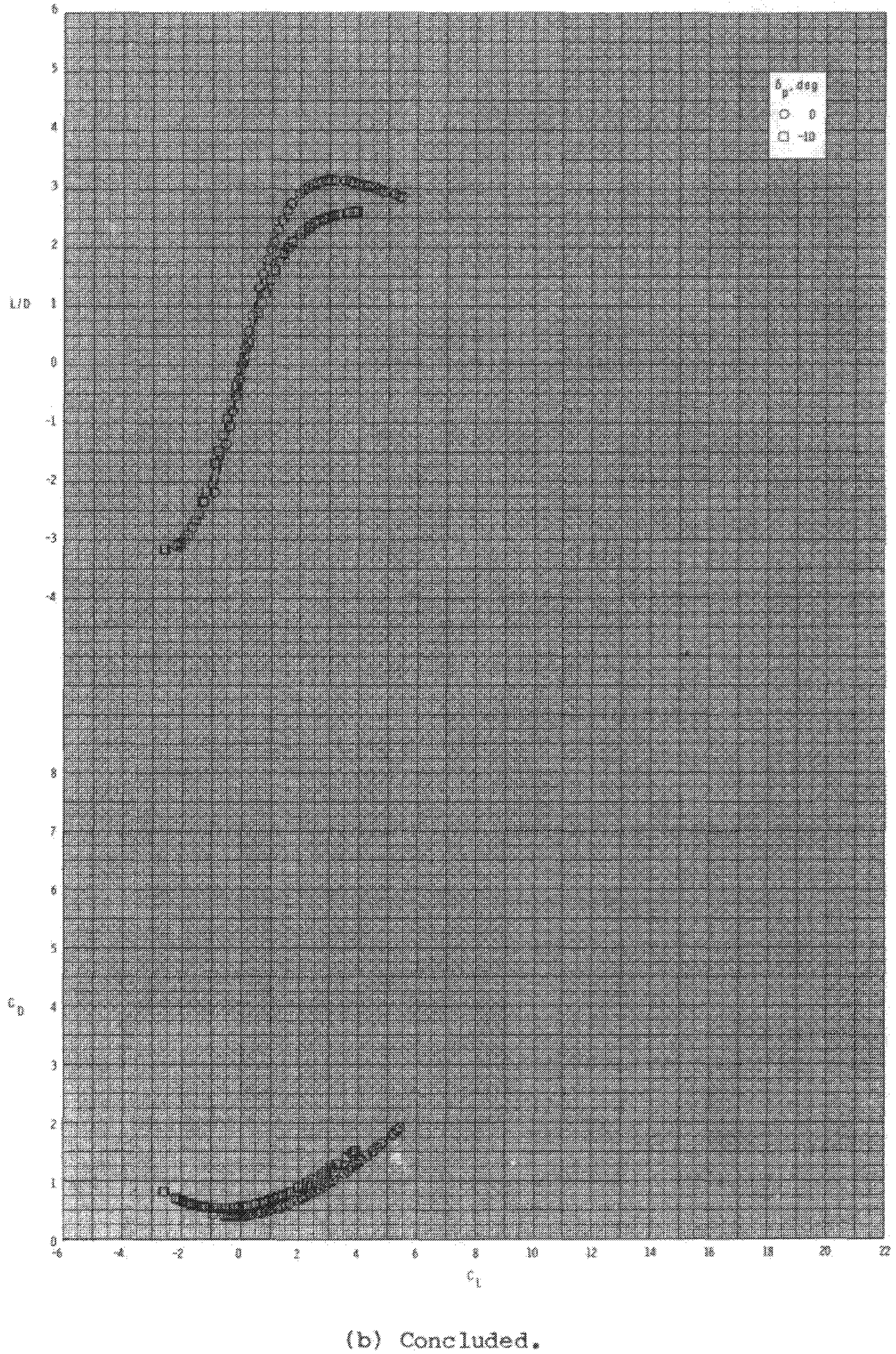

(b) Concluded.

Figure 32.- Continued.

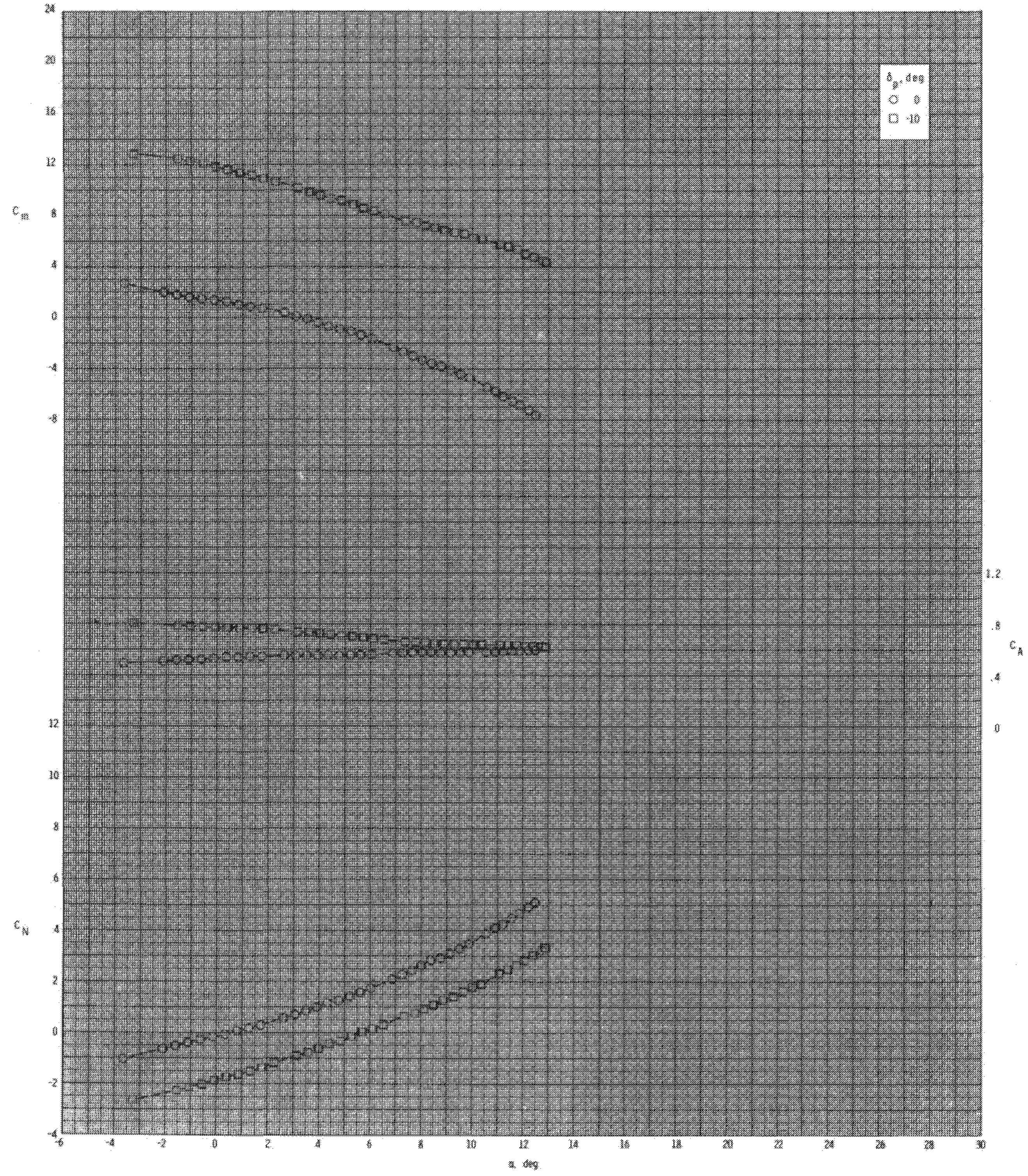

(c) M = 0.95.

Figure 32.- Continued.

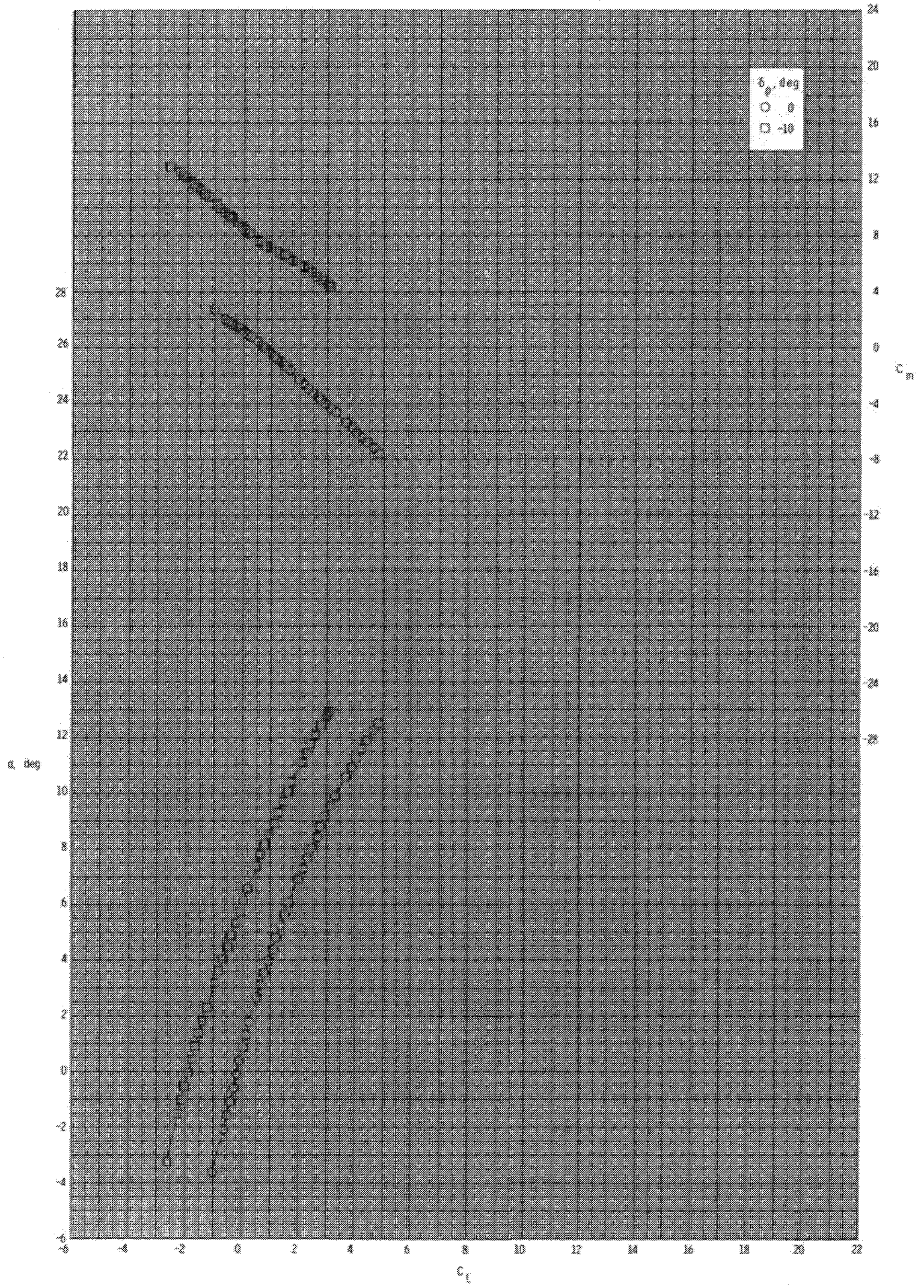

(c) Continued.

Figure 32.- Continued.

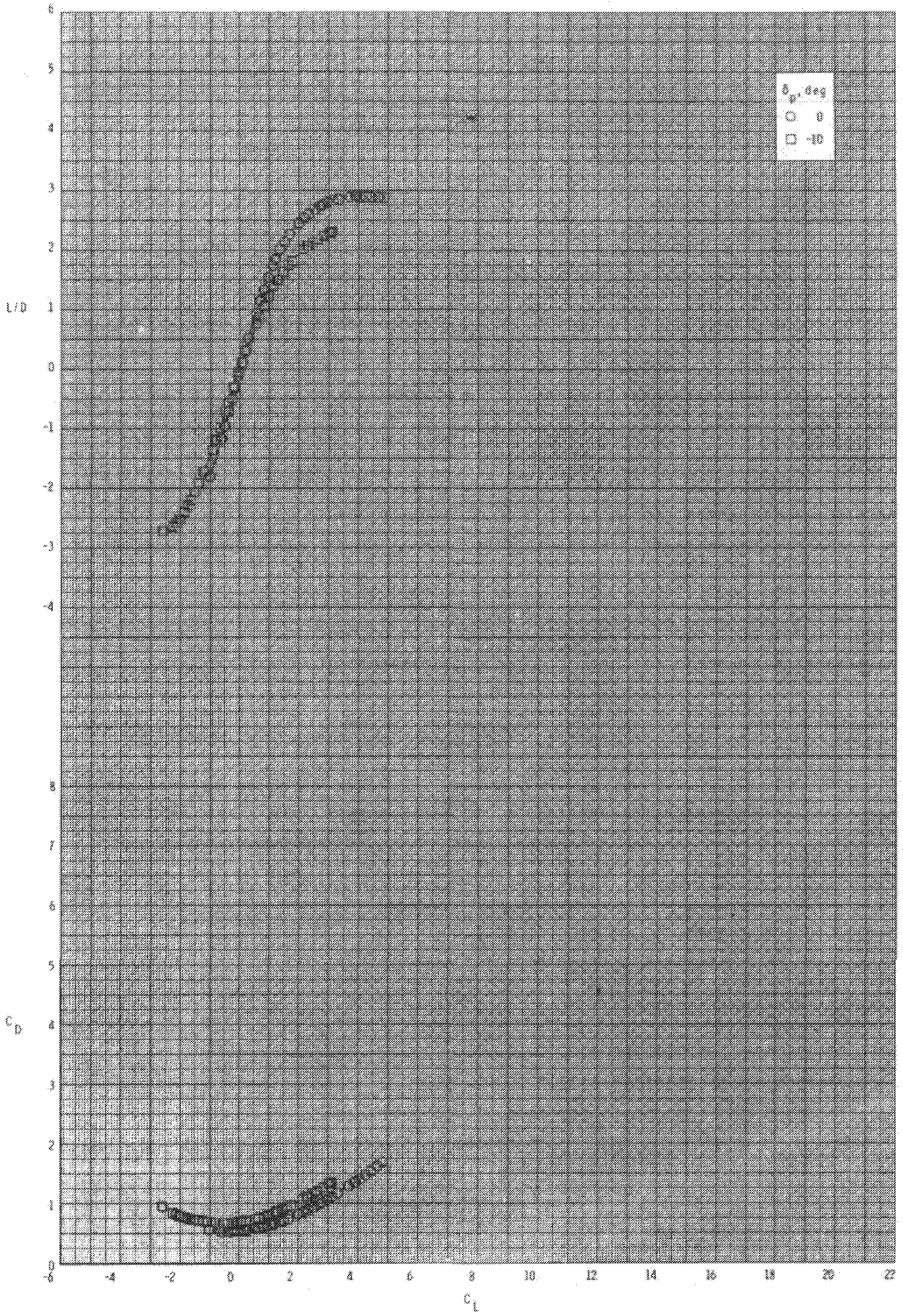

(c) Concluded.

Figure 32.- Concluded.

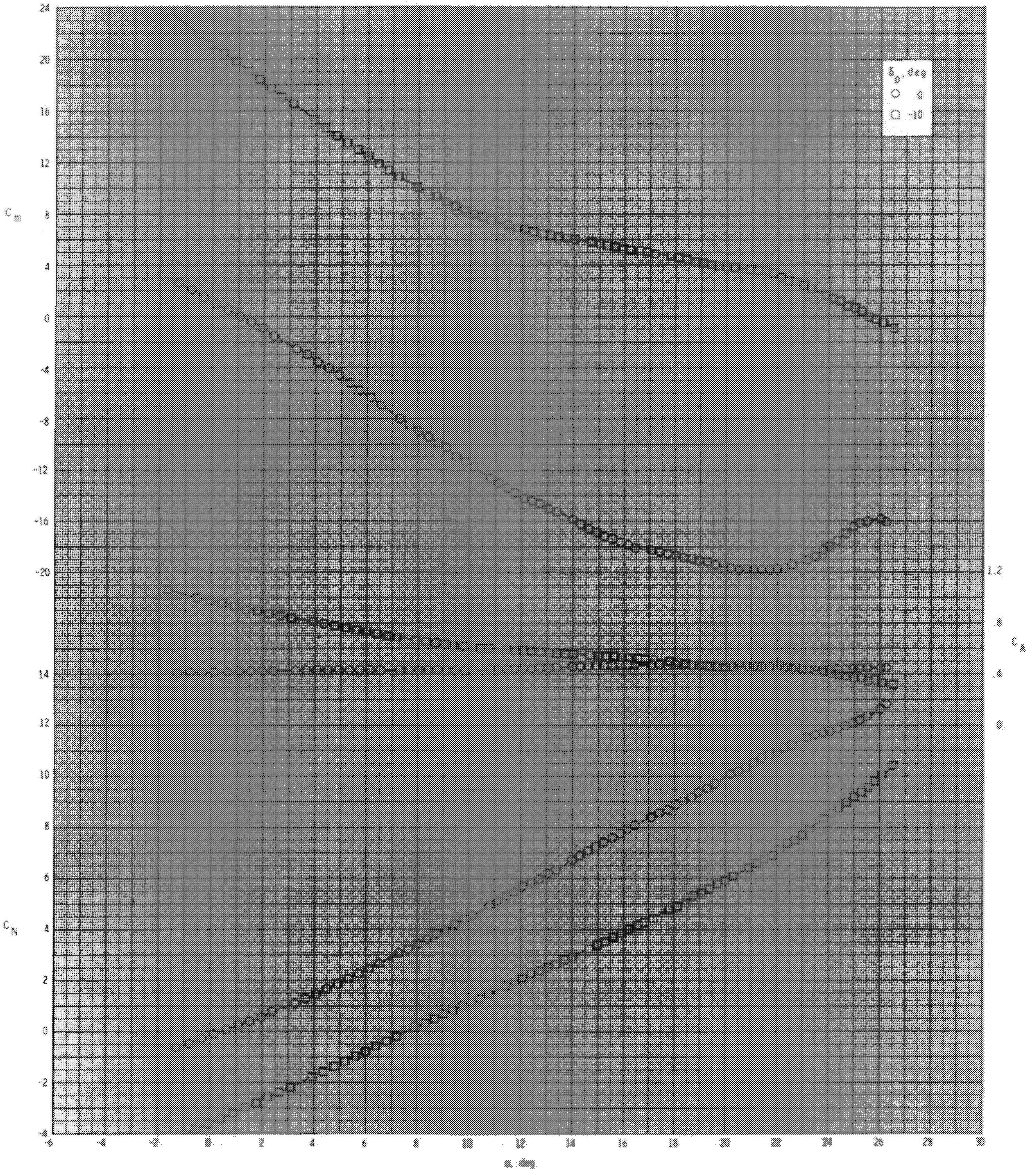

(a) M = 0.60.

Figure 33.- Pitch-control effectiveness for configuration $B_1 I_{2c} T_2$ with internal ducts closed and $\phi_I = 135°$.

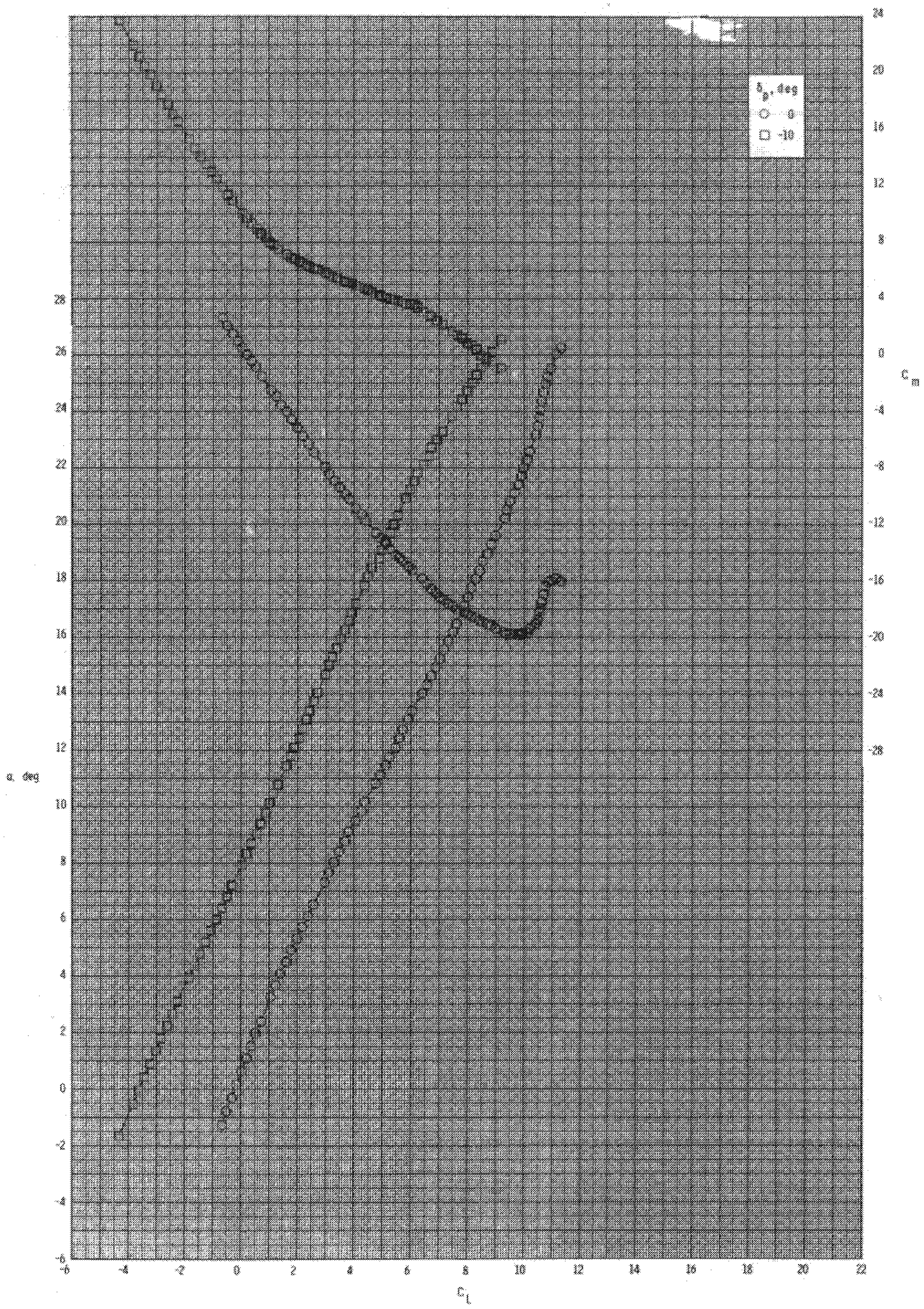

(a) Continued.

Figure 33.- Continued.

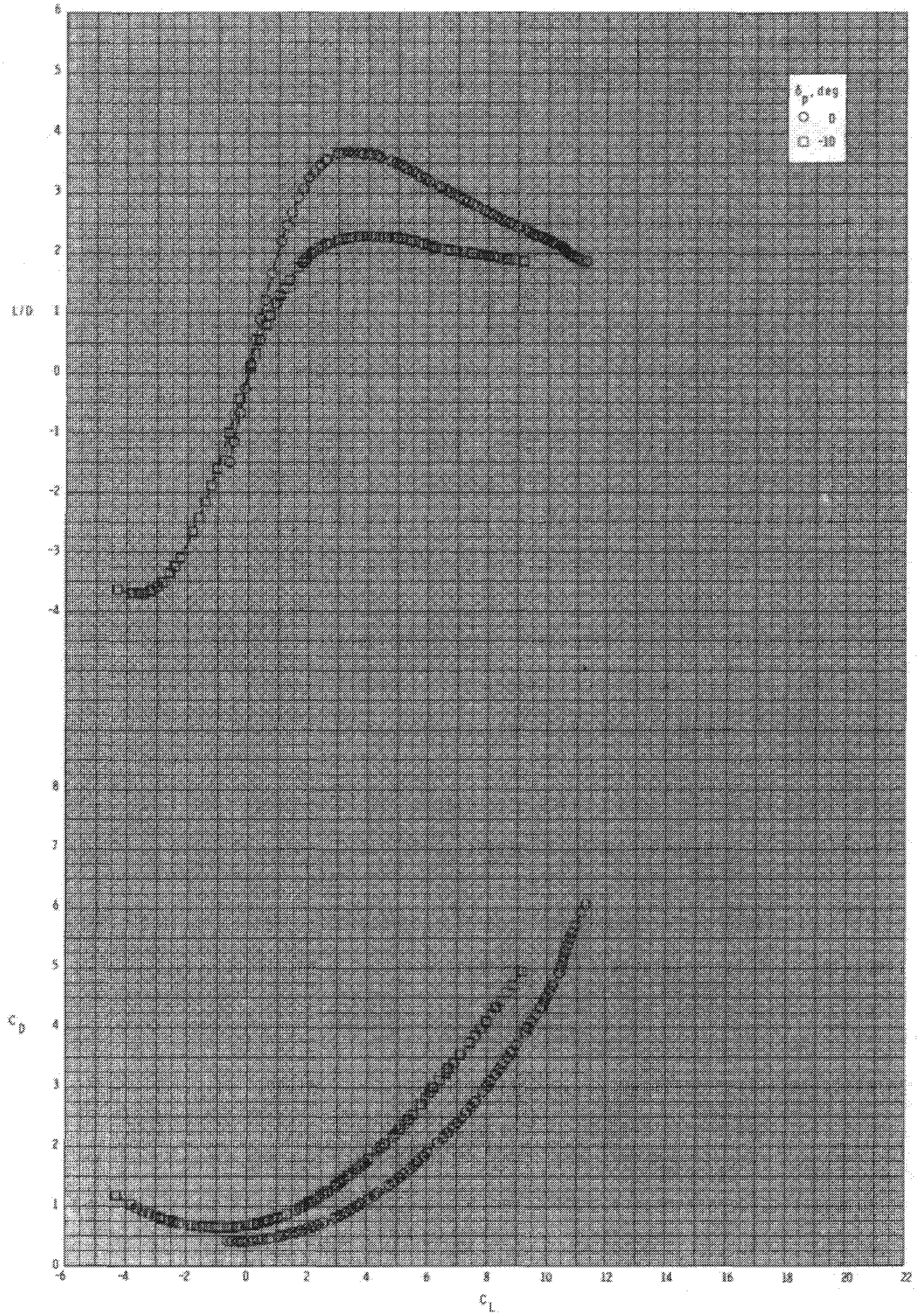

(a) Concluded.

Figure 33.- Continued.

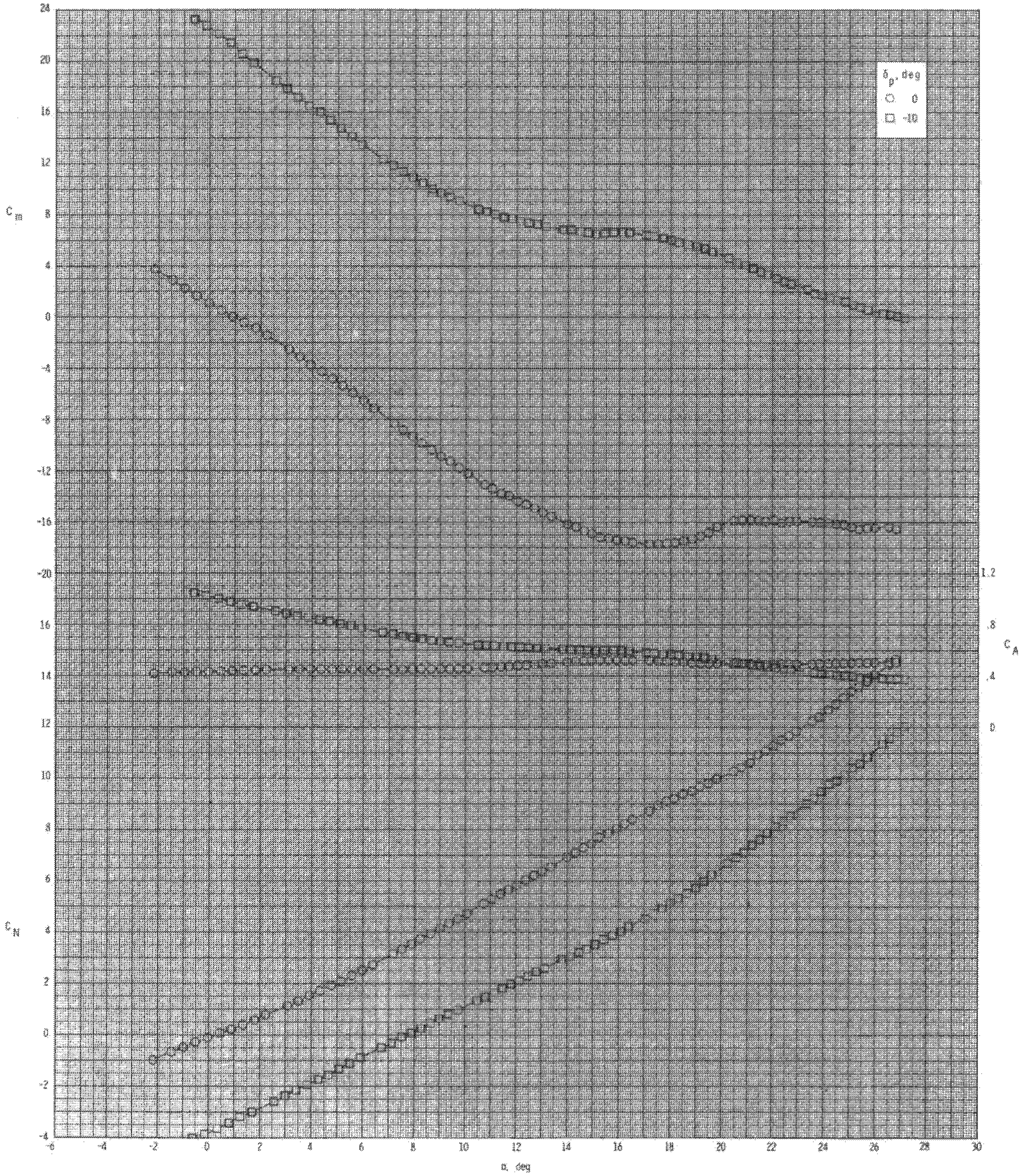

(b) M = 0.80.

Figure 33.- Continued.

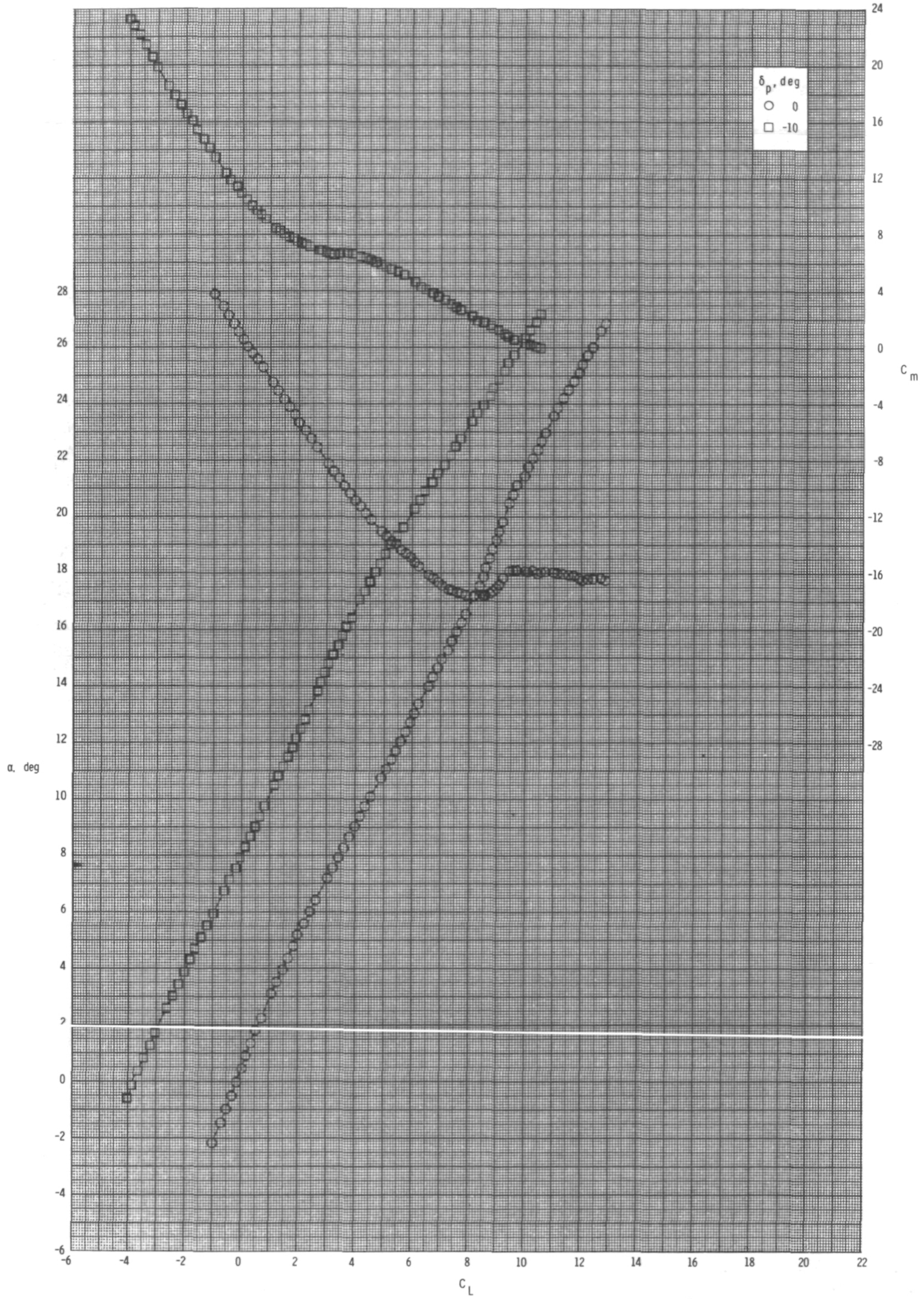

(b) Continued.

Figure 33.- Continued.

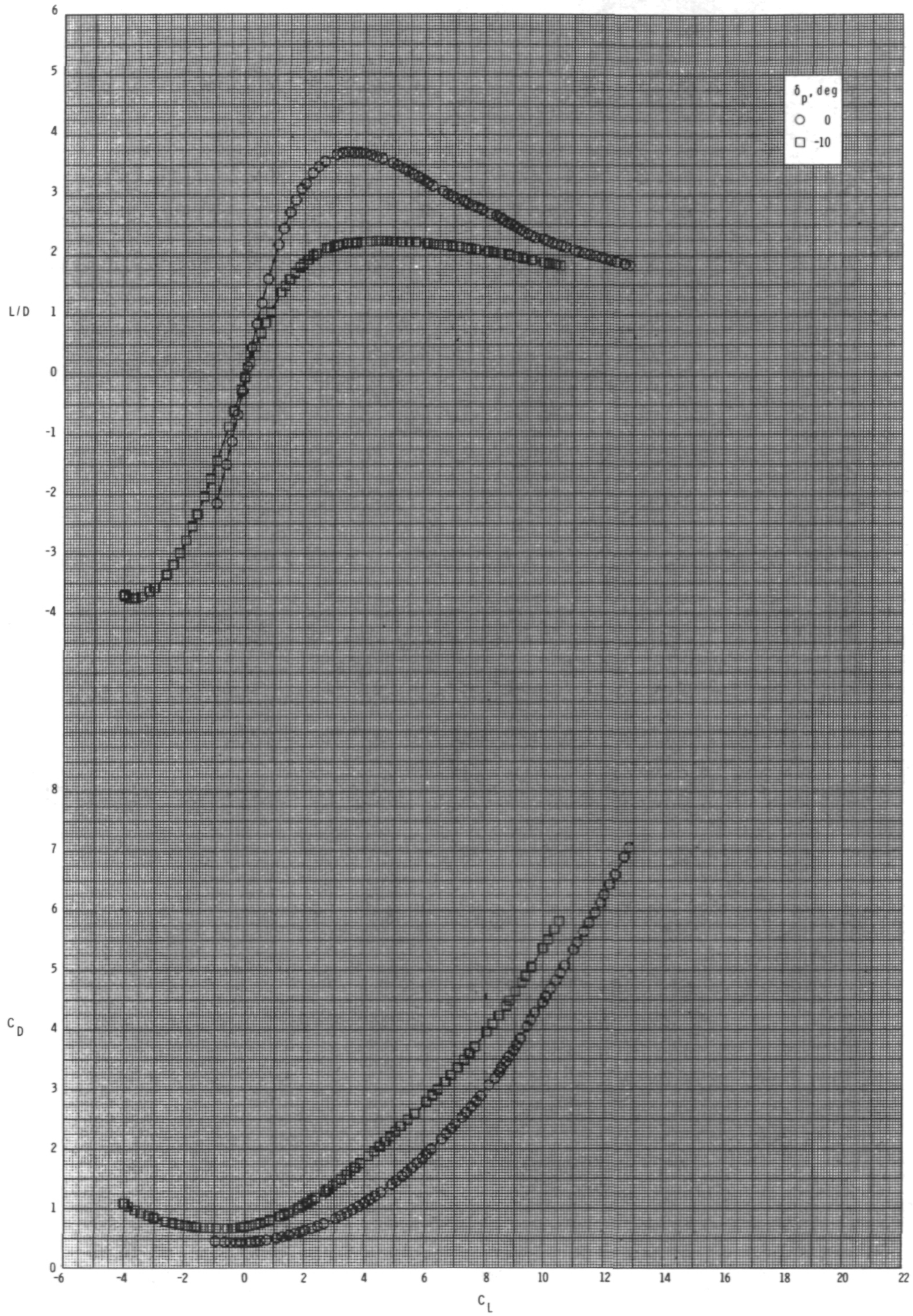

(b) Concluded.

Figure 33.- Continued.

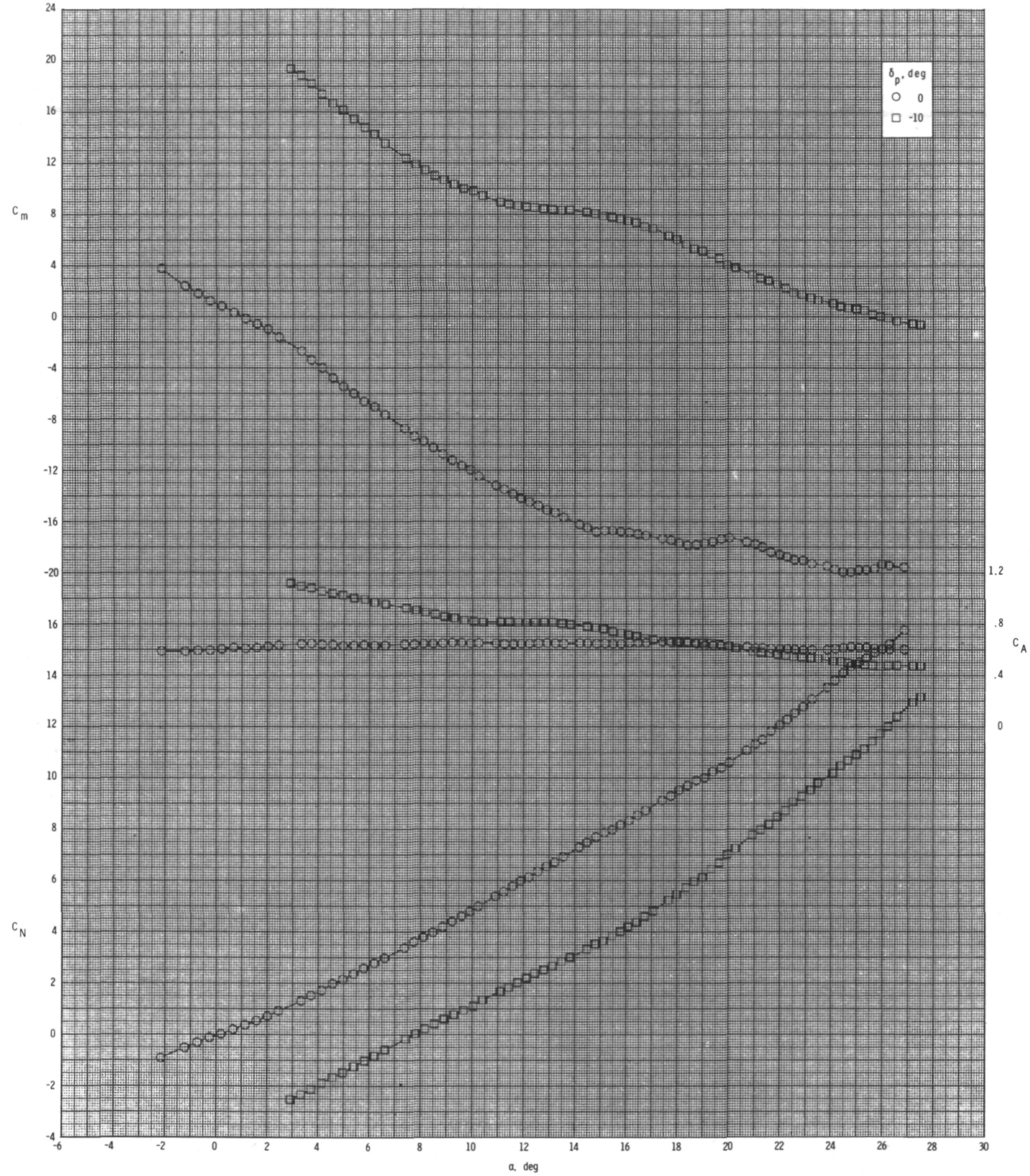

(c) M = 0.95.

Figure 33.- Continued.

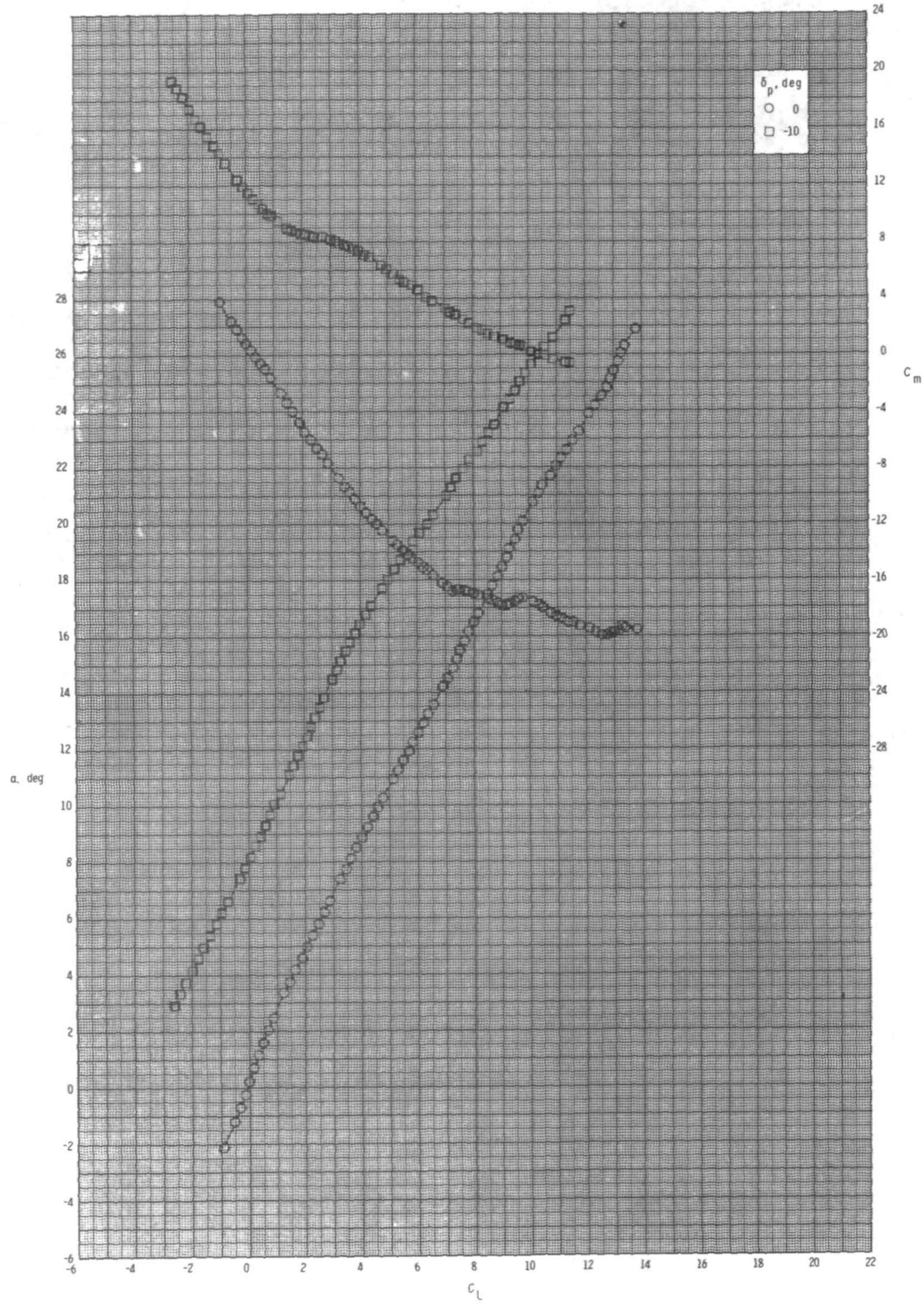

(c) Continued.

Figure 33.- Continued.

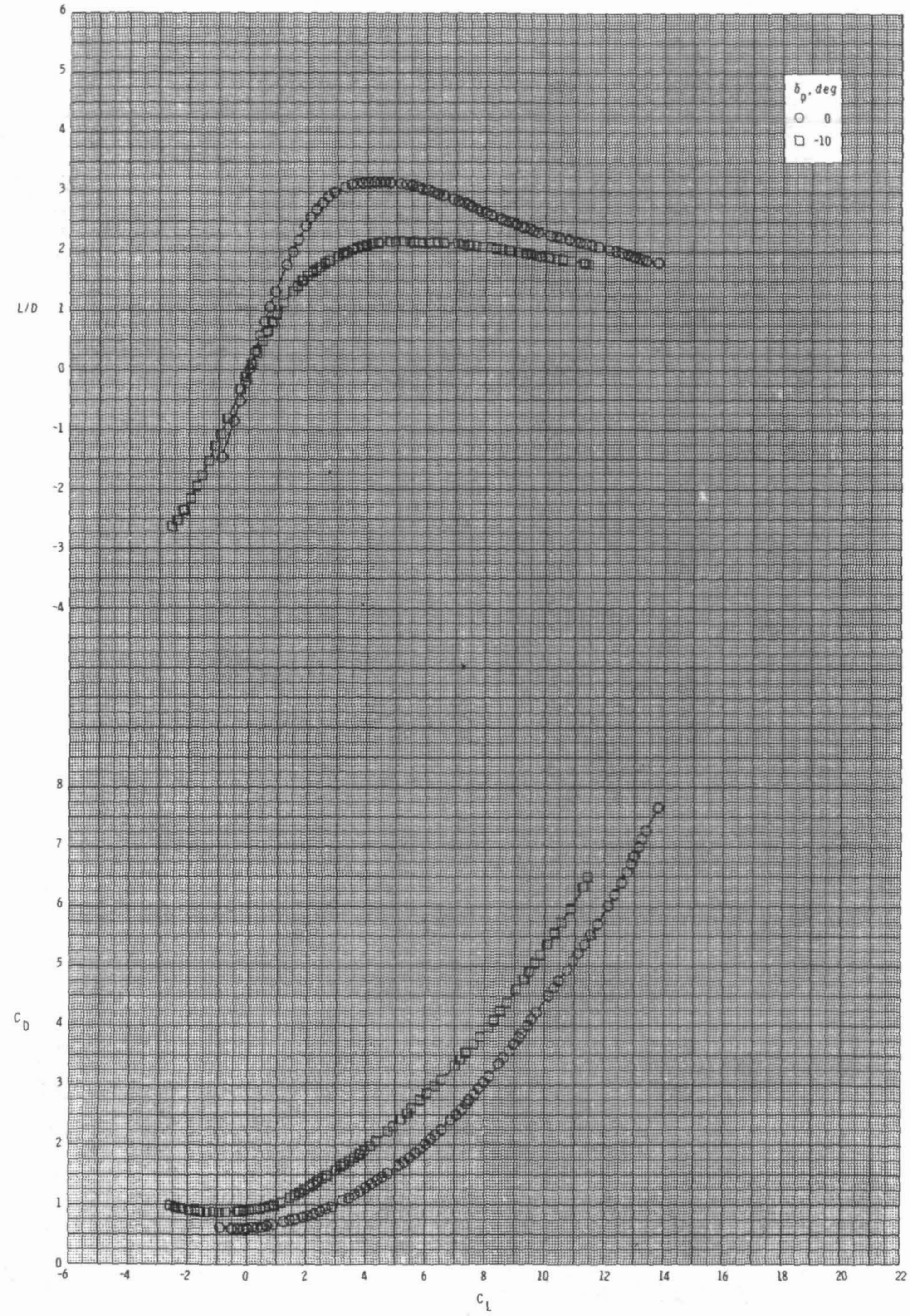

(c) Concluded.

Figure 33.- Concluded.

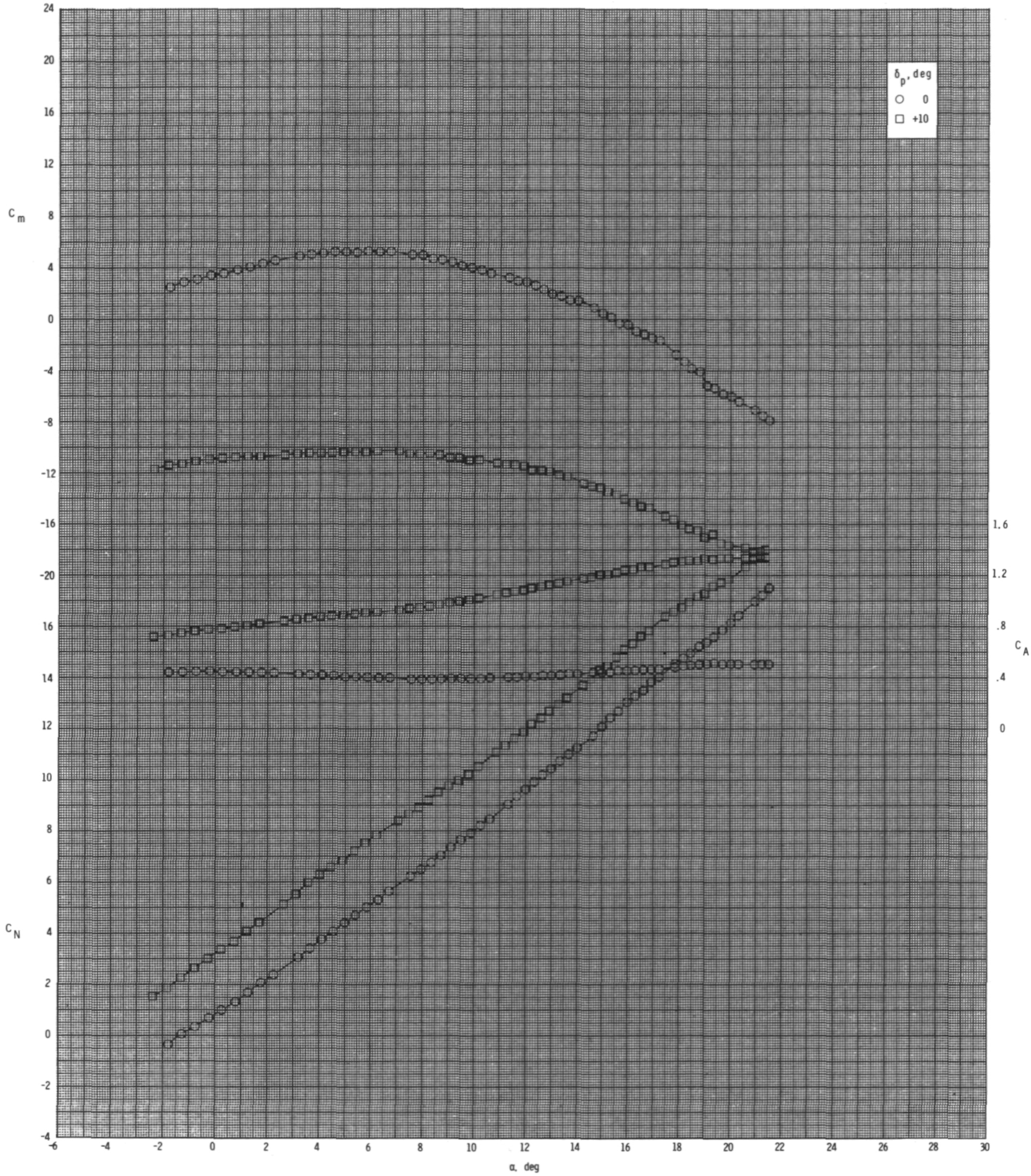

(a) M = 0.60.

Figure 34.- Pitch-control effectiveness for configuration $B_1I_{2c}W_1T_1$ with internal ducts closed and $\phi_I = 115°$.

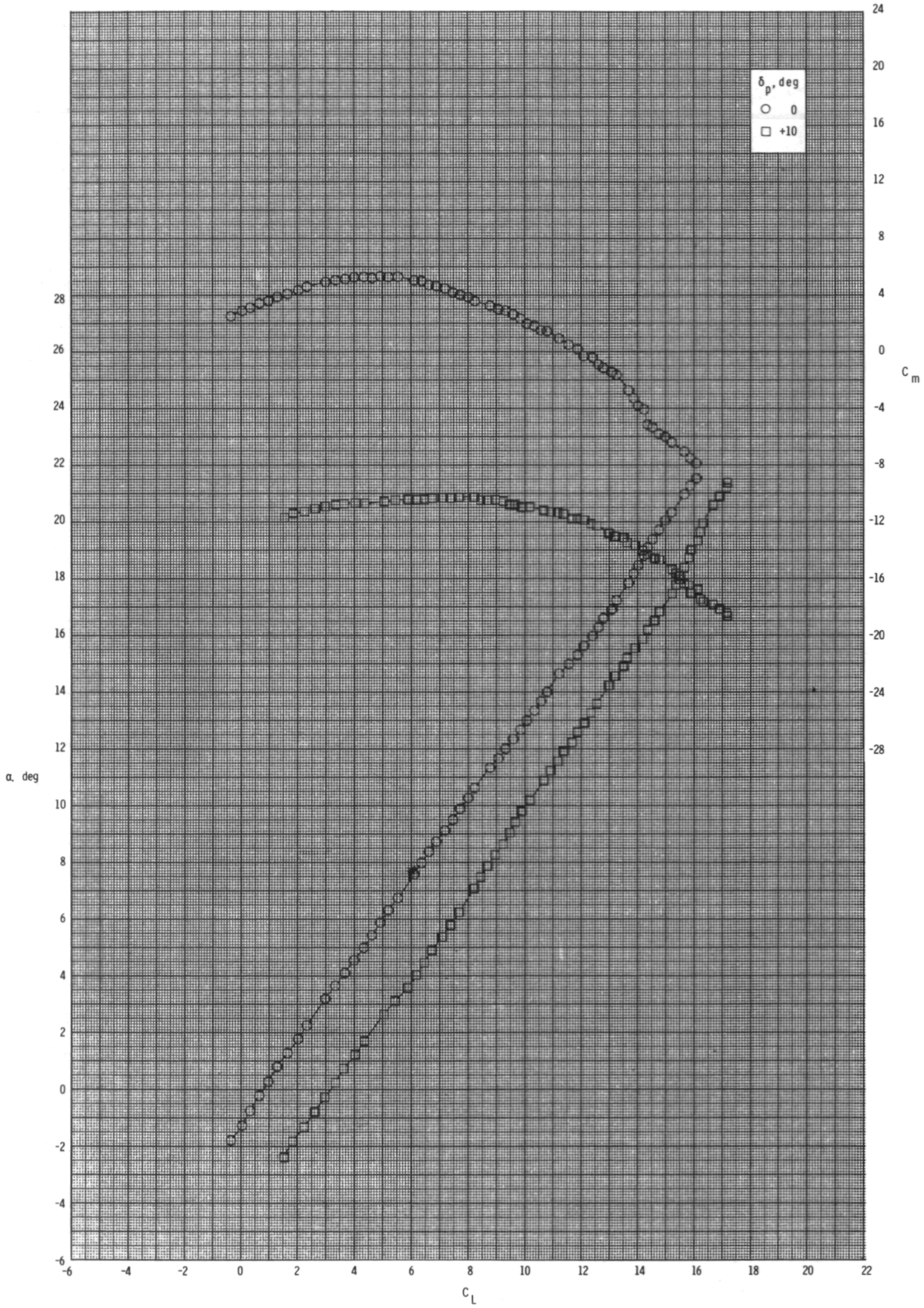

(a) Continued.

Figure 34.- Continued.

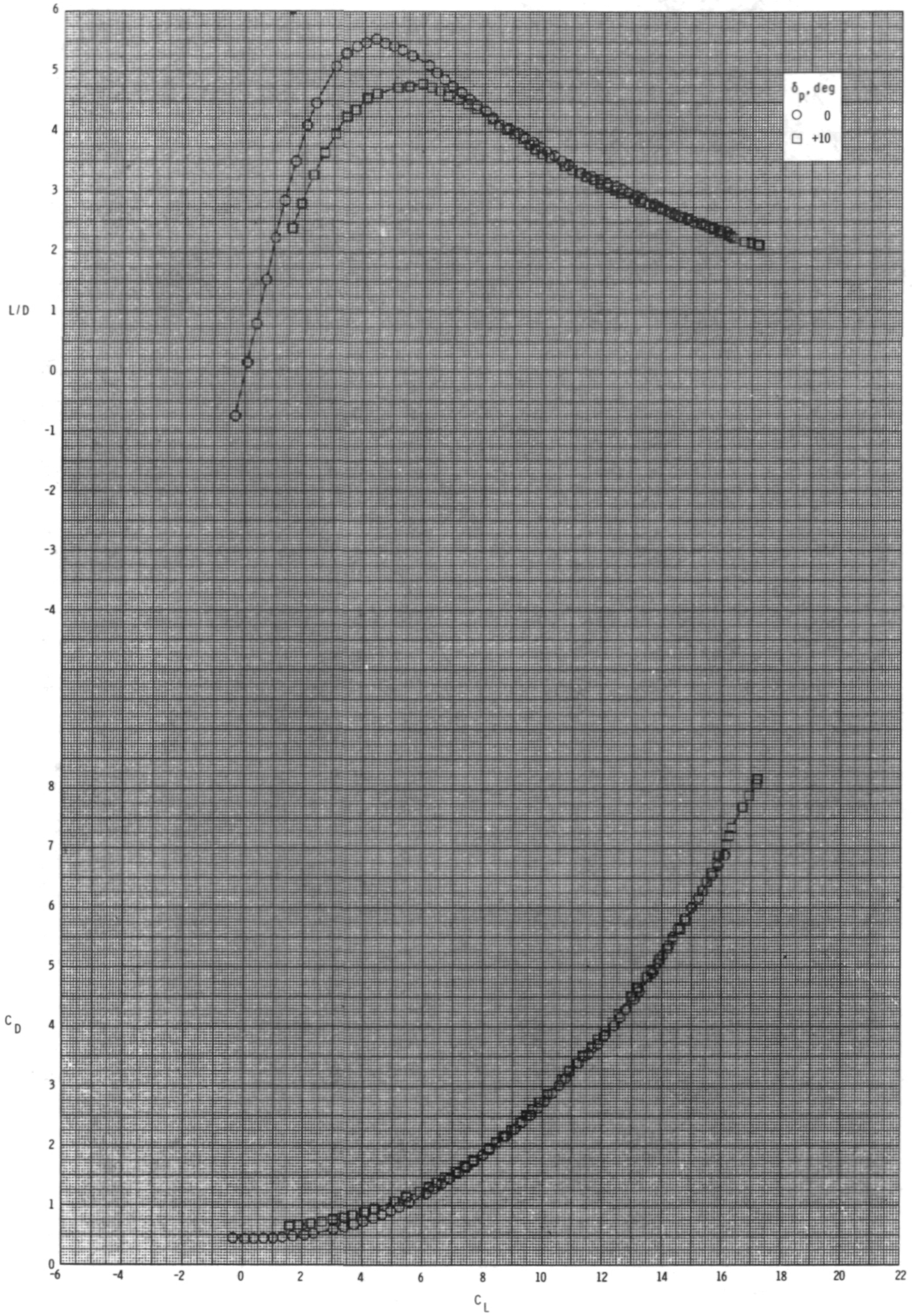

(a) Concluded.

Figure 34.- Continued.

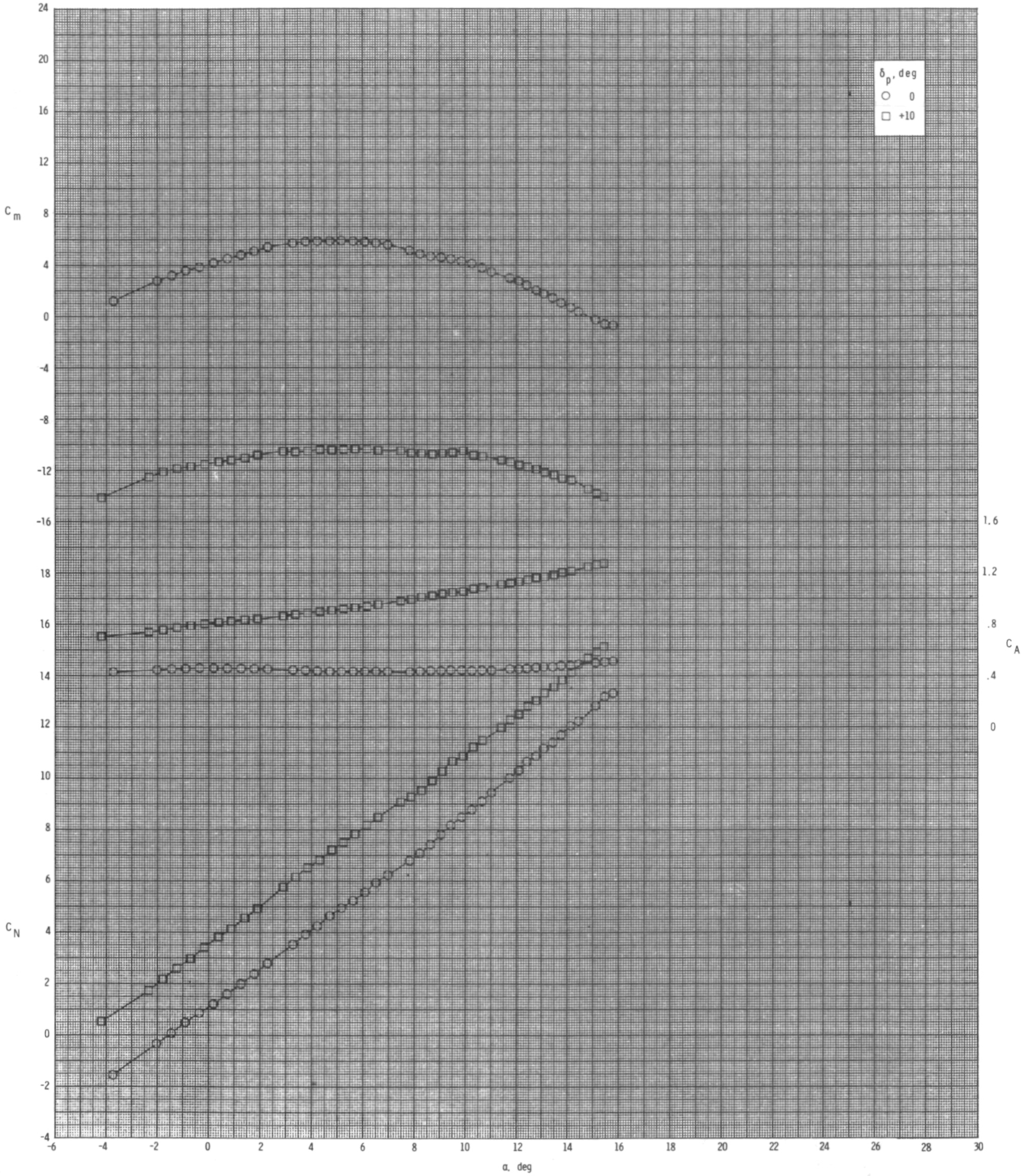

(b) M = 0.80.

Figure 34.- Continued.

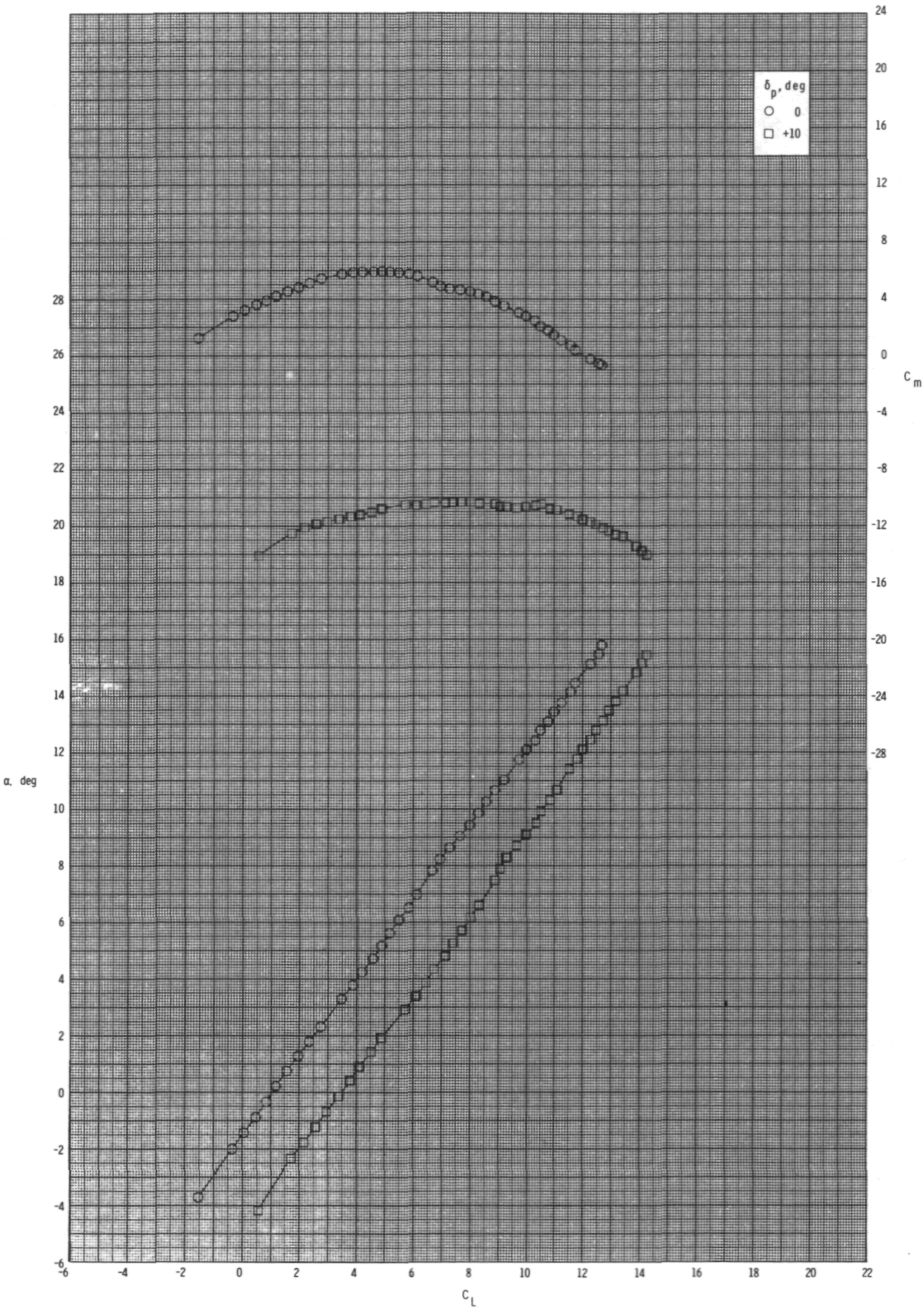

(b) Continued.

Figure 34.- Continued.

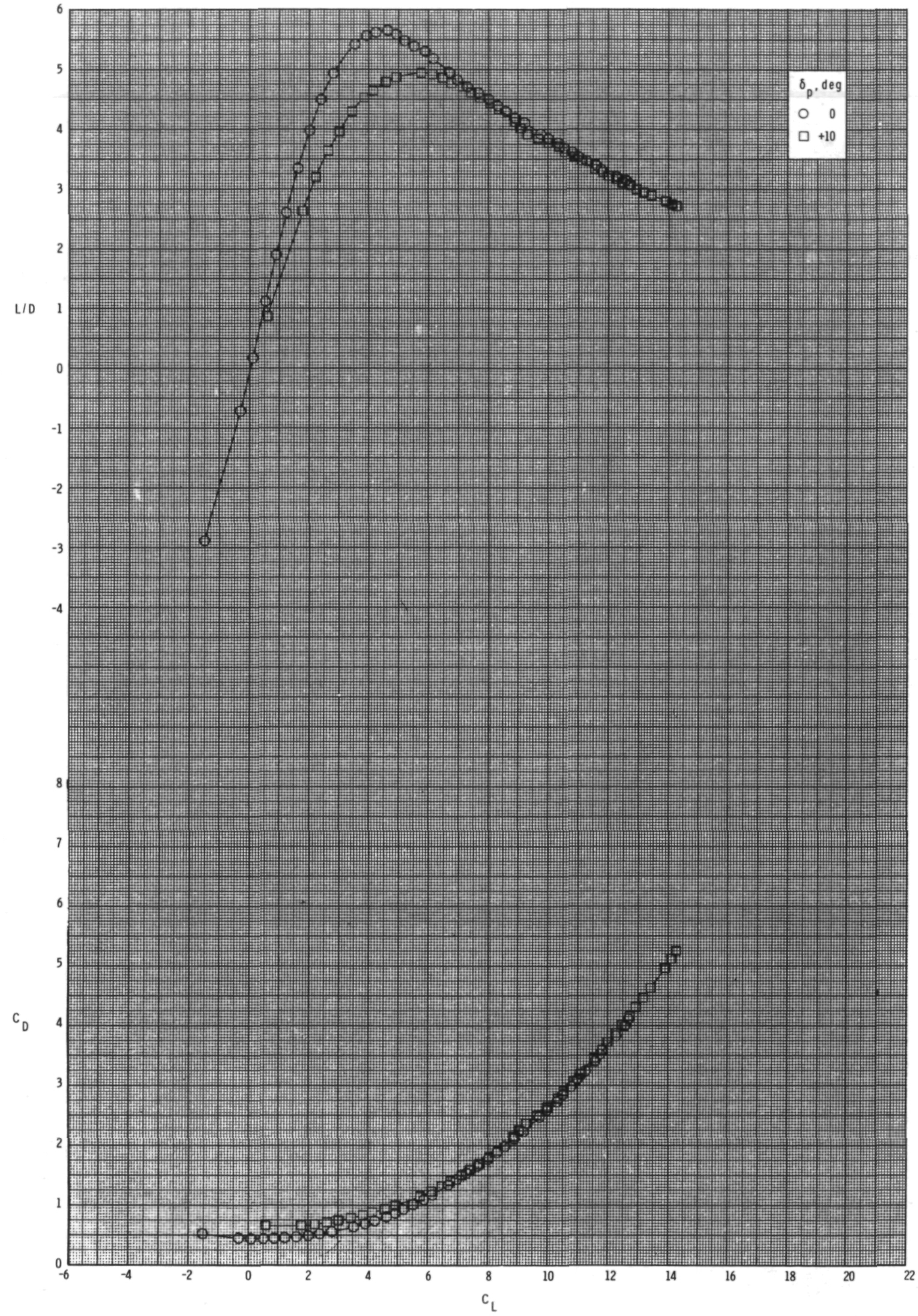

(b) Concluded.

Figure 34.- Continued.

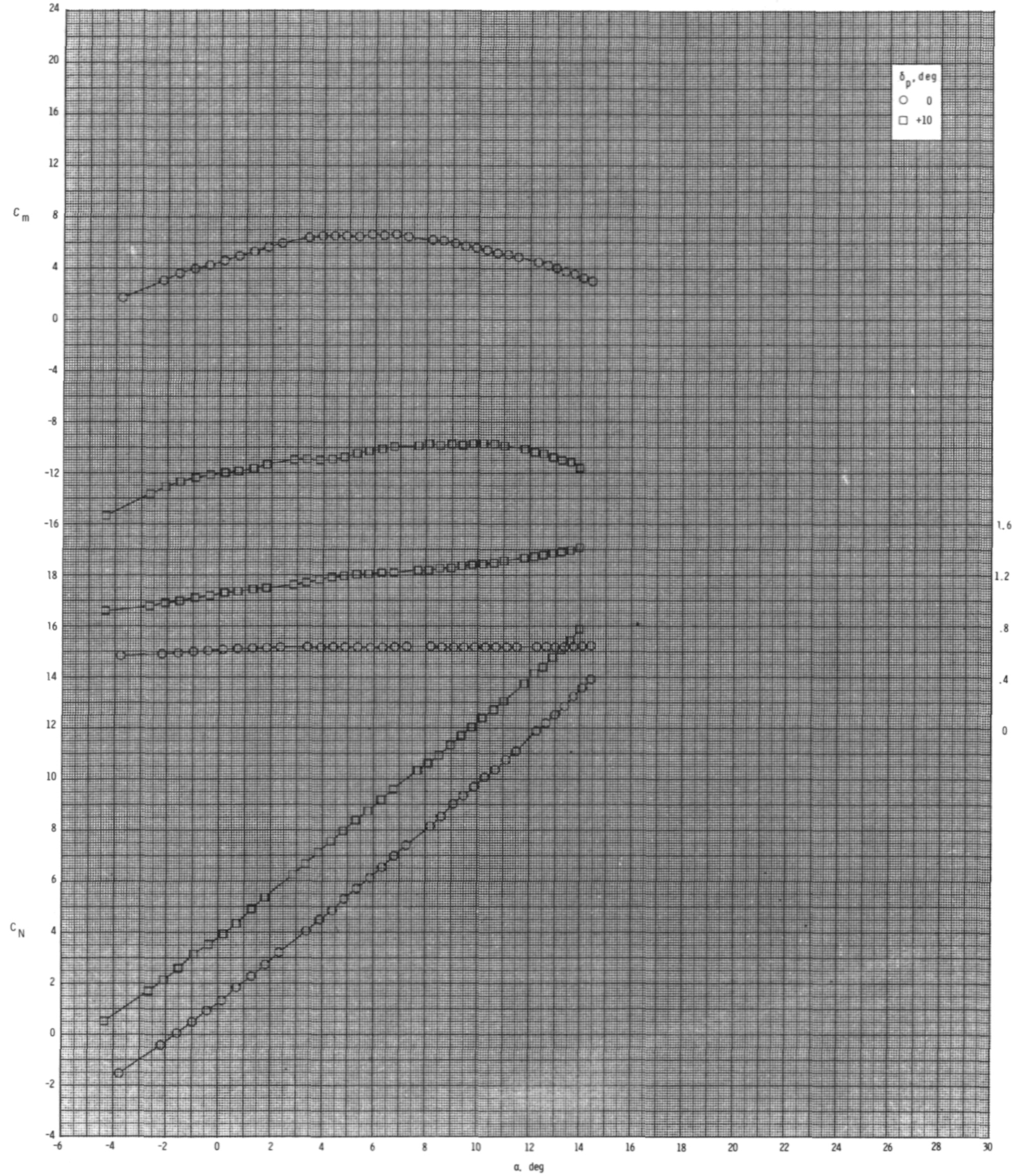

(c) M = 0.95.

Figure 34.- Continued.

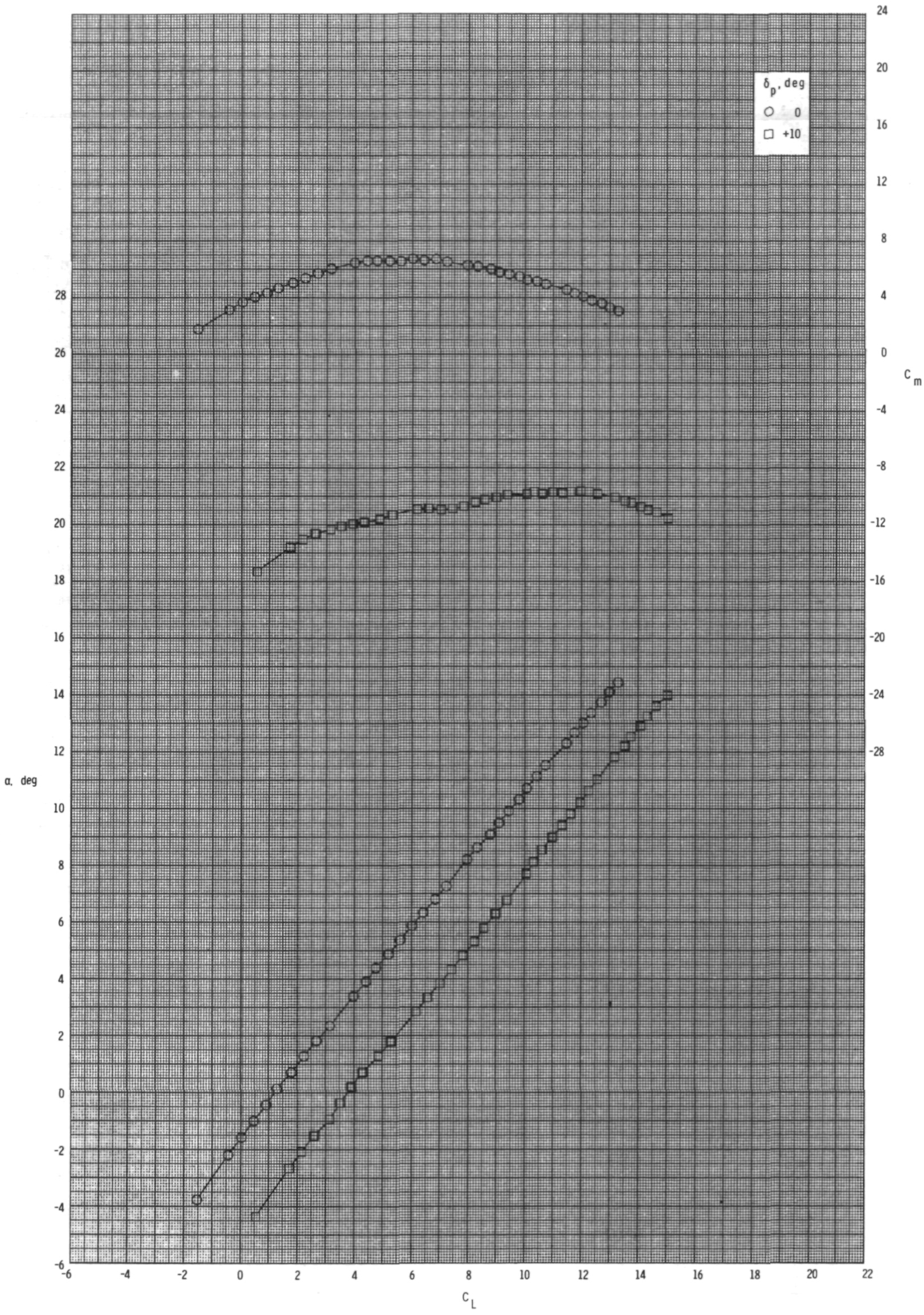

(c) Continued.

Figure 34.- Continued.

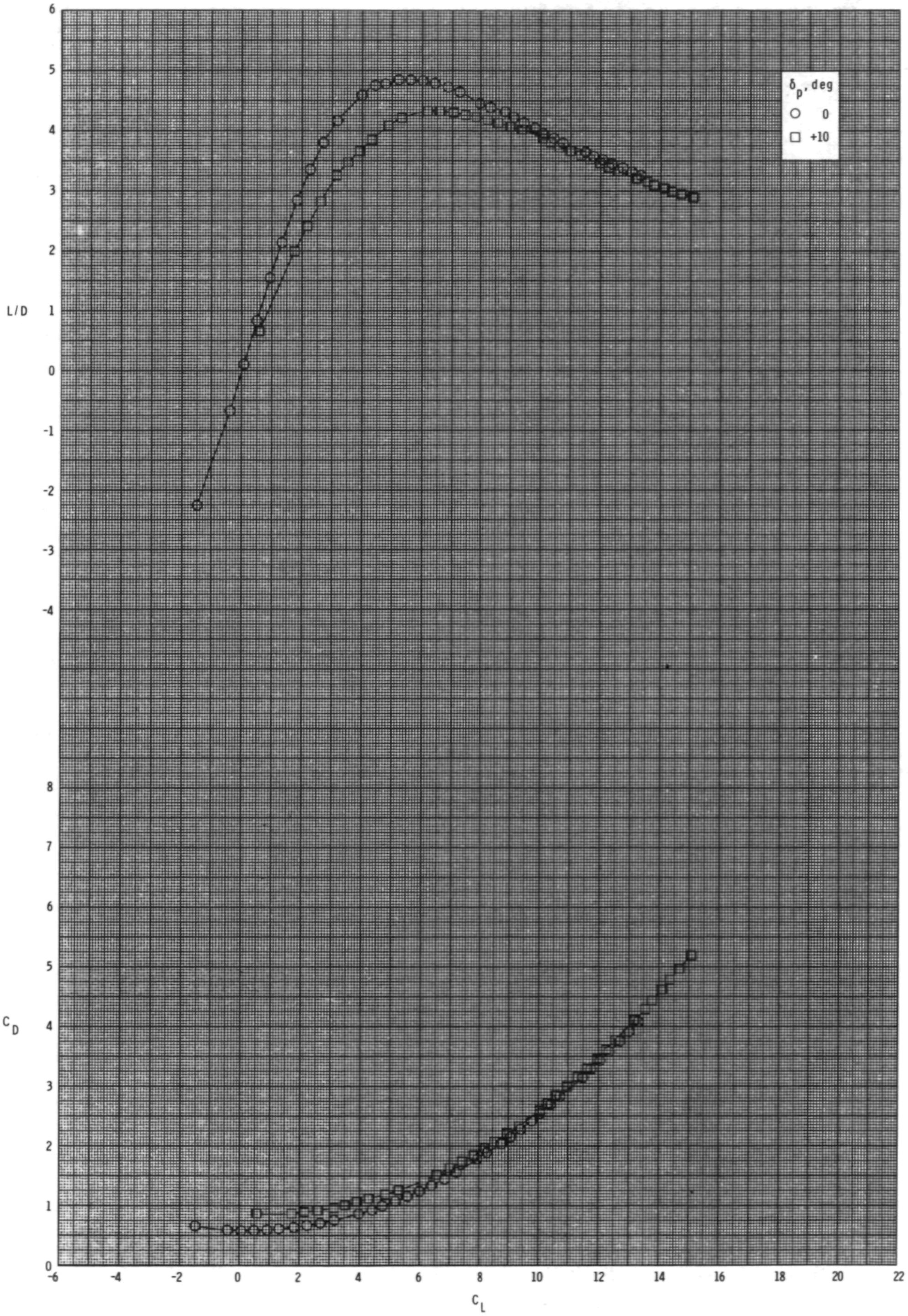

(c) Concluded.

Figure 34.- Concluded.

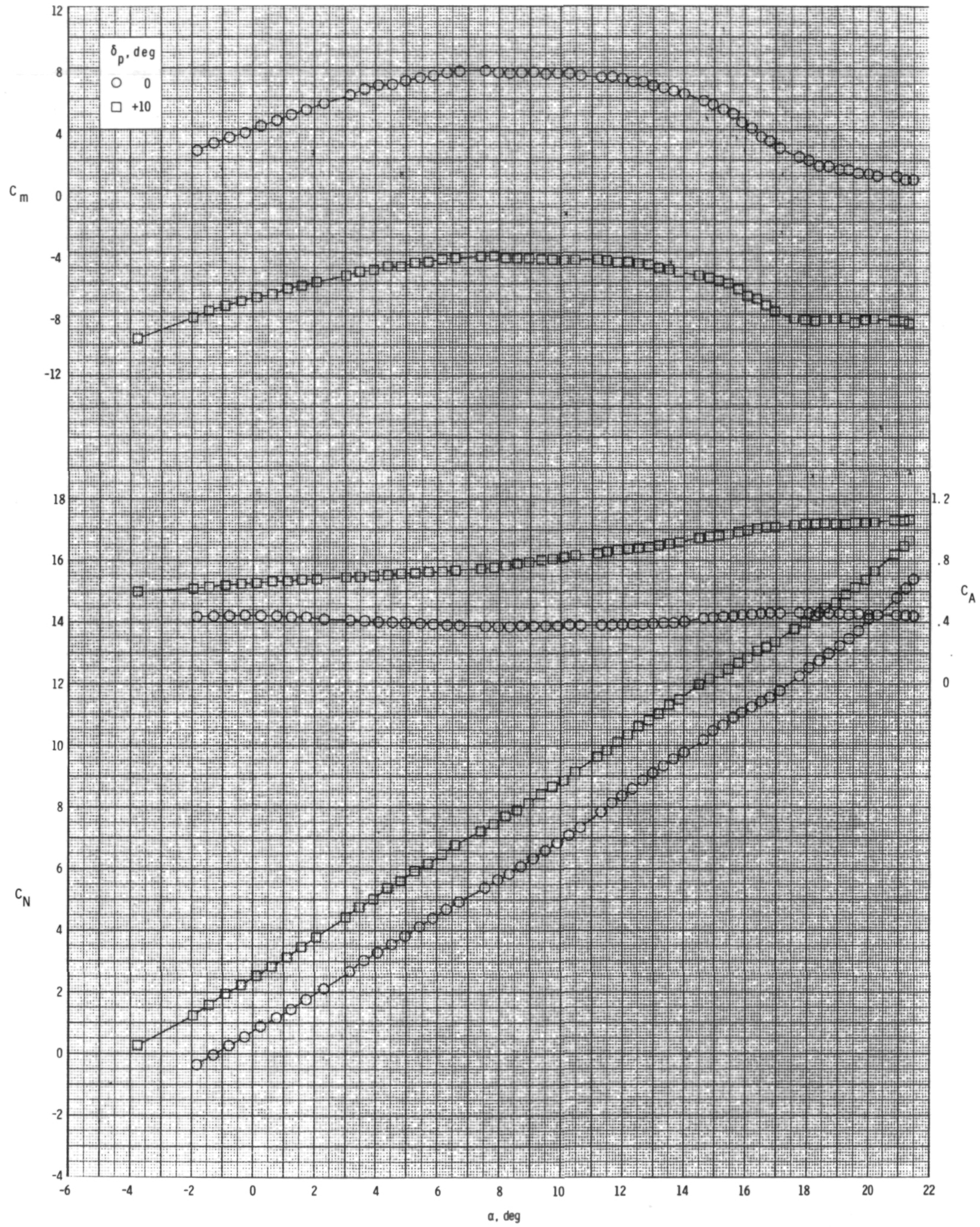

(a) M = 0.60.

Figure 35.- Pitch-control effectiveness for configuration $B_1 I_{2c} W_1 T_1$ with internal ducts closed and $\phi_I = 135°$.

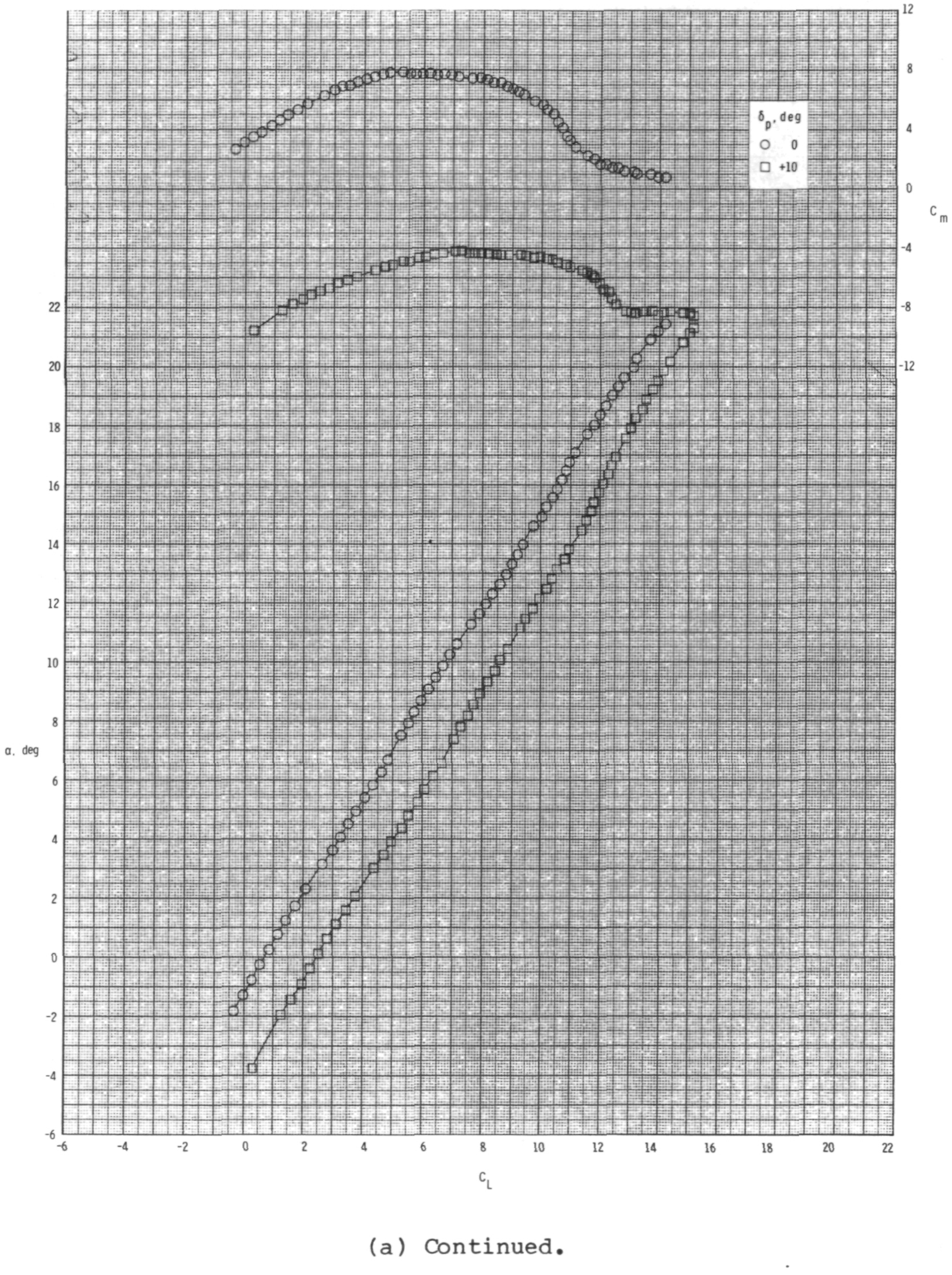

(a) Continued.

Figure 35.- Continued.

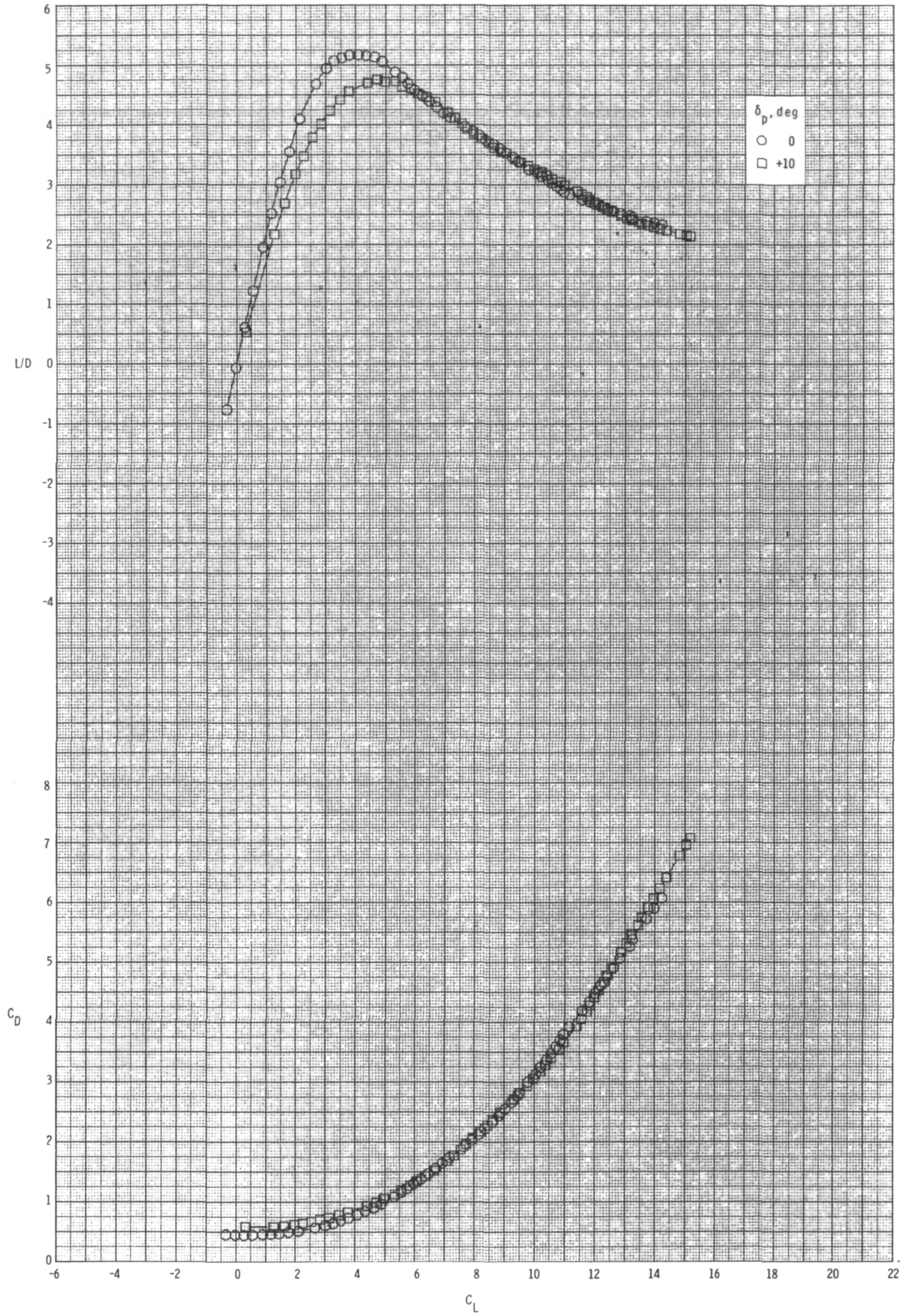

(a) Concluded.

Figure 35.- Continued.

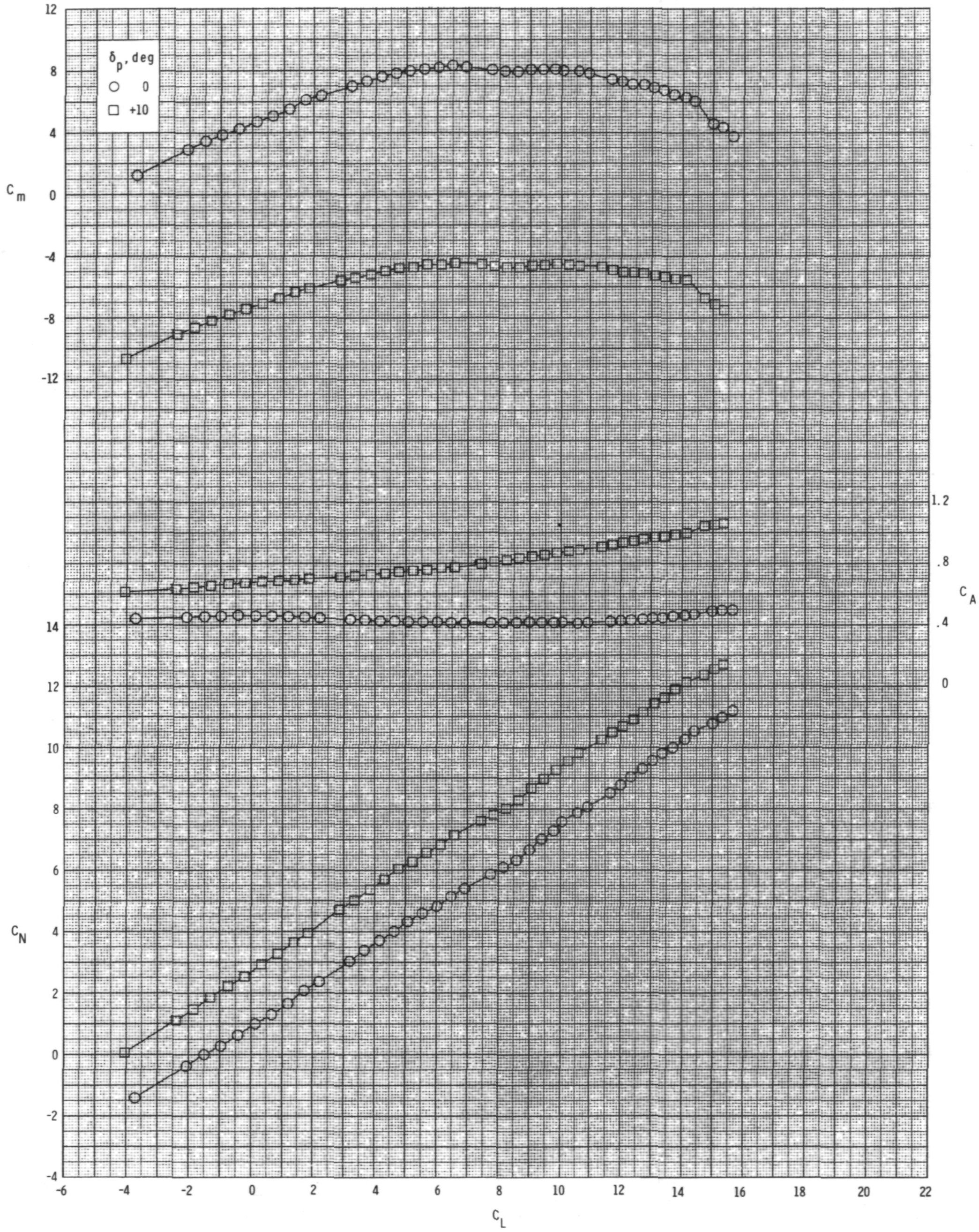

(b) M = 0.80.

Figure 35.- Continued.

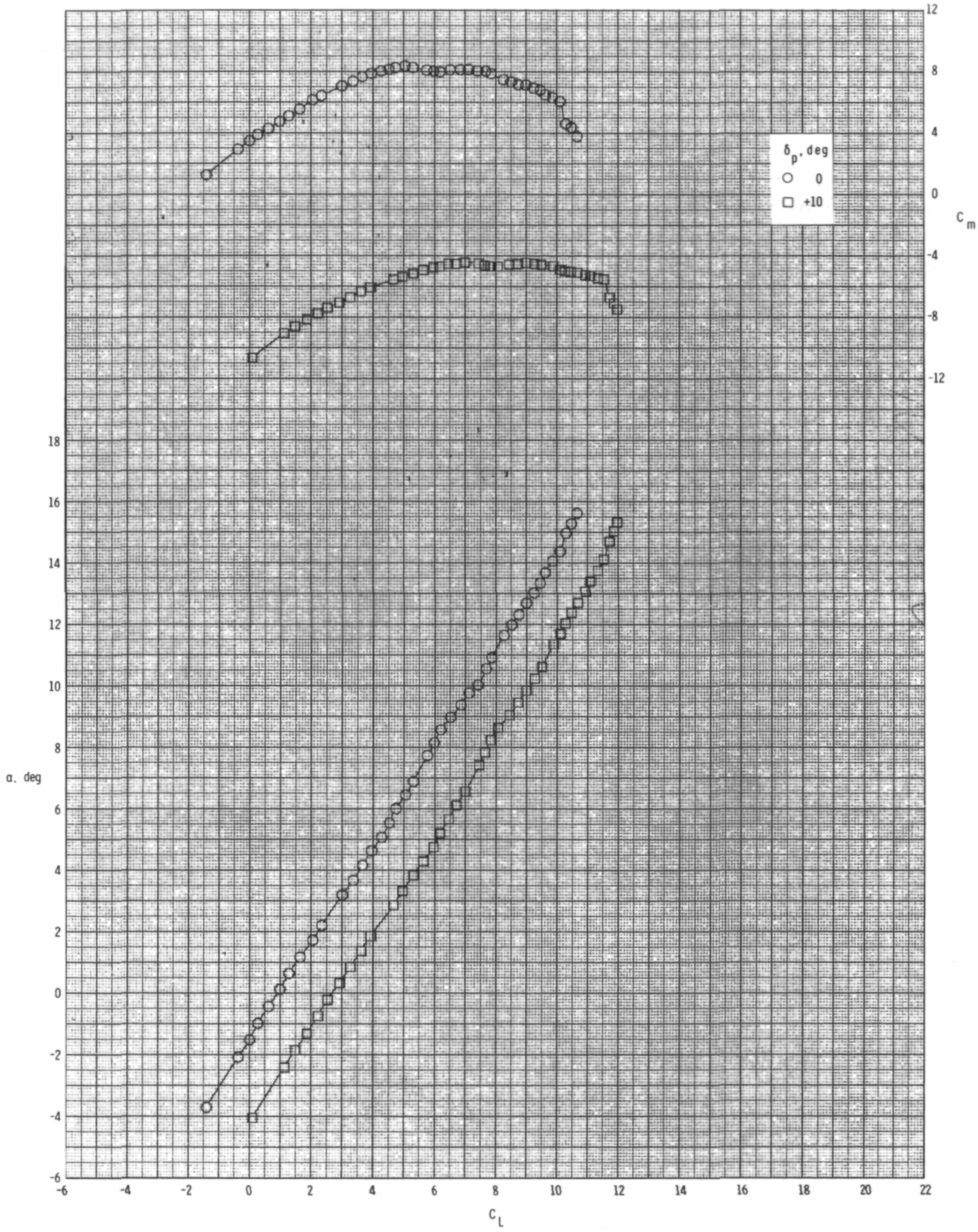

(b) Continued.

Figure 35.- Continued.

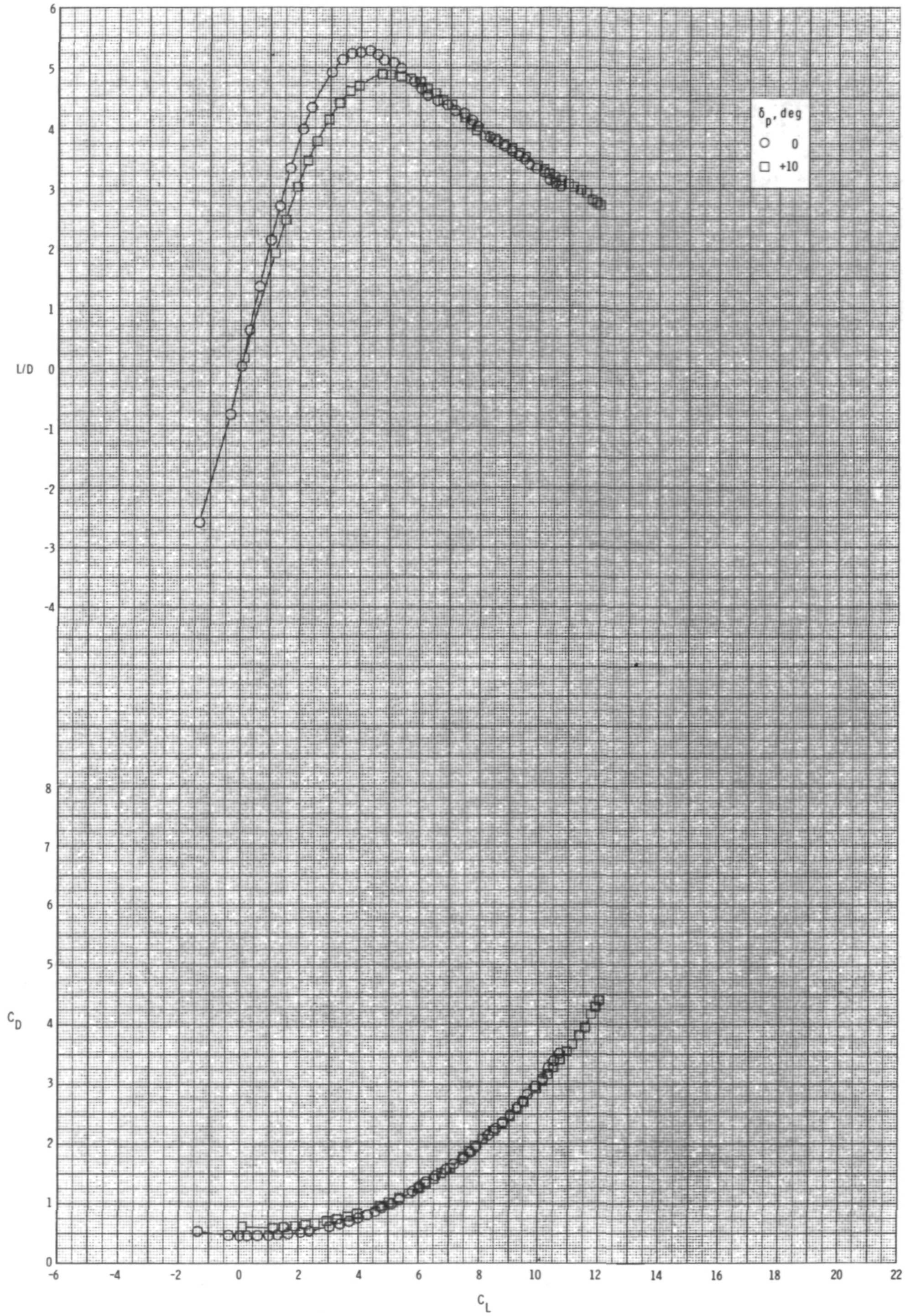

(b) Concluded.

Figure 35.- Continued.

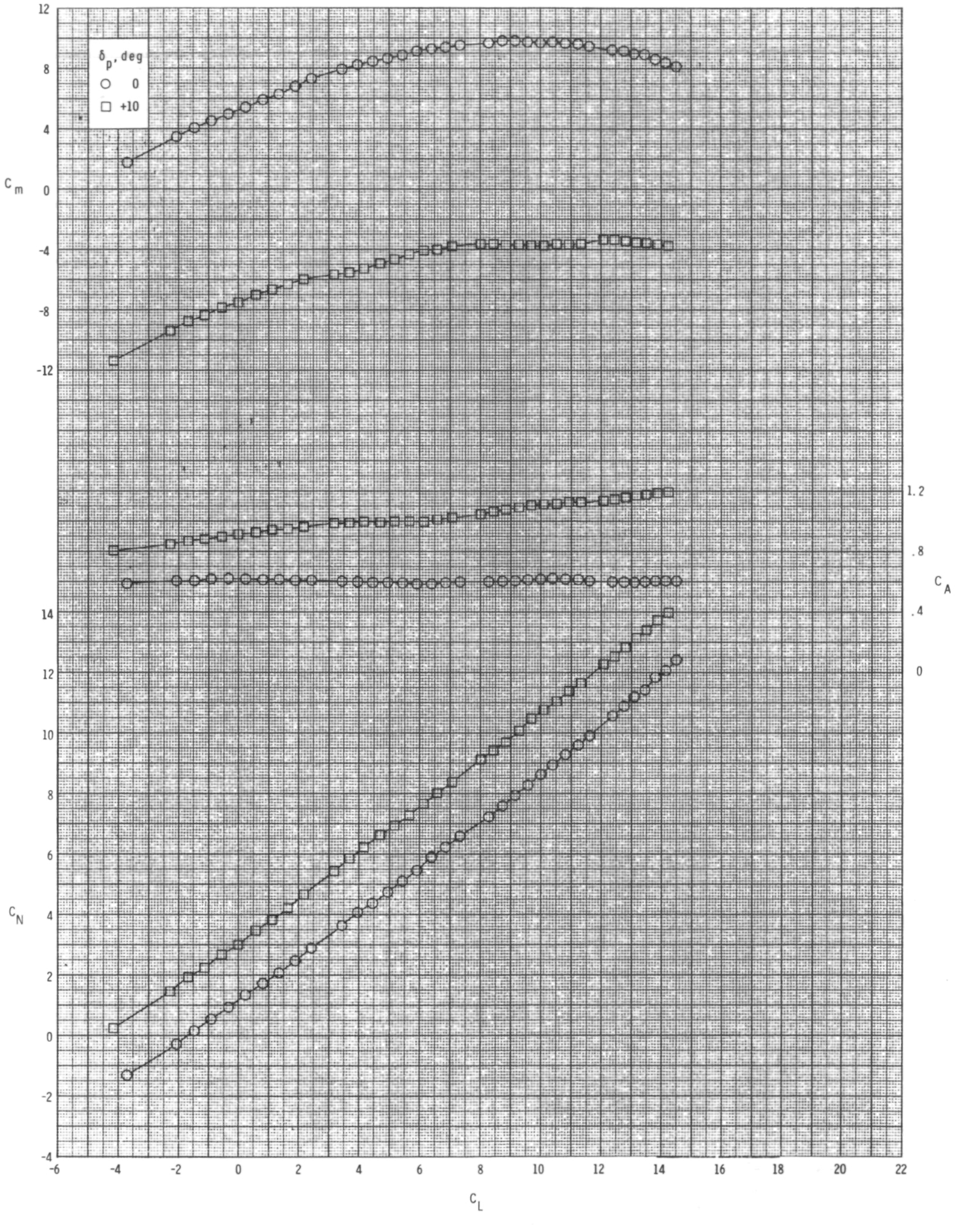

(c) M = 0.95.

Figure 35.- Continued.

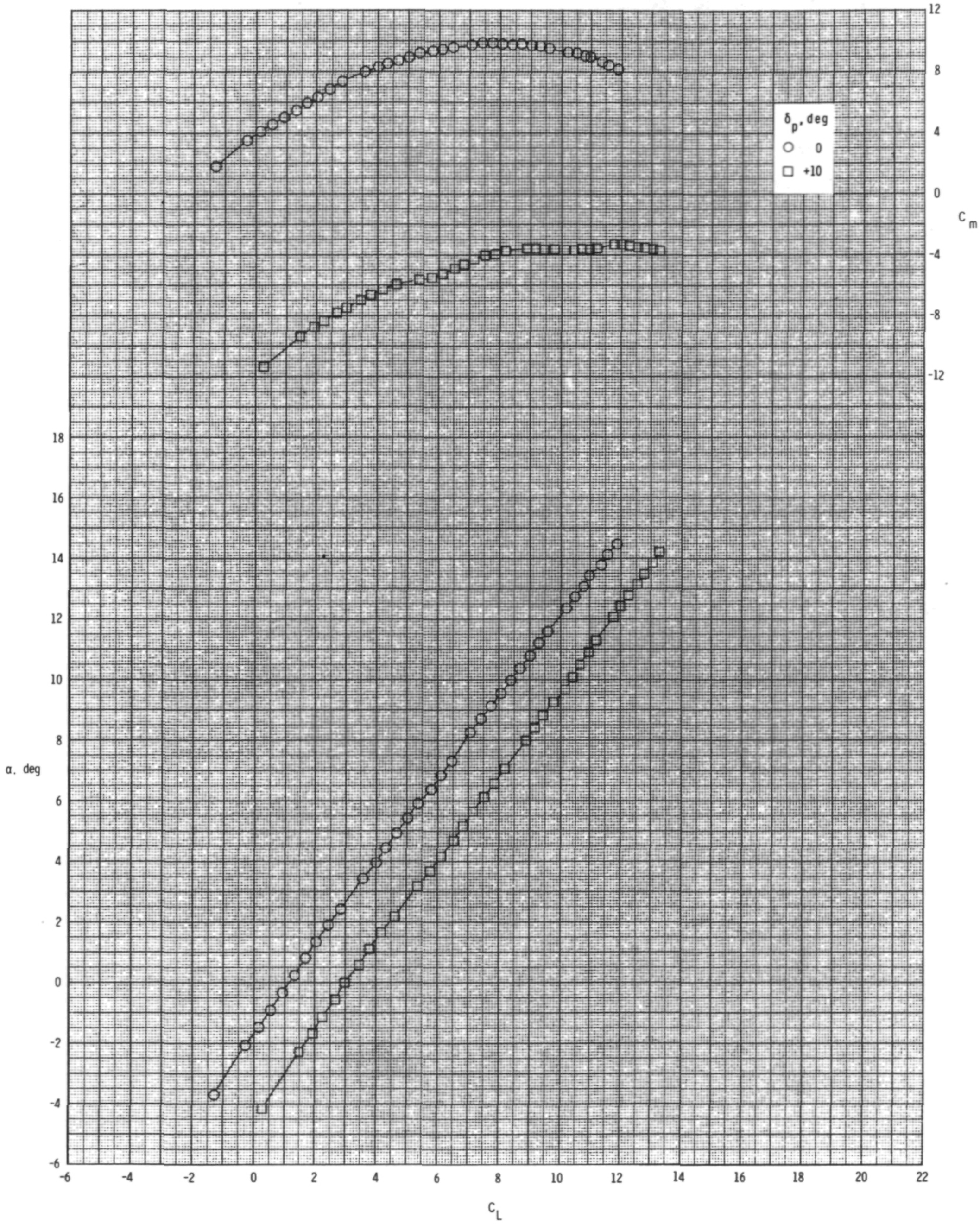

(c) Continued.

Figure 35.- Continued.

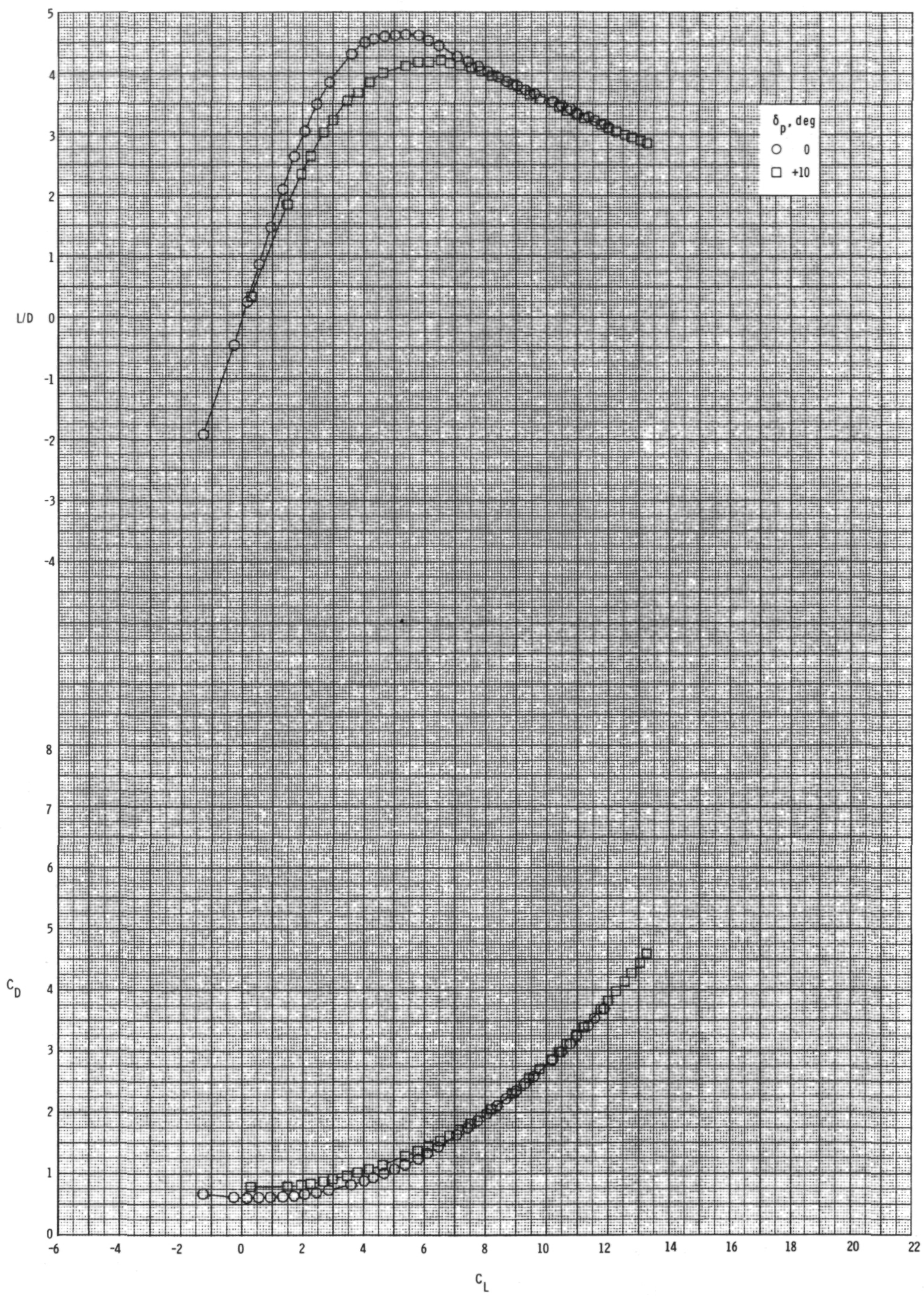

(c) Concluded.

Figure 35.- Concluded.

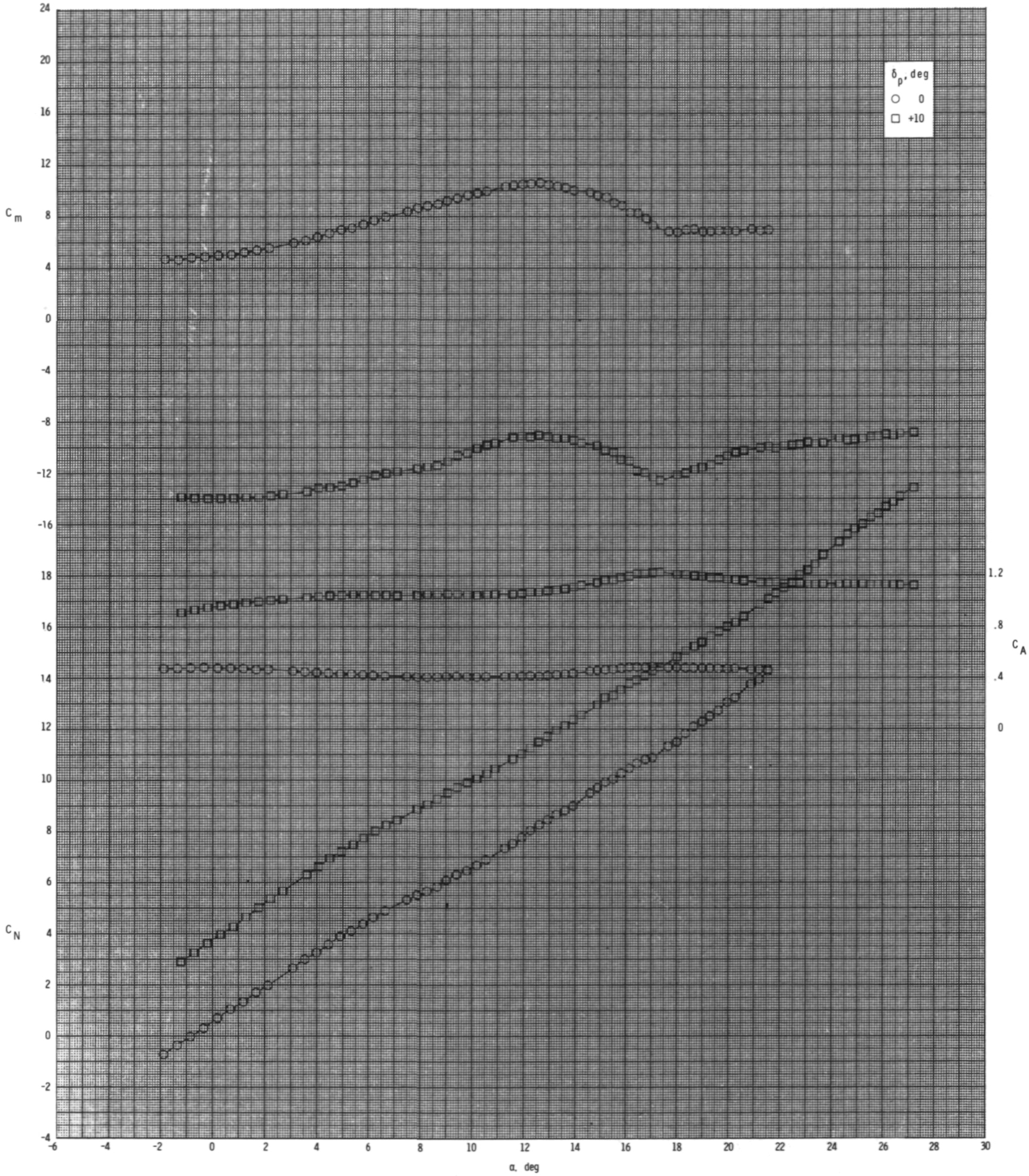

(a) M = 0.60.

Figure 36.- Pitch-control effectiveness for configuration $B_1I_{2c}W_1T_2$ with internal ducts closed and ϕ_I = 135°.

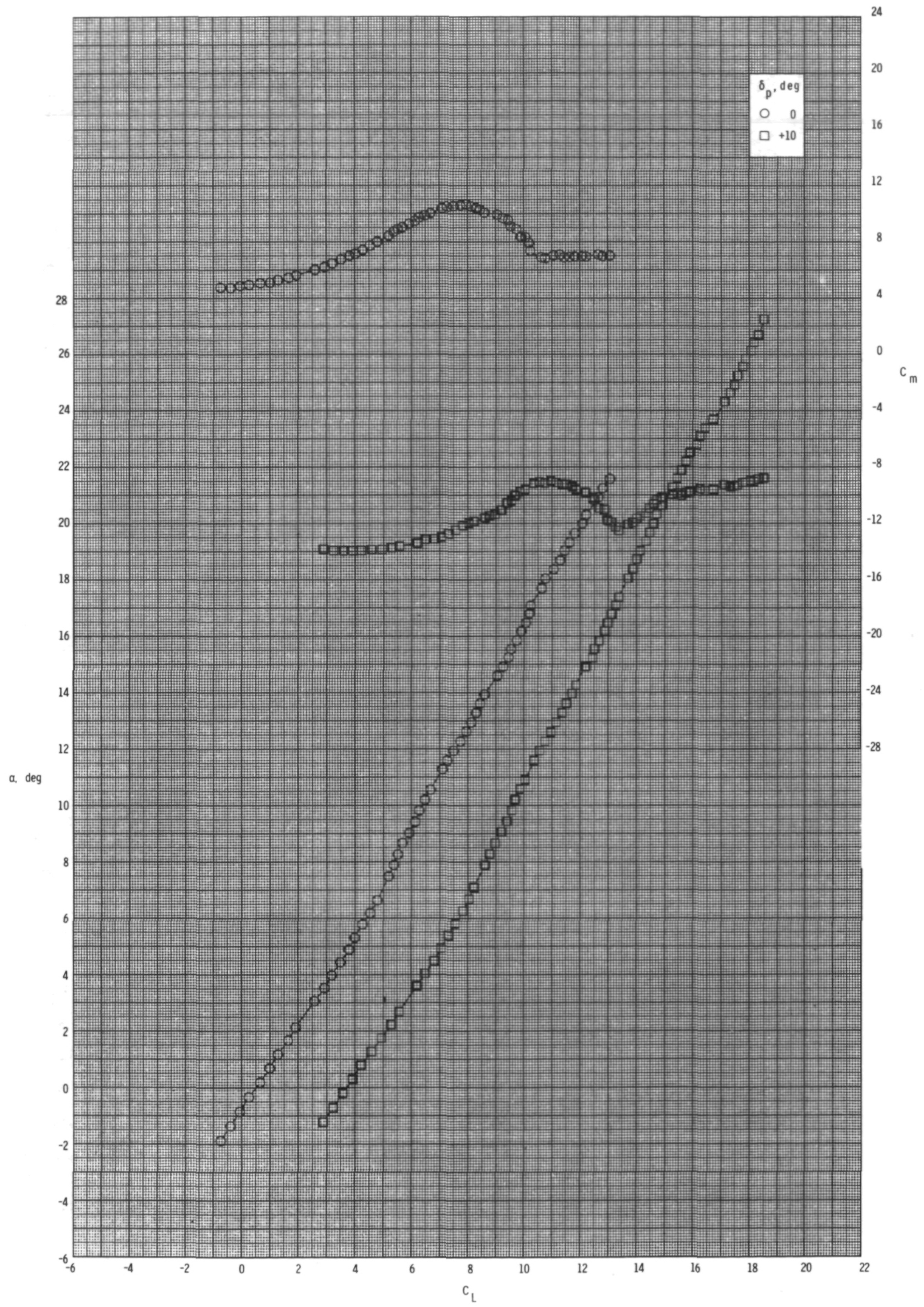

(a) Continued.

Figure 36.- Continued.

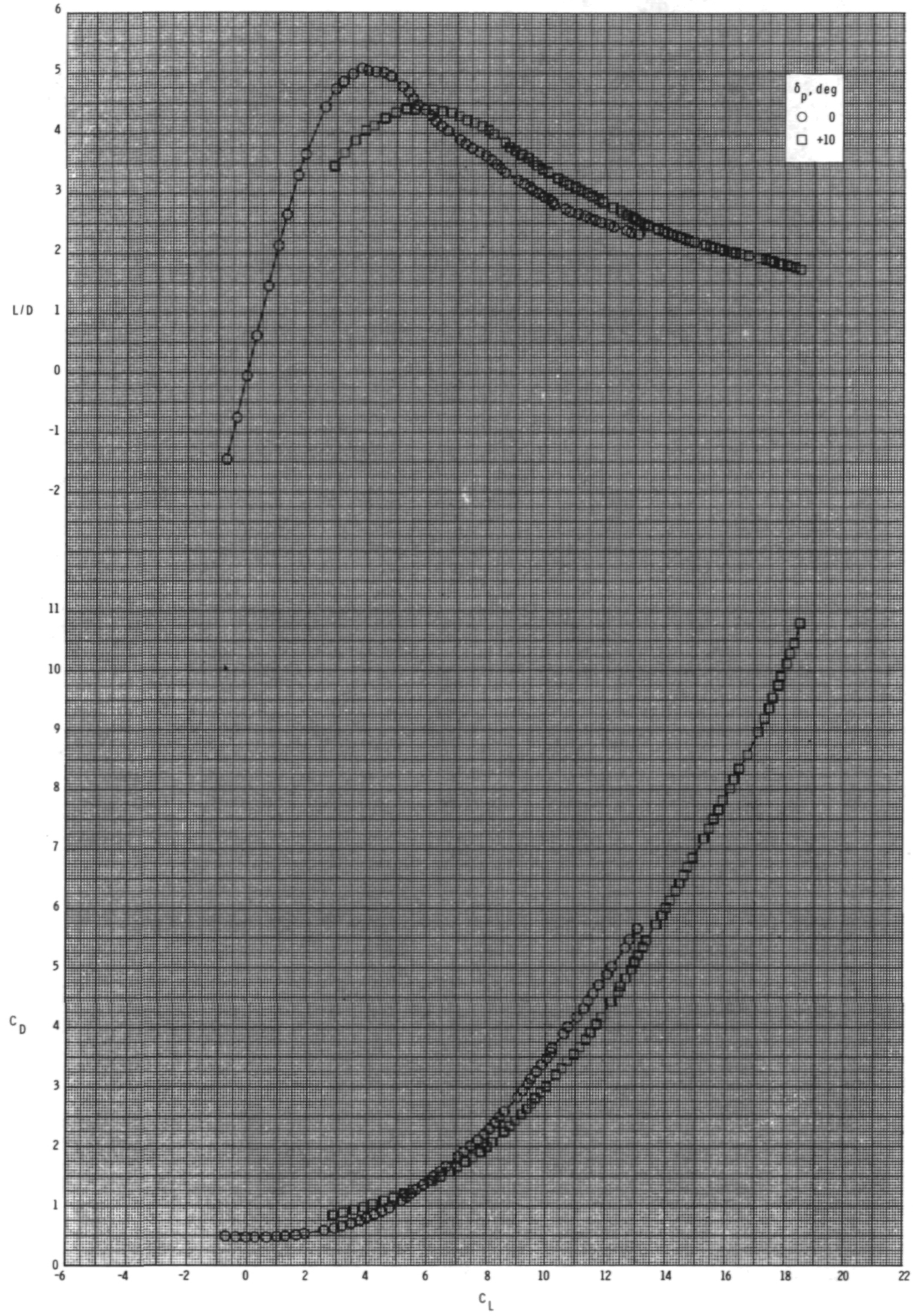

(a) Concluded.

Figure 36.- Continued.

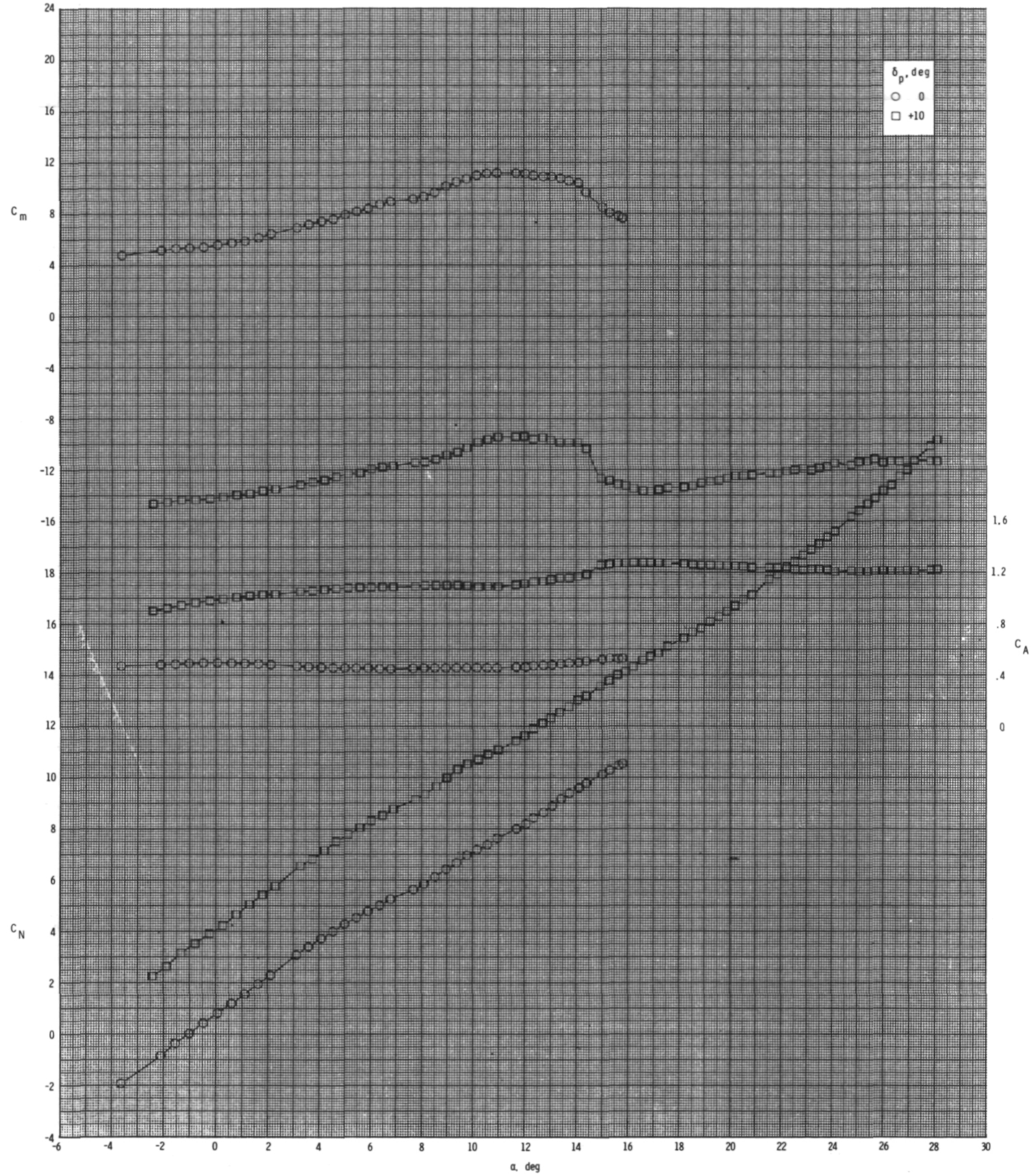

(b) M = 0.80.

Figure 36.- Continued.

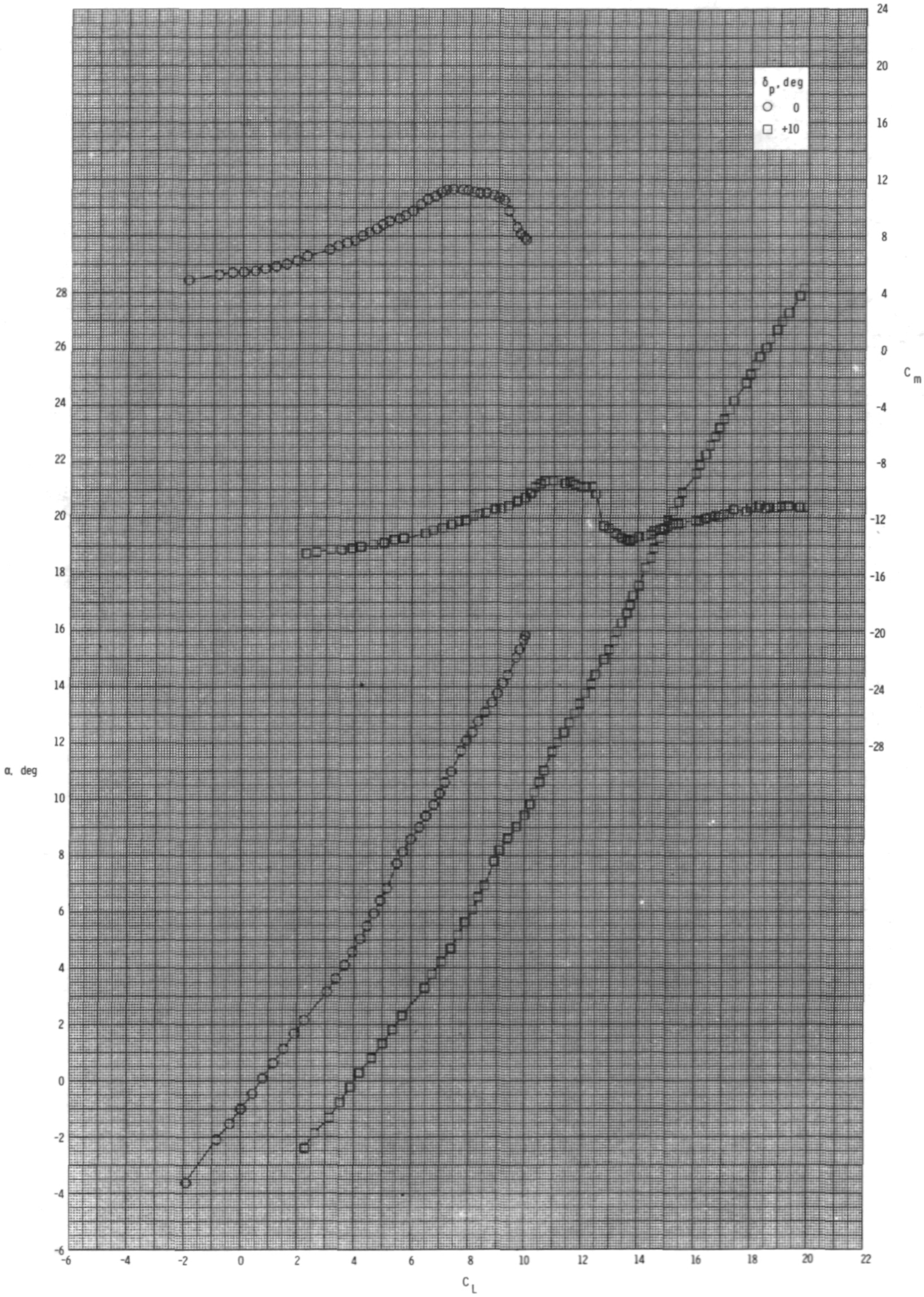

(b) Continued.

Figure 36.- Continued.

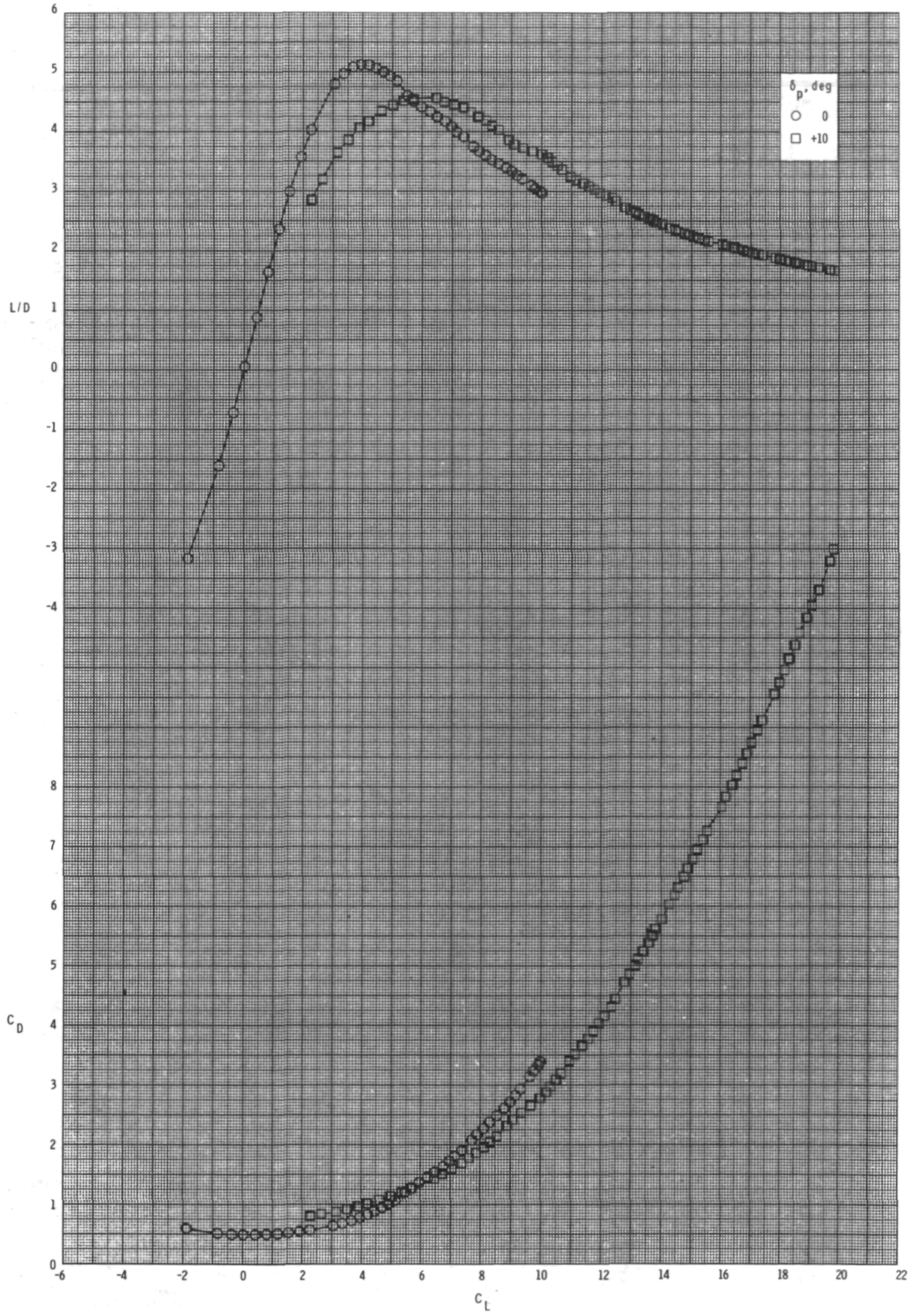

(b) Concluded.

Figure 36.- Continued.

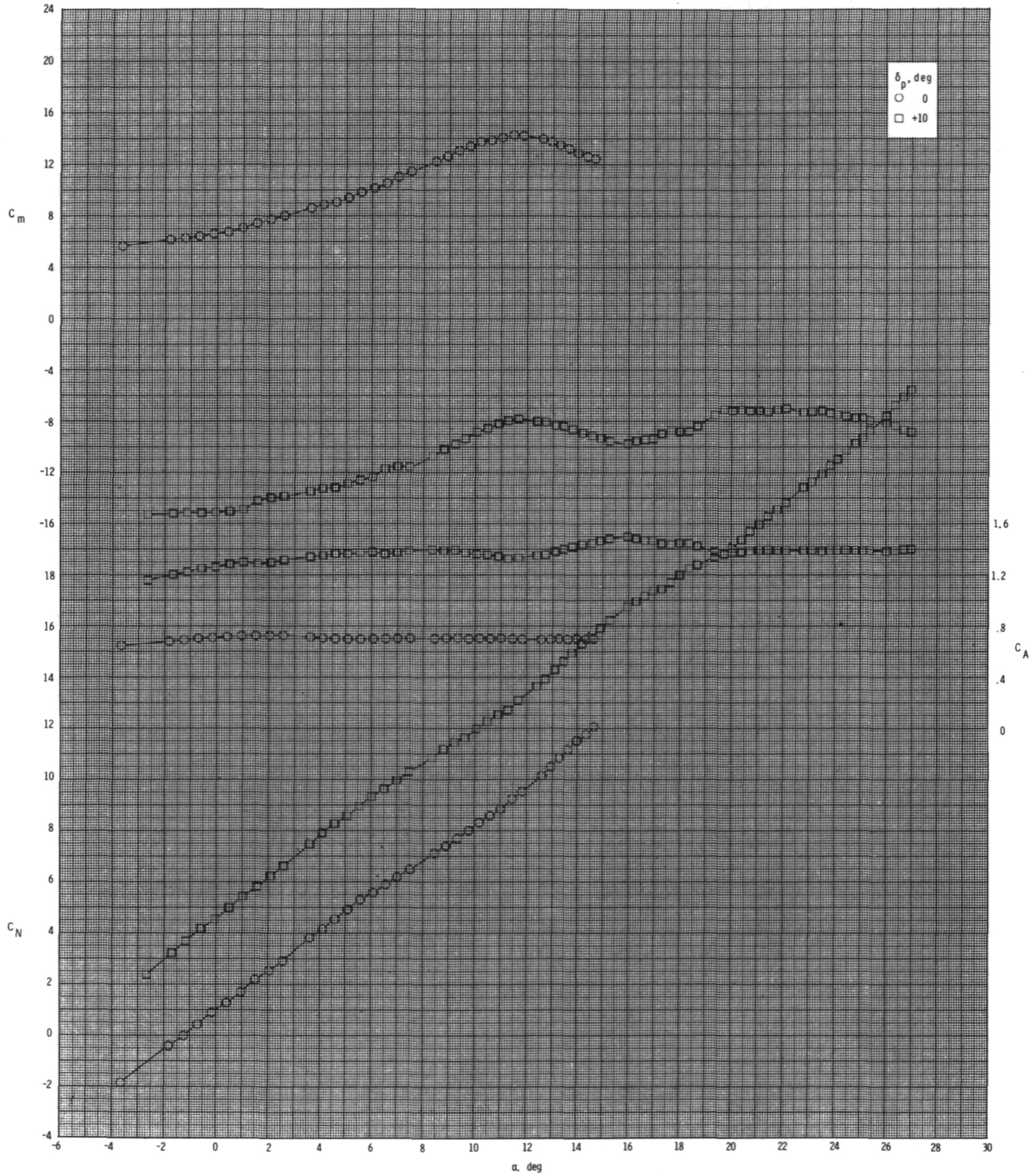

(c) M = 0.95.

Figure 36.- Continued.

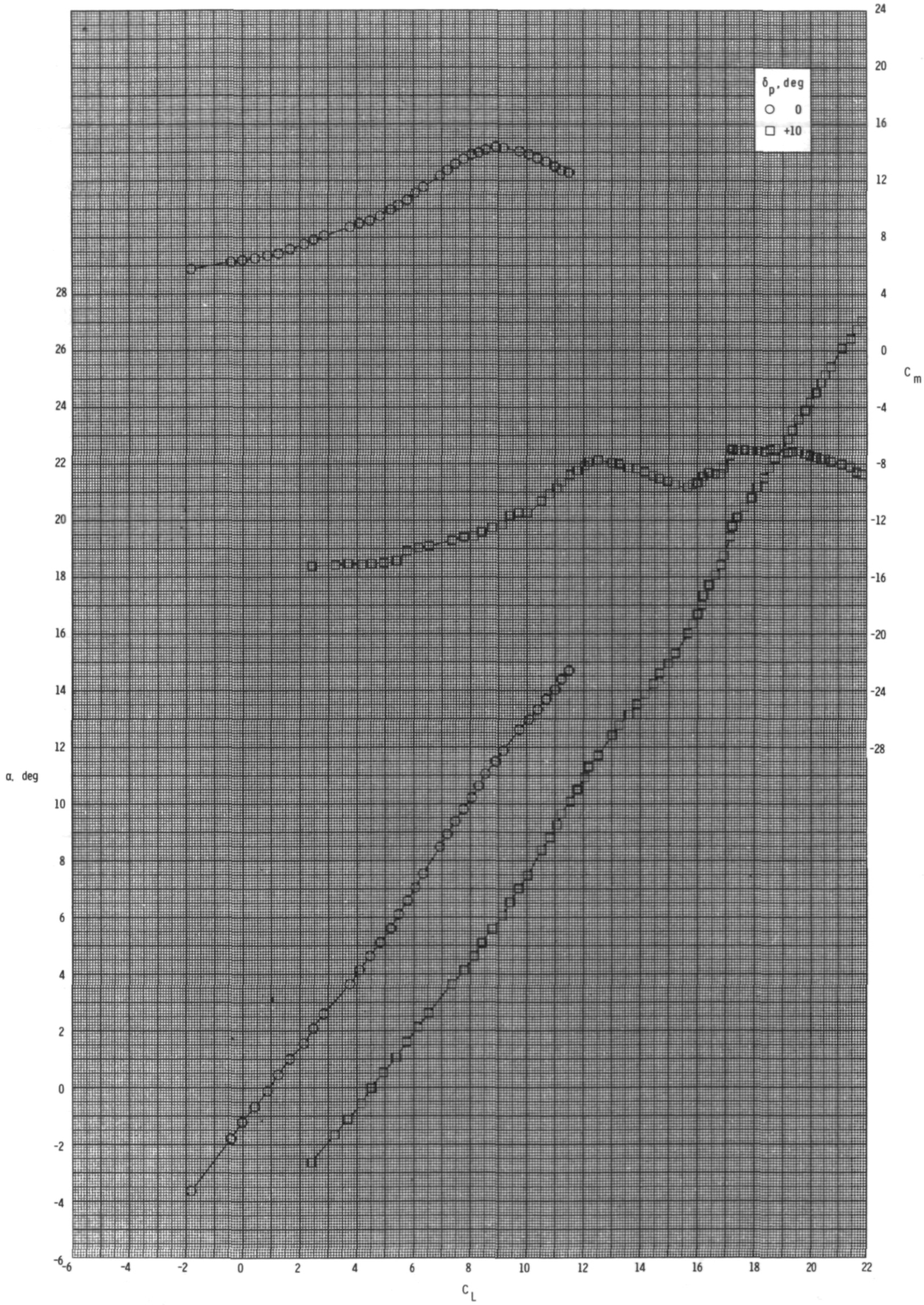

(c) Continued.

Figure 36.- Continued.

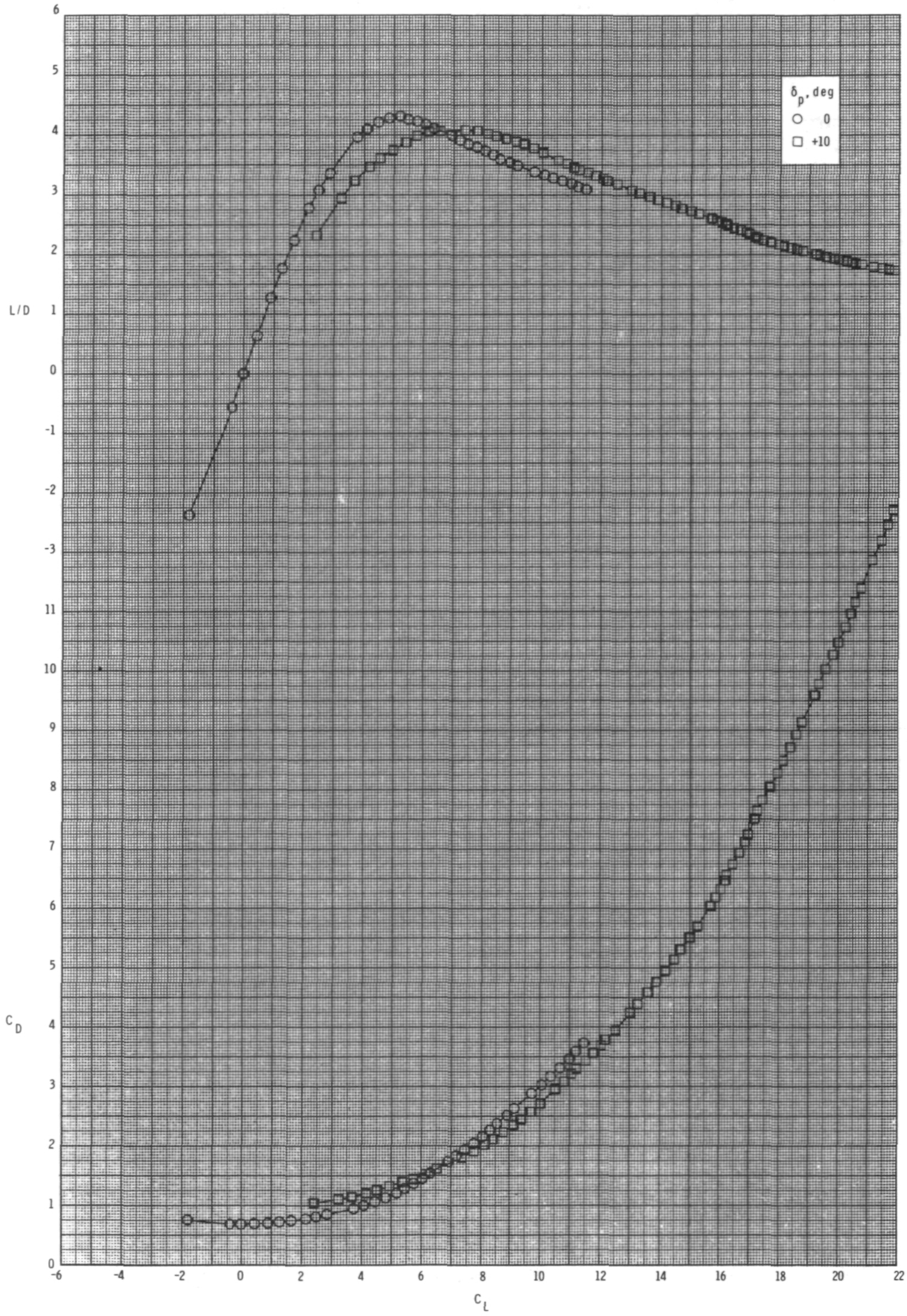

(c) Concluded.

Figure 36.- Concluded.

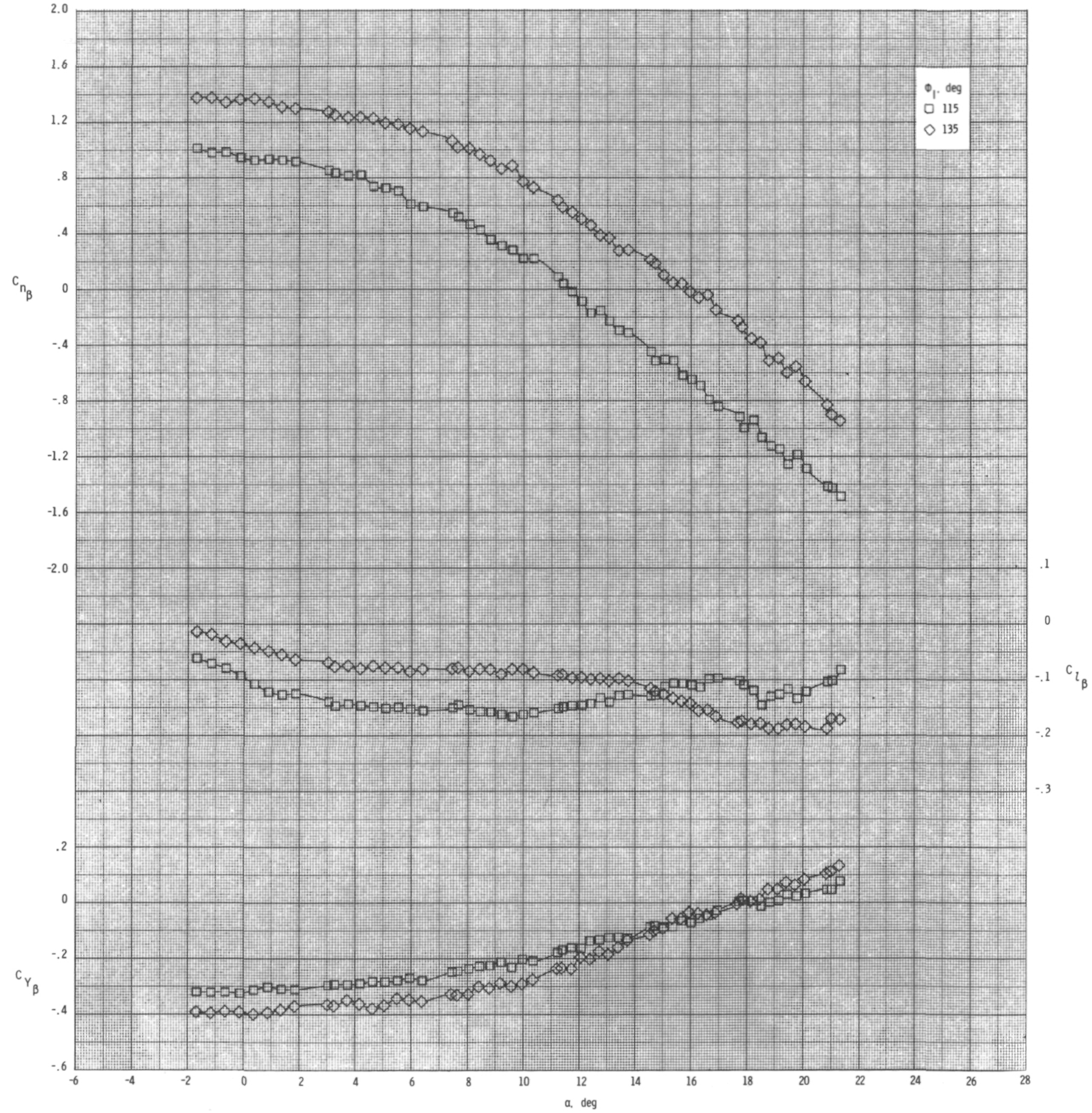

(a) M = 0.60.

Figure 37.- Effect of inlet orientation angle ϕ_I on lateral-directional stability for configuration $B_1I_{2c}W_1T_1$ with internal ducts closed and $\delta_p = 0°$.

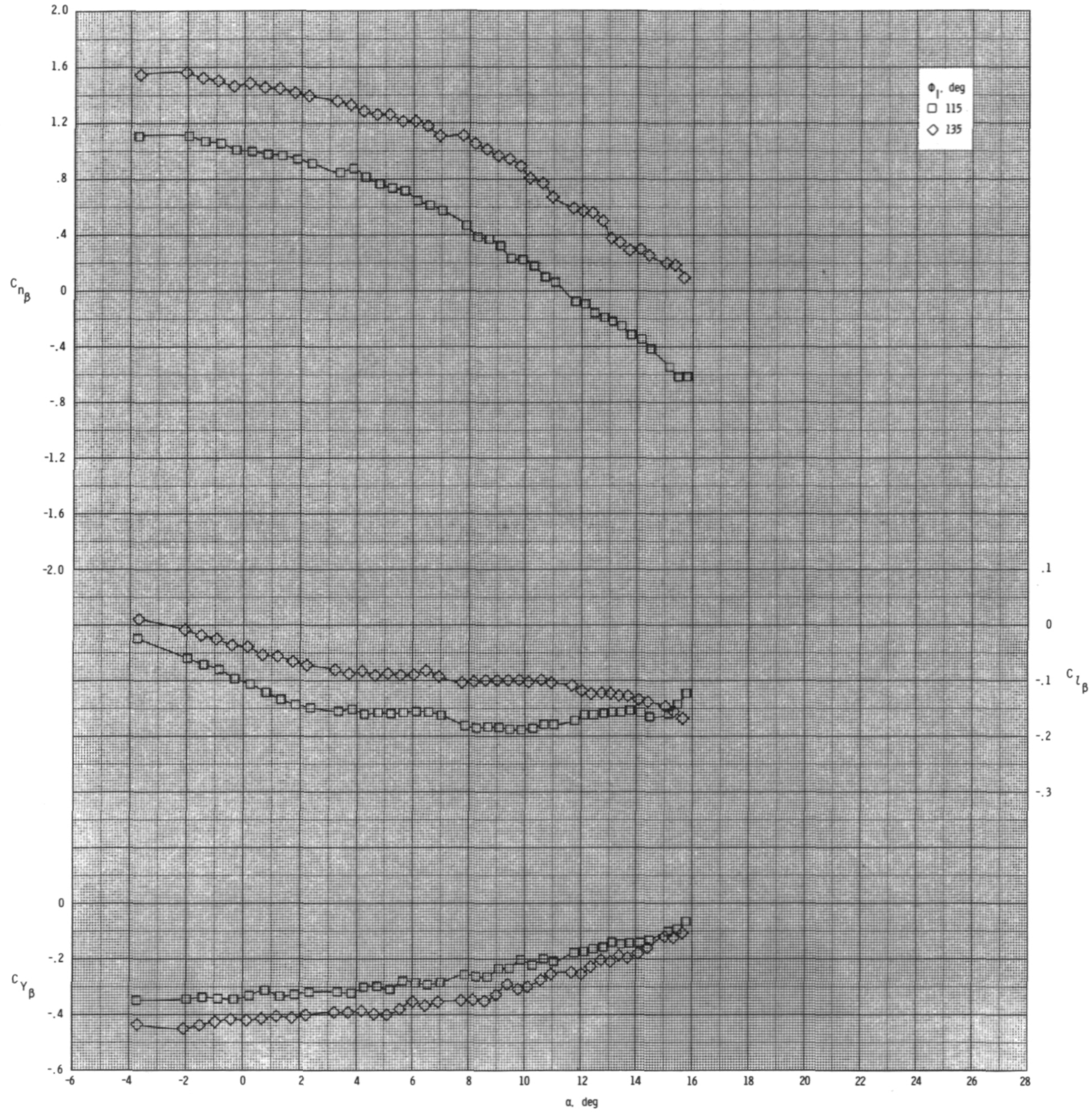

(b) M = 0.80.

Figure 37.- Continued.

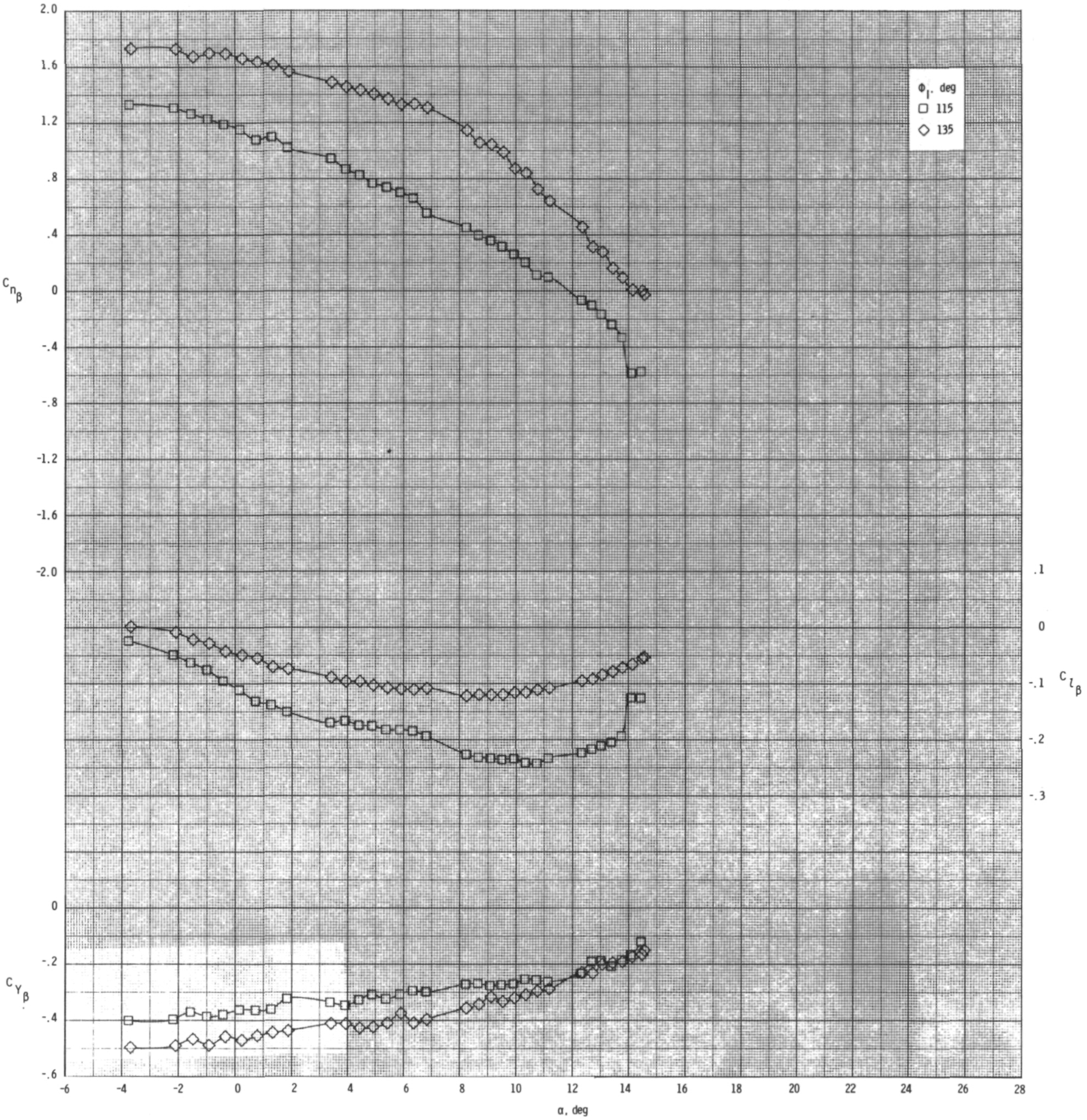

(c) M = 0.95.

Figure 37.- Concluded.

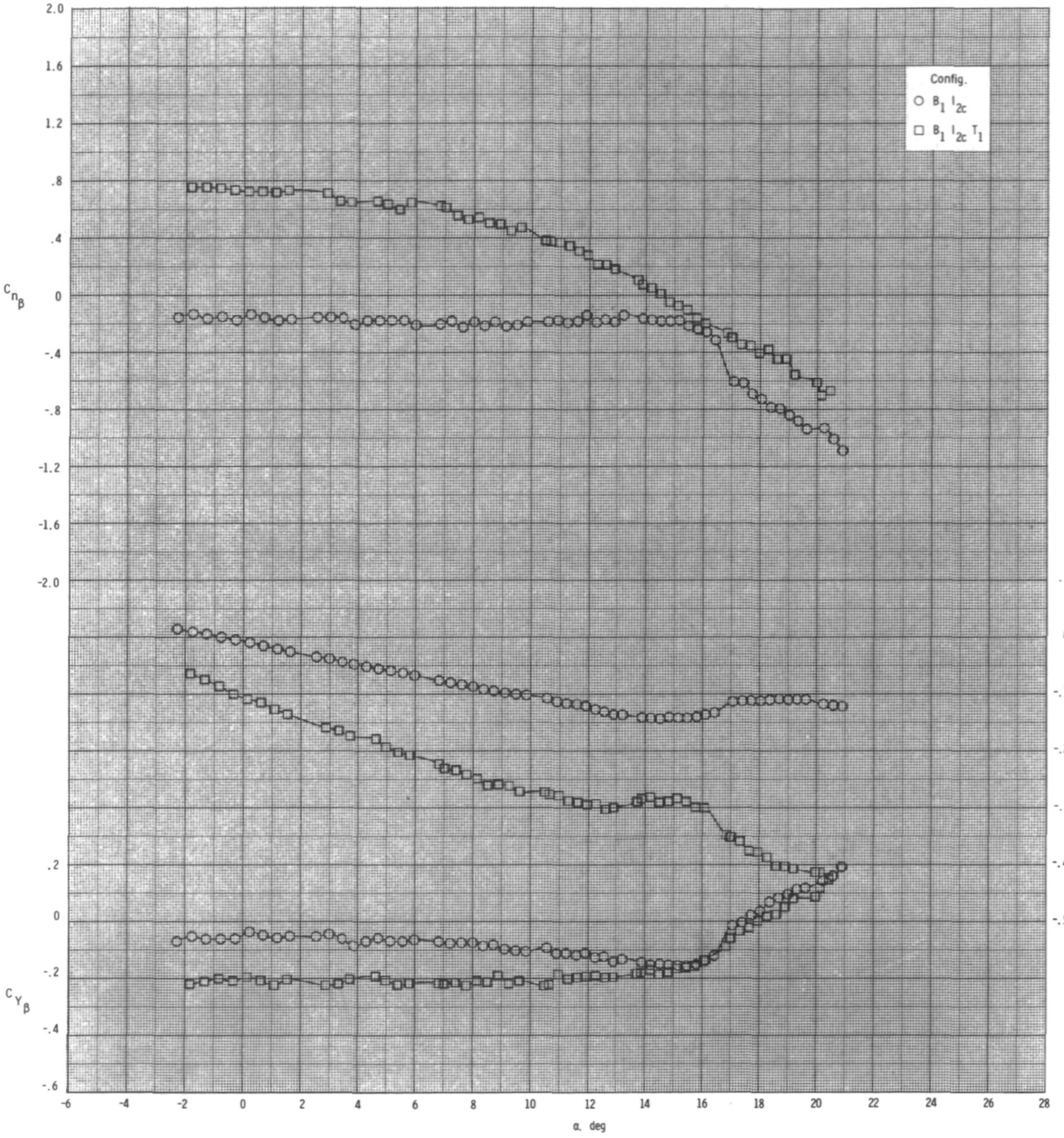

(a) M = 0.60.

Figure 38.- Effect of various model components on lateral-directional stability for 2-D inlets with internal ducts closed, inlet covers installed, $\phi_I = 90°$, and $\delta_p = 0°$.

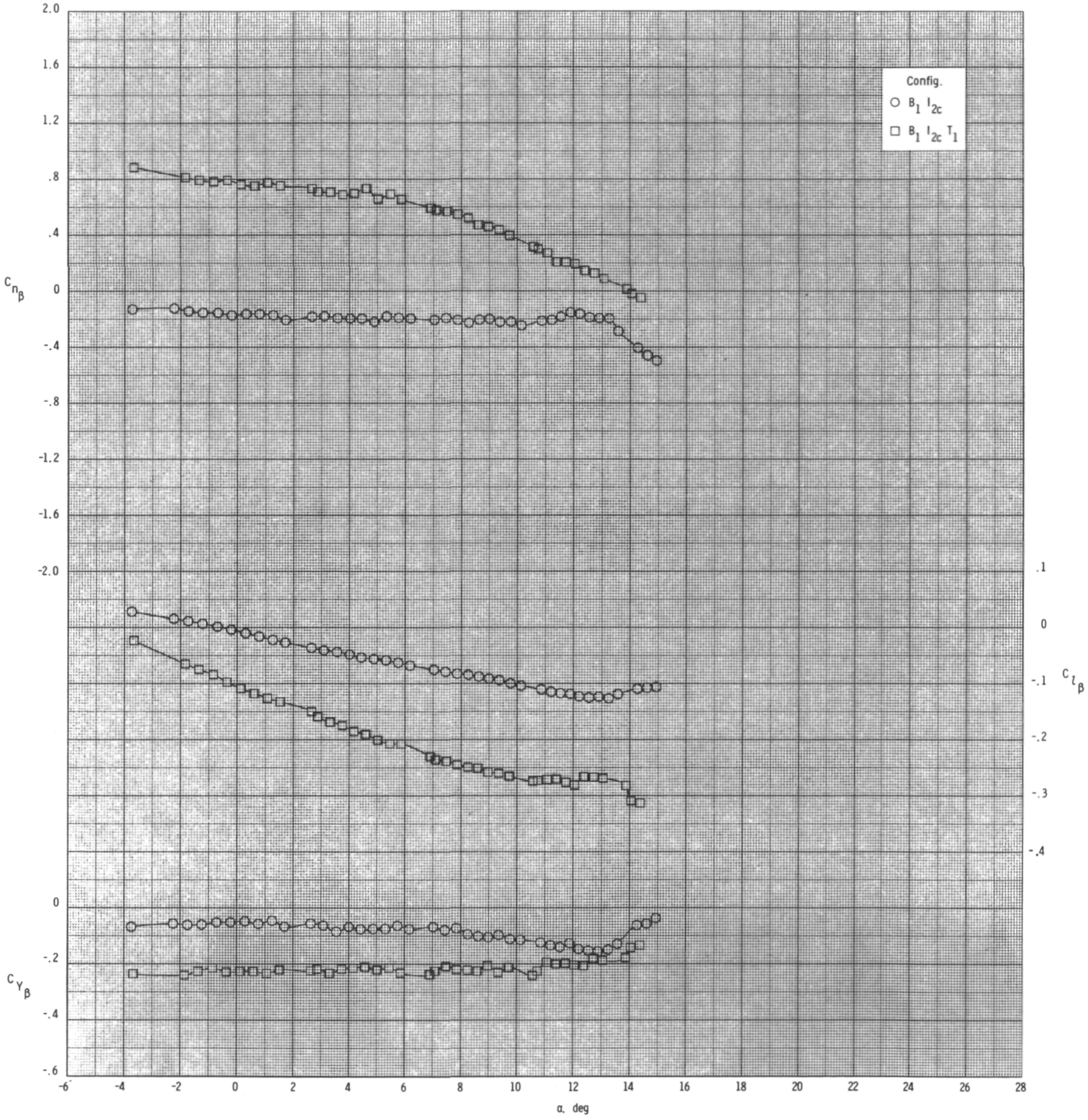

(b) M = 0.80.

Figure 38.- Continued.

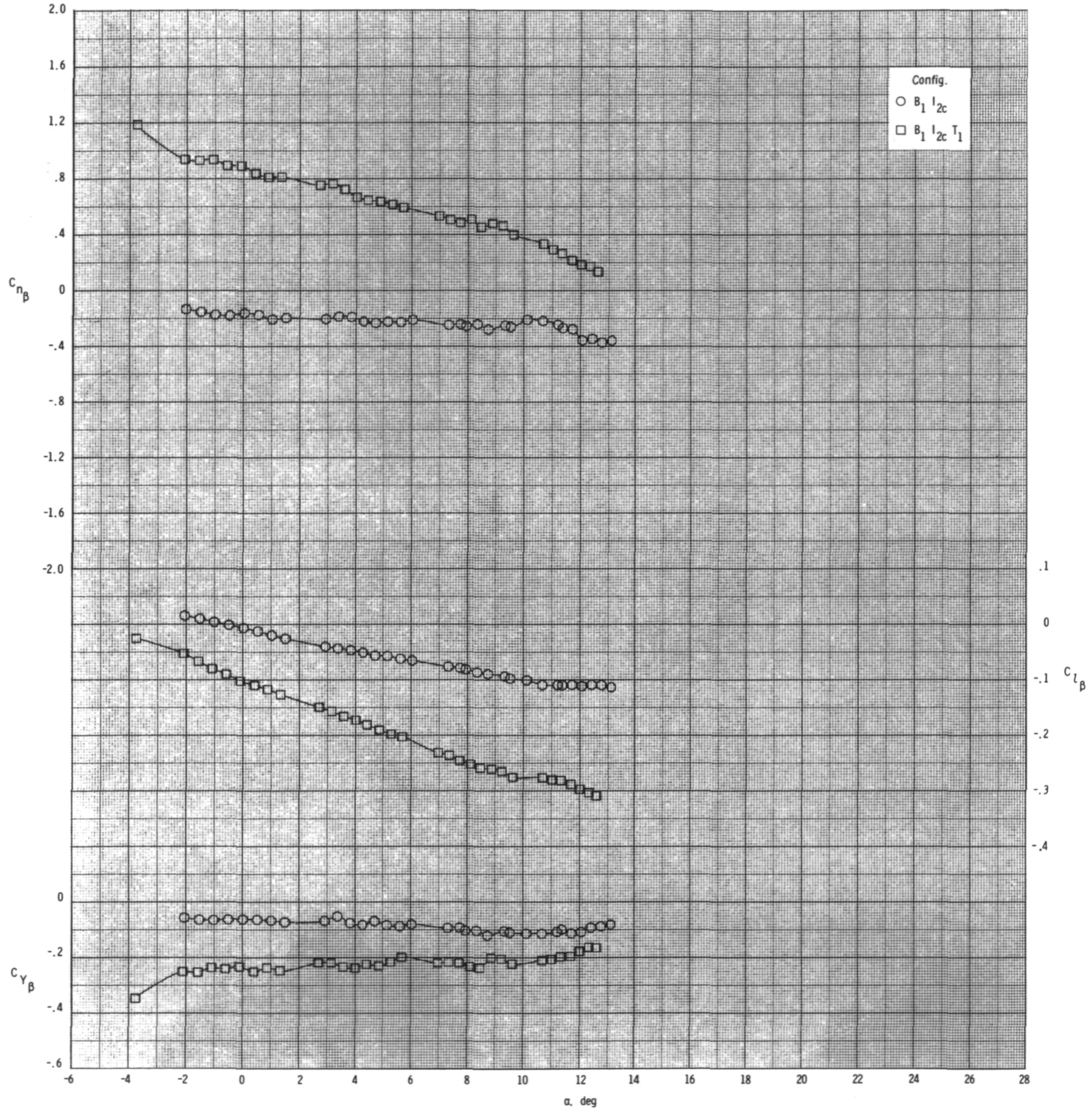

(c) M = 0.95.

Figure 38.- Concluded.

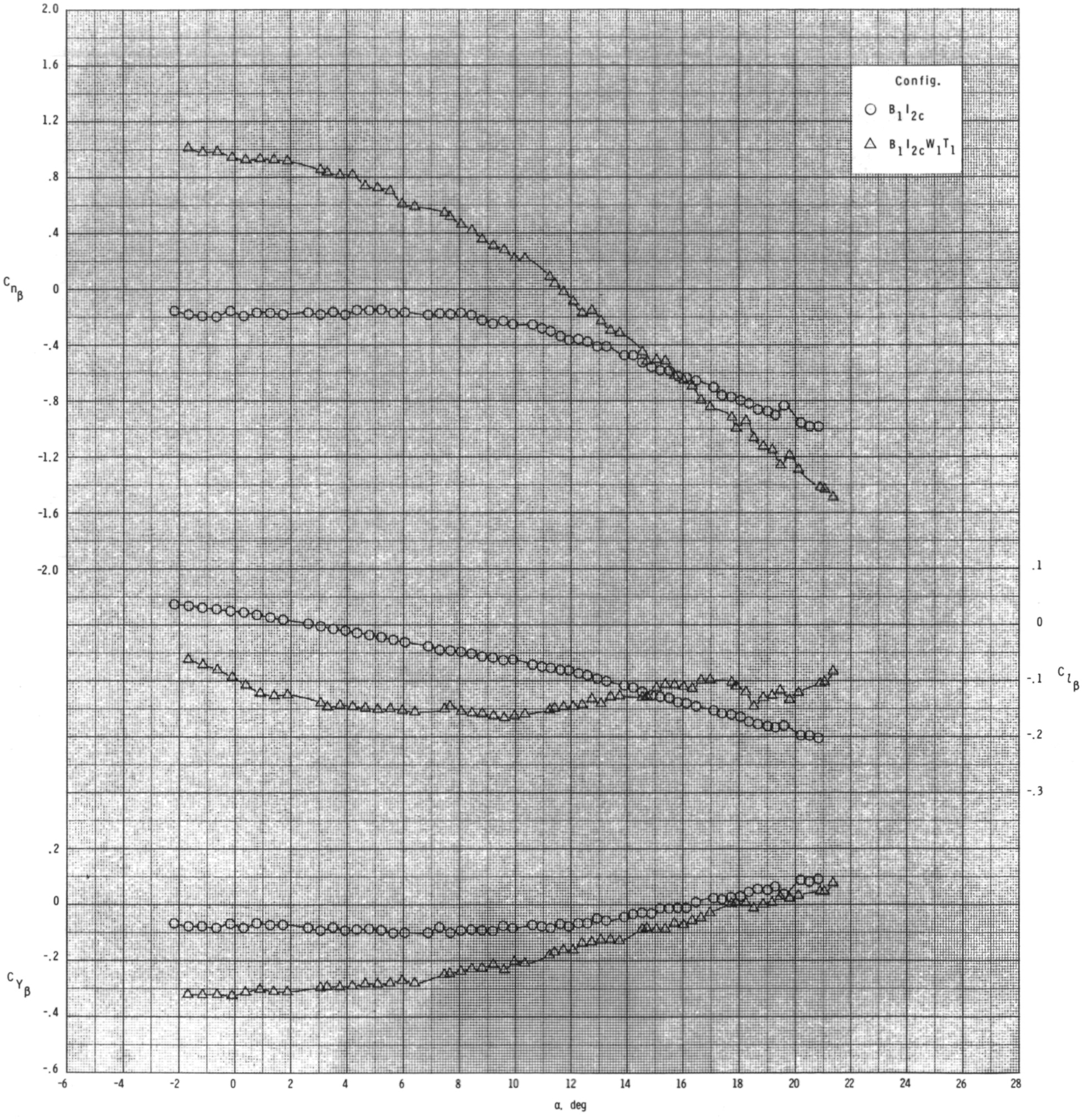

(a) M = 0.60.

Figure 39.- Effect of various model components on lateral-directional stability for 2-D inlets with internal ducts closed, inlet covers installed, $\phi_I = 115°$, and $\delta_p = 0°$.

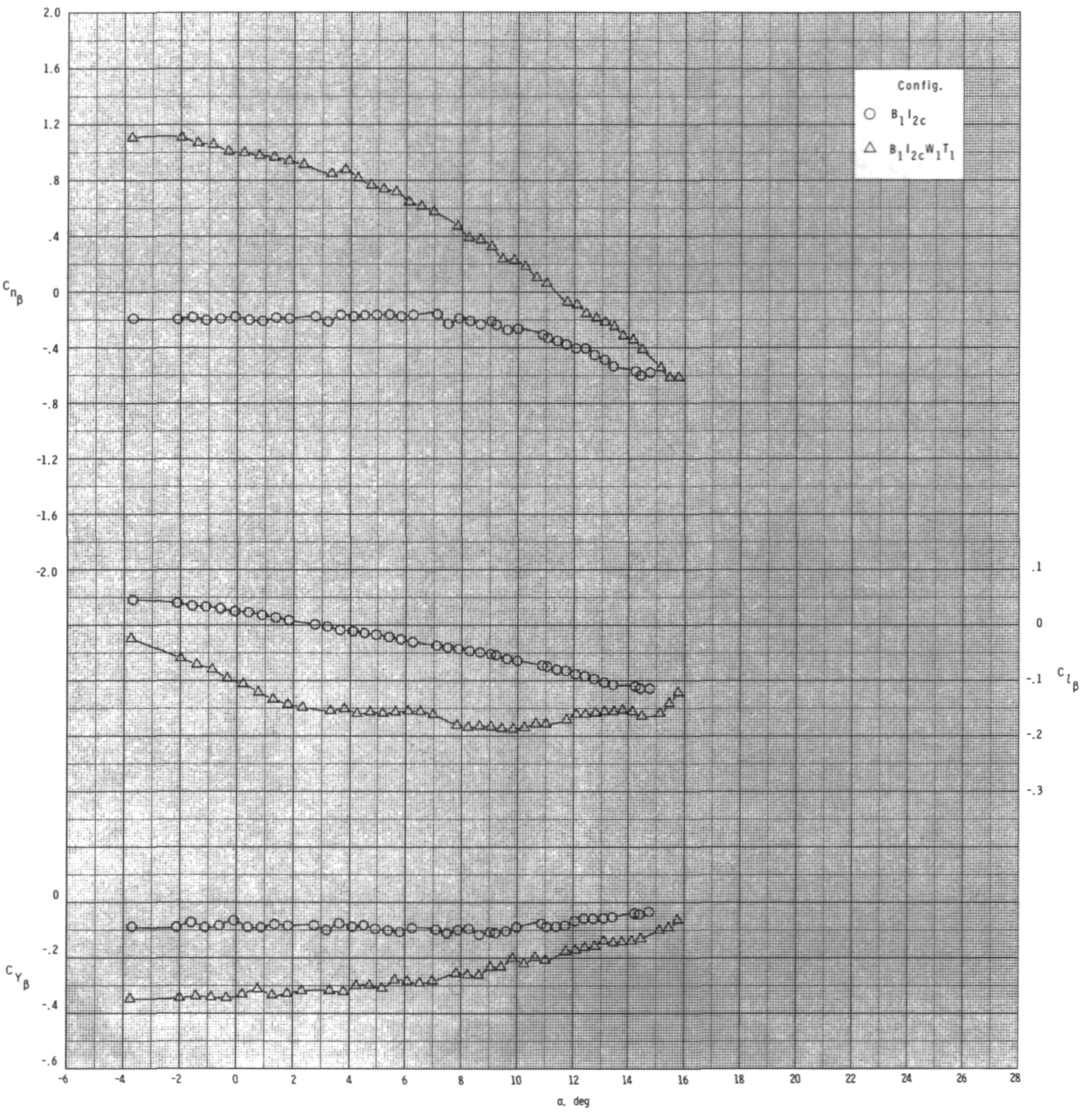

(b) M = 0.80.

Figure 39.- Continued.

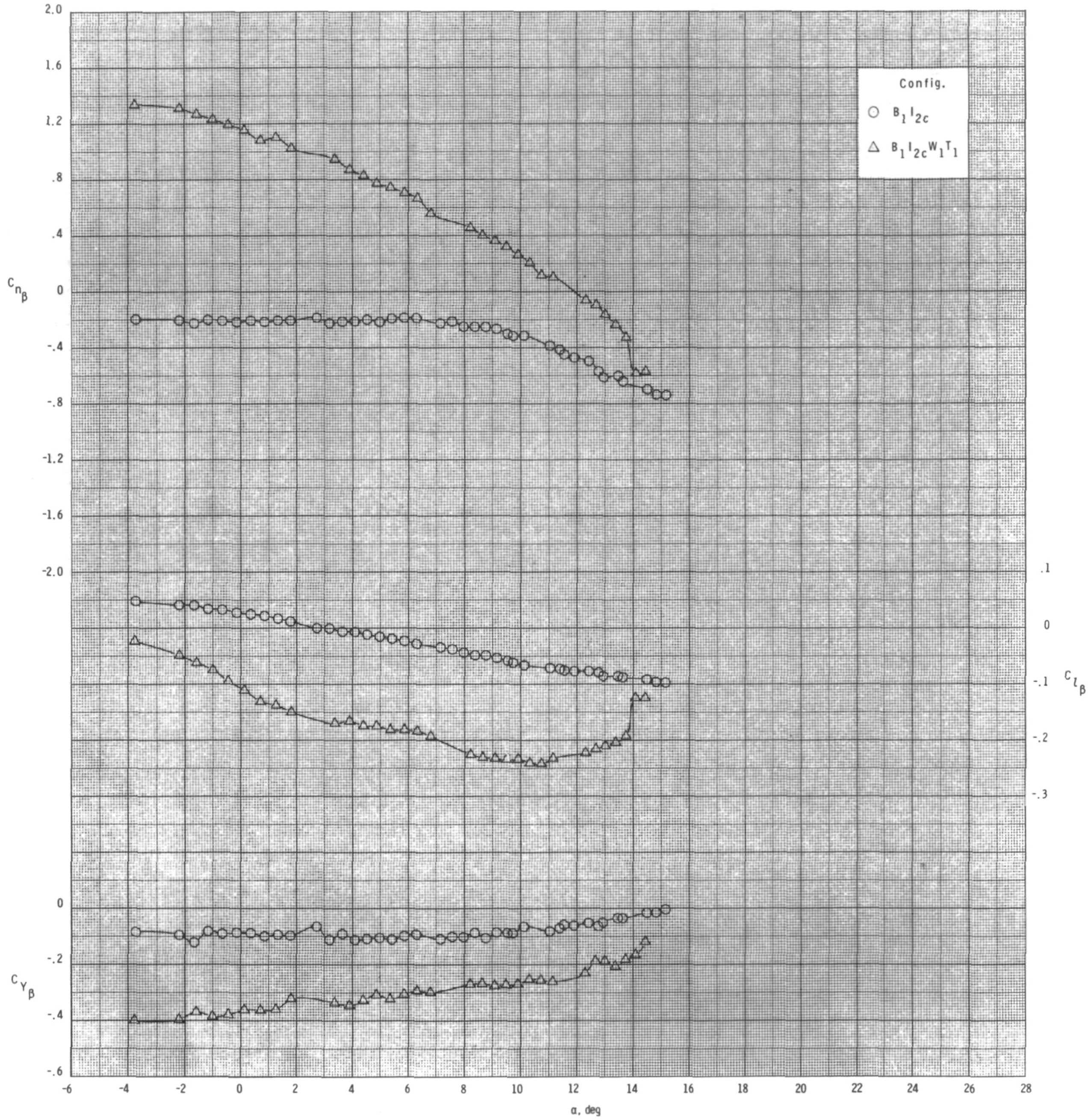

(c) M = 0.95.

Figure 39.- Concluded.

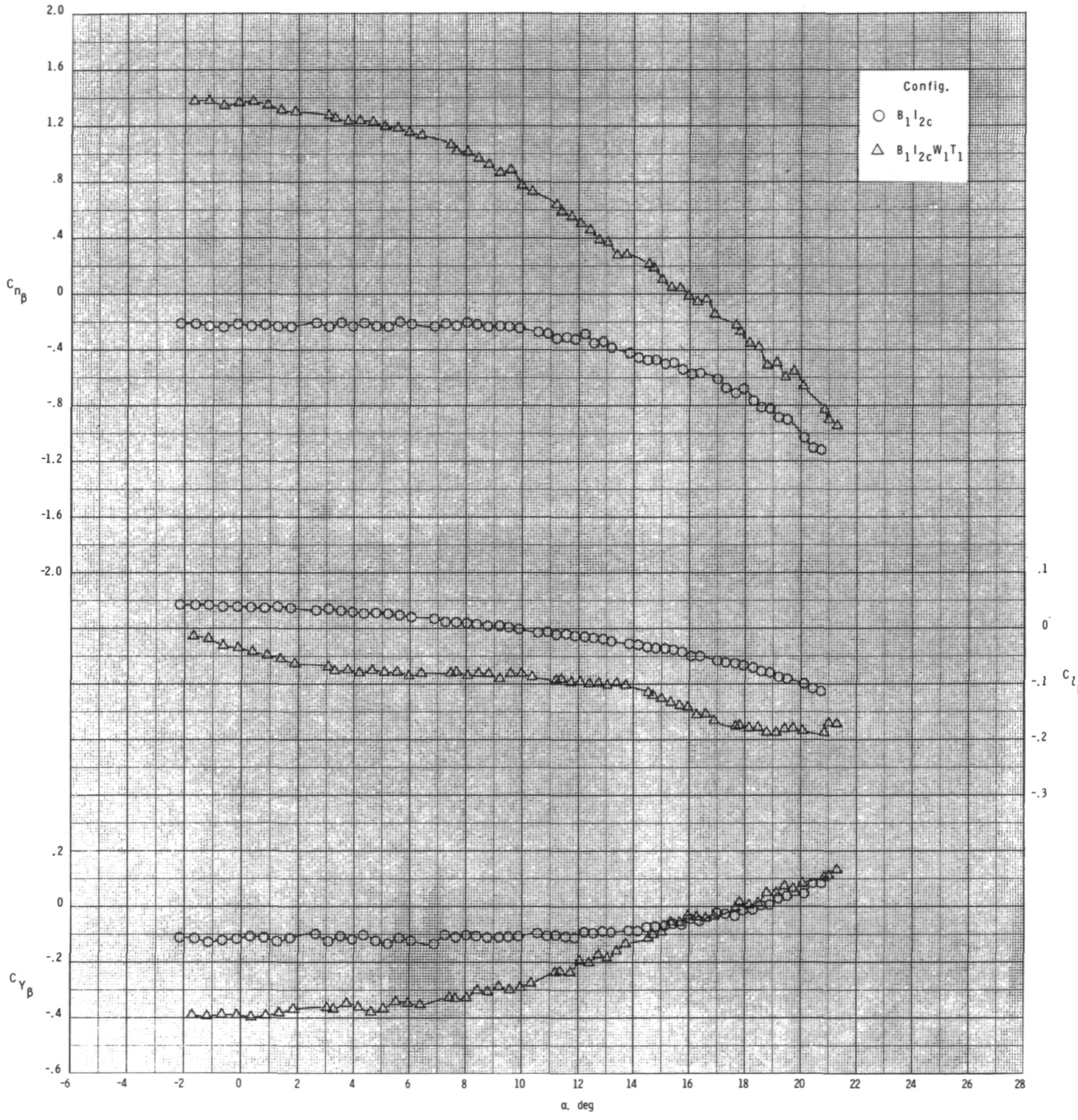

(a) M = 0.60.

Figure 40.- Effect of various model components on lateral-directional stability for 2-D inlets with internal ducts closed, inlet covers installed, T_1, $\phi_I = 135°$, and $\delta_p = 0°$.

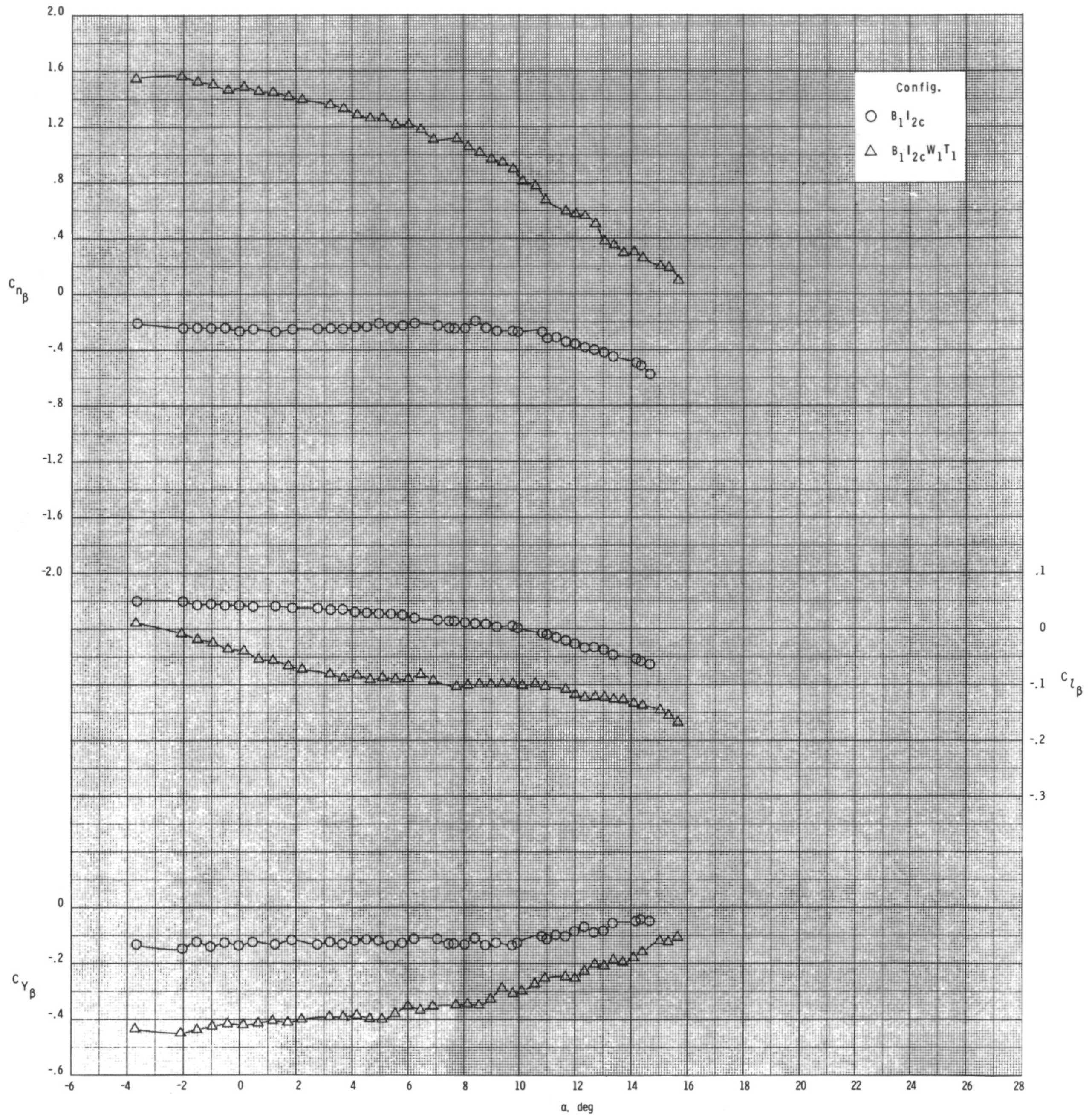

(b) M = 0.80.

Figure 40.- Continued.

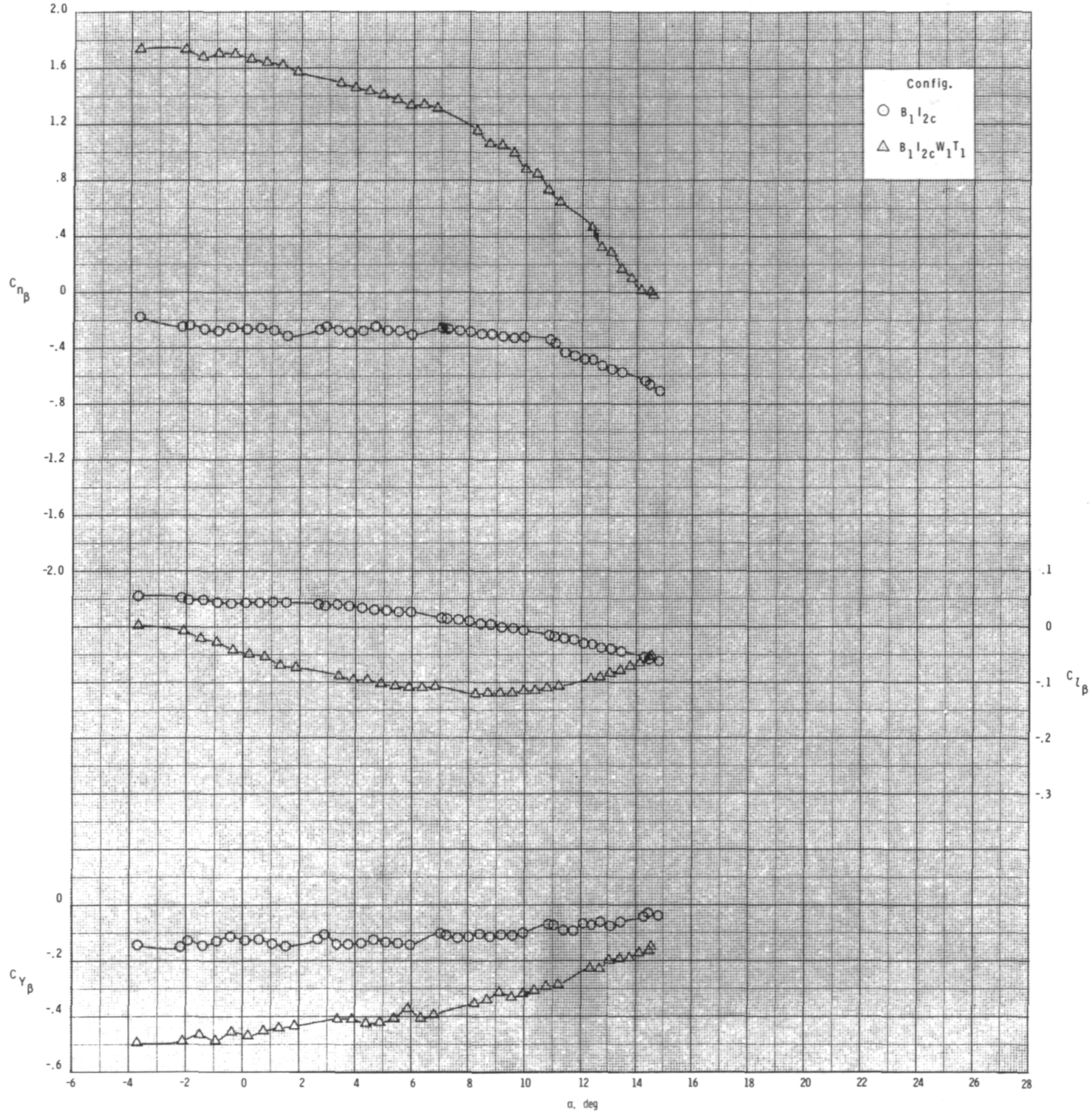

(c) M = 0.95.

Figure 40.- Concluded.

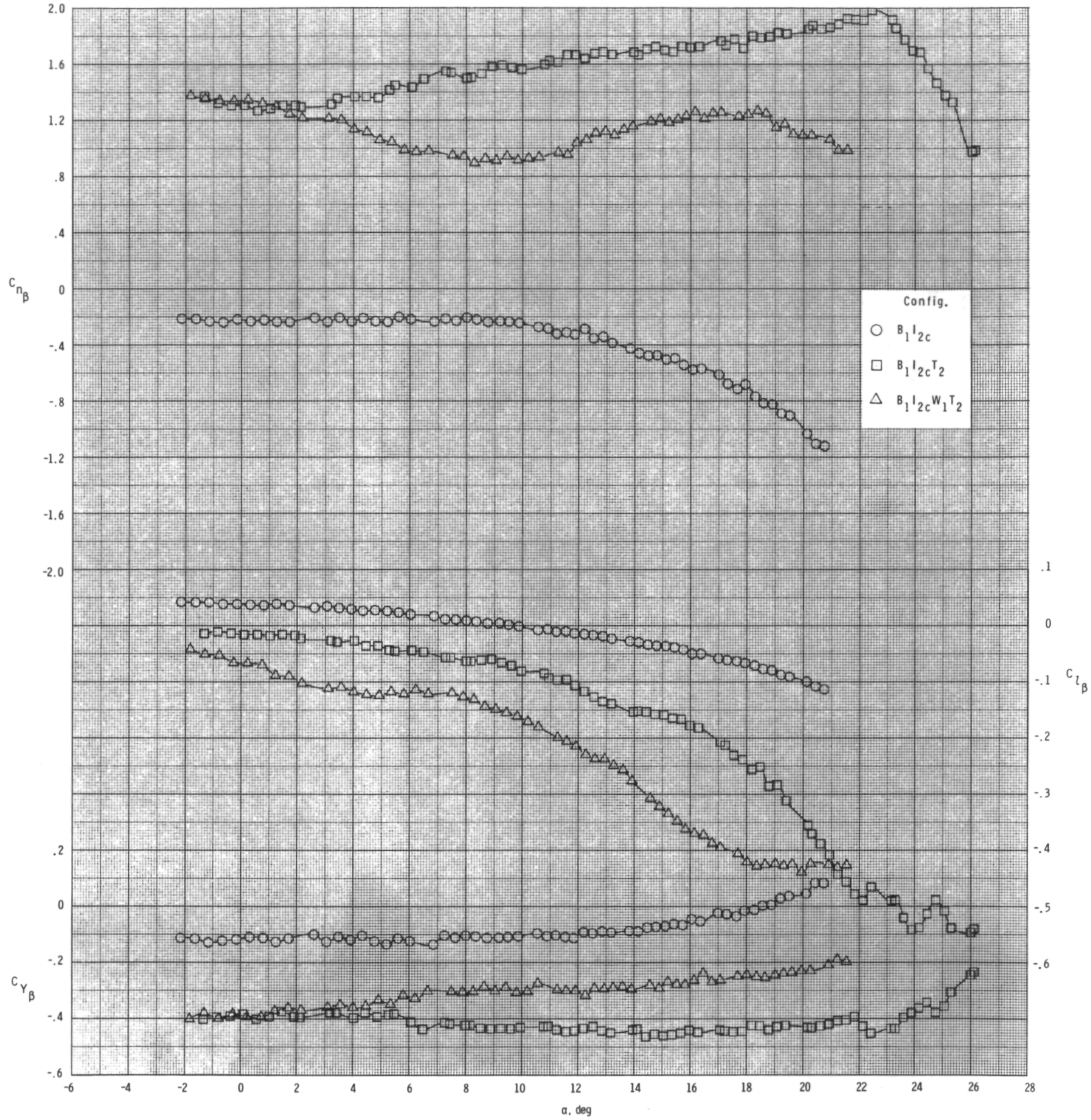

(a) M = 0.60.

Figure 41.- Effect of various model components on lateral-directional stability for 2-D inlets with internal ducts closed, inlet covers installed, T_2, ϕ_I = 135°, and δ_p = 0°.

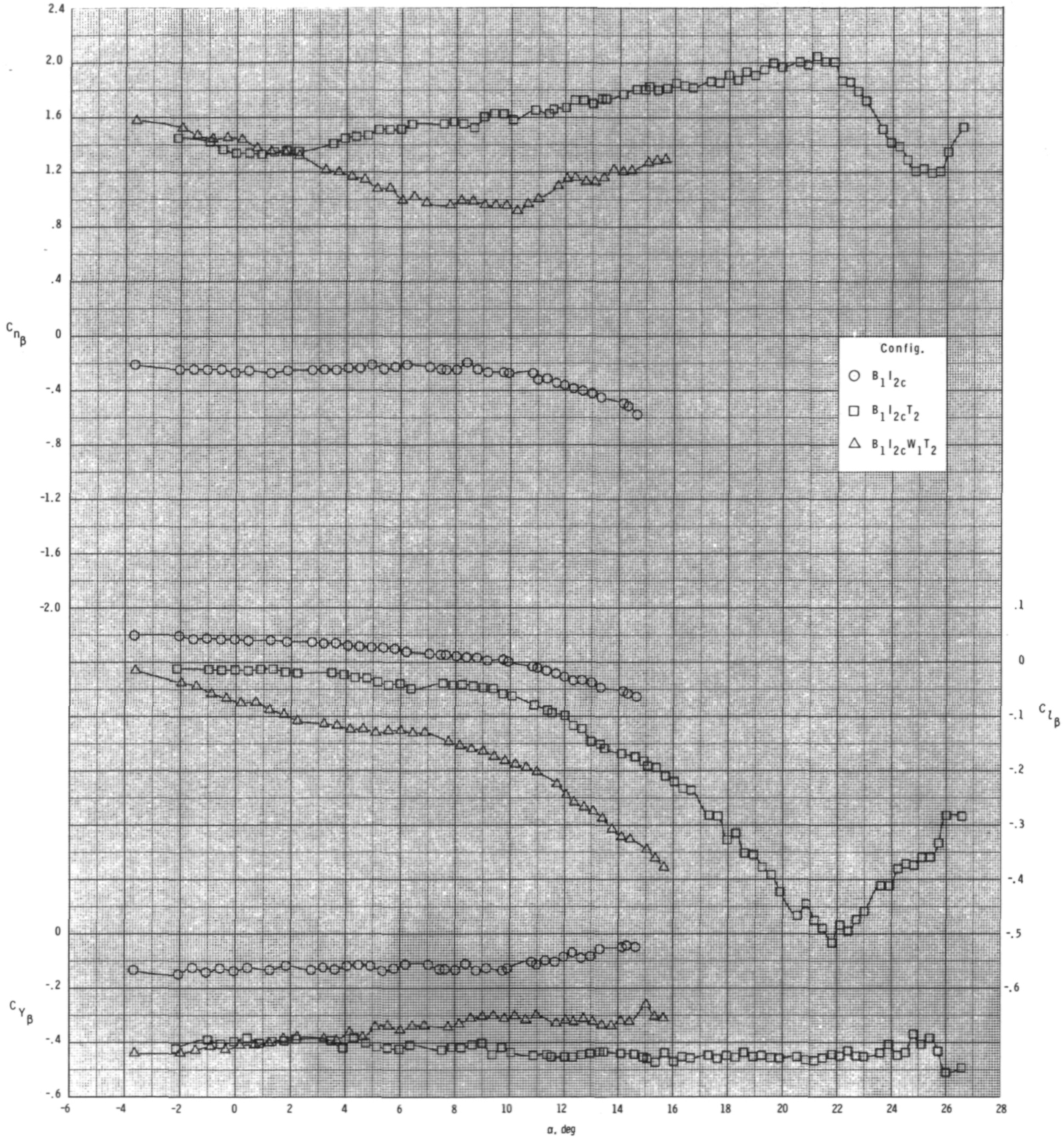

(b) M = 0.80.

Figure 41.- Continued.

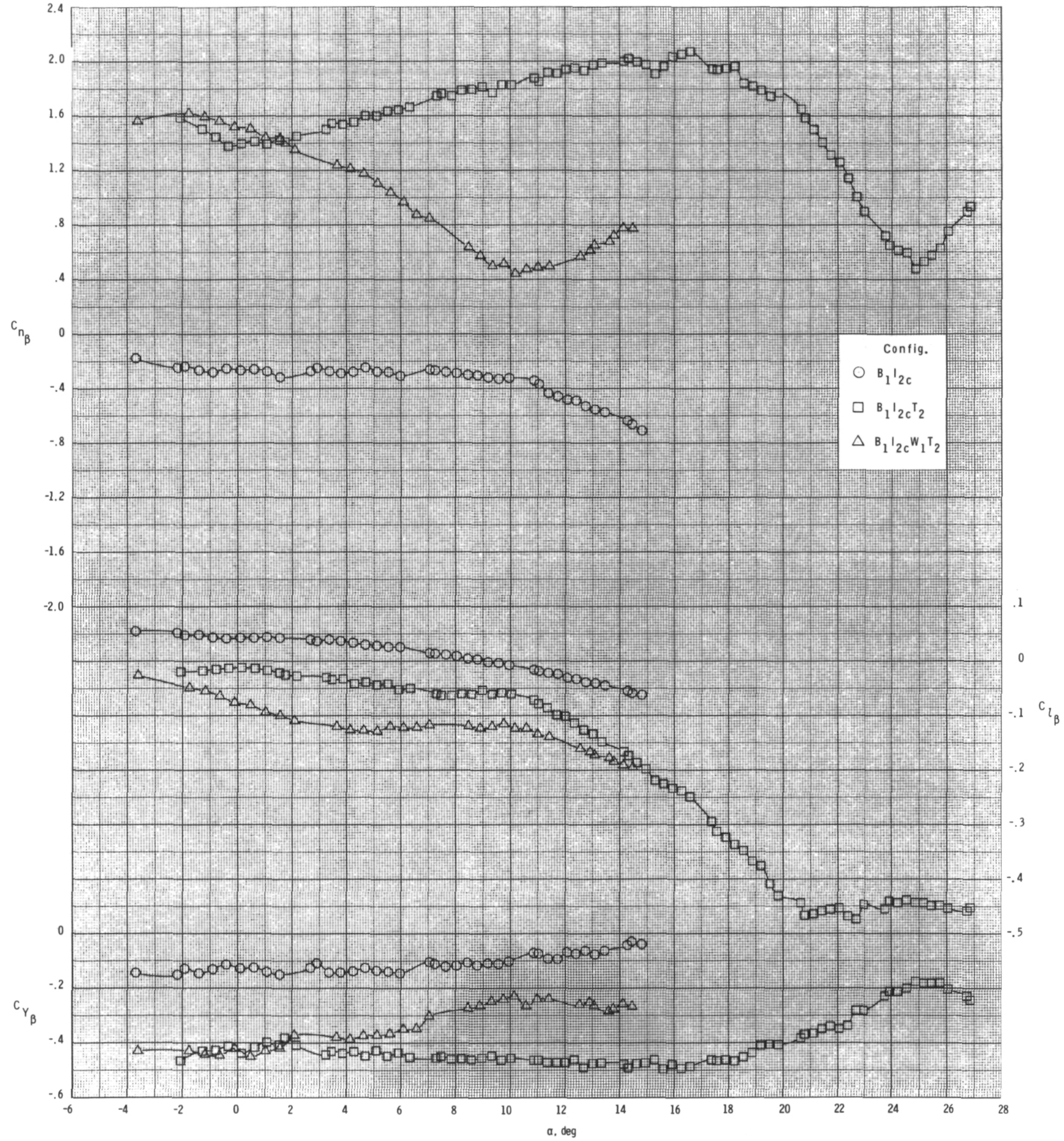

(c) M = 0.95.

Figure 41.- Concluded.

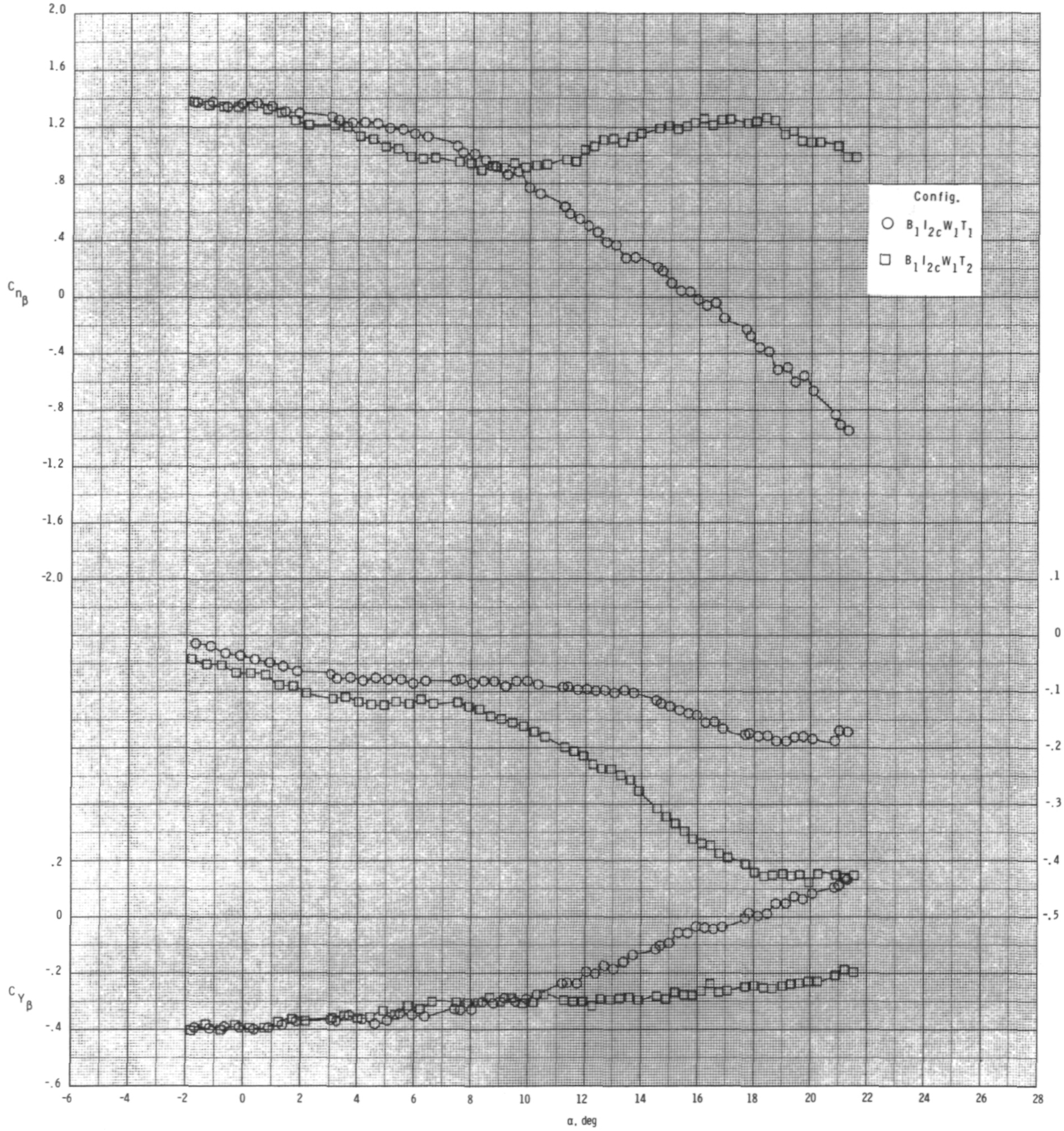

(a) M = 0.60.

Figure 42.- Effect of tail configuration on lateral-directional stability for configuration $B_1 I_{2c} W_1 T$ with internal ducts closed, $\phi_I = 135°$, and $\delta_p = 0°$.

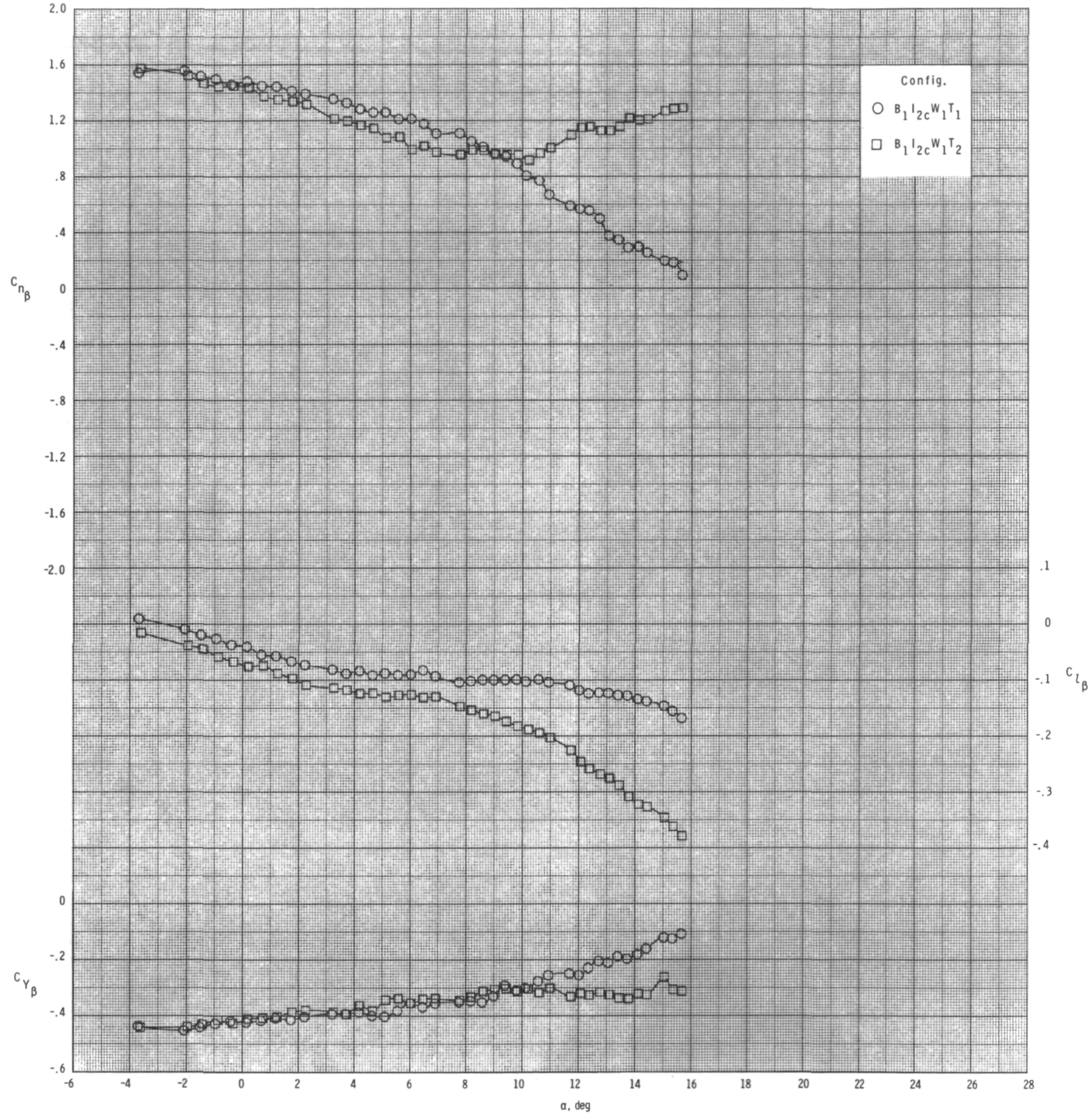

(b) M = 0.80.

Figure 42.- Continued.

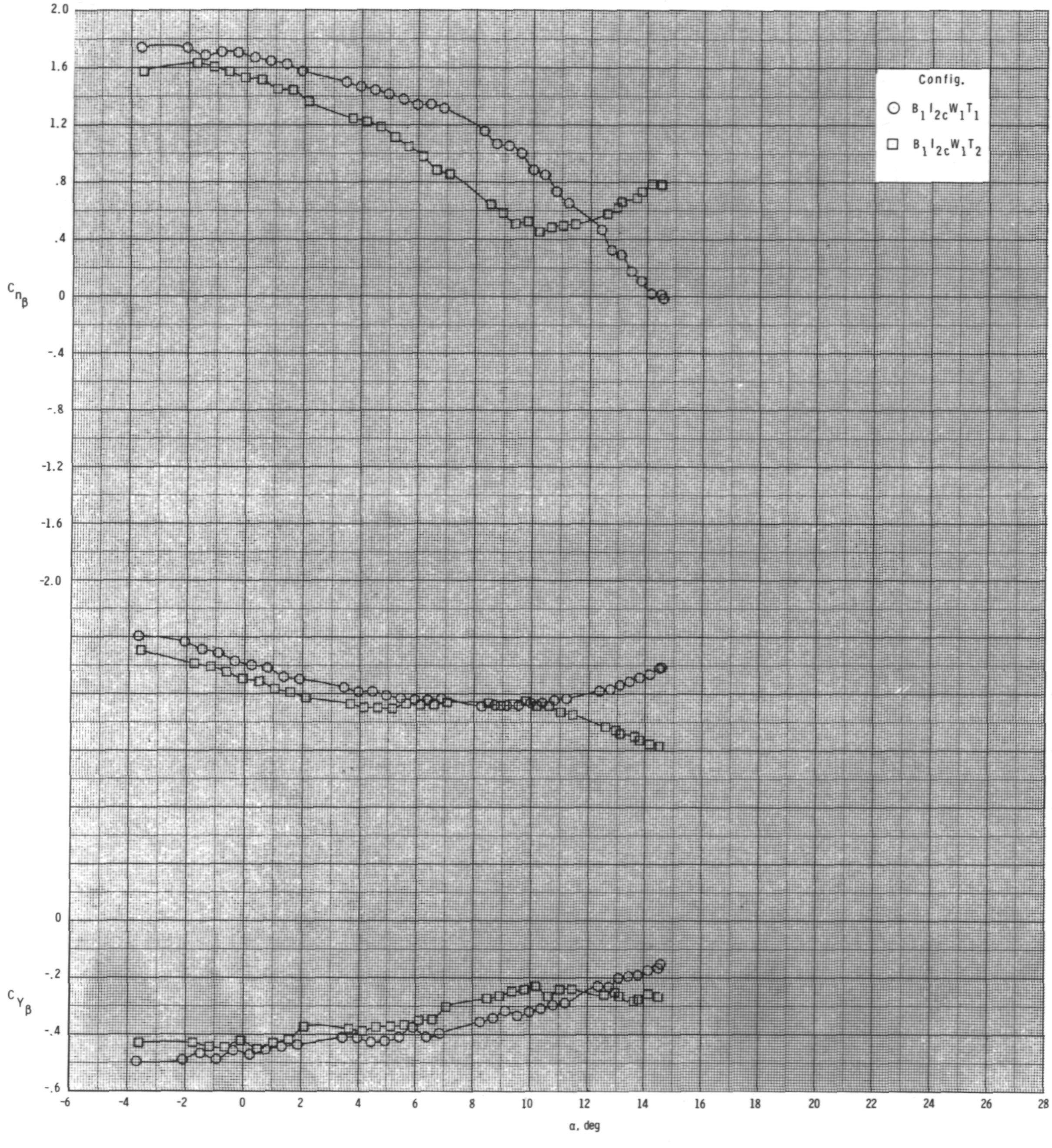

(c) M = 0.95.

Figure 42.- Concluded.

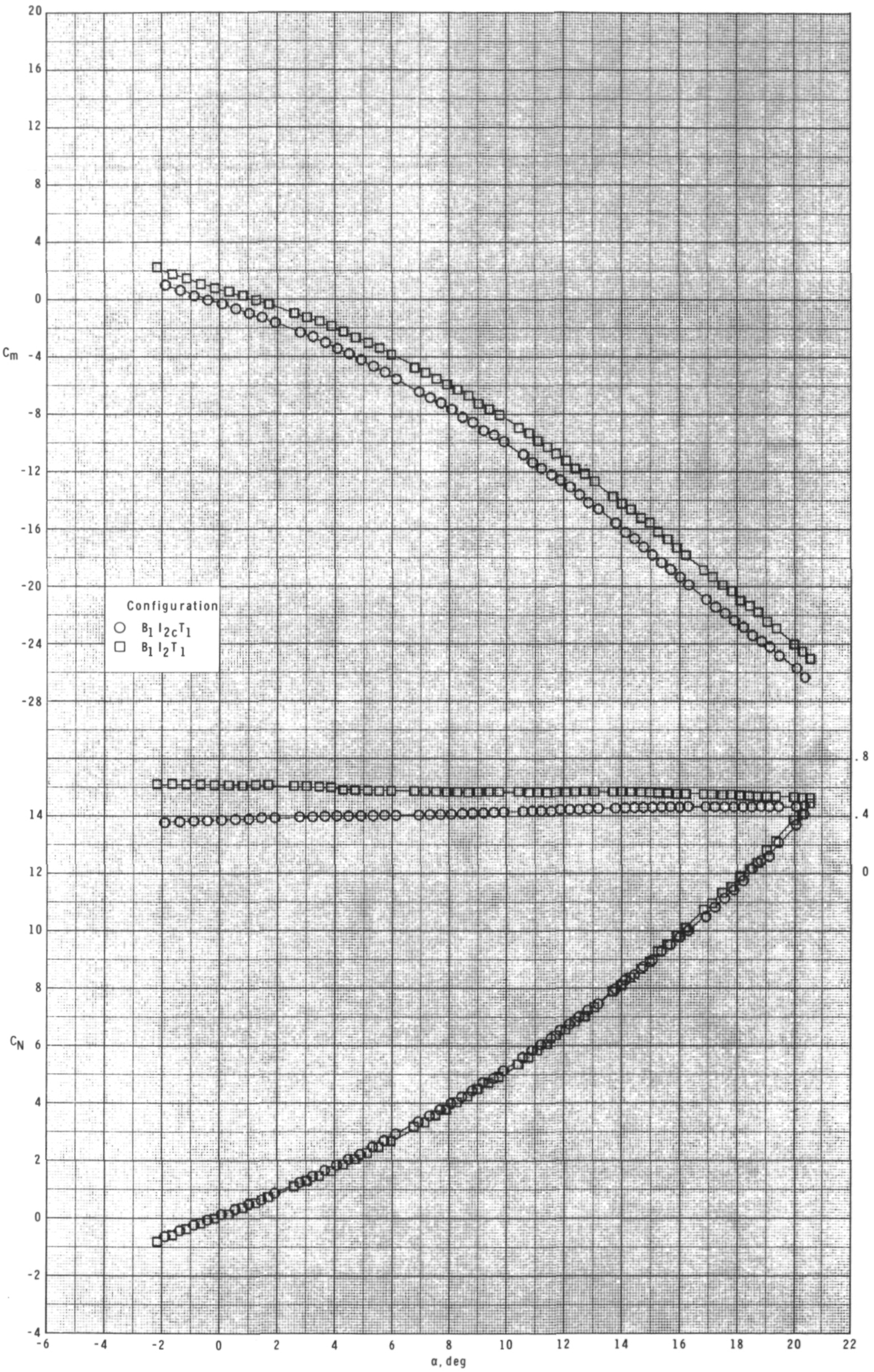

(a) M = 0.60.

Figure 43.- Effect of removing inlet covers on longitudinal aerodynamic characteristics with internal ducts closed and ϕ_I = 90°.

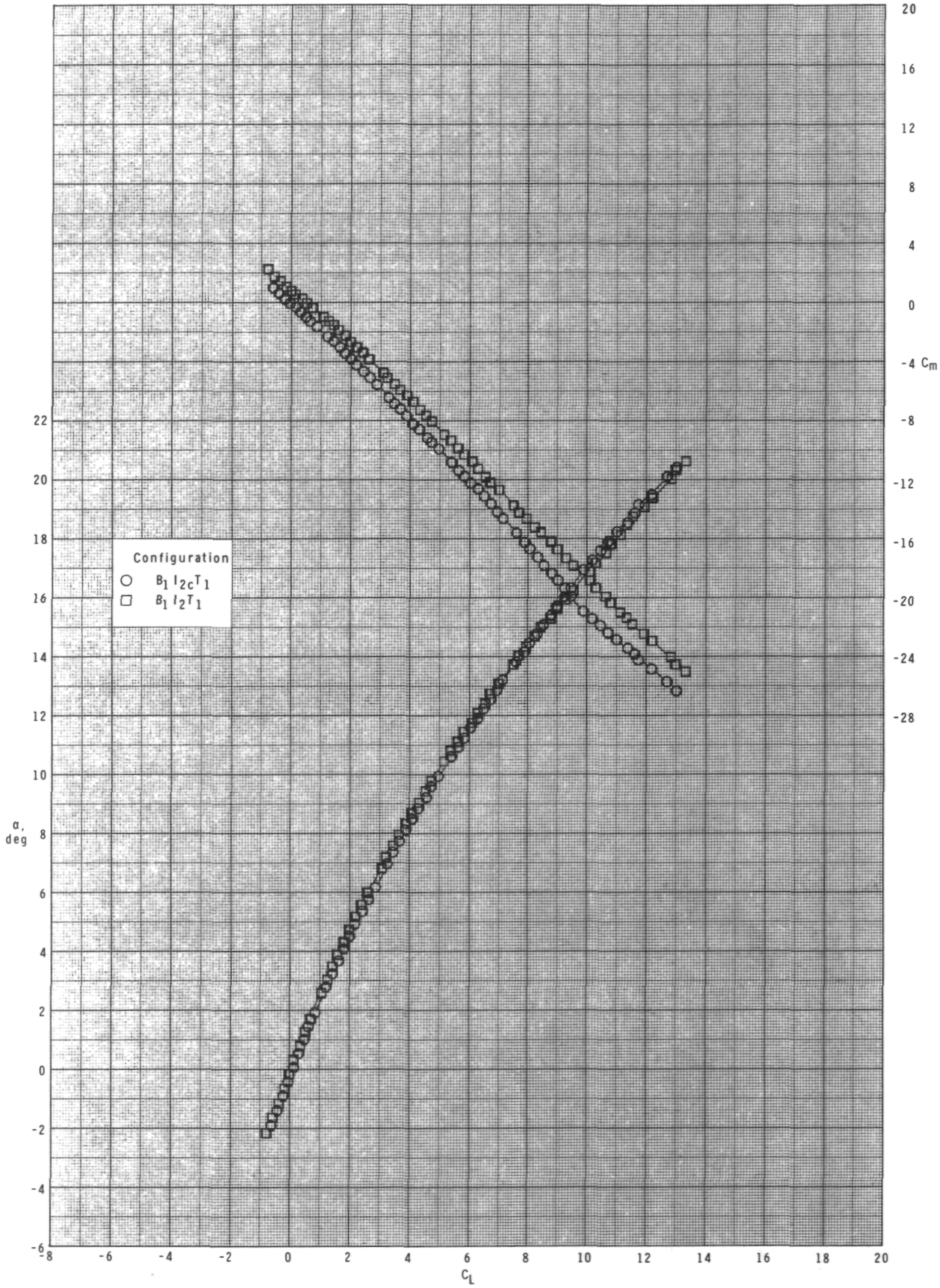

(a) Continued.

Figure 43.- Continued.

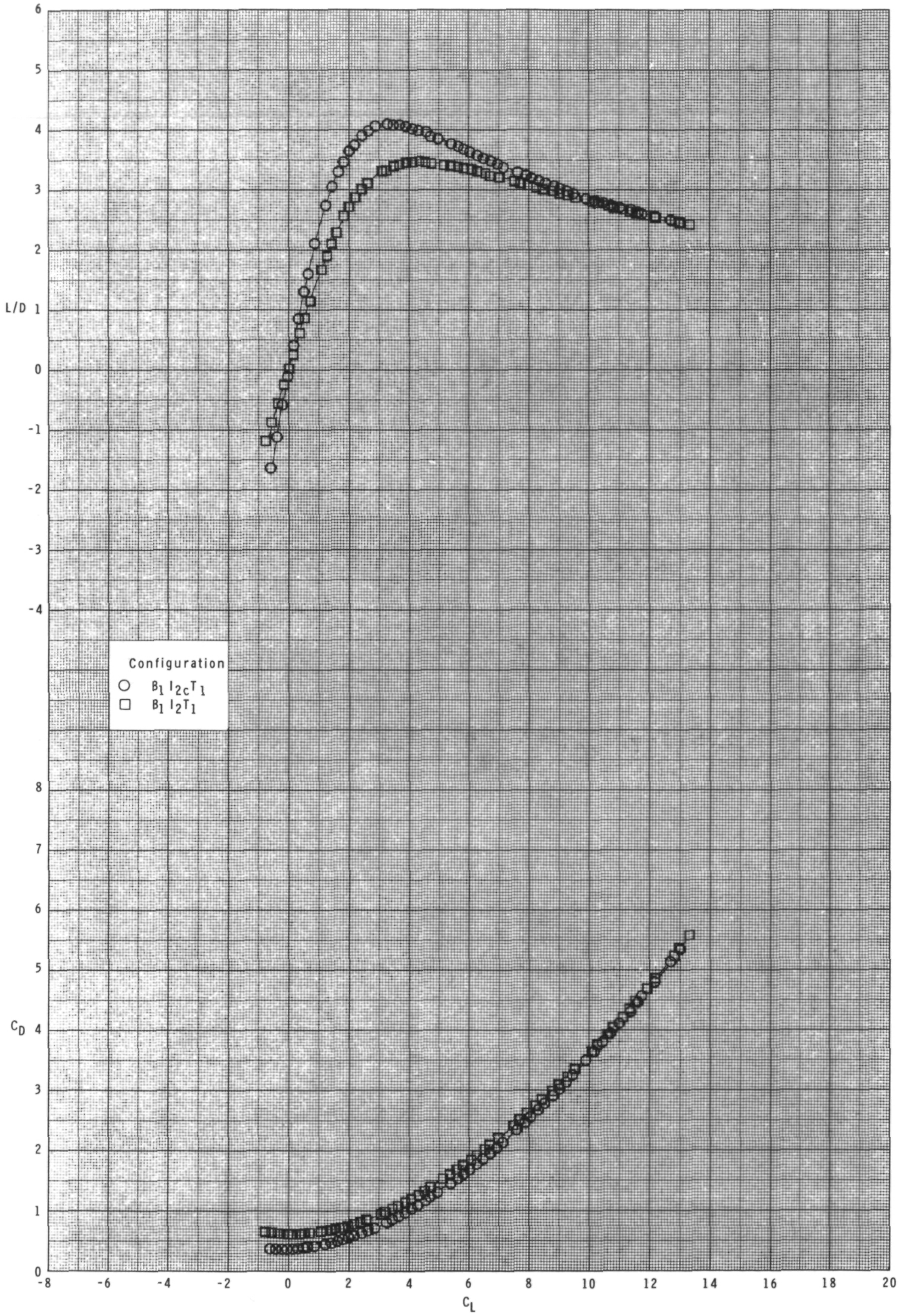

(a) Concluded.

Figure 43.- Continued.

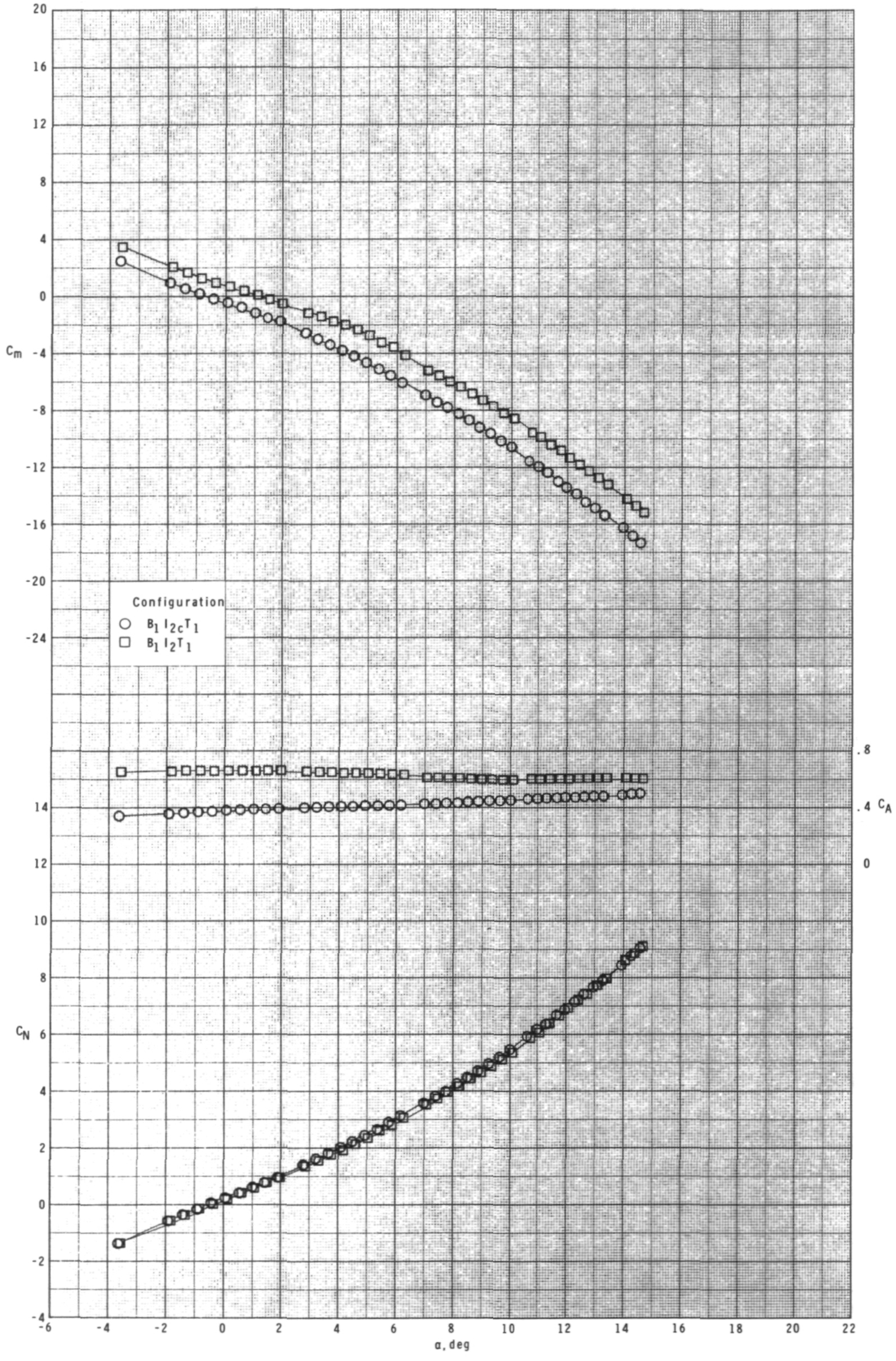

(b) M = 0.80.

Figure 43.- Continued.

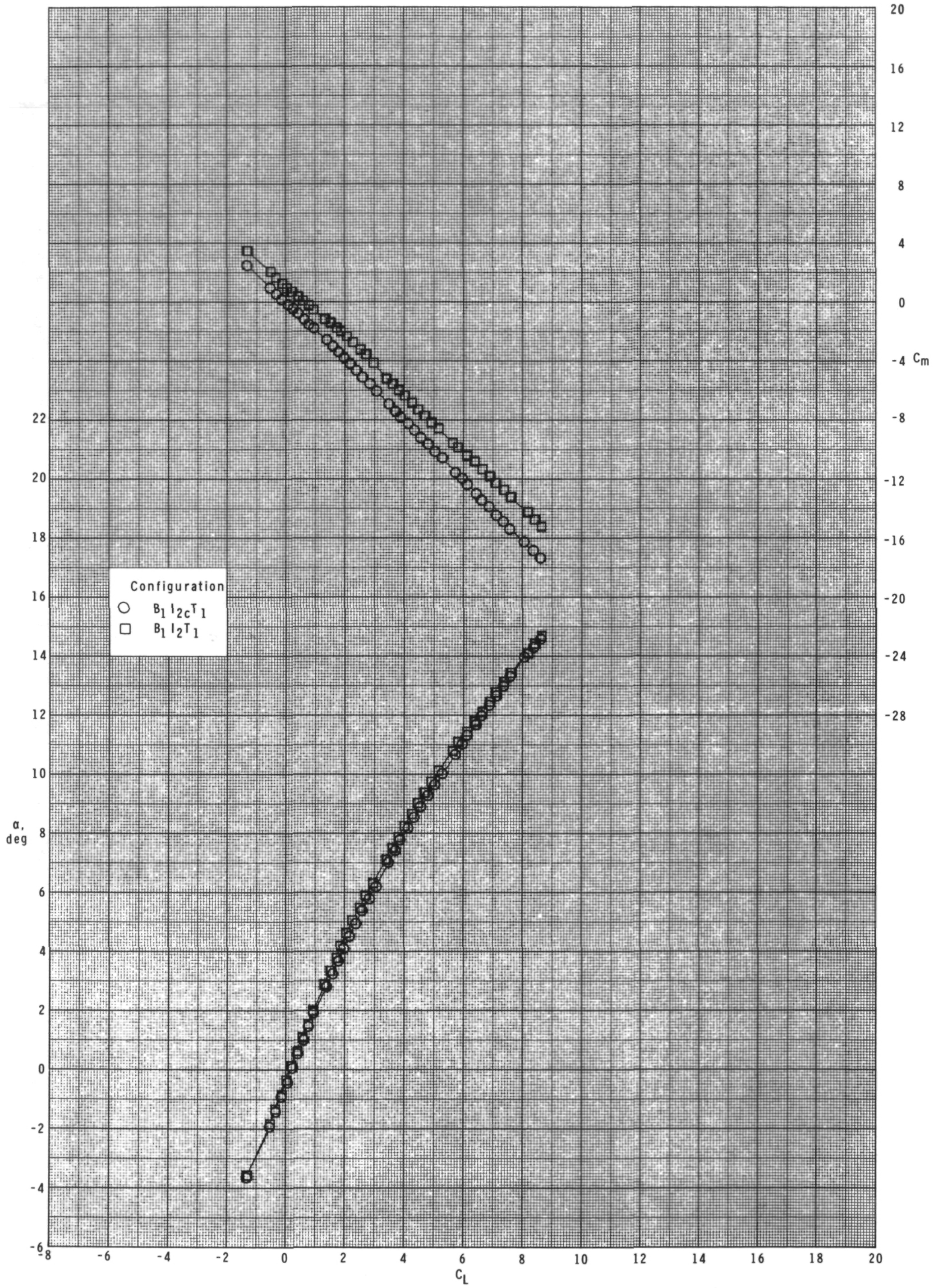

(b) Continued.

Figure 43.- Continued.

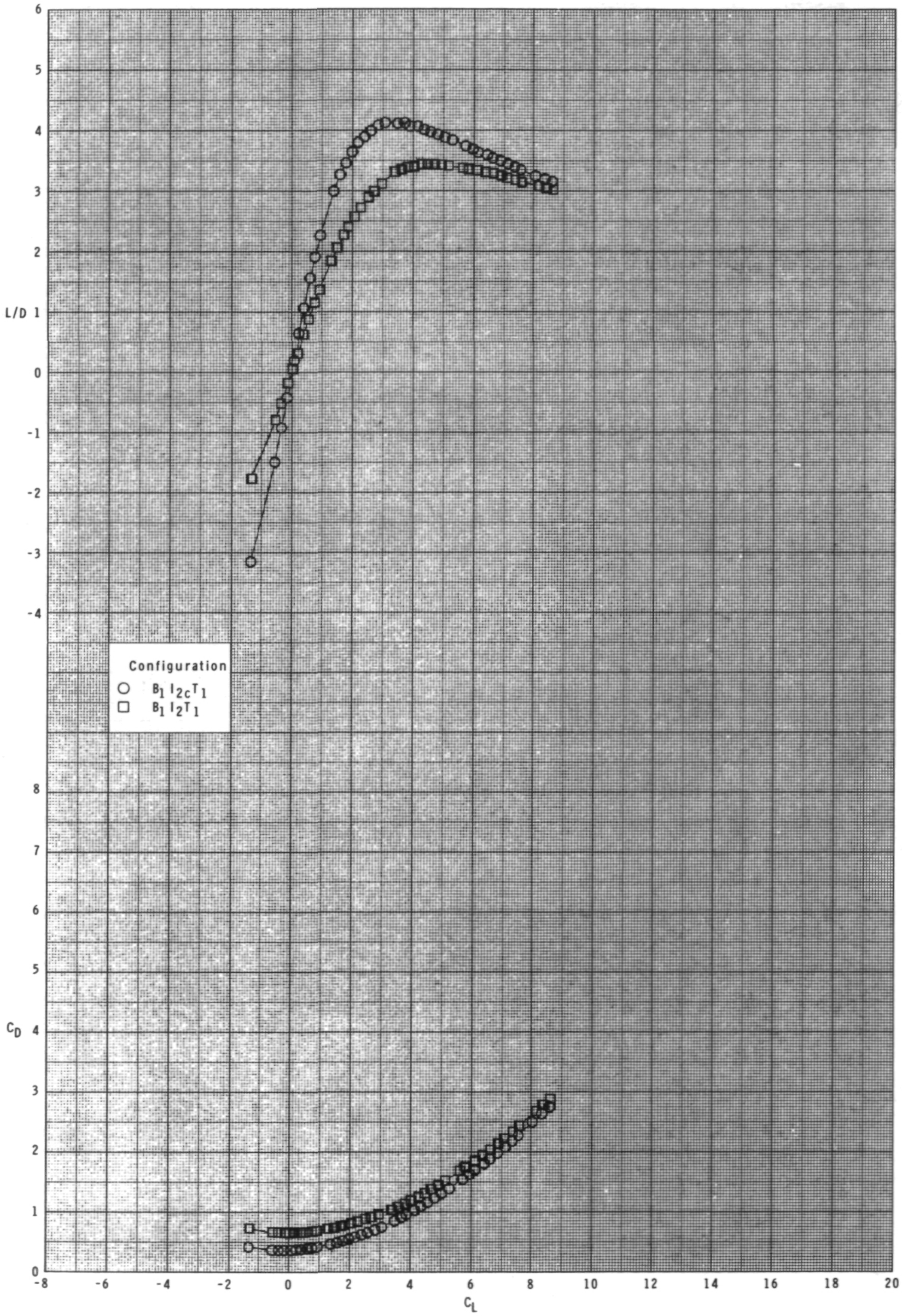

(b) Concluded.

Figure 43.- Continued.

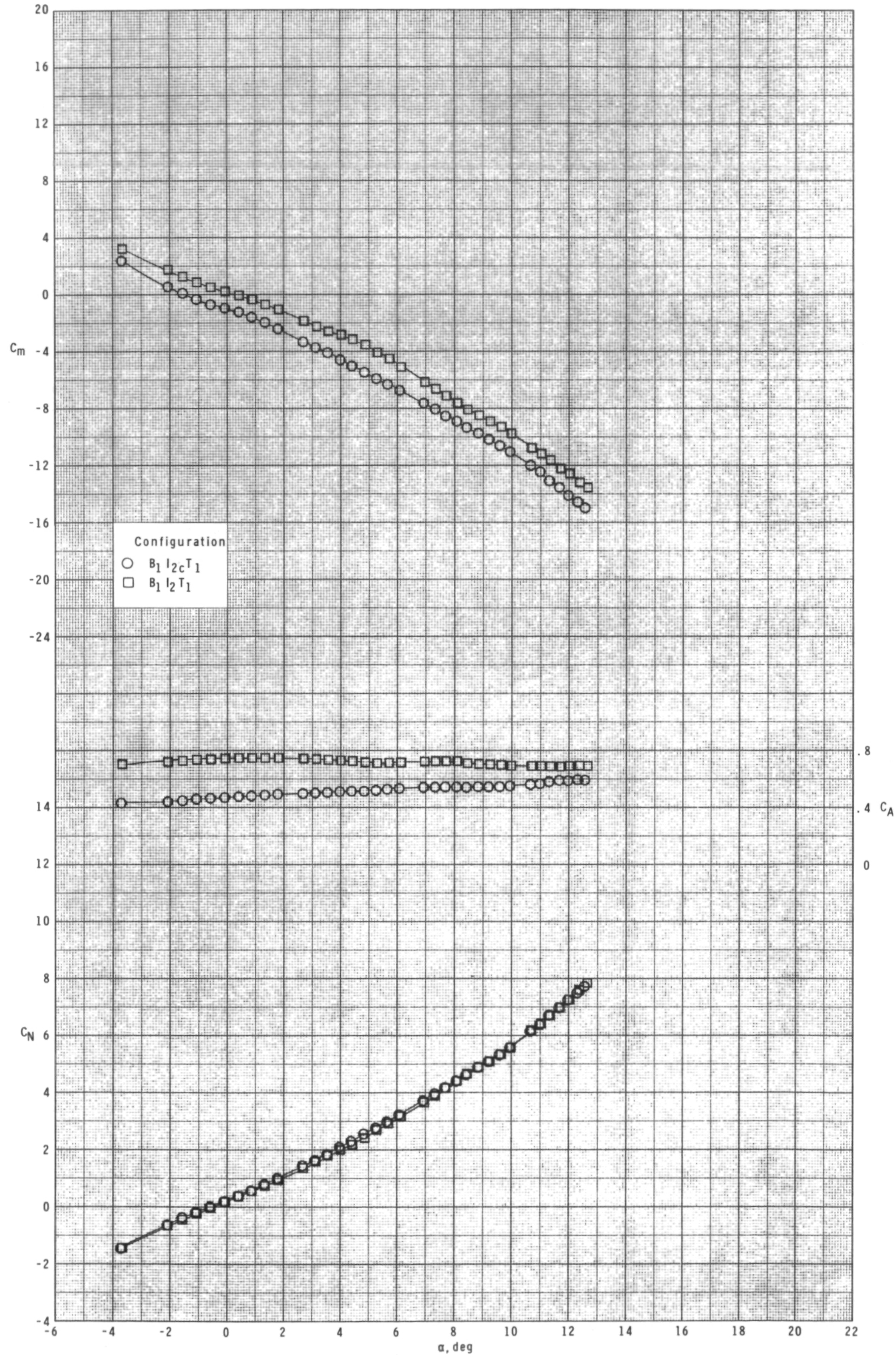

(c) M = 0.95.

Figure 43.- Continued.

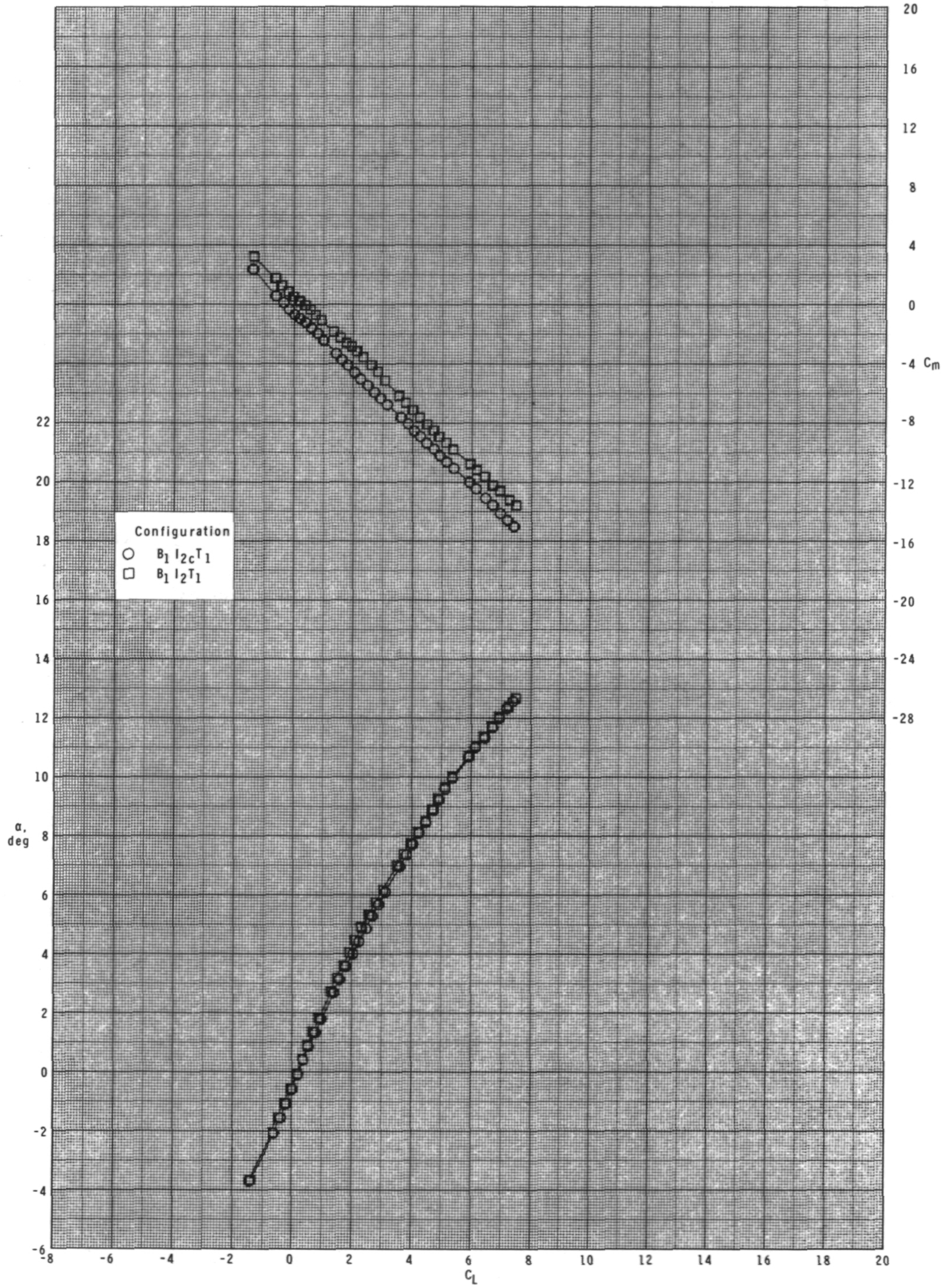

(c) Continued.

Figure 43.- Continued.

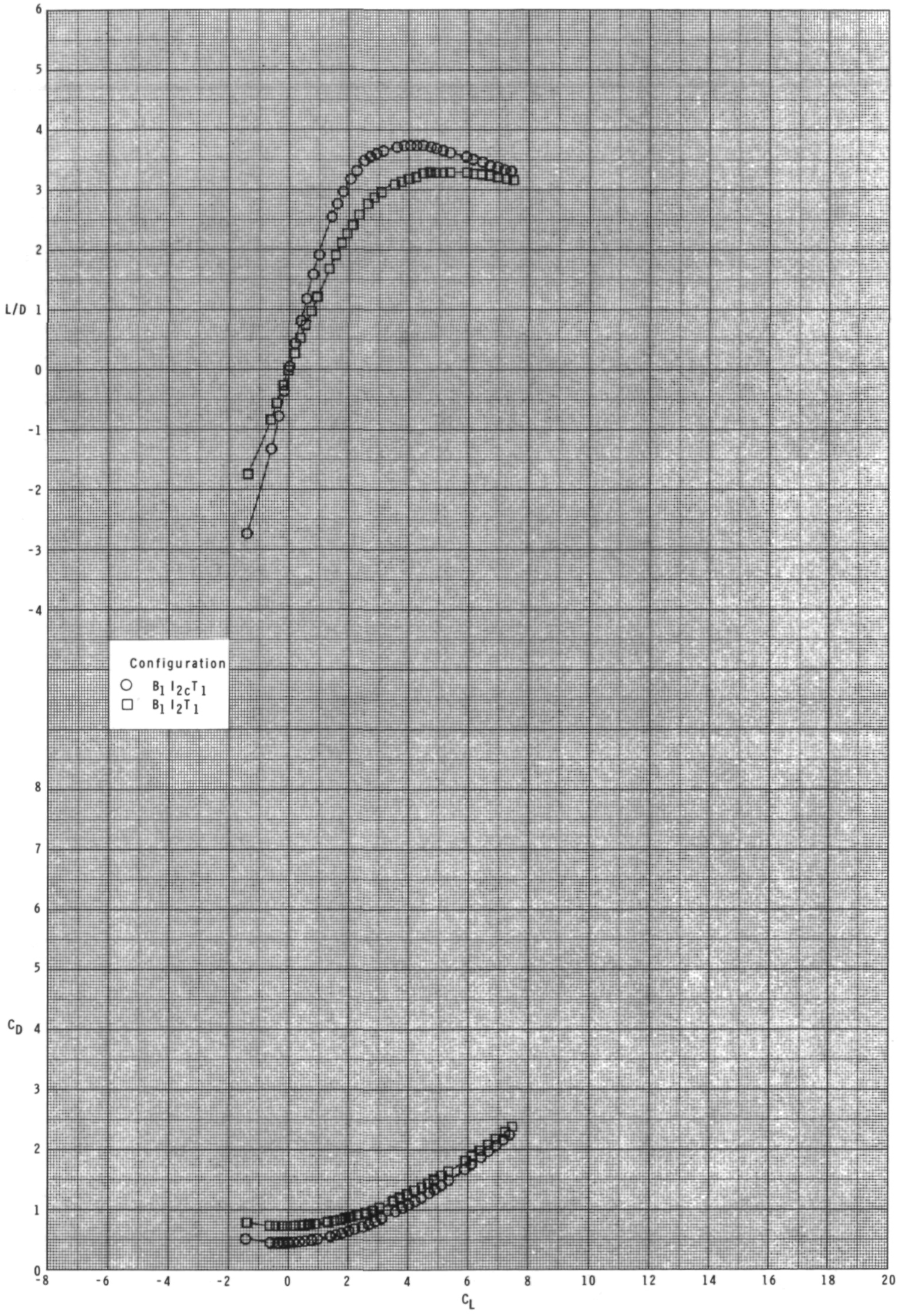

(c) Concluded.

Figure 43.- Concluded.

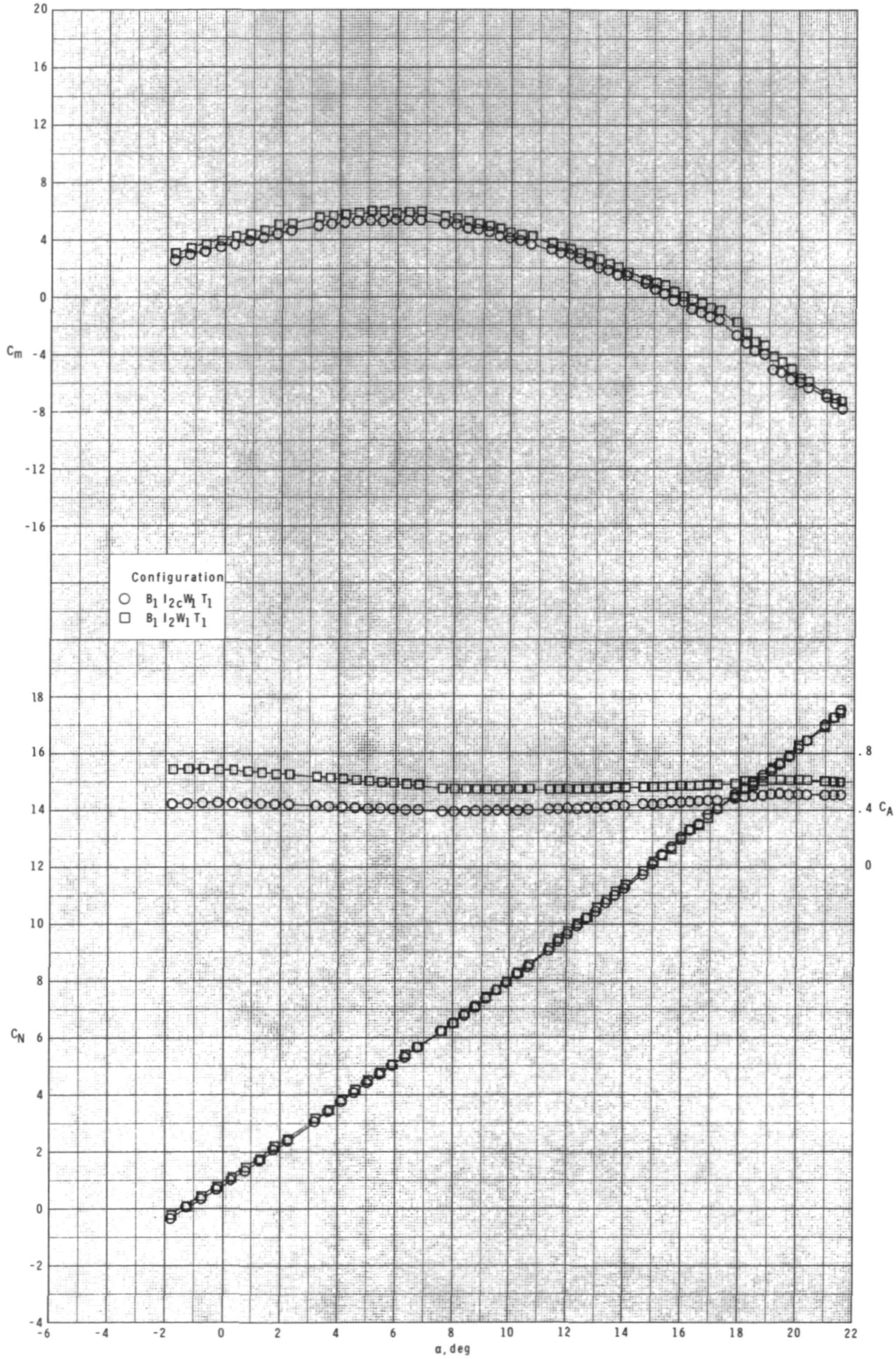

(a) M = 0.60.

Figure 44.- Effect of removing inlet covers on longitudinal aerodynamic characteristics with internal ducts closed and ϕ_I = 115°.

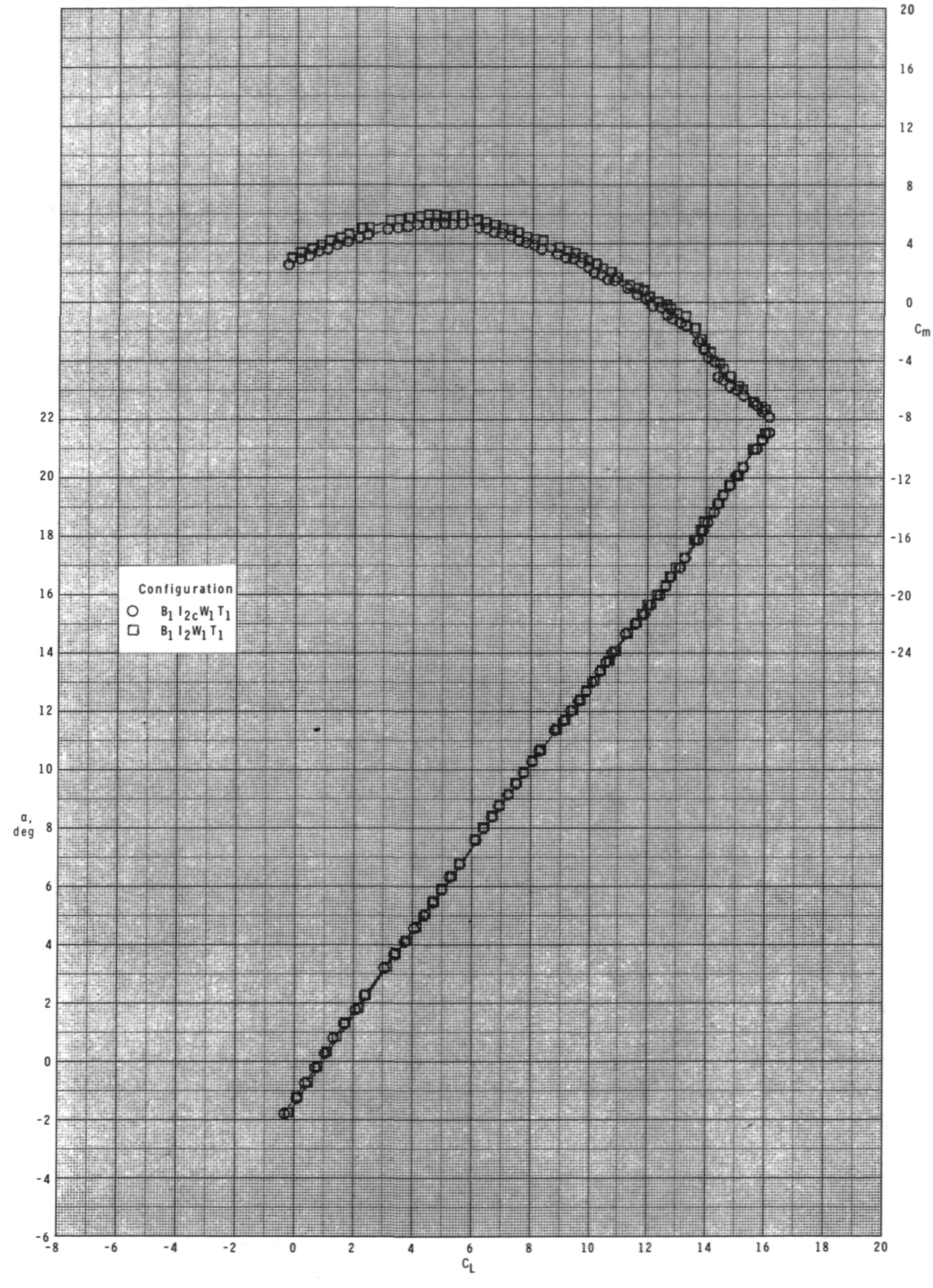

(a) Continued.

Figure 44.- Continued.

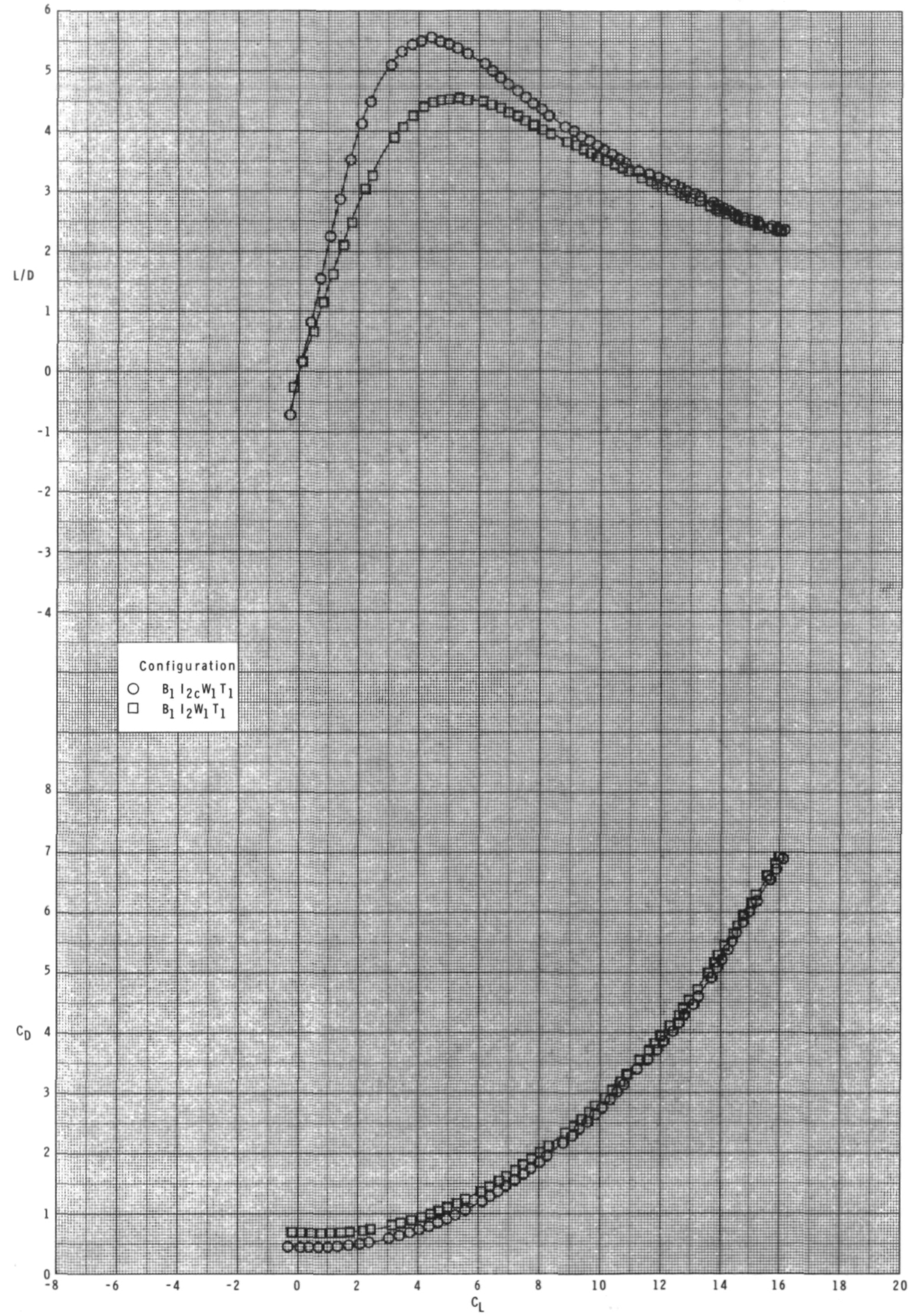

(a) Concluded.

Figure 44.- Continued.

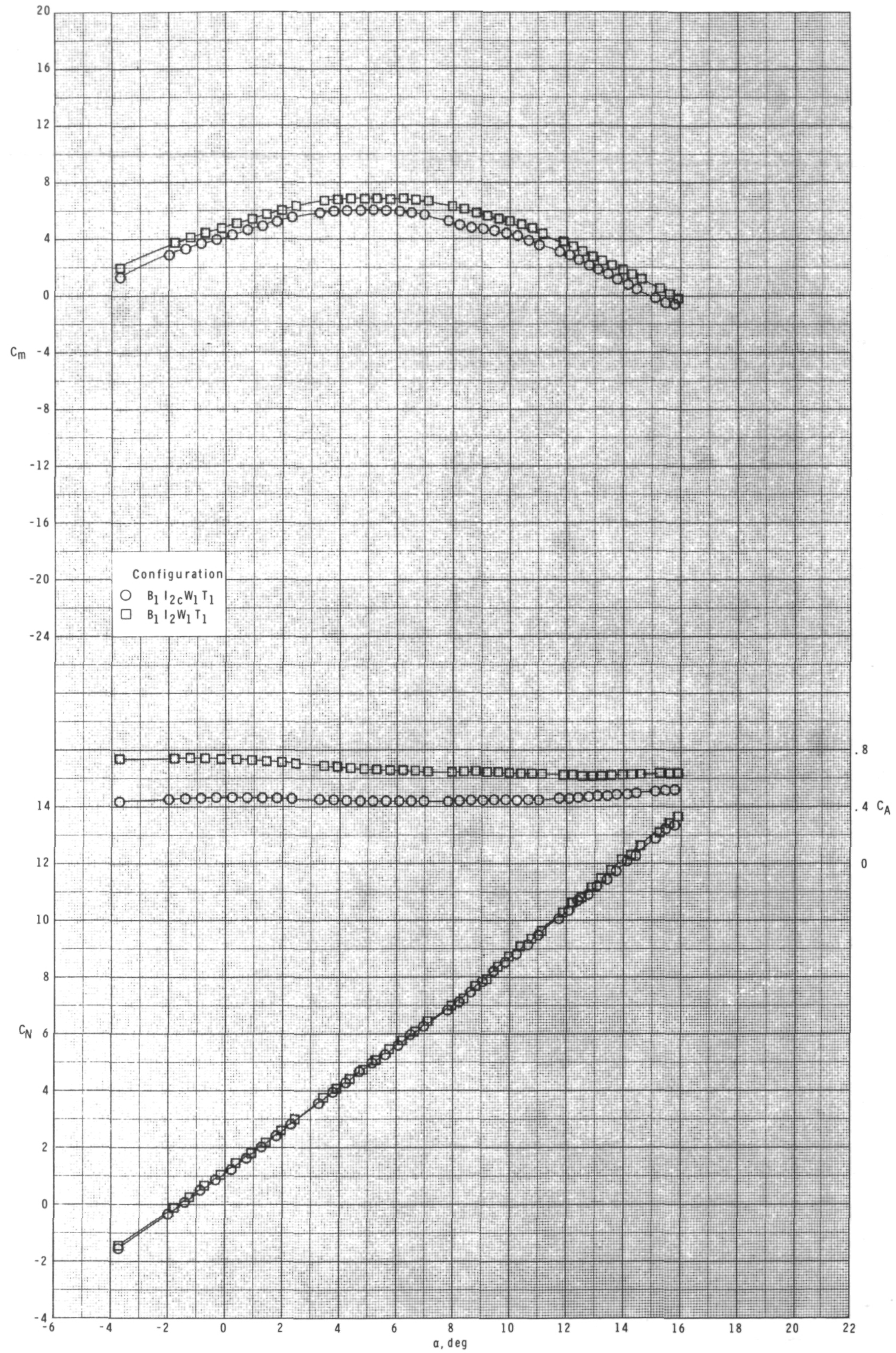

(b) M = 0.80.

Figure 44.- Continued.

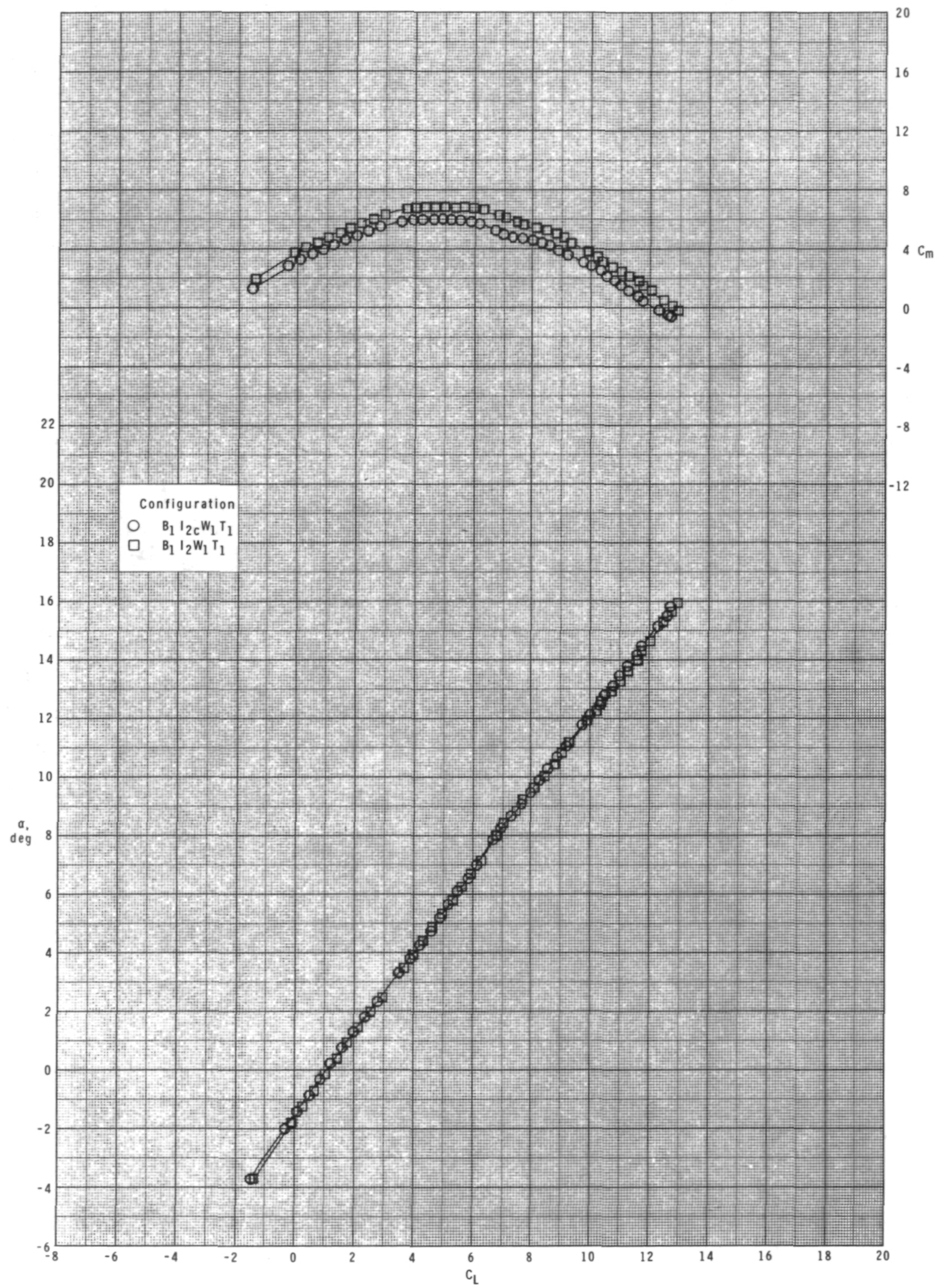

(b) Continued.

Figure 44.- Continued.

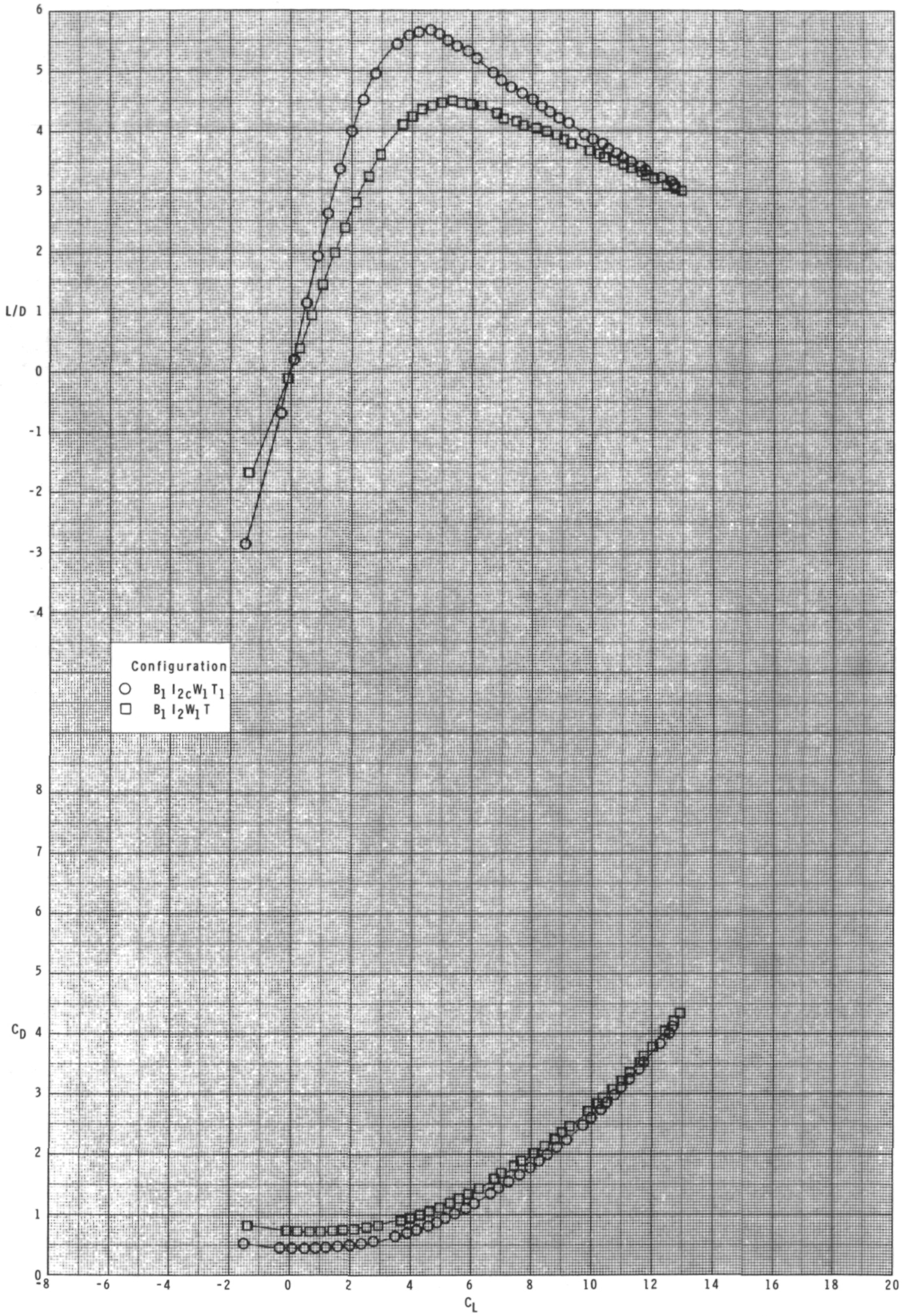

(b) Concluded.

Figure 44.- Continued.

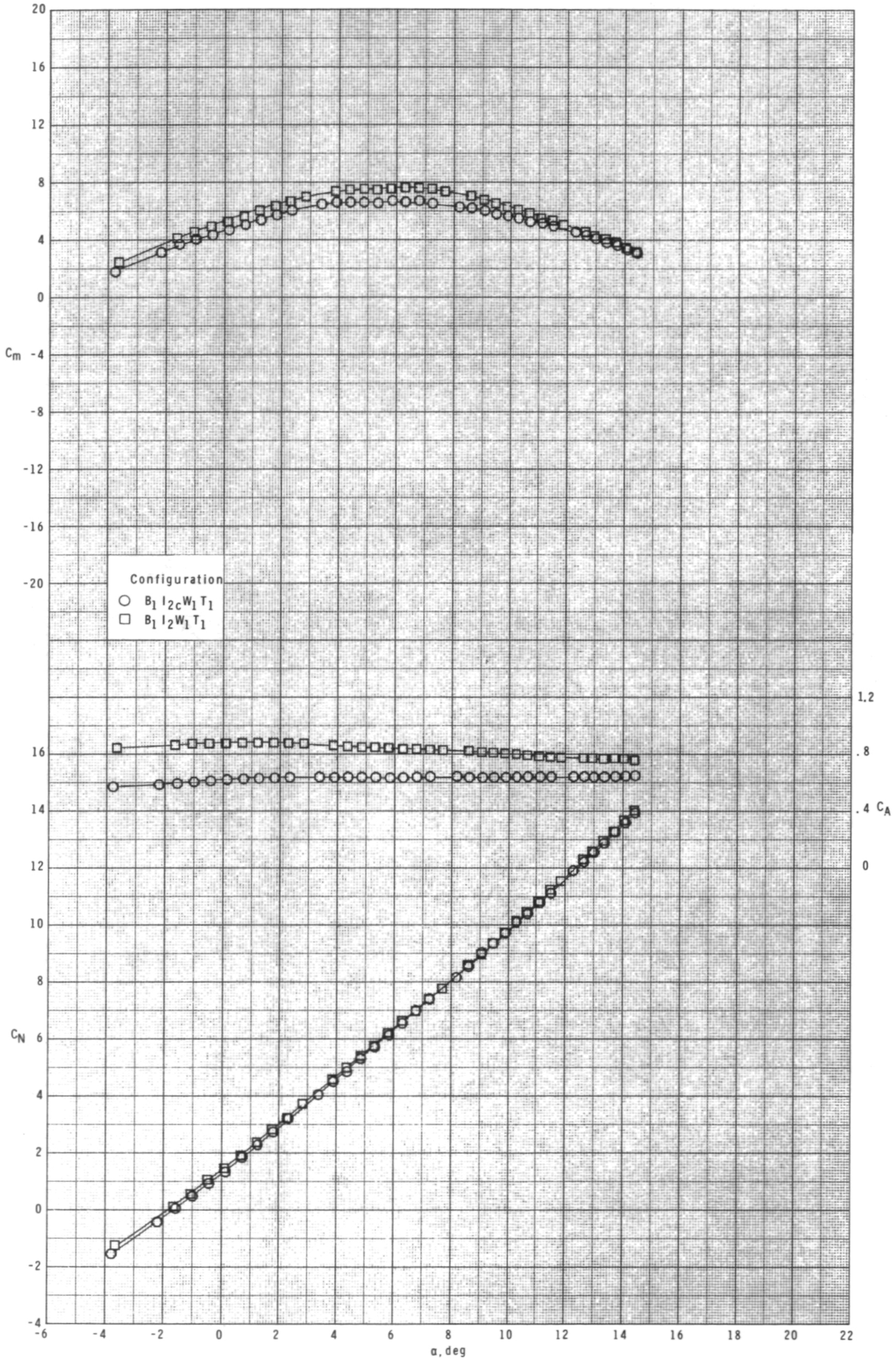

(c) M = 0.95.

Figure 44.- Continued.

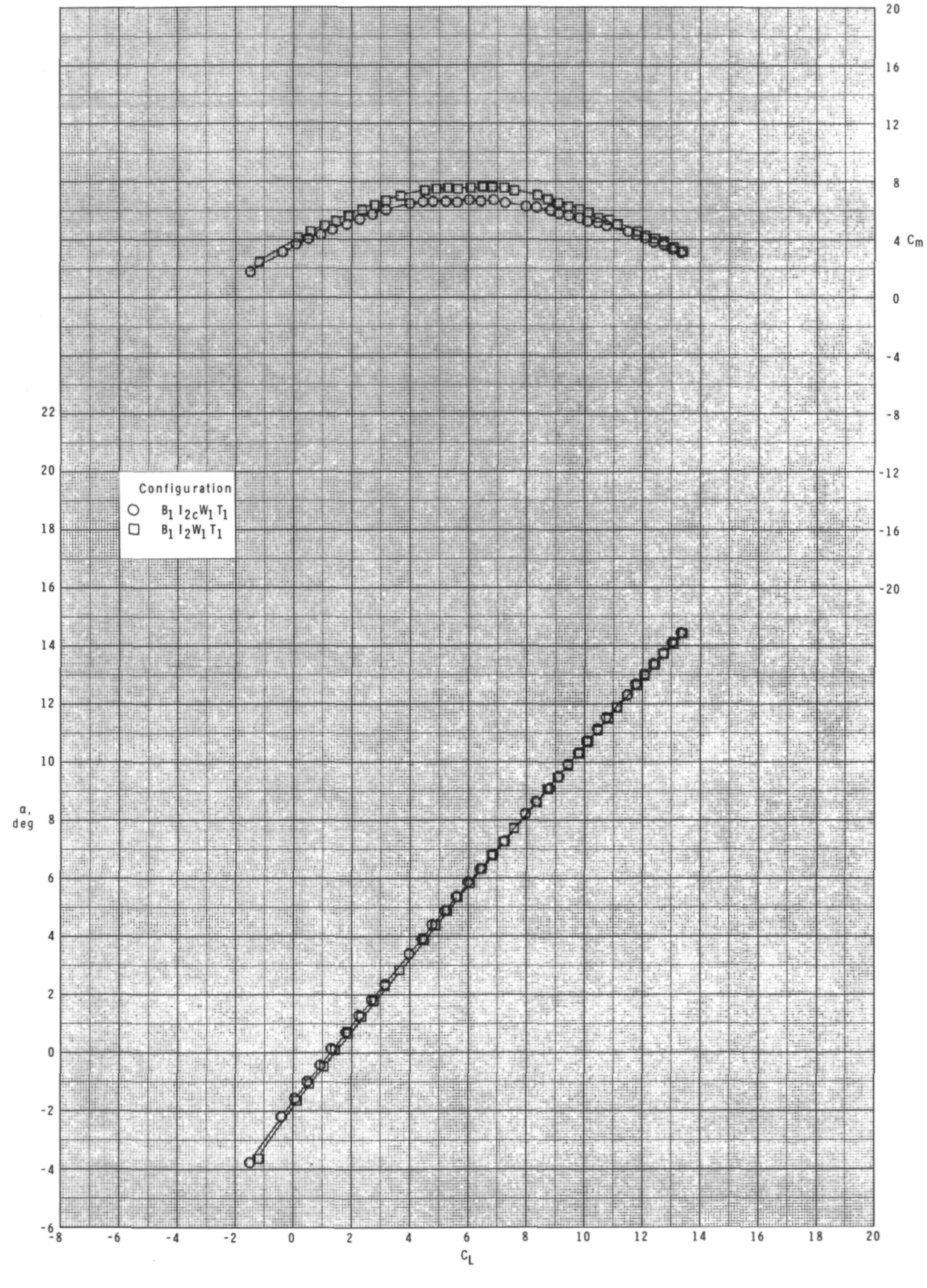

(c) Continued.

Figure 44.- Continued.

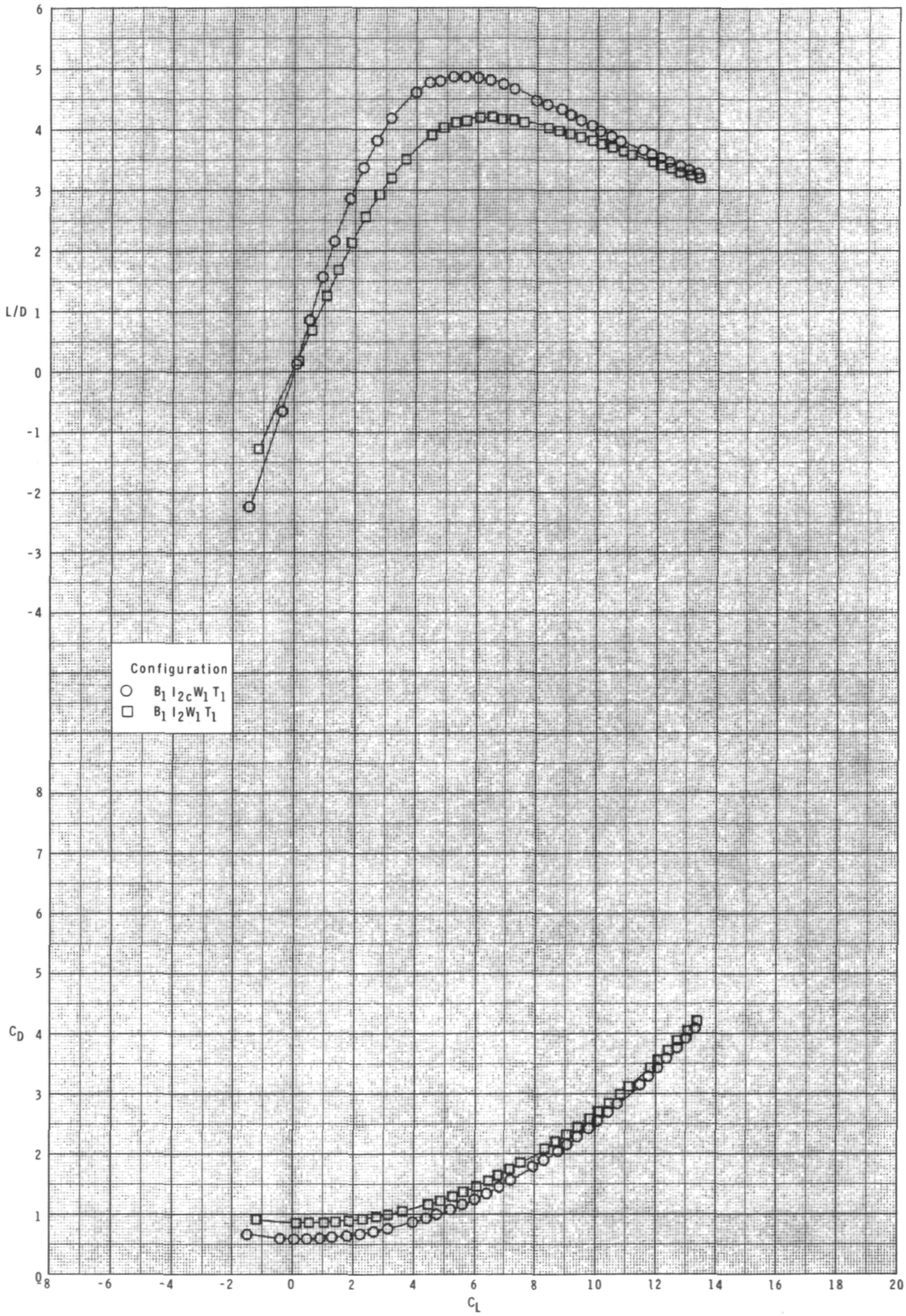

(c) Concluded.

Figure 44.- Concluded.

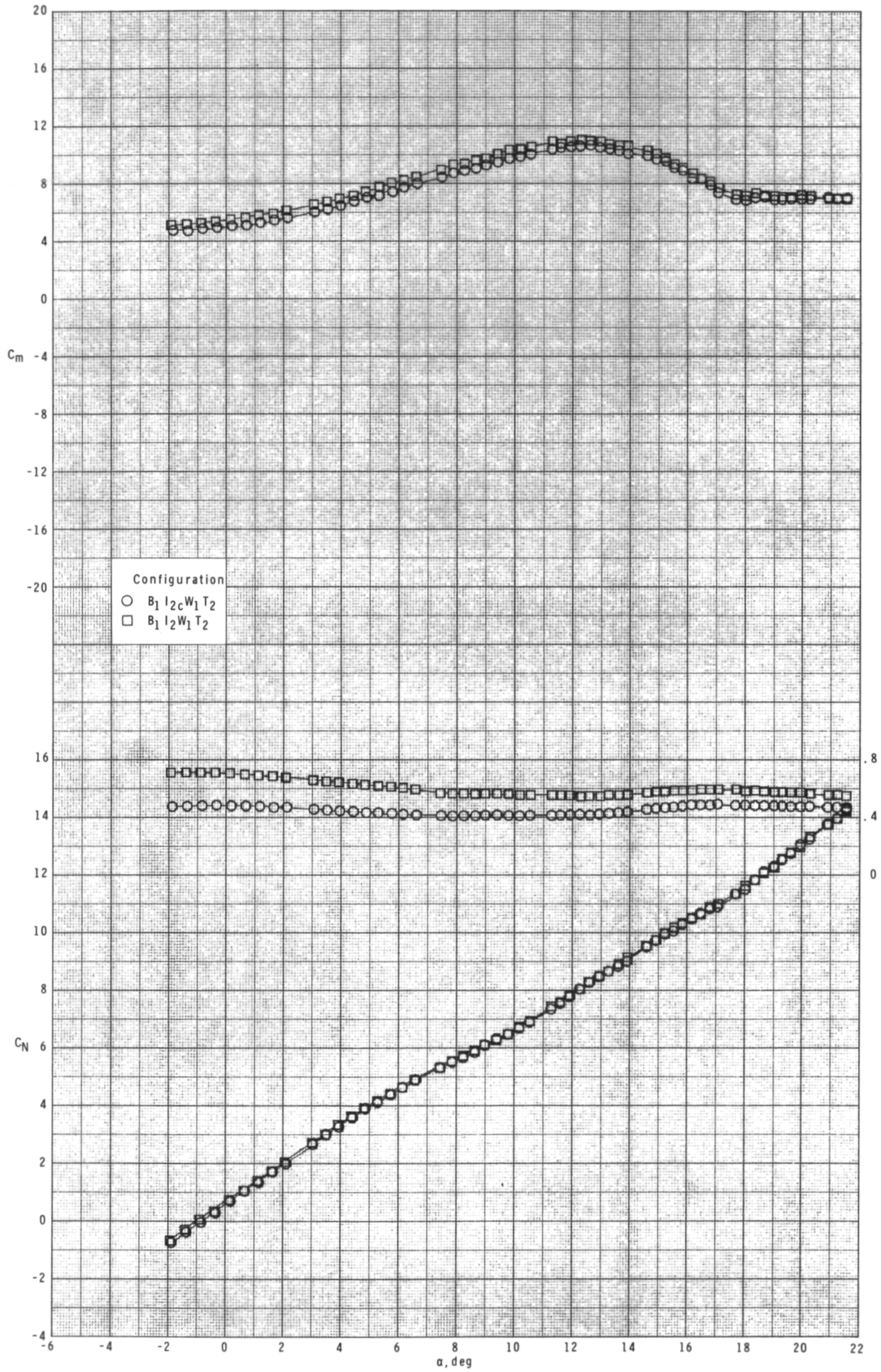

(a) M = 0.60.

Figure 45.- Effect of removing inlet covers on longitudinal aerodynamic characteristics with internal ducts closed and ϕ_I = 135°.

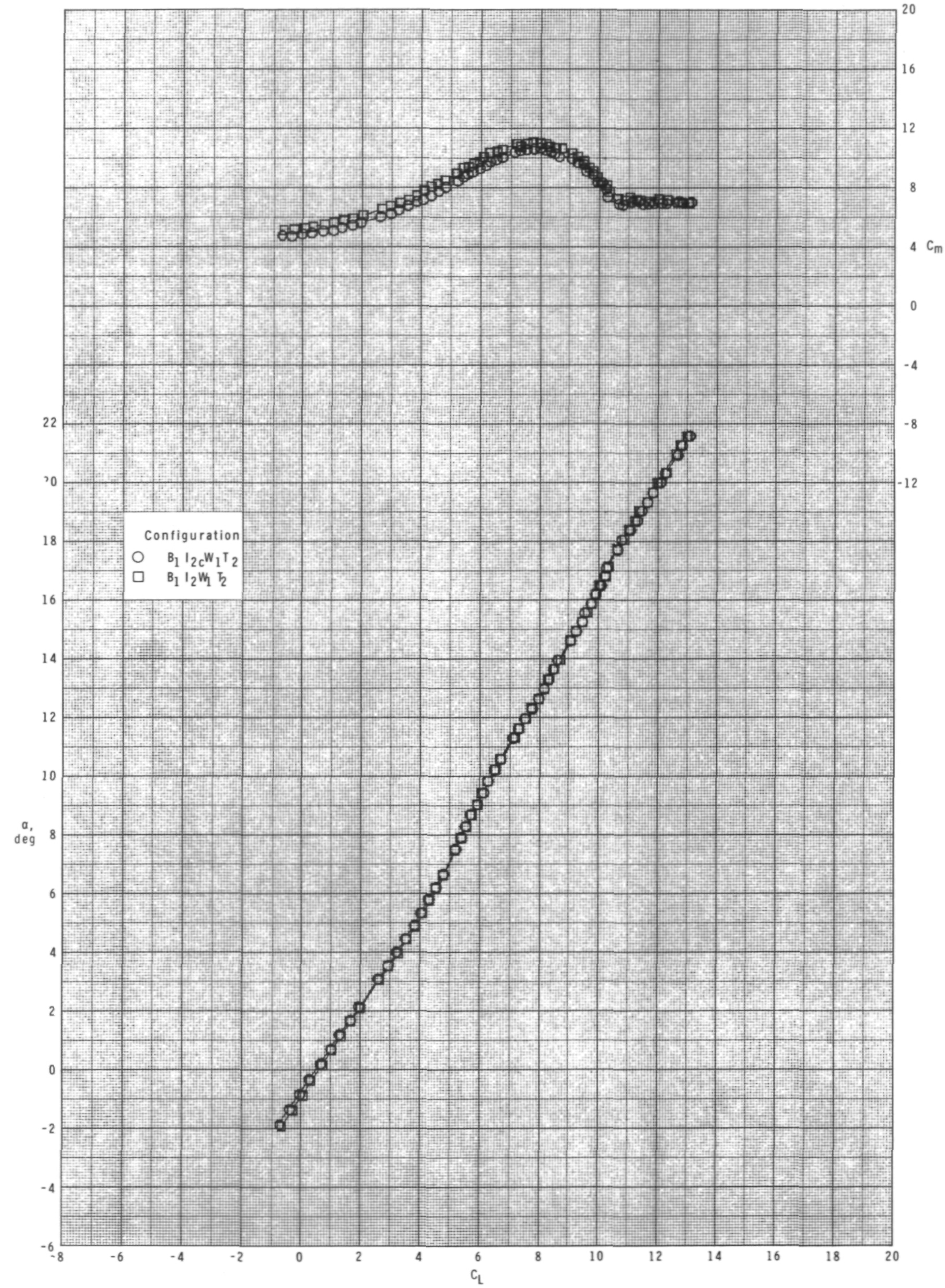

(a) Continued.

Figure 45.- Continued.

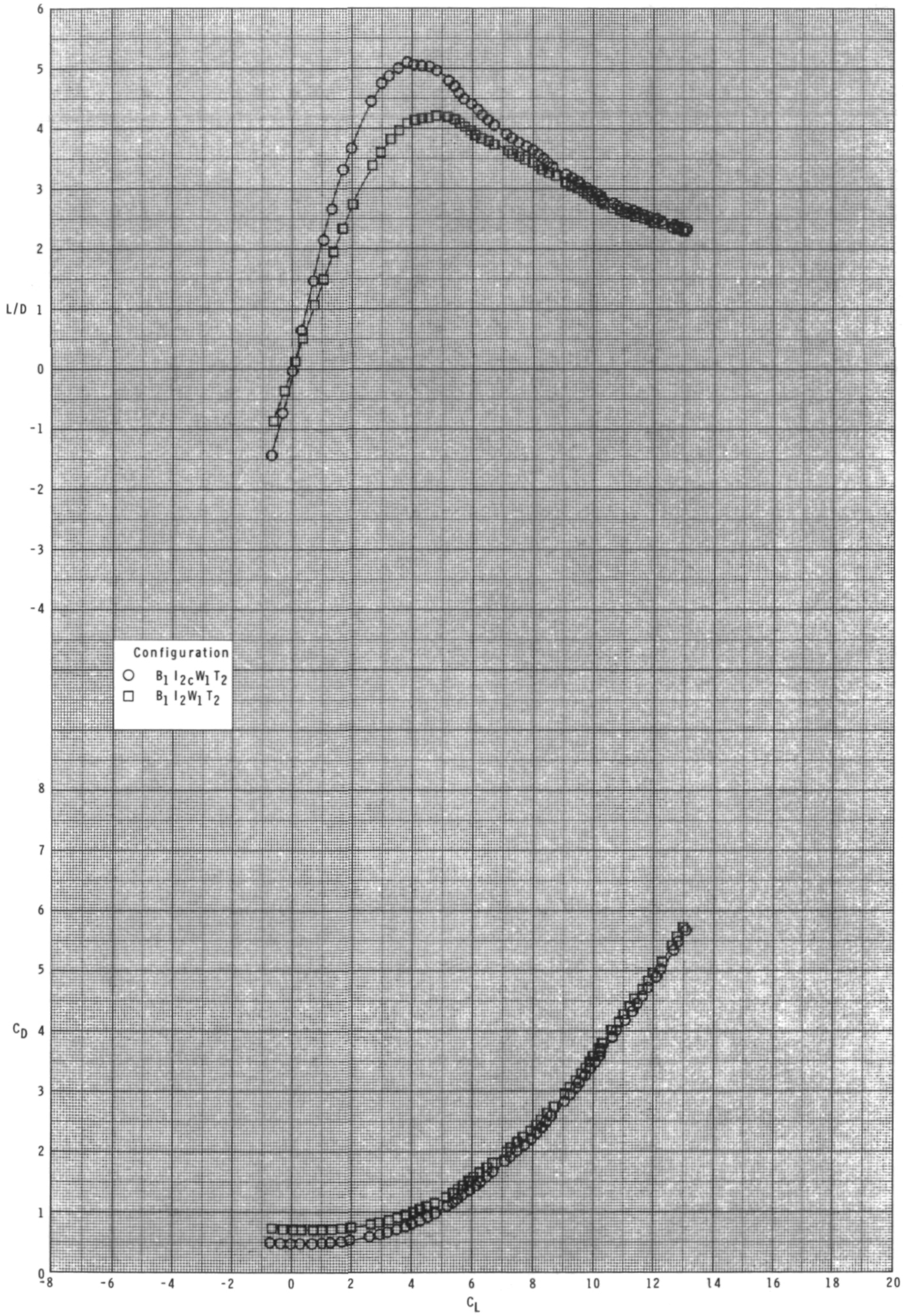

(a) Concluded.

Figure 45.- Continued.

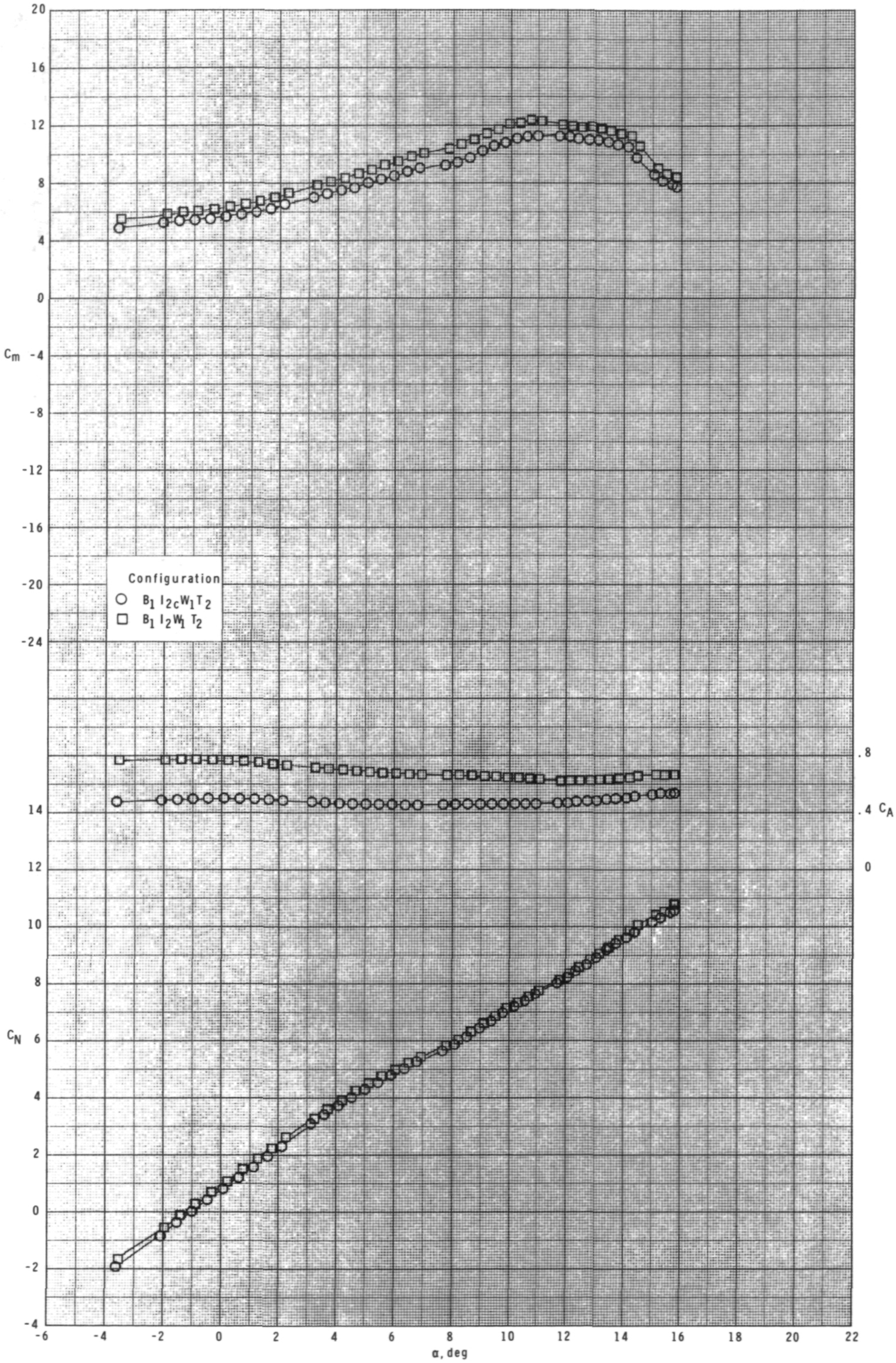

(b) M = 0.80.

Figure 45.- Continued.

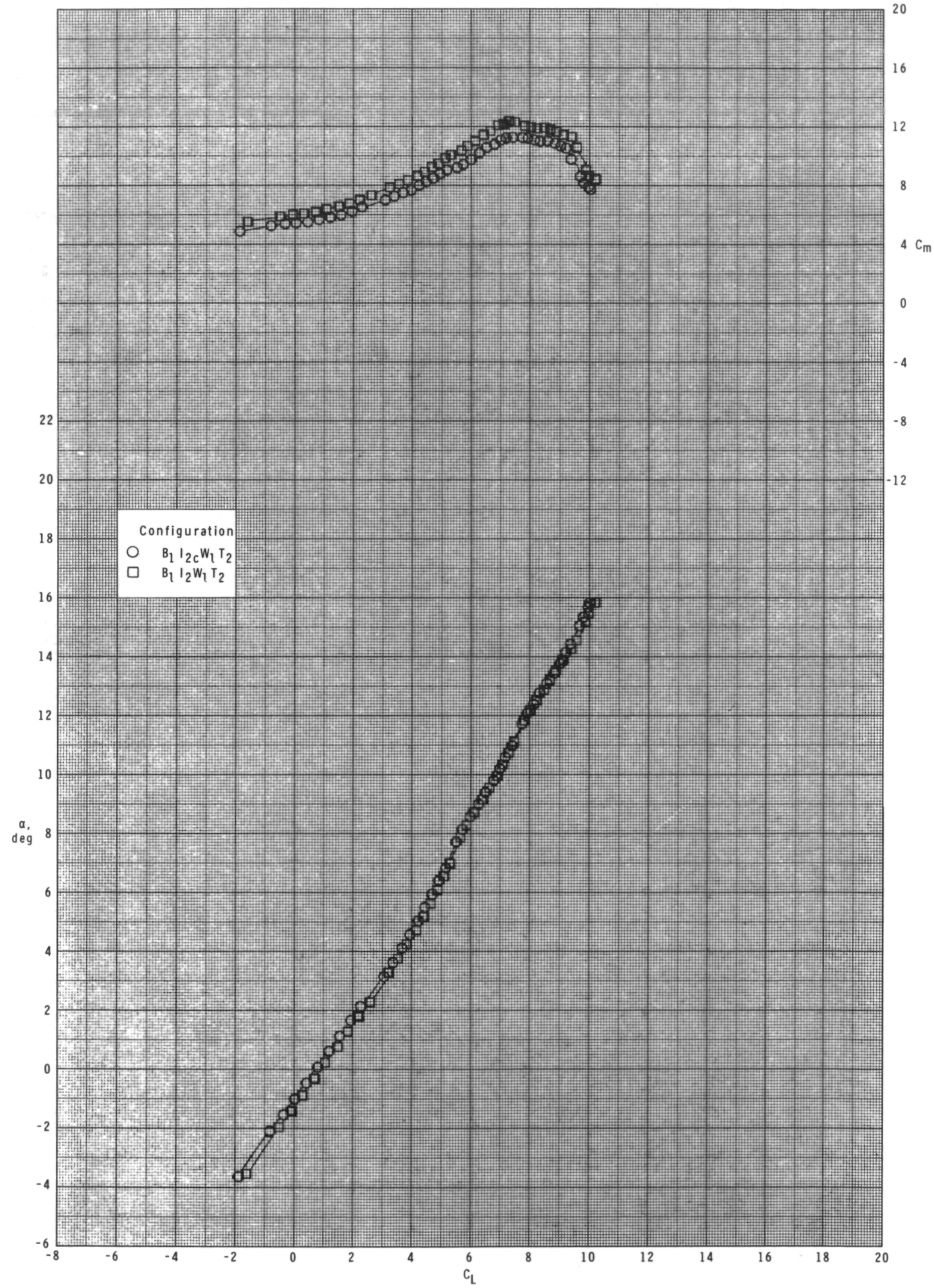

(b) Continued.

Figure 45.- Continued.

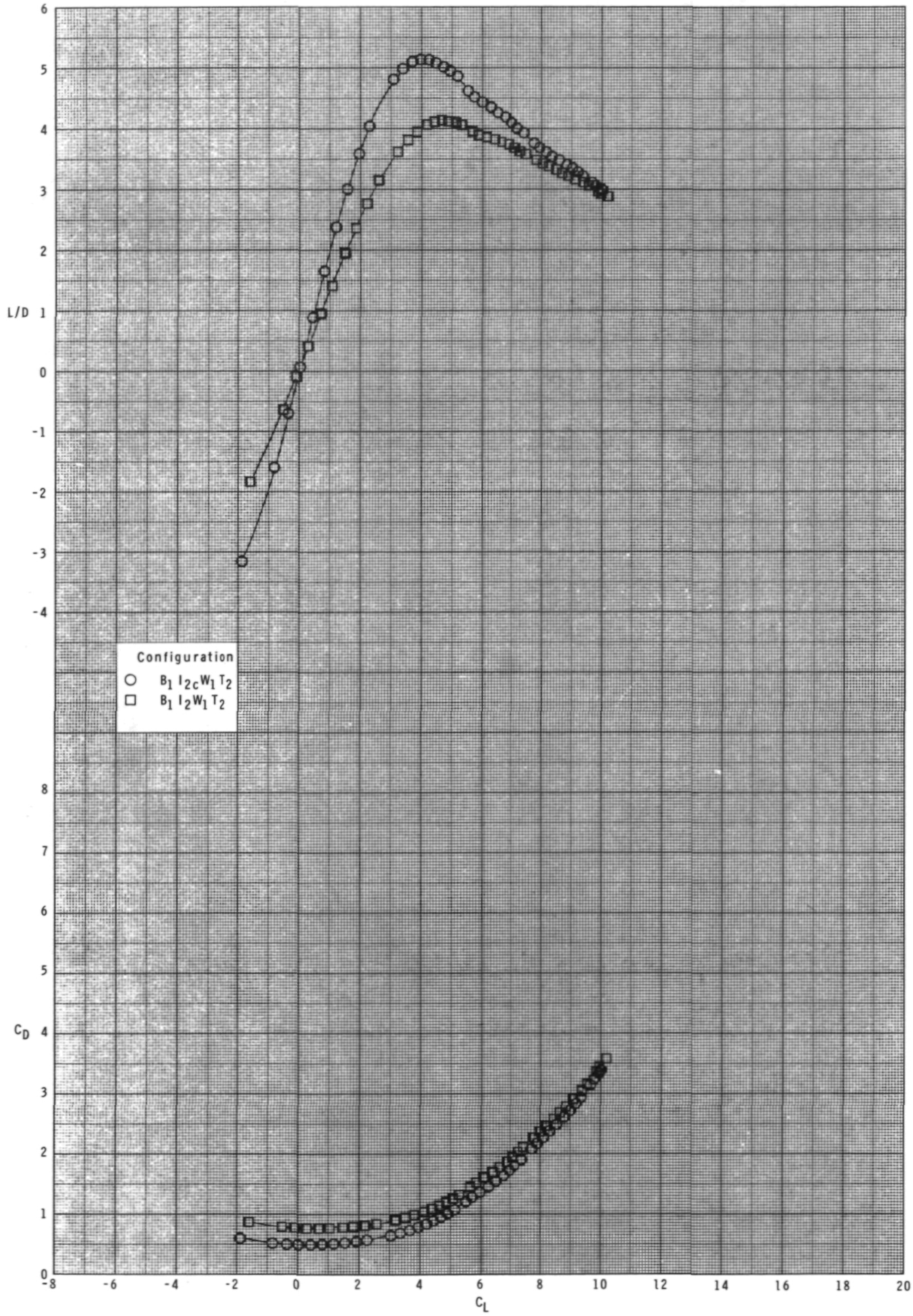

(b) Concluded.

Figure 45.- Continued.

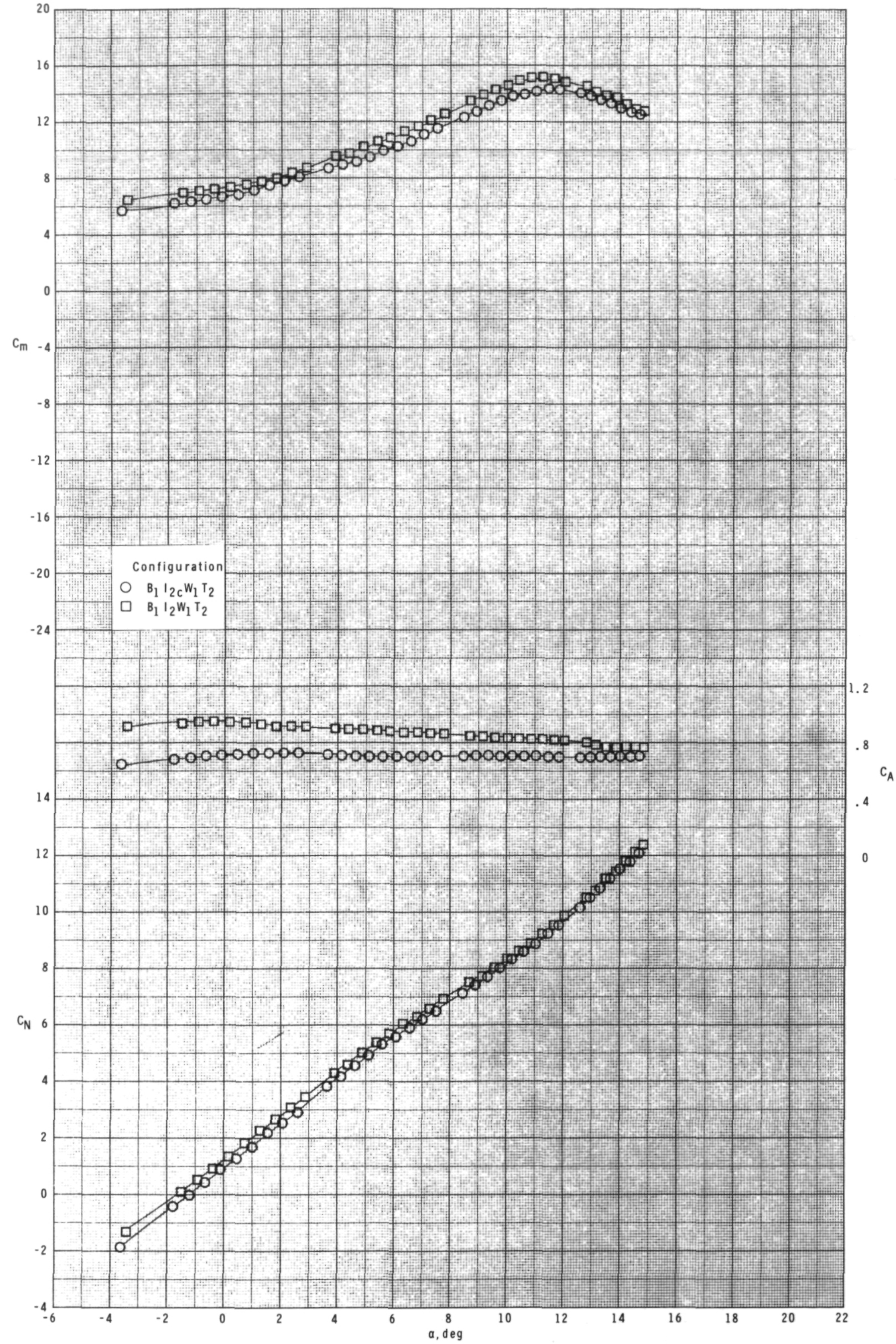

(c) M = 0.95.

Figure 45.- Continued.

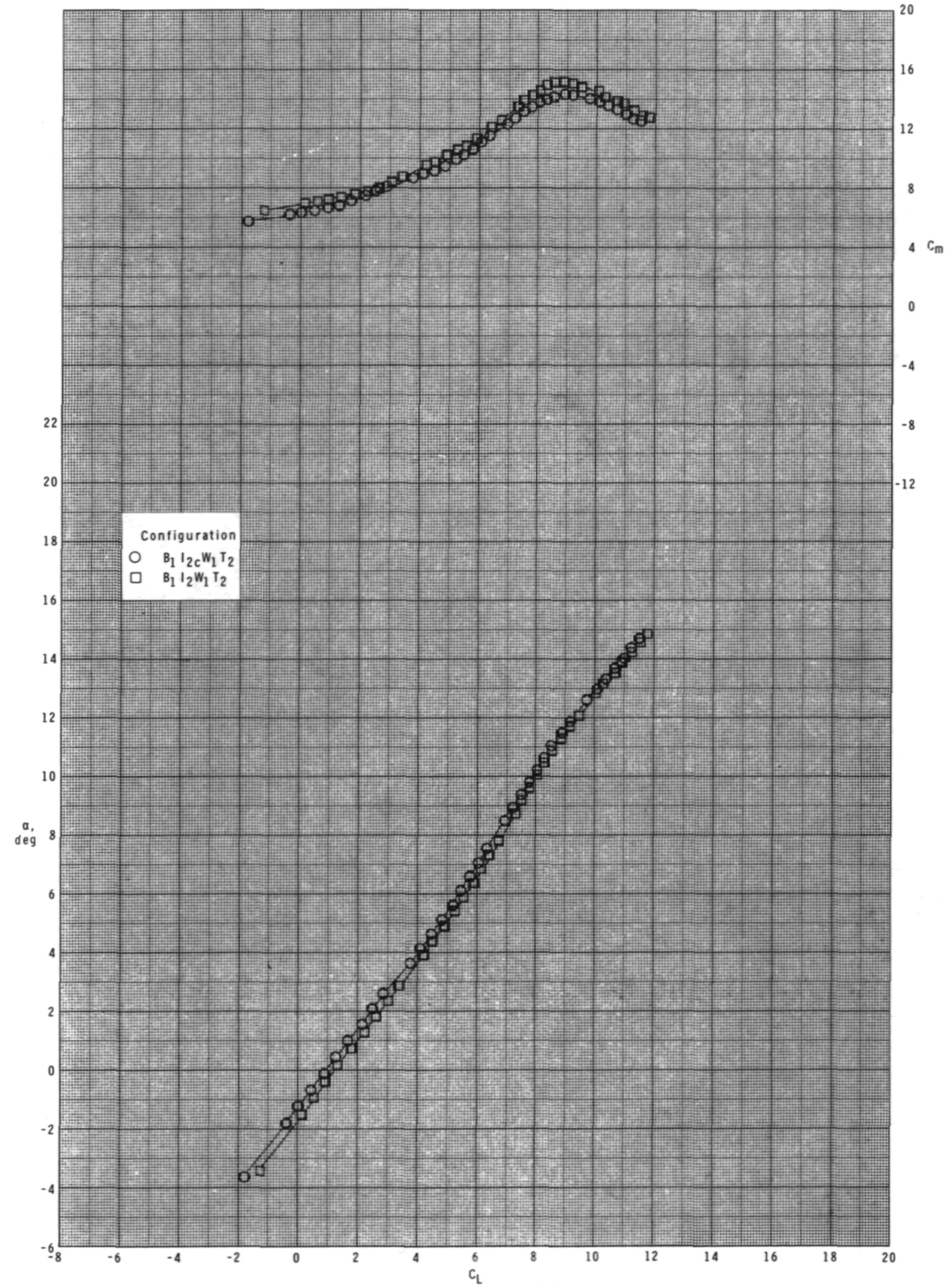

(c) Continued.

Figure 45.- Continued.

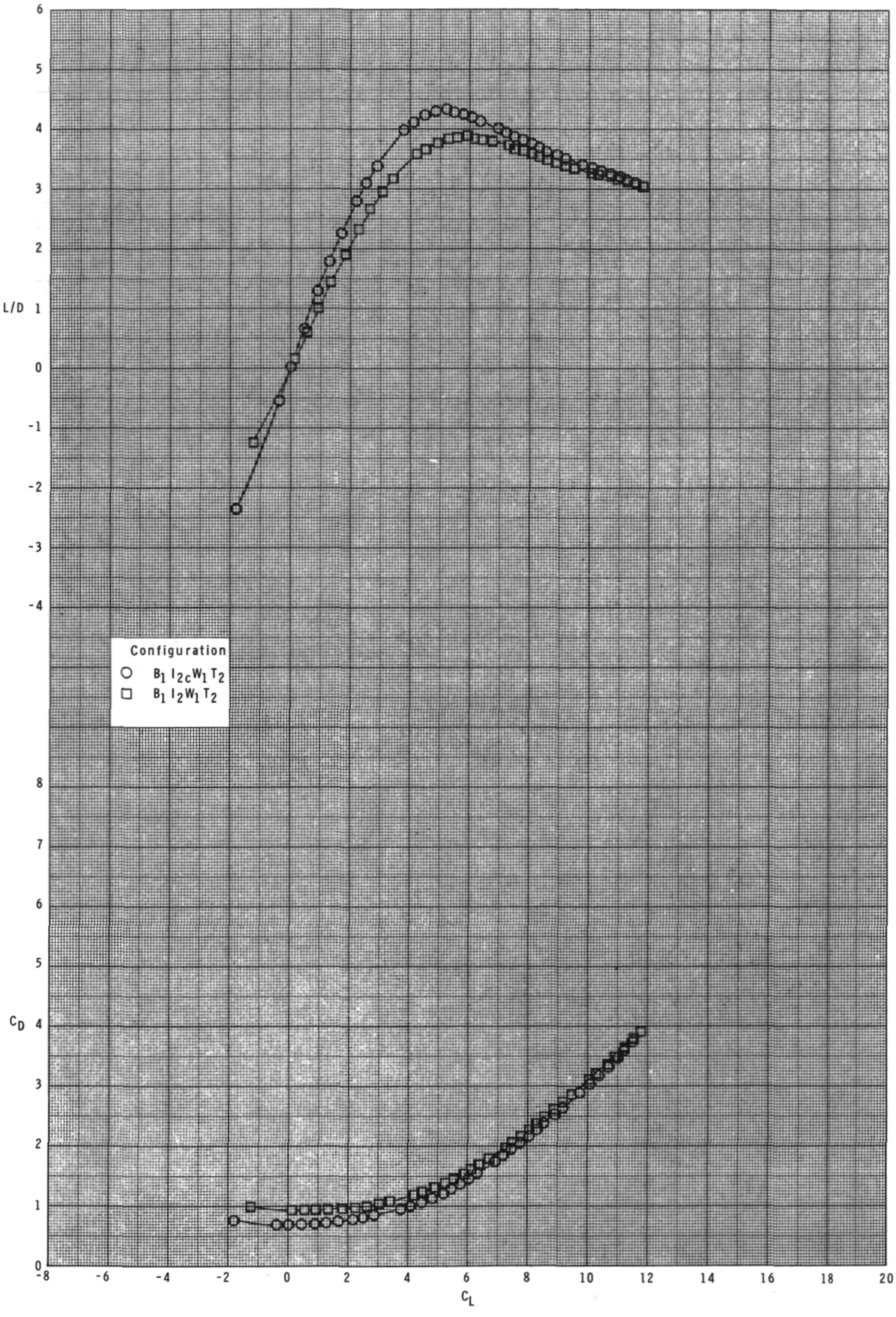

(c) Concluded.

Figure 45.- Concluded.

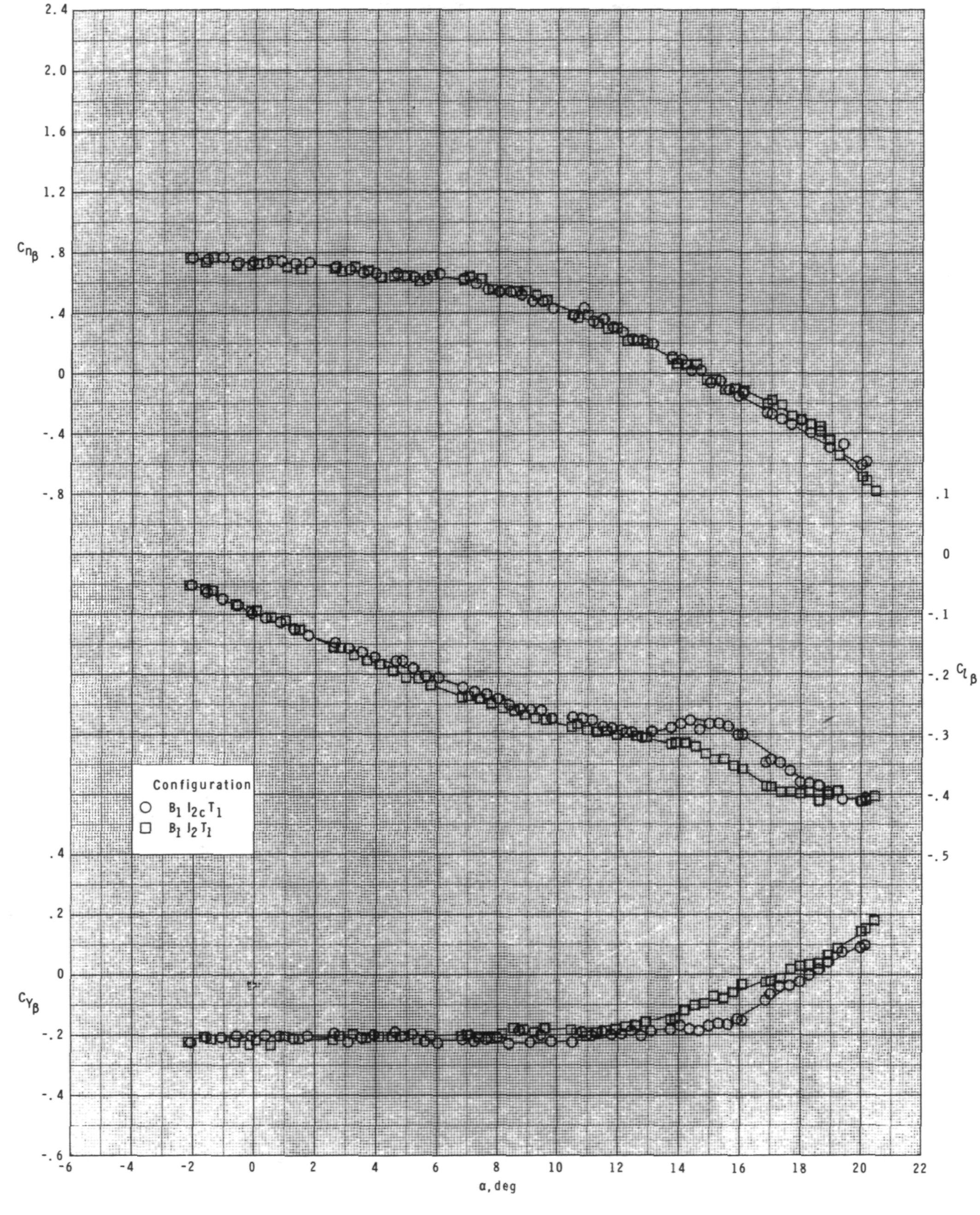

(a) M = 0.60.

Figure 46.- Effect of removing inlet covers on lateral-directional stability with internal ducts closed and $\phi_I = 90°$.

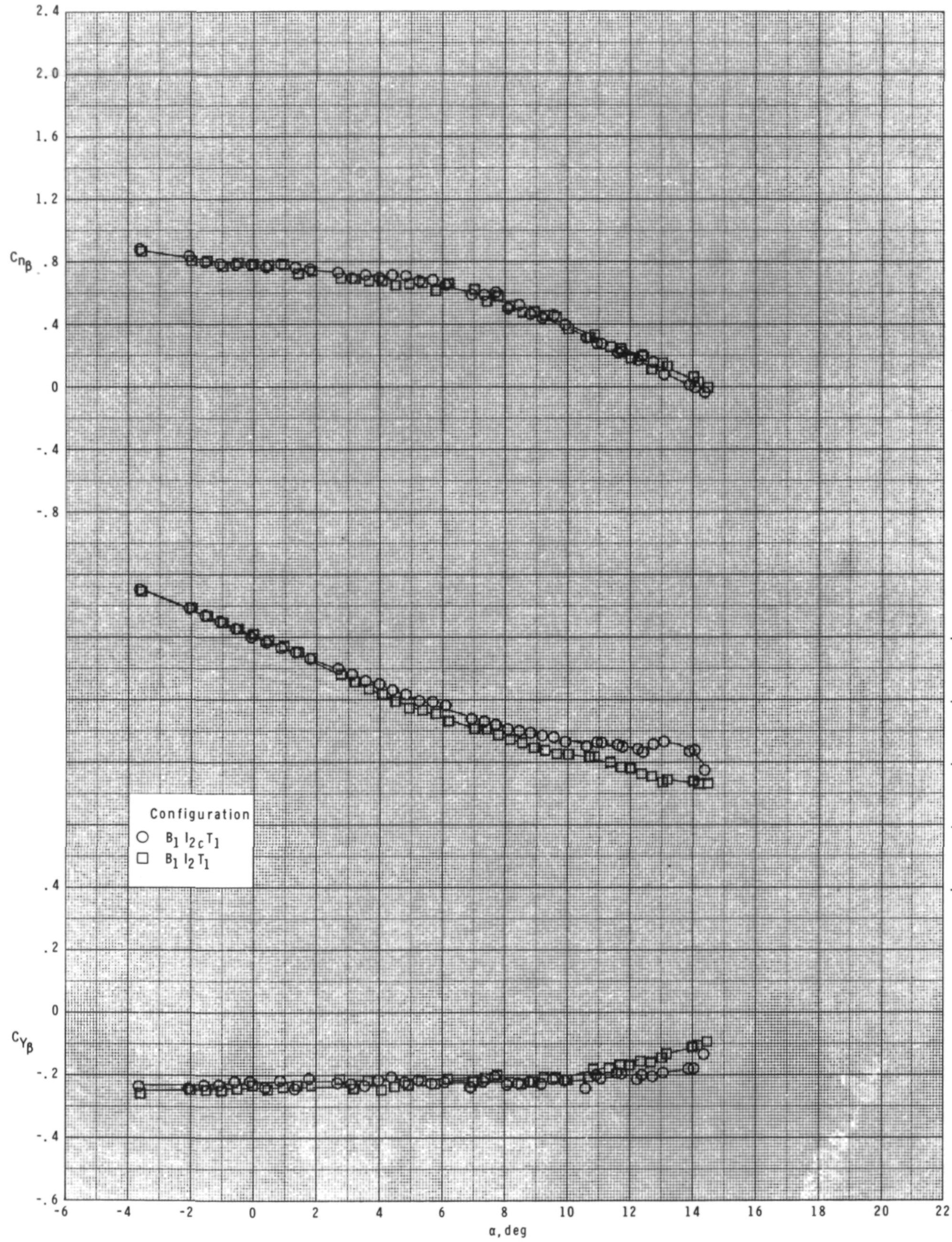

(b) M = 0.80.

Figure 46.- Continued.

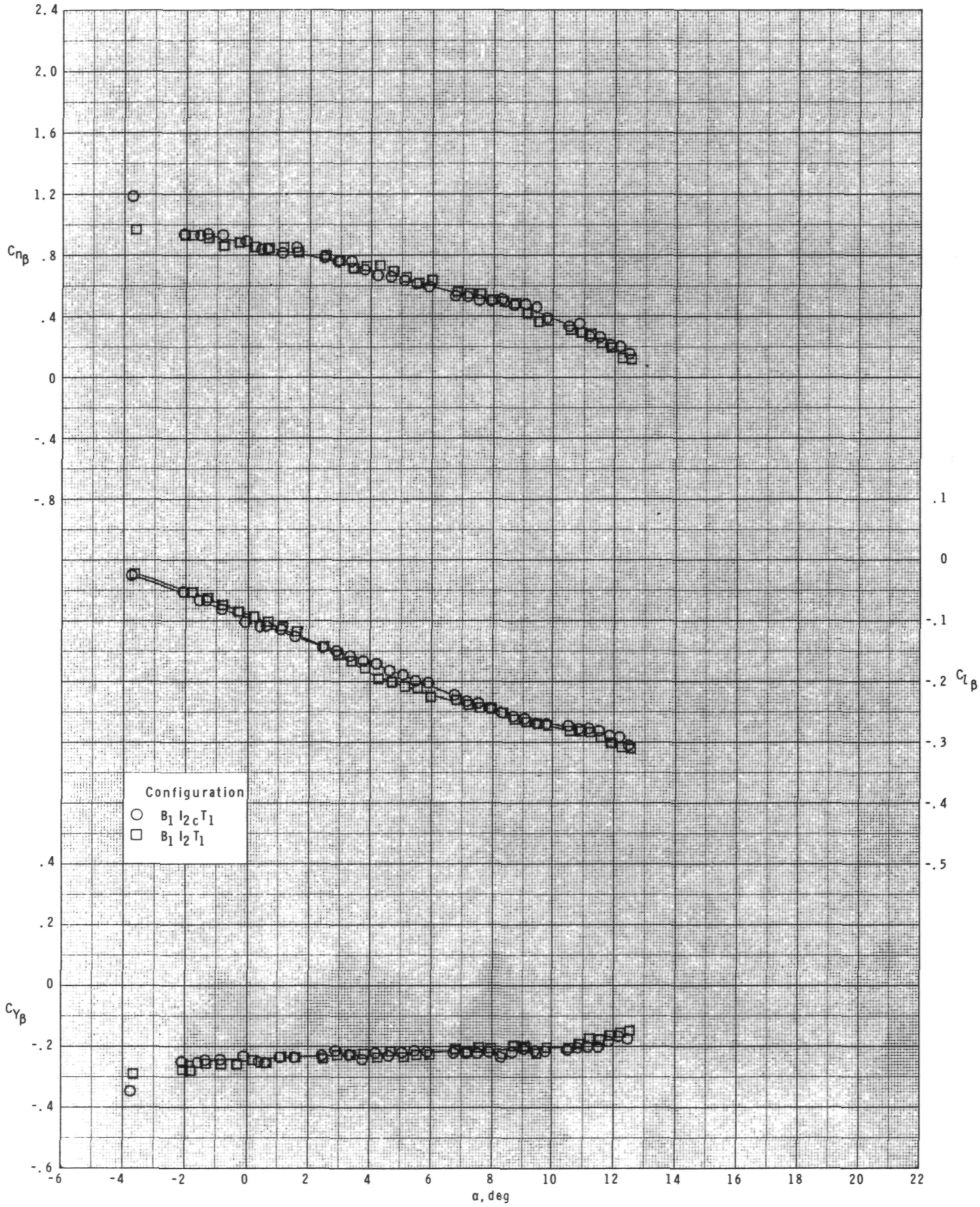

(c) M = 0.95.

Figure 46.- Concluded.

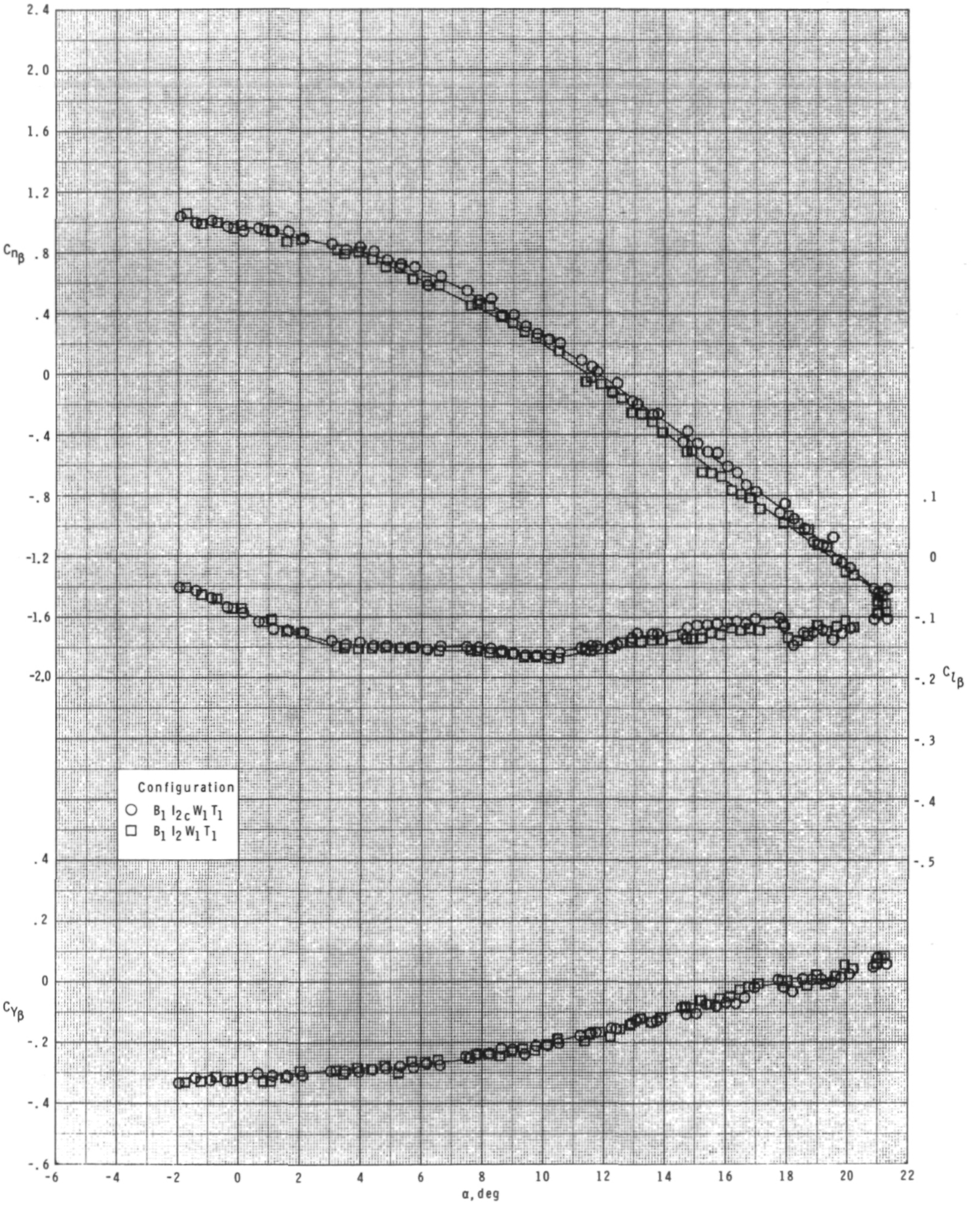

(a) M = 0.60.

Figure 47.- Effect of removing inlet covers on lateral-directional stability with internal ducts closed and $\phi_I = 115°$.

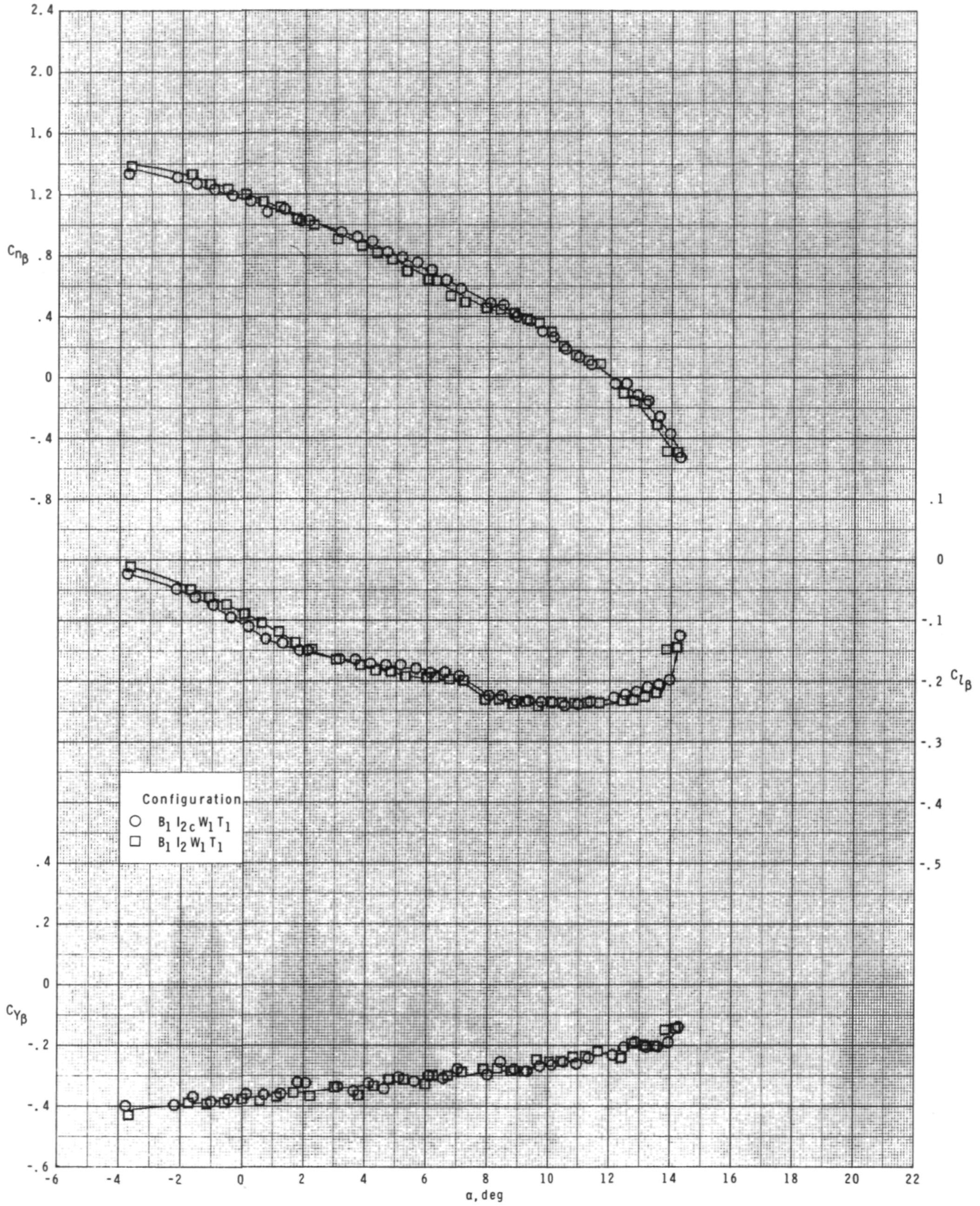

(b) M = 0.80.

Figure 47.- Continued.

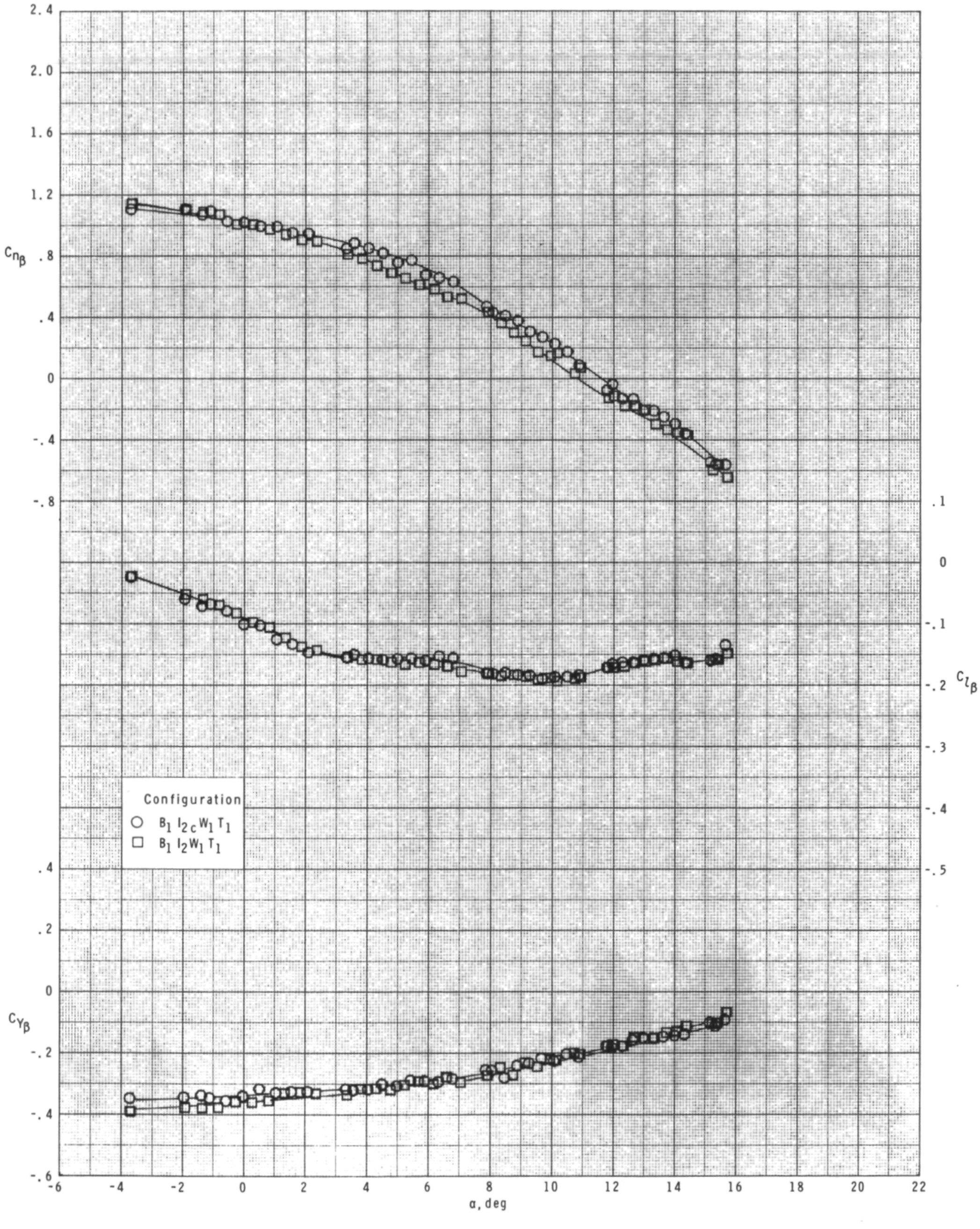

(c) M = 0.95.

Figure 47.- Concluded.

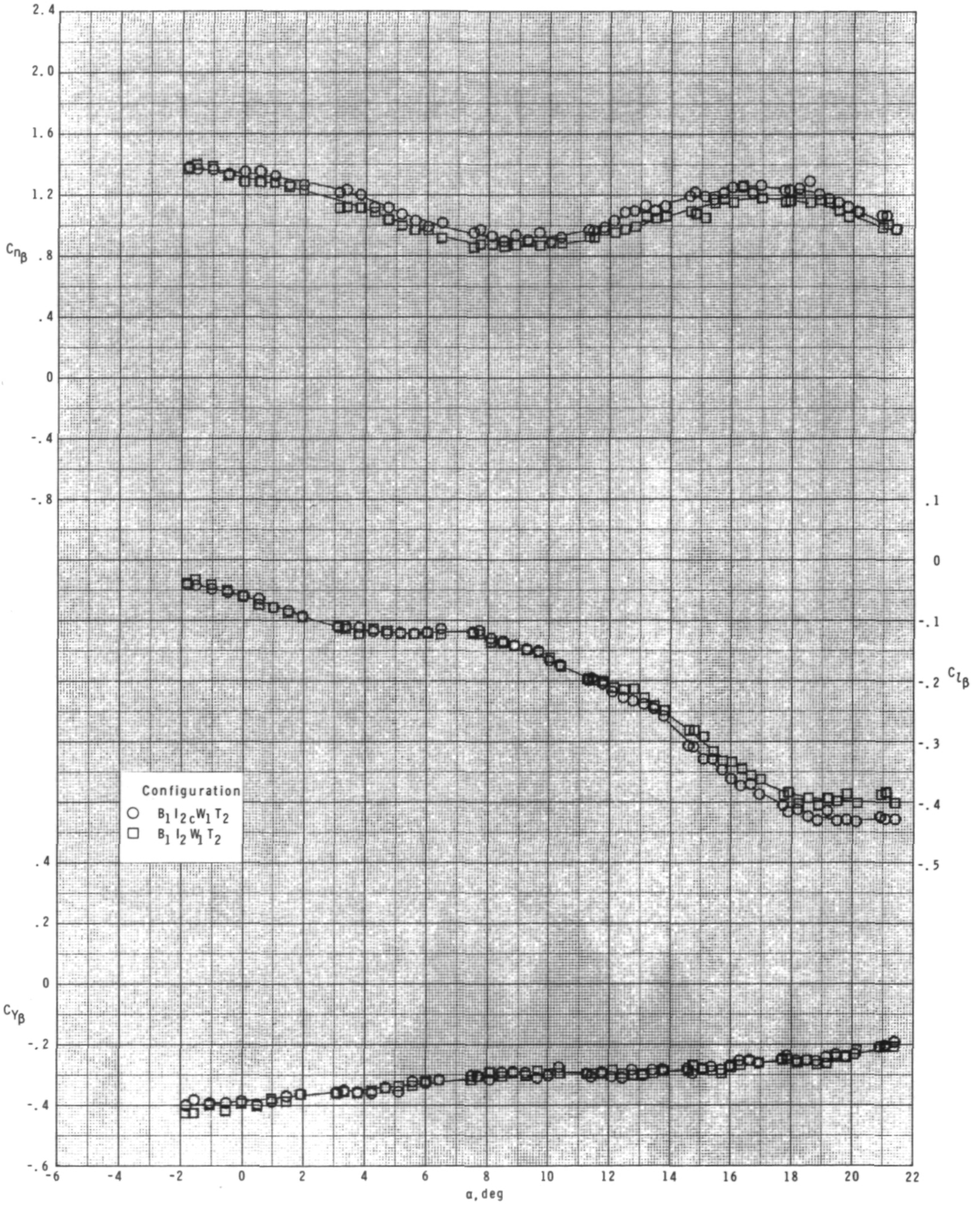

(a) M = 0.60.

Figure 48.- Effect of removing inlet covers on lateral-directional stability with internal ducts closed and ϕ_I = 135°.

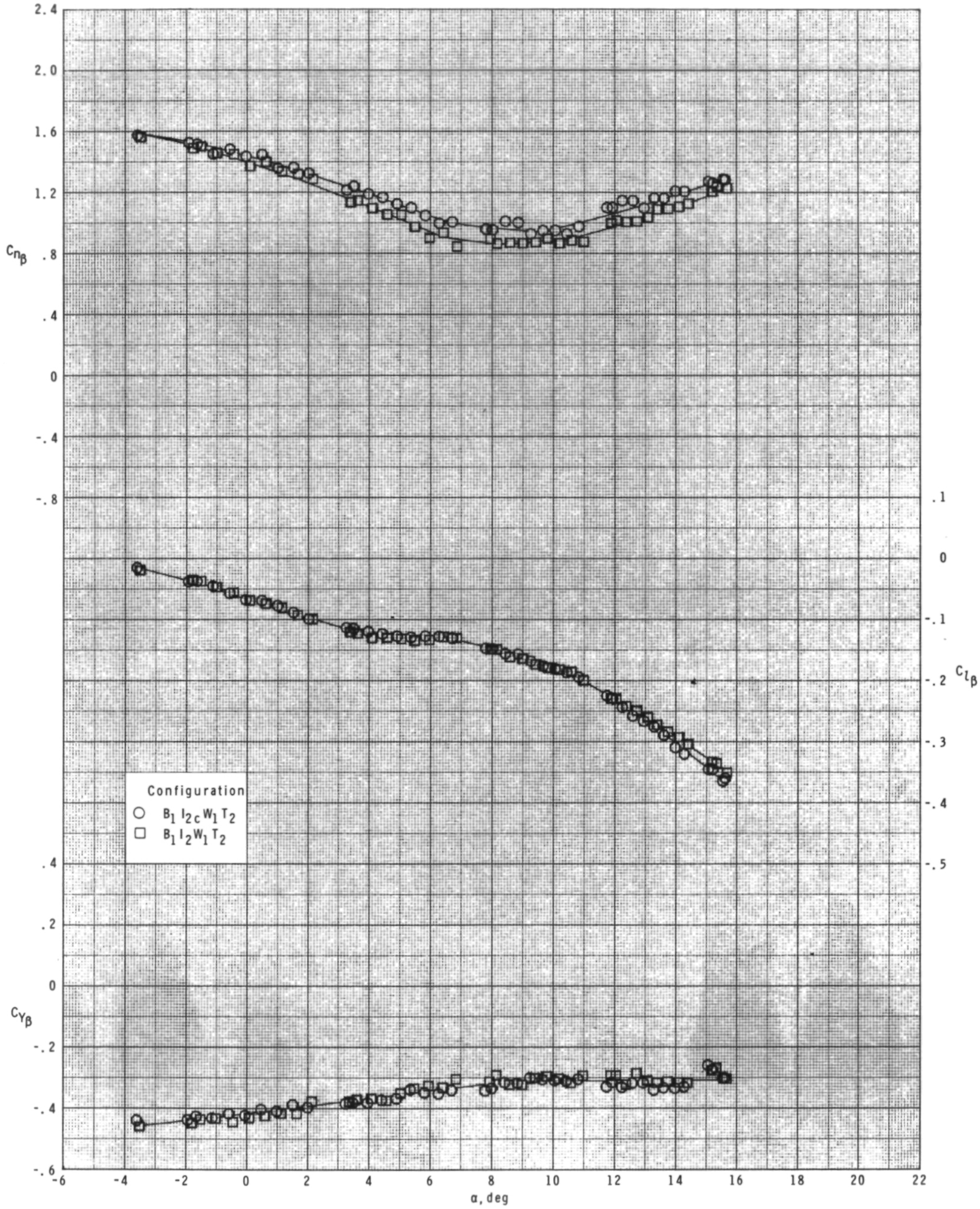

(b) M = 0.80.

Figure 48.- Continued.

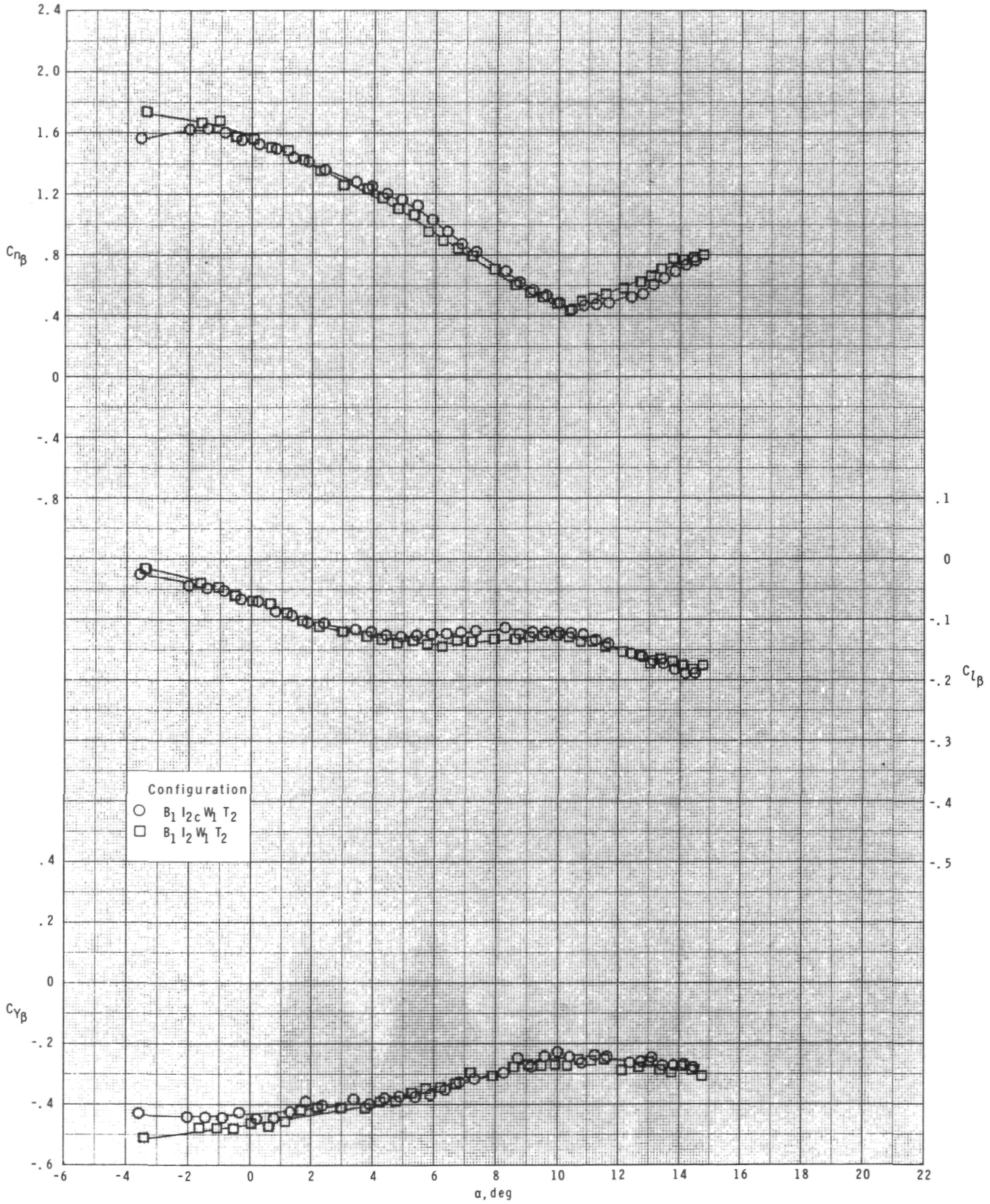

(c) M = 0.95.

Figure 48.- Concluded.

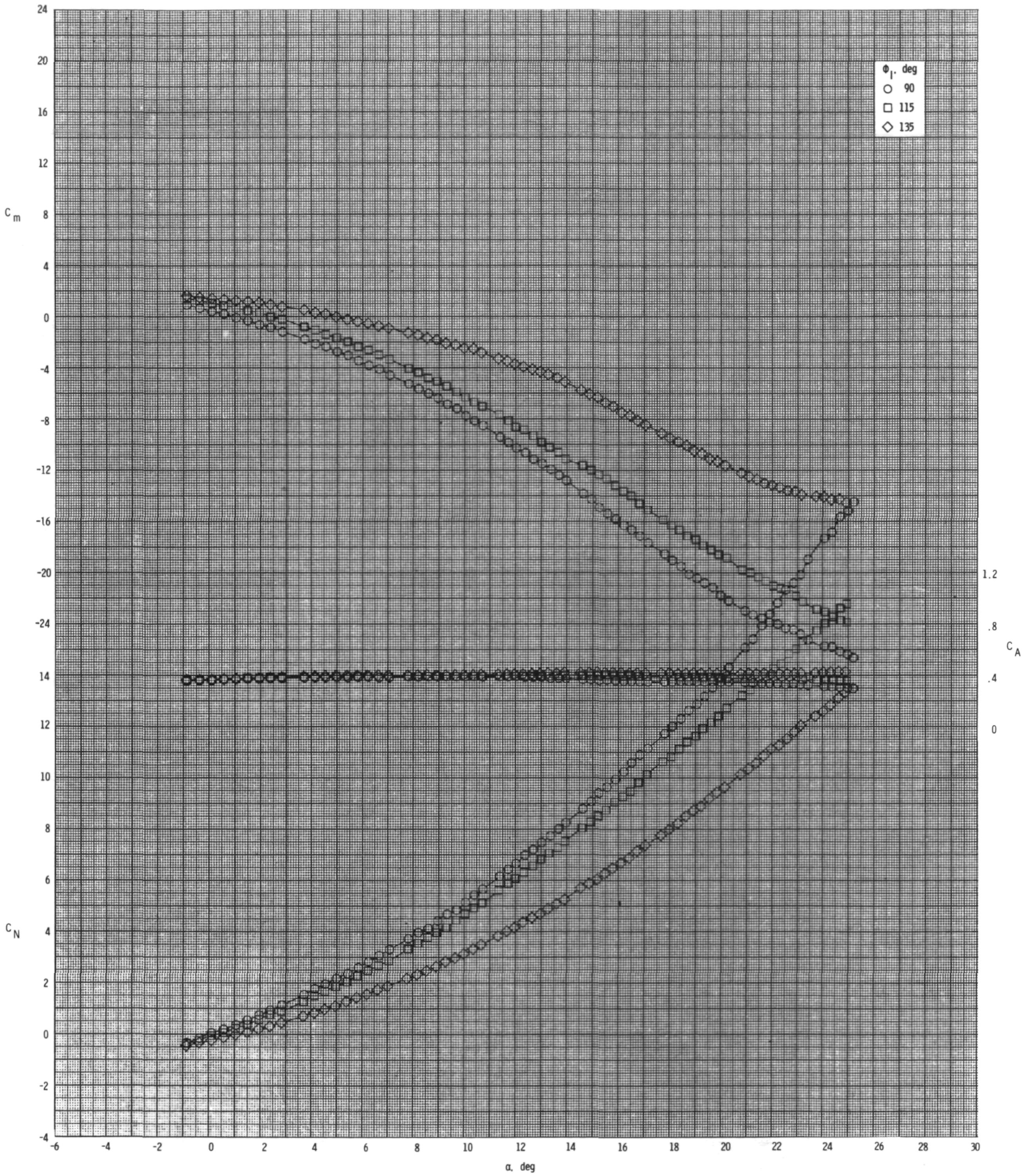

(a) M = 0.60.

Figure 49.- Effect of inlet orientation angle ϕ_I on longitudinal aerodynamic characteristics for configuration $B_1I_{3c}T_1$ with internal ducts closed and $\delta_p = 0°$.

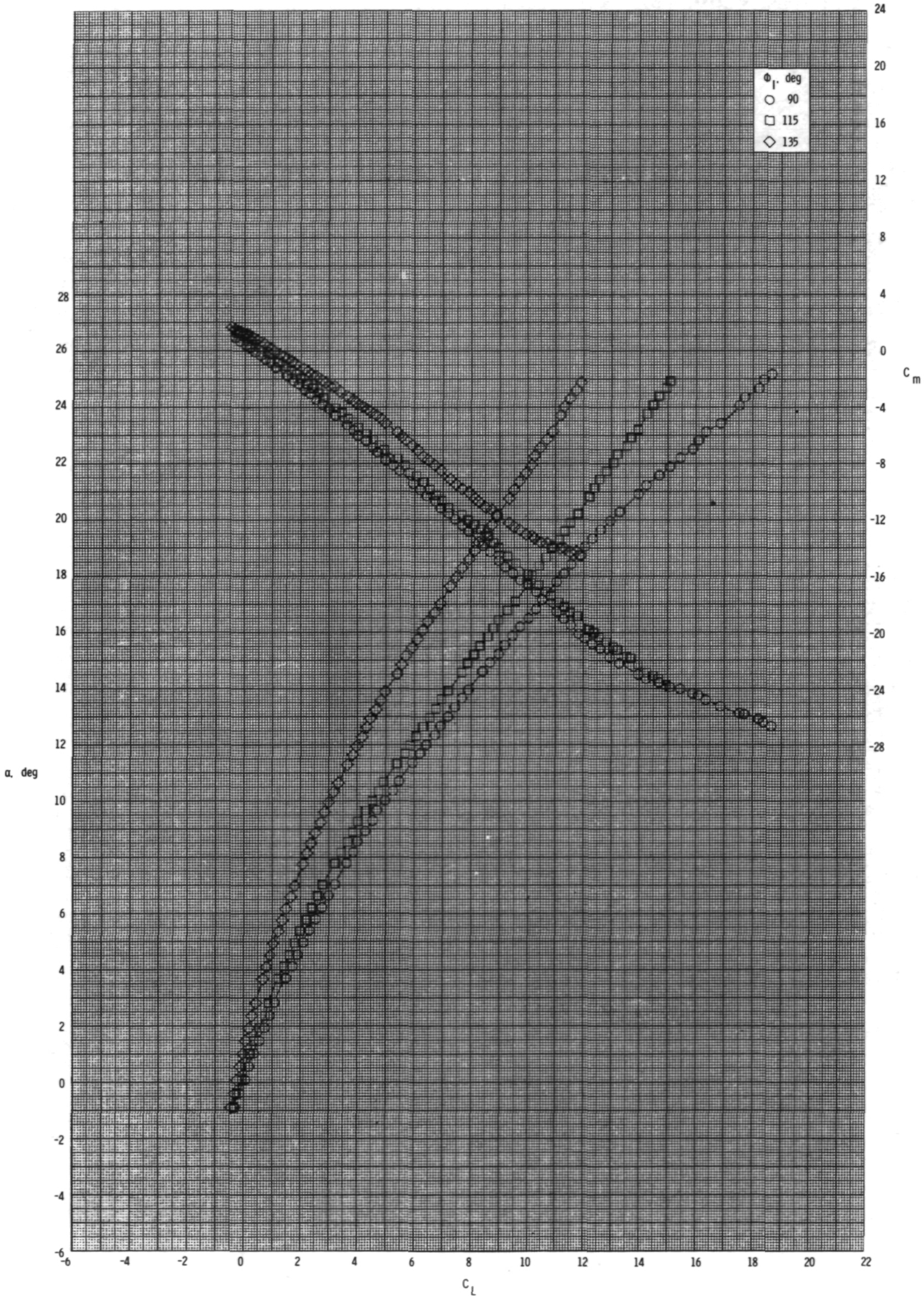

(a) Continued.

Figure 49.- Continued.

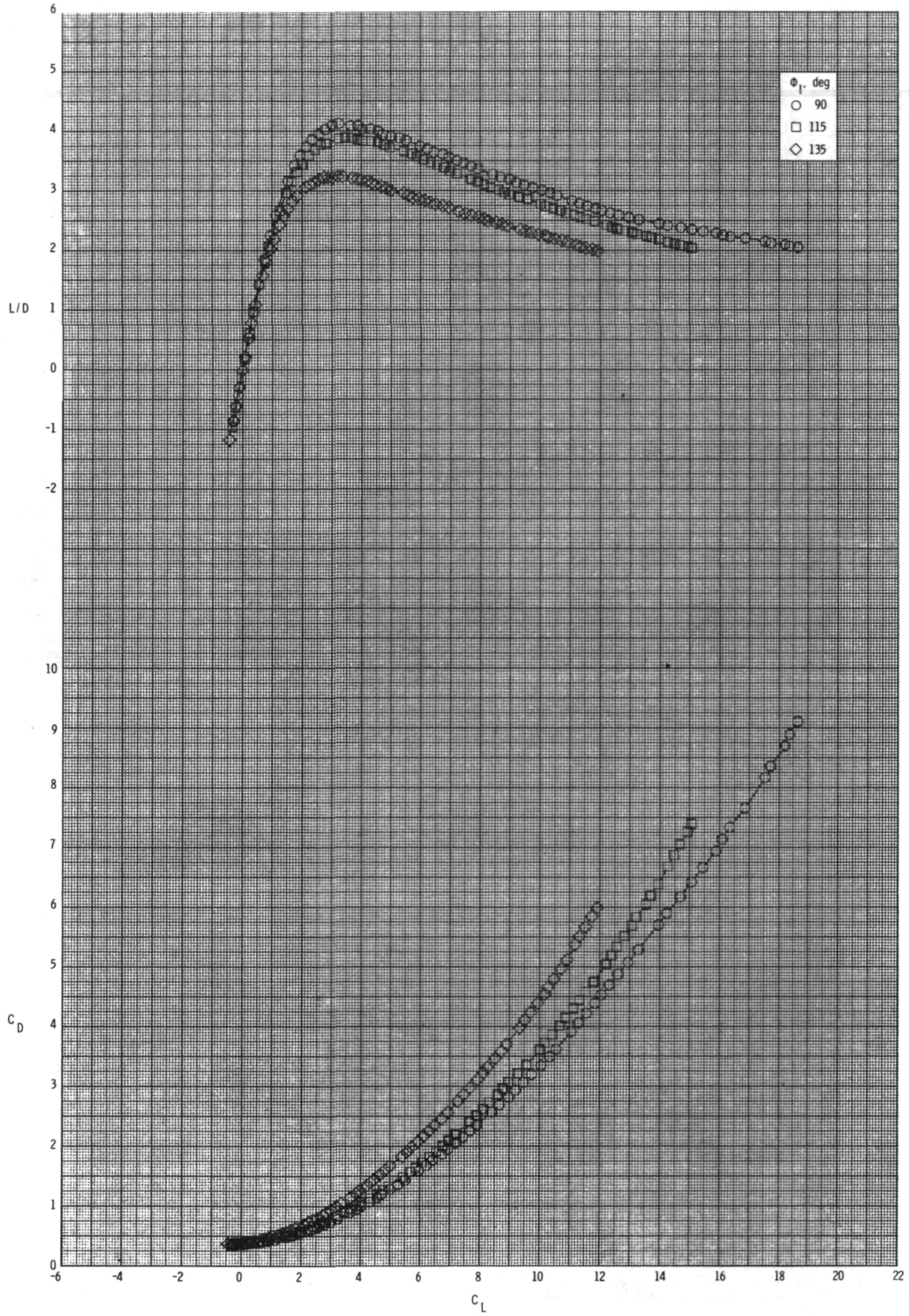

(a) Concluded.

Figure 49.- Continued.

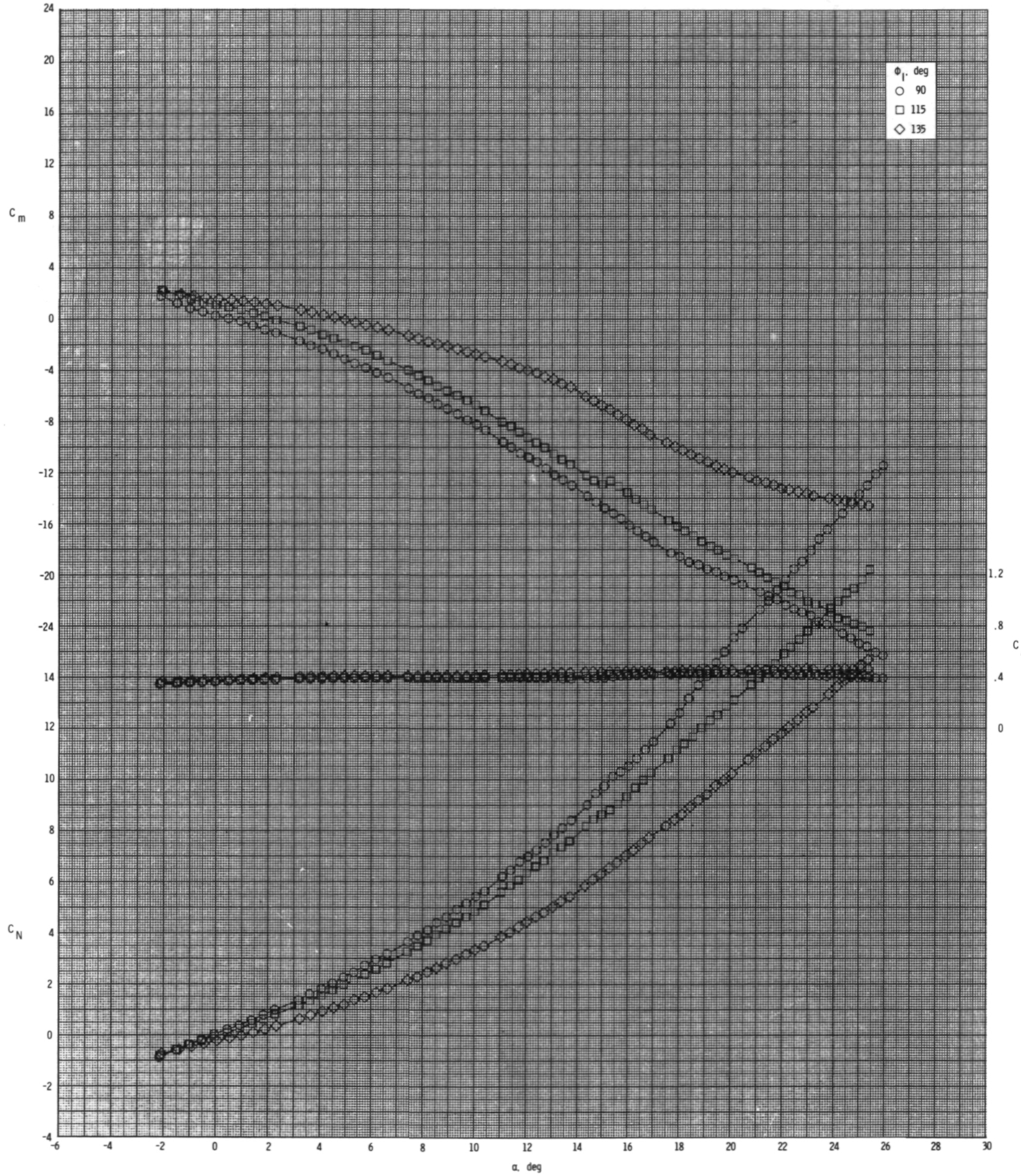

(b) M = 0.80.

Figure 49.- Continued.

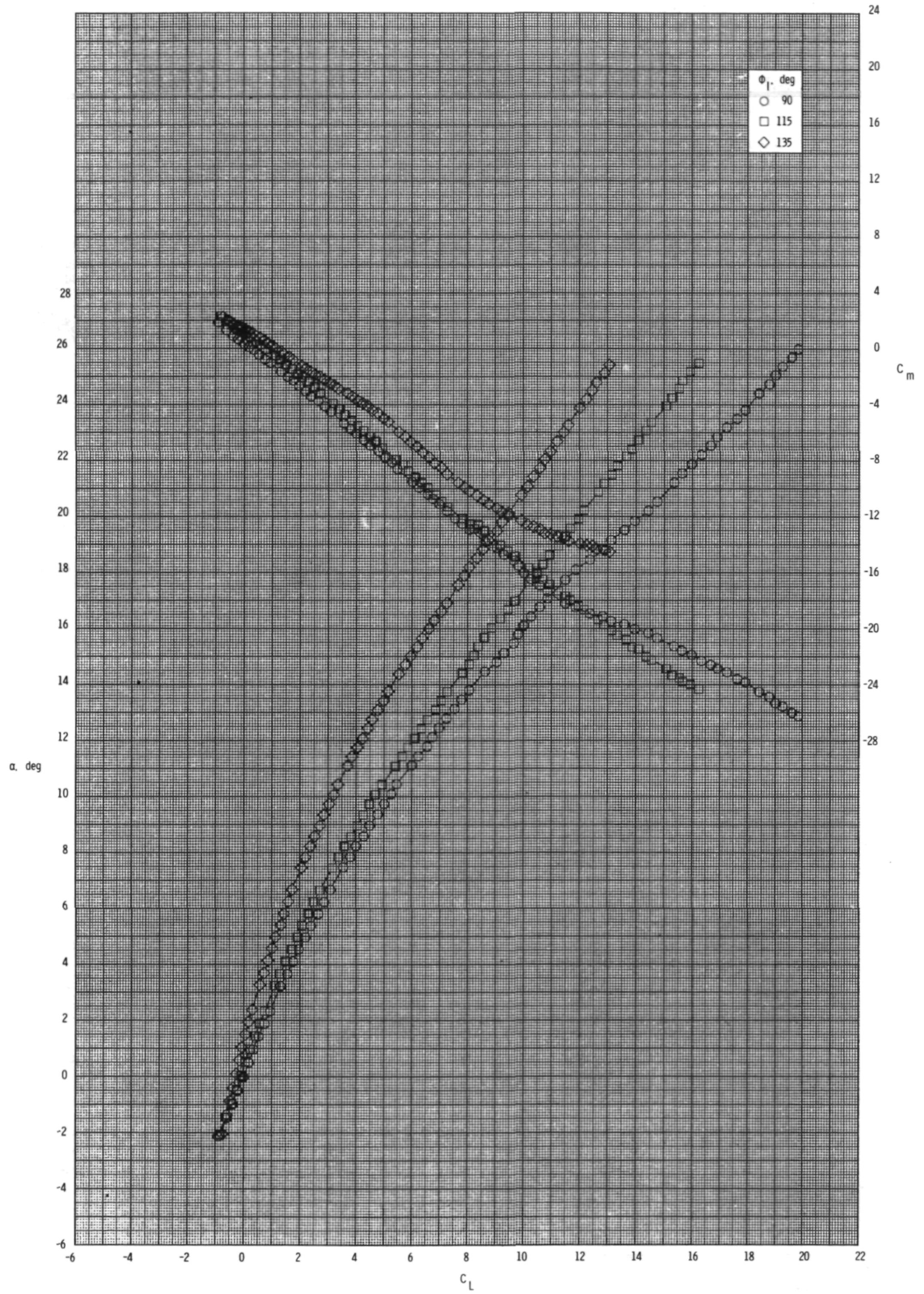

(b) Continued.

Figure 49.- Continued.

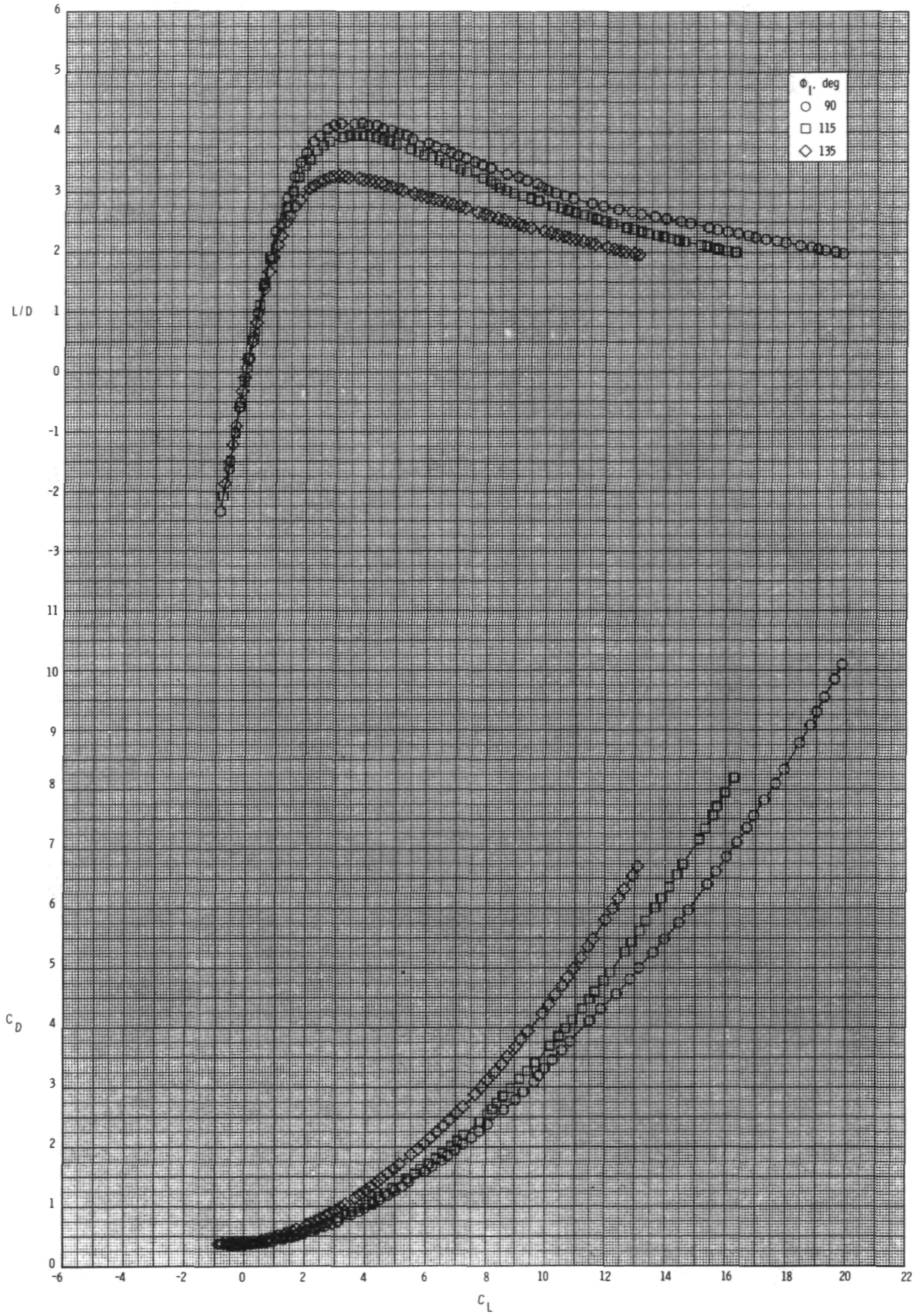

(b) Concluded.

Figure 49.- Continued.

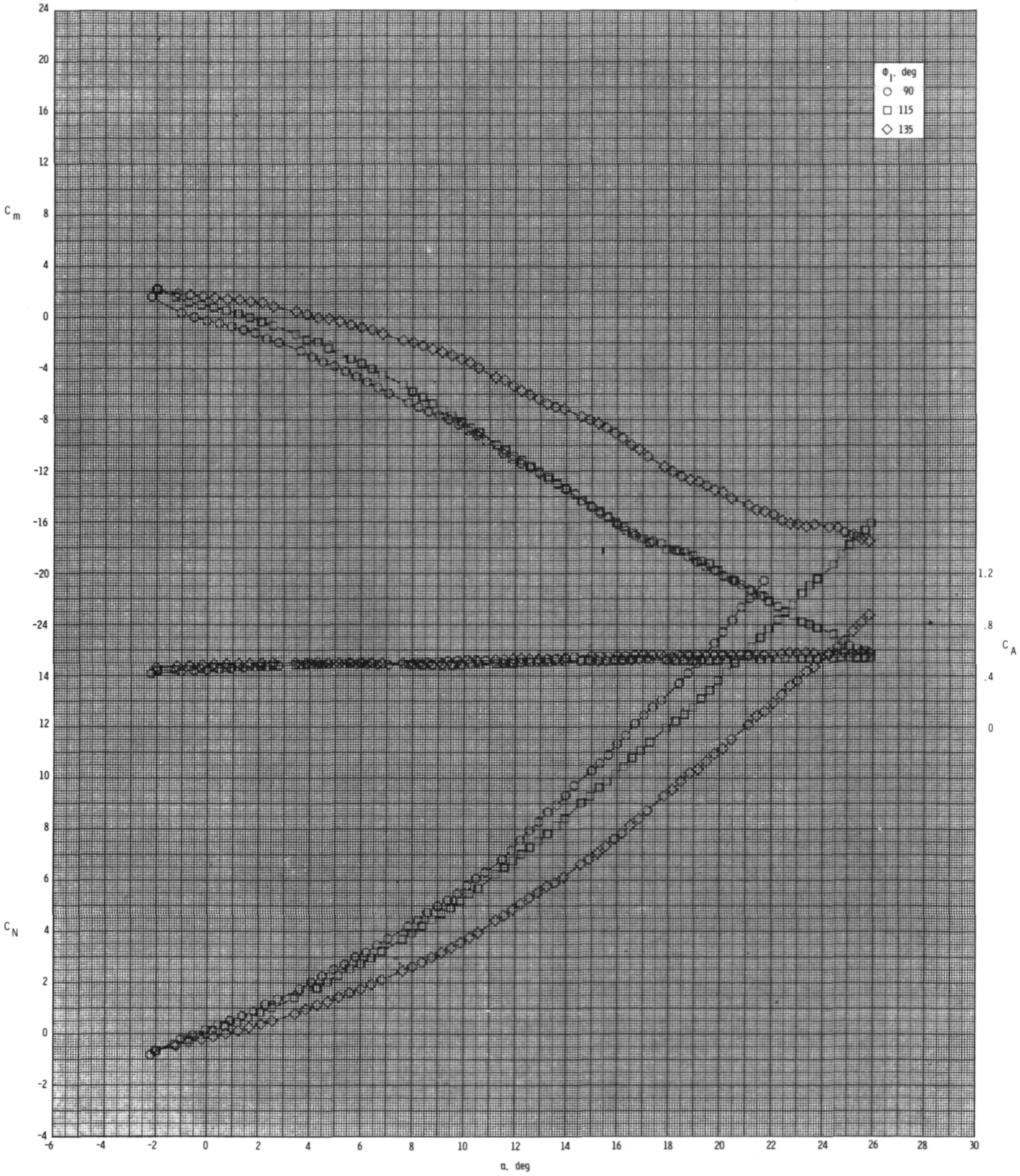

(c) M = 0.95.

Figure 49.- Continued.

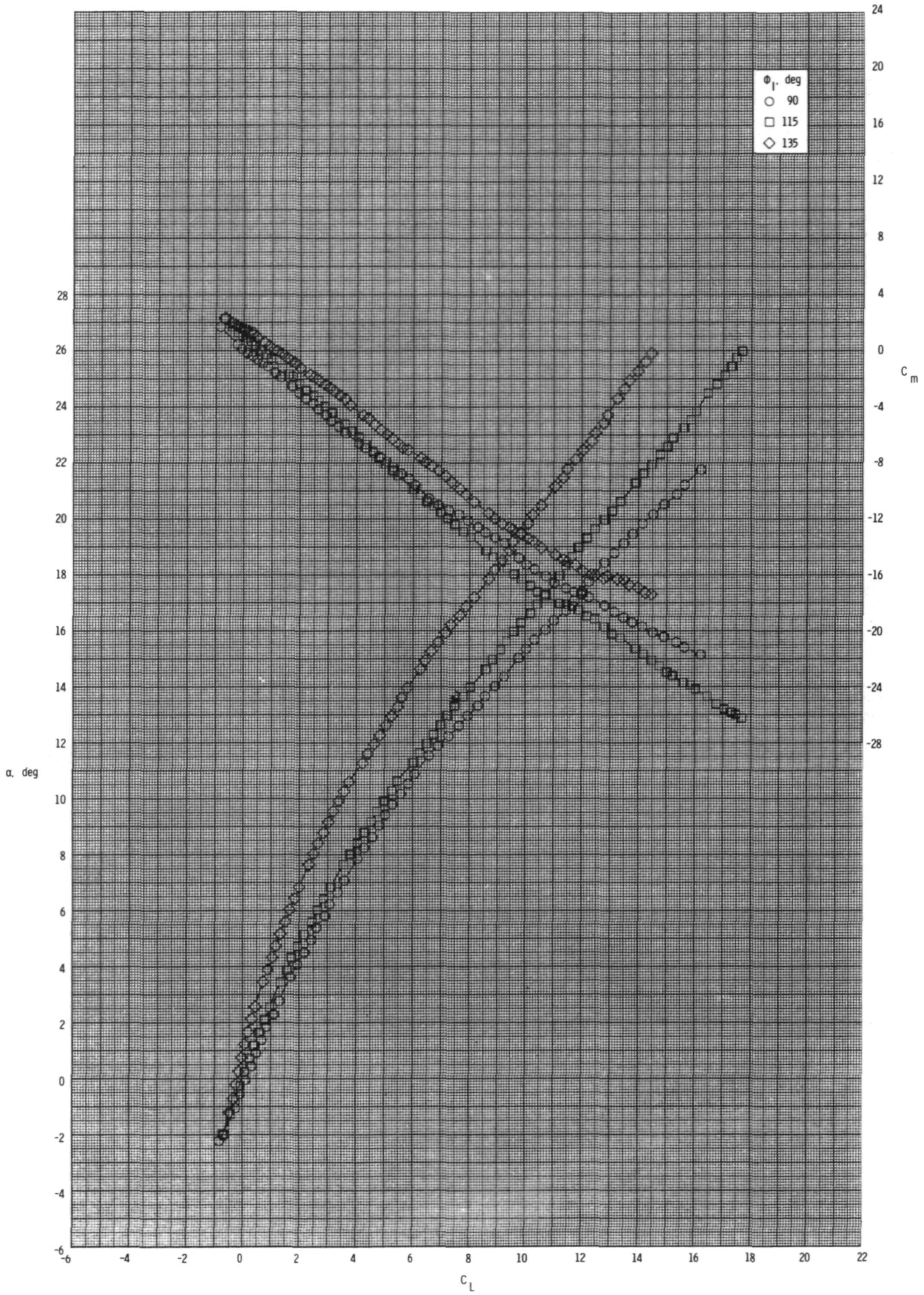

(c) Continued.

Figure 49.- Continued.

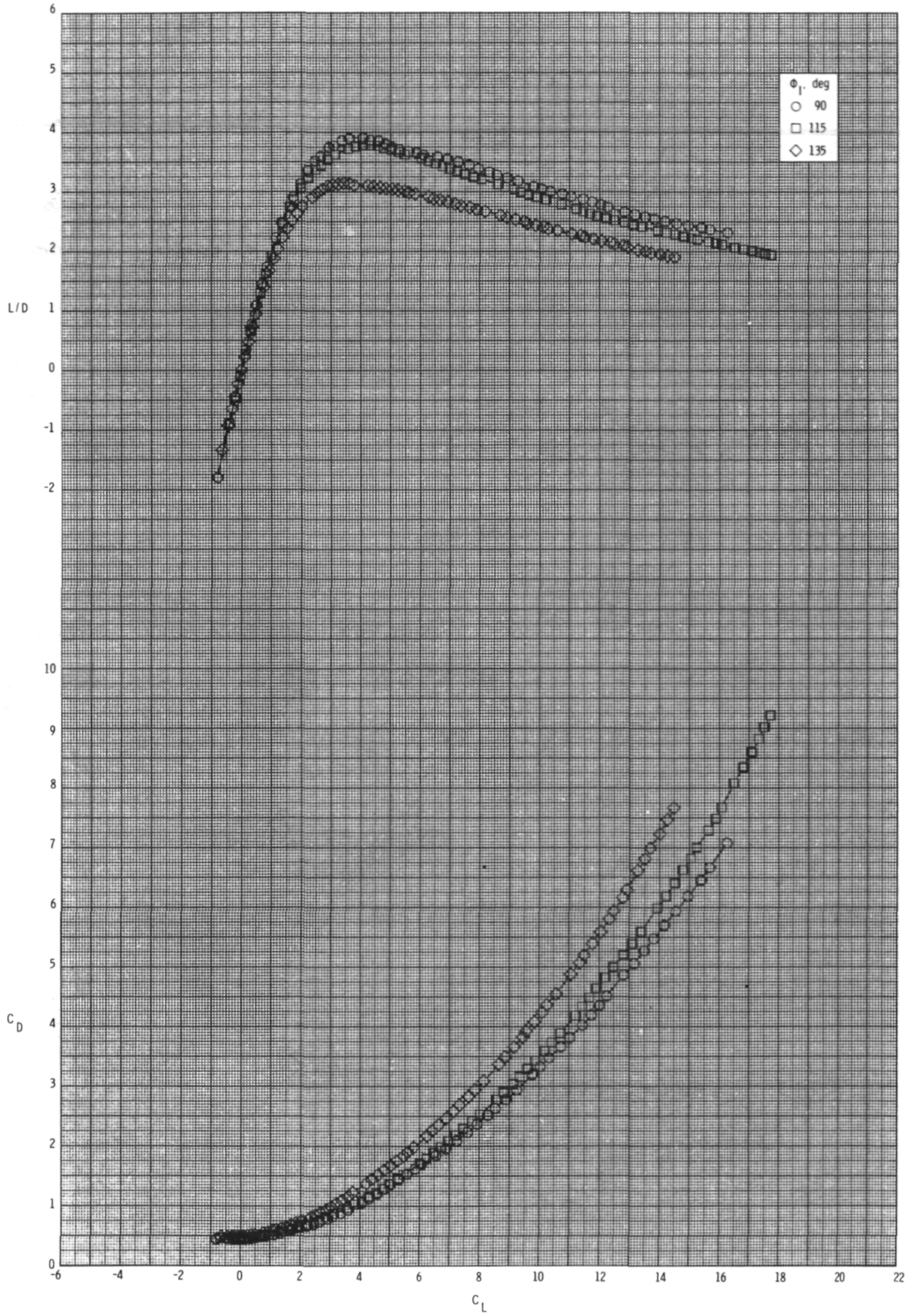

(c) Concluded.

Figure 49.- Concluded.

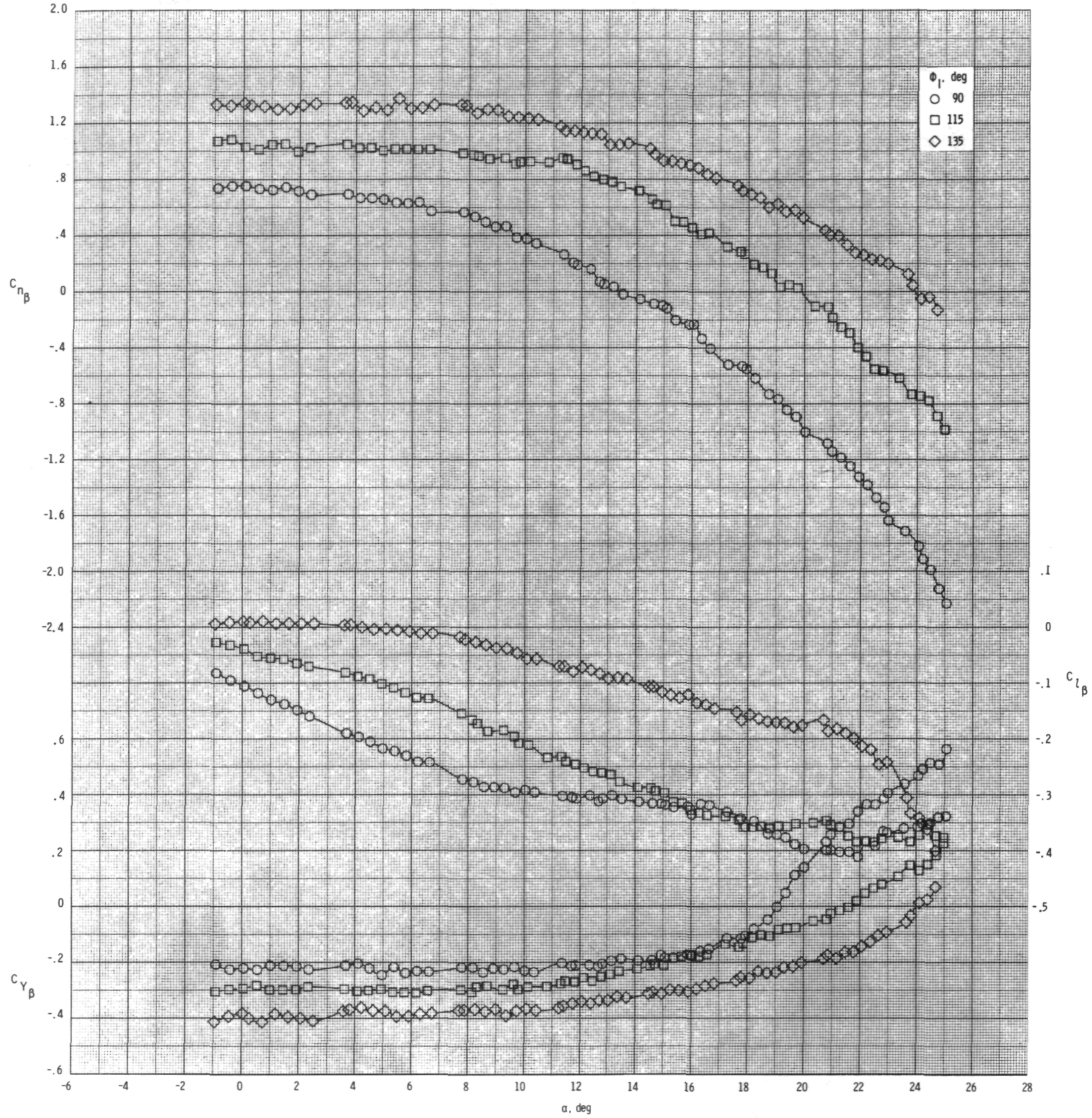

(a) M = 0.60.

Figure 50.- Effect of inlet orientation angle ϕ_I on lateral-directional stability for configuration $B_1 I_{3c} T_1$ with internal ducts closed and $\delta_p = 0°$.

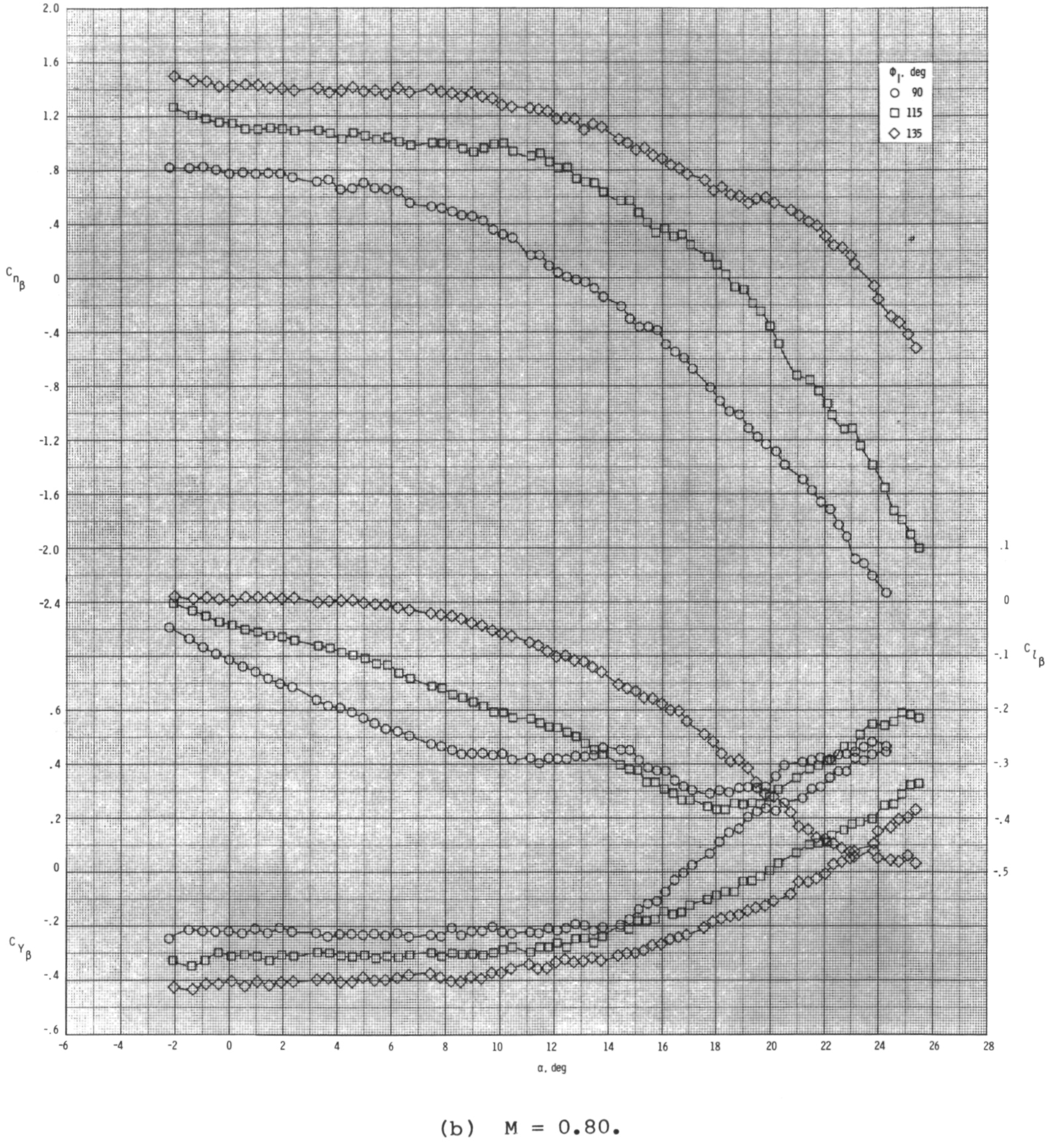

(b) M = 0.80.

Figure 50.- Continued.

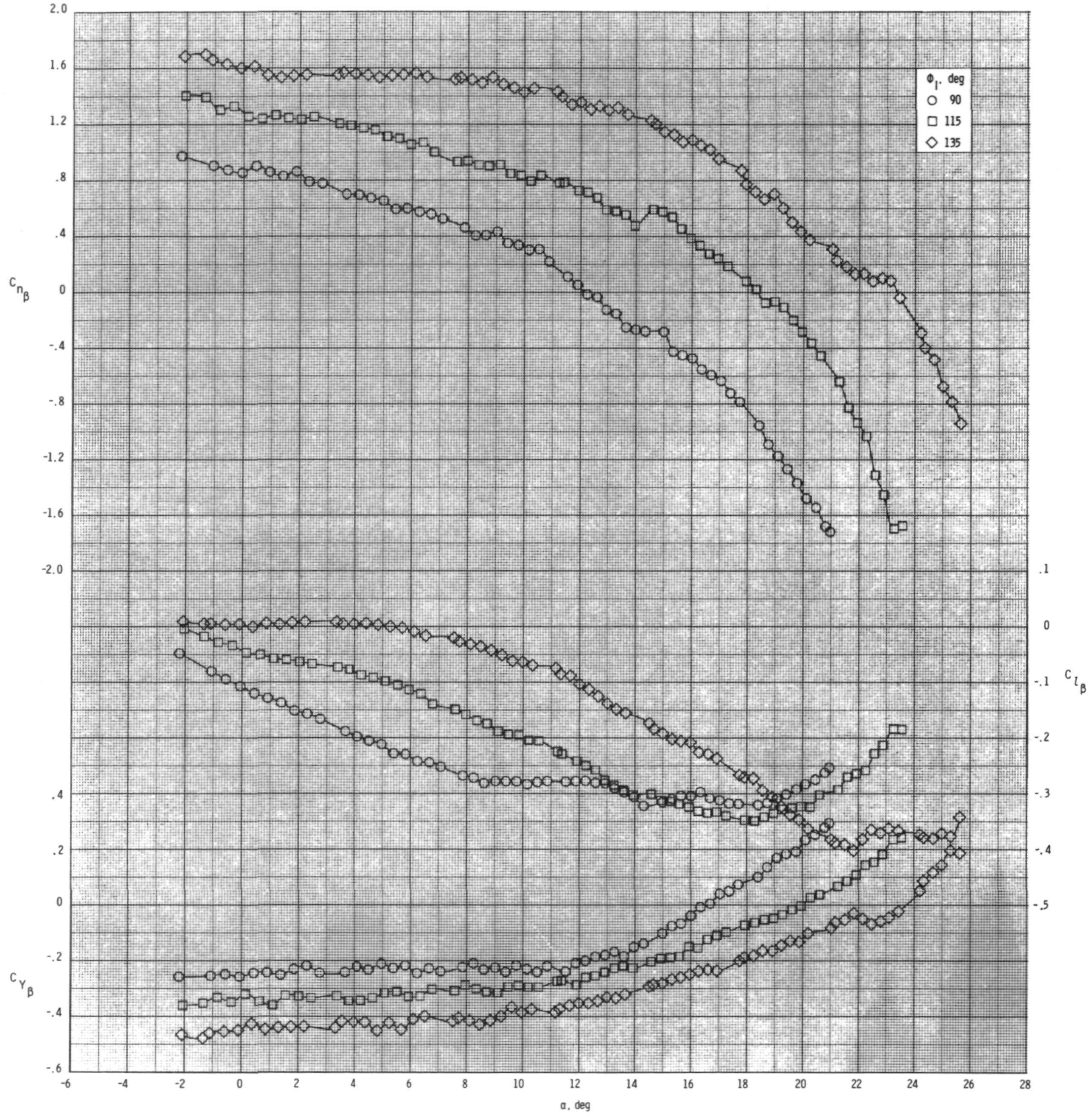

(c) M = 0.95.

Figure 50.- Concluded.

1. Report No.	2. Government Accession No.	3. Recipient's Catalog No.
NASA TM-84560		

4. Title and Subtitle	
AERODYNAMIC CHARACTERISTICS OF A SERIES OF TWIN-INLET AIR-BREATHING MISSILE CONFIGURATIONS III - AXISYMMETRIC AND TWO-DIMENSIONAL INLETS AT SUBSONIC-TRANSONIC SPEEDS	5. Report Date: March 1983
	6. Performing Organization Code: 505-43-23-02
7. Author(s): Clyde Hayes	8. Performing Organization Report No.: L-15528
9. Performing Organization Name and Address: NASA Langley Research Center, Hampton, VA 23665	10. Work Unit No.
	11. Contract or Grant No.
12. Sponsoring Agency Name and Address: National Aeronautics and Space Administration, Washington, DC 20546	13. Type of Report and Period Covered: Technical Memorandum
	14. Sponsoring Agency Code

15. Supplementary Notes

16. Abstract

A series of air-breathing missile configurations has been investigated to provide a data base for the design of such missiles. The model could be configured with either twin axisymmetric or two-dimensional inlets. Three circumferential inlet locations were investigated: 90°, 115°, and 135° from the top center. Two vertical wing locations, as well as wingless configurations, were used. Three tail configurations were formed by locating the tail surfaces either on the inlet fairing or on the inlet fairing or on fairings on the body. The surfaces were used to provide pitch control. Two-dimensional inlets with extended compression surfaces, used to improve the angle-of-attack performance of the inlets for wingless configurations, were also investigated. This report covers both the twin axisymmetric two-dimensional inlet types, without internal flow, and simulates the boost configuration of an air-breathing missile.

17. Key Words (Suggested by Author(s))	18. Distribution Statement
Air-breathing propulsion Stability and control Aerodynamic characteristics	Unclassified - Unlimited Subject Category 02

19. Security Classif. (of this report)	20. Security Classif. (of this page)	21. No. of Pages	22. Price
Unclassified	Unclassified	359	A16

For sale by the National Technical Information Service, Springfield, Virginia 22161

NASA-Langley, 1983